



**HAL**  
open science

# Nouveaux outils pour l'analyse de liaisons chimiques remarquables : caractérisation théorique de la nature des liens avec le béryllium

Oriana Brea

► **To cite this version:**

Oriana Brea. Nouveaux outils pour l'analyse de liaisons chimiques remarquables : caractérisation théorique de la nature des liens avec le béryllium. Theoretical and/or physical chemistry. Université Paul Sabatier - Toulouse III, 2017. English. NNT : 2017TOU30039 . tel-01811168

**HAL Id: tel-01811168**

**<https://theses.hal.science/tel-01811168>**

Submitted on 8 Jun 2018

**HAL** is a multi-disciplinary open access archive for the deposit and dissemination of scientific research documents, whether they are published or not. The documents may come from teaching and research institutions in France or abroad, or from public or private research centers.

L'archive ouverte pluridisciplinaire **HAL**, est destinée au dépôt et à la diffusion de documents scientifiques de niveau recherche, publiés ou non, émanant des établissements d'enseignement et de recherche français ou étrangers, des laboratoires publics ou privés.



# THÈSE

En vue de l'obtention du

## DOCTORAT DE L'UNIVERSITÉ DE TOULOUSE

Délivré par :

Université Toulouse 3 Paul Sabatier (UT3 Paul Sabatier)

---

**Présentée et soutenue par :**

**Oriana BREA NORIEGA**

Le 19/05/2017

**Titre :**

Novel Tools for the Analysis of Non-standard Chemical Bonds: Theoretical  
Insight into the Nature of Beryllium Bonds

---

ED SDM : Physicochimie théorique - COP 01

**Unité de recherche :**

Laboratoire de Chimie et Physique Quantiques (UMR5626)

**Directeur(s) de Thèse :**

Manuel YÁÑEZ MONTERO et Stefano EVANGELISTI

**Rapporteurs :**

Mariona SODUPE ROURE et Carmen BARRIENTOS BENITO

**Autre(s) membre(s) du jury :**

Manuel ÁLCAMÍ PERTEJO

Benoît BRAÏDA



# NOVEL TOOLS FOR THE ANALYSIS OF NON-STANDARD CHEMICAL BONDS:

THEORETICAL INSIGHT INTO THE NATURE OF BERYLLIUM  
BONDS

ORIANA BREA NORIEGA

*A thesis submitted for the degree of Doctor*



Departamento de Química

Facultad de Ciencias

Universidad Autónoma de Madrid

*Supervisor:* Manuel Yáñez Montero

*Co-Supervisor:* Inés Corral Pérez



Ecole doctorale Sciences de la Matière

Laboratoire de Chimie et Physique Quantiques

Université Toulouse III-Paul Sabatier

*Supervisor:* Stefano Evangelisti

*Co-Supervisor:* Thierry Leininger

Madrid, May 2017 –

©2017 by Oriana Brea Noriega

*Novel Tools for the Analysis of Non-standard Chemical Bonds: Theoretical Insight into the Nature of Beryllium Bonds.*

SUPERVISORS:

Manuel Yáñez Montero

Stefano Evangelisti

Inés Corral Pérez

Thierry Leininger

LOCATION:

Universidad Autónoma de Madrid

Facultad de Ciencias, Departamento de Química

Ciudad Universitaria de Cantoblanco, 28049, Madrid, Spain.

Université Toulouse III-Paul Sabatier

Laboratoire de Chimie et Physique Quantiques (LCPQ)

118 Rue de Narbonne, 31062, Toulouse, France.

PhD Thesis, 19 May 2017.

*A Oliver,  
por enseñarme que no existen metas imposibles de cruzar.*



*Nothing in life is to be feared, it is only to be understood.  
Now is the time to understand more, so that we may fear less.*  
— **Maria Skłodowska-Curie** .

## AGRADECIMIENTOS

---

Esta tesis no hubiera sido posible sin el gran apoyo de mi director de tesis Manuel Yáñez y la profesora Otilia Mó. Gracias infinitas por haberme recibido en su grupo, por enseñarme y guiarme durante el desarrollo de esta tesis, por crear un ambiente de trabajo increíble, por sus grandes consejos e historias, y por confiar en mí para llevar a cabo este trabajo. De igual manera, a mi co-directora de tesis Inés Corral. Gracias por todo el cariño y tiempo que has dedicado a este proyecto, por todo lo que he aprendido de ti durante esta etapa y por todos los grandes momentos que hemos compartido (no encontraré una mejor compañera de aventuras/congresos en ningún lugar del mundo).

To my thesis director Stefano Evangelisti and co-director Thierry Leininger for giving me a second home in Toulouse. Thank you for your endless patience, for introducing and teaching me a new world beyond chemistry, for helping me to survive to french bureaucracy, and for all the amazing moments we shared in the Pyrenees or having dinner at Stefano's place.

Gracias al Centro de Computación Científica de la Universidad Autónoma de Madrid por su gran servicio. Así como, al Ministerio de Educación, Cultura y Deporte de España por mi beca doctoral y a las organizaciones NEXT y Campus France por mis becas de movilidad.

Gracias a los profesores Mariona Sodupe, Manuel Alcamí, Benoît Braïda, Carmen Barrientos, Ibon Alkorta y Aurora Costales por aceptar ser parte del tribunal. Así como a Daniel Escudero por acceder a ser evaluador internacional de mi tesis.

Gracias al departamento de Química de la Universidad Autónoma de Madrid por los recursos aportados para realizar este trabajo de investigación. A todos los que hacen vida en este departamento, gracias por crear un súper ambiente de trabajo y por estar siempre dispuestos a ayudarme. Marga y Wilson, quisiera agradecerles todo su cariño y el hacer más sencillo este trabajo. Millones de gracias a los habitantes del despachin 501-A. A los que ya no están con nosotros: Ane, Juan Pablo, Martina. . . A los que siguen ahora: Enrique y Eva. Y a las que se convirtieron en indispensables en mi vida: Lara, gracias por estar siempre del otro lado de la pantalla (literal y metafóricamente), por tener siempre la respuesta correcta a todo y por todos los grandes momentos que compartimos juntas (Oviedo, boda, forever 21, navidades. . . te echo muchísimo de menos). Serris, gracias por escucharme y ayudarme a encontrar la solución perfecta a todos los problemas, por enseñarme a tener más paciencia y calma y por siempre regalarme un sonrisa. A José Manuel Segovia, gracias por hacer que nuestro trabajo sea visualmente asombroso y por hacernos sentir parte de tu familia.



Aux personnes dans l'Institut de Recherche sur les Systèmes Atomiques et Moléculaires Complexes dans l'Université Paul Sabatier. Merci beaucoup for all the interesting discussions in the group meetings (and the "Loto de Vin"), for the nice environment and for the incredible moments in the cafeteria and Dubliners. Specially, to Muammar, gracias por tu infinita paciencia, por enseñarme a ser un poco más UNIX y lo más importante, por tu amistad y la de Claudia. Ahmad, gracias por ser un gran compañero de trabajo y por las tardes al sol tomando té enseñándome una nueva perspectiva del mundo. Mina, thank you very much for all the great moments we shared in Toulouse, since dancing over tables until the nice trips, miss you girl. Stefano (the technician), thank you very very much for all your help and support during this rough time, for so many moments we shared together ("Notre Rhum qui est frais,...") and for the technical/methodological assistance.

Amigos, la familia que elegimos. Gracias a los pagafantas por hacer tan sencillo estar lejos de casa. Álvaro, gracias por todos los momentos especiales que hemos compartido, por tu eterno apoyo y por poner un poco de música en mi vida. Chiara, la mia ragazza, grazie mille bella por estar siempre dispuesta a ayudarme y por enseñarme un poco de estilo italiano, te echo mucho de menos. Darek, mi polaco favorito, gracias por tus increíbles ocurrencias, por estar siempre feliz y tener una gran historia que contar y por todo el apoyo al final, cuando más lo necesitaba. David, muchacho, eres el corazón de este grupo, gracias por estar siempre disponible para lo que sea y porque sin ti todo sería infinitamente más aburrido. Estefi, gracias por ser mamitefi, por tener siempre un consejo para dar y aportar un toque de locura a mi vida, también te extraño muchísimo. Juanjo, eres la mejor persona que existe en este planeta y tengo la suerte de contar contigo, gracias por abrir puertas cuando nadie podía abrirlas y por siempre abrir un espacio en tu (ocupada) agenda para nosotros. Patri, no podría imaginarme Madrid (o Toulouse) sin ti, gracias por ser una gran amiga, por apoyarme y soportarme desde el principio, por pegarme un poco (mucho) el acento madrileño, por . . . , son muchas cosas! Gracias por estar siempre ahí.

A toda mi familia, agradecerles todo su apoyo, tanto a los que están cerca como a los que están a millas de distancia. A mis padres, Zulia y José, gracias por enseñarme a ser la persona que soy y por apoyarme incondicionalmente en cada una de mis aventuras. A mi hermana, Marina, gracias por ser mi compañera de vida, por estar del otro lado del teléfono cuando volvía tarde a casa, por esperarme con mil planes (como si nunca hubiera estado lejos), por pretender que te interesaba en lo que he estado trabajando, y por ser la mejor hermana!

## PUBLICATIONS

---

The results of this thesis are published in the following papers:

- ***Behavior of the Position–Spread Tensor in Diatomic Systems.*** Brea, O.; El Khatib, M.; Angeli, C.; Bendazzoli, G. L.; Evangelisti, S.; Leininger, T. *Journal of chemical theory and computation*, **2013**, 9, 5286.
- ***Creating  $\sigma$ –Holes through the Formation of Beryllium Bonds.*** Brea, O.; M $\acute{o}$  O.; Y $\acute{a}$ ñez, M.; Alkorta, I.; Elguero, J. *Chemistry-A European Journal*, **2015**, 21, 12676.
- ***Intramolecular beryllium bonds. Further insights into resonance assistance phenomena.*** Brea, O.; Alkorta, I.; Corral, I.; M $\acute{o}$ , O.; Y $\acute{a}$ ñez, M.; Elguero, J. *Intermolecular interactions in crystals: Fundamentals of Crystal Engineering*; Novoa, J., Ed.; Royal Society of Chemistry: Cambridge, **2016**.
- ***Exergonic and Spontaneous Production of Radicals through Beryllium Bonds.*** Brea, O.; Alkorta, I.; M $\acute{o}$ , O.; Y $\acute{a}$ ñez, M.; Elguero, J.; Corral, I. *Angewandte Chemie*, **2016**, 128, 8878.
- ***The Spin-Partitioned Total-Position Spread Tensor: An Application to Diatomic Molecules.*** Brea, O.; El Khatib, M.; Bendazzoli, G. L.; Evangelisti, S.; Leininger, T.; Angeli, C. *The Journal of Physical Chemistry A*, **2016**, 120, 5230.
- ***On the Existence of Intramolecular One–electron Be–Be Bonds.*** Brea, O.; M $\acute{o}$ , O.; Y $\acute{a}$ ñez, M.; Alkorta, I.; Elguero, J. *Chemical Communications*, **2016**, 52, 9656.
- ***Beryllium-based Anion sponges. Close Relatives of Proton Sponges.*** Brea, O.; Corral, I.; M $\acute{o}$ , O.; Y $\acute{a}$ ñez, M.; Alkorta, I.; Elguero, J. *Chemistry-A European Journal*, **2016**, DOI: 10.1002/chem.201604325. **(Inside cover)**.
- ***Modulation of the strength of Be-Be bonds by Lewis Base coordination..*** Brea, O.; Alkorta, I.; Leininger, T. ; M $\acute{o}$ , O.; Elguero, J.; Evangelisti, S.; Y $\acute{a}$ ñez, M. ; Corral, I. **In preparation**
- ***The Total-Position Spread Tensor description of Be-carbonyl derivatives.*** Brea, O.; Leininger, T. ; Y $\acute{a}$ ñez, M. ; Corral, I.; Evangelisti, S. **In preparation**

Other results not related to the thesis subject are published in the following papers:

- ***Ga<sup>+</sup> Basicity and Affinity Scales Based on High–Level Ab Initio Calculations.*** Brea, O.; M $\acute{o}$ , O.; Y $\acute{a}$ ñez, M. *ChemPhysChem*, **2015**, 16, 3206.

- ***Why Is the Spontaneous Deprotonation of [Cu (uracil)<sub>2</sub>]<sup>2+</sup> Complexes Accompanied by Enolization of the System?***. Brea, O.; Yáñez, M.; MÓ.; Lamsabhi, A. M. *ChemPhysChem*, **2015**, 16, 2375. (Inside cover),
- ***The Total Position—Spread Tensor: Spin Partition***. El Khatib, M.; Brea, O.; Fertitta, E.; Bendazzoli, G. L.; Evangelisti, S.; Leininger, T. *The Journal of chemical physics*, **2015**, 142, 094113.
- ***Spin Delocalization in Hydrogen Chains Described with the Spin—Partitioned Total Position-Spread Tensor***. El Khatib, M.; Brea, O.; Fertitta, E.; Bendazzoli, G. L.; Evangelisti, S.; Leininger, T.; Paulus, B. *Theoretical Chemistry Accounts*, **2015**, 134, 1.

## ABSTRACT

---

The chemical bond is among the oldest and most important concepts in chemistry because it allows to describe chemical properties of a system, as well as to understand and predict chemical reactions. The main goal of this PhD thesis is to study new types of chemical interactions involving the beryllium atom. Be atom has a rich chemistry due to its low-lying  $p_{\text{Be}}$  orbitals, but its high toxicity has limited the number of experimental studies, enhancing the importance of theory in the description of Be compounds. This thesis reports the theoretical analysis of three new types of Be bonds using high-level ab-initio and Density Functional Theory, and the applications of the Total Position Spread Tensor (TPS) to molecular systems.

First, the non-covalent Beryllium Bonds (BerB). This type of bond is formed by an interaction between a Be moiety acting as a strong Lewis Acid (LA) and a Lewis Base (LB). The interaction between beryllium LA and fluorine derivatives (FR) generates a  $\sigma_{\text{hole}}$  in the fluorine atom, otherwise not possible, opening the possibility to design new materials where fluorine binds through halogen bonds. This same interaction decreases the F-R bond energy, turning the F-R homolytic dissociation in an *exothermic process*, and suggesting BerBs can be used to produce spontaneously radical species. Moreover, in this thesis, Intramolecular Beryllium Bonds (IBerB) were studied in malonaldehyde- and tropolone-like systems. This interaction is stronger in unsaturated systems than in their saturated analogues due to the increase of the acidity and basicity of the LA and LB, respectively.

Second, the intramolecular Be-Be bond in disubstituted naphthalene complexes. The anion species of 1,8-diBeY<sub>1</sub>'-naphthalene derivatives show a very strong *one-electron* Be-Be bond. This bond is eight times stronger and 0.5 Å shorter than the one in the isolated dimer. These systems present high electron affinities, which give to them an exceptional property: the ability to behave as what we have named anion sponges. It was found that the interaction between anions and Be disubstituted naphthalene is among the highest anion affinities reported in the literature for neutral compounds. This property could lead to a wide range of applications as anions receptors and sensors.

Third, the interaction between the Be<sub>2</sub> molecule and Lewis bases, which has shown to enhance the strength of the Be-Be bond compared with the isolated molecule. The non-covalent interaction in complexes of the type L: Be-Be: L decreases the distance and increases the strength of the Be-Be bond. The effect over the Be<sub>2</sub> moiety depends on the nature of the Lewis bases. The most dramatic effect occurs when L are radical species. The Be-Be bond in this type of complexes is among the strongest reported in the literature due to an increase of the Be<sub>2</sub> oxidation state from Be<sub>2</sub><sup>0</sup> to Be<sub>2</sub><sup>2+</sup>. The same effect is found in ligands with  $\pi_{\text{L}}$  orbitals, which conjugate with the  $\pi_{\text{Be}}$  orbitals and increase the oxidation state of the Be<sub>2</sub> moiety to +1. Therefore, the Be-Be interaction becomes stronger than the free Be<sub>2</sub> molecule,

although still weaker than that of complexes with radical species. At last, the complexes where the Be<sub>2</sub> moiety remains neutral and interacts with the lone pairs of the LB show, to the best of our knowledge, the strongest Be-Be bond reported in the literature for the neutral Be dimer.

Finally, the TPS is proposed as a new method for the description of chemical bonds. The TPS is quantity that describes the electron and spin fluctuation when a system is perturbed. In this PhD thesis the TPS is applied to diatomic molecules and to Be-carbonyl derivatives. The tensor shows a different behavior depending on the type of interaction, thus allowing the distinction between a covalent, ionic, charge-shift, and other types of bonds, and at the same time the tensor identifies the electron correlation nature of the system.

## RESUMEN

---

El enlace químico es uno de los conceptos más antiguos e importantes en química ya que las propiedades y la reactividad química de un sistema pueden ser explicadas tomando en cuenta este modelo. El objetivo principal de esta tesis doctoral es el estudio de nuevos tipos de enlaces químicos en los que participa el átomo de Berilio. El átomo de Be tiene una extraordinaria química debido a sus orbitales  $p_{Be}$  bajos en energía, sin embargo, el número de estudios experimentales de derivados de Be se encuentran limitados por la alta toxicidad del metal, con lo cual, la descripción teórica de los compuestos de Be adquiere mayor relevancia. Esta tesis realiza un análisis teórico de tres nuevos tipos de enlaces de Be aplicando métodos ab-initio y Teoría del Funcional de la Densidad (DFT, por sus siglas en inglés Density Functional Theory). Así como, la aplicación del Tensor de Propagación de la Posición Total (TPS, por sus siglas en inglés Total Position Spread tensor) a sistemas moleculares.

En primer lugar, el enlace no-covalente de Be (BerB, por sus siglas en inglés Beryllium Bond). Este tipo de enlace se forma por la interacción entre un derivado de Be que actúa como un Ácido de Lewis (AL) fuerte y una Base de Lewis (BL). La interacción entre AL de berilio y derivados de flúor (FR) genera un  $\sigma_{agujero}$  en el átomo de flúor, lo que permite diseñar nuevos materiales con derivados de Be unidos a través de enlaces de halógenos. Esta misma interacción debilita la fuerza del enlace F-R, convirtiendo la disociación homolítica del mismo en un *proceso exotérmico*. Por lo tanto, los BerBs pueden ser utilizados para formar especies radicalarias espontáneamente. Los Enlaces de Berilios Intramoleculares (IBerB, por sus siglas en inglés Intramolecular Beryllium Bonds) fueron estudiados en derivados del malonaldehído y tropolona. Estas interacciones intramoleculares son más fuertes en sistemas insaturados que en saturados análogos, esto se debe a que los AL y BL son más ácidos y más básicos, respectivamente.

En segundo lugar, el enlace intramolecular Be-Be en complejos disustituido de naftaleno. El enlace Be-Be en los aniones de los derivados del 1,8-diBeY<sub>1</sub>'-naftaleno es muy fuerte, y se caracteriza por ser un enlace *mono-electrónico*. Se encontró que este tipo de enlace es 0,5 Å más corto y ocho veces más fuerte que el del dímero de Be aislado. La afinidad electrónica de estos sistemas es muy alta, lo cual les da una propiedad excepcional: la habilidad de comportarse como lo que hemos denominado *esponjas de aniones*. Los resultados muestran que las afinidades aniónicas de los derivados del 1,8-diBeY<sub>1</sub>'-naftaleno se encuentra entre las más altas reportadas en la literatura, por lo que estos compuestos podrían ser aplicados como receptores y sensores de aniones.

Tercero, la interacción entre la molécula Be<sub>2</sub> y bases de Lewis, la cual ha demostrado incrementar la fuerza del enlace Be-Be respecto a la molécula aislada. La interacción no-covalente en sistemas del tipo L: Be-Be: L disminuye la distancia y aumenta la fuerza del

enlace Be-Be. El efecto sobre el monómero del  $\text{Be}_2$  dependerá de la naturaleza de la Base de Lewis. El efecto más dramático ocurre cuando L es un radical, el enlace Be-Be en este tipo de complejos se encuentra entre los más fuertes reportados en la literatura, debido a que esta interacción aumenta el estado de oxidación de  $\text{Be}_2$  a  $\text{Be}_2^{2+}$ . El mismo efecto se encontró en ligandos con sistemas de electrones  $\pi_L$ , los cuales se conjugan con los orbitales  $\pi_{\text{Be}}$ , aumentando el estado de oxidación del monómero de  $\text{Be}_2$  a  $\text{Be}_2^+$  por lo que el enlace Be-Be en este tipo de compuesto es más fuerte que la molécula  $\text{Be}_2$  aislada, pero es más débil que en los complejos con ligandos radicalarios. Finalmente, se encuentran los complejos en los que el fragmento de  $\text{Be}_2$  interactúa con un par de electrones solitarios de la base de Lewis. En este tipo de complejos  $\text{Be}_2$  se mantiene neutro, y según nuestro conocimiento son los sistemas con los enlaces Be-Be más fuertes reportados en la literatura para el dímero neutro.

Finalmente, se propone el TPS como un nuevo método para describir enlaces químicos. El TPS es una medida que describe la fluctuación electrónica y de espín cuando un sistema es perturbado. En esta tesis se estudia el comportamiento del TPS en moléculas diatómicas y en derivados del Be-carbonilo. El tensor muestra un comportamiento diferente dependiendo del tipo de enlace químico, lo cual permite hacer distinción entre enlaces covalentes, iónicos, fluctuación-carga, y otros, también es capaz de describir la naturaleza de la correlación electrónica del sistema.

## RÉSUMÉ

---

Le concept de liaison chimique compte parmi les plus importants de la chimie car il permet de décrire aussi bien les propriétés chimiques d'un système que de comprendre et prédire les réactions chimiques. L'objectif principal de cette thèse est l'étude de nouveaux types d'interactions chimiques impliquant l'atome de béryllium. L'atome Be présente d'importantes propriétés chimiques en raison de la basse énergie des orbitales  $p_{Be}$ . Compte tenu de leur toxicité, les composés de béryllium ont été relativement peu étudiés sur le plan expérimental. Renforçant ainsi l'importance de la théorie dans le domaine. Dans cette thèse, nous rapportons une analyse théorique de trois nouveaux types de liaison impliquant le béryllium en utilisant des méthodes *ab-initio* de haut niveau, la théorie de la fonctionnelle de la densité (DFT), ainsi que l'application du Tenseur de Spread de la Position Totale (TPS, pour l'acronyme en anglais Total Position Spread tensor) aux systèmes moléculaires.

Tout d'abord, la liaison béryllium non-covalente (BerB, pour l'acronyme en anglais Beryllium Bond). Ce type de liaison se forme grâce à une interaction entre un dérivé du Be agissant comme un Acide de Lewis (LA) fort et une Base de Lewis (LB). L'interaction entre un LA du béryllium et des dérivés du fluor génère un  $\sigma_{hole}$  dans l'atome de fluor, qui n'aurait pu être créé autrement, ce qui rend possible la conception de nouveaux matériaux où l'atome de fluor se lie à travers des liaisons halogènes. Cette même interaction diminue leur énergie de liaison F-R, en changeant la dissociation homolytique du F-R en un processus exothermique. Par conséquent, les BerB peuvent être utilisés pour produire spontanément des espèces radicaliques. La Liaison béryllium intramoléculaire (IBerB) ont été étudiés dans les systèmes de type malonaldéhyde et tropolone. Cette interaction intramoléculaire devient plus forte dans les systèmes insaturés, parce que la LA et la LB sont plus acides et basiques, respectivement.

Deuxièmement, la liaison Be-Be intramoléculaire dans les complexes de naphthalène doublement substitués. Les espèces anioniques dérivées du 1,8-diBeY<sub>1</sub>'-naphthalène montrent une très forte liaison Be-Be mono-électronique. Cette liaison est huit fois plus forte et 0.5Å plus courte que le dimère isolé. Ces systèmes présentent haute affinité électronique, ce qui leur donne une propriété exceptionnelle : la capacité d'agir comme des on les appelle éponges anioniques. Il a été découvert que les interactions entre les anions et le naphthalène doublement substitué présente des affinités anioniques parmi les plus élevées, comparé à ce qui a été publié dans la littérature sur les composés neutres. Ce qui pourrait conduire à une grande variété d'applications dans le domaine des récepteurs et des capteurs d'anions.

Troisièmement, l'interaction entre la molécule Be<sub>2</sub> et a LB, qui a montré pour augmenter la force de la liaison Be-Be par rapport à la molécule isolée. L'interaction non-covalentes dans les complexes du type L: Be-Be: L diminue la distance et augmente l'énergie d'interaction de la liaison Be-Be. L'effet sur la fraction Be<sub>2</sub> dépend de la nature des bases de Lewis. L'effet



le plus spectaculaire se produit lorsque la L correspond à une espèce radicale, la liaison Be-Be dans ce type de complexes compte parmi les plus fortes rapportés dans la littérature, en raison de l'augmentation de l'état d'oxydation, de  $\text{Be}_2$  à  $\text{Be}_2^{2+}$ . Le même effet se trouve dans les ligands avec des orbitales  $\pi_L$ , qui sont conjuguées avec les orbitales  $\pi_{\text{Be}}$  augmentant l'état d'oxydation du fragment de  $\text{Be}_2$  augmente à +1. L'interaction Be-Be devient alors plus forte, bien que restant toutefois plus faible que celle des complexes avec des ligands radicaux. Enfin, les complexes où la fraction  $\text{Be}_2$  interagit avec le doublet non liant de L.  $\text{Be}_2$  dans ce type de complex reste neutre, à notre connaissance, ces complexes constitue la plus forte liaison Be-Be rapporté pour le dimère neutre

Pour terminer, le TPS est proposé comme une nouvelle méthode permettant de décrire les liaisons chimiques. Le TPS est une quantité qui décrit la fluctuation des électrons et du spin lorsqu'un système est perturbé. Dans cette thèse, le TPS est appliqué à des molécules diatomiques et à des dérivés de Be-carbonyl. Le tenseur montre un comportement différent selon le type d'interaction, permettant ainsi la distinction entre des liaisons covalentes, ioniques, de changement de charge et autres, et l'identification de la nature de la corrélation électronique du système.

## CONTENTS

---

I	INTRODUCTION	1
1	INTRODUCTION	3
1.1	Beryllium Chemistry . . . . .	4
1.2	Computational Chemistry . . . . .	8
1.3	Motivation and Outline . . . . .	15
II	QUANTUM CHEMISTRY METHODS	17
2	QUANTUM CHEMISTRY METHODS	19
2.1	Hartree-Fock Theory . . . . .	20
2.1.1	Hartree-Fock Equations . . . . .	20
2.1.2	Restricted Hartree-Fock: Roothaan-Hall Equations . . . . .	23
2.1.3	Unrestricted Hartree-Fock: Pople-Nesbet Equations . . . . .	26
2.1.4	The Hartree-Fock Limit: Electron Correlation . . . . .	28
2.2	Many-Body Perturbation Theory . . . . .	29
2.2.1	Corrections to the energy . . . . .	30
2.2.2	Corrections to the wave function . . . . .	30
2.2.3	Møller-Plesset equations . . . . .	31
2.3	Configuration Interaction . . . . .	33
2.3.1	The Full CI Method . . . . .	33
2.3.2	Multi-Configurational Methods . . . . .	35
2.4	Coupled Cluster Theory . . . . .	44
2.4.1	The CCSD Method . . . . .	46
2.4.2	The CCSD(T) Method . . . . .	46
2.5	Density Functional Theory . . . . .	48
2.5.1	The Electron Density . . . . .	49
2.5.2	The Hohenberg-Kohn Theorems . . . . .	49
2.5.3	The Kohn-Sham Method . . . . .	51
2.5.4	The Exchange Correlation Energy . . . . .	53
2.5.5	Advantages and Disadvantages of DFT . . . . .	56
2.6	Basis Set . . . . .	56
2.6.1	Slater Type Orbitals . . . . .	57
2.6.2	Gaussian Type Orbitals . . . . .	57
2.6.3	Pople Basis Set . . . . .	58
2.6.4	Polarization and Diffuse Functions . . . . .	59
2.6.5	Dunning Basis Set - Correlation Consistent Basis Set . . . . .	59
2.6.6	Basis Set Superposition Error . . . . .	60
2.7	Gaussian Composite Methods . . . . .	61
2.8	Wave Function Analysis . . . . .	63

---

2.8.1	Natural Bond Orbital . . . . .	63
2.8.2	Quantum Theory of Atoms in Molecules . . . . .	65
2.8.3	Electron Localization Function . . . . .	68
2.8.4	Electron Decomposition Energy . . . . .	69
2.8.5	Total Position Spread Tensor . . . . .	72
III	CHEMICAL BONDS . . . . .	77
3	CHEMICAL BONDS . . . . .	79
3.1	Strong Interactions . . . . .	80
3.1.1	Covalent and Ionic Bonds . . . . .	80
3.1.2	Charge-Shift Bonds . . . . .	85
3.2	Weak Bonds . . . . .	87
3.2.1	Non-Covalent Bonds . . . . .	87
3.2.2	Be <sub>2</sub> Molecule . . . . .	99
IV	RESULTS . . . . .	105
4	BERYLLIUM INTERACTIONS . . . . .	107
4.1	Zero-Electrons Be Bonds . . . . .	107
4.1.1	Methodology . . . . .	108
4.1.2	Properties of the Beryllium Bonds . . . . .	110
4.1.3	Halogen Bonds in Fluorine Derivatives . . . . .	113
4.1.4	Homolytic Dissociations . . . . .	117
4.1.5	Intramolecular Beryllium Bonds: Resonance Assisted Interactions . . . . .	123
4.1.6	Conclusions . . . . .	125
4.2	One-Electron Be Bonds . . . . .	127
4.2.1	Methodology . . . . .	128
4.2.2	Properties of the one-electron Be-Be bond . . . . .	128
4.2.3	Anion Sponges . . . . .	131
4.2.4	Conclusions . . . . .	133
4.3	Four-Electrons Be Bonds . . . . .	134
4.3.1	Methodology . . . . .	135
4.3.2	The Be <sub>2</sub> molecule . . . . .	136
4.3.3	Properties of the four-electrons Be-Be bonds . . . . .	140
4.3.4	Conclusions . . . . .	146
5	THE TOTAL POSITION SPREAD TENSOR . . . . .	149
5.1	Methodology . . . . .	150
5.2	Covalent Bonds . . . . .	152
5.3	Charge-shift Bonds . . . . .	153
5.4	Ionic Bonds . . . . .	155
5.5	Weak Bonds . . . . .	157
5.5.1	Van der Waals Interactions: He <sub>2</sub> . . . . .	157
5.5.2	Be bonds: Be <sub>2</sub> and CO: Be-Be: CO. . . . .	158
5.5.3	Conclusions . . . . .	160

---

V	RÉSUMÉ SUBSTANTIEL	163
VI	BIBLIOGRAPHY	191
VII	APPENDIX	209
A	FIGURES AND ANIMATIONS	211
B	PUBLICATIONS RESULT OF THIS THESIS	215
C	JOURNAL COVERS	353

## LIST OF FIGURES

---

Figure 1.1	IR spectra of BeH <sub>2</sub> and BeH <sub>2</sub> : H <sub>2</sub> O . . . . .	12
Figure 1.2	Wave function analysis for the BeH <sub>2</sub> : H <sub>2</sub> O system . . . . .	14
Figure 3.1	Wave function analysis of strong chemical bonds . . . . .	82
Figure 3.2	Natural Bond Orbitals of strong chemical bonds . . . . .	84
Figure 3.3	Kohn-Sham molecular orbitals of the $\pi$ valence orbitals of the F <sub>2</sub> molecule . . . . .	87
Figure 3.4	Wave function analysis of non-covalent bonds . . . . .	90
Figure 3.5	IR spectrum of the LA: H <sub>2</sub> O complexes, with LA = H <sub>2</sub> O, BeH <sub>2</sub> and FCl . . . . .	91
Figure 3.6	MESPs for the CF <sub>3</sub> X molecule with X = F, Cl, Br . . . . .	94
Figure 3.7	s and p atomic orbitals of the H and Be atoms . . . . .	96
Figure 3.8	Comparison of different theoretical methods in the description of the dissociation curve of the $^1\Sigma_g$ state of the Be dimer. . . . .	100
Figure 3.9	Molecular orbital diagram for the singlet $^1\Sigma$ and the triplet $^3\Sigma$ states of the Be <sub>2</sub> molecule . . . . .	102
Figure 3.10	Comparison of the BDE for the complexes between Be <sub>2</sub> and electron donor ligands. . . . .	103
Figure 4.1	Energetic and geometric properties of the most relevant complexes showing BerBs . . . . .	111
Figure 4.2	Linear correlation between the BerB $E_{\text{int}}$ and n substitution, the Be-Y bond distance, and the value of $\rho_{\text{BCP}_{\text{BeO}}}$ , for the BeCl <sub>2</sub> : CH <sub>3-n</sub> F <sub>n</sub> OF complexes . . . . .	112
Figure 4.3	Effect of the degree of substitution in the value of $V_{\text{max}}$ of the F $\sigma_{\text{hole}}$ for Be(Y' <sub>1</sub> ) <sub>2</sub> : CH <sub>3-n</sub> F <sub>n</sub> OF complexes . . . . .	114
Figure 4.4	Contour map of $\nabla^2\rho$ for CH <sub>3-n</sub> F <sub>n</sub> OF and Be(Y' <sub>1</sub> ) <sub>2</sub> : CH <sub>3-n</sub> F <sub>n</sub> OF complexes . . . . .	115
Figure 4.5	Comparison of the MESP and F $V_{\text{max}}$ in the $\sigma_{\text{hole}}$ for the complexes between BeH <sub>2</sub> : Y and BH <sub>3</sub> : Y, with Y=MeOF, NO <sub>2</sub> F, NO <sub>3</sub> F. . . . .	115
Figure 4.6	Representation of the geometries and $E_{\text{int}}$ trends for the BeH <sub>2</sub> : CH <sub>3</sub> OF: NH <sub>3</sub> , BeCl <sub>2</sub> : CH <sub>3</sub> OF: NH <sub>3</sub> and BeCl <sub>2</sub> : CF <sub>3</sub> O-F: NH <sub>3</sub> complexes . . . . .	116
Figure 4.7	Linear correlation between the XB and BerB $E_{\text{int}}$ , the XB $E_{\text{int}}$ and $V_{\text{max}}$ in the F $\sigma_{\text{hole}}$ and, the $\angle\text{O-F-N}$ and $V_{\text{max}}$ in the F $\sigma_{\text{hole}}$ . . . . .	117
Figure 4.8	(a) Linear correlation between $\Delta H_4^\circ$ and $ \chi_B - \chi_A $ for the BeH <sub>2</sub> : FR complexes. (b) Left figure represents the values of the RSH and right figure represents the BerB $\Delta H_1^\circ$ for the BeH <sub>2</sub> : FR complexes . . . . .	118
Figure 4.9	Representation of the FNO and H <sub>2</sub> BeFNO molecules . . . . .	119

Figure 4.10	Relevant molecular structures from the dissociation profile of the $\text{Be}(\text{Y}'_1)_2$ : FF complexes, with $\text{Y}'_1$ equal to (a) H and (b) Cl . . . . .	121
Figure 4.11	Comparison of the geometries and $\Delta E_{\text{TS2}}^\ddagger$ for the TS2 in the dissociation mechanism of the $\text{BeCl}_2$ : FF complex. . . . .	122
Figure 4.12	Relevant molecular structures from the dissociation profile along the $\text{BeH}_2$ : FNO complex . . . . .	122
Figure 4.13	Proton ( $\text{H}^+\text{A}$ ) and hydride ( $\text{H}^-\text{A}$ ) affinities of malonaldehyde derivatives . . . . .	123
Figure 4.14	Linear correlation between (a) $\text{H}^+\text{A}$ , (b) $\text{H}^-\text{A}$ and $E_{\text{int}}$ . . . . .	125
Figure 4.15	Wave function analysis for the $(1,8\text{-diBeY}'_1\text{naphthalene})^-$ and $(1,8\text{-diBeY}'_1\text{naphthalene})^-$ complexes . . . . .	129
Figure 4.16	$\Delta\text{Be-Be}$ and $E_{\text{ea}}$ for $1,8\text{-diBeY}'_1\text{naphthalene}$ complexes . . . . .	130
Figure 4.17	Wave function analysis for the $(\text{L}: 1,8\text{-diBeY}'_1\text{naphthalene})^-$ complexes . . . . .	132
Figure 4.18	Linear correlation between $E_{\text{L}}^-$ and Be-Be bond distances for $(\text{L}: 1,8\text{-diBeClnaphthalene})^-$ and $(\text{F}: 1,8\text{-diBeY}'_1\text{naphthalene})^-$ complexes . . . . .	132
Figure 4.19	Anion affinities for $(\text{L}: 1,8\text{-diBeY}'_1\text{naphthalene})^-$ complexes . . . . .	133
Figure 4.20	Ground and excited states dissociation curves of the $\text{Be}_2$ molecule . . . . .	137
Figure 4.21	Representation of the CASSCF wave function analysis for the ground and excited states of the $\text{Be}_2$ molecule . . . . .	138
Figure 4.22	Molecular Orbitals associated to the $\text{Be}: \text{L}$ interaction . . . . .	146
Figure 5.1	SS-TPS and SP-TPS for covalent bonds . . . . .	152
Figure 5.2	SS-TPS for charge-shift bonds . . . . .	154
Figure 5.3	Wave function analysis of the $\text{N}_2$ molecule. . . . .	155
Figure 5.4	SS-TPS and SP-TPS for ionic bonds . . . . .	156
Figure 5.5	SS-TPS and SP-TPS for non-dynamical bonds . . . . .	159
Figure 5.6	SS-TPS and SP-TPS for carbonyl-Be complexes . . . . .	160
Figure A.1	Molecular electrostatic potentials of $\text{BeY}'_1\text{Y}'_2$ : $\text{Y}'\text{F}$ complexes. . . . .	211
Figure A.2	Animation of the dissociation profile of the $\text{BeH}_2$ : FF complexes calculated at CASPT2//CASSCF(14,9)/cc-pVTZ level of theory . . . . .	212
Figure A.3	Animation of the dissociation profile of the $\text{BeCl}_2$ : FF complexes calculated at CASPT2//CASSCF(14,9)/cc-pVTZ level of theory. . . . .	212
Figure A.4	Animation of the dissociation profile of the $\text{BeH}_2$ : FNO complexes calculated at CASPT2//CASSCF(12,9)/cc-pVTZ level of theory. . . . .	213
Figure A.5	Animation of the variation of $\nabla^2\rho$ in the relaxed scan of the Be-Be bond distance of the $\text{CO}: \text{Be-Be}: \text{CO}$ complex . . . . .	213

## LIST OF SCHEMES

---

1.1	Representation of the variation of the energy with the bond distance for a repulsive and a stable molecule. . . . .	3
1.2	Representation of beryllium hydride and halide in gas and solid state. . . . .	5
1.3	Representation of the BeY <sub>2</sub> and H <sub>2</sub> O moieties and the BeY <sub>2</sub> : H <sub>2</sub> O complex. . . . .	9
1.4	Dissociation curve of the Be <sub>2</sub> <sup>2+</sup> cation . . . . .	13
2.1	H <sub>2</sub> potential energy curves . . . . .	26
2.2	CASSCF and RASSCF spaces. . . . .	39
2.3	Matrix representation of: left CASSCF- $\hat{F}$ and right CASPT- $\hat{H}_0$ . Adapted from Helgaker[1]. . . . .	42
2.4	Matrix representation of the MS-CASPT2 effective Hamiltonian . . . . .	43
2.5	Comparison of the performance of CC and MPn methods using FCI as a reference methodology . . . . .	48
2.6	Comparison of the wave function $\Psi$ and electron density $\rho$ for the $\Sigma_g$ and $\Sigma_u$ states of the H <sub>2</sub> molecule . . . . .	50
2.7	Representation of the DFT adiabatic connection . . . . .	55
2.8	Comparison STOs vs. GTOs . . . . .	58
2.9	The convergence to the basis set limit (dash line) of the correlation energy ( $E_{\text{corr}}$ ) (full line) when the cardinal number $X$ is increased. . . . .	60
2.10	Sequence of the natural localized orbital ensemble . . . . .	65
2.11	Representation of a set of trajectories of $\nabla\rho$ ending in a critical point of $\rho$ . . . . .	66
2.12	EDA representation for the complex AB . . . . .	70
2.13	Representation of the metal-insulator property considering band gap theory and the Localization Tensor . . . . .	72
2.14	Matrix representation of the Spin Summed-Total Position Spread Tensor . . . . .	75
3.1	Timeline of modern chemical bond . . . . .	79
3.2	Representation of covalent and ionic bonds. . . . .	81
3.3	Representation of the dissociation curves of covalent and ionic bonds . . . . .	84
3.4	Comparison of the dissociation curve for charge shift and classic bonds . . . . .	86
3.5	Representation of non-covalent bonds. . . . .	89
3.6	Representation of the water dimer isomers. . . . .	92
3.7	Representation of an intramolecular RAHB . . . . .	92
3.8	Representation of the positive and negative cooperativity between BerBs and Y'Z: Y complexes, with Z = H, X. . . . .	98
4.1	Representation of the BerBs studied in this thesis . . . . .	108
4.2	Scheme of the methodology used in this thesis . . . . .	109

---

4.3	Representation of the thermodynamical cycle of the $\text{BeH}_2$ : FR dissociation into $\text{BeH}_2\text{F}\cdot + \text{R}\cdot$ . . . . .	118
4.4	Scheme of the Potential Energy Profile for the dissociation of $\text{BeH}_2$ : FR . . .	120
4.5	(a) IHB and (b) IBERB in tropolone derivatives. . . . .	124
4.6	(Z)-4-(hydroxymethylene)cyclobut-2-enone derivatives. (a) $\text{LA}=\text{ROBeH}$ and (b) $\text{LA}=\text{RCHBeH}$ . . . . .	124
4.7	1,8-diBeY <sub>1</sub> ' naphthalene derivatives studied in this thesis. . . . .	127
4.8	L: Be-Be: L complexes in groups-I, -II and -III . . . . .	134
4.9	Representation of a system without and with a NNA. . . . .	139
4.10	Formation of a NNA considering catastrophe theory and promolecular model	140
5.1	Representation of the TPS (a) perpendicular to the bond direction ( $\Lambda_{\perp}$ ) and (b) in the bond direction ( $\Lambda_{\parallel}$ ). . . . .	150



## LIST OF TABLES

---

Table 1	Theoretical Be-Be bond distances and BDE for $\text{Be}_2$ , $\text{Be}_2$ ions and L: Be-Be: L systems. . . . .	11
Table 2	Moments and cumulants for a variable X from first to third order. . .	73
Table 3	Value of $\rho$ in the NNA for the L: Be-Be: L complexes . . . . .	144
Table 4	Description of the method and basis set for the molecules studied in the analysis of the TPS . . . . .	151
Table 5	Bond dissociation energies (BDE) and equilibrium distances ( $R_e$ ) for diatomic molecules. . . . .	151











## ACRONYMS AND ATOM COLOR LEGEND

---

<b>ANO</b>	Atomic Natural Orbital	<b>HOMO</b>	Highest Occupied Molecular Orbital
<b>AO</b>	Atomic Orbitals	<b>IBerB</b>	Intramolecular Beryllium Bonds
<b>AS</b>	Active Space	<b>IHB</b>	Intramolecular Hydrogen Bonds
<b>BDE</b>	Bond Dissociation Energy	<b>IR</b>	Infrared
<b>BDH</b>	Bond Dissociation Enthalpy	<b>IRC</b>	Intrinsic Reaction Coordinate
<b>BAR</b>	Bond Activation-Reinforcement	<b>IQA</b>	Interacting Quantum Atoms
<b>BerB</b>	Beryllium Bonds	<b>LA</b>	Lewis Acid
<b>BCP</b>	Bond Critical Points	<b>LB</b>	Lewis Base
<b>BSSE</b>	Basis Set Superposition Error	<b>LCAO</b>	Linear Combination of Atomic Orbitals
<b>CASSCF</b>	Complete Active Space Self Consistent Field	<b>LIIC</b>	Liner Interpolation in Internal Coordinates
<b>CASPT2</b>	Complete Active Space Second Order Perturbation Theory	<b>LMOEDA</b>	Localized Molecular Orbital Energy Decomposition Analysis
<b>CBD</b>	Chronic Beryllium Disease	<b>LP</b>	Lone Pair
<b>CC</b>	Coupled Cluster	<b>LT</b>	Localization Tensor
<b>CI</b>	Configuration Interaction	<b>LUMO</b>	Lowest Unoccupied Molecular Orbital
<b>CS</b>	Charge-Shift	<b>MEM</b>	Maximum Entropy Method
<b>DFT</b>	Density Functional Theory	<b>MESP</b>	Molecular Electrostatic Potential
<b>EDA</b>	Energy Decomposition Analysis	<b>MP2</b>	Møller-Plesset Second Order Perturbation Theory
<b>EDD</b>	Electron Density Distribution	<b>MO</b>	Molecular Orbitals
<b>ELF</b>	Electron Localization Function	<b>MOT</b>	Molecular Orbital Theory
<b>EPR</b>	Electron Paramagnetic Resonance	<b>NBO</b>	Natural Bond Orbital
<b>FCI</b>	Full Configuration Interaction	<b>NNA</b>	Non-Nuclear Attractor
<b>GTO</b>	Gaussian Type Orbitals	<b>PES</b>	Potential Energy Surface
<b>G09</b>	Gaussian09 computational package		
<b>G4</b>	Gaussian-4 Theory		
<b>HB</b>	Hydrogen Bonds		
<b>HF</b>	Hartree Fock		

<b>QTAIM</b> Quantum Theory of Atoms in Molecules	<b>SP-TPS</b> Spin-Partitioned of the Total Position Spread Tensor
<b>RAHB</b> Resonance Assisted Hydrogen Bond	<b>TPS</b> Total Position Spread Tensor
<b>RHF</b> Restricted Hartree-Fock	<b>TS</b> Transition State
<b>RSE</b> Radical Stabilization Energy	<b>SOMO</b> Single Occupied Molecular Orbital
<b>RSH</b> Radical Stabilization Enthalpy	<b>SCF</b> Self-Consistent Field
<b>STO</b> Slater Type Orbitals	<b>UHF</b> Unrestricted Hartree-Fock
<b>SS-TPS</b> Spin-Summed of the Total Position Spread Tensor	<b>VBT</b> Valence Bond Theory
	<b>XB</b> Halogen Bonds
	<b>ZPE</b> Zero Point Energy

### Atom Color Legend

 Hydrogen	 Helium
 Lithium	 Beryllium
 Boron	 Carbon
 Nitrogen	 Oxygen
 Fluorine	 Chlorine

## Part I

### INTRODUCTION

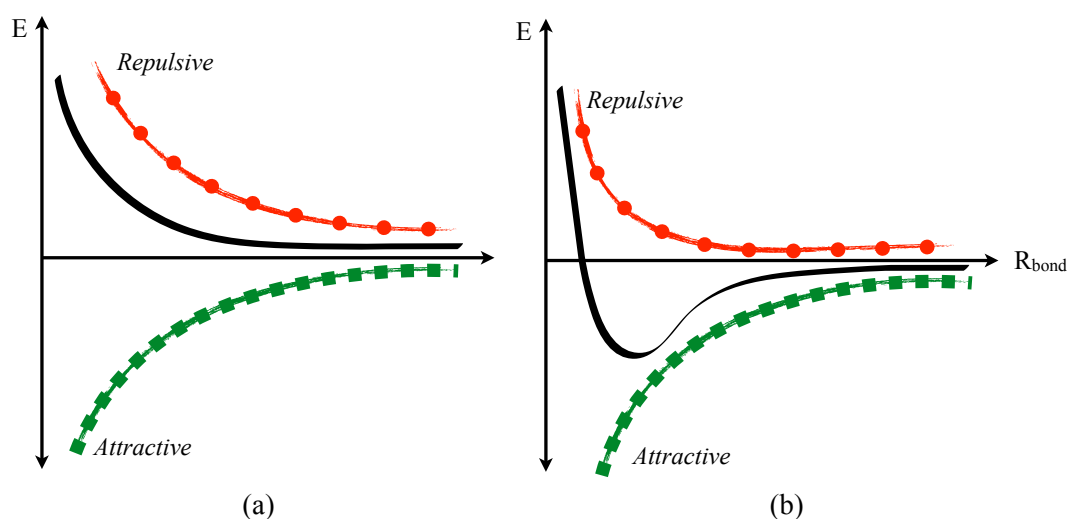
"The concept of the chemical bond is the most valuable concept in chemistry. Its development over the past 150 years has been one of the greatest triumphs of the human intellect. I doubt that there is a chemist in the world who does not use it in his or her thinking. Much of modern science and technology has developed because of the existence of this concept."

*Linus Pauling. The Nature of the Chemical Bond - 1922.*



## INTRODUCTION

One of the most important concepts in chemistry is the chemical bond. It is widely used to explain the structure, reactivity, and properties of a system, to understand trends in a group of molecules or to design new complexes with specific characteristics. The formation of chemical bonds involves three types of interactions: the nuclear and electronic repulsion and the nuclei-electron attraction. Then, for stable molecules, attractive forces must be larger than the repulsive ones (see scheme 1.1). The classic model to explain chemical bonds considers that electrons are arranged in pairs[2–4]. The bonding pair could be created by sharing electrons between atoms (covalent bonds) or by transferring electrons from one atom to another (ionic bonds).



Scheme 1.1: Representation of the variation of the energy with the bond distance for (a) a repulsive and (b) a stable molecule. The circle-red line represents repulsive forces, the square-red line attractive forces and the black-line the total energy.

Covalent and ionic interactions have been the main topic of chemical bonding studies, so they could be considered as a well-known subject. Theory has succeeded in explaining the formation and dissociation of both types of bonds, and also describing with high accuracy experimental data. Such as spectra, kinetic and thermodynamic properties and molecular structures. But most importantly, theory has elucidated the nature of both types of interactions [5]. Notwithstanding, there are still some interactions that cannot be experimentally measured or described, for example, weak interactions. There are few experimental observables that can be directly measured for this type of interactions. Instead, experimentalists measure the changes induced by the formation of weak interactions. These properties can be classified in direct and indirect observables[6–8]:

## 1. Indirect observables

- a) *Geometries* are calculated from the rotational constants obtained by microwave spectroscopy. The rotational constants for rigid molecules are determined with high accuracy, but clusters bonded by weak interactions are flexible structures. Therefore, their rotational constants are susceptible to centrifugal distortion, and the spectra of these systems have more peaks than structural parameters. Then, the geometry must be determined by an average of the vibrations.
- b) *Stabilization Enthalpies*. There are different methodologies to determine binding energies, for example by measuring the dependence of the equilibrium constant with temperature, or by calculating the dissociation energy of the monomers and the dimers upon ionization. The most accurate method to calculate binding enthalpies is the Zero Electron Kinetic Energy spectroscopy. This technique is based on the ionization of the molecule by a pulsed-field, which provides the vibrational and rotational structure of the cation. Moreover, the dissociation energy of the cation can be obtained by mass spectrometry, and the dissociation energy of the neutral species is determined from the Born-Haber cycle.

## 2. Direct observables:

*Vibrational Frequencies* are measured by Infrared (IR) or Raman spectroscopy. The formation of weak interactions induces a redshift in the stretching frequencies of the isolated monomer. The magnitude of this shift has been associated to the strength of weak interactions. For example, the formation of hydrogen bonds ( $Y'-H: Y$ ) redshifts the antisymmetric stretching vibrational mode associated to the hydrogen donor bond,  $Y'-H$ .

There are different types of weak interactions, but this thesis is mainly focused on non-covalent interactions where Be derivatives behave as Lewis acids. Experimentally, the characterization of these interactions have the additional limitation that beryllium compounds are very toxic, so there are fewer experimental studies of Be derivatives compared with other systems. Therefore, computational chemistry has become a very useful tool to overcome the experimental challenges associated with the description of Be compounds. Specifically, we have considered two types of Be derivatives: beryllium-hydrides or -halides and the  $Be_2$  molecule.

### 1.1 BERYLLIUM CHEMISTRY [9–11]

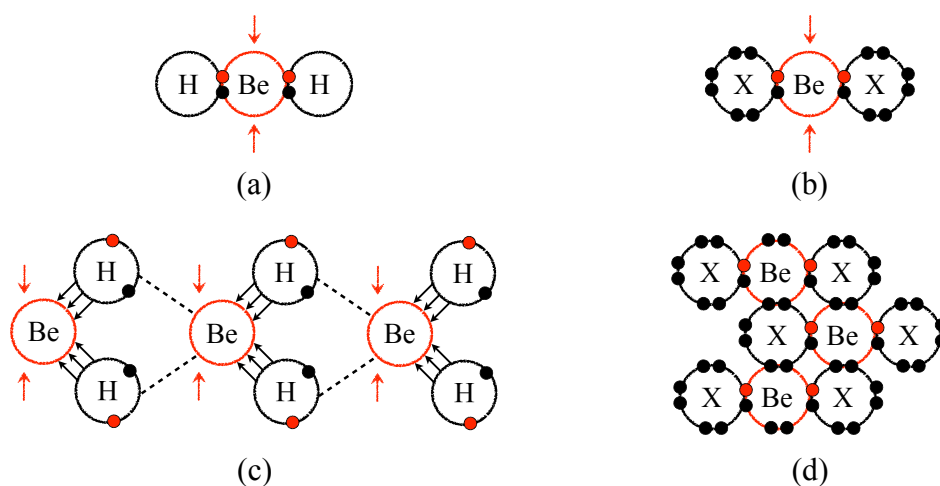
Beryllium is a steel-gray hard metallic element that normally exists in a close-packed hexagonal (hcp) crystalline form. The metal has atomic number 4 what makes it the lightest member of the family of the alkaline earth metals. The electronic configuration of the ground state is closed-shell:  $1s^2 2s^2$ . Therefore, the reactivity of the atom depends on the  $2s \rightarrow 2p$  excita-

tions, which are possible because of the low energy of the  $p_{\text{Be}}$  orbitals. The single excitation from  $2s$  to  $2p$  in Be is  $1700\text{kJ}\cdot\text{mol}^{-1}$  lower in energy than in He ( $2600\text{kJ}\cdot\text{mol}^{-1}$ ). Thus, Be can form two covalent bonds by sharing its two valence electrons, but a third or even a fourth interaction can be formed by accepting electron-lone pairs into the empty  $p_{\text{Be}}$  orbitals [12–17].

There are many types of beryllium derivatives, the most commercial high-purity compound is Beryllium oxide ( $\text{BeO}$ ).  $\text{BeO}$  exists in nature as the mineral bromellite or it can be produced by calcination of high-purity beryllium sulfate. Solid  $\text{BeO}$  has a hexagonal wurtzite structure with tetrahedral  $\text{Be}^{2+}$  and  $\text{O}^{2-}$  centers, while in gas phase it is a diatomic molecule bonded by two  $\sigma$  and two  $\Pi$  bonds.  $\text{BeO}$  ceramic shows very high thermal conductivity, heat capacity, and electrical resistivity, which are compared with pure aluminum, but it is also carcinogenic and causes Chronic Beryllium Disease (CBD) [18]. The chemical properties of the compounds studied in this thesis are briefly summarized in the next sections.

### 1.1.1 $\text{BeY}_2$ compounds

Beryllium forms a wide range of  $\text{BeY}_2$  complexes: beryllium borides, carbonites, carboxylates, halides, hydride, hydroxide, nitrate, oxalate, phosphates, sulfates, and others. Among these systems, in this thesis special attention is devoted to the compounds with  $Y = \text{H}, \text{F}$  and  $\text{Cl}$ . In general,  $\text{BeY}_2$  compounds are characterized by a high electron deficiency, which is due to the empty  $p_{\text{Be}}$  orbitals. However, crystal Be-halides are not electron-deficient compounds because the  $p_{\text{Be}}$  orbitals are filled by the lone pairs of the halogens from the layers above and below (see scheme 1.2 b).



Scheme 1.2: Representation of beryllium (a,c) hydride and (b,d) halide. Top figure represents the system in the gas phase and below in the solid state. The red arrows point to the empty  $p_{\text{Be}}$  orbitals.

*Beryllium hydride* ( $\text{BeH}_2$ ) (scheme 1.2 a). Solid state  $\text{BeH}_2$  is a three-dimensional white polymer formed by an ionic bond between  $\text{Be}^{2+}$  and  $\text{H}^-$ . The polymer is thermally stable un-



til 125°C. Above that temperature, it decomposes in atomic Be and H. Therefore, molecular BeH<sub>2</sub> is obtained by the reaction between ethereal lithium-aluminum hydride and beryllium chloride.

*Beryllium fluoride* (BeF<sub>2</sub>) is the most stable beryllium-halide. In solid state, it has a quartz-crystal structure bonded by an ionic interaction, while in gas phase it is a monomer covalently bonded. The crystal has a melting point of 552°C and sublimates at 740°C. BeF<sub>2</sub> can be produced by the reaction between gaseous hydrogen fluoride and beryllium oxide or by thermal decomposition of ammonium fluoroberyllate ((NH<sub>4</sub>)<sub>2</sub>BeF<sub>4</sub>). BeF<sub>2</sub> is thermally stable until 3000K, showing a decomposition below 50% at this temperature.

*Beryllium chloride* (BeCl<sub>2</sub>). Solid BeCl<sub>2</sub> exists in several polymorphic structures depending on the temperature. In contrast to BeF<sub>2</sub>, the Be-Cl interaction has a covalent character in both, crystal and molecular states. In gas phase, the system is formed by BeCl<sub>2</sub> dimers bonded by chlorine-bridges. The chlorine-bridges can be cleaved by increasing the temperature to obtain the BeCl<sub>2</sub> monomer. The molecule is thermally stable until 1000°C when it dissociates into Be + 2Cl. The solid compound is obtained as an anhydrous product by the reaction between BeO and chlorine at high temperatures, while gaseous BeCl<sub>2</sub> is obtained by sublimation at (350 – 360)°C.

*Beryllium Bonds* (BerB) were defined and characterized in 2009 by Yáñez, Mó and coworkers. BerBs and Hydrogen Bonds (HB) are closely related. They are the result of electrostatic interactions between a Lewis Acid (LA) and a Lewis Base (LB), but in BerBs the LA is a BeY<sub>2</sub> derivative. BerBs have been found to be up to five times stronger than HBs. The p<sub>Be</sub> orbitals increase the charge transfer from the LB towards the Beryllium-Lewis Acid (Be-LA), which is not feasible for the high energetic p<sub>H</sub> orbitals [19].

### 1.1.2 *Beryllium molecule* (Be<sub>2</sub>)

The Beryllium molecule exists as a gas dimer, which is formed by a weakly interaction between two Be atoms. The Be dimer can be prepared by deposition of Be vapor in noble gas matrices [20] or by Pulsed-Laser ablation of metal Be[21]. The last technique was used to obtain the first gas-phase spectrum of the Be<sub>2</sub> molecule, determining a Be-Be bond distance equal to 2.45Å and a Bond Dissociation Energy (BDE) of 9.45kJ·mol<sup>-1</sup>[22]. The excitation spectrum of Be<sub>2</sub> was obtained from laser vaporization of a Be surface, finding two main peaks at 461 and 359 nm<sup>-1</sup>. The lowest excitation was assigned to the <sup>1</sup>Π<sub>u</sub> → n<sup>1</sup>Σ<sub>g</sub><sup>+</sup> and the highest one to the <sup>1</sup>Σ<sub>u</sub><sup>+</sup> → n<sup>1</sup>Σ<sub>g</sub><sup>+</sup> transitions [20–23]. There are several factors associated with the scarce experimental information about Be<sub>2</sub>. The molecule dissociates at its melting and boiling points, it oxidizes easily and it is very toxic.

### 1.1.3 Toxicity [18]

The first association of Be compounds with lung diseases was observed in 1930. These studies were based on animal experimentation and in the analysis of neighborhoods surrounded by beryllium plants, finding a direct relation between the metal and a lung disease named *Berylliosis* or Chronic Beryllium Disease. There are different mechanisms for beryllium to enter in the human body, (1) ingestion, (2) inhalation or (3) absorption through the skin. The digestive system is able to eliminate the metal by excreting it in faeces without being absorbed by the bloodstream. Therefore, Be has a limited toxicity by ingestion. However, this is not the case for mechanisms (2) and (3). The metal can be deposited in the lungs by inhalation or could produce skin lesions by dermatitis contact.

CBD is a granulomatous lung disease originated by the deposit of Be in the lungs. CBD is originated by an immune-system response to the presence of Be in the human body. The mechanism of interaction between Be compounds and living cells remains unknown, then, at the moment there is not cure for CBD. The main hypothesis to explain the high toxicity of Be is that Be compounds interfere with the gene expression by Be-proteins interactions. However, there are several interpretations about the nature of this interaction, suggesting that the mechanism could depend on the type of beryllium compound.

### 1.1.4 Applications

Be metal and its derivatives have extraordinary properties despite their high toxicity, what makes them attractive compounds for engineering design. Beryllium is a very light atom but at the same time, it is among the strongest and stiffness ones. Be has the highest specific heat of any metals and its thermal conductivity is comparable with that of aluminum. Table 1 in reference [10] summarizes the applications and properties of Be compounds, some of which are described below:

#### 1. *Beryllium Metal*

- a) Nuclear power. The metal is an excellent neutron generator due to its low atomic mass, low x-ray absorption, and a high neutron scattering cross sections. Thus, Be metal is used as an initiator of nuclear fission reactions.
- b) Aerospace. Be is used in aircraft and aerospace design due to its low density, high thermal conductivity, and heat permeability. For example, Be is used in heat shields and heat collectors of space vehicles, aircraft brakes, antennas and rocket heads. The high melting point and elasticity of beryllium make it suitable as a structural material for jet aircraft and guided missiles.

2. BeO *Ceramic* is an extraordinary heat and electrical conductor. Therefore, it is used in the electronic industry for the manufacture of insulators, resistors, spark plugs and microwave tubes.
3. *Alloys* represent the major application of beryllium, but in most of them, Be is the minority component. Among their remarkable properties are their rigidity, low density, and high specific heat, thermal conductivity and melting point.

The high cost of production and toxicity have restricted the applications of Be compounds mainly to aerospace engineering and have been discriminated in other fields. The Be compounds with more applications are pure Be, BeO and Be-alloys, and regardless their extraordinary properties Be-halides and Be<sub>2</sub> have not any remarkable application.

## 1.2 COMPUTATIONAL CHEMISTRY

The main aim of this thesis is to perform a theoretical study of weak interactions involving Be. Computational chemistry is defined as a *discipline using mathematical methods for the calculation of molecular properties or for the simulation of molecular behavior. It also includes, e.g., synthesis planning, database searching, combinatorial library manipulation* [24]. The foundation of Computational Chemistry dates back to the XX century with the development of Quantum Mechanics, but it has needed almost 35 years to evolve into the discipline that is currently known. The exponential growth of technology has allowed overcoming the initial limitations of Quantum Mechanics. While in the middle of the 90's it was possible to describe systems constituted by only a few atoms, nowadays, computational chemists can describe hundreds of atoms within chemical accuracy ( $\pm 1 \text{ kcal} \cdot \text{mol}^{-1}$ ). The next sections present the theoretical description of Be-halides and hydrates, and Be<sub>2</sub>. Notice that comparison between experimental and theoretical results for Be compounds is limited by the lack of experimental data.

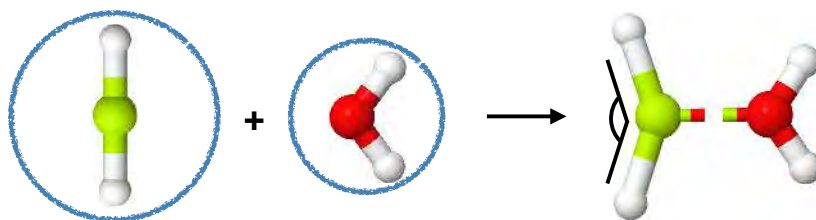
### 1.2.1 Geometries and Potential Energy Surfaces

Theoretically, it is possible to describe with high accuracy not only the ground state geometry of a system but also the most important stationary points of the Potential Energy Surface (PES). The PES of a system is the representation of its potential energy considering all possible arrangements of the atoms. The stationary points of the PES are determined by a geometry optimization. This procedure starts with an initial guess of the geometry and its Hessian, searching for the correct minimization pathway on the PES. The next step is to follow the zero-gradient of the energy respect to variations of the system coordinates until it is located a stationary point of the PES. See reference [25] for a description of the different optimization models.

Crystal Orbital Method was applied to perform the first structural study for  $\text{BeH}_2$ . The geometry of the  $\text{BeH}_2$  molecule is described by this method as linear with Be-H bond distances around of  $1.33\text{\AA}$  [26, 27]. The Be-H bond distance does not change by increasing electron correlation. The discrepancies in the bond distance between the Crystal Orbital and high correlated methods have been found to be on the order of  $0.01\text{\AA}$  [28–30]. The first experimental spectra of the  $\text{BeH}_2$  molecule was obtained almost 20 years after the first theoretical study. The structure of the molecule was determined by vibration-rotation spectroscopy, ratifying the Be-H bond distance predicted by theory [31, 32].

The first experimental evidence of molecular  $\text{BeF}_2$  and  $\text{BeCl}_2$  was reported in 1957 by using visual Gas Electron Diffraction. Both molecules were found to have a linear geometry with Be-Y bond distances equal to  $1.40\text{\AA}$  and  $1.75\text{\AA}$ , for  $Y = \text{F}$  and  $Y = \text{Cl}$ , respectively [33]. Those results were refined with more accurate experimental methods, finding a shorter Be-Y bond distance for  $\text{BeF}_2$  ( $1.37\text{\AA}$ ) and longer for  $\text{BeCl}_2$  ( $1.80\text{\AA}$ ). The  $\text{BeCl}_2$  dimer is a molecule with  $D_{2h}$  symmetry and a Cl-Be-Cl angle equal to  $135^\circ$ . The Be-Cl bond distance in the dimer was found to be longer than in the monomer, showing values between  $1.83\text{\AA}$  and  $1.96\text{\AA}$ . Theoretically, the structure of  $\text{BeF}_2$  can be accurately described at Hartree Fock (HF) level of theory, the bond distance is predicted to be  $1.37\text{\AA}$ , showing a perfect agreement with the experimental results. The difference in the Be-F bond distance between HF and Møller-Plesset Second Order Perturbation Theory (MP2) is on the order of  $0.001\text{\AA}$ . On the contrary, HF fails in the description of the  $\text{BeCl}_2$  geometry, this method overestimates the Be-Cl bond distance. The experimental value is recovered at MP2 level of theory, predicting a bond distance equal to  $1.79\text{\AA}$  [34, 35].

BerBs have been studied only theoretically. The lack of experimental evidence of this interaction is newly attributed to the high toxicity of the metal. Notwithstanding, high-level methodologies have been applied to describe this non-covalent bond. The distances between the LA and the LB were found to be below the sum of the Van der Waals radii, supporting the formation of the BerB. The formation of a BerB induces dramatic structural changes in both the Beryllium Lewis Acids (Be-LA) and the LB. The  $\text{BeY}_2$  angle in the  $\text{BeY}_2:\text{LB}$  complex deviates from linearity and the Be-Y bond distance becomes longer [19]. See scheme 1.3.



Scheme 1.3: Representation of the  $\text{BeY}_2$  and  $\text{H}_2\text{O}$  moieties and the  $\text{BeY}_2:\text{H}_2\text{O}$  complex.

The theory most widely used by computational chemists, Molecular Orbital Theory (MOT), describes  $\text{Be}_2$  as an inexistent molecule, due to its  $[\text{He}](2\sigma)^2(2\sigma^*)^2$  electron configuration. The failure of MOT is ascribed to the large electron-correlation needed to describe the bond in the Be dimer. Thus, the bonding character is only recovered by high-level multi-reference and CCSD(T) methods. For example, the Full Configuration Interaction (FCI)

method predicts a Be-Be bond distance equal to 2.47Å, which is only 0.02Å above the experimental value [36]. The  $\text{Be}_2^+$  and  $\text{Be}_2^-$  ions have shorter and stronger Be-Be bond compared to the neutral molecule. The monocation becomes stronger because the  $2\sigma^*$  orbital is not longer doubly occupied, while the monanion shows a single occupied  $3\sigma_g$  orbital. The  $\text{Be}_2^+$  geometry was determined from the rotational constants, finding a Be-Be bond distance equal to 2.211Å, which is in perfect agreement with the value predicted by MRCI (2.212Å) [23, 37–39]. To our knowledge, there is not experimental information for the anion, but its electronic structure has been studied at high-level of theory (MRCI/aug-cc-pVQZ). The Be-Be bond distance in  $\text{Be}_2^-$  is predicted to be 2.223Å [39]. Theoretically, the Be dication has been found to be metastable, because the Be-Be bond is stronger than the coulomb repulsion. The bond distance was determined by the MRCI method, finding that  $\text{Be}_2^{2+}$  has the shortest bond among the  $\text{Be}_2$  ions, 2.13Å [40].

Theoreticians have made an intensive effort to propose new  $\text{Be}_2$  derivatives with stronger Be-Be bonds. For example, the Be-Be bond distances in the complexes formed between  $\text{Be}_2$  and electron donor species have been found to be smaller than the ones reported for the  $\text{Be}_2$  ions. There have been considered different donor species in complexes of the type L: Be-Be: L. The earliest study considered carbonyl ligands. The shorter Be-Be bond have been reported for L equal to a N-heterocyclic carbene (NRC), and the strongest complex is the one formed with fluorine. The  $(\text{CO})_n$ : Be-Be:  $(\text{CO})_n$  complexes have a Be-Be bond distance around 1.855 Å for  $n = 1$  and 1.938 Å for  $n = 2$  [41, 42]. The complexes formed with NRC show distances between 1.95 – 2.00 Å, depending on the carbene substituent (R) [43]. The Be-Be bond distance with L = F was found to be approximately 2.048 Å [44]. The geometries of the complexes with carbonyl ligands were described by means of the HF method, the NRC derivatives by Density Functional Theory (DFT) and the fluorines complexes with the CCSD(T) method, but all these methods have shown to poorly describe the isolated  $\text{Be}_2$  molecule [23].

Table 1 shows the geometrical and energetics properties of  $\text{Be}_2$ ,  $\text{Be}_2$  ions and L: Be-Be: L complexes reported so far in the literature.

### 1.2.2 Vibrational Frequencies

IR spectroscopy is the most common method used to characterize non-covalent interactions and Be compounds. Indeed, for some systems, the IR spectrum is the only available experimental evidence of their existence. Theoretically, vibrational frequencies are evaluated considering the harmonic approximation. However, there are systems that cannot be described within the harmonic approximation (anharmonic systems) and the harmonic frequencies need to be corrected. The corrections could be done by scaling factors or by considering anharmonicity as a perturbation of the harmonic system.

For example, the IR spectra is the only available experimental observable for the  $\text{BeH}_2$  molecule. The experimental infrared spectra shows two mean peaks below  $2240\text{cm}^{-1}$ :  $\nu_1 =$

Table 1: Theoretical Be-Be bond distances and BDE for Be<sub>2</sub>, Be<sub>2</sub> ions and L: Be-Be: L systems.

MOLECULE	BOND DISTANCE (Å)	BDE(kJ·mol <sup>-1</sup> )
Be <sub>2</sub> [36]	2.47 [(2.47 [22])]	8.55 [(9.45 [22])]
Be <sub>2</sub> <sup>+</sup> [23]	2.21 [(2.21 [23])]	199 [(192 [23])]
Be <sub>2</sub> <sup>2+</sup> [40]	2.13	106
Be <sub>2</sub> <sup>-</sup> [39]	2.22	-
CO: Be-Be: CO [42]	1.86	42 <sup>[a]</sup>
(CO) <sub>2</sub> : Be-Be: (CO) <sub>2</sub> [41]	1.94	209
NHC: Be-Be: NHC [43]	1.95	167
NPhC: Be-Be: NPhC [43]	1.98	271
F: Be-Be: F [44]	2.05	322

<sup>[a]</sup> The BDE of the CO: Be-Be: CO complexes was calculated at HF level of theory. The remaining results in this table were calculated by considering post-HF methods. See references and text for more details.

716 and  $\nu_3 = 2255$  [31, 32]. The two peaks have been reproduced theoretically, with errors that amount (a discrepancy) between 2 and 20 cm<sup>-1</sup> depending on the method. Table 1 from reference [30] compares the BeH<sub>2</sub> vibrational frequencies at different levels of theory. The theoretical IR vibrational frequencies for Be halides are described with the same accuracy than Be hydrides. Tables 1 and 2 in reference [45] show a comparison between theoretical and experimental results. The formation of BerBs induces a redshift in the stretching vibrational modes of BeY<sub>2</sub>, which is in agreement with the results obtained upon the formation of other non-covalent interactions such as HBs (see figure 1.1).

The theoretical vibrational frequencies calculated for the Be<sub>2</sub> molecule are within the experimental error ( $\pm 2\text{cm}^{-1}$ ). Experimentally, the first vibrational frequency of the Be dimer is 222.6cm<sup>-1</sup> [23]. The predicted vibrational frequency is 222.7cm<sup>-1</sup> and 219.9cm<sup>-1</sup> at MRCI[46] and FCI[36] levels of theory, respectively.

### 1.2.3 Energetic Properties

The energetic properties calculated in this thesis (interaction energies, bond energies, bond enthalpies, and others) were determined considering the supramolecular method. The energy differences within this method are evaluated as the difference between the total complex (supersystem, AB) and the energies of subsystems (A,B),  $\Delta E = E_{(A+B)} - E_{AB}$ . There are other approaches to calculate interaction energies, such as Symmetry Adapted Perturbation Theory (SAPT) [47] and Energy Decomposition Analysis (EDA) [48, 49]. The advantage of these latter methods is that they do not only compute the strength of the interaction, but they also determine the electrostatic and orbital contributions to the interaction energies.

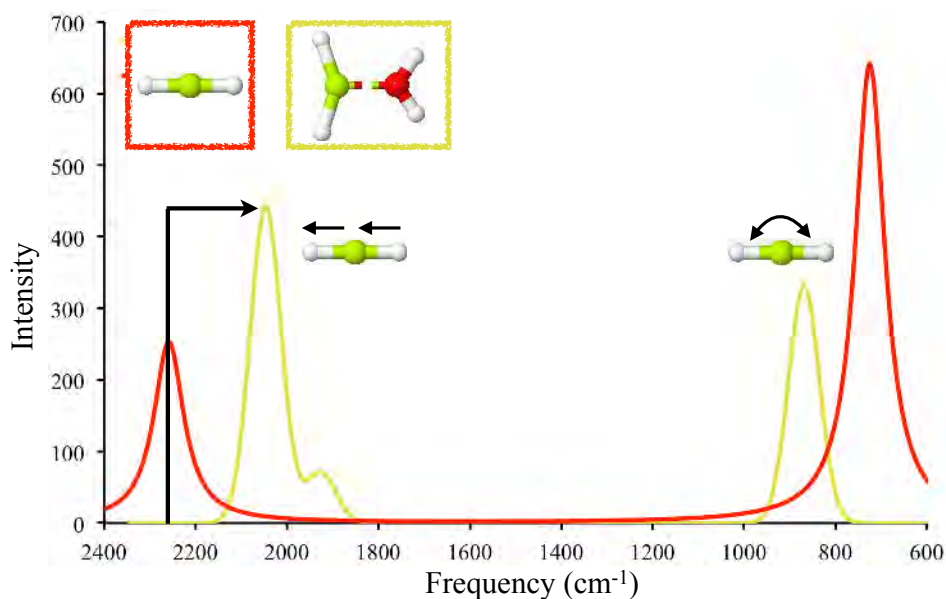
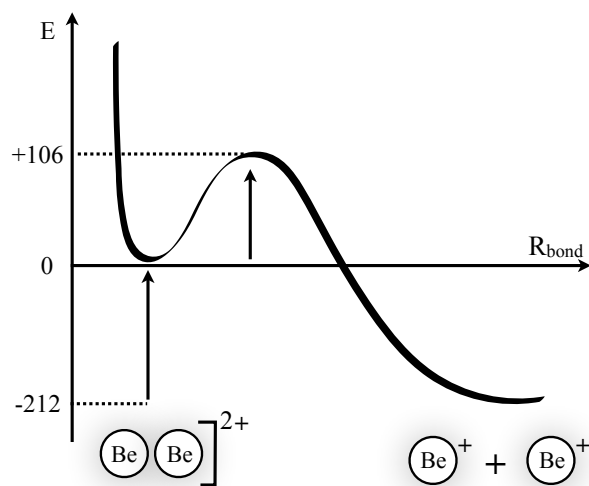


Figure 1.1: IR spectrum of  $\text{BeH}_2$  in red and  $\text{BeH}_2 : \text{H}_2\text{O}$  in yellow. The calculations were performed at B3LYP/cc-pVTZ level of theory.

BerBs have shown soaring interaction energies that in some cases can be compared with covalent bonds [19]. A remarkable property of BerBs is that they can be used to modify intrinsic energetic properties of the LB interacting with the Be-LA. For example, the interaction of Be-hydrate with derivatives of the squaric acid induces the spontaneous formation of  $\text{H}_2$ . This means that the reaction  $\text{BeH}_2 + \text{C}_4\text{H}_2\text{O}_4 \rightarrow \text{BeHC}_4\text{HO}_4 + \text{H}_2$  is exothermic [50]. The strength of non-covalent interactions can be increased by the formation of BerBs. For instance, the hydrogen bond in  $\text{BeY}_2 : \text{Y}'\text{H} : \text{Y}$  have been found to be stronger than in  $\text{Y}'\text{H} : \text{Y}$  [51, 52].

The BDE of  $\text{Be}_2$  is very sensitive to the theoretical method. The Be-Be bond energy is accurately described only by some multi-reference methodologies (FCI, MRCI, CASPT2 and CASSCF) and the single-reference method CCSD(T) (see table 1 from reference [53]). These methods are able to predict the  $\text{Be}_2$  BDE within chemical accuracy [36, 38, 54, 55]. In agreement with the bond distances, the Be-Be bond in the  $\text{Be}_2$  ions is stronger than in the neutral dimer. The theoretical BDE of  $\text{Be}_2^+$  was found to be in very good agreement with the experimental values. MRCI predicts a bond energy equal to  $192\text{kJ}\cdot\text{mol}^{-1}$  that is just  $7\text{kJ}\cdot\text{mol}^{-1}$  below the experimental result [23, 37]. In contrast to the neutral molecule, the BDE of  $\text{Be}_2^+$  is correctly described by single-reference methodologies, even though the cation is an open-shell system, showing the highly correlated Be-Be bond in the  $\text{Be}_2$  molecule. The dication molecule has a complicated PES, see scheme 1.4.  $\text{Be}_2^{2+}$  lies  $212\text{kJ}\cdot\text{mol}^{-1}$  higher in energy than the dissociation products,  $\text{Be}^+ + \text{Be}^+$ , but an energetic barrier of  $106\text{kJ}\cdot\text{mol}^{-1}$  to reach these products needs to be overcome. Therefore, the  $\text{Be}_2$  dication is predicted to be a metastable system [40].

The BDE of the L: Be-Be: L complexes are comparable with the  $\text{Be}_2$  ions (see table 1). The disubstituted complex,  $\text{CO} : \text{Be-Be} : \text{CO}$ , has only been described at HF level of the-



Scheme 1.4: Dissociation curve of the  $\text{Be}_2^{2+}$  cation. Energetics were taken from reference [40] and are in  $\text{kJ}\cdot\text{mol}^{-1}$ .

ory. The HF BDE was found to be around  $42\text{kJ}\cdot\text{mol}^{-1}$ . The tetra-substituted Be-carbonyl,  $(\text{CO})_2:\text{Be}-\text{Be}:(\text{CO})_2$  was studied at HF and MP4 level of theory, finding that HF underestimates the Be-Be bond strength by  $144\text{kJ}\cdot\text{mol}^{-1}$ . MP4 predicts a BDE of  $209\text{kJ}\cdot\text{mol}^{-1}$ . Therefore, HF fails in the description of Be-carbonyl compounds [41, 42]. The BDE of the complexes with N-heterocyclic carbenes were determined using DFT. The Be-Be bond strengths are between 166 and  $270\text{kJ}\cdot\text{mol}^{-1}$  depending on the carbenes substituents [43]. Finally, the strongest Be-Be bond has been reported for the  $\text{F}:\text{Be}-\text{Be}:\text{F}$  complexes, with a BDE almost 30 times stronger than the isolated  $\text{Be}_2$  molecule [44].

#### 1.2.4 Description of the bond

The wave function can be used to analyze the nature of the chemical bond. In this thesis, different types of wave function analysis methods were used. Among them, methods based on a topological analysis of the electron density (Quantum Theory of Atoms in Molecules (QTAIM)) or the Electron Localized Function (Electron Localization Function (ELF)). These methods not only give information about the bond strength but also about the covalent or electrostatic nature of the bond. A different approach is the Natural Bond Orbital (NBO) method. NBO consists of a sequence of localization steps to transform Atomic Orbitals (AO) into Molecular Orbitals (MO), recovering the Lewis Structure of the system. Non-covalent bonds are not described by Lewis Structures, the NBO method quantifies the energetic contribution from non-Lewis structures by perturbation theory. Therefore, the strength of non-covalent bonds can be measured within the NBO framework.

BerBs have been characterized by wave function analysis. For example, consider the wave function analysis for  $\text{BeH}_2:\text{H}_2\text{O}$  in figure 1.2. The three methods, QTAIM, ELF and NBO agree on the formation of a strong non-covalent bond between  $\text{BeH}_2$  and  $\text{H}_2\text{O}$ . QTAIM locates a saddle point of  $\rho$  between Be and O (Bond Critical Points (BCP)), the value of  $\rho$  at



the BCP is on the same order than for other non-covalent bonds. The ELF analysis locates a  $V(\text{Be}, \text{O})$  disynaptic basin, with a population close to  $2e^-$ . The NBO analysis describes the BerB as a charge transfer from the Lone Pair (LP) of O towards the  $p_{\text{Be}}$  and  $\sigma_{\text{BeH}}^*$  orbitals. The strength of the BerB is quantified considering NBO second order perturbation energy, finding a high value equal to  $147\text{kJ}\cdot\text{mol}^{-1}$ .

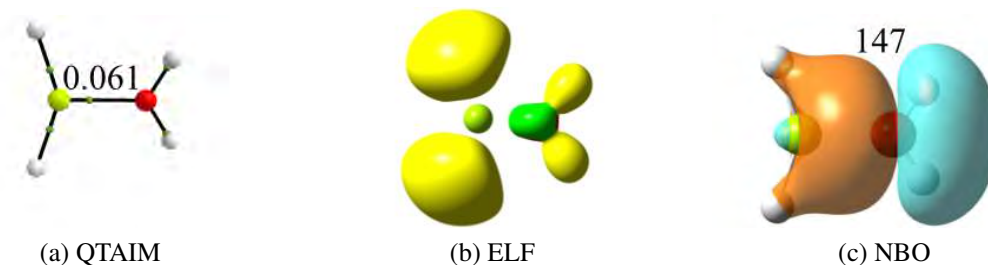


Figure 1.2: Wave function analysis for the  $\text{BeH}_2:\text{H}_2\text{O}$  system. The calculations were performed at B3LYP/cc-pVTZ level of theory.

The development of new theoretical models to understand the nature of chemical interactions is an important field to merge theory and experiments. The Total Position Spread Tensor (TPS) is a new tool that describes the electron and spin dynamics in a system. The theory behind the tensor was introduced in 1964 by Walter Khon in his exceptional study about the Theory of the Insulating State, *the essential property is this: every low-lying wave function ( $\Psi$ ) of an insulating ring breaks up into a sum of functions,  $\Psi = \sum_{-\infty}^{\infty} \Psi_M$ , which are localized in disconnected regions of the many-particle configuration space and have essentially vanishing overlap. This property is the analog of localization for a single particle and leads directly to the electrical properties characteristic of insulators*[56]. Therefore, the electrical properties of a system can be calculated from the localization of  $\Psi$ , instead of the classical band-gap theory. The theory of Khon was reformulated by Resta and co-workers to define the metal-insulator nature of solid state systems by introducing the Localization Tensor (LT). The LT is the second order cumulant of the position operator divided by the number of electrons in the system. In molecular environments, a "per-electron" quantity seems to be inappropriate. Therefore, we propose the TPS as better quantity for molecular systems, which is defined as the LT multiplied by the number of electrons. The TPS is a quantity closely related to the fluctuation of the polarization of a system [57], which seems to be an extraordinary tool to describe the nature of chemical bonds. The position operator can be formulated without considering the electronic spin, defining the Spin-Summed of the Total Position Spread Tensor (SS-TPS). On the contrary, the position operator could distinguish between  $\alpha$  and  $\beta$  electron spins, defining the Spin-Partitioned of the Total Position Spread Tensor (SP-TPS).

---

### 1.3 MOTIVATION AND OUTLINE

Chemists have developed systematic methodologies and models to analyze and synthesize new compounds. The *chemical bond* is the most important and famous one. This concept has had an enormous influence on the progress of this field, by providing understanding and classifying chemical species. The chemical bond model has been mainly used by experimental chemists, but in the last years, computational chemists have developed methods to describe chemical bonding from Quantum Mechanical results.

*The primary aim of this thesis is to perform a theoretical study of novel beryllium compounds with novel properties. As well as the application of the Total Position Spread Tensor to molecular systems.*

BerBs increase the acidity of the LB interacting with Be [58, 59]. This property was profited to modify two important properties of fluorine derivatives: (1) the strength of the F-R bonds and (2) the generation of a  $\sigma_{\text{hole}}$  in fluorine. The formation of radical species is the determining step in several chemical reactions. Therefore, Be compounds can be used to weaken F-R bonds, inducing the spontaneous formation of radical species. Fluorine is the only halogen atom not showing a  $\sigma_{\text{hole}}$ , which avoids the formation of halogen bonds in fluorine derivatives [60]. The generation of  $\sigma_{\text{hole}}$  in fluorine derivatives assisted by BerBs allows the design of new materials, where fluorine derivatives could be assembled with Lewis bases by halogen bonds. The human body has several LB sites with which BeY<sub>2</sub> derivatives can interact forming BerBs. This interaction might modify intrinsic properties of the interacting LB, suggesting an explanation to the high toxicity of BeY<sub>2</sub> compounds.

Generally, non-covalent interactions become stronger in unsaturated systems. A well-known representative of this effect are Resonance Assisted Hydrogen Bond (RAHB), which have been used to explain the stronger HB in unsaturated compounds such as the DNA nitrogen bases. Two possible explanations have been proposed for the Resonance Assistance phenomena: (1) the H-donor and -acceptor are part of the resonance structures, which increases the electrostatic interaction between them [61–63]. (2) The H-donor and -acceptor become stronger acids and bases in unsaturated systems [64–66]. In this thesis, the concept of Resonance Assistance is revised by considering a stronger non-covalent interaction, Beryllium Bonds.

The most remarkable property of amine substituted naphthalene compounds is their soaring proton affinities, for which they have been called *proton sponges* [67]. On the contrary, the high-electron deficiency of BeY<sub>2</sub> explains their high affinity to anion species. Therefore, BeY disubstituted naphthalene compounds behave as their analog amine substituted system, but instead of trapping protons they trap anions, leading to what we have named *anion sponges*. This property suggests that BeY disubstituted naphthalene derivatives could be used in the design of new electronic devices, where the performance of the device might be enhanced by the anion selectivity of Be compounds.

The complexes formed between  $\text{Be}_2$  and electron donor species  $\text{L}:\text{Be}-\text{Be}:\text{L}$  have shown to dramatically increase the strength of the Be-Be interaction [41–44]. Therefore,  $\text{L}:\text{Be}-\text{Be}:\text{L}$  systems are synthetically viable complexes. The theoretical study performed for this type of compounds has been done by means of single-reference methodologies, which do not describe correctly the isolated  $\text{Be}_2$  dimer, nor the  $\text{Be}_2$  low-lying excited states neither [53]. This thesis aims at studying  $\text{L}:\text{Be}-\text{Be}:\text{L}$  compounds considering different types of L substituents with high-level multi-reference methods. These methodologies would not only provide an accurate description of the Be-Be bond in these complexes, but also will allow the analysis of the effect of the substituents on the excited states of the  $\text{Be}_2$  moiety.

The Localization Tensor has been mainly applied to solid state systems. We would like to extend its application to molecular systems by the use of the SS-TPS and SP-TPS. These tensors allow to characterize regions of the PES with low and high electron and spin fluctuation. The behavior of the SS-TPS and SP-TPS was studied in a set of diatomic molecules showing different types of chemical bonds and in Be carbonyl derivatives.

This thesis is structured into five chapters. The thesis begins with an introduction of Be compounds and their theoretical description, chapter 1. The second chapter deals with the theoretical background of the methodology employed for this study. Chapter 3 gives a brief review of different types of chemical bonds. The bonding properties of these interactions were described by means of classical methods: Valence Bond Theory (VBT) and MOT, and new wave function analysis methodologies: QTAIM, ELF and NBO. Chapters 4 and 5 present the results and conclusions of this thesis. The fourth chapter analyses the properties of Be-compounds, while in the fifth chapter the behavior of the SS-TPS and SP-TPS for molecular systems is described.

## Part II

### QUANTUM CHEMISTRY METHODS

"Each piece, or part, of the whole of nature is always merely an approximation to the complete truth, or the complete truth so far as we know it. In fact, everything we know is only some kind of approximation because we know that we do not know all the laws as yet."

*Richard Feynman. The Feynman Lectures on Physics - 1964.*



## QUANTUM CHEMISTRY METHODS

---

The birth of Modern Quantum Chemistry is established with the discovery of the time-independent Schrödinger equation and its exact solution for the hydrogen atom in 1926 [68, 69]:

$$\hat{H}\Psi = E\Psi \quad (2.1)$$

The wave function ( $\Psi$ ) contains all the information about a system. In contrast to classically mechanics, the square of  $\Psi$  defines the *probability* to find the system at a certain position in a certain time, and not the exact position of the system. The Hamiltonian ( $\hat{H}$ ) is the operator associated with the energy of the system, and it is defined as the sum of the kinetic and the potential energies.

The Hamiltonian for a system with  $N$  electrons and  $P$  nuclei is defined as:

$$\hat{H} = - \sum_{i=1}^N \frac{1}{2} \nabla_i^2 - \sum_{A=1}^P \frac{1}{2M_A} \nabla_A^2 - \sum_{i=1}^N \sum_{A=1}^P \frac{Z_A}{r_{iA}} + \sum_{i=1}^N \sum_{j>i}^N \frac{1}{r_{ij}} + \sum_{A=1}^P \sum_{B>A}^P \frac{Z_A Z_B}{R_{AB}}, \quad (2.2)$$

where  $R$  and  $r$  are the nuclear and electronic positions, respectively.  $M$  is the nuclear ratio of the mass with respect to the electrons and  $Z$  is the atomic number. In equation 2.2 the first term corresponds to the electronic kinetic energy operator ( $\hat{T}_e$ ), the second term is the nuclear kinetic energy operator ( $\hat{T}_n$ ), the third term is the nucleus-electron coulomb attraction ( $\hat{V}_{Ne}$ ), the fourth term is the electron-electron repulsion ( $\hat{V}_{ee}$ ), and finally, the last term is the nucleus-nucleus repulsion ( $\hat{V}_{NN}$ ).

Equation 2.2 operates over the spatial coordinates of both nuclei and electrons, which makes difficult the evaluation of the energy for avarege-size systems. To overcome this problem the Born-Oppenheimer approximation was proposed, which decouples the electronic and nuclear movements accounting for the heavier mass of these latter. Thus,  $\hat{H}$  in equation 2.2 could be divided in nuclear ( $\hat{H}_p$ ) and electronic ( $\hat{H}_e$ ) contributions,

$$\hat{H}_e = \hat{T}_e + \hat{V}_{ee} + \hat{V}_{Ne} \quad (2.3a)$$

$$\hat{H}_p = \hat{T}_n + \hat{V}_{NN} \quad (2.3b)$$

In the same way, it is possible to define the electronic ( $\Psi_e$ ) and nuclear ( $\Psi_p$ ) wave functions as:

$$\Psi_e = \Psi(\mathbf{r}; \mathbf{R}) \quad (2.4a)$$

$$\Psi_p = \Psi(\mathbf{R}) \quad (2.4b)$$

here  $\Psi_e$  depends only parametrically to the nuclear positions.

Finally, the electronic solution of equation 2.1 is

$$\hat{H}_e \Psi_e = E_e \Psi_e, \quad (2.5)$$

the total energy of a system at a given state is the corresponding eigenvalue of equation 2.5 plus the nuclear potential.

Equation. 2.5 has only been exactly solved for mono-electronic systems, for which the term  $\hat{V}_{ee}$  does not exist. For poly-electronic atoms or molecules, where  $\hat{V}_{ee} \neq 0$ , it cannot be exactly solved. However, several approximations to this equation that allow determining the wave function and the energy of poly-electronic systems have been proposed.

This chapter provides a review of the approximations to the solution of the electronic Schrödinger equation used in this thesis. First, the wave function optimization methods Hartree-Fock and post Hartree-Fock will be introduced. Next, Density Functional Theory (DFT) methods that are based on the optimization of the electron density will be described. Then, the basis set functions used in this thesis will be presented. Finally, the theoretical background of wave function analysis methods is introduced.

## 2.1 HARTREE-FOCK THEORY

Hartree Fock (HF) derives from Molecular Orbital Theory (MOT) and it is the most common starting point for most of the electronic structure methods. HF theory attempts to solve the electronic Schrödinger equation based on the approximation that electrons do not interact among them, instead, each electron "feels" an average potential of the remaining electrons. Although, this appears to be a colossal approximation, it is possible to recover the main part of the electronic energy [70–72]. This section gives a brief review of the equations behind this theory for closed and open shell systems.

### 2.1.1 Hartree-Fock Equations

The wave function for a system of non-interacting electrons is defined as the *Hartree Product* ( $\Psi_{HP}$ )

$$\Psi_{HP}(\vec{x}_1, \vec{x}_2, \dots, \vec{x}_N) = \chi_1(\vec{x}_1)\chi_2(\vec{x}_2) \cdots \chi_N(\vec{x}_N), \quad (2.6)$$

where  $\chi$  are spin orbitals and  $\mathbf{x}_1$  symbolizes the space coordinates ( $r_1$ ) of an electron including its spin coordinate ( $s_1$ ).  $\Psi_{\text{HP}}$  does not satisfy the *antisymmetry principle*, which states that an electronic wave function should be antisymmetric to the interchange of the particles coordinates. This is just a general form of the *Pauli exclusion principle*, which prevents two electrons occupying the same quantum state.

The antisymmetry of the wave function can be introduced by the use of **Slater determinants**. For a system with two electrons,  $\Psi$  is a linear combination of the two possible  $\Psi_{\text{HP}}$

$$\Psi(\vec{\mathbf{x}}_1, \vec{\mathbf{x}}_2) = \frac{1}{\sqrt{2}} [\chi_1(\vec{\mathbf{x}}_1)\chi_2(\vec{\mathbf{x}}_2) - \chi_2(\vec{\mathbf{x}}_1)\chi_1(\vec{\mathbf{x}}_2)], \quad (2.7)$$

where  $1/\sqrt{2}$  is the normalization factor. Equation 2.7 can be generalized for an N-electron system and rewritten as a determinant:

$$\Psi(\vec{\mathbf{x}}_1, \vec{\mathbf{x}}_2, \dots, \vec{\mathbf{x}}_N) = \frac{1}{\sqrt{N!}} \begin{vmatrix} \chi_1(\vec{\mathbf{x}}_1) & \chi_2(\vec{\mathbf{x}}_1) & \cdots & \chi_N(\vec{\mathbf{x}}_1) \\ \chi_1(\vec{\mathbf{x}}_2) & \chi_2(\vec{\mathbf{x}}_2) & \cdots & \chi_N(\vec{\mathbf{x}}_2) \\ \vdots & \vdots & \vdots & \vdots \\ \chi_1(\vec{\mathbf{x}}_N) & \chi_2(\vec{\mathbf{x}}_N) & \cdots & \chi_N(\vec{\mathbf{x}}_N) \end{vmatrix} \quad (2.8)$$

This determinant has N *indistinguishable* electrons occupying N spin orbitals. Considering properties of determinants, the exchange of two electron coordinates corresponds to the exchange of two rows of the determinant, which implies a change in the sign of the determinant. Then, Slater determinants are antisymmetric.

The notation of Slater determinants can be simplified considering only their diagonal elements. The ground state wave function of an N-electron system can be written as:

$$|\Psi_0\rangle = |\chi_1\chi_2 \cdots \chi_a\chi_b \cdots \chi_N\rangle, \quad (2.9)$$

where  $\chi_N$  represents the set of occupied spin orbitals.

The electronic Hamiltonian is approximated by considering the sum between a *core-Hamiltonian operator* ( $\hat{h}$ ) and the Hartree-Fock potential ( $v^{\text{HF}}$ ). The *Fock operator* ( $\hat{f}$ ), for a single electron is defined as:

$$\hat{f}(1) = \hat{h}(1) + v^{\text{HF}}(1), \quad (2.10)$$

where:

- $\hat{h}$  corresponds to the kinetic and potential energies of an electron:

$$\hat{h}(1) = -\frac{1}{2}\nabla_1^2 - \sum_A \frac{Z_A}{r_{1A}} \quad (2.11)$$



- $v^{\text{HF}}$  describes the interaction between an electron in  $\chi_a$  and the potential of a second electron in  $\chi_b$ . This potential approximates the electron-electron interaction to an electron-field interaction:

$$v^{\text{HF}}(1) = \sum_b (\hat{J}_b(1) - \hat{K}_b(1)), \quad (2.12)$$

where  $\hat{J}_b$  and  $\hat{K}_b$  are the coulomb and exchange operators, respectively.

The coulomb operator represents the repulsion between an electron in  $\chi_a$  and a second electron in  $\chi_b$ :

$$\hat{J}_b(1) = \int \frac{|\chi_b(2)|^2 d\vec{x}_2}{r_{12}}, \quad (2.13)$$

The exchange operator does not have a classical interpretation like the coulomb operator. This operator is a consequence of the wave function antisymmetry.  $\hat{K}_b(1)$  is defined by its effect when operates on a spin orbital  $\chi_a(1)$ :

$$\hat{K}_b(1)\chi_a(1) = \left[ \int \chi_b^*(2) \frac{1}{r_{12}} \chi_a(2) d\vec{x}_2 \right] \chi_b(2) \quad (2.14)$$

The Hartree-Fock energy expression for a single electron is

$$\hat{f} |\chi_a\rangle = \varepsilon_a |\chi_a\rangle, \quad (2.15)$$

where  $\varepsilon_a$  is the orbital energy of  $\chi_a$ .

Equation 2.15 is an pseudo-eigenvalue equation, in which the  $\chi_a$  orbital is optimized in order to obtain the lowest possible value for the energy,  $\varepsilon_a$  (*variational principle*). This is considered a non-linear equation because both  $\hat{f}$  and  $\varepsilon$  depend on the spin-orbital. Thus, equation 2.15 can only be solved through an iterative procedure. The *Self-Consistent Field (SCF)* is the iterative method applied to solve the Hartree-Fock equations. This method considers a guess of  $\chi$  to determine an initial  $v^{\text{HF}}$ . The initial effective potential allows calculating a new set of spin orbitals that minimizes the orbital energy, and the procedure continues until self-consistency is reached.

Finally, the total electronic energy is calculated from the wave function obtained from the optimized orbitals. However,  $E_e \neq \sum_a \varepsilon_a$ , actually:

$$E_e = \sum_a \varepsilon_a - \frac{1}{2} \sum_a \sum_b \langle \chi_a | \hat{J}_b - \hat{K}_b | \chi_a \rangle = \sum_a \varepsilon_a - \frac{1}{2} \sum_a \sum_b \langle ab | ab \rangle \quad (2.16)$$

The sum over  $\varepsilon_a$  overestimates the total energy because the coulomb and exchange integrals are evaluated for each orbital energy,  $\varepsilon_a$ . For example, let us consider consider a system with two electrons  $l$  and  $m$ , when the energy of electron  $l$  is added to the energy of electron  $m$ , the electron-electron contributions are included twice.

So far, we have provided a formal formulation of the Hartree-Fock method. The representation of the spin orbitals leads to integro-differential equations that can only be solved for no more than a few atoms. The solution to these equations for more complicated systems, such as molecules, was introduced by Roothaan and Hall in 1951 by expanding the spin orbitals as Linear Combination of Atomic Orbitals (LCAO) [73, 74].

The use of the LCAO approximation to determine the electronic energy is explained in the following sections. However, the formulation of the method depends on the spin properties of the system and is different for closed- and open-shell electronic configurations. For systems with an even number of electrons organized in pairs, Roothaan and Hall proposed the Restricted Hartree-Fock (RHF) method. On the other hand, for an odd number of electrons or open-shell systems, the Unrestricted Hartree-Fock (UHF) method proposed by Pople and Nesbet should be applied [75].

### 2.1.2 Restricted Hartree-Fock: Roothaan-Hall Equations

Closed-shell systems have not only an even number of electrons, but also, the orbitals have only zero or double occupancy, in such a way that both  $\alpha$  and  $\beta$  spin orbitals have the same spatial functions.

In order to ensure that the only difference is the spin function  $s_\alpha$  and  $s_\beta$ ,  $\Psi$  is defined for  $N/2$  doubly occupied Molecular Orbitals (MO). The wave function in equation 2.9 can be written in a MO basis by considering:

$$\chi_i(\vec{x}) = \begin{cases} \psi_i(\vec{r})\alpha(\sigma) = \psi_i \\ \psi_i(\vec{r})\beta(\sigma) = \bar{\psi}_i \end{cases} \quad (2.17)$$

and the wave function of the ground state of a restricted closed-shell system is

$$|\Psi_{\text{RHF}}\rangle = |\psi_1\bar{\psi}_1\psi_2\bar{\psi}_2\cdots\psi_\alpha\bar{\psi}_\alpha\psi_\beta\bar{\psi}_\beta\cdots\psi_{N/2}\bar{\psi}_{N/2}\rangle. \quad (2.18)$$

The MOs ( $\psi_i$ ) can be expanded on the basis of  $K$  known spatial basis functions ( $\phi_p$ ) (LCAO approximation):

$$\Psi_i = \sum_p^K C_{pi}\phi_p. \quad (2.19)$$

Therefore, the energy is calculated by minimizing the MO coefficients ( $C_{pi}$ ) instead of the spin orbitals.

The substitution of the MO expansion in equation 2.15 yields an integro-differential equation for  $C_{pi}$

$$\hat{f}(1) \sum_p^K C_{pi}\phi_p(1) = \epsilon_i \sum_p^K C_{pi}\phi_p(1). \quad (2.20)$$

This equation can be converted into a matrix equation multiplying by  $\phi_q^*(1)$  on the left:

$$\sum_p^K F_{qp} C_{pi} = \varepsilon_i \sum_p^K S_{qp} C_{pi}, \quad (2.21)$$

or,

$$\mathbf{FC} = \mathbf{SC}\varepsilon. \quad (2.22)$$

The matrices in equation 2.22 are defined as:

- $\mathbf{F}$  is the Fock matrix, with elements  $F_{qp} = \int \phi_q^*(1) \hat{f}(1) \phi_p(1) d\vec{r}_1$ .
- $\mathbf{S}$  is the overlap matrix, with elements  $S_{qp} = \int \phi_q^*(1) \phi_p(1) d\vec{r}_1$ .
- $\mathbf{C}$  is the matrix containing the orbitals coefficients.
- $\varepsilon$  is a diagonal matrix representing the orbital energies.

The Fock matrix is constructed from the elements of the Fock operator in equation 2.10:

$$\begin{aligned} F_{qp} &= \int \phi_q^*(1) \hat{f}(1) \phi_p(1) d\vec{r}_1 \\ &= \int \phi_q^*(1) \hat{h}(1) \phi_p(1) d\vec{r}_1 + \sum_a^{N/2} \int \phi_q^*(1) [2\hat{J}_a(1) - \hat{K}_a(1)] \phi_p(1) d\vec{r}_1 \\ &= H_{qp}^{\text{core}} + \sum_a^{N/2} 2(qp|aa) - (qa|ap), \end{aligned} \quad (2.23)$$

where the core-Hamiltonian ( $H_{qp}^{\text{core}}$ ) matrix and the physical notation for the coulomb and the overlap integrals have been introduced. The matrix elements involving the one-electron operator  $\hat{h}(1)$  are grouped in  $H_{qp}^{\text{core}}$  ( $T_{qp} = \int \phi_q^*(1) [-\frac{1}{2}\nabla_1^2] \phi_p(1) d\vec{r}_1$  and  $V_{qp}^{\text{Ne}} = \int \phi_q^*(1) \left[ -\sum_A \frac{Z_A}{|\mathbf{r}_1 - \mathbf{R}_A|} \right] \phi_p(1) d\vec{r}_1$ ). Thus, the Fock matrix can be rewritten in the LCAO formalism, considering one- and two-electron terms

$$\begin{aligned} F_{qp} &= H_{qp}^{\text{core}} + \sum_a^{N/2} \sum_{st} C_{sa} C_{ta}^* [2(qp|ts) - (qs|tp)] \\ &= H_{qp}^{\text{core}} + \sum_{st} \mathbf{D}_{st} \left[ (qp|ts) - \frac{1}{2}(qs|tp) \right] \\ &= H_{qp}^{\text{core}} + \mathbf{G}_{qp}. \end{aligned} \quad (2.24)$$

here  $\mathbf{D}$  is the first-order density matrix and  $\mathbf{G}_{qp}$  the two-electron term of the Fock Matrix. Notice that only  $\mathbf{G}_{qp}$  depends on the orbital coefficients.

The basis functions used in the LCAO expansion are non-orthogonal sets. Therefore, the orbitals coefficients cannot be obtained from the diagonalization of the Fock matrix. There

are several procedures to orthogonalize basis functions, in such a way that the  $\mathbf{S}$  matrix is eliminated and the eigenvalue problem is simplified to  $\mathbf{FC} = \mathbf{C}\varepsilon$ . A simple (and computational inexpensive) procedure is to consider a new coefficient matrix  $\mathbf{C}'$  related to  $\mathbf{C}$  by the expression:

$$\mathbf{C}' = \mathbf{X}^{-1}\mathbf{C} \quad \Rightarrow \quad \mathbf{C} = \mathbf{X}\mathbf{C}', \quad (2.25)$$

where  $\mathbf{X}$  satisfies  $\mathbf{X}^\dagger\mathbf{S}\mathbf{X} = 1$ , that is  $\mathbf{X} = \mathbf{S}^{-1/2}$ .

Substituting equation 2.25 in equation 2.22 and multiplying by  $\mathbf{X}^\dagger$  yields

$$(\mathbf{X}^\dagger\mathbf{F}\mathbf{X})\mathbf{C}' = (\mathbf{X}^\dagger\mathbf{S}\mathbf{X})\mathbf{C}'\varepsilon \quad (2.26a)$$

$$(\mathbf{S}^{-1/2}\mathbf{F}\mathbf{S}^{-1/2})\mathbf{C}' = (\mathbf{S}^{-1/2}\mathbf{S}\mathbf{S}^{-1/2})\mathbf{C}'\varepsilon, \quad (2.26b)$$

If a new Fock matrix is defined as  $\mathbf{F}' = \mathbf{X}^\dagger\mathbf{F}\mathbf{X}$ , the Roothaan-Hall equation can be rewritten as:

$$\mathbf{F}'\mathbf{C}' = \mathbf{C}'\varepsilon. \quad (2.27)$$

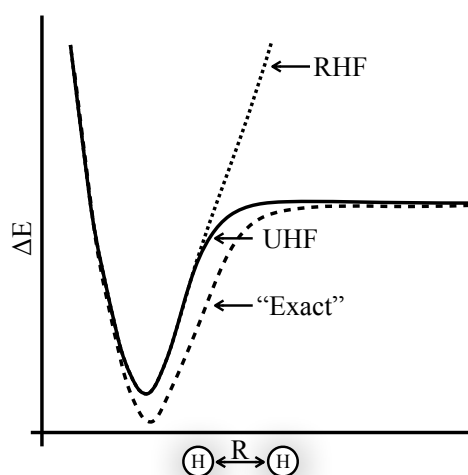
As for the Hartree-Fock equations, the previous equation does not have a direct solution because the Fock matrix also depends on the orbital coefficients. As a consequence, the Roothaan-Hall equations have to be solved iteratively. Finally, the SCF procedure can be summarized in 13 steps:

1. Indicate the molecule characteristics: nuclear coordinates ( $R_A$ ), number of electrons ( $N$ ), atomic numbers ( $Z_A$ ), and basis set ( $\phi_p$ ).
2. Calculate one-electron ( $H_{qp}^{\text{core}}, S_{qp}$ ) and two-electron ( $(qp|st)$ ) integrals.
3. Diagonalize the overlap matrix ( $\mathbf{S}$ ) and obtain the appropriate transformation matrix ( $\mathbf{X}$ ).
4. Consider a guess for the density matrix  $\mathbf{D}_0$ . The extended Hückel method is commonly used to calculate  $\mathbf{D}_0$ .
5. Calculate the matrix  $\mathbf{G}$  using  $\mathbf{D}$  and  $(qp|st)$ .
6. Obtain the Fock matrix  $\mathbf{F}$  from  $\mathbf{G}$  and  $H_{qp}^{\text{core}}$ .
7. Determine the transformed Fock matrix  $\mathbf{F}'$  using  $\mathbf{X}$ .
8. Diagonalize  $\mathbf{F}'$  to obtain  $\mathbf{C}'$  and  $\varepsilon$ .
9. Calculate the coefficient matrix ( $\mathbf{C}$ ) from  $\mathbf{C}'$  and  $\mathbf{X}$ .
10. Evaluate a new density matrix  $\mathbf{D}_n$  from  $\mathbf{C}$ .
11. If  $\mathbf{D}_n = \mathbf{D}_{n-1}$  within a established convergence criteria, the procedure has converged and goes to (13). Otherwise the SCF procedure continues and go to (12).

12. Replace  $\mathbf{D}_{n-1}$  with  $\mathbf{D}_n$  and go back to (5).
13. Determine  $\Psi$  from  $\mathbf{C}, \mathbf{D}, \mathbf{F}$ , and compute the properties of the system.

### 2.1.3 Unrestricted Hartree-Fock: Pople-Nesbet Equations

Open-shell systems do not have an even number of electrons or not all the electrons are arranged into pairs (for example  $\text{O}_3$ ). This means that the wave function cannot be described by  $N/2$  doubly occupied orbitals as in the procedure described in section 2.1.2. Many chemical processes are driven by open-shell systems (for example radicals or excited states), which RHF is not able to describe. A simple process like the homolytic dissociation of the  $\text{H}_2$  becomes a big problem for HF (see scheme. 2.1). RHF correctly describes the  $\Sigma_g$  state of the molecule at its equilibrium position, but at long distance, the RHF solution leads to the heterolytic cleavage. The correct homolytic dissociation is only recovered using the UHF method.



Scheme 2.1:  $\text{H}_2$  potential energy curves. The dotted line is the RHF solution, solid line the UHF and the dashed line the exact solution. Adapted from Szabo [76].

There are two approximations to treat open-shell systems: Restrict-Open-shell Hartree-Fock (ROHF) and UHF. In the ROHF method, all electrons are treated as in the RHF approximation except the unpaired electrons, while within the UHF  $\alpha$  and  $\beta$  electrons are no longer treated in the same spatial conditions. Thus, the flexibility of  $\Psi_{\text{UHF}}$  with respect to the  $\Psi_{\text{ROHF}}$  decreases the variational energy. However, the UHF wave function is not an eigenfunction of the spin operator  $S^2$  and could be contaminated by highest spin multiplicity states.

To build up the  $|\Psi_{\text{UHF}}\rangle$  using the UHF formalism, two sets of MO  $|\Psi_i^\alpha\rangle$  and  $|\Psi_i^\beta\rangle$  are needed. In the LCAO formalism,

$$\Psi_i^\alpha = \sum_p^K C_{pi}^\alpha \phi_p. \quad (2.28)$$

$$\Psi_i^\beta = \sum_p^K C_{pi}^\beta \phi_p. \quad (2.29)$$

but now, both  $\mathbf{C}^\alpha$  and  $\mathbf{C}^\beta$  coefficients must be minimized.

Substituting each wave function expansion in the Hartree-Fock equation (2.15), and multiplying by  $\phi_q^*$  on the left

$$\sum_p^K C_{pi}^\alpha \hat{f}_\alpha(1) \phi_p(1) = \epsilon_a^\alpha \sum_p^K C_{pi}^\alpha \phi_p(1). \quad \sum_p F_{qp}^\alpha C_{pi}^\alpha = \epsilon_a^\alpha \sum_p S_{qp} C_{pi}^\alpha. \quad (2.30)$$

$$\sum_p^K C_{pi}^\beta \hat{f}_\beta(1) \phi_p(1) = \epsilon_a^\beta \sum_p^K C_{pi}^\beta \phi_p(1). \quad \sum_p F_{qp}^\beta C_{pi}^\beta = \epsilon_a^\beta \sum_p S_{qp} C_{pi}^\beta. \quad (2.31)$$

The overlap matrix  $S_{qp}$  remains as in the RHF formalism, but not the Fock matrix  $F_{qp}^\sigma$ . For  $\sigma = \alpha$ :

$$F_{qp}^\alpha = \int \phi_q^* \hat{f}_\alpha(1) \phi_p(1) d\vec{r}(1), \quad (2.32)$$

with  $\hat{f}_\alpha = \hat{h}(1) + \sum_a^{N^\alpha} [\hat{J}_a^\alpha(1) - \hat{K}_a^\alpha(1)] + \sum_a^{N^\beta} \hat{J}_a^\beta(1)$ . The operators  $\hat{J}_a^\alpha(1)$  and  $\hat{K}_a^\alpha(1)$  have the same formulation as in restricted formalism.

Pople and Nesbet introduced for the first time the UHF matrix equations were,

$$\mathbf{F}^\alpha \mathbf{C}^\alpha = \mathbf{S} \mathbf{C}^\alpha \epsilon^\alpha \quad (2.33a)$$

$$\mathbf{F}^\beta \mathbf{C}^\beta = \mathbf{S} \mathbf{C}^\beta \epsilon^\beta. \quad (2.33b)$$

The density matrix is also partitioned considering the  $\alpha$  and  $\beta$  electronic spin components (**D**),

$$D_{st}^\alpha = \sum_a^{N^\alpha} C_{sa}^\alpha (C_{ta}^\alpha)^*, \quad (2.34)$$

$$D_{st}^\beta = \sum_a^{N^\beta} C_{sa}^\beta (C_{ta}^\beta)^*, \quad (2.35)$$

and the total density matrix  $\mathbf{D}^\top$  is the sum of its spin components.

The final expression of the spin partitioned Fock matrices is

$$F_{qp}^\alpha = H_{qp}^{\text{core}} + \sum_s \sum_t D_{st}^\top (qp|ts) - D_{st}^\alpha (qs|tp). \quad (2.36)$$

$$F_{qp}^{\beta} = H_{qp}^{\text{core}} + \sum_s \sum_t D_{st}^T(qp|ts) - D_{st}^{\beta}(qs|tp). \quad (2.37)$$

Equations 2.33a and 2.33b are solved in a similar way as the Roothan-Hall equations. The main difference is that the two Fock matrices are diagonalized simultaneously, because  $F^{\alpha}$  and  $F^{\beta}$  depend on both  $C^{\alpha}$  and  $C^{\beta}$ .

#### 2.1.4 The Hartree-Fock Limit: Electron Correlation

Electron correlation ( $E_{\text{corr}}$ ) is divided in Exchange electron correlation (Pauli exclusion principle,  $E_{\text{corr}}^{\text{XC}}$ ) and Coulomb electron correlation (electron-electron interaction,  $E_{\text{corr}}^{\text{ee}}$ ). The Hartree-Fock approximation accurately describes the  $E_{\text{corr}}^{\text{XC}}$  by considering Slater determinants, but it fails describing  $E_{\text{corr}}^{\text{ee}}$  because the wave function corresponds to non-interacting electrons.

- Exchange electron correlation is correctly described by the use of Slater determinants. Therefore, the accuracy of  $E_{\text{corr}}^{\text{XC}}$  depends only on the size of the basis set. For an infinite number of basis functions, it is possible to recover the total  $E_{\text{corr}}^{\text{XC}}$ . Currently, the computational resources allow to include large basis set, until the *Hartree-Fock limit* is reached. The HF limit is the best possible solution within HF approximation, which is an increase of the flexibility of the basis leads to a negligible change in the energy.
- Coulomb electron correlation is defined as the difference between the Exact non-relativistic ( $E_0$ ) and the HF limit ( $\epsilon_0$ ) energies

$$E_{\text{corr}}^{\text{ee}} = \epsilon_0 - E_0, \quad (2.38)$$

$E_{\text{corr}}^{\text{ee}}$  is not an easy to compute quantity. It has also two components: *dynamical correlation* and *non-dynamical correlation*. The goal of Post Hartree-Fock methods is to recover both:

- Dynamical correlation describes the electron movement. In HF theory an electron moves in the average potential created by the remaining electrons. Then, does not account for such type of correlation. There are several approaches to include dynamical correlation: Perturbation Theory, Configuration Interaction, Coupled-Cluster, and others.
- Non-Dynamical correlation is a consequence of the mono configurational character of the HF wave function. The main approach to include non-dynamical correlation is to introduce more than one determinant in the wave function, with methods such as Multi-configurational SCF (MCSCF).

In the following sections, Post Hartree-Fock methods are going to be introduced. Generally,  $E_{\text{corr}}^{\text{ee}}$  is simply called "electron correlation" because the exchange part is correctly determined by HF. Therefore, in the following, the coulomb electron correlation will be referred as electron correlation.

## 2.2 MANY-BODY PERTURBATION THEORY

Many-Body Perturbation Theory (MBPT) is applied to introduce electronic correlation to the well-known HF result, under the assumption that the correction (electron correlation energy) is much smaller than the HF energy. This is a non-variational method, therefore, the calculated MBPT energy can be an upper bound of the exact energy. But as an advantage, this is a *size-consistent* method, that is, the energy of the system  $E(A + B)$  is equal to sum of the fragments  $E(A) + E(B)$ . There are different models to apply perturbation theory. This section describes the *Rayleigh-Schrödinger Perturbation Theory* (RSPT) [77, 78].

The Hamiltonian is split into two parts, a zero<sup>th</sup>-order Hamiltonian ( $\hat{H}_0$ ) plus a perturbation ( $V$ ).  $\hat{H}_0$  is the Hartree-Fock hamiltonian, whose eigenvalues and eigenfunctions are known.

$$\hat{H} = \hat{H}_0 + \lambda V, \quad (2.39)$$

$\lambda$  is an ordering parameter indicating the order of the perturbation. For  $\lambda = 0$  the solution is equal to the unperturbed system, generally the HF solution. Whereas for  $\lambda = 1$  the exact hamiltonian is recovered. It is possible to expand both the energy and the wave function as a Taylor series in  $\lambda$ :

$$E_i = E_i^{(0)} + \lambda E_i^{(1)} + \lambda^2 E_i^{(2)} + \cdots + \lambda^n E_i^{(n)} \quad (2.40)$$

$$|\Psi\rangle_i = |\Psi_i^{(0)}\rangle + \lambda |\Psi_i^{(1)}\rangle + \lambda^2 |\Psi_i^{(2)}\rangle + \cdots + \lambda^n |\Psi_i^{(n)}\rangle \quad (2.41)$$

Replacing the energy and wave function expansions in the Schrödinger equation

$$\begin{aligned} & (\hat{H}_0 + \lambda V)(|\Psi_i^{(0)}\rangle + \lambda |\Psi_i^{(1)}\rangle + \lambda^2 |\Psi_i^{(2)}\rangle + \cdots + \lambda^n |\Psi_i^{(n)}\rangle) \\ &= (E_i^{(0)} + \lambda E_i^{(1)} + \lambda^2 E_i^{(2)} + \cdots + \lambda^n E_i^{(n)})(|\Psi_i^{(0)}\rangle + \lambda |\Psi_i^{(1)}\rangle \\ &+ \lambda^2 |\Psi_i^{(2)}\rangle + \cdots + \lambda^n |\Psi_i^{(n)}\rangle), \end{aligned} \quad (2.42)$$

This equation only holds if the  $\lambda^n$  coefficients are equal on both sides. Then, collecting equal coefficients:

$$\hat{H}_0 |\Psi_i^{(0)}\rangle = E_i^{(0)} |\Psi_i^{(0)}\rangle \text{ for } \lambda^0 \quad (2.43a)$$

$$\hat{H}_0 |\Psi_i^{(1)}\rangle + V |\Psi_i^{(0)}\rangle = E_i^{(0)} |\Psi_i^{(1)}\rangle + E_i^{(1)} |\Psi_i^{(0)}\rangle \text{ for } \lambda^1 \quad (2.43b)$$

$$\hat{H}_0 |\Psi_i^{(2)}\rangle + V |\Psi_i^{(1)}\rangle = E_i^{(0)} |\Psi_i^{(2)}\rangle + E_i^{(1)} |\Psi_i^{(1)}\rangle + E_i^{(2)} |\Psi_i^{(0)}\rangle \text{ for } \lambda^2, \quad (2.43c)$$



and so on until  $\lambda^n$ . From equations 2.43, it is possible to calculate  $E$  and  $\Psi$  at any correction order.

### 2.2.1 Corrections to the energy

Equation 2.43a is the expression for the unperturbed system (zero<sup>th</sup>-order correction), which corresponds to the HF solution. The first order correction to the energy is obtained by multiplying equation 2.43b by  $\langle \Psi_i^{(0)} |$

$$\langle \Psi_i^{(0)} | \hat{H}_0 | \Psi_i^{(1)} \rangle + \langle \Psi_i^{(0)} | V | \Psi_i^{(0)} \rangle = \hat{E}_{(0)} \langle \Psi_i^{(0)} | \Psi_i^{(1)} \rangle + E_i^{(1)} \langle \Psi_i^{(0)} | \Psi_i^{(0)} \rangle. \quad (2.44)$$

Considering: the orthogonality relation  $\langle \Psi_i^{(0)} | \Psi_i^{(n)} \rangle = 0$ , the orthonormalization of the functions  $\Psi_i^{(n)}$ , and the  $\hat{H}$  hermiticity ( $\langle \Psi_i^{(0)} | \hat{H}_0 | \Psi_i^{(1)} \rangle = \hat{E}_0 \langle \Psi_i^{(0)} | \Psi_i^{(1)} \rangle$ )

$$E_i^{(1)} = \langle \Psi_i^{(0)} | V | \Psi_i^{(0)} \rangle. \quad (2.45)$$

The same procedure can be applied for  $n = 2$  to obtain the correction to the energy at second order:

$$E_i^{(2)} = \langle \Psi_i^{(0)} | V | \Psi_i^{(1)} \rangle. \quad (2.46)$$

The energy of order  $k$  depends on the 0<sup>th</sup> and  $(k - 1)$ <sup>th</sup> order wave functions. The general expression for the correction at  $k$ <sup>th</sup>

$$E_i^k = \langle \Psi_i^{(0)} | V | \Psi_i^{(k-1)} \rangle. \quad (2.47)$$

Finally, the total electronic energy is

$$E_i = E_i^{(0)} + \sum_{k>0}^k \langle \Psi_i^{(0)} | V | \Psi_i^{(k-1)} \rangle. \quad (2.48)$$

### 2.2.2 Corrections to the wave function

The first-order correction to the wave function is obtained from equation 2.43b. First, this equation is multiplied by  $\langle \Psi_j^0 |$

$$\langle \Psi_j^{(0)} | \hat{H}_0 | \Psi_i^{(1)} \rangle + \langle \Psi_j^0 | V | \Psi_i^{(0)} \rangle = E_i^{(0)} \langle \Psi_j^{(0)} | \Psi_i^{(1)} \rangle + E_i^{(1)} \langle \Psi_j^{(0)} | \Psi_i^{(0)} \rangle, \quad (2.49)$$

where  $\langle \Psi_j^{(0)} | \Psi_i^{(1)} \rangle$  is a measure of the effect of  $\Psi_i$  over a function  $\Psi_j$  of the unperturbed system,  $\langle \Psi_j^{(0)} | \Psi_i^{(1)} \rangle = c_j^{(1)}$ . Considering:  $\langle \Psi_j^{(0)} | \Psi_i^{(0)} \rangle = 0$  and ( $\langle \Psi_j^{(0)} | \hat{H}_0 | \Psi_i^{(1)} \rangle = \hat{E}_0 \langle \Psi_j^{(0)} | \Psi_i^{(1)} \rangle$ )

$$c_j^{(1)} = \frac{\langle \Psi_j^{(0)} | V | \Psi_i^{(0)} \rangle}{E_i^{(0)} - E_j^{(0)}} \quad (2.50)$$

The first-order correction  $\Psi_i^{(1)}$  can be obtained as an expansion of  $\Psi_j^{(0)}$  with  $c_j^{(1)}$  coefficients, which is only possible for a complete set of basis functions (in practice  $\Psi_i^{(0)}$  is a finite set of functions).

$$\Psi_i^{(1)} = \sum_j c_j^{(1)} \Psi_j^{(0)} = \sum_{j \neq i} \frac{\langle \Psi_j^{(0)} | V | \Psi_i^{(0)} \rangle}{E_i^{(0)} - E_j^{(0)}} \Psi_j^{(0)}, \quad (2.51)$$

and  $\Psi_i$  at first-order correction is

$$\Psi_i = \Psi_i^{(0)} + \Psi_i^{(1)} = \Psi_i^{(0)} + \sum_j c_j^{(1)} \Psi_j^{(0)} = \Psi_i^{(0)} + \sum_{j \neq i} \frac{\langle \Psi_j^{(0)} | V | \Psi_i^{(0)} \rangle}{E_i^{(0)} - E_j^{(0)}} \Psi_j^{(0)}. \quad (2.52)$$

The energy at 2nd-order correction can be calculated from  $\Psi_i^{(1)}$ ,

$$E_i^{(2)} = \sum_{j \neq i} \frac{|\langle \Psi_j^{(0)} | V | \Psi_i^{(0)} \rangle|^2}{E_i^{(0)} - E_j^{(0)}} \quad (2.53)$$

### 2.2.3 Møller-Plesset equations

The theory described in the previous sections was postulated by Møller and Plesset in 1934 as a special case of the RSPT. However, the formulation implemented in most of the computational packages was introduced almost 40 years later by Binkley and Pople [79, 80].

The zero<sup>th</sup>-order Hamiltonian is defined as the sum of the Fock operators:

$$\hat{H}^{(0)} = \sum_i \hat{f}_i. \quad (2.54)$$

The zero<sup>th</sup>-order wave function and energy correspond to the HF solution:  $\Psi_i^{(0)} = \Psi^{\text{HF}}$  and  $E_i^{(0)} = \sum_a \varepsilon_a$ .

The correction  $V$  introduces the term  $\frac{1}{r_{ij}}$  (electron-electron interaction), but it also has to be considered that  $E_i^{(0)}$  is an upper bound of the real HF energy,

$$V = \sum_{i < j} \frac{1}{r_{ij}} - \sum_b (\hat{J}_b - \hat{K}_b). \quad (2.55)$$

The 1<sup>st</sup>-order correction to the energy is formulated from equation 2.45 and  $V$ :

$$\begin{aligned}
 E_i^{(1)} &= \langle \Psi^{\text{HF}} | V | \Psi^{\text{HF}} \rangle \\
 &= \langle \Psi^{\text{HF}} | \sum_{i < j} \frac{1}{r_{ij}} | \Psi^{\text{HF}} \rangle - \langle \Psi^{\text{HF}} | \sum_b (\hat{J}_b - \hat{K}_b) | \Psi^{\text{HF}} \rangle \\
 &= \frac{1}{2} \sum_a \sum_b \langle ab || ab \rangle - \sum_a \langle a | \sum_b (\hat{J}_b - \hat{K}_b) | a \rangle \\
 &= -\frac{1}{2} \sum_a \sum_b \langle ab || ab \rangle.
 \end{aligned} \tag{2.56}$$

And the energy:

$$\begin{aligned}
 E_i &= E_i^{(0)} + E_i^{(1)} \\
 &= \sum_i \varepsilon_i - \frac{1}{2} \sum_a \sum_b \langle ab || ab \rangle = E^{\text{HF}}
 \end{aligned} \tag{2.57}$$

The first perturbative correction only gives back the HF energy. This implies that in order to recover electron correlation it is necessary to go beyond 1<sup>st</sup>-order perturbation theory. However, to derive the second order correction of the energy, the first order correction to the wave function needs to be known (equation 2.53)

$\Psi_i^{(1)}$  is defined in equation 2.52, where  $\Psi_j^{(0)}$  and  $E_j^{(0)}$  are the only unknown terms of this equation.  $\Psi_j^{(0)}$  is an excited function from  $\Psi_i^{\text{HF}}$ , but which type of excitation?

- Singly excited functions:  $\langle \Psi_a^r | V | \Psi_i^{\text{HF}} \rangle = 0$  (the Brillouin theorem)
- Doubly excited functions:  $\langle \Psi_{ab}^{rs} | V | \Psi_i^{\text{HF}} \rangle = \langle ab || rs \rangle$
- Triply excited functions:  $\langle \Psi_{abc}^{rst} | V | \Psi_i^{\text{HF}} \rangle = 0$ .  $\hat{H}$  is a bi-electronic operator, thus, triple or higher excitations do not interact with  $\Psi_i^{\text{HF}}$ .

Then, for  $\Psi_j^{(0)} = \Psi_{ab}^{rs}$  only double excitations are considered (in Møller-Plesset Second Order Perturbation Theory (MP2)). The first correction to the wave function is defined as:

$$\Psi_i^{(1)} = \sum_{\substack{a < b \\ r < s}} c_{ab}^{rs} \Psi_{ab}^{rs} \tag{2.58}$$

The final unknown term in the energy expression is  $E_j^{(0)}$ :

$$E_j^{(0)} = \hat{H}_0 | \Psi_{ab}^{rs} \rangle = E_i^{(0)} - (\varepsilon_a + \varepsilon_b - \varepsilon_r - \varepsilon_s), \tag{2.59}$$

and,

$$E_i^{(0)} - E_j^{(0)} = \varepsilon_a + \varepsilon_b - \varepsilon_r - \varepsilon_s. \tag{2.60}$$

Finally, the energy corrected to second order is defined as:

$$\begin{aligned}
 E_i &= E_i^{(0)} + E_i^{(1)} + E_i^{(2)} \\
 &= E^{\text{HF}} + \sum_{\substack{a>b \\ r>s}} \frac{|\langle \Psi_{ab}^{rs} | V | \Psi_i^{\text{HF}} \rangle|^2}{E_i^{(0)} - E_j^{(0)}} \\
 &= E^{\text{HF}} + \sum_{\substack{a>b \\ r>s}} \frac{\langle ab || rs \rangle^2}{\epsilon_a + \epsilon_b - \epsilon_r - \epsilon_s},
 \end{aligned} \tag{2.61}$$

This equation is known as MP2 and it recovers between 80 – 90% of electron correlation. The remaining electron correlation can be calculated taking further the perturbation formalism, and considering the methods MP3, MP4, MP5 and MP6 for the corrections of third, fourth, fifth and sixth order, respectively. However, the evaluation of higher order corrections of the wave function increases dramatically the computational effort and time.

## 2.3 CONFIGURATION INTERACTION

The HF wave function has a mono determinantal character, corresponding to a single electronic configuration. A "simple" approach introducing electron correlation is to consider other possible electronic configurations, and thus, their determinants in the wave function. Finally, the electronic energy is obtained by diagonalizing the N-electron Hamiltonian considering the variational principle. This approach is called *Configuration Interaction (CI)*. The CI method provides a scheme to obtain the exact energy for an infinite basis set. However, basis sets are in practice finite and for very large basis set  $\Psi$  could become very large, making the diagonalization of  $\hat{H}$  a very hard task [81, 82].

In this section CI methods are presented, considering the complete (Full Configuration Interaction (FCI)) and its truncated solutions. Multi-configurational approaches that are based on the CI methodology will also be introduced.

### 2.3.1 The Full CI Method

Equation 2.9 in page 21 shows the determinantal representation of the HF wave function for occupied spin orbitals ( $\chi_1, \chi_2, \dots, \chi_a, \chi_b, \dots, \chi_N$ ), but up to  $(2K - N)$  virtual spin orbitals are also obtained at HF level of theory ( $\chi_{N+1}, \chi_{N+2}, \dots, \chi_r, \chi_s, \chi_t, \chi_u, \dots, \chi_{2K-N}$ ), where  $K$  is the number of basis set functions and  $N$  is the number of electrons. Therefore, it is possible to build new determinants promoting electrons from occupied to virtual orbitals:

- Singly excited determinants ( $|\Psi_a^r\rangle$ ), where an electron has been excited from an occupied ( $\chi_a$ ) to a virtual orbital ( $\chi_r$ ).

- Doubly excited determinants ( $|\Psi_{ab}^{rs}\rangle$ ), where two electrons have been excited from two occupied ( $\chi_a, \chi_b$ ) to two virtual orbitals ( $\chi_r, \chi_s$ ).
- ...

The Configuration Interaction (CI) wave function can be expressed as linear combination of all the determinants. The introduction of this flexibility in the wave function allows recovering the electron correlation.

$$|\phi_0\rangle = \sum_I |\Psi_I\rangle = c_0 |\Psi_0\rangle + \sum_{ar} c_a^r |\Psi_a^r\rangle + \sum_{\substack{a<b \\ r<s}} c_{ab}^{rs} |\Psi_{ab}^{rs}\rangle \dots, \quad (2.62)$$

this expansion goes up to  $\binom{2K}{N}$  determinants, with  $2K$  one-electron spin orbitals.

Equation 2.62 is the *Full CI wavefunction*. The number of determinants increases rapidly with the number of atoms and basis set, but this expansion can be truncated without affecting the results. Determinants with different spin do not mix and can be therefore eliminated. For example, for a system of singlet multiplicity, all the determinants with a different number of  $\alpha$  and  $\beta$  electrons can be discarded.

To express the FCI energy it is convenient to consider an intermediate normalized form of  $|\phi_0\rangle$ ,

$$\langle \Psi_0 | \phi_0 \rangle = 1 \quad (2.63)$$

It is possible to normalize  $|\phi_0\rangle$  by multiplying each term of the expansion by a constant,  $|\phi'_0\rangle = c' |\phi_0\rangle$  in such a way that  $\langle \phi'_0 | \phi_0 \rangle = 1$ .

The main aim is to determine the correlation energy. The Schrödinger equation ( $\hat{H} |\phi_0\rangle = \varepsilon_0 |\phi_0\rangle$ ) can be expressed as a function of the correlation energy considering equation 2.38

$$(\hat{H} - E_0) |\phi_0\rangle = (\varepsilon_0 - E_0) |\phi_0\rangle = E_{\text{corr}} |\phi_0\rangle \quad (2.64)$$

Multiplying both sides by  $\langle \Psi_0 |$

$$\langle \Psi_0 | (\hat{H} - E_0) | \phi_0 \rangle = E_{\text{corr}} \langle \Psi_0 | \phi_0 \rangle = E_{\text{corr}} \quad (2.65)$$

and introducing the intermediate normalized expansion of 2.62

$$\langle \Psi_0 | (\hat{H} - E_0) | \phi_0 \rangle = \langle \Psi_0 | (\hat{H} - E_0) \left( |\Psi_0\rangle + \sum_{ct} c_c^t |\Psi_c^t\rangle + \sum_{\substack{c<t \\ d<u}} c_{ct}^{du} |\Psi_{ct}^{du}\rangle \dots \right) \quad (2.66)$$

The correlation energy is defined as:

$$E_{\text{corr}} = \sum_{\substack{a<b \\ r<s}} c_{ab}^{rs} \langle \Psi_0 | \hat{H} | \Psi_{ab}^{rs} \rangle, \quad (2.67)$$

considering the Brillouin theorem  $\langle \Psi_0 | (\hat{H} - E_0) | \Psi_c^t \rangle = 0$ , and eliminating the matrix elements differing by more than two spin-orbitals with respect to  $\Psi_0$  (Slater–Condon rules).

Equation 2.67 suggests that the correlation energy only depends on double excitations. However, the coefficients  $c_{ab}^{rs}$  consider higher order excitations, what makes the size of the FCI matrix to be giant. Then, the FCI method can hardly be employed for systems larger than light diatomic molecules.

The first attempt to decrease the size of the CI matrix is the so called *truncated-CI* methods: CID only considers double excitations, CISD includes single and double excitations, and going further is not computationally feasible. The disadvantage of these methods is that they are not *size-consistent*, preventing the correct description of dissociation processes. Some corrections have been proposed to solve the *size-consistency* problems: Davidson correction (based on perturbative corrections) [83], Average Coupled-Pair Function (based on Coupled Cluster theory) [84], Quadratic CISD (the quadratic terms are included as a product of double excitations) [85], and others.

### 2.3.2 Multi-Configurational Methods

Until now two approaches to calculate electron-correlation have been described. Perturbation theory and CI methods. The first is size consistent but does not account for non-dynamical electron correlation. On the contrary, the second includes non-dynamical electron correlation but it is not size consistent. And, there are some processes in chemistry, however, where it is essential to consider non-dynamical electron correlation and size consistent methodologies. For example:

- Dissociation processes.
- Configuration degeneracy.
- Excited states

Multi-Configurational Self-Consistent Field (MCSCF) methods are non-dynamical electron correlation and size consistent methodologies. They are also based in a truncation of the CI matrix, but following a different approach than for *truncated-CI*.

#### 2.3.2.1 Multi-Configurational Self-Consistent Field (MCSCF)

The MCSCF wave function is

$$|\Psi_{\text{MCSCF}}\rangle = \sum_{\text{I}} C_{\text{I}} |\Psi_{\text{I}}\rangle, \quad (2.68)$$

where  $\Psi_I$  are Slater determinants for different configurations constructed from orthonormal spin-orbitals, and  $C_I$  are the CI coefficients. In this method both, the expansion and the orbital coefficients are optimized.

The MCSCF expression of the energy will be derived in the second quantization framework. The spin-dependent terms of the Hamiltonian are not included in order to express the methodology in terms of the spin summed excitation operators  $\hat{E}_{ij}$

$$\hat{E}_{ij} = \hat{a}_{i\alpha}^\dagger \hat{a}_{j\alpha} + \hat{a}_{i\beta}^\dagger \hat{a}_{j\beta}, \quad (2.69)$$

here  $\hat{a}_i^\dagger$  is the creation operator able to add an electron in orbital  $i$ , and  $\hat{a}_i$  is the annihilation operator that removes an electron from orbital  $j$ .

Some properties of  $\hat{E}_{ij}$ :

- The commutator relation:  $[\hat{E}_{ij}, \hat{E}_{kl}] = \hat{E}_{il}\delta_{jk} - \hat{E}_{kj}\delta_{il}$ .
- The adjoint operator:  $\hat{E}_{ij}^\dagger = \hat{E}_{ji}$ .
- The operations over orbitals, considering  $n$  as the orbital occupation number (0,1,2):

$$\hat{E}_{ij} |n_1, \dots, n_i, n_j, \dots, n_N\rangle = \begin{cases} 0 & \text{for } n_i = 2, n_j = 0, i \neq j \\ n_i |n_1, \dots, n_i, n_i, \dots, n_N\rangle & \text{for } i = j \end{cases} \quad (2.70)$$

Having introduced second quantization, the next step is to define the operators and matrix elements in this formalism. For an independent spin **one-electron operator**  $\hat{F}$ :

$$\hat{F} = \sum_i \sum_j F_{ij} \hat{E}_{ij}, \quad (2.71)$$

where  $F_{ij} = \int \phi_i^*(1) \hat{F}(1) \phi_j(1) d\vec{r}_1$ . The sum and the integral are defined in the molecular orbitals basis.

The matrix elements of this operator are related to the first-order reduced density matrix. Consider a matrix element of  $\hat{F}$  between two Slater determinants  $|m\rangle$  and  $|n\rangle$

$$\langle m | \hat{F} | n \rangle = \sum_i \sum_j F_{ij} \langle m | \hat{E}_{ij} | n \rangle = \sum_i \sum_j F_{ij} D_{ij}^{mn}, \quad (2.72)$$

where  $D_{ij}^{mn}$  are the *one-electron coupling coefficients*. For a wave function of the type  $|\Psi\rangle = \sum_m c_m |m\rangle$ , the first-order density matrix is defined as  $D_{ij} = \sum_m \sum_n c_m^* c_n D_{ij}^{mn}$ .

The next step consists in deriving the independent spin **two-electron operator**  $\hat{G}$ :

$$\hat{G} = \frac{1}{2} \sum_{i,j} \sum_{k,l} g_{ijkl} (\hat{E}_{ij} \hat{E}_{kl} - \delta_{jk} \hat{E}_{il}), \quad (2.73)$$

where  $g_{ijkl} = \int \phi_i^*(1)\phi_j(1)(r_{12}^{-1})\phi_k^*(2)\phi_l(2)dV_1dV_2$ . The sum and the integral are defined in the molecular orbitals basis.

Similarly, the matrix elements of  $\hat{G}$  are related to the second-order reduced density matrix. Repeating the previous strategy, the matrix elements between Slater determinants are

$$\langle m|\hat{G}|n\rangle = \sum_{i,j} \sum_{k,l} g_{ijkl} \frac{1}{2} \langle m|\hat{E}_{ij}\hat{E}_{kl} - \delta_{jk}\hat{E}_{il}|n\rangle = \sum_{i,j} \sum_{k,l} g_{ijkl} P_{ijkl}^{mn}, \quad (2.74)$$

where  $P_{ijkl}^{mn}$  are the *two-electron coupling coefficients*. The second order density matrix is  $P_{ijkl} = \sum_m \sum_n c_m^* c_n P_{ijkl}^{mn}$ .

The final step is to formulate the Hamiltonian and the electronic energy. The Hamiltonian operator is,

$$\hat{H} = \sum_i \sum_j h_{ij} \hat{E}_{ij} + \frac{1}{2} \sum_{i,j} \sum_{k,l} g_{ijkl} (\hat{E}_{ij}\hat{E}_{kl} - \delta_{jk}\hat{E}_{il}), \quad (2.75)$$

here  $h_{ij}$  and  $g_{ijkl}$  are the one- and two-electron integrals, respectively. The energy is calculated as the expectation value of  $\hat{H}$  over a wave function of the type 2.68,

$$E = \langle \Psi|\hat{H}|\Psi\rangle = \sum_i \sum_j h_{ij} D_{ij} + \sum_{i,j} \sum_{k,l} g_{ijkl} P_{ijkl}. \quad (2.76)$$

where the orbital and CI coefficients are in the  $\mathbf{D}$  and  $\mathbf{P}$  density matrices.

As was stated previously, the energy is determined by optimizing the CI and the orbitals coefficients. However, the MCSCF convergence is not easy, then there are different types of approaches to optimize the coefficients. The *Newton-Raphson* method is a second order method that considers not only the gradient but also the hessian to find the optimal parameters [86]. The *Super-CI* optimization finds the optimal wave function by annihilating the singly excited configurations in an iterative procedure [87]. Both methods have advantages and disadvantages. Computationally, the *Super-CI* method is more demanding but the coefficients always converge to a local minimum.

The complicated procedure inherent to the optimization of the MCSCF wave function justifies that not many computationally packages implement/improve this methodology, compared to other single-reference methods. Two of the most widely used programs implementing MCSCF algorithms are MOLCAS[88] and MOLPRO[89]. Both of them were used in this thesis for MCSCF calculations. MOLCAS optimization methods relies in the original *Super-CI* and new updates of this approach[87, 90, 91], while MOLPRO uses an update of the quadratically convergent theory proposed by Werner and Meyer[92, 93].

### 2.3.2.2 Complete Active Space Self-Consistent Field

The only CI approach that preserves *size-consistency* is FCI. An approximation is to constrain the FCI calculation to a selected space of the wave function while the others are treated at



HF level of theory. This method is the so called Complete Active Space Self Consistent Field (CASSCF) and was introduced in 1980 by Roos and co-workers [87, 90].

The CASSCF wave function ( $\Psi_{\text{CASSCF}}$ ) is divided into four spaces, see scheme 2.2:

- *Core orbitals*. This space is formed by doubly occupied orbitals that are optimized at HF theory. These orbitals are kept frozen and cannot be rotated to the active space during the orbital optimization.
- *Inactive and Virtual orbitals*. These spaces are formed by doubly occupied (inactive) and empty (virtual) orbitals. These orbitals can be rotated into the active space during the orbital optimization.
- *Active orbitals*. This is the most important space in the  $\Psi_{\text{CASSCF}}$ . It is formed by a subspace of orbitals with fractional occupation number comprised between 0 – 2, and where FCI is applied. Then, the choice of the active space determines the accuracy of the CASSCF result.

The CASSCF calculation begins with a FCI procedure including all possible determinants in the active space. The next step is a MCSCF calculation, where the wave function is defined as 2.68. The energy is calculated following the formalism in section 2.3.2.1. However, as FCI calculations, this method is limited by the number of Configuration State Functions (CSFs) defined by the active space ( $N_{\text{CAS}}$ ).  $N_{\text{CAS}}$  is a space composed by  $n$  electrons and  $m$  orbitals, with a total spin  $S$ . The number of CSFs is calculated by the Weyl formula:

$$N_{\text{CAS}} = \frac{2S + 1}{m + 1} \binom{m + 1}{\frac{1}{2}n - S} \binom{m + 1}{\frac{1}{2}n + S + 1}. \quad (2.77)$$

Then, for a singlet state system with 14 active electrons and 14 active orbitals, the number of CSFs is equal to 2760615, which is close to the limit for this type of calculations. According to previous works, the CASSCF limit is around 12-16 orbitals. Finally, a common notation to indicate the method and the size of the active space is CASSCF( $n, m$ ).

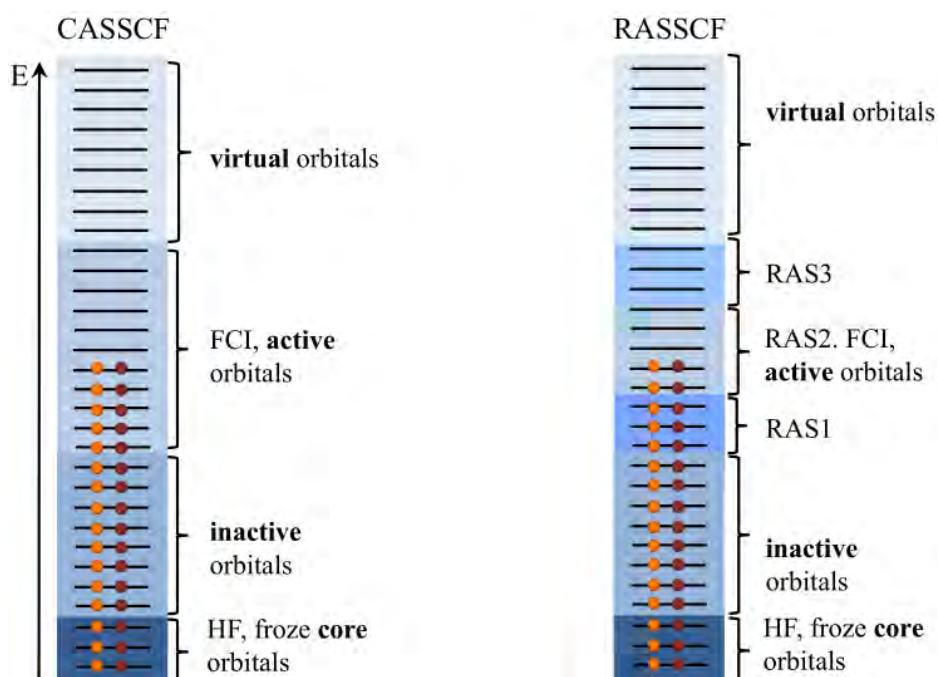
In the last years, several approximations to increase the size of the active space have been proposed. The Restricted Active Space SCF (RASSCF) approximation is among them. It is a simple technique in which the active space is further divided into three subspaces (see scheme 2.2):

1. *Core orbitals*
2. *Inactive orbitals*
3. *Active orbitals*
  - a) RAS1: are doubly occupied orbitals that only allow a fix number of holes (defined by the user).

- b) RAS 2: all possible excitations are included in this space, is equivalent to the active orbitals in the CASSCF partition.
- c) RAS 3: are empty orbitals that only allow a fix number of electrons (defined by the user).

#### 4. Virtual orbitals

The success of this scheme is that for specific problems double excitations from or to some particular orbitals are not reasonable. But there is also a disadvantage, the orbital rotation within the three RAS-subspaces should be possible, diffculting the convergence of the RASSCF wave function.



Scheme 2.2: Left CASSCF and right RASSCF spaces.

Having discussed how to compute the MCSCF energy and wave function, the end of this section introduces some practical information about the calculations.

#### Active Space

The accuracy of the CASSCF method depends on the Active Space (AS). An incorrect AS could deliver energies higher than the HF result. There are no rules for choosing the correct AS, but below are listed some hints that can be taken into account:

- *Occupancy*: orbitals with occupancy number higher than 1.99 or lower than 0.01 could be left outside of the active space. In general, excitations within this type of orbitals do not have an important contribution to the wave function.

- *Energy*: occupied orbitals with low energy and virtual orbitals with high energy should also be left outside of the active space. As in the case of the occupancy criteria, excitations from or to these type of orbitals are not expected to have a significant contribution to the wave function.
- *Orbitals*: balanced active spaces are very much preferred. A well-balance active space includes each bonding and its corresponding anti-bonding orbitals. Also important, if the molecule has degenerated orbitals, all of them must be included in the AS.
- *System*: the system under study also provides indications about the active space that should be used. In an excited state investigation, the nature of the excitation has a fundamental role in the choice of the AS. For the description of  $\Pi \rightarrow \Pi^*$  excitations, the AS should contain (if possible) the complete set of  $\Pi$  orbitals, while for the description of  $n \rightarrow \Pi^*$  transitions the lone pairs (LP) must be also included. Another example is bond dissociations, for instance, the AS for the  $F_2 \rightarrow F(^2P) + F(^2P)$  dissociation must consider that at long distances the six  $p_F$  atomic orbitals become degenerated. Therefore, all  $p_F$  orbitals should be included in the AS (10,6). This AS preserves the size consistency of the method and represents a good balance space.
- "*Chemical intuition*": finally it is always useful to use the knowledge about the system.

### State Average CASSCF

One of the advantages of performing a FCI calculation within a particular active space is that not only the ground state is calculated, but also higher lying electronically excited states. This becomes important when the ground state is energetically degenerate to other electronic states or in excited state calculations. The correct procedure is to consider a state average solution of the MCSCF equations, where the energy is calculated averaging over  $M$  states:

$$E_{\text{aver}} = \sum_I w_I E_I, \quad (2.78)$$

here  $w_I$  are weight factors of each state, and each  $E_I$  is calculated by equation 2.76.

A big advantage of SA-CASSCF calculation is that the only "extra effort" that needs to be done is the calculation of average single state density matrices, and as the final result, a set of optimized orthogonal orbitals for  $M$  average states and  $M$  CI vectors are obtained. The disadvantages of the method: (1) the quality of the result decreases with an increasing number of  $M$ , for big values of  $M$  the final orbitals do not describe any of the  $M$  states. (2) *Root flipping* during the MCSCF calculation. Sometimes the desired root (state) is exchanged with a lower or higher energy state, which will probably cause a convergence failure. (3) Computational time increases with the number of  $M$ , because there are  $M$  MCSCF matrices to be diagonalized.

### 2.3.2.3 Multi-Configurational and Perturbative Methods: Complete Active Space and Second order Perturbation Theory

The previous section has shown how to introduce static correlation through MCSCF methods. A common (and computationally "inexpensive") approach introducing dynamic correlation is to use second order perturbation theory (see section 2.2). Hence, in this section one of the most used methods, Complete Active Space Second Order Perturbation Theory (CASPT2) is described [94, 95]. This method follows a conventional MP2 scheme but on multi-determinantal wave functions.

The CASPT2 method attempts to stay as close as possible to the Møller-Plesset scheme, then, it is worth to recall two equations from Perturbation Theory:

1. The RSPT first order correction to the wave function from equation 2.43b can be rewritten as:

$$\left(\hat{H}_0 - E^{(1)}\right) |\Psi^{(1)}\rangle = \left(E^{(0)} - V\right) |\Psi^{(0)}\rangle. \quad (2.79)$$

2. The definition of the second order correction to the energy:

$$E^{(2)} = \langle \Psi^{(0)} | V | \Psi^{(1)} \rangle. \quad (2.46)$$

From the above equations the only known terms are  $\Psi^{(0)}$  and  $V$ . The zero-order wave function is the CASSCF solution ( $\Psi^{(0)} = \Psi_{\text{CASSCF}}$ ) and the perturbation  $V$  is equivalent to that of Møller-Plesset method (see equation 2.55). The definition of the zero-order Hamiltonian is one of the most important components of Multi-Configurational Perturbative Methods. Several  $\hat{H}_0$  have been proposed, but the CASPT2 approach has shown to give accurate results.

In Møller-Plesset Theory the zero-order Hamiltonian is defined as a sum of Fock operators. However, a Fock operator able to operate over multi-configurational wave functions ( $\Psi_{\text{CASSCF}}$ ) needs to be formulated. In the second order formalism, the CASSCF Fock operator is defined as:

$$\hat{F} = \sum_{qp} f_{qp} \hat{E}_{qp} = \sum_{qp} \left( \hat{h}_{qp} + \sum_{st} D_{st} \left[ (qp|ts) - \frac{1}{2}(qs|tp) \right] \right) \hat{E}_{qp}, \quad (2.80)$$

where  $f_{qp}$  is the fock operator in the Roothan-Hall derivation for close-shell systems. The Fock matrix in CASPT2 can be simplified including the CASSCF wave function partition, that is to say the matrix is divided in inactive (i), active (a) and virtual (v) orbitals.

$$\begin{aligned} \hat{F} = & \sum_i \varepsilon_i \hat{E}_{ii} + \sum_a \varepsilon_a \hat{E}_{aa} + \sum_i \varepsilon_v \hat{E}_{vv} \\ & + \sum_{ia} f_{ai} [\hat{E}_{ia} + \hat{E}_{ai}] + \sum_{iv} f_{vi} [\hat{E}_{iv} + \hat{E}_{vi}] + \sum_{av} f_{va} [\hat{E}_{av} + \hat{E}_{va}], \end{aligned} \quad (2.81)$$

see scheme 2.3 for a matrix representation of the Fock matrix  $\hat{F}$  in the CASSCF representation.

To formulate the zero-order Hamiltonian, it has to be considered that  $\Psi_{\text{CASSCF}}$  is not an eigenfunction of  $\hat{F}$ , and then,  $\hat{H}_0$  is derived as a projection of the Fock operator in the CASSCF basis

$$\hat{H}_0 = \hat{H}_{\text{CASSCF}} = \hat{P}_{\text{CASSCF}} \hat{F} \hat{P}_{\text{CASSCF}}. \quad (2.82)$$

This guarantees, when  $\Psi_{\text{CASSCF}} = \Psi_{\text{RHF}}$ , the CASPT2 and MP2 solutions to be equal.

The CASPT2  $\hat{H}_0$  is defined as the sum of four subspaces: (1) CASSCF, the reference wave function. (2) K, the complementary CASSCF space. (3) SD, all single and double excitations respect to CASSCF. (4) X, the remaining excitations.

$$\begin{aligned} \hat{H}_0 &= \hat{H}_{\text{CASSCF}} + \hat{H}_{\text{SD}} \\ &= \hat{P}_{\text{CASSCF}} \hat{F} \hat{P}_{\text{CASSCF}} + \hat{P}_{\text{K}} \hat{F} \hat{P}_{\text{K}} + \hat{P}_{\text{SD}} \hat{F} \hat{P}_{\text{SD}} + \hat{P}_{\text{X}} \hat{F} \hat{P}_{\text{X}}. \end{aligned} \quad (2.83)$$

The matrix representation of the zero-order Hamiltonian avoids long perturbative expansions (see scheme 2.3).

		$\hat{F}$		
		$i_{\text{orb}}$	$a_{\text{orb}}$	$v_{\text{orb}}$
$i_{\text{orb}}$	$i_{\text{orb}}$	$\epsilon_i$	$f_{ia}$	X
	$a_{\text{orb}}$	$f_{ai}$	$\epsilon_a$	$f_{av}$
$v_{\text{orb}}$	$v_{\text{orb}}$	X	$f_{vi}$	$\epsilon_v$

		$\hat{H}_0$			
		CAS	SD	TQ	...
CAS	CAS	$\hat{F}$	X	X	X
	SD	X	$\hat{F}$	X	X
	TQ	X	X	$\hat{F}$	X
	...	X	X	X	$\hat{F}$

Scheme 2.3: Matrix representation of: left CASSCF- $\hat{F}$  and right CASPT- $\hat{H}_0$ . Adapted from Helgaker[1].

The first order correction to the wave function is defined with  $\hat{H}_0$ , but it has to be considered which are the configurations interacting with the CASSCF wave function. In the CASPT2  $\hat{H}_0$ , only the configurations in the SD subspace interact with the CASSCF subspace, then only single and double excitations are included in  $\Psi^{(1)}$ ,

$$\Psi^{(1)} = \sum_{\text{qpst}} C_{\text{qpst}} |\text{qpst}\rangle = \sum_{\text{qpst}} C_{\text{qpst}} (\hat{E}_{\text{qp}} \hat{E}_{\text{st}} |\Psi_{\text{CASSCF}}\rangle), \quad (2.84)$$

where the indices q and t correspond to occupied orbitals (inactive or active), and p and s stand for empty orbitals (active or virtual). Knowing  $\Psi^{(1)}$  the second order correction is calculated through equation 2.46.

Multi-State CASPT2 (MS-CASPT2)[96]

In the previous section, CASPT2 theory was explained for a single reference state, but as was stated before, there are several cases in chemistry where the reference wave function has a multiconfigurational character.

MS-CASPT2 performs  $M$  single state calculations by using an effective Hamiltonian, with elements:

$$(H_{\text{eff}})_{ij} = \delta_{ij}E_i + \langle (\Psi_{\text{CASSCF}})_i | \hat{H} | (\Psi^{(1)})_j \rangle, \quad (2.85)$$

where  $E_i$  are the CASSCF energies, and the second term is the 2<sup>nd</sup> order correlation energy ( $e_{ij}$ ).

The diagonal terms of the matrix correspond to the single state CASPT2 energies and the off-diagonal elements are the coupling between these single states. The MS-CASPT2 energies are calculated diagonalizing ( $H_{\text{eff}}$ ), see scheme 2.4.

	1	2	3	n
1	$E_1^{PT2}$	$\Delta_{12}^{PT2}$	$\Delta_{13}^{PT2}$	$\Delta_{1n}^{PT2}$
2	$\Delta_{21}^{PT2}$	$E_2^{PT2}$	$\Delta_{23}^{PT2}$	$\Delta_{2n}^{PT2}$
3	$\Delta_{31}^{PT2}$	$\Delta_{32}^{PT2}$	$E_3^{PT2}$	$\Delta_{3n}^{PT2}$
n	$\Delta_{n1}^{PT2}$	$\Delta_{n2}^{PT2}$	$\Delta_{n3}^{PT2}$	$E_n^{PT2}$

Scheme 2.4: Matrix representation of the MS-CASPT2 effective Hamiltonian. The diagonal terms  $E_i^{PT2}$  are the energies of the  $i^{\text{th}}$  state, and the off-diagonal terms  $\Delta_{ij}^{PT2}$  are the effective coupling between the  $i^{\text{th}}$  and  $j^{\text{th}}$  states.

The final MS-CASPT2 perturbatively modified wave function is defined as:

$$\Psi_p = \sum_i C_{pi} |\Psi_{\text{CASSCF}}\rangle + \Psi_p^{(1)}, \quad (2.86)$$

where  $\Psi_p^{(1)}$  is the first-order correction to the wave function for the state  $p$ .

### IPEA and Level shifts [97–100]

IPEA (Ionization Potential-Electron Affinity) and level shifts are modifications of the CASPT2 theory to solve some of its inherent problems:

1. Level shifts [101–103]. From perturbation theory, the second order correction to the energy is inversely proportional to the energy expression,  $E^{(0)} - E_i^{(0)}$  (2.51). In some cases, an  $i^{\text{th}}$  state with an energy close to  $E^{(0)}$  becomes part of the SD space (intruder state), making this energy difference insignificant. This means that  $\Psi^{(1)}$  would be enormous and perturbation theory is not valid any more to describe this system. An easy solution is to include a shift ( $\epsilon$ ) in the zero-order Hamiltonian in equation 2.79, thus, the denominator is deviated from zero:  $(E^{(0)} - E_i^{(0)}) \rightarrow (E^{(0)} - E_i^{(0)} + \epsilon)$ .
2. IPEA shift [104] corrects a systematic error of the CASPT2 original formulation. This method underestimates the energy of those processes where the number of paired electrons is changed (such as dissociation and atomization energies) and excitation energies, which is caused by an underestimation of open-shell states energies. By default, the IPEA shift includes a  $0.25\text{au}$  shift-parameter in  $H_0$ . This parameter was tested for several cases giving the optimal value for the system energy.

## 2.4 COUPLED CLUSTER THEORY

Coupled Cluster (CC) theory is a post-HF method in which size consistency is preserved and the difficulties associated with the choice of the AS of CASSCF are circumvented. However, Coupled Cluster (CC) methods are not variational and are single-reference ( $\Psi_{\text{HF}}$ ). Inspired in CI methods, electron correlation is included adding excited terms to the wave function, but in CC methods, the excitations are evaluated by exponentials of the *cluster operator*.

The *cluster operator* ( $T$ ) is an excitation operator defined by the sum of single ( $T_1$ ), double ( $T_2$ ), triples ( $T_3$ ) and so on excitation operators:

$$T = T_1 + T_2 + T_3 + \dots, \quad (2.87)$$

$T_i$  is described in analogy with the CI excited configurations, as:

$$T_1 = \sum_{a,r} t_a^r a_r^\dagger a_a \quad (2.88a)$$

$$T_2 = \sum_{a>b} \sum_{r>s} t_{ab}^{rs} a_s^\dagger a_b a_r^\dagger a_a, \quad (2.88b)$$

where  $t$  are the cluster amplitudes.

The breaking point with CI methods is the definition of the wave function, in CC  $\Psi$  is an exponential function:

$$\Psi_{\text{CC}} = \exp(T)\Psi_{\text{HF}}, \quad (2.89)$$

in which  $\exp(T)$  can be expanded in a Taylor series:

$$\begin{aligned} \exp(T) = & 1 + T_1 + T_2 + T_3 + \dots \\ & + \frac{1}{2!} T_1^2 + T_1 T_2 + \frac{1}{3!} T_1^3 + \frac{1}{4!} T_1^4 + \frac{1}{2!} T_1^2 T_2 + T_1 T_3 + \frac{1}{2!} T_2^2 \dots, \end{aligned} \quad (2.90)$$

The terms  $T_1, T_2, T_3, \dots$  are named connected terms, while  $T_1^2, T_1 T_2, \dots$  are the disconnected terms.

What is the advantage of  $\Psi_{CC}$ ? Equation 2.89 can be rewritten in:

$$\Psi_{CC} = \prod (1 + T_1 + T_2 + T_3 + \dots) \Psi_{HF}. \quad (2.91)$$

The previous equation shows that  $\Psi_{CC}$  has two remarkable properties: (1) the excitations are additive as in the case of the CI methods and (2) the wave function has a multiplicative property that allows preserving size consistency with truncated expansions. However, this representation of  $\Psi$  has also disadvantages, the evaluation of the cluster amplitudes cannot be achieved by solving a set of linear equations (as the case of CI methods), and the variational principle can no longer be applied. Then, several derivations to solve Coupled Cluster equations have been proposed.

The *projected coupled cluster equations* are among the alternatives to determine the cluster amplitudes. The full coupled cluster wave function satisfies the Schrödinger equation  $\hat{H}\exp(T)|\Psi_{HF}\rangle = E\exp(T)|\Psi_{HF}\rangle$ , but this is not the case for truncated wave functions. Then, projections over  $|\Psi_{HF}\rangle$  and excited determinants  $|\Psi_\mu\rangle$  are used to build a set of algebraic equations to obtain  $E_{corr}$  and  $T$ .

- **Energy:** Projecting over  $|\Psi_{HF}\rangle$

$$\langle\Psi_{HF}|\hat{H}\exp(T)|\Psi_{HF}\rangle = E \quad (2.92a)$$

$$\langle\Psi_{HF}|(\hat{H} - E_0)\exp(T)|\Psi_{HF}\rangle = E_{corr}, \quad (2.92b)$$

and the general CC correlation energy is defined as:

$$E_{corr} = \langle\Psi_{HF}|\hat{W}\exp(T)|\Psi_{HF}\rangle, \quad (2.93)$$

with  $\hat{W} = \hat{H} - E_0$

- **Cluster amplitudes:** Projecting over  $|\Psi_\mu\rangle$

$$\langle\Psi_\mu|\hat{W}\exp(T)|\Psi_{HF}\rangle = E_{corr} \langle\Psi_\mu|\exp(T)|\Psi_{HF}\rangle. \quad (2.94)$$

Equations 2.92 and 2.94 are known as the *unlinked CC equations*.

The evaluation of the full coupled cluster wave function is not computationally feasible and becomes necessary to truncate  $T$ . The truncated  $\Psi_{CC}$  should include at least double excitations in order to recover electron correlation, and in this particular case where  $T = T_1 + T_2$ , the method corresponds to the so-called CCSD. Higher excitation operators have small contributions to the  $E_{corr}$  and their evaluation is computationally more demanding. A common approach is to introduce triple excitations using perturbation theory [CCSD(T)]. In the following sections, both CCSD and CCSD(T) methodologies are explained, using the unlinked CC equations.



### 2.4.1 The CCSD Method [105, 106]

The CCSD wave function is defined as:

$$\Psi_{\text{CCSD}} = \exp(T_1 + T_2)\Psi_{\text{HF}} = \left(1 + T_1 + T_2 + \frac{1}{2}(T_1 + T_2)^2 + \dots\right)\Psi_{\text{HF}}. \quad (2.95)$$

$\Psi_{\text{CCSD}}$  not only includes double excitation terms in the wave function, higher excitations are considered through the disconnected contributions. For example, quadruple excitations are described by the  $T_2^2$  term, even though, the  $T_4$  and the  $T_3T_1$  terms are neglected.

The unknown terms in  $\Psi_{\text{CCSD}}$  are the single ( $t_a^r$ ) and double ( $t_{ab}^{rs}$ ) cluster amplitudes. These are obtained by projecting single ( $\Psi_a^r$ ) and double ( $\Psi_{ab}^{rs}$ ) excited determinants over  $|\Psi_{\text{HF}}\rangle$ . Finally, the energy is calculated as in equation 2.93.

**Energy:** Projecting over  $|\Psi_{\text{HF}}\rangle$

$$E_{\text{corr}} = \langle\Psi_{\text{HF}}|\hat{W}\exp(T_1 + T_2)|\Psi_{\text{HF}}\rangle \quad (2.96a)$$

$$E_{\text{corr}} = \langle\Psi_{\text{HF}}|\hat{W}\exp(1 + T_2 + \frac{1}{2}T_1^2)|\Psi_{\text{HF}}\rangle. \quad (2.96b)$$

In the previous equations, the Brillouin theorem and Slater-Condon rules were considered. These equations show that the energy depends only on single and double amplitudes independently of the  $T$  truncation.

**Cluster amplitudes:** Projecting over  $|\Psi_a^r\rangle$  and  $|\Psi_{ab}^{rs}\rangle$

$$\langle\Psi_a^r|\hat{W}\exp(T_1 + T_2)|\Psi_{\text{HF}}\rangle = E_{\text{corr}} \langle\Psi_a^r|\exp(T_1 + T_2)|\Psi_{\text{HF}}\rangle \quad (2.97a)$$

$$\langle\Psi_a^r|\hat{W}\exp(1 + T_1 + T_2 + \frac{1}{2}T_1^2 + T_1T_2 + \frac{1}{6}T_1^3)|\Psi_{\text{HF}}\rangle = t_a^r E_{\text{corr}}, \quad (2.97b)$$

the single cluster amplitude depends on single, double and **triple** excitations.

$$\langle\Psi_{ab}^{rs}|\hat{W}\exp(T_1 + T_2)|\Psi_{\text{HF}}\rangle = E_{\text{corr}} \langle\Psi_{ab}^{rs}|\exp(T_1 + T_2)|\Psi_{\text{HF}}\rangle \quad (2.98a)$$

$$\langle\Psi_{ab}^{rs}|\hat{W}\exp(1 + T_1 + T_2 + \frac{1}{2}T_1^2 + T_1T_2 + \frac{1}{6}T_1^3 + \frac{1}{2}T_2^2 + T_1^2T_2 + \frac{1}{24}T_1^4)|\Psi_{\text{HF}}\rangle = (t_{ab}^{rs} + t_a^r t_b^s - t_a^s t_b^r) E_{\text{corr}}, \quad (2.98b)$$

the double cluster amplitudes depend on single, double, triple and **quadruple** excitations.

Finally, the cluster amplitudes are optimized through an iterative method.

### 2.4.2 The CCSD(T) Method

The CCSD model is a good approximation for small systems with few interacting electrons. Notwithstanding, connected triples need to be frequently included to have a complete de-

scription of many electrons systems. In the first instance, explicitly triple excitations could be introduced ( $T = T_1 + T_2 + T_3$ , CCSDT), but this would increase the cost of the method scaling from  $N^6$  (CCSD) to  $N^8$ . Therefore, CCSDT cannot be used for the study of medium size systems. A very common approach is to use perturbation theory to treat the triple excitations, CCSD(T)[107].

The CCSD(T) method does not simply include triple excitations from the Møller-Plesset scheme. There have been an evolution of the method by improving its accuracy without increasing the computational time:

1. *CCSD-T(4)*: in this method triple excitations are included from Møller-Plesset fourth-order perturbation theory (MP4), which scales as  $N^7$ , but it is not an iterative procedure.
2. *CCSD + T(CCSD)*: the next step was the use of the CCSD optimized amplitudes ( $t_{ab}^{rs}$ ) in the MP4 calculation, instead of the first-order amplitudes as in the original MP4.
3. *CCSD(T)*: the final improvement was to include a fifth order perturbation term that only involves single amplitudes.

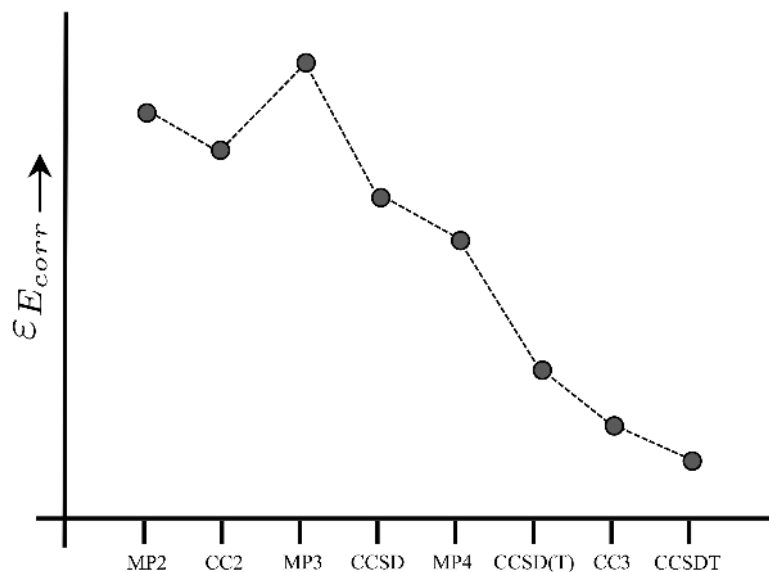
Then, CCSD(T) computational time is much worth reasonable than that of CCSDT and the results have shown that it is one of the most accurate methods for medium size systems. Actually, CCSD(T) is the most common benchmark method for single-reference problems.

Other attempts to decrease computational time are the  $n^{\text{th}}$ -order *Approximated Coupled-Cluster (CCn)*, which are iterative methods that neglect some terms in the  $T$  expansion (but yet conserving size consistency). In the CCn approximation all terms of order  $n$  and higher are discarded. The  $n$  higher amplitudes are calculated as first-order parameters, in terms of a fluctuation potential associated to the  $n - 1$  excitations (the fluctuation potential is defined as the difference between the Hamiltonian and the Fock operator). The CCn method equivalent to CCSD(T) is CC3 [108], CCSD(T) is less expensive than CC3 because triple excitations are not variationally included, but as a disadvantage, there is not a wave function associated to the CCSD(T) approximation.

Scheme 2.5 summarizes the error associated to the  $E_{\text{corr}}$  of CC and MPn methods for the water molecule, using FCI as a reference method. The importance of triple excitations to recover correlation energy is clear from this scheme (2.5), CCSD(T), CC3 and CCSDT have the best performance from all the methods, however, their scaling are also higher.

#### 2.4.2.1 Multi-configuration character, $\tau_1$ diagnostic[109]

The application of the CCSD method to single-reference systems recovers between 90 – 95% of electronic correlation. But, as was discussed in previous sections, not all the systems are single-reference. In CCSD, the orbitals are optimized for a single configuration (HF orbitals),



Scheme 2.5: Comparison of the performance of CC and MPn methods using FCI as a reference methodology.  $\epsilon E_{\text{corr}}$  is the error for the correlation energy and the calculations were performed for the water molecule. Adapted from Helgaker [1].

then, when excited configurations have a bigger weight in the wave function, those orbitals are not optimal anymore.

The relaxation of the orbitals is related to single excitations. For multi-configurational wave functions it is expected a large contribution from  $t_a^r$ . The  $\tau_1$  diagnostic is proposed as a measure of the multi-configurational character of the wave function, by considering the single excitations weight:

$$\tau_1 = \frac{|t_a^r|}{\sqrt{N}}, \quad (2.99)$$

with  $N$  equal to the number of electrons. A value of  $\tau_1$  bigger than 0.02 suggests that the wave function has a non-negligible multi-configurational character.

## 2.5 DENSITY FUNCTIONAL THEORY

The previous sections describe wave function based methods, DFT is a different approach based on the optimization of the electron density ( $\rho(\mathbf{r})$ ). Why does this represent an advantage? Because the wave function has a dependency on the coordinates of the  $N$  electrons in the system ( $3N$ ), while  $\rho$  is a spatial function that depends only on the 3 spatial coordinates. The main objective of DFT is to derive equations in which the physical observables are a function of the electron density, instead of using quantum chemical operators. This means that it is necessary to build a Hamiltonian depending on the electron density.

This section provides a brief review on DFT, as well as on the method introduced by Khon and Shawn to evaluate the electronic energy.

### 2.5.1 The Electron Density

The wave function for a system with  $N$  electrons was defined at the beginning of the chapter,  $\Psi(x_1, x_2, \dots, x_a, \dots, x_N)$ . The square of  $\Psi$  is the probability distribution to find electron 1 between  $x_1 + dx_1$ , electron 2 between  $x_2 + dx_2, \dots$ , electron  $N$  between  $x_N + dx_N$ . The probability to find an electron  $a$  independently of the position of the other electrons is defined as the integration of  $|\Psi|^2$  respect to all the coordinates except  $x_a$ :

$$dx_a \left( \int \dots \int |\Psi(\vec{x}_1, \vec{x}_2, \dots, \vec{x}_a, \dots, \vec{x}_N)|^2 d\vec{x}_1 d\vec{x}_2 \dots d\vec{x}_N \right). \quad (2.100)$$

The electrons are *indistinguishable* particles and therefore the  $N$  electrons must have the same probability distribution. The probability to find *any* of the  $N$  electrons in  $x_a + dx_a$  can be defined as the multiplication of equation 2.100 by  $N$ .

$$\left( N \int \dots \int |\Psi(\vec{x}_1, \vec{x}_2, \dots, \vec{x}_a, \dots, \vec{x}_N)|^2 d\vec{x}_1 d\vec{x}_2 \dots d\vec{x}_N \right) = \rho(\vec{x}) \quad (2.101)$$

$\rho(\vec{x})$  is the so-called density function. The electron density ( $\rho(\vec{r})$ ) is obtained integrating with respect to the spin coordinate  $s_a$

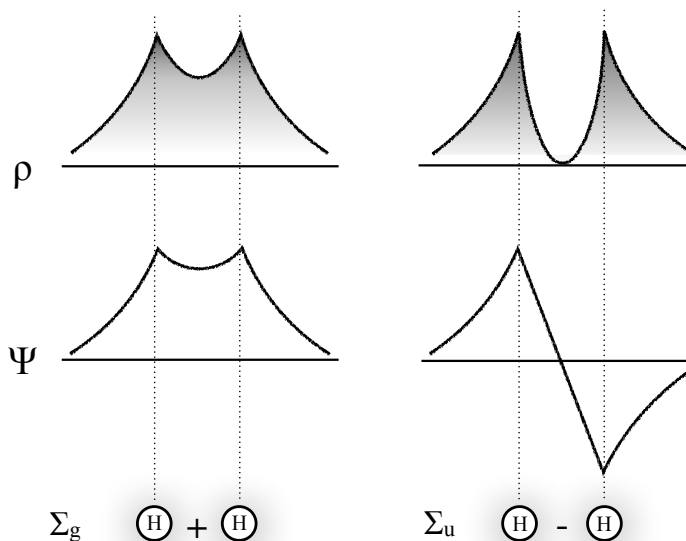
$$\left( N \int \dots \int |\Psi(\vec{x}_1, \vec{x}_2, \dots, \vec{x}_a, \dots, \vec{x}_N)|^2 ds_a d\vec{x}_1 d\vec{x}_2 \dots d\vec{x}_N \right) = \rho(\vec{r}) \quad (2.102)$$

Scheme 2.6 compares  $\Psi$  and  $\rho$  for the  $\Sigma_g$  and  $\Sigma_u$  states of the  $H_2$  molecule.  $\rho$  for the  $\Sigma_g$  state shows three regions where there is a maximum of probability to find an electron: the nuclei and the bonding regions, while in the  $\Sigma_u$  state the probability in the bonding region goes to zero. Some of the properties of  $\rho$  are shown in this scheme (2.6): (1) is always a positive value, (2) goes to zero at long distances, and (3) the area below  $\rho$  is equal to the number of electrons ( $\int \rho(\vec{r}) d\vec{r}_a = N$ ).

**The electron density is the fundamental quantity of DFT.** However, it was needed 40 years to proof that the energy of a system could be calculated from  $\rho$ .

### 2.5.2 The Hohenberg-Kohn Theorems

The backbone of modern Density Functional Theory are the two theorems proposed by Hohenberg and Kohn in 1964[110]:



Scheme 2.6: Comparison of the wave function  $\Psi$  and electron density  $\rho$  for the  $\Sigma_g$  and  $\Sigma_u$  states of the  $\text{H}_2$  molecule. The horizontal full black line represent values equal to zero.

### 2.5.2.1 The First Theorem: Existence Theorem

The external potential  $V_{\text{Ne}}(\mathbf{r})$  is (to within a constant) a unique functional of  $\rho(\mathbf{r})$ ; since, in turn  $V_{\text{ext}}(\mathbf{r})$  fixes  $\hat{H}$  we see that the full many particle ground state is a unique functional of  $\rho(\mathbf{r})$ .

The first theorem is an existence theorem, it proofs that the electron density is a unique quantity able to describe a unique system. Then, it is possible to describe the electronic properties using  $\rho$ .

*Proof:* consider two different external potentials  $V_{\text{Ne}1}(\mathbf{r})$  and  $V_{\text{Ne}2}(\mathbf{r})$ . Both of them give the same  $\rho$ , but different Hamiltonians and wave functions:  $\hat{H}_1$  and  $\Psi_1$ , and  $\hat{H}_2$  and  $\Psi_2$ .

The expectation values of  $\hat{H}_1$  using  $\Psi_2$ , and  $\hat{H}_2$  using  $\Psi_1$  are evaluated using the variational theorem:

$$\begin{aligned} E_1 < \langle \Psi_2 | \hat{H}_1 | \Psi_2 \rangle &= \langle \Psi_2 | \hat{H}_2 | \Psi_2 \rangle + \langle \Psi_2 | \hat{H}_1 - \hat{H}_2 | \Psi_2 \rangle \\ &= E_2 + \int \rho(\vec{r}) [V_{\text{Ne}1}(\vec{r}) - V_{\text{Ne}2}(\vec{r})] d\vec{r} \end{aligned} \quad (2.103)$$

$$\begin{aligned} E_2 < \langle \Psi_1 | \hat{H}_2 | \Psi_1 \rangle &= \langle \Psi_1 | \hat{H}_1 | \Psi_1 \rangle + \langle \Psi_1 | \hat{H}_2 - \hat{H}_1 | \Psi_1 \rangle \\ &= E_1 + \int \rho(\vec{r}) [V_{\text{Ne}2}(\vec{r}) - V_{\text{Ne}1}(\vec{r})] d\vec{r} \end{aligned} \quad (2.104)$$

Adding equation 2.103 to 2.104 it is found a contradiction:

$$E_1 + E_2 < E_2 + E_1, \quad (2.105)$$

which shows that two different external potentials cannot be associated to the same electron density, indicating a direct relation between  $\rho$  and  $\Psi$ :  $\rho(\mathbf{r}) \Rightarrow v_{\text{ext}}(\mathbf{r}) \Rightarrow \hat{H} \Rightarrow \Psi$ .

The main consequence of this theorem is that  $\rho$  can be used to determine all the expectation values of any observable of a system, among them, the electronic energy. The electronic energy can be written as functional of  $\rho$ :

$$\begin{aligned} E[\rho] &= V_{\text{Ne}}[\rho] + T_{\text{ee}}[\rho] + V_{\text{ee}}[\rho] \\ &= V_{\text{Ne}}[\rho] + F[\rho], \end{aligned} \quad (2.106)$$

where  $F[\rho]$  is a universal functional of  $\rho$ , in which are grouped all the terms that do not depend on  $v_{\text{ext}}(\mathbf{r})$ .

### 2.5.2.2 The Second Theorem: Variational Theorem

*The electronic density of a non-degenerate ground state can be calculated evaluating the density that minimizes the ground state energy.*

$$E_0 \leq E[\tilde{\rho}], \quad (2.107)$$

where  $E_0$  is the ground state energy, and  $E[\tilde{\rho}]$  is the ground state energy as a functional of a trial density. These energies are equal only if  $\tilde{\rho} = \rho$ .

Equation 2.107 is the equivalent of the variational principle in wave function methods. Therefore, the energy obtained from a trial  $\rho$  always represents an upper bound to the real ground state energy. In order to minimize the energy functional with respect to  $\rho(\mathbf{r})$ , the *Euler-Lagrange equation* is used. This equation uses the Lagrange minimization of a function, and  $(\int \rho(\vec{r}) d\vec{r}) - N = 0$  as a constraint.

$$\mu = \frac{\partial E[\rho]}{\partial \rho(\mathbf{r})} = v_{\text{ext}}(\mathbf{r}) + \frac{\partial F[\rho]}{\partial \rho(\mathbf{r})}, \quad (2.108)$$

The most complex term in equation 2.108 is the universal functional  $F[\rho]$ . The exact expression of this functional is unknown and the use of an approximate  $F[\rho]$  invalidates the second theorem. Thus, the variational principle can no longer be used to minimize the energy.

### 2.5.3 The Kohn-Sham Method[111]

The Kohn-Sham method is an alternative solution for equation 2.106. The main idea is to describe the main part of the kinetic energy using molecular orbitals and to solve  $N$  orbitals equations instead of a single equation (2.108).

Kohn and Sham defined the universal functional as

$$F[\rho] = J[\rho] + T_s[\rho] + E_{\text{XC}}[\rho], \quad (2.109)$$

where  $J[\rho]$  is the Hartree Coulomb repulsion

$$J[\rho] = \frac{1}{2} \iint \frac{\rho(1)\rho(2)}{r_{12}} d\vec{r}_1 d\vec{r}_2, \quad (2.110)$$

$T_s[\rho]$  is the kinetic energy of a system of non-interacting electrons with density  $\rho$  as in the HF method.

$$T_s[\rho] = \sum_i^N \langle \Psi_i | -\frac{1}{2} \nabla^2 | \Psi_i \rangle. \quad (2.111)$$

where  $\Psi_i$  is a single determinant wave function built by a Slater Determinant of Kohn-Sham orbitals ( $\phi_{KS}$ ).

The final term is the *exchange-correlation energy*  $E_{XC}[\rho]$ , where are collected all the approximations done in equations 2.110 and 2.111.  $E_{XC}[\rho]$  is considered the *key* quantity of DFT methods.

$$E_{XC}[\rho] = [(T[\rho] - T_s[\rho]) + (V_{ee}[\rho] - J[\rho])] \quad (2.112)$$

The Hamiltonian for this system can be defined as:

$$\hat{H} = - \sum_i^N \frac{1}{2} \nabla_i^2 + \sum_i^N V_{eff}(r_i), \quad (2.113)$$

and finally the *Kohn-Sham eigenvalue equation can be formulated*

$$\left( - \sum_i^N \frac{1}{2} \nabla_i^2 + \sum_i^N V_{eff}(r_i) \right) \Psi_i(r) = \epsilon_i \Psi_i(r). \quad (2.114)$$

The coefficients of  $\Psi_i$  are minimized through an SCF procedure similar to the one explained before for HF:

1. Select an initial set of  $\phi_{KS}^0$  orbitals.
2. Calculate the electron density ( $\rho^0$ ) with the  $\phi_{KS}$  guess.
3. Define  $E_{XC}$  and determine  $V_{eff}$ .
4. Solve the *Kohn-Sham eigenvalue equation* and obtain a new set of  $\phi_{KS}^n$ .
5. Evaluate the new electron density ( $\rho^n$ ).
6. If the convergence criterion is reached the SCF procedure has finished, otherwise go back to step (3) using  $\rho^n$ .

### 2.5.4 The Exchange Correlation Energy

As already stated before, the  $E_{XC}[\rho]$  is the fundamental quantity for DFT. The Kohn-Sham eigenvalue equation would be the exact solution for the electronic problem with the exact exchange-correlation functional. The main issue is that the definition of  $E_{XC}[\rho]$  is unknown, and therefore,  $E_{XC}[\rho]$  must be approximated in practical calculations. This section collects the most common approximations to the  $E_{XC}[\rho]$  functional.

#### 2.5.4.1 The Local Density Approximation (LDA)

The LDA approximation considers a uniform electron gas system moving on a positive background charge distribution leading to a neutral ensemble. This system has a finite number of electrons  $N$  and volume  $V$ , and therefore, its electron density is finite and constant ( $\rho = N/V$ ). The exchange-correlation energy for a constant  $\rho$  is a local quantity that depends only on the electron density,

$$E_{XC}^{LDA}[\rho(\vec{r})] = \int \rho(\vec{r}) \epsilon_{XC}^{LDA}[\rho(\vec{r})] d\vec{r} \quad (2.115)$$

here  $\epsilon_{XC}^{LDA}[\rho]$  is the exchange-correlation energy for a particle, which is defined as the sum of the exchange ( $\epsilon_X$ ) and correlation ( $\epsilon_C$ ) energies

$$\epsilon_{XC}^{LDA}[\rho(\vec{r})] = \epsilon_X^{LDA}[\rho(\vec{r})] + \epsilon_C^{LDA}[\rho(\vec{r})] \quad (2.116)$$

The exchange contribution can be calculated analytically from the HF result as

$$\epsilon_X^{LDA}[\rho(\vec{r})] = -\frac{3}{4} \left( \frac{3}{\pi} \right)^{1/3} \int \rho(\vec{r})^{4/3} d\vec{r}. \quad (2.117)$$

On the contrary,  $\epsilon_C^{LDA}[\rho]$  does not have an analytical expression and several approximations to the correlation energy have been proposed. Ceperley and Alder used quantum Monte Carlo to simulate a uniform electron gas, and  $\epsilon_C^{LDA}[\rho]$  was calculated by subtraction from equation 2.116 [112]. Vosko, Wilk and Nusair considered a different approach, they derived a complex representation for  $\epsilon_C^{LDA}[\rho]$  based in the analytic representation of high and low density limits, the functional is named VWN[113].

The LDA exchange-correlation functional using the HF exchange and the VWN correlation functionals is termed SVWN. The LDA functionals are widely applied in periodic metallic systems in which the electrons behave as a uniform electron gas moving through the surface. However, LDA functionals do not describe the electron polarization in molecular systems, and as a consequence, this type of functionals tend to overbind molecules.

The electron density of unrestricted systems is treated considering the Local Spin Density Approximation (LSDA), which applies the LDA functional considering the  $\alpha$  and  $\beta$



electronic spin. The unrestricted DFT method is similar to UHF. The electron density is calculated considering the contributions from  $\rho^\alpha = \sum_i^{N_\alpha} \Psi_i^\alpha$  and  $\rho^\beta = \sum_i^{N_\beta} \Psi_i^\beta$ , and a Kohn-Sham eigenvalue equation is evaluated for  $\alpha$  and for  $\beta$  spin (see equation 2.114).

#### 2.5.4.2 General Gradient Approximation (GGA)

LDA functionals consider the electron density as a constant, which is far from true in molecular environments. The first idea for introducing a not-homogeneous  $\rho$  is to consider not only the density at a certain position but the variation around it (the density gradient). This is the so-called GGA approximation.

The exchange functional has a simple derivation because the analytical expression is known:

$$E_X^{\text{GGA}}[\rho(\vec{r})] = \int \rho^{4/3}(\vec{r}) f(x) d\vec{r} \quad (2.118)$$

where  $f$  is a gradient expansion. Several  $f$  have been proposed, one of the most used is the Becke expansion introduced in 1988 (B88X)[114]

$$f(x) = C_X + \beta \left( \frac{x^2}{1 + 6\beta x \cdot \text{arcsinh}(x)} \right). \quad (2.119)$$

here the  $\beta$  parameter is determined by a fit to atomic exchange energies of noble gases.

The correlation functional has been approximated by several approaches. Lee, Yang and Parr (LYP) developed a functional based on the correlation energy of the Helium atom[115]. The complex LYP functional is combined with the B88X exchange functional to give the famous BLYP functional, which is considered the responsible for the remarkable increase of DFT calculations in the 90s. There is an improvement in the results going from LDA to GGA functionals. The geometries are closer to the experimental values, but they fail in the description of long-range interactions and underestimate chemical reaction barriers.

The next step to improve GGA functionals is to include the laplacian of  $\rho$ , which leads to the so-called **meta-GGA functionals**. The *Minnesota* functionals of Truhlar and coworkers are among the most well-known functionals in this family and have shown an important improvement respect to other functionals. However, they involve an important number of semi-empirical parameters. For example, the Minnesota M06-L functional[116] has 36 parameters in contrast with the single parameter GGA-BLYP functional.

#### 2.5.4.3 Hybrid Functionals. The Adiabatic Connection

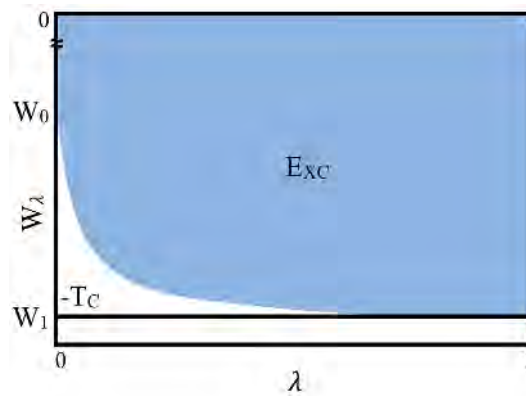
The larger contribution to the total  $E_{XC}$  energy is from the exchange component, and this term has the advantage that the exact expression is known from the HF solution. Therefore, a

simple and accurate method is to consider the HF expression of  $\epsilon_X$  and to approximate only  $\epsilon_C$ . The adiabatic connection shows the link between a system of non-interacting electrons and the real interacting system

$$E_{XC}[\rho] = \int_0^1 W_\lambda d\lambda, \quad (2.120)$$

where  $\lambda$  is the coupling parameter between the real and the non-interacting system, and  $W$  is the electron-electron interaction energy ( $W_\lambda = \langle \Psi_\lambda | \hat{V}_{ee} | \Psi_\lambda \rangle - J[\rho]$ ).

Scheme 2.7 shows a representation of the adiabatic connection.  $\lambda = 0$  corresponds to a non-interacting electron system, while  $\lambda = 1$  corresponds to the real system with electron-electron interaction. For  $\lambda = 0$  there is a contribution from  $-T_C$  ( $-T_C = T_s - T$ ), indicating that the non-interacting electron system is not completely described by  $E_{XC}$ . The exact wave function of this system has an important contribution from a Slater determinant constructed of  $\phi_{KS}$  orbitals, which can be calculated as in the HF method (see equation 2.111).



Scheme 2.7: Representation of the adiabatic connection. The blue area is the  $E_{XC}$  and the white area is  $-T_C = T_s - T$ .  $W_0$  is the exact orbital exchange and  $W_1 = V_{ee} - J$ . Adapted from reference [25].

Hybrid functionals attempt to model  $W$ . The functional of Becke approximates  $W$  as a linear equation

$$W_\lambda = a + b\lambda \quad (2.121)$$

where  $a$  and  $b$  are fitted to obtain the exact values of  $W_0$  and  $W_1$ . The exact values are defined as: (1)  $W_0 = E_X^0$ , where  $E_X^0$  is the exchange energy of a non-interacting electron system ( $E_X^0 = -\frac{1}{4} \int \int \frac{\rho_1(1,2)^2}{r_{12}} d\vec{r}_1 d\vec{r}_2$ , the HF solution); and (2)  $W_1 = V_{ee} - J$ .

Becke approximates  $W_0 = a = E_X^0$  and  $W_1 = a + b = E_{XC}^{LSDA}$ ,

$$E_{XC}[\rho] = a + \frac{b}{2} = \frac{1}{2}E_X^0 + \frac{1}{2}E_{XC}^{LSDA} \quad (2.122)$$

This equation is known as the *half-and-half* functional[117], which generally does not have a good performance.

The *half-and-half* functional could be considered the "father" of *hybrid* functionals. The most successful improvement in the development of DFT functionals has been to optimize the amount of  $E_X^0$  included in the functional. The B3 functional from Becke includes 3 parameters fitted to atomic and molecular data, this functional associated to the LYP correlation functional gives the famous B3LYP exchange-correlation functional [115, 118]

$$\text{B3LYP} = (1 - A)E_X^{\text{LSDA}} + AE_X^0 + B\Delta E_X^{\text{B88}} + (1 - C)E_C^{\text{VWN}} + CE_C^{\text{LYP}} \quad (2.123)$$

here  $A=0.2$ ,  $B=0.72$  and  $C=0.81$ .

### 2.5.5 Advantages and Disadvantages of DFT

DFT is the most cost-effective method to achieve chemical accuracy compared with wave function methods. However, it does not represent the best option in all the cases. The main advantages and disadvantages of DFT are summarized in the following:

- The elucidation of molecular structures is the main advantage of the DFT methods. The accuracy of the geometry parameters can be superior to wave function methods. Also, vibrational frequencies are in good agreement with high-level ab-initio methodologies.
- The characterization of open-shell systems is easier because the KS determinants show very low levels of spin contamination, even in those cases where post-HF methods show high spin contamination.
- The excited states. Even if the Hohenberg-Kohn theorem states that the electron density has sufficient information to determine excited states properties, the definition used for the  $E_{XC}$  functionals limits the use of this method to the ground state.
- Systems with long-range interaction and charge transfer complexes. The Van der Waals interactions,  $\pi$ -stacking and heavy-atom-heavy-atom interactions are not well described by DFT. However, DFT results could be improved by considering diffuse functions in the basis set, functionals specially parameterized to describe non-covalent interactions or dispersion corrections.
- The exchange-correlation functionals. There is not a straight strategy to develop better global functionals. Therefore, each functional has been improved to correctly describe a specific type of system.

## 2.6 BASIS SET

The basis set is a mathematical description of atomic orbitals, which are combined to build the wave function. There are different types of basis set, and the choice must be done consid-

ering the nature of the system and the computational time needed to evaluate the bi-electronic integrals.

### 2.6.1 Slater Type Orbitals (STO)[119]

Slater orbitals are the product of a radial function that depends on the nucleus-electron distance,  $r$  and a spherical harmonic,  $Y_{l,m}(\theta, \varphi)$

$$\phi^{\text{STO}}(\alpha, n, l, m; r, \theta, \varphi) = Qr^{n-1}e^{-\alpha r}Y_{l,m}(\theta, \varphi) \quad (2.124)$$

where  $Q$  is a normalization constant and  $\alpha$  is the orbital exponent.  $n$ ,  $l$ , and  $m$  are the principal, angular momentum and magnetic quantum numbers, respectively.

STOs provide an accurate description of the behavior of the electrons close to the nuclei, and at long distances, only a few STOs are needed to represent the flexibility of the valence electrons. The disadvantage of this type of functions is the evaluation of the bi-electronic integrals, because there is not an analytical representation for the  $e^r$  function. Thus, the  $e^r$  function must be integrated by numerical approximations that are computationally very demanding.

### 2.6.2 Gaussian Type Orbitals (GTO)[120]

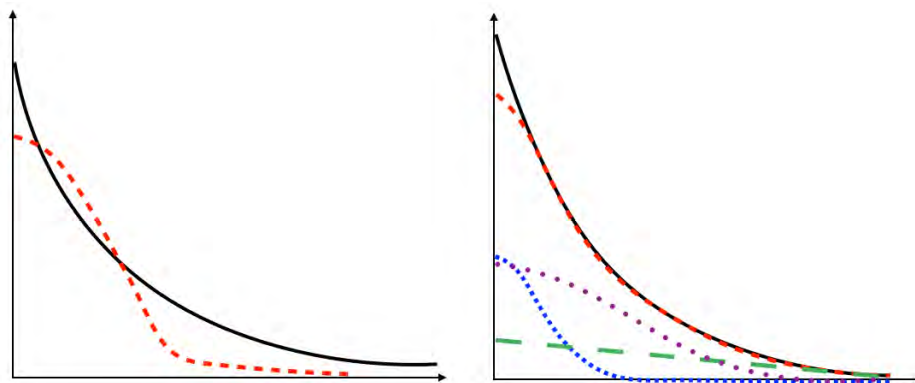
The best solution to avoid the problem associated with the evaluation of two-electron integrals, when the dominant part is  $e^{-\alpha r}$ , is to use a gaussian function  $e^{-\alpha r^2}$ . Gaussian functions lead to two-electron integrals than can be calculated analytically.

$$\phi^{\text{GTO}}(\alpha, n, l, m; r, \theta, \varphi) = Qr^{2n-l-2}e^{-\alpha r^2}Y_{l,m}(\theta, \varphi), \quad (2.125)$$

However, the use of a single GTO fails in the description of electron-nucleus interactions. For distances close to the nucleus, a GTO is not able to reproduce the maximum of the electron density, and at long distances, the function goes too rapidly to zero (see scheme 2.8).

The solution is to consider a linear combination of GTOs to emulate a STO. In this way, we will have a good behavior at all distances, preserving the simple evaluation of the integrals associated to GTOs (see scheme 2.8).

$$\phi_i = \sum_i^M a_i \varphi_i, \quad (2.126)$$



Scheme 2.8: Left, comparison of a STO (black-solid line) respect to a GTO (red-dashed line). Right, representation of a STO (black-solid line) and a STO-3G (red-dashed line), the STO-3G basis function is the sum of the remaining functions.

where  $M$  is the number of combined GTOs.  $\phi_i$  and  $\varphi_n$  are the contracted and primitive gaussian functions, respectively. The coefficients  $\alpha_i$  are optimized to fit the contracted function to a STO and preserve normalization.

### 2.6.3 Pople Basis Set

#### 2.6.3.1 Minimal Basis Set [121]

The  $\phi_{\text{STO-MG}}$  basis sets were introduced in 1969 and are known as minimal basis set because they only employ enough functions to contain all the electrons of the neutral ground state for each particular atom. This means, one s function for H and He, two s and three p functions for atoms from Li to Ne, three s and six p functions for atoms from Na to Ar, and so on. There have been formulated  $\phi_{\text{STO-MG}}$  with the size of the expansion ( $M$ ) from 2 to 6. The result is more accurate for higher values of  $M$ , but the computational time also increases. The main disadvantage of these basis sets is their inability to describe the polarization of the electron density.

#### 2.6.3.2 Split Basis Set [122]

The idea behind this basis set is to increase the flexibility of the minimal basis set by introducing more than a contracted basis function. They are named according to the number of basis used to describe the orbitals: *double*  $\zeta$  basis set uses two contracted basis function, *triple*  $\zeta$  basis set used three contracted basis, and so on.

The Pople split basis set divides the orbitals in core and valence orbitals. The core orbitals are described with a unique contracted function but with a high number of primitives because these are the orbitals contributing most to the electronic energy. The valence orbitals are

described with more than one contracted basis functions, but expanded with a smaller number of primitives because these orbitals define the reactivity of the system and need to be more flexible.

The nomenclature of Pople for basis set specifies the number of primitives used to represent each contracted function, and it uses a hyphen symbol to separate the primitives used for the expansion of the core and valence orbitals. For example, the most common Pople basis sets are the 6-31G[123–125] and 6-311G[126, 127], which are *double*  $\zeta$  and *triple*  $\zeta$  basis set in the valence shell, respectively. In these examples, both basis sets describe the core orbitals with a unique contraction of six gaussians (first term, 6-), but the difference between them is the description for the valence orbitals. The 6-31G basis set uses a contraction of three gaussians plus a gaussian function, while the 6-311G uses a contraction of three gaussians plus two unique gaussian functions.

#### 2.6.4 Polarization and Diffuse Functions

*Polarization Functions.* Split basis sets improve the description of the polarization of the electron density, but yet is not enough. A solution to this problem is to increase the number of functions with high angular momentum. Polarization functions should be included considering a *well-balanced basis set*. For example, a 3s2p1d is considered a balance basis set, while 3s2p2d or 3s2p1d1f are unbalanced basis sets. In notation of Pople, polarization functions are added between parenthesis at the end of the basis set: 6-31G(3df,2p). This double  $\zeta$  basis set includes *d* and *f* functions for heavy atoms, and *p* functions to hydrogen atoms[128–131].

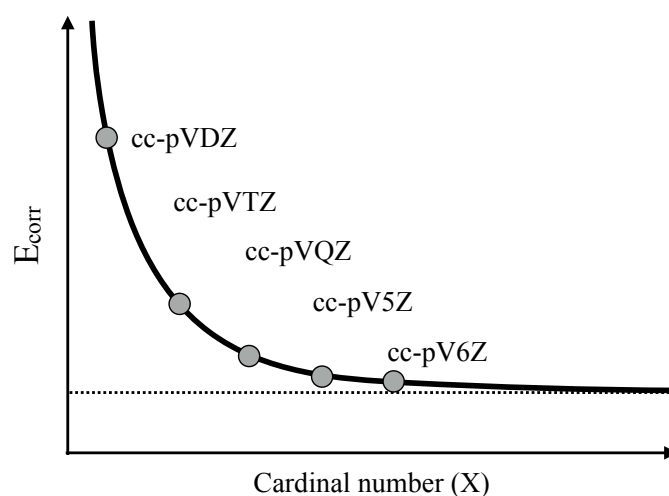
*Diffuse Functions.* There are some chemical systems in which interactions occur at long range distances, for example: non-covalent interactions, anions, Van der Waals, and others. For a correct description of these types of systems, functions with small exponents are needed (wide shape). For Pople basis sets, diffuse functions are indicated with a + symbol. The 6-31+G adds diffuse function to heavy atoms, while 6-31++G includes diffuses functions for all atoms [132].

#### 2.6.5 Dunning Basis Set - Correlation Consistent Basis Set (ccBS)

Pople split-valence basis sets are optimized for the ground state of the HF solution, which means that they consider an uncorrelated system. On the contrary, the ccBS basis sets are optimized for post HF methods, including single and double excitations. They are named cc-pVXZ, where p stands for polarized and V for valence. X is known as the *cardinal number*, for X = 2 the basis set has a double  $\zeta$  quality, X = 3 has a triple  $\zeta$  quality, and so on. For example, for an atom of the first-row the cc-pVDZ contains (9s5p1d) primitives and [3s2p1d] contracted functions [133], the cc-pVTZ increases the number of functions to (10s5p2d1f)

primitives and [4s3p2d1f] contracted [134], the cc-pVQZ has (12s6p3d2f1g) primitives and [5s4p3d2f1g] contracted sets [135].

The cc-pVXZ basis sets have the advantage that they could be systematically improved. This means that the result converges to the basis set limit when the size of the basis ( $X$ ) increases. The basis set limit could also be obtained by an extrapolation procedure (see scheme 2.9). These basis functions only include polarization function, diffuse functions are included with an extra function with a small exponent for each angular momentum. The prefix *aug* is added to indicate that diffuse functions are considered in the basis set, for example there are *aug-cc-pVDZ*, *aug-cc-pVTZ*, *aug-cc-pVQZ* ... basis set [134, 135].



Scheme 2.9: The convergence to the basis set limit (dash line) of the correlation energy ( $E_{\text{corr}}$ ) (full line) when the cardinal number  $X$  is increased.

In this thesis, both Pople and Dunning basis sets were used.

### 2.6.6 Basis Set Superposition Error: Counterpoise Correction

The Basis Set Superposition Error (BSSE) is associated with the use of finite basis sets in the calculation of energy differences. Consider the process  $AB \rightarrow A + B$ , in the complex  $AB$  the basis function of  $A_{AB}$  overlaps with the functions of  $B_{AB}$ , what does not occur in  $A_A + B_B$ . Therefore, the energies differences  $\Delta E = E(A + B) - E(AB)$  need to be corrected since  $E(A + B)$  and  $E(AB)$  are computed within different basis sets. The counterpoise correction (CPC) for BSSE evaluates each fragment in their own and in the complex basis sets.

For systems in which the formation of  $AB$  does not involve big geometrical deformations, the CPC to the interaction energy has an easy evaluation

$$E_{\text{int}}^{\text{CPC}}(AB) = E_{AB}^{\text{AB}}(AB) - E_A^{\text{AB}}(A) - E_B^{\text{AB}}(B), \quad (2.127)$$

here the subscripts indicate the basis set and the superscript the geometry.  $E_{AB}^{\text{AB}}(AB)$  is the energy of the complex  $AB$  calculated in the geometry and the basis set of  $AB$ .  $E_A^{\text{AB}}(A)$  is the

energy of the monomer  $A$  calculated in the equilibrium geometry of  $A$  but within the basis in the complex  $AB$ , and the same applies for  $E_B^{AB}(B)$ .

When the rupture of the  $A$ - $B$  bond is followed by significant geometry reorganizations, the energy of the process corresponds to the Bond Dissociation Energy (BDE) and not to the  $E_{\text{int}}$ . The BDE of a system is the sum of the  $E_{\text{int}}$  plus the deformation energy. Then, the CPC is more complicated than in equation 2.127

$$\begin{aligned} \text{BDE}^{\text{CPC}}(AB) &= E_{AB}^{AB}(AB) - E_A^A(A) - E_B^B(B) - E_{AB}^{AB}(A) + E_{AB}^A(A) - E_{AB}^{AB}(B) + E_{AB}^B(B) \\ &= [E_{AB}^{AB}(AB) - E_{AB}^{AB}(A) - E_{AB}^{AB}(B)] + [E_{AB}^A(A)] + [E_{AB}^B(B) - E_B^B(B)] \\ &= \Delta E_{\text{int}}^{\text{CP}} + \Delta E_{\text{def}}^A(A) + \Delta E_{\text{def}}^B(B) \end{aligned} \quad (2.128)$$

## 2.7 GAUSSIAN COMPOSITE METHODS

Gaussian Composite Methods (Gx) are part of the family of quantum chemistry composite methods or thermochemical recipes. These methods combine complex energy calculations to predict thermodynamic properties with high accuracy. Indeed, Gx methods show errors within the chemical accuracy. The first method was proposed by John Pople and it was named Gaussian-1 (G1)[136, 137], later Gaussian-2 (G2)[138], Gaussian-3 (G3)[139] and finally Gaussian-4 (G4)[140] were introduced. In this thesis was used the latest Gaussian method, G4, which is described below:

1. The geometry optimization is performed at B3LYP/6-31G(2df,2p).
2. The frequencies are calculated at the same level of theory than the geometry optimization, obtaining the Zero Point Energy (ZPE).
3. The Hartree-Fock energy limit  $E_{\text{HF}/\text{limit}}$  is determined using a linear two-point extrapolation scheme of Dunning aug-cc-pVXZ basis sets.

$$E(\text{HF}/\text{aug-cc-pVXZ}) = E_{\text{HF}/\text{limit}} + B \exp(-\alpha X) \quad (2.129)$$

here  $\alpha$  is an adjustable parameter. The method uses  $X = 4$  and  $5$  (aug-cc-pVQZ and aug-ccpV5Z basis sets) and  $\alpha = 1.63$ . The aug-cc-pVQZ and aug-ccpV5Z basis sets were modified to decrease the computational time, but without a reduction of the method accuracy.

4. The correlation energy is calculated considering corrections to the MP4/6-31G(d) energy.
  - a) Correction for diffuse functions:

$$\Delta E(+) = E[\text{MP4}/6-31 + \text{G}(d)] - E[\text{MP4}/6-31\text{G}(d)] \quad (2.130)$$



b) Correction for polarization functions:

$$\Delta E(2df, p) = E [\text{MP4/6-31G}(2df, p)] - E [\text{MP4/6-31G}(d)] \quad (2.131)$$

c) Correction for correlation effects beyond MP4 using CC theory

$$\Delta E(\text{CC}) = E [\text{CCSD(T)/6-31G}(d)] - E [\text{MP4/6-31G}(d)] \quad (2.132)$$

d) Correction for larger basis set effects and nonadditivity of the previous basis set:

$$\begin{aligned} \Delta E(\text{G3LargeXP}) &= E [\text{MP2(full)/G3LargeXP}] \\ &\quad - E [\text{MP2/6-31G}(2df, p)] \\ &\quad - E [\text{MP2/6-31} + \text{G}(d)] \\ &\quad + E [\text{MP2/6-31G}(d)] \end{aligned} \quad (2.133)$$

The G3LargeXP basis set corresponds to a modified 6-311+G(3d2f,2df) basis set. For instance, core polarization functions are included.

5. Combination of energies in step (4) plus Spin-Orbit (SO) correction:

$$\begin{aligned} \Delta E(\text{combined}) &= E [\text{MP4/6-31G}(d)] + \Delta E(+)+\Delta E(2df, p) \\ &\quad + \Delta E(\text{G3LargeXP}) + \Delta E(\text{HF}) + \Delta E(\text{SO}) \end{aligned} \quad (2.134)$$

where  $\Delta E(\text{HF}) = E_{\text{HF/limit}} - E_{\text{HF/G3LargeXP}}$ , and  $\Delta E(\text{SO})$  is obtained from high level methods.

6. Higher Level Corrections (HLC) are added empirically.

$$E_e(\text{G4}) = E(\text{combined}) + E(\text{HLC}), \quad (2.135)$$

here  $E(\text{HLC})$  is defined as:

$$E(\text{HLC}) = \begin{cases} -An\beta, & \text{for closed-shell molecules} \\ -A'n\beta - B(n\alpha - n\beta), & \text{for open-shell molecules} \\ -Cn\beta - D(n\alpha - n\beta), & \text{for atoms} \end{cases} \quad (2.136)$$

$n\alpha$  and  $n\beta$  are the number of  $\alpha$  and  $\beta$  valence electrons, with  $n\alpha > n\beta$ . The coefficients  $A$ ,  $A'$ ,  $B$ ,  $C$  and  $D$  correspond to empirical parameters, which were selected to reproduce experimental results of the G3/05 test set. These coefficients are equal to  $A = 6.947$ ,  $A' = 7.128$ ,  $B = 2.441$ ,  $C = 7.116$ ,  $D = 1.414$ , all values are in m.a.u.

7. The G4 energy is calculated adding the ZPE correction to the  $E_e(\text{G4})$  energy.

$$E_0(\text{G4}) = E_e(\text{G4}) + E(\text{ZPE}) \quad (2.137)$$

## 2.8 WAVE FUNCTION ANALYSIS

The wave function of a system is determined from the approximations introduced in the previous sections, but up to now, it has only been explained how to calculate the electronic energy from the wave function (or the electron density for DFT). However, there is much more information that can be extracted from  $\Psi$ , besides the energetic properties. In this section, different methodologies used to perform a chemical analysis from the quantum mechanics results are described. In other words,  $\Psi$  is used to determine or to describe properties that are well known for (general) chemists, specially *chemical bond*. The theoretical background of wave function analysis method is introduced in this section, while their applications as chemical bonds descriptors are explained in next chapter.

Five types of wave function analysis methods were used in this thesis: Natural Bond Orbital (NBO), Quantum Theory of Atoms in Molecules (QTAIM), Electron Localization Function (ELF), Energy Decomposition Analysis (EDA), and Total Position Spread Tensor (TPS). QTAIM and ELF are topological analysis in real space of two different properties obtained from  $\Psi$ . In the first case,  $\rho$  and  $\nabla^2\rho$  are analyzed, while in the second case the electron pair localization function is examined. NBO is based in an orbital localization procedure to recover basic chemical properties such as: Lewis Structures, MO hybridization, resonance, and others. EDA decomposes the electron energy into contributions from different fragments (defined by the user), and even more, the interaction energy between the fragments is divided into electrostatic and covalent components, allowing to quantify the strength and to describe the nature of the interaction. Finally, the TPS measures how the electronic fluctuation takes places when  $\Psi$  is perturbed.

### 2.8.1 Natural Bond Orbital [141]

The NBO analysis is a set of procedures to obtain the NBO orbitals from the first-order density matrix  $\mathbf{D}$ . The method is summarized in scheme 2.10 and an explanation of the procedure is given in this section.

The main "ingredient" of this method is  $\mathbf{D}$  that is constructed from **Atomic Orbitals** at a given basis set and optimized by ab-initio or DFT methods. The **Natural Orbitals (NOs)** are obtained from a diagonalization of  $\mathbf{D}$ , the eigenvectors are the NOs and the eigenvalues their occupation numbers. The NOs can be reorganized considering the atom over which is centered each basis, in such a way that  $\mathbf{D}$  could be rewritten as atomic matrix blocks. For example for atoms A, B, C ...

$$\mathbf{D} = \begin{bmatrix} \mathbf{D}^{AA} & \mathbf{D}^{AB} & \mathbf{D}^{AC} & \dots \\ \mathbf{D}^{AB} & \mathbf{D}^{BB} & \mathbf{D}^{BC} & \dots \\ \mathbf{D}^{AC} & \mathbf{D}^{BC} & \mathbf{D}^{CC} & \dots \\ \vdots & \vdots & \vdots & \ddots \end{bmatrix} \quad (2.138)$$

The **Pre-Natural Atomic Orbitals (PNAOs)** are obtained by a diagonalization of each block matrix. This means that the PNAOs of atom  $A$  are the eigenvalues of the block matrix centers on  $A$ , and so on. PNAOs are a non-orthogonal set of orbitals. Accordingly, it is not possible to recover the total number of electrons from their occupancy. The orthogonalization of the PNAOs gives the **Natural Atomic Orbitals (NAOs)** [142, 143]. Scheme 2.10 shows how to go from Atomic Orbitals (AO) to NAOs, where the electronic configuration of the isolated atoms is almost recovered. The atomic charges are calculated from the diagonal elements of the NAO matrix blocks. **Natural Hybrid Orbitals (NHOs)**[144] are optimized linear combinations of NAOs, for a given atom  $A$ :  $\text{NHO}_A = \sum_K c_K \text{NAO}_K(A)$ .

**NBOs** are defined considering the occupation and the number of atomic centers of the NAOs and the NHOs:

- Core NBO (CR) are constructed from pure NAOs.
- Lone pairs NBO (LP) are composed by a single NHO,  $\text{NBO}(A) = \text{NHO}(A)$ .
- Bonding NBO (BD) are normalized linear combinations of two bonding NHOs.

$$\text{NBO}(AB) = c_A \text{NHO}(A) + c_B \text{NHO}(B) \quad (2.139)$$

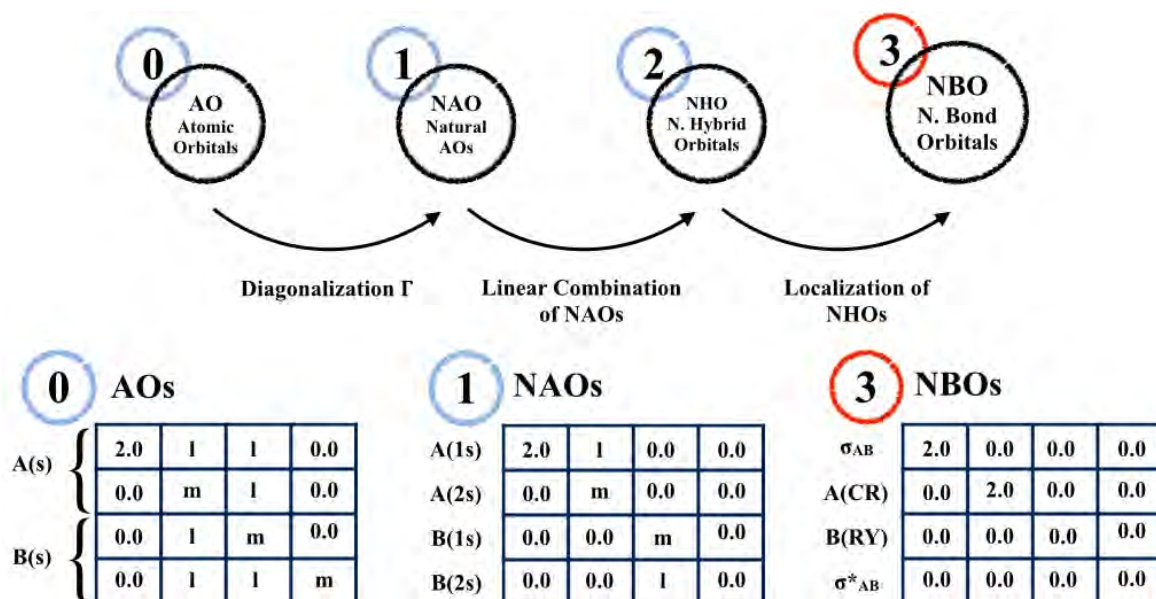
where  $c_A$  and  $c_B$  are polarization coefficients that are optimized considering that  $c_A^2 + c_B^2 = 1$ . The values of these coefficients define the type of the interaction between atoms  $A$  and  $B$ , for covalent bonds  $c_A = c_B$  and for ionic bond  $c_A \gg c_B$ .

- Anti Bonding NBO (BD\*) are the orthogonal complement of the BD orbitals,  $\text{NBO}^*(AB) = c_A \text{NHO}(A) - c_B \text{NHO}(B)$ .
- Ryberg NBO (RY\*) are monocenter orbitals that complete the basis of the NBO. They are derived from the extra valence of NAOs.

The energy associated to the NBOs could be divided into two contributions: Lewis contribution ( $E_{\text{CR}} + E_{\text{LP}} + E_{\text{BD}}$ ) plus non-Lewis contribution ( $E_{\text{BD}^*} + E_{\text{RY}^*}$ ). Generally, the Lewis contribution represents around 99% of the orbital energy, and the non-Lewis contribution is negligible. The non-Lewis contributions can be quantified by perturbation theory, considering that  $E_{\text{Lewis}} \gg E_{\text{non-Lewis}}$ . The second order non-Lewis energies are calculated as:

$$\Delta\epsilon_{\text{non-Lewis}}^{(2)} = -2 \frac{\langle \text{NBO}_{\text{Lewis}} | \hat{F} | \text{NBO}_{\text{non-Lewis}} \rangle^2}{\epsilon_{\text{non-Lewis}} - \epsilon_{\text{Lewis}}} \quad (2.140)$$

here  $\hat{F}$  is the Fock or Kohn-Sham operator and  $\epsilon$  is the energy of the orbitals.



Scheme 2.10: Above, sequence of the natural localized orbital ensemble: Atomic Orbitals (AO)  $\Rightarrow$  Natural Atomic Orbitals (NAO)  $\Rightarrow$  Natural Hybrid Orbitals (NHO)  $\Rightarrow$  Natural Bond Orbital (NBO). Below: Representation of the one-electron density matrix  $\mathbf{D}$  for the most relevant steps in the sequence, where  $m$  and  $l$  are orbitals with fractional occupations between 1.0-2.0 and 0.1-0.9 respectively.

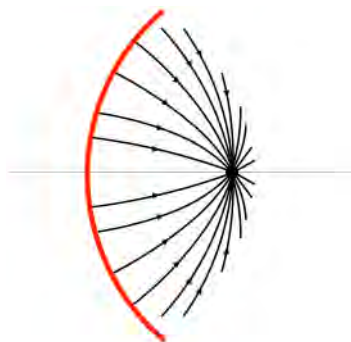
### 2.8.2 Quantum Theory of Atoms in Molecules[145]

This method is based on the definition of atoms as building blocks of molecules using quantum mechanics rules. The advantage is that the wave function can be used to describe chemical bonds based on atomic contributions. Therefore, it is possible to define the energy of the system as the sum of the atomic energies, and explain how the atoms bond each other to build a molecule.

#### 2.8.2.1 Quantum Atom

The definition of a quantum atom inside of a molecule was extensively studied by Richard Bader and coworkers. They proof that there is a region in the real subspace limited by a zero flux in the gradient vector field ( $\nabla\rho = 0$ , see scheme 2.11) and a well-defined kinetic energy, which represents an atom inside of a molecule.

There are two main advantages related to this definition: (1) it is possible to describe atoms and bonds inside of a molecule using a topological analysis of  $\rho$  and  $\nabla^2\rho$ , and (2) it allows to evaluate the energy of each atom inside a molecule.



Scheme 2.11: Representation of a set of trajectories of  $\nabla\rho$  ending in a critical point of  $\rho$ . The red line shows the zero flux gradient region ( $\nabla\rho = 0$ ). This region defines an interatomic surface inside of a molecule and the optimal path to connect the atoms.

### 2.8.2.2 Topological Analysis of $\rho$ and $\nabla^2\rho$

The electron density is a non-homogeneous function with regions where  $\rho$  is maximum or minimum. The description of these regions or *critical points* (CPs) gives information about the properties of a molecule. CPs are located considering the positions where the gradient of  $\rho$  vanishes, and they are classified according to the signature and the weight of the Hessian of  $\rho$ . The signature ( $\sigma$ ) is the algebraic sum of the eigenvalues of the Hessian and the weight ( $\omega$ ) is the number of non-zero eigenvalues. All CPs of molecules at or close to an energetically-stable geometrical configuration of the nuclei are of weight three ( $\omega = 3$ ). When  $\omega \neq 3$ , the CP is named *catastrophe point* because tiny variations of  $\rho$  could lead to its disappearance or its evolution into a  $\omega = 3$  CP. The CP are labeled as  $(\omega, \sigma)$ , for  $\omega = 3$  there are 4 type of CPs :

1. **(3, -3)**, Nuclear Critical Points (NCP).
2. **(3, -1)**, Bond Critical Points (BCP).
3. **(3, +1)**, Ring Critical Points (RCP).
4. **(3, +3)**, Cage Critical Points (CCP).

Negative values of  $\sigma$  imply there is an increase of the electron density in that direction of the real space, while positive values indicate a decrease of  $\rho$ . In the NCP  $\rho$  is maximum in all directions, while in Bond Critical Points (BCP)  $\rho$  is minimum in the bond direction and maximum in the other two directions. The case of RCP and CCP is similar but with a decrease of  $\rho$ . In the first case, the electron density decreases along any of the axes that define the ring and increases in the direction outside of the ring, and in the second case, there is a decrease of  $\rho$  in all directions.

$\nabla\rho$  defines *bond paths*, they connect two NCP when there is a BCP between them. This description gives a more realistic picture of how atoms bond each other, instead of just considering the shortest distance between the nuclei. *Bond paths* are calculated by evaluating  $\nabla\rho$

at a point  $r_0$  and following the direction in which  $\rho$  increases, by considering small variations of  $r$  ( $\Delta r$ ). The paths closing rings and cages are combinations of *bond paths*, and the graphical representation of all *bond paths* and CPs of a system defines the so-called *molecular graph*.

The laplacian of the electron density  $\nabla^2\rho$  is the second property of  $\rho$  that is analyzed in this thesis. It is defined as the sum of the eigenvalues of the Hessian:  $\nabla^2\rho = \lambda_1 + \lambda_2 + \lambda_3$ . The sign of  $\nabla^2\rho$  is related to the energetic properties of a molecule and also to the distribution of  $\rho$  at a certain position. The relation with the energy is given by:

$$2T_\rho(r) + V_\rho(r) = \frac{1}{4}\nabla^2\rho(r) \quad (2.141)$$

here  $T_\rho(r)$  is the kinetic energy density and  $V_{\rho(r)}$  the electronic potential energy density. The sign of  $\nabla^2\rho$  is analyzed by considering second derivative properties: a negative value corresponds to a local maximum, while a positive value corresponds to a local minimum of  $\rho$ .

$\nabla^2\rho < 0$ : these are regions where  $\rho$  is maximum, indicating that the electron density is built up around this position. From the energetics, the electronic potential must be the dominant term in equation 2.141 because  $T_\rho(r)$  is always positive. This implies that at the BCP the negative eigenvalues ( $\lambda_1$  and  $\lambda_2$ ) have a bigger contribution respect to the positive eigenvalue ( $\lambda_3$ ).

$\nabla^2\rho > 0$ : these are regions where  $\rho$  is minimum, indicating that the electron density is depleted in these areas. In this case, the dominant term in equation 2.141 is the kinetic energy density, and at the BCP the positive eigenvalue  $\lambda_3$  has the bigger contribution to  $\nabla^2\rho$ .

Another indicator calculated from  $\nabla^2\rho$  is the ellipticity ( $\epsilon$ ) at the BCP:

$$\epsilon = \frac{\lambda_1}{\lambda_2} - 1 \quad (2.142)$$

$\epsilon$  measures how the symmetry of  $\rho$  around the BCP is. For  $\epsilon = 0$  there is a cylindrically symmetric electron density distribution, and bigger values of  $\epsilon$  indicate an increase of the asymmetry of  $\rho$ .

### 2.8.2.3 Energy Partition

The energy of an atom is calculated considering the virial theorem and integrating over the volume ( $\Omega$ ) of the atom:

$$\int_{\Omega} dr [2T_\rho(r) + V_\rho(r)] = \frac{1}{4} \int_{\Omega} dr \nabla^2\rho(r) = 2T(\Omega) + V(\Omega) = 0 \quad (2.143)$$

The calculation of  $T(\Omega)$  is much less expensive than  $V(\Omega)$ . Therefore, it is convenient to consider that  $V(\Omega) = -2T(\Omega)$ , and that the total atomic energy is

$$E_\Omega = T(\Omega) + V(\Omega) = -T(\Omega) \quad (2.144)$$

the total energy of the molecule is recovered by adding all the atomic contributions ( $E_{\Omega}$ ).

Other approaches have been proposed to calculate the atomic energies. Among them is the *Interacting Quantum Atoms (IQA)* introduced by Pendás and coworkers [146]. The advantage of this partition is that it splits the two-center energies in classical and quantum contributions to the energy, providing information about the type of interaction between the two centers involved in a bond. However, this method is computationally rather expensive because it needs to evaluate the second order density matrix.

### 2.8.3 Electron Localization Function

The ELF method performs a topological analysis of the Electron Localized Function. This function was introduced by Becke and Edgecombe and it is based on the localization of pairs of electrons, due to their remarkable role in chemistry: bonding, lone pair, ... orbitals [147].

#### 2.8.3.1 Definition of the ELF function

The ELF function was proposed as a measure of the probability to find a pair of electrons. This probability is represented by a Lorentzian distribution

$$\text{ELF} = \eta(\mathbf{r}) = \frac{1}{1 + \left(\frac{D_{\sigma}(\mathbf{r})}{D_{\sigma}^0(\mathbf{r})}\right)^2}, \quad (2.145)$$

where  $D_{\sigma}(\mathbf{r})$  is the difference between the real kinetic energy and the von Weizsacker kinetic energy function, and  $D_{\sigma}^0(\mathbf{r})$  is the kinetic energy of a homogeneous electron gas. They are defined as:

$$D_{\sigma}(\mathbf{r}) = \frac{1}{2} \sum_i |\nabla \phi_i|^2 - \frac{1}{8} \frac{|\nabla \rho_{\sigma}(\mathbf{r})|^2}{\rho_{\sigma}(\mathbf{r})} \quad (2.146a)$$

$$D_{\sigma}^0(\mathbf{r}) = \frac{3}{5} (6\pi^2)^{2/3} \rho_{\sigma}^{5/3}(\mathbf{r}) \quad (2.146b)$$

The values of  $\eta$  are between 0 and 1. For  $\eta = 1$ , there is a high probability of finding an electron-pair at a position ( $\mathbf{r}$ ), while for  $\eta = 0$  the probability is close to zero.

#### 2.8.3.2 Topological Analysis of ELF [148]

The topological analysis of  $\eta$  is similar to the one previously exposed for  $\rho$ . Therefore,  $\nabla \eta = 0$  defines the critical points of the function and the Hessian classifies them. In analogy with the QTAIM analysis:

1. **(3,-3)** attractors.
2. **(3,-1)** and **(3,1)** are saddle points.
3. **(3,3)** repellers.

The critical points are connected by a gradient path defined by  $\nabla\eta$ . The gradient path of the attractor CP is considered a special case: the set of points whose gradient paths finish at the same attractor are named *basin*. The *basins* are classified by the synaptic order and the number of atoms over where it is centered:

1. Monosynaptic basins are centered over an atom and can be attributed to the core or lone pairs. For atom A the basin is indicated as  $V(A)$ .
2. Disynaptic basins are centered over two atoms and can be attributed to chemical bonds. For atoms A and B, the basin is indicated as  $V(A,B)$ .
3. Polysynaptic basins are centered over more than two atoms and are attributed to more delocalized chemical bonds.

### 2.8.3.3 ELF quantities

The value to quantify a critical point in QTAIM is the magnitude of  $\rho$  at the CP. In ELF the basins are quantified by their electron population ( $\tilde{N}(\Omega)$ ). The population is calculated by the integration of the electron density in the basin area:

$$\tilde{N}(\Omega) = \int_{\Omega} \rho(\mathbf{r}) d\mathbf{r} \quad (2.147)$$

The number of electrons of the system is recovered by the sum of all  $\tilde{N}(\Omega)$ .

The *covariance matrix* measures the difference between the quantum and the localized system. In particular, its diagonal elements  $\langle \text{cov}(\Omega_i, \Omega_j) \rangle$ , indicate the quantum mechanical uncertainty of the population of the basins, describing the magnitude of electron delocalization in a system[149, 150]

$$\langle \text{cov}(\Omega_i, \Omega_j) \rangle = \int_{\Omega_i} \int_{\Omega_j} \pi(\mathbf{r}_1, \mathbf{r}_2) d\mathbf{r}_1 d\mathbf{r}_2 - \tilde{N}(\Omega_i)\tilde{N}(\Omega_j) \quad (2.148)$$

here  $\pi(\mathbf{r}_1, \mathbf{r}_2)$  is the pair density. .

### 2.8.4 Electron Decomposition Energy

The EDA method is not a topological analysis like QTAIM or ELF. This method is based on the decomposition of the electronic energy, in order to determine the interaction energy between fragments in a molecule[48, 49]. However, the difference between the EDA interaction



energy and the BDE should be recalled. When a molecule is dissociated there is a geometrical rearrangement from reactant to products, and this geometry relaxation is not considered in EDA

$$\text{BDE} = \Delta E_{\text{int}} + \Delta E_{\text{def}} \quad (2.149)$$

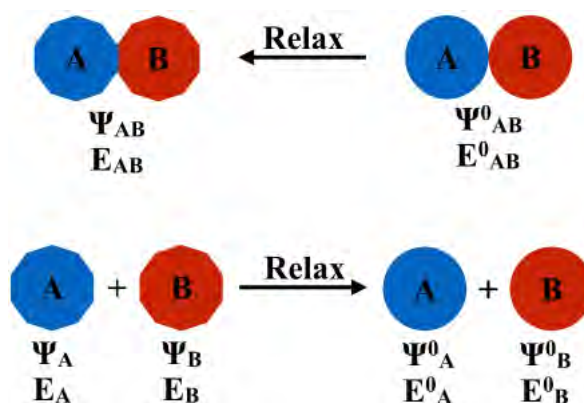
here  $\Delta E_{\text{int}}$  is the EDA interaction energy and  $\Delta E_{\text{def}}$  is the deformation energy associated to the geometry relaxation.

#### 2.8.4.1 EDA Method

The EDA interaction energy is defined as:

$$\Delta E_{\text{int}} = \Delta E_{\text{elstat}} + \Delta E_{\text{Pauli}} + \Delta E_{\text{orb}}, \quad (2.150)$$

Let us consider a system AB composed by the fragments A and B.  $\Psi_{AB}$  and  $E_{AB}$  are the wave function and energy of AB.  $\Psi_A$  and  $\Psi_B$  are the wave functions of the fragments within the geometry in the complex with energies  $E_A$  and  $E_B$ . The fragments in their ground state are indicated by the superscript  $^0$ .  $\Psi_A^0$  and  $\Psi_B^0$  are the wave functions of the fragments in their ground state geometries with energies  $E_A^0$  and  $E_B^0$ .  $E_{AB}^0$  is the energy of the complex formed by the fragments A and B within their ground state geometries (see scheme 2.12).



Scheme 2.12: EDA representation for the complex AB. The irregular shapes represent the geometry of the atoms A and B within the complex AB, and the circles represent the geometry of the atoms A and B in their ground state.

The terms in equation 2.150 for the AB system are defined as:

- $\Delta E_{\text{elstat}}$  is the quasi-classical electrostatic (coulomb) interaction. It is calculated considering the interaction between the frozen charge densities of A and B at the geometry in the complex AB:

$$\begin{aligned} \Delta E_{\text{elstat}} = & \sum_{\alpha \in A} \sum_{\beta \in B} \frac{Z_{\alpha} Z_{\beta}}{R_{\alpha\beta}} + \int V_B(\vec{r}) \rho_A(\vec{r}) d\vec{r} \\ & + \int V_A(\vec{r}) \rho_B(\vec{r}) d\vec{r} + \iint \frac{\rho_A(\vec{r}_1) \rho_B(\vec{r}_2)}{r_{12}} d\vec{r}_1 d\vec{r}_2. \end{aligned} \quad (2.151)$$

- $\Delta E_{\text{Pauli}}$  is the exchange (Pauli) repulsion. It is calculated considering an overlap of  $\Psi_A$  and  $\Psi_B$  without an orbital relaxation

$$\Delta E_{\text{Pauli}} = E_{AB}^0 - E^0, \quad (2.152)$$

here  $E^0$  is an intermediate state of  $\Psi^0 = Q\hat{A}\{\Psi_A\Psi_B\}$ .  $\Psi^0$  corresponds to the antisymmetrized and renormalized (Q) product  $\Psi_A\Psi_B$  ( $\hat{A}$ ).

- $\Delta E_{\text{orb}}$  is the orbital relaxation contribution. It is calculated considering a redistribution of electrons in order to recover the electronic state of the system AB.

$$\Delta E_{\text{orb}} = E_{AB} - E_{AB}^0. \quad (2.153)$$

The orbital interactions can be divided considering the nature of the contributions,  $\sigma, \pi, \dots$ . For the EDA method, these contributions are separated according to the irreducible representation of the point group of the system AB.

#### 2.8.4.2 EDA-NOCV (-Natural Orbitals for Chemical Valence)[151]

The EDA method cannot describe the nature of the orbital interactions for molecules without symmetry. In order to solve this problem, the EDA-NOCV method divides the orbital interaction considering pairwise contributions from the interacting fragments, and the energy is calculated considering the Extended Transition State (ETS) method.

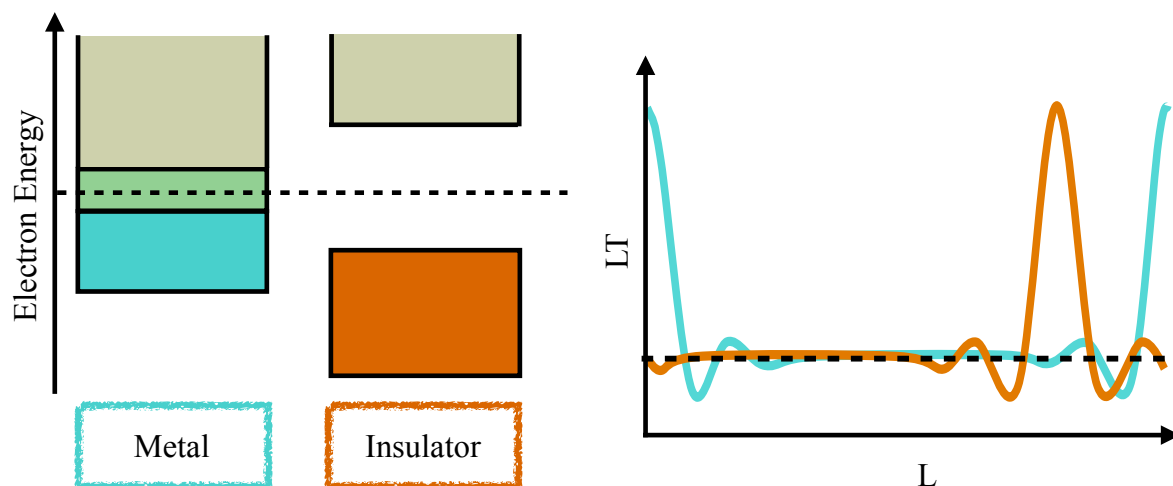
The NOCV ( $\Psi_k^{\text{NOCV}}$ ) were introduced by Nalewajski-Mrozek [152–155]. They are defined as the eigenvectors that diagonalize the deformation density matrix ( $\Delta D$ ).  $\Psi_k^{\text{NOCV}}$  can be formulated in terms of pairs of complementary eigenfunctions ( $\Psi_k^{\text{NOCV}}, \Psi_{-k}^{\text{NOCV}}$ ), with  $v_k^{\text{NOCV}}$  and  $v_{-k}^{\text{NOCV}}$  eigenvalues. Finally,  $\Delta E_{\text{orb}}^{\text{NOCV}}$  is derived considering the ETS method.

$$\Delta E_{\text{orb}}^{\text{NOCV}} = \sum_k \Delta E_{\text{korb}}^{\text{NOCV}} = \sum_k v_k^{\text{NOCV}} \left[ -F_{-k,-k}^{\text{TS}} + F_{k,k}^{\text{TS}} \right] \quad (2.154)$$

where  $-F_{-k,-k}^{\text{TS}}$  and  $F_{k,k}^{\text{TS}}$  are Transition State (TS) Kohn-Sham matrices. These matrices are the potential of a geometry between the complex AB and their dissociated fragments A and B. The partition of  $\Delta E_{\text{korb}}^{\text{NOCV}}$  considering the different components of a chemical bond ( $\sigma, \pi, \dots$ ) is done by a visual inspection of the k deformation density matrix ( $\Delta\rho_k^{\text{NOCV}}$ ).

### 2.8.5 Total Position Spread Tensor

The Total Position Spread Tensor ( $\Lambda$ ) is a quantity closely related to the Localization Tensor (LT), as it consists in the LT multiplied by the number of electrons in the system. The LT was introduced in the context of the theory of Khon for the description of electrical properties. The most remarkable property of this tensor is its ability to relate the metal/insulator nature of a system and the delocalization of the wave function, instead of the classical band structure definition [56]. In 1999 Resta and Sorella proposed a quantitative formulation of the LT for solid-state matter, which describes the electron fluctuation without the expensive calculation of an excited state: LT diverges for metals (high electron fluctuation, small gap), whereas it remains constant for insulators (small electron fluctuation, high gap), see scheme 2.13 [156–159]. The advantage of the TPS over the LT is its size-consistency, making it a superior indicator for molecular systems. Both quantities (TPS and LT) are second order cumulants, therefore before introducing the TPS formalism it is important to recall what cumulants are and which properties they have.



Scheme 2.13: Representation of the metal-insulator property considering band gap theory (left) and the Localization Tensor (right) for a periodic system in a cubic box of side  $L$  (adapted from [160]). Metals are represented in green and insulators in orange.

#### 2.8.5.1 Moments and Cumulants [161, 162]

*Moments* ( $\mu$ ) are quantities that describe the shape of a set of points, being the moments up to second order the most commonly used. For a variable  $X$ , the *zeroth* order of  $\mu$  corresponds to the total value of  $X$ , while the first and second orders of  $\mu$  are the mean value and variance of  $X$ , respectively. For instance, consider that  $X$  represents positions of a random walk:  $\mu_{0\text{th}}$  is the sum of the positions of the walk,  $\mu_{1\text{st}}$  is the average of the walk positions, and  $\mu_{2\text{nd}}$  is the deviation from the mean value squared of  $X$  during the walk.

Moments are generated from the moment generating function ( $M(\xi)$ ):

$$M(\xi) = \exp^{\xi X} = 1 + \xi X + \dots + \frac{\xi^r X^r}{r!} = \sum_{r=0}^{\infty} \frac{\mu_r \xi^r}{r!}, \quad (2.155)$$

where  $\mu_r$  is the moment of order  $r^{\text{th}}$ .

*Cumulants* ( $k$ ) are defined as linear combinations of moments, which are generated by the cumulant generating function ( $K(\xi)$ ):

$$K(\xi) = \log M(\xi) = \sum_{r=0}^{\infty} \frac{k_r \xi^r}{r!}, \quad (2.156)$$

here  $k_r$  is the cumulant of order  $r^{\text{th}}$ . The moments and cumulants for a variable  $X$  from first to third order are reported in table 2.

Table 2: Moments and cumulants for a variable  $X$  from first to third order.

ORDER	MOMENT ( $\mu$ )	CUMULANT ( $k$ )
1	$\langle X_1 \rangle$	$\langle X_1 \rangle$
2	$\langle X_1 X_2 \rangle$	$\langle X_1 X_2 \rangle - \langle X_1 \rangle \langle X_2 \rangle$
3	$\langle X_1 X_2 X_3 \rangle$	$\langle X_1 X_2 X_3 \rangle - \langle X_3 \rangle \langle X_1 X_2 \rangle - \langle X_2 \rangle \langle X_1 X_3 \rangle - \langle X_1 \rangle \langle X_2 X_3 \rangle + 2 \langle X_1 \rangle \langle X_2 \rangle \langle X_3 \rangle$

The most relevant properties of cumulants are:

- They are zero if the variables are not dependent on them.
- They can only be represented by moments of equal or lower rank.
- They are additive. When  $X$  is a molecular property the cumulant of that property is size-consistent.
- The diagonal elements of a cumulant correspond to the variance, which is always a positive quantity.
- The cumulants of order equal or higher than 2 are invariant under the translation of the origin.

The TPS is the second order cumulant of the position operator ( $\hat{R}$ ). When the spin of the electron is neglected the tensor is named Spin-Summed of the Total Position Spread Tensor (SS-TPS), when the spin components  $\sigma_\alpha$  and  $\sigma_\beta$  are introduced, the tensor is named Spin-Partitioned of the Total Position Spread Tensor (SP-TPS).

### 2.8.5.2 Spin-Summed TPS

The SS-TPS is defined as the a second order cumulant (see table 2) with X equal to the total position operator  $\hat{R}$ :

$$\Lambda = \langle \Psi | \hat{R}_i \hat{R}_j | \Psi \rangle - \langle \Psi | \hat{R}_i | \Psi \rangle \langle \Psi | \hat{R}_j | \Psi \rangle \quad (2.157)$$

where i and j correspond to a coordinate axis x, y or z.  $\hat{R}$  for an N-electron system is defined as:

$$\hat{R} = \sum_l^N \hat{r}_l \quad (x, y, z) \quad (2.158)$$

The most complex term in equation 2.157 is the bi-electronic operator  $\langle \Psi | \hat{R}_i \hat{R}_j | \Psi \rangle$ . Let us consider the analysis for a component of  $\hat{R}$ , the zz component (i = j = z).

$$\begin{aligned} \hat{R}_z^2 &= \left( \sum_l^N \hat{r}_l^z \right)^2 = \underbrace{(\hat{r}_1^z)^2 + (\hat{r}_2^z)^2 + \dots + (\hat{r}_N^z)^2}_{\text{one-electron operator}} + \underbrace{\hat{r}_1^z \hat{r}_2^z + \dots}_{\text{two-electron operator}} \\ &= \underbrace{\sum_l^N (r_l^z)^2}_{\text{one-electron operator}} + \underbrace{\sum_l^N \sum_{m \neq l}^N \hat{r}_l^z \hat{r}_m^z}_{\text{two-electron operator}} \\ &= \hat{R}_z^m + \hat{R}_z^b \end{aligned} \quad (2.159)$$

then  $\Lambda_{zz}$  is defined as:

$$\Lambda_{zz} = \langle \hat{R}_z^2 \rangle - \langle \hat{R}_z \rangle^2 = \langle \hat{R}_z^m \rangle + \langle \hat{R}_z^b \rangle - \langle \hat{R}_z \rangle^2 \quad (2.160)$$

The same procedure is applied to calculate the remaining diagonal elements of the  $\Lambda$  matrix (xx and yy), and also the nondiagonal terms considering  $i \neq j$ . See scheme 2.14 for a representation of the  $\Lambda$  matrix.

### 2.8.5.3 Spin-Partitioned TPS

The SP-TPS considers the electronic spin, at difference with the SS-TPS. Thus,  $\hat{R}$  is defined as:

$$\hat{R}_\sigma = \sum_{l=1}^N \hat{r}_l \hat{n}_{\sigma l} \quad (x, y, z) \quad (2.161)$$

where  $\hat{n}_\sigma$  is the particle number operator for  $\alpha$ -spin ( $\hat{n}_\alpha$ ) and  $\beta$ -spin ( $\hat{n}_\beta$ ). The total position operator is

$$\hat{R} = \hat{R}_\alpha + \hat{R}_\beta \quad (2.162)$$

$\Lambda_{xx}$	$\Lambda_{xy}$	$\Lambda_{xz}$
$\Lambda_{yx}$	$\Lambda_{yy}$	$\Lambda_{yz}$
$\Lambda_{zx}$	$\Lambda_{zy}$	$\Lambda_{zz}$

Scheme 2.14: Matrix representation of the SS-TPS. The eigenvalues of the SS-TPS matrix measure the electron fluctuation in the direction of the corresponding eigenvector.

and the square of  $\hat{R}$  is

$$\hat{R}^2 = \hat{R}_\alpha^2 + \hat{R}_\beta^2 + \hat{R}_\alpha \hat{R}_\beta + \hat{R}_\beta \hat{R}_\alpha \quad (2.163)$$

Therefore, considering equations 2.157 and 2.163 the spin-partitions are defined as:

$$\Lambda_{\alpha\alpha} = \langle \Psi | \hat{R}_\alpha^2 | \Psi \rangle - \langle \Psi | \hat{R}_\alpha | \Psi \rangle^2 \quad (2.164a)$$

$$\Lambda_{\beta\beta} = \langle \Psi | \hat{R}_\beta^2 | \Psi \rangle - \langle \Psi | \hat{R}_\beta | \Psi \rangle^2 \quad (2.164b)$$

$$\Lambda_{\alpha\beta} = \langle \Psi | \hat{R}_\alpha \hat{R}_\beta | \Psi \rangle - \langle \Psi | \hat{R}_\alpha | \Psi \rangle \langle \Psi | \hat{R}_\beta | \Psi \rangle \quad (2.164c)$$

$$\Lambda_{\beta\alpha} = \langle \Psi | \hat{R}_\beta \hat{R}_\alpha | \Psi \rangle - \langle \Psi | \hat{R}_\beta | \Psi \rangle \langle \Psi | \hat{R}_\alpha | \Psi \rangle \quad (2.164d)$$

and the SS-TPS is equal to the sum of the four components

$$\Lambda = \Lambda_{\alpha\alpha} + \Lambda_{\beta\beta} + \Lambda_{\alpha\beta} + \Lambda_{\beta\alpha} \quad (2.165)$$

Some properties of the TPS partitions:

- $\Lambda_{\alpha\beta}$  and  $\Lambda_{\beta\alpha}$  are identical because the commutator between  $\hat{R}_\alpha$  and  $\hat{R}_\beta$  vanishes.
- $\Lambda_{\alpha\beta}$  and  $\Lambda_{\beta\alpha}$  are cumulants of different sets of variables. This means that they are not second order cumulants and therefore they could be positive or negative quantities.
- $\Lambda_{\alpha\alpha}$  and  $\Lambda_{\beta\beta}$  are equal for closed-shell systems.
- $\Lambda_{\alpha\alpha}$  and  $\Lambda_{\beta\beta}$  are second order cumulants, which means they hold the properties described before for the SS-TPS.

#### 2.8.5.4 Polarization: Relation between the TPS and Chemical Bonds

There are different types of chemical bonds (see chapter 3 for more details), however, they share some common features among them. After the formation of a bond a polarization of

the electron density of the atoms involved in the molecule takes place, which depends on the type and strength of the interaction. The *mean square quantum fluctuation of the ground-state polarization* is defined from the mean-square of the dipole moment  $\hat{d}$  [57]:

$$\langle \Delta \hat{d}^2 \rangle = \langle \hat{d}^2 \rangle - \langle \hat{d} \rangle^2 = -e[\langle \hat{R}^2 \rangle - \langle \hat{R} \rangle^2] \quad (2.166)$$

where  $e$  is the electron charge.

There is an obvious relation between equations 2.166 and 2.157. The SS-TPS is a qualitative measure of the variation of the polarization in a system. Therefore, the TPS could be a useful tool to describe the nature of chemical bonds.

## Part III

### CHEMICAL BONDS

"The general idea was that with old-fashioned chemical concepts, which at first seemed to have their counterparts in MQM, the more accurate the calculations become, the more the concepts tend to vanish into thin air. So we have to ask, should we try to keep these concepts -do they still have a place- or should they be relegated to chemical history."

*Robert S. Mulliken.*

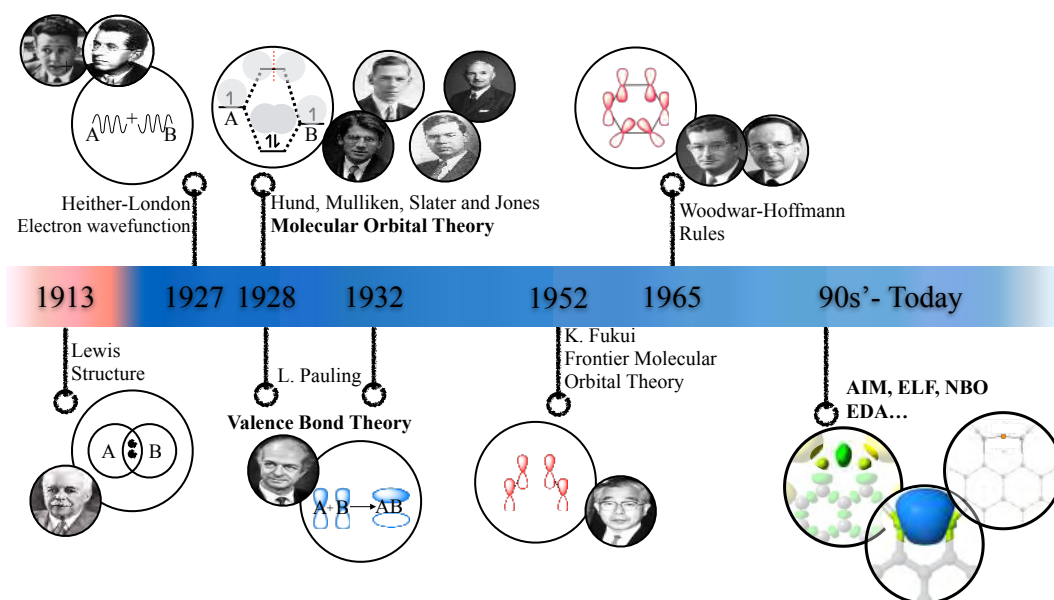
*Molecular Scientists and Molecular Science: Some Reminiscences-1965.*





## CHEMICAL BONDS

The interest in the chemical bonding is prior to the birth of Chemistry as a science. For instance, people have been always trying to understand how the primary building blocks of nature are glued, how substances can be transformed into new compounds or why some materials show specific properties. However, the concept of modern *chemical bond* was not introduced until 1916, when Gilbert Lewis proposed that atoms are bonded by a pair of electrons[2], and even now Lewis diagrams are frequently used to describe the molecular structure of a system. Lewis model is enough to provide a simple and intuitive description of the structure of a molecule and allows to explain qualitatively the trends in chemical properties and reactivity. The foundation of Quantum Mechanics (QM) propitiated the refinement of this old model with localized electrons. Two important theories to explain chemical bonds based in QM were proposed: (1) *Valence Bond Theory (VBT)* [3, 4, 163–165] and (2) *Molecular Orbital Theory (MOT)* [166–170]. VBT is an extension of the Lewis model, where the wave function is constructed by a combination of Lewis structures. In contrast, MOT does not localize the electrons in bonds between atoms. Instead, they are distributed around the nuclei using the wave function to represent the electronic arrangement, without any chemical meaning.



Scheme 3.1: Timeline of modern chemical bond. The most relevant models and theories developed in the last century to describe the chemical bond are divided in two periods: before (red) and after (blue) Quantum Mechanics.

The two theories are widely used in chemistry, but the application of MOT in the development of *ab-initio* and Density Functional Theory (DFT) computational methods has left behind VBT in computational chemistry. The main consequence of the popularity of MOT is that standard descriptors of chemical bonds (Lewis structure, hybridization, bond order, . . .) have lost interest to this discipline. To bring together both theories, wave function analysis methods (Quantum Theory of Atoms in Molecules (QTAIM), Electron Localization Function (ELF), Natural Bond Orbital (NBO), . . .) have been developed. These approaches recover the chemical descriptors from the wave function, which is calculated from *ab-initio* or DFT methods. The theory behind these methods was explained in section 2.8, and the present chapter describes how to characterize different types of chemical bonds using wave function analysis methods [171–174]. There are several types of chemical bonds, here are introduced the most relevant for this thesis, with a special emphasis on the interactions involving the beryllium atom.

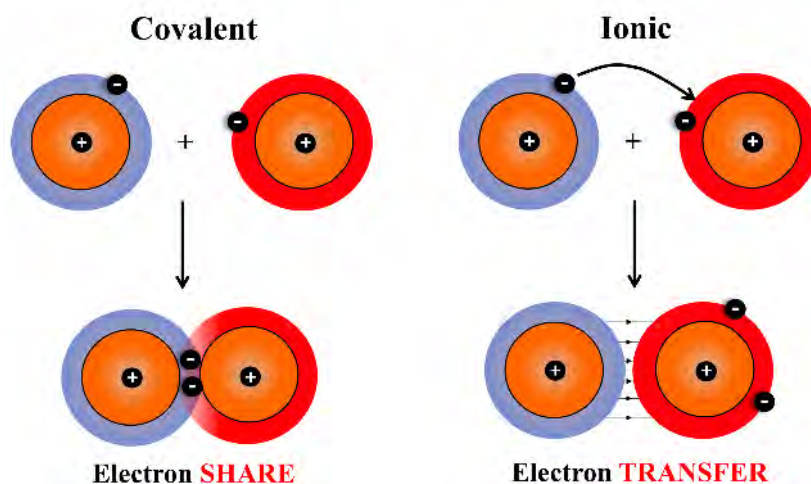
### 3.1 STRONG INTERACTIONS

The atoms linked through strong interactions require an enormous amount of energy to split them apart, this is due to the transferred or the shared of electrons between them. The energy required to break a bond depends on the type of the interaction. For example the bond enthalpy of the C=C double bond is  $682 \text{ kJ} \cdot \text{mol}^{-1}$ , of the ionic LiF bond is  $577 \text{ kJ} \cdot \text{mol}^{-1}$ , and of the  $\text{F}_2$  molecule is only  $157 \text{ kJ} \cdot \text{mol}^{-1}$  [175]. The main classification of strong interactions is into covalent and ionic bonds, and the main difference between them is the synergy between the atoms. In covalent bonds the atoms share electrons  $\phi_{\text{cov}} = (\text{A} \cdot \cdot \text{B})$ , whilst in the second case, the electrons are transferred from one atom to the other  $\phi_{\text{ion}} = (\text{A}^+ \text{B}^-)$ .

#### 3.1.1 Covalent and Ionic Bonds

The IUPAC defines a covalent bond as *a region of relatively high electron density between nuclei which arises at least partly from sharing of electrons and gives rise to an attractive force and characteristic internuclear distance*. The ionic bond is also a strong interaction but with a different nature, it is defined as *the bond between atoms with sharply different electronegativities. In strict terms, an ionic bond refers to the electrostatic attraction experienced between the electric charges of a cation and an anion, in contrast with a purely covalent bond* [24] (see scheme 3.2).

According to the classic bonding theories, the covalent bond is formed when there is an overlap of Atomic Orbitals (AO). The VBT description of covalent bonds shows a wave function of the type:  $\Psi_{\text{VB}} = c_1 \phi_{\text{cov}} + c_2 \phi_{\text{ion}}$ , where  $c_1 \gg c_2$ . In contrast, the ionic bond is formed from an electron transfer from the less to the more electronegative atom, and in the  $\Psi_{\text{VB}}$   $c_2 \gg c_1$ . The description using MOT is similar, but as was explained before it corresponds to a more mathematical representation. The covalent bond is described by two



Scheme 3.2: Representation of covalent (left) and ionic (right) bonds. The covalent interaction is characterized by an overlap of the electron density of the atoms, while the ionic is represented by an electrostatic interaction induced by a permanent dipole originated from an electron transfer.

electrons (from different atoms) occupying a bonding molecular orbital. Considering a Linear Combination of Atomic Orbitals (LCAO) wave function:  $\Psi_{MO} = \phi_A + \phi_B$  and  $\Psi_{MO}^* = \phi_A - \phi_B$ . Here, the square of  $\Psi_{MO}$  and  $\Psi_{MO}^*$  represent the probability to find an electron in the internuclear region or in the nuclei region, respectively (see scheme 2.6). For covalent bonds, there is a maximum probability of finding an electron pair in the bonding region, and it is represented with a doubly occupied  $\Psi_{MO}$  and an unoccupied  $\Psi_{MO}^*$ . MOT describes the ground state of an ionic molecule as the state in which ionic species are more stable than the neutral atoms. In this case, the electron density is delocalized around the AOs of each ion instead of at the internuclear region, and the ions hold together because of the electrostatic interaction between the two permanent charges. The LCAO wave function for ionic bonds is similar to that of covalent interactions, but instead of combining the AO of the neutral atoms those of the ionic functions are combined:  $\Psi_{MO} = \phi_{A^+} + \phi_{B^-}$  and  $\Psi_{MO}^* = \phi_{A^+} - \phi_{B^-}$ .

The methods described in section 2.8 can be applied to measure the strength of a chemical bond. The value of  $\rho$  at the Bond Critical Points (BCP) and the population of the disynaptic basin are directly related to the bond energy. The NBO analysis quantifies the energy of the orbitals, which allows estimating the energy difference between bonding and anti-bonding orbitals. The Energy Decomposition Analysis (EDA) approach calculates the bond energy and its contributions. These methods also give information about the nature of the bond [171–174].

Covalent interactions are characterized by a region where electrons are shared. This region is localized between the two bonded atoms, while in ionic bonds the electron density is concentrated around the interacting atoms. As a consequence, each type of bond presents a different topology of  $\rho$  and  $\nabla^2\rho$ . The QTAIM analysis locates a BCP for both types of interactions with a high value of  $\rho$  (of the order of  $\sim 0.1$  au). The position of the BCP is related to the electronegativity difference between the atoms participating in the bond. Therefore, for

covalent bonds (atoms of similar electronegativity) the BCP is approximately in the middle region between the atoms, and for ionic bonds (atoms with very different electronegativity) the BCP shifts closer to the less electronegative atom.  $\nabla^2\rho$  at the position of the BCP measures the distribution of  $\rho$  (see section 2.8.2.2 for a description of the  $\nabla^2\rho$  topology). For covalent bonds, the electron density is concentrated at the saddle point and this translates into a negative sign of  $\nabla^2\rho$ . For ionic bond  $\rho$  is depleted at the position of the BCP and thus the laplacian shows a positive sign (see figure 3.1a and 3.1b).

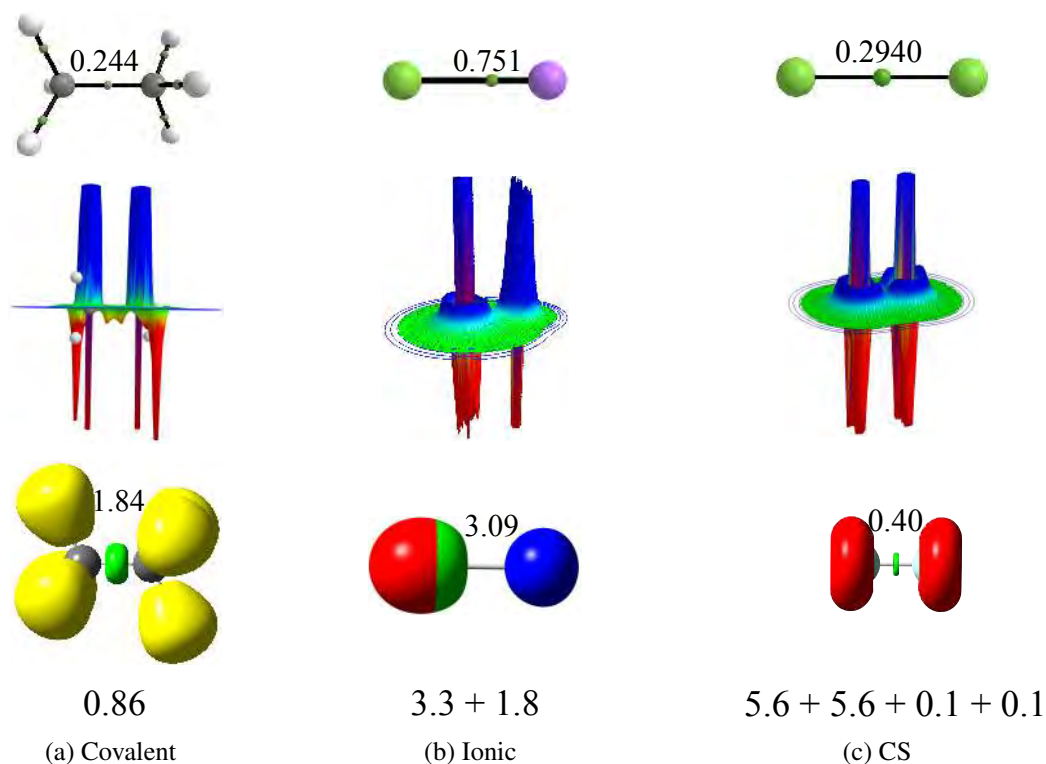


Figure 3.1: Wave function analysis of strong chemical bonds in:  $\text{H}_3\text{C}-\text{CH}_3$  (for covalent bond),  $\text{LiF}$  (for ionic bond) and  $\text{F}_2$  (for charge-shift bond). From the top to the bottom is represented: (1) the QTAIM molecular graph and the value of  $\rho$  ( $\text{au}$ ) at the BCP; (2) the relief map of  $\nabla^2\rho$ , the color scale is: blue  $> 1$ , cyan  $> 0.5$ , green  $> -0.5$ , yellow  $> -1$ , red  $< -1$ ; (3) the ELF representation of the basins and their populations, the color scale is: disynaptic basins involving H atoms are in yellow, monosynaptic basins associated with lone pairs are in red, and disynaptic basins or trisynaptic basins involving heavy atoms are in green; (4) The diagonal elements of the covariance matrix for the valence electrons of heavy atoms. The calculations were performed at B3LYP/cc-pVTZ level of theory.

Considering again equation 2.141, which describes the relation between  $\nabla^2\rho$  and the energy density:

$$2T_\rho(\mathbf{r}) + V_\rho(\mathbf{r}) = \frac{1}{4}\nabla^2\rho(\mathbf{r}). \quad (2.141)$$

From this expression is complicated to interpret the atomic energy contributions because there is a 2:1 relation between  $T_\rho$  and  $V_\rho$ . Hence, it has been proposed the *local energy density* ( $H_\rho$ ) as a better energetic descriptor of the chemical bond [145]

$$H_\rho(\mathbf{r}) = \frac{1}{4}\nabla^2\rho(\mathbf{r}) - T_\rho(\mathbf{r}) = T_\rho(\mathbf{r}) + V_\rho(\mathbf{r}). \quad (3.1)$$

$H_\rho$  is always negative for covalent bonds and positive for ionic. This means covalent bonds have a greater contribution from the electron-electron interaction, while ionic bonds have a higher contribution from the electronic kinetic energy.

The ELF method does a topological analysis of the Electron Localized Function ( $\eta$ ) to localize pairs of electrons. In covalent bonds, the higher probability to find an electron pair is between the bonded atoms, while in an ionic interactions it is close to the more electronegative atom. Therefore, the basins for each type of interaction are located in different positions: *the disynaptic basin  $V(A,B)$  is centered on the bond area for covalent bonds and over one of the atoms for ionic bonds.* The population of these basins is around to  $2e^-$  for a single bond,  $4e^-$  for a double bond, and so on. The covariance matrix (equation 2.148 in page 69) also gives indications about the type of interaction. For covalent bonds in which the electrons are localized in the bond area, small values are expected for  $\langle \text{cov}\Omega_i, \Omega_j \rangle$ , while in ionic bonds  $\langle \text{cov}\Omega_i, \Omega_j \rangle$  has bigger values because of the electron charge transfer between the atoms. See figures 3.1a and 3.1b.

The NBO and EDA analyses have an intuitive interpretation for each bond type. NBO describes covalent bonds with a  $[A \cdots B]$  Lewis structure. The bonding hybrid orbital (BD(AB)) is built by two NHOs centered on two atoms, contributing in the same amounting to BD(AB) ( $c_A = c_B$ , see equation 2.139 in page 64). The bond order of BD(AB) is determined from the NAOs. The EDA shows a high contribution from the orbital relaxation partition ( $\Delta E_{\text{orb}}$ ). As has been recalled before, covalent bonds are based in an orbital overlap of the atoms involved in the interaction. However, the remaining components of the EDA partition: Electrostatic ( $\Delta E_{\text{elstat}}$ ) and Pauli repulsion ( $\Delta E_{\text{Pauli}}$ ), have also an important contribution to the interaction energy. For the ethane molecule,  $\Delta E_{\text{Pauli}}$  is bigger than  $\Delta E_{\text{orb}}$ , but this difference is compensated by  $\Delta E_{\text{elstat}}$ , demonstrating that electrostatic interactions are also relevant in covalent bonds. On the contrary, the interaction energy of ionic bonds have a bigger contribution from  $\Delta E_{\text{elstat}}$ . The NBO analysis for ionic bonds recovers a  $[A^+B^-]$  Lewis structure. Therefore, there are not bonding by molecular orbitals. The NBO for the ethene and LiF are shown in 3.2a and 3.2b, respectively. The ethene molecules presents an overlap of the electron density between the C atoms, while for LiF there is not a bonding region.

### 3.1.1.1 Covalent vs. Ionic Dissociations: Avoided crossings

Chemical bonds dissociation curves are a relevant subject in this thesis. The importance of this type of calculation is twofold. First, to study the nature of the wave function for different

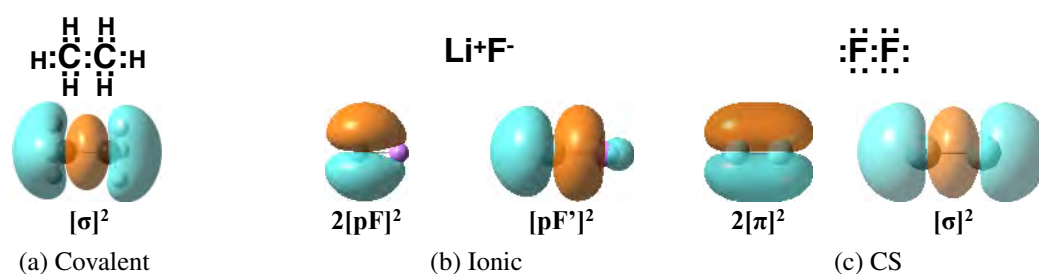
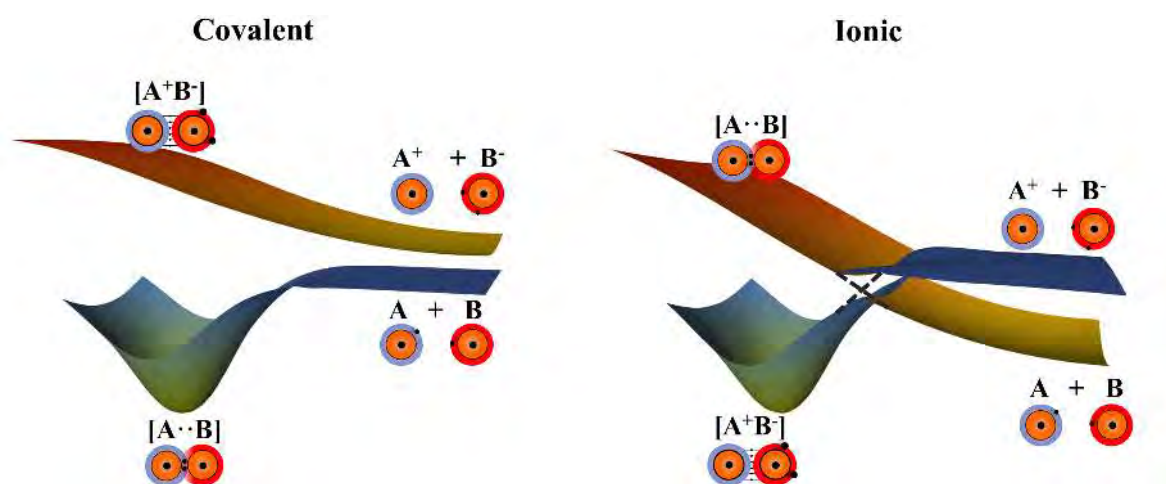


Figure 3.2: Natural Bond Orbitals of strong chemical bonds in:  $\text{H}_3\text{C}-\text{CH}_3$  (for covalent bond),  $\text{LiF}$  (for ionic bond) and  $\text{F}_2$  (for charge-shift bond). The calculations were performed at B3LYP/cc-pVTZ level of theory.

types of chemical bonds using the Total Position Spread Tensor (TPS) analysis. And second, to have not only the thermodynamic, but also the kinetic description of bond dissociations.

The Potential Energy Surface (PES) for the dissociation of covalent and ionic bonds are disparate, as illustrated in scheme 3.3. In both cases, the main dissociation channel is the homolytic dissociation of the bond in which the products are the neutral radicals  $\text{A}\cdot + \text{B}\cdot$ . However, the initial states are different. The covalent ground state wave function is defined as  $\Psi_{\text{cov}} = \phi_{\text{A}} \pm \phi_{\text{B}}$ . This function dissociates into the most stable products  $\text{A}\cdot + \text{B}\cdot$ , but the ionic wave function  $\Psi_{\text{ion}} = \phi_{\text{A}}^+ \pm \phi_{\text{B}}^-$  dissociates in the ionic products  $\text{A}^+ + \text{B}^-$ . This means that for ionic dissociations, there must be a crossing of states in the PES along the dissociation coordinate. According to the non-crossing rules, the PES of two electronic states of the same symmetry cannot cross. Then, for a system where  $\Psi_{\text{cov}}$  and  $\Psi_{\text{ion}}$  share symmetry, the degeneracy point in ionic dissociations is described by an *avoiding crossing*, beyond which the covalent potential becomes the ground state and the ionic potential the excited state. See scheme 3.3.



Scheme 3.3: Representation of the dissociation curves of covalent (left) and ionic (right) bonds.

Considering the wave function  $\Psi = c_1\phi_{\text{cov}} + c_2\phi_{\text{ion}}$ . The Slater determinant of  $\Psi$  is

$$\begin{vmatrix} \hat{H}_{11} - E_{11} & \hat{H}_{12} \\ \hat{H}_{21} & \hat{H}_{22} - E_{22} \end{vmatrix} \begin{vmatrix} c_1 \\ c_2 \end{vmatrix} = 0 \quad (3.2)$$

Interstate degeneracy occurs when  $\hat{H}_{11} = \hat{H}_{22}$  and  $\hat{H}_{12} = \hat{H}_{21} = 0$ , and this is only possible if two independent nuclear coordinates are considered. Therefore, a state crossing is clearly impossible for diatomic molecules. As was stated in the previous chapter, poli-electronic systems are very often treated within the Born–Oppenheimer approximation. This approximation describes the electronic structure of a system considering a unique nuclear state, which is not the case of state-crossing regions. Therefore, the crossing of two surfaces is strictly forbidden under this approximation.

### 3.1.2 Charge-Shift Bonds

The localization of the electron pair in covalent and ionic bonds is very well defined, but there is an intermediate type of bond introduced in 2005 by Shaik and co-workers, named *Charge-Shift (CS) Bonds*, where electronic localization is not so obvious [176]. The definition of these bonds was based on a VBT description. According to this theory, charge-shift bonds are interactions characterized by a mixture between the  $\phi_{\text{cov}}$  and the  $\phi_{\text{ion}}$  configurations. For example, consider a charge-shift bond with a dissociation curve as that in scheme 3.4 and a VBT wave function  $\Psi_{\text{VB}} = c_1\phi_{\text{cov}} + c_2\phi_{\text{ion}}$ . The dissociation energy of the system is defined as

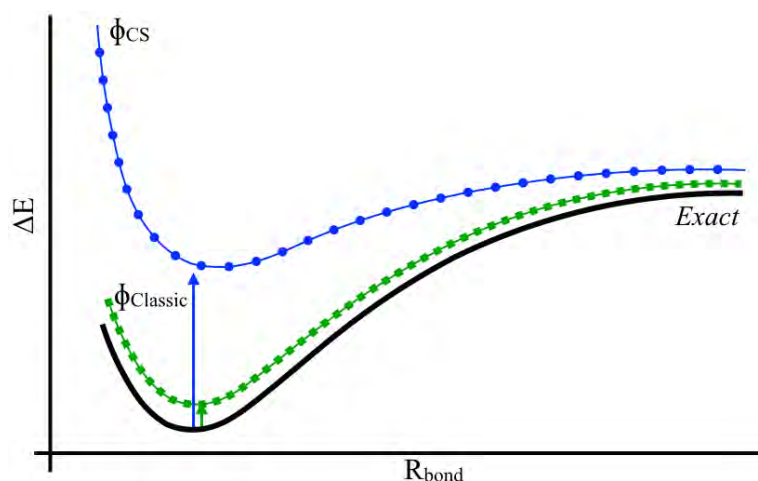
$$D_e = D_{\text{classic}} + \text{RE} \quad (3.3)$$

where  $D_{\text{classic}}$  is the energy of the component with the higher contribution to  $\Psi_{\text{VB}}$  ( $\phi_{\text{cov}}$  or  $\phi_{\text{ion}}$ ) and RE is the Resonance Interaction energy defined as the energy difference between the exact solution and  $D_{\text{classic}}$ . For classic bonds, RE has a small contribution to the dissociation energy (green arrow in scheme 3.4) and the systems are correctly described by considering only the  $\phi_{\text{cov}}$  or  $\phi_{\text{ion}}$  solution. On the other hand, charge-shift bonds have a big contribution from RE (blue arrow in scheme 3.4). Thus, the system cannot longer be described exclusively by  $\phi_{\text{cov}}$  or  $\phi_{\text{ion}}$ , but by means of a resonance between both states.

The  $F_2$  molecule is a representative of charge-shift bonds. For several years this molecule has been classified as a covalent system. However, it was found that the  $\phi_{\text{cov}}$  solution has a repulsive character, and therefore, RE has an important contribution to  $D_e$ . The description of charge-shift bonds using wave function analysis methods is not simple. It is necessary a combination of methods to understand the nature of this type of bond. Figure 3.1c shows QTAIM and ELF results for the  $F_2$  molecule:

- **The QTAIM analysis** shows a strong interaction ( $\rho = 0.29$ ), which is characterized by a depletion of the electron density at the BCP. See the positive  $\nabla^2\rho$  in figure 3.1c. Then, according to the QTAIM analysis, the  $F_2$  bond is a strong electrostatic interaction, contradicting with the classical covalent description of this molecule.





Scheme 3.4: Comparison of the dissociation curve for charge shift and classic bonds. The black full line represents the exact dissociation curve, the green-squared line represents classic bonds ( $\phi_{\text{Classic}} = \phi_{\text{cov}}$  or  $\phi_{\text{ion}}$ ), and the blue-dotted line represents the charge-shift bonds ( $\phi_{\text{CS}}$ ). The arrows show the contribution of the RE to the exact energy, notice that RE is almost negligible for classic bonds but it has a big contribution for charge-shift bonds.

- **The ELF analysis** shows a weak interaction between the fluorine atoms. The  $V(\text{F}, \text{F})$  disynaptic basin is located between the F atoms, but the population is lower than  $0.5e^-$  (see figure 3.1c). However, the high values of the diagonal elements of the covariance matrix indicate an electron fluctuation between the valence basins of the fluorine atoms.
- **The NBO analysis** shows a pure covalent interaction. There is a  $\sigma_{\text{F-F}}$  bond with a population equal to  $2e^-$  and a negligible contribution from the non-Lewis structures.

Thus, the wave function analysis performed for  $\text{F}_2$  gives inconsistent results. The  $\text{F}_2$  molecule for some methods predicts a covalent character and for others ionic. But if all the interpretations are analyzed together, the results recover consistency and are in agreement with the VBT description. The value of  $\rho$  at the BCP, the positive value of  $\nabla^2\rho$  and the small population of the  $V(\text{F}, \text{F})$  basin are caused by a high concentration of  $\rho$  in the bonding region, but in constant motion. This electron fluctuation also explains why charge-shift bonds cannot be properly described through a localization method, such as NBO. Overall, all methods agree to define the F-F bond as a mixture between covalent and ionic structures. The physical explanation of the electron fluctuation in charge-shift bonds has been done considering Pauli repulsion.  $\text{F}_2$  or isoelectronic systems have a  $\pi$  cloud around the chemical bond. The ground state stabilizes when there is a fluctuation of this cloud, instead of localized  $\pi$  orbitals that would repel each other (see figure 3.3).

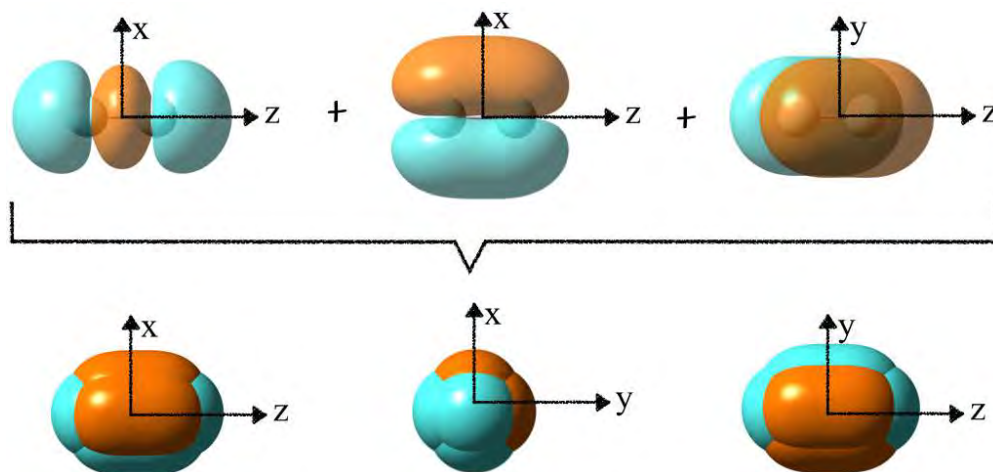


Figure 3.3: Kohn-Sham molecular orbitals of the  $\pi$  valence orbitals of the  $F_2$  molecule. Top MOs correspond to the  $\sigma$  and  $\pi$  orbitals of the molecule. Bottom MOs represent the  $\pi$  cloud. The calculation was performed at B3LYP/cc-pVTZ level of theory.

## 3.2 WEAK BONDS

The systems bonded through weak interactions can be easily dissociated without the use of a large amount of energy. The importance of this interaction is however not related to its strength, but to the incredible properties that the systems held because of them. For example, these bonds are associated with the structure of proteins and nucleic acids[177, 178], the properties of water[179], the design of new materials[180–182] and many other applications. Non-covalent interactions are the most common weak interactions in chemistry and biology and are an important subject of this thesis. This section focussed on the principal characteristics of three type of non-covalent bonds: hydrogen, halogen and beryllium bonds, and also on the appropriate methodology to describe them.  $Be_2$  molecule is not bonded through a non-covalent bond, but it is considered a weak interaction. The features of this particular bond are also described in this section.

### 3.2.1 Non-Covalent Bonds

Non-Covalent or Van der Waals interactions were introduced in 1870 by Van der Waals to explain the interactions involved in liquid He. He discovered that there are attractive forces between the closed-shell He atoms, which were considered a new type of bond. Since 1870 there has been much interest in this type of interactions, and also a great progress in the description of non-covalent bonds. The attraction forces have been identified as electrostatic, induction and dispersion, and in general, the biggest contribution is from the electrostatic interaction. As was stated in the introduction, experimentally, non-covalent bonds ( $Y'-H: Y$ ) are characterized by Infrared (IR) absorption or Raman vibrational spectroscopy, showing a shift and a higher intensity of the  $Y'-H$  symmetric-stretching vibrational modes [6–8].

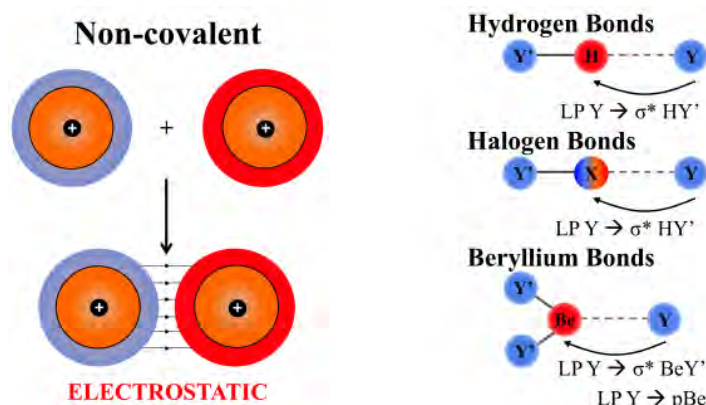
The strength and the electrostatic nature are the main differences between non-covalent and covalent interactions. On the other hand, ionic and non-covalent interactions share the same electrostatic component, although the interacting species in ionic bonds are ions with permanent opposite charge, while in non-covalent interactions the interaction is between permanent dipoles (or multipoles). Therefore, non-covalent bonds are weaker than covalent and ionic bonds, no matter, the nature of the interaction. Non-covalent bonds are long-range interactions due to their electrostatic nature, while for covalent bonds after 4Å there is no longer an overlap of the electron density or a chemical bond, the non-covalent interactions are in a wide range of distances from 4 up to 100Å.

The QM description of non-covalent bonds needs to consider the intrinsic characteristics of the bond. For instance, the basis set must include polarization and sometimes diffuse functions to account for long-range interactions. The electrostatic nature of these interactions cannot be described by a system of non-interacting electrons or by a linear combination of Slater determinants, indicating that dynamic correlation has a big contribution to the interaction energy. Therefore, methods like Hartree Fock (HF) or Complete Active Space Self Consistent Field (CASSCF) cannot correctly describe non-covalent bonds. The use of DFT methods for this type of interactions is controversial because these methods do not account for dispersion forces. Then, for interactions in which the role of dispersion is negligible such as many hydrogen bonds, DFT performs correctly. But for the case of  $\pi$  stacking interactions, in which dispersion forces have an important role, DFT fails. For example, pure DFT is not able to describe the DNA double helix[8, 183]. Empirical corrections have been introduced to remove the dispersion errors. Among them it is worth mentioning Grimme corrections[184] and Truhlar functionals [185, 186], which have shown excellent performance.

### 3.2.1.1 Hydrogen Bonds

Hydrogen Bonds (HB) are the most common non-covalent interactions. They have an important role in essential compounds like water and DNA. The incredible properties and structure of the water are due to the association of water molecules through HBs, and the DNA replication is produced through HBs pairing of the nucleotides. The IUPAC defines this interaction as *a form of association between an electronegative atom and a hydrogen atom attached to a second, relatively electronegative atom. It is best considered as an electrostatic interaction, heightened by the small size of hydrogen, which permits proximity of the interacting dipoles or charges*[24]. In scheme 3.5, the electronegative atom attached to the hydrogen atom is  $Y'$  and is labeled *proton donor*, while the electronegative atom acting as a Lewis Base (LB) ( $Y$ ) is named *proton acceptor*.

There are three types of forces taking part in a HB. As it has been already pointed out, the main one is electrostatic, but there is also an orbital overlap and a charge transfer between the hydrogen donor and acceptor. Due to the last two contributions, the exclusive electrostatic nature of HBs has been questioned, suggesting a non-negligible covalent character in this interaction[8, 141]. Figure 3.4a shows the wave function analysis for the water dimer, but



Scheme 3.5: Representation of non-covalent bonds. The different types of non-covalent interactions are also shown.  $Y'Z$  represents the Lewis acid (with  $Z = \text{H, Be, X}$ ),  $Y$  is the Lewis base, and  $X$  is a halogen atom.

these results can be generalized for most of HBs. The oxygen atom acting as a H-donor is represented as  $O'$ . According to QTAIM, NBO and EDA there is a weak electrostatic interaction with a covalent component:

- **The QTAIM analysis** finds a BCP between the monomers with a small value of  $\rho$  of the order  $\sim 0.01 \text{ au}$ . This value has been associated to the strength of the non-covalent bond. Because of the electrostatic nature of the interaction, the analysis of  $\nabla^2\rho$  is similar to that of ionic bonds,  $\nabla^2\rho > 0$  which indicates a depletion of  $\rho$  at the BCP, and that the biggest contribution to the energy comes from the kinetic term  $T_\rho$  [171]. The difference between ionic and non-covalent bonds is the bond strength because in ionic bonds there is a bigger polarization of the electron density, then  $\rho$ ,  $\nabla^2\rho$  and  $T_\rho$  are also bigger compared to HBs. For example,  $\nabla^2\rho$  is 10 bigger for  $\text{LiF}$  than for  $(\text{H}_2\text{O})_2$ . The strength of the interaction defines two types of HBs: weak and strong. In strong HBs there is a bigger charge transfer from Lone Pair  $(\text{LP})_{\text{O}} \rightarrow \sigma_{\text{O}'\text{H}}^*$  and the  $\nabla^2\rho$  could be negative[187], like in covalent interactions.
- **The NBO second order energies** can be used to quantify the strength of HBs. The interaction energy of the water dimer is estimated to be  $33 \text{ kJ} \cdot \text{mol}^{-1}$ , which shows the weak interaction between the monomers. The interaction energy is associated to a charge transfer from the LP of the oxygen (*H-donor*) to the  $\sigma_{\text{O}'\text{H}}^*$  (*H-acceptor*). This charge transfer is an evidence of the covalent character of the interaction [141].
- **The EDA** partition of the interaction energy describes the electrostatic nature of the HBs with a big contribution from  $\Delta E_{\text{elstat}}$ . However, it also finds a minor contribution from  $\Delta E_{\text{orb}}$ . The  $\Delta E_{\text{orb}}$  component indicates that there is an orbital relaxation involved in the formation of HBs, which means there is a covalent character associated to the interaction[188].

**The ELF analysis** does not locate a disynaptic basin between the  $\text{H}_2\text{O}$  monomers, this could be interpreted as a signature of a pure electrostatic interaction. The ELF description

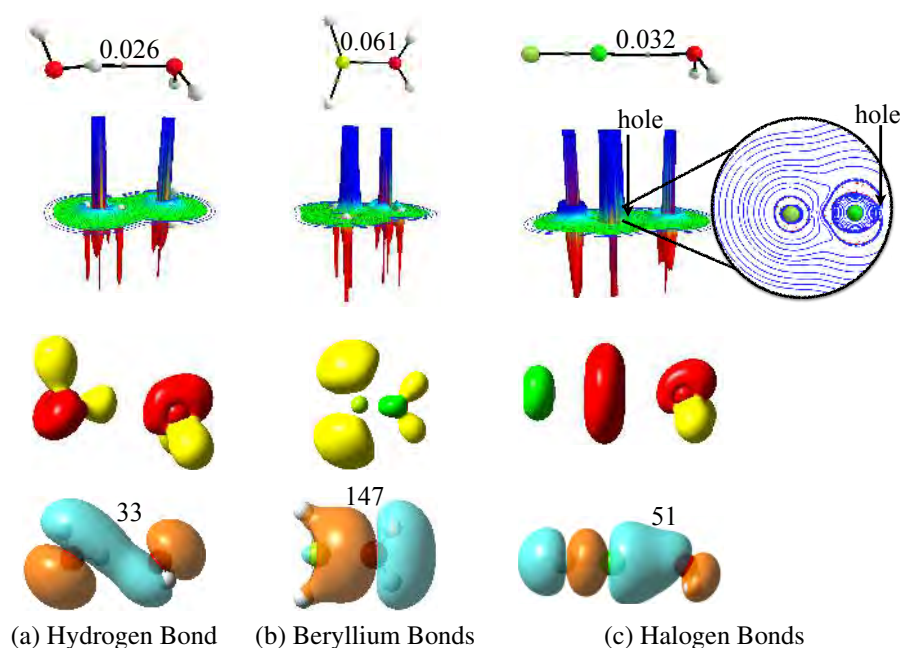


Figure 3.4: Wave function analysis of non-covalent bonds:  $\text{H}_2\text{O}:\text{H}_2\text{O}$  (hydrogen bonds),  $\text{BeH}_2:\text{H}_2\text{O}$  (beryllium bonds) and  $\text{FCl}:\text{H}_2\text{O}$  (halogen bonds). From the top to the bottom it is represented: (1) the QTAIM molecular graph and the value of  $\rho$  at the  $\text{BCP}_{\text{HY}}$ ; (2) the relief map of  $\nabla^2\rho$ ; 3) the ELF representation of the basins and their populations; 4) the NBO molecular orbitals and the second order perturbation energy associated to the charge transfer from the  $\text{LB}\rightarrow\text{LA}$ . The contour map of the  $\nabla^2\rho$  for the XB is also reported, the arrow shows the position of the hole in the halogen atom. The calculations were performed at B3LYP/cc-pVTZ level of theory. Same conventions as in figure 3.1 page 82.

of this interaction can be done considering the variation of the population of the basins of the hydrogen donor and acceptor upon the formation of the HB. For instance, in the water dimer, there is an increase in the population of the  $V(\text{O}', \text{H})$  basin and a decrease in  $V(\text{O})$ . Therefore, even though a disynaptic basin  $V(\text{H}, \text{O})$  is not located, there is a charge transfer from O to  $\text{O}'\text{H}$ , indicating that the ELF analysis is in agreement with the previous methods. The location of a  $V(\text{H}, \text{O})$  basin depends on the strength of the interaction, the increase of the covalent character in strong HBs originates a disynaptic basin  $V(\text{H}, \text{O})$  [189].

In general, HBs have been described as an electrostatic interaction with a covalent character. This description is also in agreement with VBT. According to this method, there are three main structures contributing to HBs: (1)  $\text{Y}'\text{H}:\text{Y}$ , (2)  $\text{Y}'^-:\text{H}^+:\text{Y}$ , and (3)  $\text{Y}'^-:\text{HY}^+$ . The first structure has the biggest contribution in the  $\Psi_{\text{VB}}$  for a HB. It represents the dipole-dipole interaction. The second structure shows the ionic character of the interaction, this component has also a considerable contribution to  $\Psi_{\text{VB}}$ , but yet not as big as the first one. Finally, the third structure is the covalent contribution to the wave function, which although small, it is different to zero, ratifying the small covalent character of the interaction. The study of the water dimer was done for the first time by Pauling. He found that the main

contribution (65%) is from structure (1), but the third covalent structure has also a small contribution (5%) [4].

HBs can be also characterized by the geometric and spectroscopic transformations undergone by the moieties after the interaction. The H-Y' bond becomes longer and there is a bigger polarization in the direction of the bond. The increase of the bond length produces a redshift and an increase in the transition intensity in the IR spectrum (see figure 3.5).

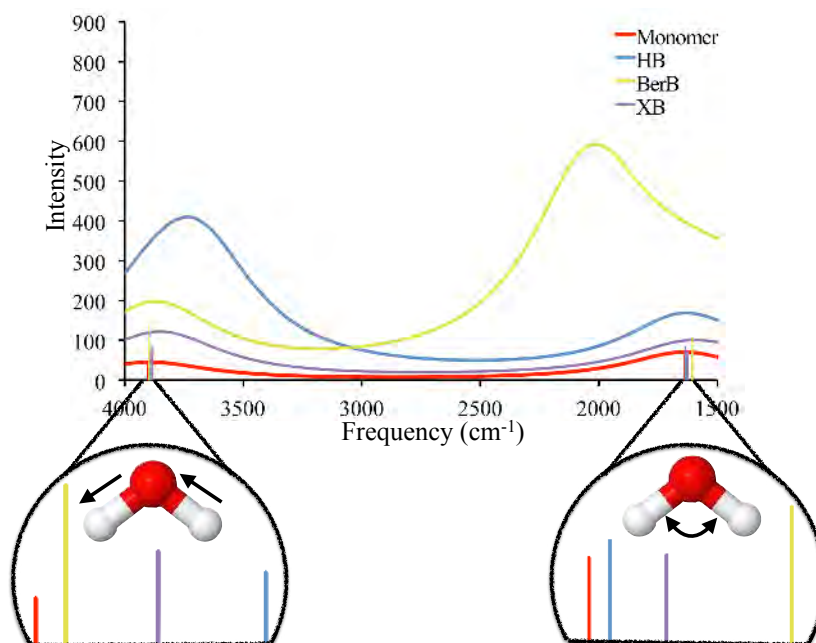
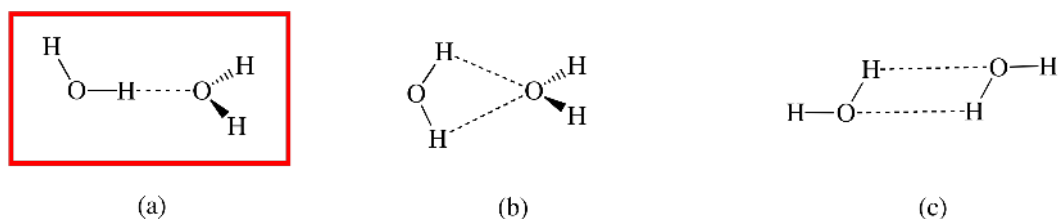


Figure 3.5: IR spectrum of the LA: H<sub>2</sub>O complexes. The water monomer is represented in red, the HB with LA = H<sub>2</sub>O in blue, the BerB with LA = BeH<sub>2</sub> in yellow, and the XB with LA = FCl in purple. The insets show the peaks for the antisymmetric stretching and bending for the H<sub>2</sub>O moiety acting as a LB. The calculations were performed at the B3LYP/cc-pVTZ level of theory.

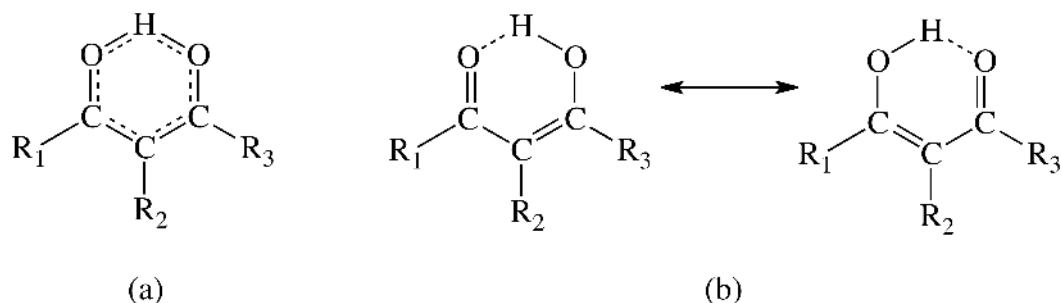
Other experimental methods such as nuclear magnetic resonance (NMR) and X-ray spectroscopy also provide information about the bond. The geometrical conformation is also associated with the strength of this interaction. The three possible isomers for the water dimer are shown in scheme 3.6. There are two important parameters, the O'-H bond length and the O'-H: O angle. Among the three isomers, the most stable is highlighted with red. For the most stable complex, the proton donor O'-H covalent bond is longer and defining a nearly 180° angle with the O atom from the proton acceptor. This orientation increases both the dipole-dipole interaction and the charge transfer from the hydrogen acceptor to the donor [6–8].



Scheme 3.6: Representation of the water dimer isomers, squared in red the most stable structure.

### Resonance Assisted Hydrogen Bonds

Resonance Assisted Hydrogen Bond (RAHB) is among the stronger HBs in which the complexes are neutral (one of the strongest HB is found in the  $[\text{FH}: \text{F}]^-$  anion [190]). The bond was introduced in 1989 by Gilli and co-workers and was explained as a HB in which *the proton donor and proton acceptor are connected by a  $\pi$  system, in such a way that the resonance structures (see scheme 3.7) enhance the strength of HBs* [61]. The model was based on the geometric parameters obtained by X-ray diffraction of  $\beta$  diketones. Initially, the interaction was explained considering only the electrostatic nature of the bonds, and the increase of the strength of HBs was attributed to the fluctuation of a negative charge induced by the resonance effect [62]. Later, the covalent character of the interaction was described using VBT, indicating that the strength of RAHBs was a blend between the electrostatic interaction enhancement by the  $\pi$  system, plus a covalent contribution [63].



Scheme 3.7: Representation of an intramolecular RAHB based on references [61, 62]. (a) The delocalized resonance structure and (b) the contributing structures.

The RAHBs became a popular concept to explain chemical reactivity. A well-known application is the description of the strong interaction between the base pairs of the DNA. However, the theoretical description of RAHB disagrees in the correlation between the  $\pi$  delocalization and the interaction energies. The degree of delocalization in these systems have been studied by considering the electron donor or attractor capacity of the substituents R (see scheme 3.7a), and also the size and unsaturation of the  $\pi$  system. In none of the cases, it was found a relationship between the increase of the resonance effect and the HB interaction energy. Alternatively, the increase of the interaction energy ( $E_{\text{int}}$ ) has been explained due to an increment in the basicity and acidity of the H- donor and acceptor, caused by unsaturated moieties [64–66]. The NMR analysis of systems with Intramolecular Hydrogen Bonds (IHB)

does not find a relation between the interaction energies of saturated and unsaturated systems with the proton chemical shift or the coupling constant ( $J$ ). Instead, it was proposed that IHBs are stronger in unsaturated systems because of the favorable arrangement of the  $\sigma$  skeleton of the molecule. The  $\pi$  system in unsaturated compounds induces a decrease of the distance between the proton donor and acceptor [191–194]. The EDA analysis is in agreement with this result. A study of several systems holding RAHBs with different degrees of unsaturation found that the biggest contribution to  $\Delta_{\text{orb}}$  comes from the  $\sigma$  and not from the  $\pi$  partition [195–197]. On the other hand, the Block Localized Wave Function (BLWF) method finds a relation between the HB interaction energy and the involvement of the  $\pi$  resonance. The result of this analysis is in agreement with the description of Gilli: RAHB is an electrostatic interaction improved by a  $\pi$  delocalization with a small covalent contribution [198]. Also in agreement with this result, the NMR description of the Paramagnetic Spin Orbital (PSO) and the Spin Dipolar (SP) components of  $J$  show that the strength of the HB depends on the  $\pi$  delocalization of the system [199].

In order to clarify the nature of RAHBs, Pendás and coworkers have performed a QTAIM and Interacting Quantum Atoms (IQA) analysis of the bond. They considered different systems with IHB like those in scheme 3.7 and their corresponding non-HB structures. The analysis of the delocalization indexes and the atomic charges shows an increase of the electron delocalization when the IHB is formed. The IQA method established that the electron reorganization primarily involved the  $\sigma$  bonds, while the  $\pi$  system cooperates in the electron redistribution. The nature of the interaction was studied considering two approaches: (1) the hydrogen was substituted by a point charge, finding that this model system describes correctly the delocalization indexes of the real system, and (2) the IQA energy partition finds that the main contribution to the IHB interaction energy is from the electrostatic components of the energy. These results suggest that *it is the IHB what enhances the  $\pi$  delocalization, and not the other way around* [200].

### 3.2.1.2 Halogen Bonds

The first report of complexes bonded by a halogen atom acting as a Lewis Acid (LA) and a LB dates back to the 19<sup>th</sup> century, when were described the compounds formed between halogen dimers and ammonia or methylamines [201, 202]. However, the *halogen bond* concept was not coined until the 20<sup>th</sup> century, when in 1978 Dumas used this term to explain the interaction between halogens derivatives (ClR and BrR) and Lewis bases in crystal structures [203]. In 2013, the IUPAC introduced a formal definition for this type of bond: *a halogen bond occurs when there is evidence of a net attractive interaction between an electrophilic region associated with a halogen atom in a molecular entity and a nucleophilic region in another, or the same, molecular entity*. Therefore, Halogen Bonds (XB) have been compared with HBs, where the H atom is replaced by a halogen atom (X) (see scheme 3.5). The surprising feature of this interaction is that both subunits are well-known electron donor species: a halogen and a lewis base, but as was stated in the IUPAC definition, there is an electron



deficient region in the halogen atoms that allows them to behave as electron acceptors. This region is named  $\sigma_{\text{hole}}$ .

The origin of the  $\sigma_{\text{holes}}$  is explained considering the electronic configuration of halogens. Halogen atoms have two doubly occupied p orbitals and a half occupied p orbital. This feature makes the atom not perfectly spherically symmetric and with a positive electrostatic potential in the direction of the half-filled orbital. When the halogen atom forms a X-Y' covalent bond, there is a redistribution of the electron density in which there is a fluctuation of  $\rho$  towards Y'. This preserves the positive electrostatic potential of the free halogen atoms, and which is oriented in the bond direction ( $\sigma_{\text{hole}}$ , see figure 3.6) [204–206]. The magnitude of the positive potential in the  $\sigma_{\text{hole}}$  is associated with the strength of the XB. The higher the positive potential, the stronger the non-covalent interaction. Thus, the electrostatic potential of halogen derivatives can be considered a good measure of its capacity to form XBs [207, 208].

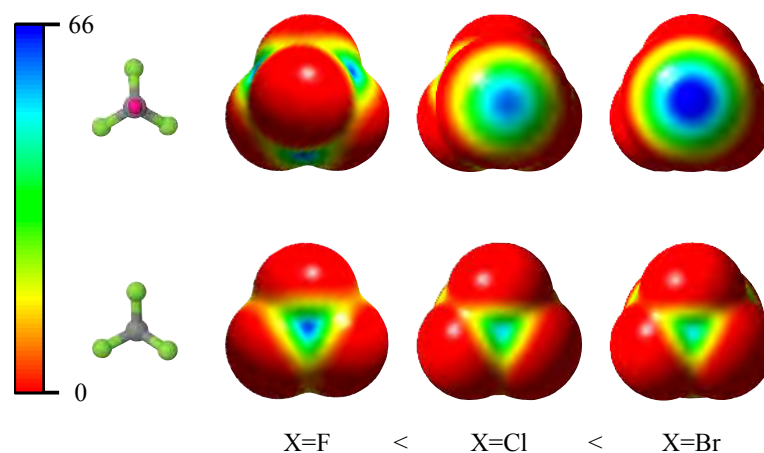


Figure 3.6: MESP for the  $\text{CF}_3\text{X}$  molecule with  $\text{X} = \text{F}, \text{Cl}, \text{Br}$ . The pink dot represents the position of the halogen atom(s) and the values of the potential are in  $\text{kJ}\cdot\text{mol}^{-1}$ . The calculations were performed at the B3LYP/cc-pVTZ level of theory.

### Molecular Electrostatic Potential

The nuclei and electrons produce an heterogeneous electrostatic potential ( $V(\mathbf{r})$ ) in a molecule, which can be calculated from the wave function of the molecular system,

$$V(\vec{r}) = \sum_{A=1}^P \frac{Z_A}{|\mathbf{R}_A - \mathbf{r}|} - \int \frac{\rho(\vec{r}')}{|\mathbf{r}' - \mathbf{r}|} d\vec{r}', \quad (3.4)$$

The MESP defines regions dominated by the nuclei (positive areas) or the electrons (negative areas). These areas give extra information about the molecule reactivity, like predicting which regions of the system are attractors of Lewis bases or Lewis acids. The MESP in this thesis are calculated over a surface of the molecule, defined as a three-dimensional  $0.001 e^{-\text{\AA}}$  contour of the electron density (Van der Waals surface).

The  $\sigma_{\text{hole}}$  is not only the signature of XB, but it is the responsible of the main characteristics and advantages of this interaction:

- The localization of the  $\sigma_{\text{hole}}$  makes XBs a **directional** interaction, in general the  $Y'X$ : Y angle is close to  $180^\circ$  [204–206, 208].
- The  $\sigma_{\text{hole}}$  strength can be **tuned** considering the electron withdrawing nature of both X and  $Y'$ . The strength of the  $\sigma_{\text{hole}}$  decreases when the electronegativity of X increases, which decreases with the size of the atom. Then, the strength of the  $\sigma_{\text{hole}}$  follows the trend:  $I > Br > Cl > F$  (see figure 3.6). The increase of the electron withdrawing strength of  $Y'$  also increases the positive potential of the  $\sigma_{\text{hole}}$  [208, 209]. For example,  $CF_3Cl$  has a  $\sigma_{\text{hole}}$  but the  $CH_3Cl$  molecule does not.
- In general, fluorine does not form XBs because of its high electronegativity. F is able to withdraw electron density from  $Y'$  and there is no longer a half filled p orbital, preventing the formation of a  $\sigma_{\text{hole}}$  (see figure 3.6). The same explanation can be applied for molecules where the electronegativity difference between X and  $Y'$  is soaring, for instance the  $CH_3Cl$  molecule. However, as was pointed out above, the strength of the  $\sigma_{\text{hole}}$  increases when  $Y'$  is an electron withdrawing group. For high electron withdrawing groups, like  $CN$ [60, 210],  $NC-C\equiv C$ ,  $F_3CC\equiv C$ ,  $FC\equiv C$  [210] and  $CF_3SO_2OCO$  [211], it has been found a shadow  $\sigma_{\text{hole}}$  in the fluorine atom.

The directionality and the possibility to control the strength of the interaction makes XBs a suitable tool to design new drugs or materials. In biological systems, halogen bonds are related to ligand binding, recognition, equilibrium geometries, molecular folding, and other types of interactions [205, 212, 213]. The application of XBs in the design of new crystal materials is wide, for example in new molecular conductors, super conductors, non-linear optical materials, liquid crystals, nanomaterials, anion transport, and many other applications [60, 205, 214–218]. Another interesting feature of using XBs to design new molecules is their emission properties. For example, halogen bonds have been used to induced phosphorescence in amino acids [219] and crystal materials [217].

The interaction can be characterized by spectroscopic and wave function analyses. The shifts and intensities in the IR and NMR spectra are similar to those discussed before for HBs, and are illustrated in the IR spectrum of the  $FCl:H_2O$  complex in figure 3.5 [207, 215, 220, 221]. The nature of this interaction can be compared with HBs. There is an electrostatic interaction between the positive potential of the  $\sigma_{\text{hole}}$  and the LB with a not negligible covalent character. The wave function analysis for the  $FCl:H_2O$  complex is presented in figure 3.4c. The QTAIM analysis describes it as an interaction between two closed-shell systems, the  $BCP_{XY}$  shows a small value of  $\rho$  and a negative value of  $\nabla^2\rho$ . The ELF calculation does not locate a disynaptic basin between the halogen and the LB, but there is a decrease in the population of the  $V(O)$  monosynaptic basin and an increase in  $V(F, Cl)$ , which is consistent with the charge transfer found within the NBO second order analysis of the non-Lewis contributions. The NBO analysis quantifies the interaction with a magnitude of  $51 \text{ kJ} \cdot \text{mol}^{-1}$ .

In general, the strength of XBs is comparable or higher than HBs. Eskandari proposed an interesting interpretation of halogen bonds based on the analysis of the topology of  $\nabla^2\rho$ . According to this study, XBs are a lump-hole interaction, where the hole can be seen as a region in front of the halogen atom where  $\nabla^2\rho$  is positive (see figure 3.4c), and the lump is the LP of the Lewis base [222]. A further investigation using the same analysis showed that even though CNF has a  $\sigma_{\text{hole}}$ , the  $\nabla^2\rho$  does not show a hole, indicating that possibly the interaction between CNF and Lewis bases should not be classified as a halogen bond. Actually, alternatively, the label *fluorine bond* was proposed for systems where there is an electrostatic interaction between a F atom and a LB [223].

It has been shown that XBs are able to cooperate with other non-covalent interactions. When XBs and HBs are part of the same system, there is an enhancement of the strength of both interactions [224–226]. In this thesis, the cooperativity between XB and Beryllium Bonds (BerB) was studied in systems where  $X = \text{F}$ .

### 3.2.1.3 Beryllium Bonds

BerBs were first defined and characterized in 2009 by Yáñez and coworkers. They are non-covalent interactions where the Lewis acid is a beryllium derivative ( $\text{BeY}'_1\text{Y}'_2$ , see scheme 3.5). There is a close relation between BerBs and HBs. The nature of these interactions is mainly electrostatic. However, it has been found that BerBs are up to five times stronger than their HBs analogues, because the low-lying  $p_{\text{Be}}$  orbitals favors a charge transfer from the LB towards these orbitals, something impossible for the highly energetic  $p_{\text{H}}$  orbitals [19] (see figure 3.7).

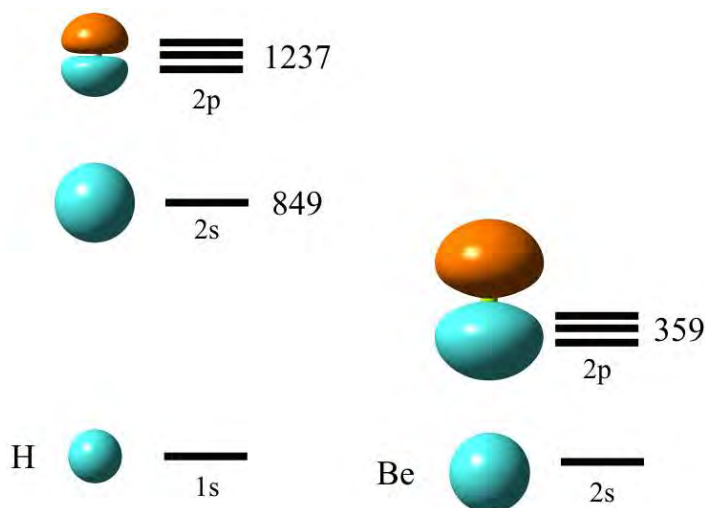


Figure 3.7: s and p atomic orbitals of the H and Be atoms. The values are in m.a.u. and the calculations were performed at the CCSD/cc-pVTZ level of theory.

The methodology to describe BerBs was assessed using the CCSD(T) method as a benchmark. It has been found that Møller-Plesset Second Order Perturbation Theory (MP2) is able

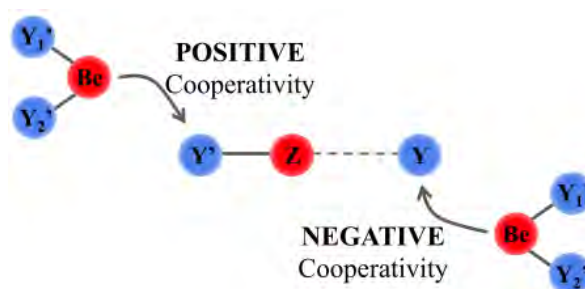
to reproduce the CCSD(T) interaction energies ( $E_{\text{int}}$ ), while DFT-B3LYP overestimates the bond strength, but it describes correctly the trends in  $E_{\text{int}}$ . The failure of B3LYP to describe long-range interaction was described at the beginning of this chapter. The incorrect behavior of B3LYP describing BerBs can be corrected considering the functional of Truhlar M06-2X, or others including dispersion corrections. A triple  $\zeta$  basis set is flexible enough to describe this interaction. The error introduced with the basis set was calculated using a quintuple  $\zeta$  basis as a benchmark, and the differences were found to be negligible [19, 227, 228].

The wave function analysis of BerBs shows similarities between this interaction and HBs. The main difference is that BerBs are stronger than their HBs analogues [19, 227]. The stronger Be interaction is reflected in the increase of  $\rho$  at the  $\text{BCP}_{\text{BeY}}$  and in the population of the  $V(\text{Be}, \text{Y})$  disynaptic basin. For example, when the Lewis base is  $\text{H}_2\text{O}$  (see figure 3.4 in page 90) the ELF method locates a disynaptic basin for the BerB but it does not for the HB. The interaction energies calculated with NBO are in agreement with the QTAIM and ELF descriptions. As was pointed before, BerBs interaction energies are larger than for their corresponding HBs, which is due to an additional donation from the  $\text{LP}_{\text{Y}}$  to the  $\text{p}_{\text{Be}}$  orbitals. The interaction between those orbitals leads to geometrical deformations. The Lewis acid experiences a bending of the  $\text{Y}'_1\text{BeY}'_2$  angle due to a  $sp$  hybridization of the Be atom, and an increase of the  $\text{Y}'\text{Be}$  bond distance, as a consequence of the charge transfer from the  $\text{LP}_{\text{Y}} \rightarrow \sigma_{\text{BeY}'}^*$ . It has been calculated that these geometrical distortions represent around 30% of BerBs interaction energies [229]. IR spectroscopy can also be used to describe the formation of a BerB. The  $\text{Y}'\text{Be}$  antisymmetric stretching is redshifted while the symmetric mode is blue shifted after the formation of the complex [19], see figure 3.5. Recently, the energetic partition of the BerBs interaction energies was analyzed by means of DFT-SAPT [228], IQA and NEDA [230]. In agreement with the wave function analysis methods, the main contribution to the interaction energy is electrostatic, with a covalent character coming from the charge transfer from the LB to  $\text{Y}'_1\text{BeY}'_2$  moiety.

Despite its interest, the chemistry of beryllium has not been deeply studied because of the high toxicity of the metal. Computational chemistry represents an important tool to study the properties of beryllium derivatives. An extensive work on Be complexes has been performed by the group of Yáñez and MÓ at the Universidad Autónoma de Madrid (UAM) and by Alkorta and Elguero at the Consejo Superior de Investigaciones Científicas (CSIC) to describe the properties of beryllium bonds. One of their most remarkable findings is that it is possible to modify intrinsic chemical properties of different types of systems using this interaction. Some of the most important results are summarized below:

*Modulating non-covalent interactions*, cooperativity effects are found when more than one non-covalent interaction occur in a particular system. The cooperativity effects could be positive and thus the strength of all the interactions would increase (positive cooperativity) or it could be negative, with a decrease in the strength of at least one of the interactions (negative cooperativity). BerBs can act as positive or negative cooperative interactions (see scheme 3.8). Systems holding simultaneously a BerB and a HB have shown an increase in the strength of the HB when the Be atom interacts with the proton donor, since upon the

formation of the BerB the  $Y'H$  bond weakens due to the charge transfer from the  $\sigma_{Y'H}$  to the Be derivative. On the other hand, when the Be atom interacts with the proton acceptor, there is a polarization of the electron density of the Y atom in the direction of the BerB, instead of the HB, and the strength of this latter decreases [50–52]. The same effect is found for BerB and XB. The XB is stronger when the Be interacts with the halogen donor because the association of the Be derivatives increases the positive potential of the  $\sigma_{hole}$  [231, 232]. The positive cooperativity between BerB and HB or XB increases both interaction energies, but in all the cases described before it was found that the beryllium bond is always the strongest interaction.



Scheme 3.8: Representation of the positive and negative cooperativity between BerBs and  $Y'Z:Y$  complexes, with  $Z = H, X$ .

*Modulating acidity*, among the amazing features of beryllium bonds it is worth highlighting the increase of the acidity of both Lewis bases and acids interacting with the Be-derivative ( $BeY_1'Y_2'$ ). In fact, the intrinsic acidity of the systems can be raised up to  $150\text{kJ} \cdot \text{mol}^{-1}$  and placing beryllium complexes in the same group as very strong acids like HF, HCl,  $\text{HClO}_4$ . This acidity enhancement can be explained by considering the stabilization of the anion formed after the proton loss. The interaction between  $BeY_1'Y_2'$  and the anions is up to 5 times stronger than the interaction with the neutral moieties [58, 59, 233].

*Modulating reactivity*, the effects of BerBs described above have a big effect on the chemical reactivity. It has been found that endothermic reactions become exothermic and spontaneous after the formation of the non-covalent interaction.

- The *spontaneous formation of ion pairs* in gas phase is possible in systems in which the Be atom interacts with the proton or halogen donor and the acceptor species is a strong LB, since the ionic products  $[Y_1'BeY_2']^- + [ZY]^+$  (with  $Z = H, X$ ) are more stable than the neutrals [58, 232].
- The *keto-enol tautomerism* in biological building blocks has always been an important subject to explain cell damage. The interconversion of formamide into the corresponding enol tautomer becomes spontaneous when formamide interacts with Be-hydride or Be-halides. In the case of nucleobases, in contrast, this non-covalent interaction decreases the energetic barriers associated with the formation of the enol tautomer and also increases the stability of the enol product [234, 235].

- *Hydrogen storage.* The interaction of  $\text{BeH}_2$  with squaric acid derivatives [236] and carboxylic acids [237] leads to spontaneous  $\text{H}_2$  loss. This means, the  $\text{BeH}_2 + \text{RCOOH} \rightarrow \text{BeH} + \text{RCOO} + \text{H}_2$  reaction is exothermic.

### 3.2.2 $\text{Be}_2$ Molecule

The description of the beryllium molecule is a challenge for theoretical methods because this molecule is characterized by a highly correlated-electron ground state. However, until 1984, the experimental description of this system was also a challenge. The first attempt to synthesize the molecule was in 1929 by Herzberg, who detected instead beryllium oxide ( $\text{BeO}$ ) [238, 239]. This finding is in agreement with the zero bond order predicted by MOT and other theoretical methodologies, for which  $\text{Be}_2$  is an inexistent molecule [240–242]. The development of methods including electronic correlation allowed a better description of the molecule, and at the end of 1970 and beginning of 1980, it was suggested that the Be dimer is bonded through a weak Van der Waals interaction. This Van der Waals minimum was located at long internuclear distances ( $\sim 4 \text{ \AA}$ ) [243–245]. Later, in 1983 Full Configuration Interaction (FCI) calculations predicted an associative curve for the Be molecule with a well-depth around  $2.5 \text{ \AA}$  [246]. A year after, Bondybey and coworkers reported the first gas phase spectrum of the  $\text{Be}_2$  molecule. Experiments actually revealed that  $\text{Be}_2$  is characterized by a bond length of  $2.45 \text{ \AA}$  at the equilibrium and a small Bond Dissociation Energy (BDE) ( $9.45 \text{ kJ} \cdot \text{mol}^{-1}$ ) [21, 22], which is in agreement with the earliest theoretical results. Subsequent theoretical studies were able to reproduce these experimental results. See table 1 from reference [53] for a summary of the different approaches and results obtained for this molecule from 1962 to 1993.

The previous chapter explained the difficulties of recovering the electron correlation energy. In some systems, this component of the electronic energy represents a small portion of the total energy. However, this is not the case of the  $\text{Be}_2$  molecule. Figure 3.8 shows the dissociation curve computed for different types of methods, some of the general trends are discussed below:

- *Repulsive methods:* HF and CASSCF show a repulsive curve for the  $\text{Be}_2$  molecule. According to these methods, in the gas phase, the Be dimer would exist as two isolated Be atoms. HF failure is due to the lack of electron correlation of this method, whilst *full valence* CASSCF calculation shows the importance of dynamical correlation in the description of this molecule. A deeper analysis of the CASSCF result is performed in section 4.3.2.
- *Van der Waals methods:* the increase of dynamical correlation results in a shallow minimum around  $4 \text{ \AA}$  that corresponds to a Van der Waals complex. This behavior is representative of the CCSD method, similar curves were also reported for other methods [243–245].

- *Bond methods:* the correct description of the  $\text{Be}_2$  bond is only achieved with high-level methodologies, such as CCSD(T) and Complete Active Space Second Order Perturbation Theory (CASPT2). This recalls the importance of direct triple excitation in CC theory, and that the CASSCF solution is improved after including dynamical correlation with CASPT2. MP2 and DFT-B3LYP describe correctly the position of the equilibrium distance, but respectively, under and overestimate the Bond Dissociation Energy (BDE). The inaccuracy of MP2 is attributed to the neglect of triplet excitations in the electron correlation. DFT, in turn, fails to describe long-range interactions.

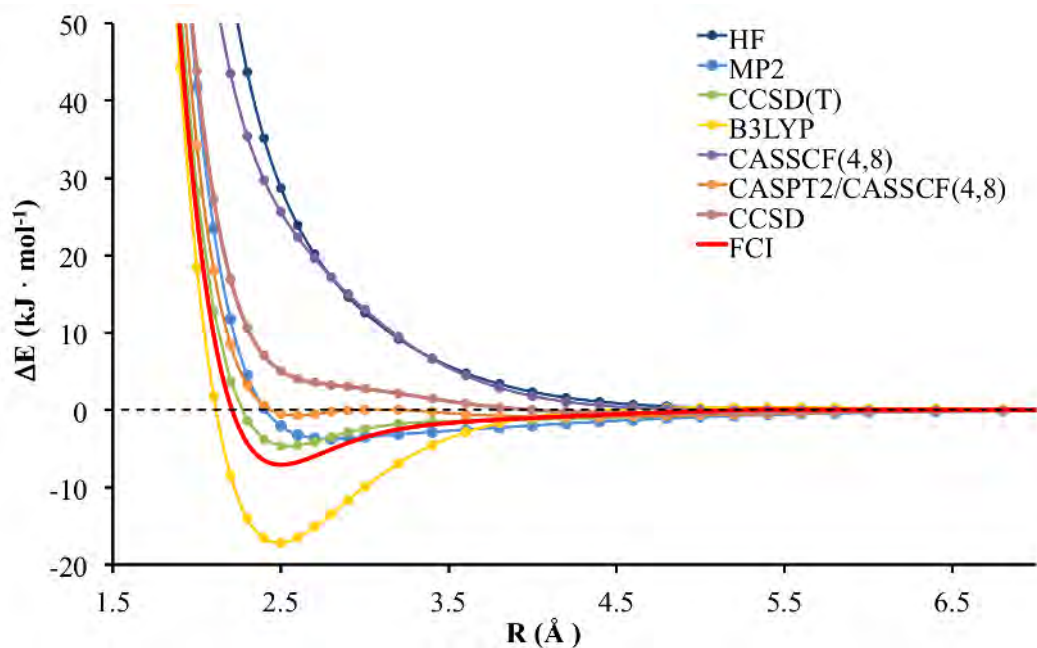


Figure 3.8: Comparison of different theoretical methods in the description of the dissociation curve of the ground state of the Be dimer. The calculations were performed with the cc-pVTZ basis set.

Figure 3.8 shows that the solution closer to the FCI result is obtained with the CCSD(T) approach. However, the wave function of the  $\text{Be}_2$  ground state has shown a multi-reference character, thus, a correct description of this system needs to consider more than one Slater determinant[54, 55], which is not the case of  $\Psi_{\text{CCSD}}$ . Therefore,  $\Psi_{\text{Be}_2}$  must be calculated considering multi-reference methods. The importance of dynamical correlation becomes clear from the HF result, without dynamical correlation the system has a repulsive character. The failure of the CASSCF method could lead to a misinterpretation of the importance of non-dynamical correlation. The occupation of the Highest Occupied Molecular Orbital (HOMO) and the Lowest Unoccupied Molecular Orbital (LUMO) in the ground state wave function is around 1.7 and 0.2, respectively, ratifying the multi-configurational character of the wave function, but CASSCF does not account for dynamic correlation.

The theoretical description of this system is complicated. Therefore, the main studies of the Be dimer focus in the role of the electron correlation in the replication of the few exper-

imental data available, thus, a deep analysis of its bonding properties has not been done yet. The nature of the Be-Be bond is not completely understood, the covalent character of the interaction is not widely accepted because of the small dissociation energy and the double occupation of the  $2\sigma^*$  orbital. The EDA analysis highlights the role of the p orbitals of the Be atoms in the  $\text{Be}_2$   $\sigma_{\text{BeBe}}$  bond. The major component of the interaction energy is from  $\Delta_{\text{orb}}$ , but when the p orbitals are not considered the interaction becomes repulsive because of a major contribution from  $\Delta_{\text{pauli}}$  [247]. The importance of the p orbitals in the  $\sigma_{\text{BeBe}}$  bond is ratified by the multi-reference and the TPS analysis of the wave function. ElKhatib et al. describe the Be-Be bond as a *non-dynamical correlated bond, based in the mixture of the two quasi-degenerated orbitals s and p* [54].

### 3.2.2.1 The triplet state of the $\text{Be}_2$ molecule

Much less effort has been invested in the description of the triplet state of the beryllium molecule compared to the singlet ground state ( $^1\Sigma^+$ ). The ground state of the molecule has an electronic configuration  $[\text{He}](2\sigma)^2(2\sigma^*)^2$ , where the doubly occupied  $2\sigma^*$  orbital is close in energy to the p orbitals. This electronic configuration does not only increase the non-dynamical character of the Be-Be bond but also decreases the energy gap between the ground and the excited states. The lowest excited state ( $^3\Sigma^+$ ) corresponds to a single excitation from the  $2\sigma^*$  to the bonding p orbitals ( $3\sigma$ ). This triplet state has been described considering different types of methodologies, among which, the theoretical studies performed by Evangelisti and coworkers using FCI with a large basis set [36, 248] and the experimental work done by Bondybey in 2008 [23] can be highlighted.

The triplet state lies around  $90 \text{ kJ} \cdot \text{mol}^{-1}$  higher in energy than the singlet ground state (adiabatic excitation). This state has a stronger Be-Be bond, with a  $0.35\text{\AA}$  shorter bond distance and 18 times higher dissociation energy. Figure 3.9 shows the molecular orbital diagrams for both singlet and triplet states. The increase in the bond strength of the triplet state can be explained considering two arguments: (1) in the singlet state, the  $2\sigma^*$  orbital is doubly occupied while in the triplet state it is singly occupied, and (2) the energy difference between the  $2\sigma$  and  $2\sigma^*$  orbitals increases in the triplet state. The nature of the bond of the triplet state has been also scarcely studied. Section 4.3.2 shows the result of the wave function analysis for this state.

### 3.2.2.2 The strength of the $\text{Be}_2$ derivatives

The strength of the Be dimer has been widely discussed from both the experimental and the theoretical points of view. As was stated in the introduction, synthetically  $\text{Be}_2$  represents a challenge. Therefore, theoreticians have been proposing new Be derivatives, without the experimental challenges of the isolated dimer. For instance, the complexes formed by the interaction between  $\text{Be}_2$  and electron donor species, which has shown higher BDE and shorter Be-Be bond lengths (see figure 3.10).



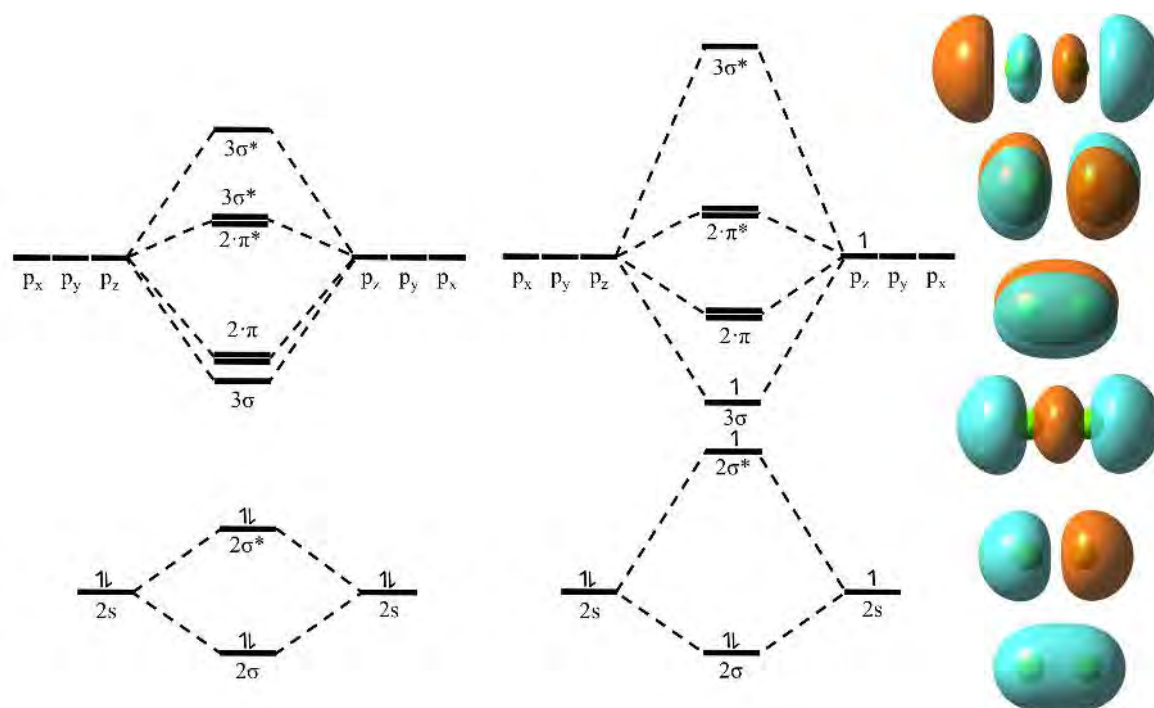


Figure 3.9: Molecular orbital diagram for the singlet  $^1\Sigma^+$  (left) and the triplet  $^3\Sigma^+$  (right) states of the  $\text{Be}_2$  molecule. The diagrams were calculated at CASSCF(4,16)/cc-pVTZ level of theory.

Among the first studies that considered this approach were the  $\text{CO}_n : \text{Be-Be} : \text{CO}_n$  complexes proposed in 1994 by Sunil[41]. The Be-carbonyl derivatives were studied using HF and perturbation theory. These studies predicted a double bond in the complexes for  $n = 2$ . Two different arguments were considered to explain the reinforcement of this bond: (1) a delocalization between the  $\pi_{\text{CO}}$  and  $p_{\text{Be}}$  orbitals is responsible of the double Be-Be bond, and (2) the existence of a C-Be-Be three-center bond [249, 250]. However, as was stated in the introduction, HF does not give an accurate description of these type of systems. Despite the limitations in the theoretical description of Be-carbonyl compounds, the interest about these complexes increased, and as predicted by theory the complexes with  $n = 1, 2$  were detected by IR spectroscopy [42].

Later in 2013, it was found that the complexes formed between  $\text{Be}_2$  and N-heterocyclic carbenes (NRC) present short Be-Be distances, which are among the shortest Be-Be bonds reported in the literature. The study was performed using DFT with a triple-zeta basis set, considering both the singlet and triplet state of the complexes. The authors of this study considered the NRC : Be-Be : NRC system, with several R substituent, such as R = H, methyl (Me) and phenyl (Ph). Very short Be-Be distances were reported for the complexes with Me, with a bond distance of  $1.949\text{\AA}$ , that is  $0.5\text{\AA}$  shorter than in the free Be dimer. However, the Me-complex does not exhibit the strongest Be-Be bond, which was found in the complex with R = Ph. This was rationalized considering the electronic state of  $\text{Be}_2$  in the complex. For R = H and Me, the most stable state is the triplet, showing a shorter Be-Be bond distance. For R = Ph, the ground state was found to be a singlet and here the BDE

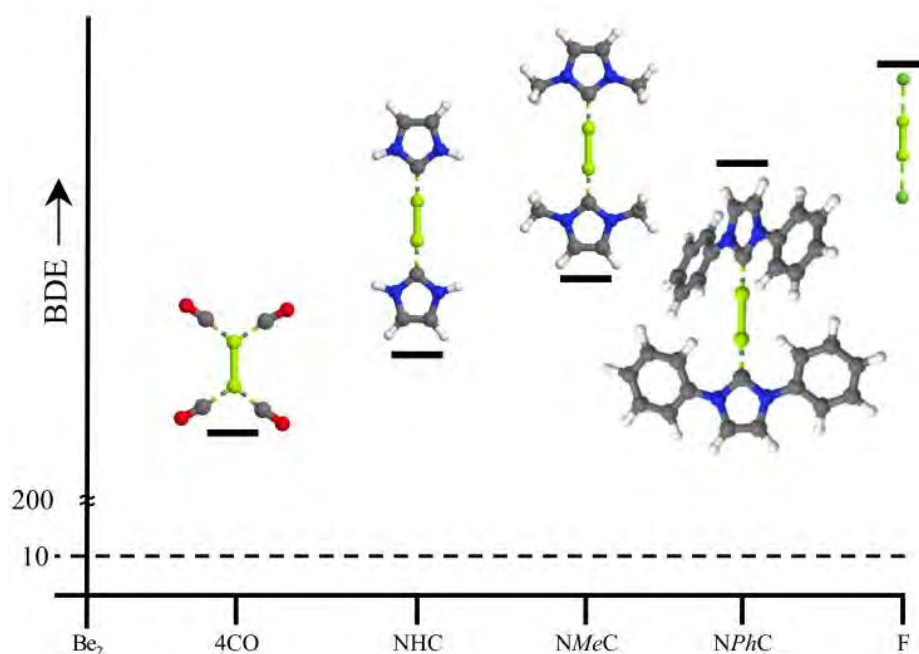


Figure 3.10: Comparison of the BDE for the complexes between  $\text{Be}_2$  and electron donor ligands. BDE taken from: 4-CO[41], NRC[43] and F[44]. The dotted line represents the BDE of the isolated  $\text{Be}_2$  molecule. The H atoms are shown in white, Be atoms in green-chartreuse, C atoms in grey, N atoms in blue, O atoms in red and F atoms in green.

increases by more than  $220 \text{ kJ} \cdot \text{mol}^{-1}$  with respect to the isolated dimer. The nature of the NRC: Be interaction was investigated using the EDA-NOCV method. The bond analysis shows that the interaction between the Be atoms and the NRC has a big covalent character. In fact,  $\Delta E_{\text{orb}}$  represents almost 50% of the interaction energy, with a charge transfer from the  $\sigma_{\text{Be-Be}}$  orbital towards the NRC and from the  $\pi_{\text{NRC}}$  orbitals to the  $\text{Be}_2$  moiety, both of them contributing to the same extent [43].

The NRC: Be-Be: NRC complexes were considered the strongest complexes involving the Be dimer until 2016, when the F: Be-Be: F system was proposed. The BDE of this complex amounts to  $322 \text{ kJ} \cdot \text{mol}^{-1}$  and the bond length is  $2.048 \text{ \AA}$ . This bond is shorter than in the isolated dimer but yet it is longer than in the complexes with NRC [44]. As already pointed out, the ground state of the complexes with NRC is predicted to be a triplet state, or the ground-singlet state has degenerated with an triplet-excited state. This is, however, not the case of the complexes with fluorine, showing a longer bond length even when the BDE is higher. The same year, a second work proposed a series of complexes with Be-Be bonds in the range of  $1.728 \text{ \AA}$  to  $1.866 \text{ \AA}$ , NRC:  $\text{Y}'_1\text{Be-BeY}'_2$ : NRC (with  $\text{Y}'_1=\text{Y}'_2=\text{H}$ ). These compounds have the shortest Be-Be bond distances reported to date in the literature[251]. Two features were combined to design complexes with ultra short Be-Be bond lengths: (1) a vertical Be-Be axis interacting with the ligand in a star shape as in the  $\text{C}_2\text{Be}_4\text{H}_4$  complexes [252], and (2) the electron donor capacity of the NRC ligands. The analysis of the bond was performed using the Adaptive Natural Density Partitioning (AdNDP) method, which describes the interaction as a *four-center two-electron  $\pi$ -bond delocalized over the*

NRC:  $Y_1'Be-BeY_2'$ : NRC system. However, it has been found that in this type of complexes in which  $Be_2$  is part of a cyclic structure there is not a real bond, even though the bond distance is ultra short. The QTAIM analysis does not locate a Be-Be BCP, instead it is found a ring critical point in the  $Y_1'Be-BeY_2'$  moiety [253, 254].

## Part IV

### RESULTS

"A detective with his murder mystery, a chemist seeking the structure of a new compound, use little of the formal and logical modes of reasoning. Through a series of intuitions, surmises, fancies, they stumble upon the right explanation, and have a knack of seizing it when it once comes within reach."

*Gilbert Lewis. The Anatomy of Science - 1926.*



## BERYLLIUM INTERACTIONS: ZERO, ONE AND FOUR ELECTRONS Be BONDS

---

### 4.1 ZERO-ELECTRONS Be BONDS

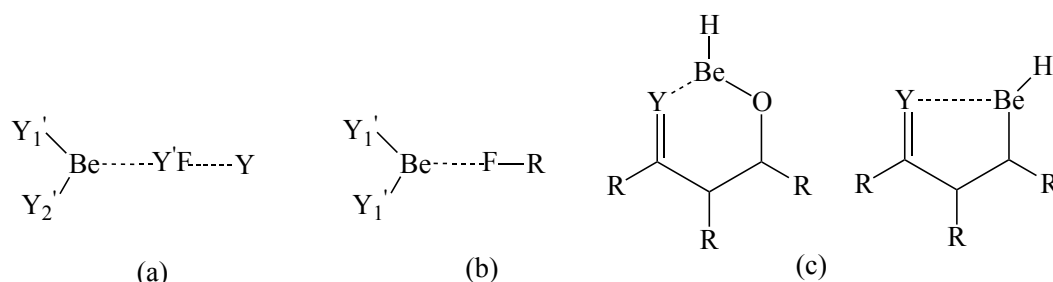
The zero-electrons Beryllium Bonds (BerB) are non-covalent interactions between Be-Lewis Acid (LA) and Lewis Base (LB). The properties and advantages of this interaction were described in section 3.2.1.3. This thesis studies the influence of BerBs over three types of chemical processes:

*Formation of Halogen Bonds (XB) in fluorine compounds:* there is consensus in the literature on the fact that fluorine derivatives only show  $\sigma_{\text{hole}}$  when the halogen atom is bonded to very electron withdrawing groups. In this work, the generation of a F  $\sigma_{\text{hole}}$  has been studied in systems of the type  $\text{BeY}'_1\text{Y}'_2: \text{Y}'\text{F}$ . These studies also discuss their ability to form XB with a LB (Y) (see scheme 4.1a). The effect of the strength of BerBs in the  $\sigma_{\text{hole}}$  was analyzed by increasing the acidity of  $\text{BeY}'_1\text{Y}'_2$ , by considering  $\text{Y}'_1 = \text{H, F, Cl}$  and  $\text{Y}'_2 = \text{H, F, Cl}$ . As explained in previous chapters, the electron withdrawing power of  $\text{Y}'\text{F}$  has an important role in the occurrence of F  $\sigma_{\text{hole}}$  and, therefore, different substituents were considered  $\text{Y}' = \text{CH}_3\text{O}(\text{MeO}), \text{Cl}, \text{NO}_2\text{F}, \text{NO}_3\text{F}$  and  $\text{CNF}$ . Finally, the influence of Y basicity in the strength of the XB with  $\text{Y} = \text{NH}_3, \text{CHN}, \text{N}(\text{CH}_3)_3$  and F was also studied.

*Formation of neutral radical species:* the formation of radical species requires a large amount of energy for the cleavage of covalent bonds. In order to decrease these energetic barriers, the assistance of BerBs in the homolytic dissociation of fluorine derivatives,  $\text{Be}(\text{Y}'_1)_2: \text{F-R}$ , to produce neutral radicals,  $(\text{Y}'_1)_2\text{BeF}\cdot + \text{R}\cdot$  was considered (see scheme 4.1b). The influence of  $\text{Be}(\text{Y}'_1)_2$  acidity in the Bond Dissociation Energy (BDE) was studied increasing the electronegativity of  $\text{Y}'_1$  from H to Cl. The effect of the nature of R in  $\text{Be}(\text{Y}'_1)_2: \text{F-R}$  was also evaluated, by considering the radical stability of  $\text{R}\cdot$  and also the electronegativity difference between F and  $\text{R} = \text{CH}_3, \text{NH}_2, \text{OH}, \text{F}, \text{SiH}_3, \text{PH}_2, \text{SH}, \text{Cl}$  and  $\text{NO}$ .

*Formation of Intramolecular Beryllium Bonds (IBerB):* the concept of Resonance Assisted Hydrogen Bond (RAHB) has been revisited considering the stronger non-covalent interaction which results after replacing a H atom by BeH in malonaldehyde and tropolone derivatives (see scheme 4.1c). The effect of the Be-acceptor basicity was studied considering  $\text{Y} = \text{O}, \text{NH}$ , while the degree of unsaturation and the flexibility of the  $\sigma$  skeleton was analyzed with different R substituents. The acidity of BeH was modulated by the group to which the Be atom is bonded. A higher acidity is expected when BeH is bonded to

the hydroxyl group (-OBeH) or a lower acidity when it is bonded to the alkyl group (-CBeH).

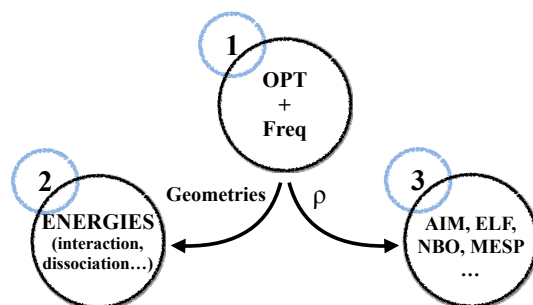


Scheme 4.1: Representation of the BerBs studied in this thesis. (a) The  $\text{BeY}_1'\text{Y}_2'$ :  $\text{Y}'\text{F}$ :  $\text{Y}$  complexes involved in the formation of halogen bonds. (b) The  $\text{Be}(\text{Y}_1')$ :  $\text{F-R}$  complexes involved in the formation neutral radicals. (c) IBerBs in malonaldehyde and tropolone derivatives.

#### 4.1.1 Methodology

The methodology employed in the present thesis is summarized in scheme 4.2. The stationary points of the Potential Energy Surface (PES) were located by geometry optimizations and were classified as local or global minima or as saddle points by an evaluation of the harmonic vibrational frequencies. For some of these species, the thermodynamical properties were also calculated. The electron density of the optimized structures was used to perform a wave function analyses, while the energetics were refined at a higher level of theory. The geometry optimization is a procedure that demands many computational resources because the first (and sometimes second) derivatives of the energy with respect to the geometrical parameters must be evaluated at each optimization step. Density Functional Theory (DFT) and MP2 methods combined with a double-zeta basis set represent a good performance/cost ratio for geometry relaxation [255–257]. Notwithstanding, the geometries were validated considering larger basis set and other highly correlated methods. Double-zeta basis sets are flexible enough to describe the geometries, but not so much to obtain accurate energetic properties [258–264]. Therefore, the basis set was increased to calculate reliable interaction ( $E_{\text{int}}$ ) and dissociation energies. The previous methods are only suitable for single-reference systems, for systems with a multi-reference character Complete Active Space Second Order Perturbation Theory (CASPT2)/Complete Active Space Self Consistent Field (CASSCF) methodology was employed. The geometry optimizations were performed considering a minimal Active Space (AS), while final energies were calculated within an extended AS. The methods applied to describe each system are explained below.

The complexes considered in the study of XBs and IBerBs are closed-shell molecules correctly described by single-reference methods. The structures in the analysis of XBs were optimized using the MP2/aug-cc-pVDZ level of theory. The performance of the double-zeta basis set was assessed considering a triple-zeta basis, finding negligible differences. The IBerB geometries were calculated with the B3LYP functional and the Pople 6-31G+(d,p)



Scheme 4.2: Scheme of the methodology used in this thesis: (1) the geometry is relaxed to a stationary point characterized through a vibrational frequency calculation. (2) Energetics were recomputed at a higher level of theory. (3) Finally, a wave function analysis of the system is performed to characterize the bonding properties

basis set. B3LYP geometries were validated considering MP2 geometries, and it was found that even when DFT overestimates the Be: O=C interactions, it correctly describes the geometrical and energetic trends. The situation is different for the Be derivatives precursors of radicals because the homolytic rupture of bonds is a multi-reference process. In the reaction:



the reactants are closed-shell molecules that could be studied using MP2, DFT or Coupled Cluster (CC) methods, while the radical products may have a wave function with a multi-reference character. The geometry optimization of reactants and products was performed with single-reference methods: CCSD(T)/cc-pVTZ and B3LYP/6-31G(2df,p) and, compared with the multi-reference method CASPT2//CASSCF(10,6)/cc-pVTZ, finding a very good agreement between the three methods, see tables S1, S2 and S3 from appendix B.2. MP2 and B3LYP calculations were performed with the Gaussian09 computational package (G09) [265], while for the CCSD(T)/cc-pVTZ and CASPT2//CASSCF(10,6)/cc-pVTZ MOLPRO 2015 was instead employed [89].

Different methodologies were also considered to calculate the energetic properties. BeRBs and XBs interaction energies in the  $\text{BeY}'_1\text{Y}'_2: \text{Y}'\text{F}$ : Y complexes were calculated at CCSD(T)/aug-cc-pVDZ//MP2/aug-cc-pVDZ using G09, while for IBeRBs, they were evaluated maintaining the B3LYP functional of the geometry optimization, but with the larger basis set 6-311G(2df,p). For a selected group of complexes, these energies were assessed using G4 theory, finding a good agreement between B3LYP and G4. Newly, the multi-reference character of the  $\text{Be}(\text{Y}'_1)_2: \text{F-R}$  BDEs was tested by comparing the CASPT2//CASSCF(14,9)/cc-pVTZ//CASPT2//CASSCF(10,6)/cc-pVTZ with single-reference results (CCSD(T)/cc-pVTZ and G4), showing a good agreement between the three methods. The enthalpy of reaction ( $\Delta H_{\text{reac}}$ ) is a better measurement of the energy required to cleave a bond over the BDE.  $\Delta H_{\text{reac}}$  was calculated at G4 level of theory, considering that composite methods have shown to predict thermodynamic properties within chemical accuracy [140]. The G4 calculations were performed with G09. The BDE or  $\Delta H_{\text{reac}}$  predict whether a reaction is thermodynamically favored, but not kinetically due to the existence of a high energetic barrier along the



dissociation coordinate that could trap the population in the minimum. The kinetic stability of reaction 4.1 was determined by locating the Transition State (TS) and mapping the dissociation process. The first order saddle points were calculated at CASPT2/CASSCF(14,9)/cc-pVTZ level of theory using the computational program MOLCAS 7.8 [88]. The AS used for BeH<sub>2</sub>: FF in reaction 4.1 is shown in figure S7 from appendix B.2, but a similar AS was employed for BeCl<sub>2</sub>: FF and BeH<sub>2</sub>: FNO. The AS for the geometry optimizations includes the p valence orbitals of the FR molecule, while final energies were computed including the  $\sigma_{\text{BeH}}$  orbitals. The AS of the products were selected to preserve the same set of orbitals as in the reactants.

The wave function analysis was performed at B3LYP level of theory with the same basis set used in the geometry optimization. The disadvantage of considering  $\Psi_{\text{MP2}}$  is the lack of contributions from triplet excitations (see equation 2.58). Quantum Theory of Atoms in Molecules (QTAIM) calculations were performed with the AIMAll computational package [266], the Natural Bond Orbital (NBO) with NBO-3.1 [267], the Electron Localization Function (ELF) calculation with the TopMod program [268–270] and the Molecular Electrostatic Potential (MESP) with the Multiwfn program [271]. The electrostatic potential in the  $\sigma_{\text{hole}}$  ( $V_{\text{max}}$ ) was determined by locating the maxima of the MESP on the surface. This calculation was also performed with the Multiwfn program.

#### 4.1.2 Properties of the Beryllium Bonds

The energetics and some relevant geometric parameters for several complexes studied in this thesis are shown in figure 4.1. The effect of the acidity of the Be-derivatives (Be(Y'<sub>1</sub>)<sub>2</sub>) is evaluated by comparing complexes containing BeH<sub>2</sub> and BeCl<sub>2</sub>, and the effect of the strength of the Y-R Lewis base by increasing the electronegativity of the Be-acceptor. Figure 4.1a shows that the strength of this non-covalent interaction goes from 2 to 150 kJ·mol<sup>-1</sup>, which depends on the acidity and basicity of the LA and LB, respectively. In the following, in the formation of BerBs, the atoms interacting with Be will be highlighted in red

The higher acidity of Be(Y'<sub>1</sub>)<sub>2</sub> increases the strength of the BerB and decrease the Be: Y bond length (see figures 4.1a and 4.1b). The electron acceptor capacity of Be(Y'<sub>1</sub>)<sub>2</sub> is larger for more electronegative Y'<sub>1</sub> substituent, increasing the strength of this non-covalent interaction. BerBs also becomes stronger when YR is more basic. This effect is illustrated by increasing the fluorine substitution in the BeY'<sub>1</sub>Y'<sub>2</sub>: CH<sub>3-n</sub>F<sub>n</sub>OF complexes. The substitution of H atoms by more electronegative elements increase the acidity of the CH<sub>3-n</sub>F<sub>n</sub> group. Therefore, there is a decrease of the electron donor capacity of the Be-acceptor (O atom) and also in the strength of the BerBs, as can be seen in figure 4.2a. This figure shows a linear correlation between the decrease of the donor capacity of the LB and the  $E_{\text{int}}$ . The values for  $n = 2$  are out of the linear regression, indicating that going from  $n = 1$  to  $n = 2$  the variation of the LB basicity is insignificant. However, there is not always a linear relation between the increase of  $n$  and the acidity of the group. For example, BF<sub>3</sub> is a stronger acid

than  $\text{BH}_3$ , but not the monosubstituted and disubstituted derivatives [272, 273], and the same is found when  $\text{BeH}_2$  is monosubstituted by F [59, 229].

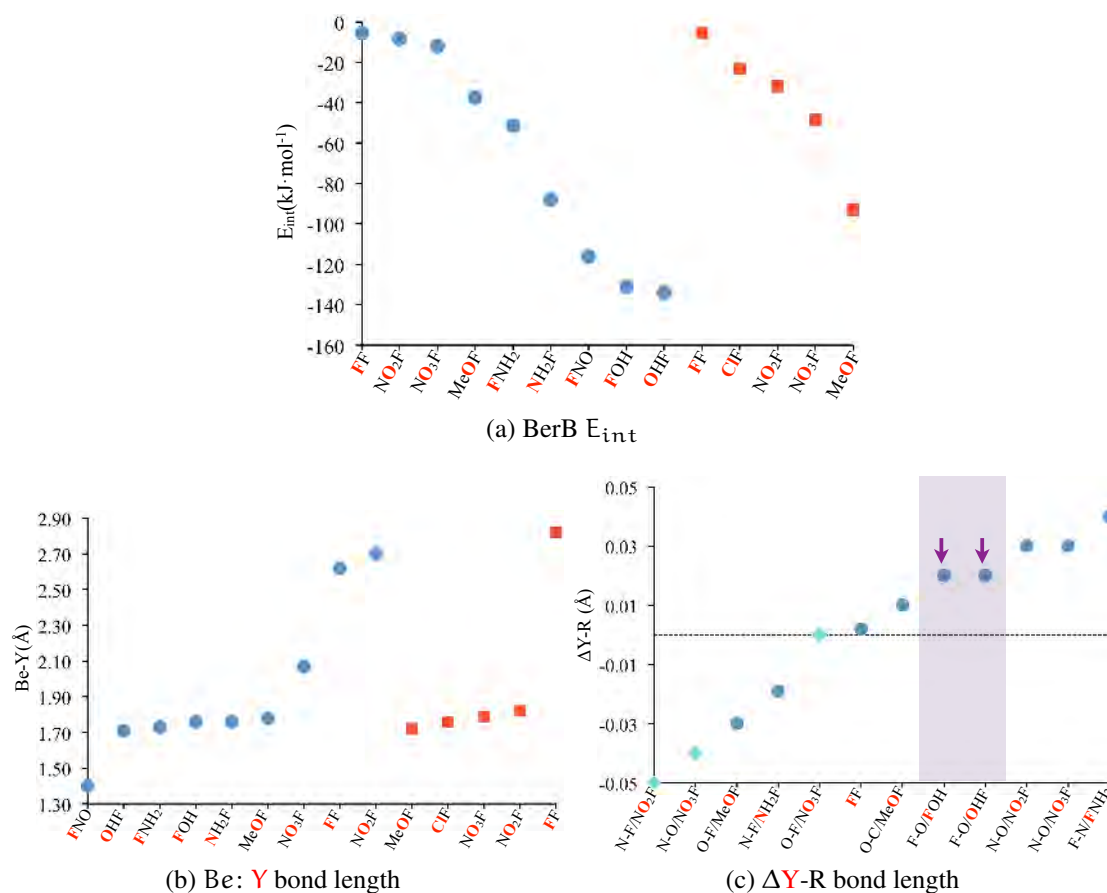


Figure 4.1: Energetic and geometric properties of the most relevant  $\text{Be}(Y_1')_2: \text{YR}$  complexes, the atoms interacting with Be are highlighted in red. The complexes formed with  $Y_1' = \text{H}$  are represented with blue circles and  $Y_1' = \text{Cl}$  with red squares. (a) Represents  $E_{\text{int}}$ , negative values show a stabilization of the YR moiety after the formation of BerBs (previous page). (b) Represents the bond length of the non-covalent interaction ( $\text{Be}: \text{Y}$ ). (c) Shows the variation of the Y-R bond length for the complexes with  $Y_1' = \text{H}$  with respect to the isolated YR moiety, for which negative and positive values represent a decrease and an increase of the bond length, respectively. The diamonds make references to the bonds of the remote groups to the BerB.  $\Delta Y\text{-R}$  for  $\text{BeH}_2: \text{FNO}$  is equal to  $1.19\text{\AA}$  (not included in the figure). All values were calculated at CCSD(T)/cc-pVDZ.  $E_{\text{int}}$  are in  $\text{kJ}\cdot\text{mol}^{-1}$  and the bond distances in  $\text{\AA}$ .

The  $\text{Be}: \text{Y}$  distances lie in wide range between  $1.3 - 2.4\text{\AA}$ , but by comparing figures 4.1a and 4.1b there is not a linear relation between the  $\text{Be}: \text{Y}$  distances and the  $E_{\text{int}}$  ( $R^2 = 0.5$ ). The complexes in figures 4.1a and 4.1b can be considered as an heterogeneous group. The atoms involved in the Y-R bond are different among the complexes, in some of the compounds there is a formation of not only a BerB but also a dihydrogen bond (such as  $\text{BeH}_2: \text{FNH}_2$  and  $\text{BeH}_2: \text{FOH}$ ), or the interaction between Be and Y is strong enough to form a covalent interaction (for example the  $\text{BeH}_2\text{F}: \text{NO}$  complex). Therefore, the relation between  $E_{\text{int}}$  and  $\text{Be}: \text{Y}$  distances has been analyzed in a more homogenous subensemble:

the complexes between  $\text{BeY}'_1\text{Y}'_2$  and  $\text{CH}_{3-n}\text{F}_n\text{OF}$ . The linear relation between  $E_{\text{int}}$  and the Be: O bond length, and between  $E_{\text{int}}$  and  $\rho$  at the Be: O Bond Critical Points (BCP) for the  $\text{BeY}'_1\text{Y}'_2$ :  $\text{CH}_{3-n}\text{F}_n\text{OF}$  complexes is represented in figures 4.2b and 4.2c, in both cases the values of  $R^2$  are higher than 0.9. Then, both the Be: O bond length and  $\rho_{\text{Be: O}}$  are indicators of the strength of the non-covalent interaction, when they are considered within an homogenous group. The value for  $n = 2$  is also slightly out of the linear correlation in figure 4.2.

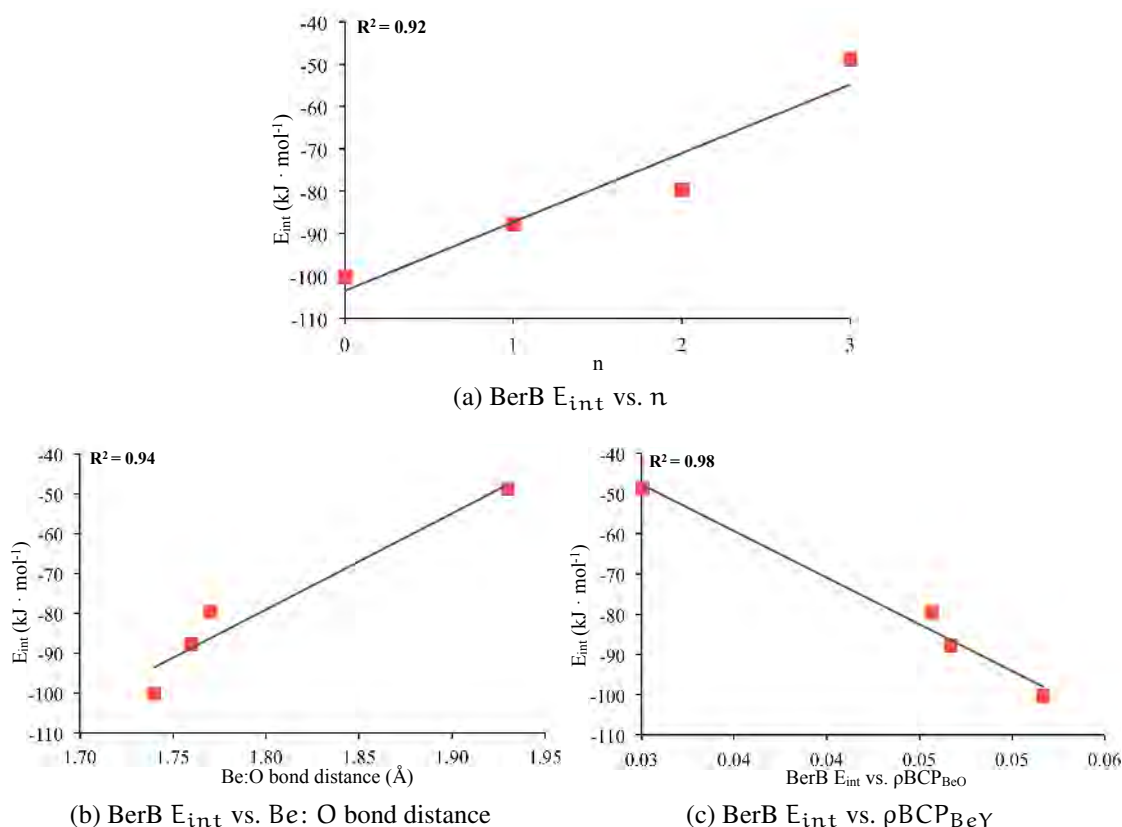


Figure 4.2: Linear correlation between (a) the BerB  $E_{\text{int}}$  and  $n$  substitution, (b) the BerB  $E_{\text{int}}$  and the Be-Y bond distance and (c) the BerB  $E_{\text{int}}$  and the value of  $\rho$  at the  $\text{BCP}_{\text{BeO}}$ , for the  $\text{BeCl}_2$ :  $\text{CH}_{3-n}\text{F}_n\text{OF}$  complexes.  $E_{\text{int}}$  (in  $\text{kJ} \cdot \text{mol}^{-1}$ ) were calculated at CCSD(T)/aug-cc-pVDZ//MP2/aug-cc-pVDZ, Be: O bond distances are in  $\text{\AA}$  and were calculated at MP2/aug-cc-pVDZ, and  $\rho_{\text{BCP}_{\text{BeO}}}$  are in au and were calculated at B3LYP/aug-cc-pVDZ level of theory.

The variations in the geometries of the LB are explained considering:

1. *The Bond Activation-Reinforcement (BAR) rule* [274]. This rule predicts the changes in the strength of an A-B bond when an electron withdrawing substituent  $Y'$  is attached to the bond. Let us assume that A is more electronegative than B. If  $Y'$  is attached to A, then the A-B bond becomes weaker. Conversely, if  $Y'$  is attached to B, the A-B bond becomes stronger. In the first case the charge transfer from A to  $Y'$  enhances the electronegativity of A (already large) and A recovers part of this charge by depopulating the A-B bonding region in which its orbitals participate. In the second case the phe-

nomenon is the same. The electronegativity of B is enhanced upon the attachment of  $Y'$ , but since A is more electronegative than B, this latter can only polarize the charge from A into the bonding area and the bond becomes reinforced.

2. *The protonation of alcohols.* There has been an extensive research in the effect of protonation on C-H BDEs of alcohols,  $[\text{CH}_3\text{OH}_2]^+ \rightarrow [\text{H}\cdot + \cdot\text{CH}_2\text{OH}_2]^+$ . Upon protonation, there is an increase of the oxygen electronegativity, inducing a decrease in the bond length of the remote groups (C – H) with respect to the protonation center (OH) [275, 276]. The effect of BerBs is similar than the one found for the alcohols protonations. After the formation of the non-covalent interaction there is an increase of the Be-acceptor (Y) electronegativity, therefore it is expected a decrease in the bond length of the remote groups.

The variations in the Y-R bond for the  $\text{Be}(Y'_1)_2: \text{YR}$  complexes follow the BAR rule in most of the complexes (see figure 4.1c). For example, consider  $\text{YR} = \text{MeOF}$  with the oxygen atom as the beryllium acceptor. The oxygen atom is less electronegative than fluorine atom, becoming the O-F bond shorter. Compared with the situation before, the O-C bond distance becomes longer because the oxygen atom is more electronegative than the carbon atom. The same behavior was found for the remaining complexes, except when  $\text{FR} = \text{FOH}$ . According to the BAR rule, when O is the Be-acceptor (less electronegative group) it is expected an increase of the F-O bond. However, as can be seen in figure 4.1c highlighted in purple, independently of the Be-acceptor, F or O, the F-O bond always becomes longer compared with the isolated LB. This behavior remains when the basis set is increased or different methodologies (MP2, CASPT2 and B3LYP) are considered, and it is also in agreement with the values of  $\rho$  at the  $\text{BCP}_{\text{FO}}$  (see figure S1 from appendix B.2). The geometries changes in the remote groups upon  $\text{BeY}'_1\text{Y}'_2$  complexation are shown in blue-diamonds in figure 4.1c, and for all the systems there is a decrease of the these bond distances due to the increase of the electronegativity of the Be-acceptor, which is consistent with the results obtained for the protonation of alcohols. In summary, the largest variations in figure 4.1c are found when Be interacts with the most electronegative atom, because the difference in the electronegativity between Y and R becomes larger, enhancing the depopulation of the Y-R and the remote bonds.

#### 4.1.3 Halogen Bonds in Fluorine Derivatives

The formation of BerBs generates a  $\sigma_{\text{hole}}$  in fluorine atoms in complexes such as  $\text{Be}(Y'_1)_2: Y'F$ . This non-covalent interaction increases the  $Y'$  electronegativity due to the charge donation from  $Y'$  towards  $\text{Be}(Y'_1)_2$ , and which results in transformations of the  $Y'F$  moiety that follow the BAR rule. In most of the compounds the  $Y'-F$  bond becomes shorter upon the formation of BerBs (see figure 4.1c), which has been explained as polarization of F orbitals into the bonding region. Then, the  $p_{\text{F}}$  orbital in the  $Y'F$  bond direction is preserved as singly occupied ( $\sigma_{\text{hole}}$ ). The F  $\sigma_{\text{hole}}$  in  $\text{Be}(Y'_1)_2: Y'F$  is deeper when the strength of the

BerB is increased, as can be seen figure 4.3 for  $\text{Be}(Y'_1)_2: \text{CH}_{3-n}\text{F}_n\text{OF}$  with  $Y'_1$  equal to H and Cl. A deep analysis of the formation of  $\sigma_{\text{hole}}$  in fluorine derivatives can be found in appendix B.1.

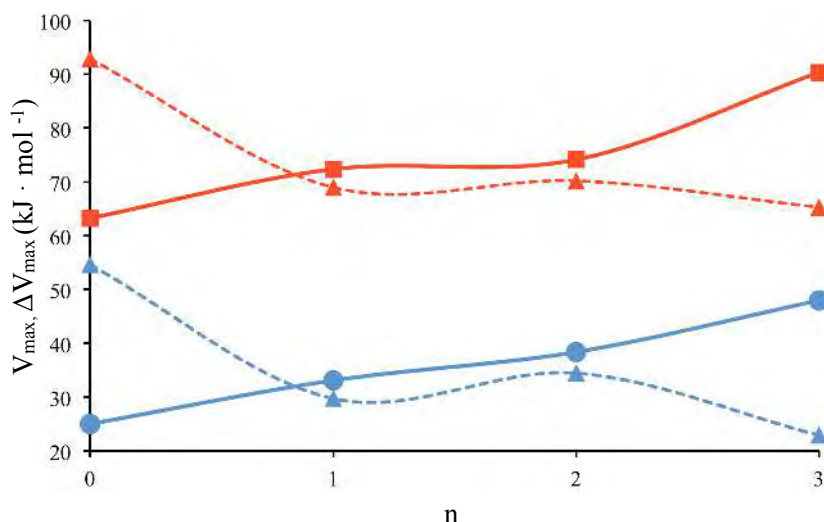


Figure 4.3: Effect of the degree of substitution in the value of  $V_{\text{max}}$  of the  $\sigma_{\text{hole}}$  for  $\text{Be}(Y'_1)_2: \text{CH}_{3-n}\text{F}_n\text{OF}$  complexes ( $n = 0, 1, 2, 3$ ). The complexes formed with  $Y'_1 = \text{H}$  are represented in blue and  $Y'_1 = \text{Cl}$  in red. Blue squares and red circles represent the values of  $V_{\text{max}}$  in the  $\sigma_{\text{hole}}$  and the triangles  $\Delta V(r)$  ( $\Delta V(r) = V(r)_{\text{BerB}} - V(r)_{\text{no-BerB}}$ ). All values are in  $\text{kJ}\cdot\text{mol}^{-1}$  and were calculated at B3LYP/aug-cc-pVDZ level of theory.

The effect of the substituent in the strength of the  $\sigma_{\text{hole}}$  is illustrated considering the  $\text{Be}(Y'_1)_2: \text{CH}_{3-n}\text{F}_n\text{OF}$  system in figure 4.3. The acidity of  $\text{CH}_{3-n}\text{F}_n\text{O}$  increases with  $n$ , inducing two main changes in the systems: (1) the BerB becomes weaker and (2)  $\text{CH}_{3-n}\text{F}_n\text{O}$  is a more powerful electron withdrawing group. Thus, the  $\sigma_{\text{hole}}$  becomes stronger for higher values of  $n$ , but the BerB weakens (see figures 4.2a and 4.2a). The *negative cooperativity* is represented in figure 4.3, while the value of  $V(r)$  (full line) increases with  $n$ , there is a decrease in  $\Delta V(r)$  (dashed lines,  $\Delta V(r) = V(r)_{\text{BerB}} - V(r)_{\text{no-BerB}}$ ). The changes of  $V_{\text{max}}$  when  $n$  is increased from 1 to 2 is small. The most dramatic result is when  $Y'_1 = \text{Cl}$  (red-□ line), where the figure shows a flat behavior between  $n = 1, 2$ , again the consecutive substitution of H by a more electronegative atom does not translate into a linear increase of the electron withdrawing power of  $\text{CH}_{3-n}\text{F}_n\text{OF}$ .

The formation of a  $\sigma_{\text{hole}}$  has been described using a topological analysis of  $\nabla^2\rho$ . The  $\sigma_{\text{hole}}$  is characterized by an area with a negative value of  $\nabla^2\rho$  located ahead the halogen atom (see section 3.2.1.2), but as can be seen in figure 4.4 there is not such an area around fluorine independently of the strength of the Lewis acid (see figures 4.4b and 4.4c) or the nature of the substituent (see figure 4.4d). However, these results are not in agreement with the MESP shown in appendix B.1 (figures 1, 4 and 6).

Other non-covalent interactions were also considered to generate a  $\sigma_{\text{hole}}$  in fluorine derivatives. Figure 4.5 shows the MESP for the complexes with  $\text{BH}_3$ , and even though in

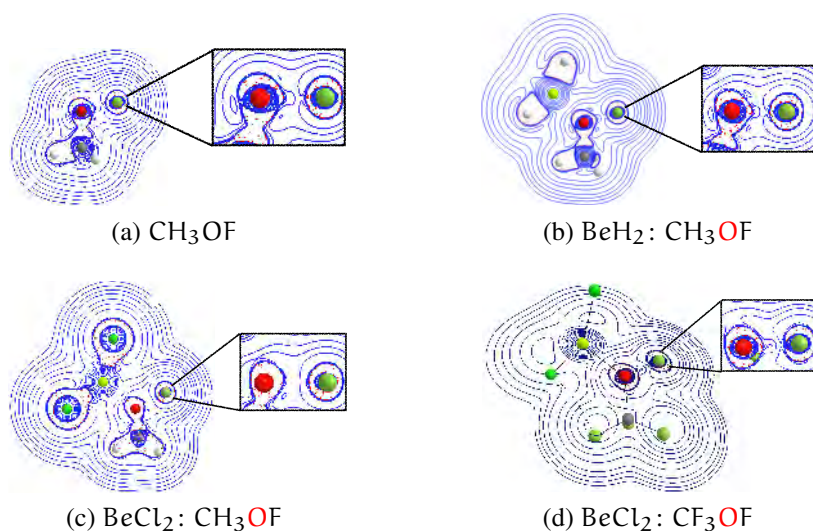


Figure 4.4: Contour map of  $\nabla^2\rho$  for  $\text{CH}_{3-n}\text{F}_n\text{OF}$  and  $\text{Be}(\text{Y}'_1)_2:\text{CH}_{3-n}\text{F}_n\text{OF}$  complexes. Red lines corresponds to negative values and blue lines to positive values of the laplacian. The insets are focussed on the fluorine atom. The contour maps were calculated at B3LYP/aug-cc-pVDZ level of theory.

some complexes a  $\sigma_{\text{hole}}$  is generated, the values of  $V_{\text{max}}$  are smaller compared to the analogue Be complexes. Indeed, while  $\text{CH}_3\text{OF}$  shows a  $\sigma_{\text{hole}}$  when interacting with  $\text{BeH}_2$ , it does not with  $\text{BH}_3$ . According to reference [59], the acidity of unsaturated LB increases with the formation of both non-covalent interactions, Be and B bonds. However, the effect is greater for  $\text{Be}(\text{Y}'_1)_2$  derivatives than for analogous complexes with  $\text{B}(\text{Y}'_1)_3$ . Therefore, the smaller  $V_{\text{max}}$  values in the complexes with  $\text{BH}_3$  are due to a higher basicity of fluorine in borane complexes, with respect to the systems with  $\text{BeH}_2$ .

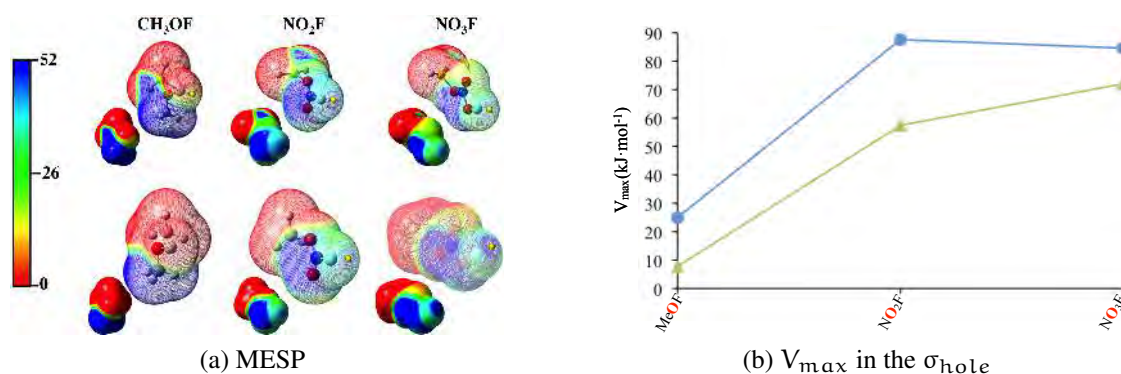


Figure 4.5: Comparison of the MESP and  $V_{\text{max}}$  in the  $\sigma_{\text{hole}}$  for the complexes between  $\text{BeH}_2:\text{Y}$  and  $\text{BH}_3:\text{Y}$ , with  $\text{Y}=\text{MeOF}$ ,  $\text{NO}_2\text{F}$  and  $\text{NO}_3\text{F}$ . (a) Shows the MESP for the complexes with  $\text{BeH}_2$  (on top) and with  $\text{BH}_3$  (bottom). (b)  $V_{\text{max}}$  for the complexes with  $\text{BeH}_2$  (in blue-circles) and  $\text{BH}_3$  in (green-triangles). All values are in  $\text{kJ}\cdot\text{mol}^{-1}$  and were calculated at B3LYP/aug-cc-pVDZ.

Generally,  $Y'F: Y$  compounds do not form XBs, while  $BeY'_1Y'_2: Y'F: Y$  complexes do. The formation of XBs does not only depend on the strength of the LA or the LB, but also in the cooperativity between the non-covalent interactions, BerB and XB. When the acidity of F is smaller than the  $BeY'_1Y'_2$  moiety, the LB prefers to interact with the metal instead of the halogen, see  $BeH_2: CH_3OF: NH_3$  in figure 4.6. If F is more acidic than  $Be(Y'_1)_2$  there is a formation of a XB, which is ratified by the presence of a  $BCP_{FY}$  with values of  $\rho$  in the order of  $0.01 a.u.$  (see figure 5 from appendix B.1). The formation of  $BeY'_1Y'_2: Y'F: Y$  complexes ratifies the presence of a  $\sigma_{hole}$  in fluorine derivatives, even though  $\nabla^2\rho$  does not behave as in the complexes with heavier halogens. Appendix B.1 describes all the complexes studied in this thesis. The  $BeCl_2: CH_{3-n}F_nOF: NH_3$  system is used to illustrate the properties of the interaction.

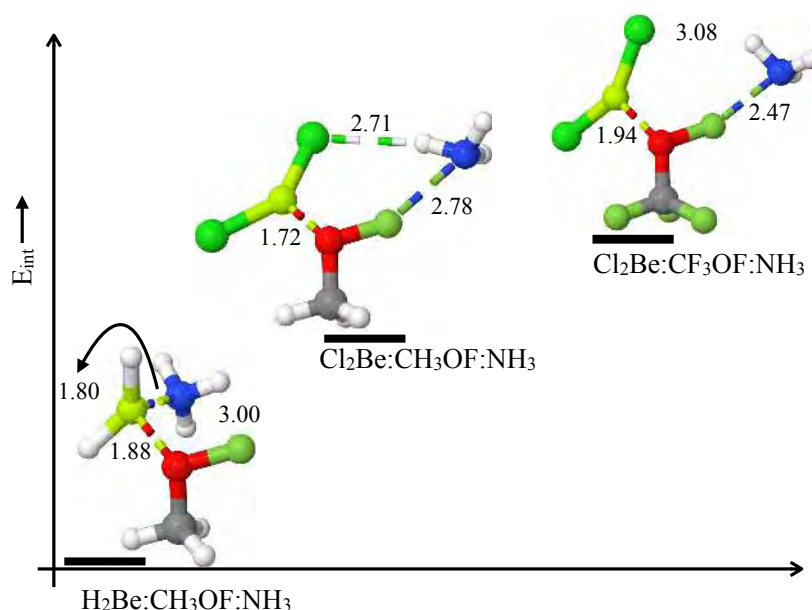
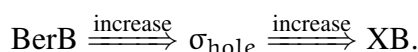


Figure 4.6: Representation of the geometries and  $E_{int}$  trends for the  $BeH_2: CH_3OF: NH_3$ ,  $BeCl_2: CH_3OF: NH_3$  and  $BeCl_2: CF_3OF: NH_3$  complexes. The interaction energy between F and  $NH_3$  increases from left to right and the most relevant bond distances are in Å. The geometrical parameters were calculated at MP2/aug-cc-pVDZ level of theory.

Figures 4.7a and 4.7b show a linear correlation between the strength of the XB and both the BerB and  $V_{max}$ , so that



This synergy is represented in the complexes in figure 4.6, while in the  $BeH_2: CH_3OF: NH_3$  system it is found only a  $Be: NH_3$  interaction, in the  $BeCl_2: CH_3OF: NH_3$  complex there is an  $F: NH_3$  XB. However, in the  $BeCl_2: CH_3OF: NH_3$  compound,  $NH_3$  still interacts with  $BeCl_2$  through a  $Cl: H_3N$  hydrogen bond, and as a consequence the  $O-F-N$  arrangement is not linear. The directionality of the XB can be recovered by increasing the strength of the  $\sigma_{hole}$ . For example,  $\angle O-F-N$  becomes close to  $160^\circ$  for  $BeCl_2: CF_3OF: NH_3$  (see figures 4.6 and 4.7c). The cooperativity between the non-covalent interactions was found to

be positive, hence after the formation of the XB there is an increase of  $\rho$  at the BCP<sub>BeY'</sub> (see figure 5 from appendix B.1).

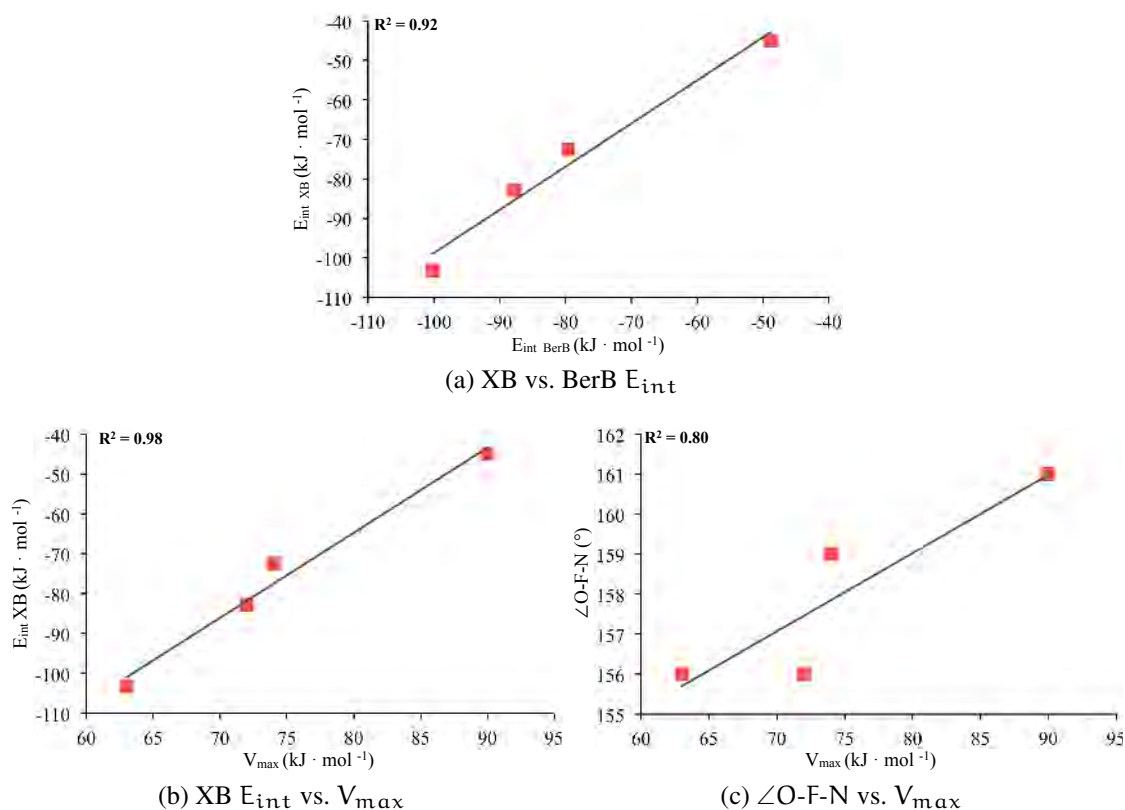


Figure 4.7: Linear correlation between (a) the XB and BerB  $E_{int}$ , (b) the XB  $E_{int}$  and  $V_{max}$  in the  $F\sigma_{hole}$  and (c) the  $\angle O-F-N$  and  $V_{max}$  in the  $F\sigma_{hole}$ , for the  $BeCl_2:CH_{3-n}F_nOF:NH_3$  complexes, with  $n = 1, 2, 3$ .  $E_{int}$  and  $V_{max}$  are in  $kJ \cdot mol^{-1}$ , the first were calculated at CCSD(T)/aug-cc-pVDZ//MP2/aug-cc-pVDZ and the second at B3LYP/aug-cc-pVDZ level of theory.  $\angle O-F-N$  is in degrees ( $^{\circ}$ ) and was calculated at MP2/aug-cc-pVDZ level of theory.

#### 4.1.4 Homolytic Dissociations

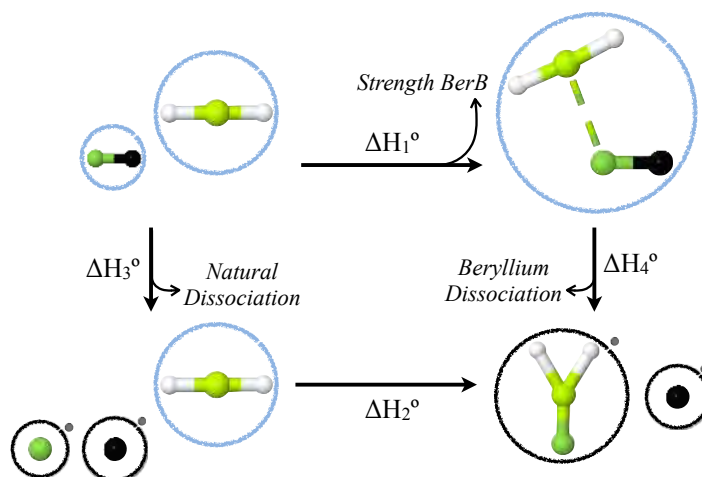
The Bond Dissociation Enthalpy (BDH) of the  $BeH_2:F-R$  complexes or  $\Delta H_4^{\circ}$  (see scheme 4.3) are in table 1 from appendix B.2.

The trends in the dissociation enthalpies of  $BeH_2:F-R$  can be explained by considering the electronegativity difference between F and R [277, 278]. Pauling electronegativity difference,  $|\chi_B - \chi_A|$ , is defined as:

$$\Delta(AB) = E(AB) - \frac{E(AA) + E(BB)}{2} \quad (4.2a)$$

$$|\chi_B - \chi_A| = 0.102 \left| \sqrt{\Delta(AB)} \right| \quad (kJ \cdot mol^{-1}) \quad (4.2b)$$





Scheme 4.3: Representation of the thermodynamical cycle of the  $\text{BeH}_2:\text{FR}$  dissociation into  $\text{BeH}_2\text{F}\cdot + \text{R}\cdot$ .

The relation between  $\Delta H_4^\circ$  and  $|\chi_B - \chi_A|$  is shown in figure 4.8a. The values of  $|\chi_B - \chi_A|$  were calculated for the isolated FR monomers, considering that after the formation of the BerB,  $|\chi_{\text{F}\cdot} - \chi_{\text{R}\cdot}| \sim |\chi_{\text{BeH}_2\text{F}} - \chi_{\text{R}\cdot}|$ . Figure 4.8a shows a linear relation between  $\Delta H_4^\circ$  and  $|\chi_B - \chi_A|$ ,  $R^2 > 0.90$ , except for the  $\text{BeH}_2:\text{FNO}$  complex (pointed with a red arrow). The geometries of the  $\text{BeH}_2:\text{FNO}$  and FNO are shown in figure 4.9, and it is clear from this figure that there is a change in  $|\chi_B - \chi_A|$  going from FNO to  $\text{BeH}_2:\text{FNO}$ . The high stability of the  $\text{NO}\cdot$  radical enhances a strong Be-F interaction, and also a very weak F-N bond. Therefore  $|\chi_{\text{F}\cdot} - \chi_{\text{NO}\cdot}| \approx |\chi_{\text{BeH}_2\text{F}} - \chi_{\text{NO}\cdot}|$ .

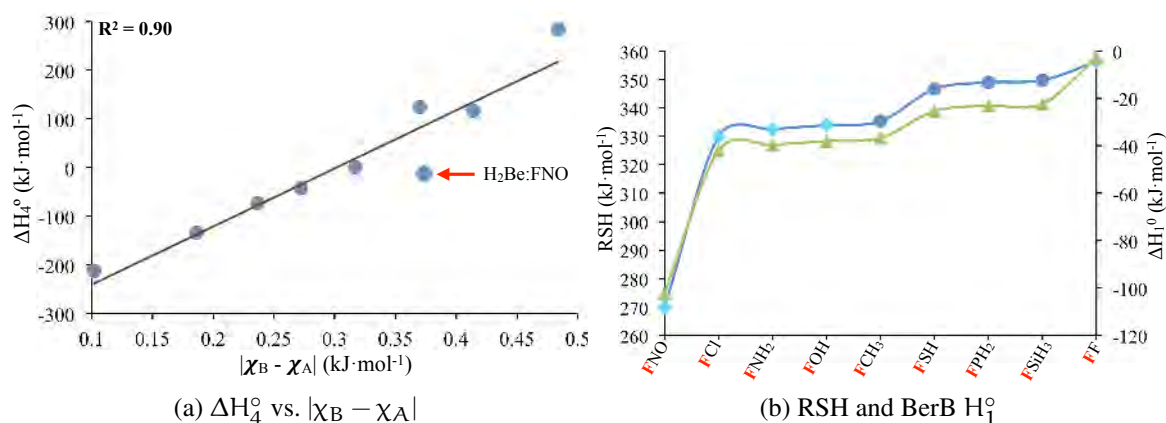


Figure 4.8: (a) Linear correlation between  $\Delta H_4^\circ$  and  $|\chi_B - \chi_A|$  for the  $\text{BeH}_2:\text{FR}$  complexes. (b) Left figure represents the values of the RSH (blue-circles) and right side represents the BerB  $\Delta H_1^\circ$  (green-triangles) for the  $\text{BeH}_2:\text{FR}$  complexes. Cyan-diamonds show the complexes with negative  $\Delta H_4^\circ$ . All values are in  $\text{kJ}\cdot\text{mol}^{-1}$  and were calculated at G4 level of theory.



Figure 4.9: Representation of the (a) FNO and (b)  $\text{BeH}_2\text{FNO}$  molecules. The most important atomic distances are shown in Å. The FNO and  $\text{BeH}_2\text{F}$ : NO geometry optimizations were performed at CASPT2//CASSCF(9,6)/cc-pVTZ and CASPT2//CASSCF(12,9)/cc-pVTZ, respectively.

The comparison of the natural BDH ( $\Delta H_3^\circ$ ) and Be-assisted BDH ( $\Delta H_4^\circ$ ) was performed considering the thermodynamic cycle for the different F-R LBs (see scheme 4.3) and table 1 from appendix B.2). The most surprising result is that while  $\Delta H_3^\circ$  is always positive,  $\Delta H_4^\circ$  is negative for highly electronegative R groups (NO, Cl,  $\text{NH}_2$ , OH and F). That is, the F-R bond dissociation becomes an *exothermic* reaction after the formation of BerBs.

The striking differences between  $\Delta H_3^\circ$  and  $\Delta H_4^\circ$  can be understood considering the Radical Stabilization Energy (RSE). This concept was introduced by Radom and coworkers in 2001 to measure the stability of radicals species after a perturbation of the system[279]. However, in this thesis the RSH instead of RSE will be used. RSH for reaction 4.3 is defined as the difference between the natural BDH ( $\Delta H_1^\circ$ ) and the Be-assisted BDH ( $\Delta H_4^\circ$ ):

$$\Delta H_3^\circ = (\text{F}\cdot + \text{R}\cdot) - \text{FR} \quad (4.3a)$$

$$\Delta H_4^\circ = (\text{BeH}_2\text{F}\cdot + \text{R}\cdot) - \text{BeH}_2:\text{FR} \quad (4.3b)$$

$$\text{RSH} = \Delta H_3^\circ - \Delta H_4^\circ = \text{BeH}_2:\text{FR} + \text{FR} - (\text{BeH}_2\text{F}\cdot + \text{F}\cdot) \quad (4.3c)$$

Figure 4.8b shows that RSH is always positive and very large for the  $\text{BeH}_2:\text{FR}$  complexes. These positive values of RSH indicate that  $\text{BeH}_2\text{F}\cdot$  is a more stable radical than  $\text{F}\cdot$ , decreasing the bond enthalpy of  $\text{BeH}_2:\text{FR}$  with respect to FR. The same figure (4.8b) compares the RSH and the BerB  $E_{\text{int}}$  ( $\Delta H_1^\circ$ ), showing two parallel curves. This is not surprising because the difference between these quantities is the enthalpy of formation of the Be radicals ( $\Delta H_2^\circ$ ), and in figure 4.8b the formation of the  $\text{BeH}_2\text{F}\cdot$  neutral radical is the only one considered.

$$\Delta H_1^\circ - \text{RSH} = (\text{BeH}_2\text{F}\cdot) - (\text{BeH}_2 + \text{F}\cdot) = \Delta H_2^\circ \quad (4.4)$$

$\Delta H_2^\circ$  for the  $\text{BeH}_2:\text{FR}$  complex only changes when the basic site is R instead of F.

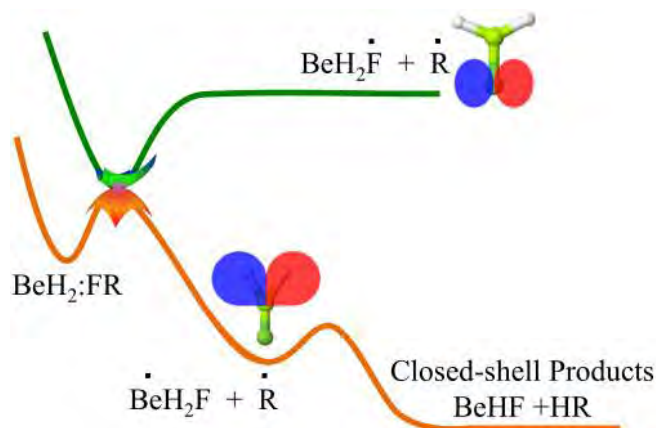
The RSH of  $\text{BeH}_2:\text{OHF}$  and  $\text{BeH}_2:\text{NH}_2\text{F}$  is almost  $200 \text{ kJ}\cdot\text{mol}^{-1}$  smaller than for  $\text{BeH}_2:\text{FR}$ , indicating that it is required much more energy to obtain  $\text{BeH}_2\text{R}\cdot$  than  $\text{BeH}_2\text{F}\cdot$ . In contrast,  $\Delta H_1^\circ$  is higher in absolute value for  $\text{BeH}_2:\text{RF}$  than for  $\text{BeH}_2:\text{FR}$  ( $\text{BeH}_2:\text{FNH}_2 = -40$  vs.  $\text{BeH}_2:\text{NH}_2\text{F} = -78$  and  $\text{BeH}_2:\text{FOH} = -38$  vs.  $\text{BeH}_2:\text{OHF} = -51$ , all values are in  $\text{kJ}\cdot\text{mol}^{-1}$ ). Therefore, the decrease in the BDEs is related to the stability of the  $\text{BeH}_2\text{Y}\cdot$  radical, rather than to the strength of the BerB.

The analysis of the electron configuration of the  $\text{BeH}_2\text{F}\cdot$  neutral radical is shown in figure S3 from appendix B.2. The product of the natural dissociation of the  $\text{F}_2$  molecule are two fluorine atoms with an electronic configuration  $[\text{He}]2s^22p^5$ . The dissociation products of the  $\text{BeH}_2:\text{FF}$  complex is the  $\cdot\text{BeH}_2\text{F}$  and  $\text{F}\cdot$  neutral radicals. The F atom in  $\cdot\text{BeH}_2\text{F}$  has a noble gas configuration  $[\text{Ne}]$  and the Single Occupied Molecular Orbital (SOMO) is localized in the  $\sigma_{\text{BeH}}$  molecular orbital. This electron migration towards the F atom highly stabilizes the  $\cdot\text{BeH}_2\text{F}$  radical. The  $\text{BeH}_2\text{F}\cdot$  excited state where F preserves the electron configuration of atomic fluorine ( $[\text{He}]2s^22p^5$ ) lies more than  $400\text{kJ}\cdot\text{mol}^{-1}$  higher in energy, which is close to the RSE calculated for the  $\text{BeH}_2:\text{FR}$  complexes.

Reaction 4.1 is exothermic for the substituents  $\text{R} = \text{F}, \text{NH}_2, \text{OH}, \text{NO}$ , and  $\text{Cl}$ . However, the spontaneity of this reaction depends on the energetic barrier associated to the crossing between the  $\cdot\text{BeH}_2\text{F}$  and the  $\text{BeH}_2\text{F}\cdot$  states. Nevertheless, there are secondary closed-shell products that are energetically more stable than the radicals,



The dissociation of the  $\text{BeH}_2:\text{F-R}$  complexes occurs via a two-step mechanism: first the radical species are formed, and second, their reorganization leads to the final closed-shell products. See scheme 4.4 for a representation of the reaction mechanism. The first height of the energetic barrier determines the spontaneity of the electron migration process from the Be moiety towards fluorine, and that of the second TS defines the lifetime of the radicals or the spontaneity of formation of the closed-shell products.



Scheme 4.4: Scheme of the Potential Energy Profile for the dissociation of  $\text{BeH}_2:\text{FR}$ . In green the formation of the  $\text{BeH}_2\text{F}\cdot + \text{R}\cdot$  radical products is represented. In orange, the formation of the  $\cdot\text{BeH}_2\text{F} + \text{R}\cdot$  radical products, finally evolving to the  $\text{HBeF} + \text{HR}$  closed-shell products.

Below, the reaction mechanism for three systems is described:

1.  $\text{BeH}_2:\text{FF}$  is the system with the more negative bond enthalpy.
2. The comparison between the previous system and  $\text{BeCl}_2:\text{FF}$  allows studying the effect of the acidity of the Be monomer in the reaction mechanism.

3. The stability of leaving  $R\cdot$  is studied by comparing the  $\text{NO}\cdot$  and the  $\text{F}\cdot$  radicals, considering  $\text{BeH}_2:\text{FNO}$ . This comparison is very relevant because  $\text{NO}\cdot$  is a rather stable radical.

The reaction profiles for  $\text{BeH}_2:\text{FF}$  and  $\text{BeCl}_2:\text{FF}$  can be found in appendix B.2 (figures 2 and S5), and the most relevant structures are collected in figure 4.10. The reaction path is similar for both complexes. There is a first step in which Be intercalates between the F atoms forming a three-membered ring and assisting the rupture of the F-F bond. The energetic barriers associated to the first step are below the Zero Point Energy (ZPE) of both,  $\text{BeH}_2:\text{FF}$  and  $\text{BeCl}_2:\text{FF}$ , and hence the radical species are expected to be produced spontaneously. The unpaired electrons are located over the  $\text{Be}(\text{Y}'_1)_2$  group and the leaving F atom. The main difference between the two complexes is that for  $\text{BeCl}_2:\text{FF}$ , the radical complex is an intermediate species, while for  $\text{BeH}_2:\text{FF}$  the radical evolves spontaneously without a second TS to the final closed-shell products. The second energetic barrier for  $\text{BeCl}_2:\text{FF}$  was estimated using a Linier Interpolation in Internal Coordinates (LIIC) from the intermediary to the closed-shell products. The estimated value which corresponds to an upper bound of the real barrier is predicted to be higher than the ZPE of the intermediary, indicating that this is not necessarily a spontaneous process. As already stated above,  $\text{BeH}_2:\text{FF}$  is expected to dissociate into the closed-shell final products in a spontaneous manner, since no energetic barriers were found to separate neither the reactants from the intermediates, nor the latter from the final products. The increase in the acidity of  $\text{Be}(\text{Y}'_1)_2$  was however found to increase the barrier separating the radicals from the closed shell products, suggesting that the final product reorganization might not be spontaneous in the  $\text{BeCl}_2:\text{FF}$  complex. See figures A.2 and A.3 in the electronic version of this thesis for animations of the reaction profiles.

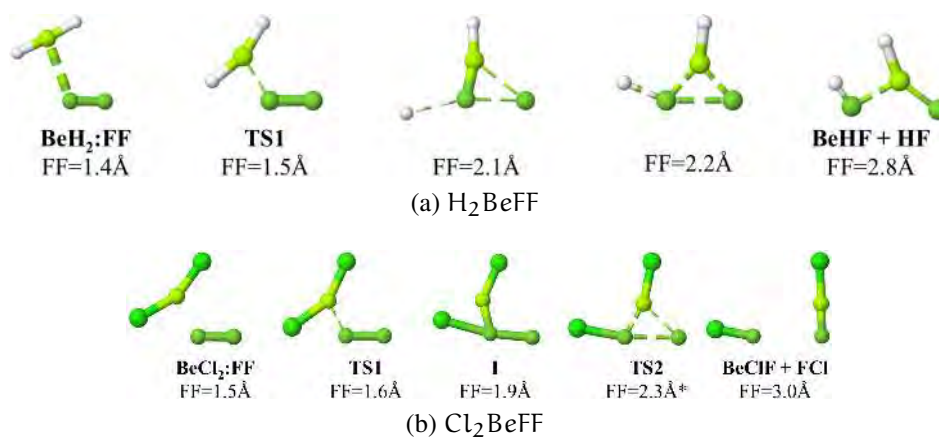


Figure 4.10: Relevant molecular structures from the dissociation profile of the  $\text{Be}(\text{Y}'_1)_2:\text{FF}$  complexes, with  $\text{Y}'_1$  equal to (a) H and (b) Cl. The potential energy profiles were calculated at CASPT2//CASSCF(14,9)/cc-TZVP level of theory and all values are in Å.

It was not possible to locate the second TS associated to the reaction mechanism of the  $\text{BeCl}_2:\text{FF}$  at CASPT2/CASSCF level of theory, but it was at CC2 and MP2. The optimized geometries were found to be similar to the ones predicted using the LIIC method, see figure 4.11 for a comparison of geometries and  $\Delta E_{\text{TS2}}^\ddagger$ . According to the LIIC dissociation path in

figure S5 from appendix B.2, the profile for this TS has a narrow shape along the reaction coordinate; this makes difficult to locate the second TS and becomes even more complicated when multi-reference optimization algorithms are used.

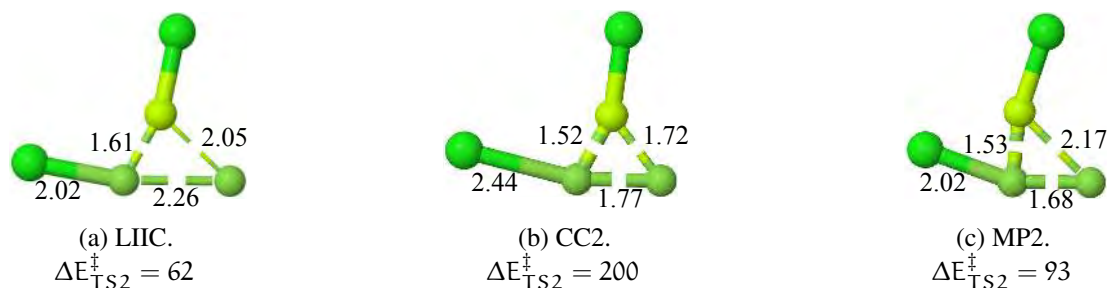


Figure 4.11: Comparison of the geometries and  $\Delta E_{TS2}^{\ddagger}$  for the TS2 in the dissociation mechanism of the  $\text{BeCl}_2:\text{FF}$  complex. The geometrical parameters were calculated considering a cc-pVTZ basis set and all values are in Å.  $\Delta E_{TS2}^{\ddagger}$  were calculated at CASPT2//CASSCF(14,9)/cc-pVTZ//method/cc-pVTZ, over the geometries determined with method= LIIC, CC2 and MP2. All values are in  $\text{kJ}\cdot\text{mol}^{-1}$ .

Figure S6 in appendix B.2 shows the reaction mechanism for the  $\text{BeH}_2:\text{FNO}$  system and the most relevant geometries are in figure 4.12. The ground state of this system has already a partial radical character, with the unpaired electrons located on the BeH and the NO moieties. Considering scheme 4.4, the first local minimum of this complexes does not exist and the TS to reach the closed-shell products was found to be below the ZPE of the complex. Therefore,  $\text{HBeF} + \text{HON}$  are produced spontaneously, and subsequently evolve to the  $\text{HBeF} + \text{HNO}$  final products. See figure A.4 in the electronic version of this thesis for an animation of the reaction profile.

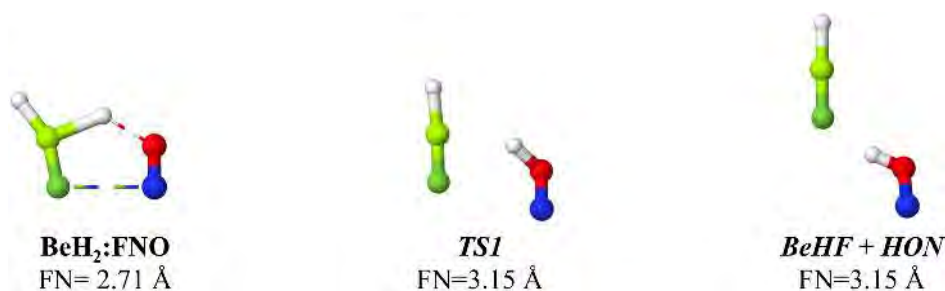


Figure 4.12: Relevant molecular structures from the dissociation profile along the  $\text{BeH}_2:\text{FNO}$  complex. The reaction profiles were calculated at CASPT2//CASSCF(12,9)/cc-pVTZ level of theory and all values are in Å.

The heterolytic dissociation yielding ion-pair products was also considered. Table 2 from appendix B.2 shows the dissociation enthalpies for all possible reactions for the  $\text{BeH}_2:\text{FCl}$  complex, and although the  $\text{BerB}$  decreases  $\Delta H$ , yet the heterolytic dissociations are endothermic.

## 4.1.5 Intramolecular Beryllium Bonds: Resonance Assisted Interactions

The resonance phenomena in Hydrogen Bonds (HB) was introduced in section 3.2.1.1. In this thesis we studied an analogue interaction, but by replacing the H atom by the  $\text{BeY}'_1$  group in malonaldehyde and tropolone derivatives (see scheme 4.1c and appendix B.3). Similarly to Intramolecular Hydrogen Bonds (IHB), IBerBs are stronger in unsaturated systems. The strongest IBerB in unsaturated systems is reflected by a larger value of  $\rho$  at the  $\text{BCP}_{\text{BeY}}$ , compared to the saturated derivatives. For the unsaturated complexes,  $\rho$  is of the same order as covalent interactions ( $0.1 \text{ au}$ ), while for their analogous saturated derivatives the values are around  $0.04\text{-}0.06 \text{ au}$ . The strength of IBerBs was estimated by comparing the relative stability of closed and open structures, with  $E_{\text{int}}$  spreading along a broad interval between  $40$  and  $160 \text{ kJ}\cdot\text{mol}^{-1}$ . Moreover, in agreement with the QTAIM analysis, the IBerB interaction energies for the unsaturated derivatives are up to twice higher than the saturated ones (see figures 1-4 and 6 from appendix B.3). The strong non-covalent interaction in the closed structures was analyzed considering: (1) the resonance assistance phenomena, (2) the effect of the  $\sigma$  skeleton and (3) the acidity and the basicity of the Be- donors and acceptors, respectively.

The decrease in the grade of unsaturation weakens the IBerB, but the analysis of the contributing resonance structures of the unsaturated system does not show any structure where the Be-Y group participates. This indicates that IBerBs are not stabilized by the resonance of the system (see schemes 4 and 5 from appendix B.3). The proton ( $\text{H}^+ \text{A}$ ) and hydride ( $\text{H}^- \text{A}$ ) affinities of the closed structures are shown in figure 4.13.

$$\text{H}^+ \text{A} = [\text{RC} = \text{Y} + \text{H}^+] - [\text{RC} = \text{YH}]^+ \quad (4.6a)$$

$$\text{H}^- \text{A} = [\text{RBeHH}]^- - [\text{RBeH} + \text{H}^-] \quad (4.6b)$$

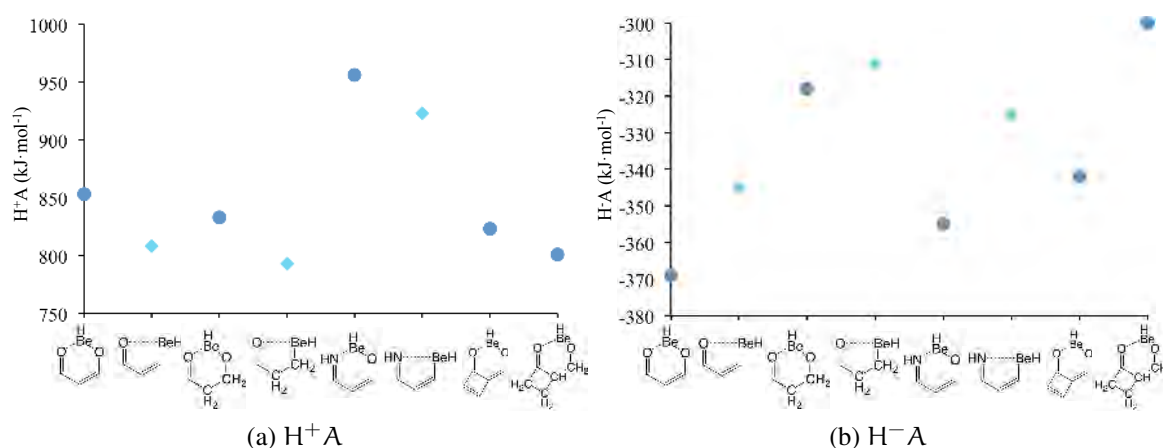
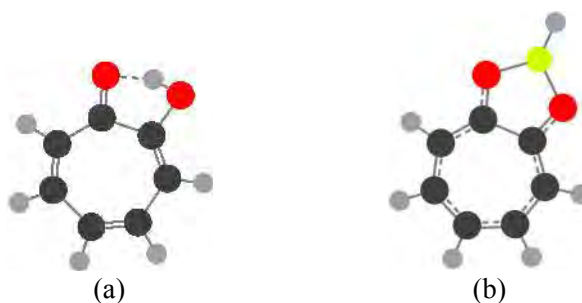


Figure 4.13: (a) Proton ( $\text{H}^+ \text{A}$ ) and (b) hydride ( $\text{H}^- \text{A}$ ) affinities of malonaldehyde derivatives. Blue-circles correspond to the unsaturated structures and cyan-diamonds to the saturated analogues. All values are in  $\text{kJ}\cdot\text{mol}^{-1}$  and were calculated at G4 level of theory.

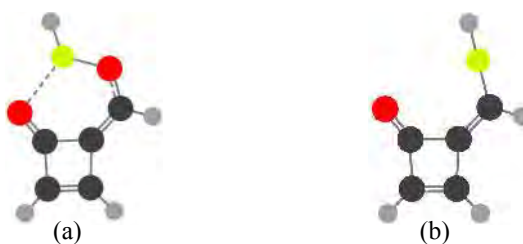
Figure 4.13 shows that the unsaturated systems have higher  $H^+A$  and lower  $H^-A$  with respect to their saturated counterparts. This indicates that the rise in the strength of the IBerB is due to an increase of the basicity of Y and the acidity of BeH, and not to resonance assistance. Consistently, when Y is exchanged from O to NH, the higher basicity of the amide group enhances the strength of the BerB. Moreover, when BeH is attached to an alkyl rather than the carbonyl group, the acidity of the Be derivative decreases and also the strength of the non-covalent interaction.

The results obtained show that the resonance structures do stabilize the systems. But contrary to what has been proposed, the resonance interaction is enhanced by the formation of IBerBs. Tropolone derivatives are a good example of this cooperativity. The IHB in tropolone is not strong enough to delocalize the  $\pi$  cloud in the ring as it is represented in scheme 4.5a, the ring shows alternating double bonds. The increase of the strength of the intramolecular interaction after substituting a H by BeH reorganizes the electron density, and the seven-membered ring has almost an aromatic character. See appendix B.3 for a description of other tropolone derivatives.



Scheme 4.5: (a) IHB and (b) IBerB in tropolone derivatives.

The effect of the flexibility of the  $\sigma$  skeleton was investigated by attaching R to a four-membered ring, finding that IBerBs becomes weaker for more rigid skeletons. Figure 4.13 shows that constrained  $\sigma$  skeletons decrease the acidity of BeH and the basicity of the carbonyl groups. Indeed, there is no formation of an IBerB, when BeH and R are attached to an alkyl group and a to a four membered ring, respectively (see scheme 4.6b). In general, therefore, IBerB as their analogous IHB are stronger because the resonance enhances the acidity and basicity of the Be-donor and acceptors, respectively, but not due to the participation of the non-covalent interactions in the resonance structures.



Scheme 4.6: (Z)-4-(hydroxymethylene)cyclobut-2-enone derivatives. (a)  $LA=ROBeH$  and (b)  $LA=RCHBeH$ .

Figure 4.14 describes the relation between the strength of IBeRBs and  $H^+A$  and  $H^-A$ . The first conspicuous result is that while there is almost a linear correlation between  $H^-A$  and  $E_{int}$  (figure 4.14b), there is not such a relation between  $H^+A$  and  $E_{int}$  (figure 4.14a). According to this figure (4.14), the stronger IBeRBs are not formed by a combination of the stronger LA and LB. For LA equal OBeH group, the stronger Be: Y interaction takes places with the stronger LB (Y = NH) and the second most acidic OBeH group. On the other hand, for LA equal CBeH group, the stronger IBeRB occurs with the most acid CBeH group and the second most basic group (Y=O). The lack of correlation between  $E_{int}$  and  $H^+A$  and  $H^-A$  is attributed to the fact that the LA and the LB are part of the same system, influencing each other.

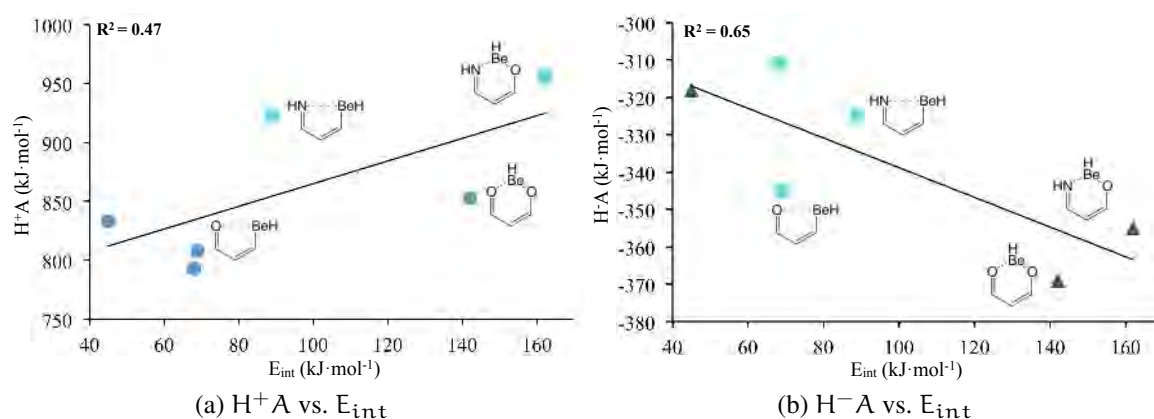


Figure 4.14: Linear correlation between (a)  $H^+A$ , (b)  $H^-A$  and  $E_{int}$ . Cyan-square symbols represent in (a) the complexes formed with the strongest LB (RNH), and in (b) the complexes formed with the weaker LA (CBeH). Energetics were calculated at G4 level of theory and are in  $\text{kJ}\cdot\text{mol}^{-1}$ .

#### 4.1.6 Conclusions

*Beryllium bonds can be used to modify important properties of a system: they generate a  $\sigma_{hole}$  in fluorine derivatives and they induce the spontaneous formation of radical species. The analysis of IBeRBs is another proof that the strongest non-covalent bonds in unsaturated systems are due to an enhancement of the LA and LB strength, and not to assistance resonance phenomena.*

Inter and Intramolecular BeRBs are strong non-covalent interactions caused by a charge transfer from the lone pairs of the LB towards the  $p_{Be}$  orbitals, showing interaction energies up to  $150 \text{ kJ}\cdot\text{mol}^{-1}$ . The nature of this interaction is electrostatic with a non-negligible covalent character. The formation of this non-covalent interaction leads to geometric deformations in both the LA and the LB, the  $Y'_1BeY'_2$  angle is no longer linear and the variations in the bond lengths of the LB depends on the nature of the base. Finally, it is possible to modulate the strength of the BeRB by increasing the acidity of the LA or the basicity of the LB.



The increase of the electronegativity of the Be-acceptor in the LB induces the generation of  $\sigma_{\text{hole}}$  in fluorine, otherwise inexistent. The presence of a  $\sigma_{\text{hole}}$  in the F atom allows the formation of XBs. The strength of both the  $\sigma_{\text{hole}}$  and XBs can be modulated by increasing the strength of BerBs or the acidity of the fluorine substituent. Non-covalent interactions with borane derivatives also produce a  $\sigma_{\text{hole}}$  in fluorine, but in this case the  $\sigma_{\text{hole}}$  were found to be less deeper compared to beryllium derivatives.

The electronic rearrangement originated by the creation of BerBs can affect the bond strength of the LB (weakening), and surprisingly in some cases, homolytic bond cleavage reactions can become exothermic. The dramatic reduction of the bond enthalpies is due to the stabilization of the radical products, where the SOMO is not longer located in the LB but at the Be moiety. The dissociation profiles do not show energetic barriers for the formation of the radical species, which can further evolve, sometimes spontaneously to closed-shell products.

IBerBs in unsaturated systems were found to be stronger than in their saturated analogues. The strength of this interaction is due to an increase of both the acidity and basicity of the LA and LB, respectively. These findings do not support the concept of RAHB, actually, it is the non-covalent interaction what enhances the resonance interaction and not the opposite.

### Conclusiones

*Los enlaces de Berilio (BerBs, por sus siglas en inglés Beryllium Bonds) pueden ser utilizados para modificar propiedades importantes de un sistema: estos enlaces generan un  $\sigma_{\text{agujero}}$  en compuestos de flúor e inducen la formación espontánea de especies radicalarias. Nuestro estudio sobre enlaces de Berilio Intramoleculares (IBerB, por sus siglas en inglés Intramolecular Beryllium Bonds) ratifica que las interacciones no-covalentes son más fuertes en sistemas insaturados debido a un aumento de acidez del Ácido de Lewis (AL) y de basicidad de la Base de Lewis (BL), y no como ha sido propuesto anteriormente, ocasionado por el fenómeno de asistencia por resonancia.*

Los BerBs inter- e intra-moleculares son interacciones no-covalentes muy fuertes originadas por la transferencia de carga del par de electrones no compartidos (LP, por sus siglas en inglés Lone Pairs) de la BL hacia los orbitales  $p_{\text{Be}}$ , presentando energías de interacción que alcanzan los  $150 \text{ kJ}\cdot\text{mol}^{-1}$ . La naturaleza de este tipo de enlace es electrostática, sin embargo, también tienen un componente covalente. La formación de BerBs deforma las geometrías tanto del AL como de la BL, el ángulo  $Y'_1\text{Be}Y'_2$  ya no es lineal y las variaciones en la BL dependen de la naturaleza de la base. Finalmente, es posible controlar la fortaleza de los BerBs aumentando la acidez del AL o la basicidad de la BL.

La formación de BerBs aumenta la electronegatividad del átomo aceptor de Be en la BL, permitiendo formar un  $\sigma_{\text{agujero}}$  en el átomo de flúor, lo cual sería imposible sin la cooperación de esta interacción no-covalente. Por lo tanto, es posible formar enlaces de halógenos (XB, por sus siglas en inglés Halogen Bonds) en complejos de F asistidos por BerBs. La

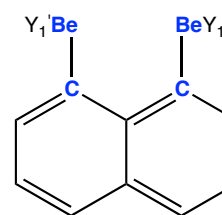
fortaleza de los XBs puede ser controlada considerando la fuerza del BerB o la acidez del derivado de F. Las interacciones no-covalentes con compuestos derivados de borano también permiten generar un  $\sigma_{\text{agujero}}$  en el átomo de F, sin embargo, este agujero es menos profundo que el formado con derivados de Be.

La formación de BerBs produce una reorganización de la estructura electrónica de la BL, lo cual debilita la fuerza de sus enlaces, y sorprendentemente, en algunos compuesto la disociación homolítica se convierte en un proceso exotérmico. La extraordinaria disminución en las entalpías de enlace se debe a la gran estabilización de los productos radicalarios, en los cuales el Orbital Molecular Ocupado por un Solo electrón (SOMO, por sus siglas en inglés Singly Occupied Molecular Orbital) se encuentra localizado en el fragmento de Be y no en la BL. De acuerdo con los perfiles de disociación, no existen barreras energéticas en la formación de especies radicalarias asistidas por Be. Y en algunos sistemas, estas especies radicalarias también evoluciona espontáneamente a productos de capa-cerrada.

Los IBerBs son más fuertes en sistemas insaturados en comparación a sus compuestos saturados análogos. La mayor fortaleza de enlace en los sistemas insaturados se debe a un aumento de acidez y basicidad del AL y la BL, respectivamente. Estos resultados no respaldan el concepto de Enlaces de Hidrógeno Asistidos por Resonancia (RAHB, por sus siglas en inglés Resonance Assisted Hydrogen Bond), incluso, hemos encontrado que es la interacción no-covalente lo que aumenta la interacción por resonancia y no lo contrario.

## 4.2 ONE-ELECTRON Be BONDS

One-electron bonds can be found in anions formed by electron attachment or in cations formed by electron loss. The incredible characteristics of this type of interactions is that they do not follow the classical electron pair description of the chemical bond introduced by Lewis and supported by Pauling. However, it was Pauling himself who proposed one-electron bonds in 1931, in order to explain the bonding properties in several types of molecules, among them the  $B_2H_6$  system [165]. The one-electron B-B bond was experimentally described by Electron Paramagnetic Resonance (EPR) [280] and X-ray crystallography [281], and theoretically, has been characterized considering wave function analysis [282]. The formation of the B-B one-electron bond has been attributed to the B low-lying p orbitals of the atom. The p orbitals of the Be atom are also low lying energy orbitals. Thus, we can defined *one-electron Be bonds* as the interactions following electron attachment in which the unpaired electron is between the Be moieties. One-electron Be-Be atoms are studied in this thesis by considering the anions of 1,8-diBeY<sub>1</sub>'naphthalene, with Y<sub>1</sub>' = H, F, Cl, Br, CH<sub>3</sub>, NH<sub>2</sub>, OH, CF<sub>3</sub>, C(CF<sub>3</sub>)<sub>3</sub>, NF<sub>2</sub>, OF, CN, NO<sub>2</sub>, SOH, t-Bu, Ph. See scheme 4.7.



Scheme 4.7: 1,8-diBeY<sub>1</sub>'naphthalene derivatives studied in this thesis.

#### 4.2.1 Methodology

The neutral 1,8-diBeY<sub>1</sub>' naphthalene compounds are closed-shell systems that can be correctly described using single-reference methodologies, but this is not the case of its anions. The multi-reference character of the radical anions was tested for a selected set of complexes, by comparing B3LYP and CASSCF(5,6) geometries combined with the 6-31+G(d,p) basis set. The (5,6) AS was selected to include the valence orbitals of the Be atoms plus the unpaired electron. The differences were found to be of the order of 0.05 Å for the Be-Be, Be-Y<sub>1</sub>' and Be-C bond distances (see figure S2 from appendix B.4). The B3LYP/6-31+G(d,p) geometries of the disubstituted naphthalene derivatives were assessed by considering CCSD(T)/cc-pVDZ calculations, being negligible the differences between the geometries obtained with both methods (see figure S1 from appendix B.4). The effect of the size of the basis set was also studied. The geometries were optimized at CC2/cc-pVDZ and CC2/cc-pVTZ level of theory (see figure S3 from appendix B.4). According to our results, there is a good agreement between these two methods. Then, the optimization of the neutral and anion species of the disubstituted naphthalene derivatives was performed with the B3LYP/6-31+G(d,p) method. The DFT calculations were performed with G09, the CCSD(T) with MOLPRO 2015, and the CC2 optimizations with the TURBOMOLE program [283].

The energetics were calculated enhancing the flexibility of the basis set up to the 6-311+G(3df,2p). The nature of the one-electron Be-Be bond was described by using three different approaches: QTAIM, ELF and NBO. The strength of the interaction was quantified using EDA as implemented in the ADF program [284–286]. The QTAIM, ELF and NBO analyses were carried out using the same programs described in section 4.1.1.

#### 4.2.2 Properties of the one-electron Be-Be bond

All possible isomers of the neutral and anionic structures of beryllium di-substituted naphthalenes derivatives were explored. The most stable structures are those where the Be, C, C, Be atoms (highlighted in blue in scheme 4.7) are in the same plane (see appendix B.4). The most dramatic change going from the neutral to the anionic system is the decrease of the Be-Be bond distance and the Y<sub>1</sub>'-Be-C angle (see figure 4.15b). These variations ( $\Delta_{\text{Be-Be}} = \text{Be-Be}_{\text{neutral}} - \text{Be-Be}_{\text{anion}}$ ) are independent of the Y<sub>1</sub>' substituent, because the Be-Be bond distance in all the anions studied in this thesis is equal to 2.3 Å. Therefore, the wide range of  $\Delta_{\text{Be-Be}}$  (0.5 - 1.0 Å) is ascribed to the geometries of the neutral complexes. Notice that the Be-Be bond distance in (1,8-diBeY<sub>1</sub>' naphthalene)<sup>-</sup> compounds is 0.15 Å shorter than in the free Be<sub>2</sub> molecule, indicating a stronger Be-Be bond in the anions than in the isolated Be<sub>2</sub> molecule.

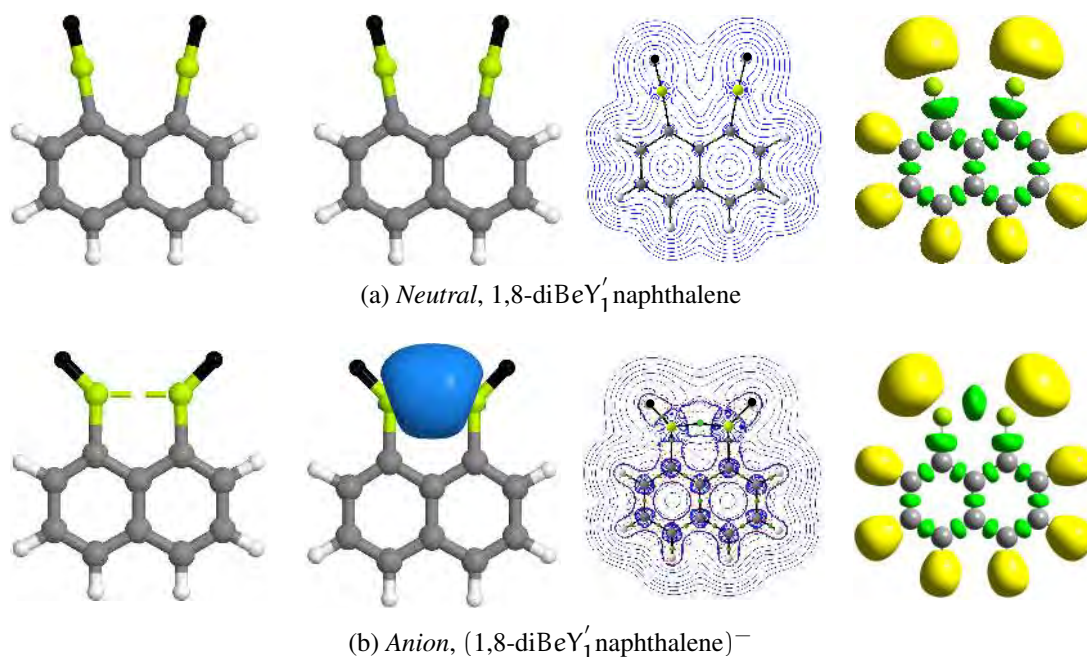


Figure 4.15: Wave function analysis for (a) the 1,8-diBeY<sub>1</sub>'naphthalene and (b) [1,8-diBeY<sub>1</sub>'naphthalene]<sup>-</sup> complexes. The first column shows the geometry with Y<sub>1</sub>' groups highlighted in black. Second column shows the one-electron Be-Be NBO orbital. Third column shows the molecular graph and  $\nabla^2\rho$  contour map, the BCPs are represented with green dots, the blue lines denote regions where  $\nabla^2\rho$  is positive and red lines where it is negative. Fourth column shows the ELF plots, yellow lobes correspond to disynaptic basins involving hydrogen atoms, green lobes correspond to disynaptic basins between heavy atoms and red basins denote monosynaptic basins associated with lone-pairs. All calculations were performed at B3LYP/6-31+G(d,p) level of theory.

Figure 4.16 summarizes  $\Delta_{\text{Be-Be}}$  for all Y<sub>1</sub>'Be substituents considered in this work. The effect of the acidity of the Y<sub>1</sub>'Be group in the neutral complexes is opposite than for BerBs. The Be-Be bond in the neutral 1,8-diBeY<sub>1</sub>'naphthalene compounds is shorter ( $\Delta_{\text{Be-Be}}$  is smaller) for the complexes where Y<sub>1</sub>' are electron donor groups. For example, the Be-Be bond length is shorter for 1,8-diBeHnaphthalene than for 1,8-diBeClnaphthalene derivatives, while for BeY<sub>1</sub>'Y<sub>2</sub>: YR (BerBs), the Be: Y bond is shorter for the beryllium halides. BerBs are interactions between an electron-deficient and an electron-donor group, while Be-Be interactions take place between two electron-deficient atoms. Steric effects have also an important role in the trend of  $\Delta_{\text{Be-Be}}$  in figure 4.16, while in neutral compounds bulky Y<sub>1</sub>' groups lead to rather long Be-Be distances, in the anions Be-Be bond distances are independent of Y<sub>1</sub>'. For instance,  $\Delta_{\text{Be-Be}}$  is twice for C(CF<sub>3</sub>)<sub>3</sub> than for CF<sub>3</sub>.

The short and constant values of the Be-Be bond distances in the anions is ascribed to the formation of an one-electron Be-Be bond. This extra electron instead of being delocalized around the aromatic naphthalene rings is mainly localized between the BeY<sub>1</sub>' groups, compensating the electron deficiency of the Be moieties in the neutral compounds. The wave function analysis confirms the formation of this special Be-Be bond in (1,8-diBeY<sub>1</sub>'naphthalene)<sup>-</sup>

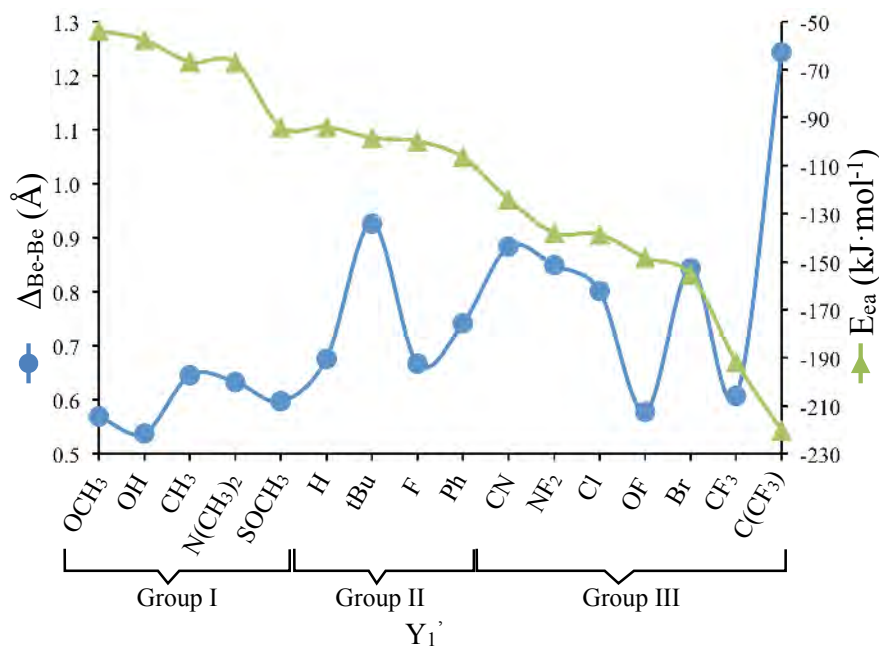


Figure 4.16:  $\Delta\text{Be-Be}$  (blue-circles) and Electron Affinities ( $E_{ea}$ , green-triangles) for 1,8-diBeY<sub>1</sub>' naphthalene complexes.  $\Delta\text{Be-Be}$  are in Å. Geometry optimization and energetics were computed at B3LYP/6-31+G(d,p) and at B3LYP/6-311G(3df,2p) level of theory, respectively.

compounds. The QTAIM analysis shows a Be-Be BCP in the anions, at difference with the analysis of the neutrals. The values of  $\rho$  are around of 0.03au and according to the negative values of  $\nabla^2\rho$ , the interaction has a covalent character. The NBO analysis localizes singly occupied  $\sigma$  bonds formed mainly by combinations of the  $2s_{\text{Be}}$  Atomic Orbitals (AO), which does not exist in the neutral complexes (see figure 4.15). ELF calculations on the neutral species do not locate disynaptic basins between the Be atom. However, the anions show  $V(\text{Be}, \text{Be})$  basins with populations close to  $1e^-$  (see figure 4.15). The energetic properties are in agreement with the wave function analysis. The Localized Molecular Orbital Energy Decomposition Analysis (LMOEDA) predicts a Be-Be bond with a strength of  $74\text{kJ}\cdot\text{mol}^{-1}$  and with a maximum contribution from the  $\Delta_{\text{orb}}$  partition. This ratifies the covalent character of the interaction. Isodesmic reactions find analogous values for  $E_{\text{int}}$  (see appendix B.5). The strength of the Be-Be interaction in the  $(1,8\text{-diBeY}_1'\text{naphthalene})^-$  derivatives was estimated to be around  $80\text{kJ}\cdot\text{mol}^{-1}$ , which is almost eight times stronger than for free  $\text{Be}_2$  molecule. All in all, the geometrical, bonding and energetic analyses recognize the formation of a one-electron Be-Be in  $(1,8\text{-diBeY}_1'\text{naphthalene})^-$  derivatives.

The formation of the one-electron Be-Be bond is due to an increase in the electron affinity ( $E_{ea}$ ) of the anion; while for naphthalene  $E_{ea}$  is positive ( $7.5\text{kJ}\cdot\text{mol}^{-1}$ ) for the 1,8-diBeY<sub>1</sub>' naphthalene derivatives these values are negative and lie within a wide range depending on the electronic nature Y<sub>1</sub>' (see figure 4.16). Y<sub>1</sub>' substituent can be classified into three different categories: (I) Y<sub>1</sub>' is an electron donor group which decreases the acidity of BeY<sub>1</sub>', thus making  $E_{ea}$  more positive, (III) Y<sub>1</sub>' is an electron withdrawing group leading to

the opposite effect to group I, and in the middle (II) where there is a mixture between substituents classically classified as group I or III. The variation of  $E_{ea}$  in this group is small ( $\sim 2\text{kJ}\cdot\text{mol}^{-1}$ ) what translates into an almost a horizontal line in graph 4.16. According to the  $Y'_1$  NBO charges, the  $\text{Be}Y'_1$  substituents in group-II become slightly more negative when are attached to the 1,8-di $\text{Be}Y'_1$ naphthalene complexes, indicating that they behave as weak electron withdrawing groups. Figure 4.16 does not show a linear correlation between  $\Delta_{\text{Be-Be}}$  and  $E_{ea}$ . As explained above, the bond distance does not depend exclusively on the nature of  $Y'_1$ . Consider for instance the steric effect of  $Y'_1$  in the neutral complexes.  $E_{ea}$  is only 12% more negative in  $\text{C}(\text{CF}_3)_3$  compared to  $\text{CF}_3$ , while the bond distance is twice as large for the  $\text{C}(\text{CF}_3)_3$  derivatives than in  $\text{CF}_3$  ones.

### 4.2.3 Anion Sponges

The ability to accept and extra electron between the Be atoms suggests that Beryllium disubstituted naphthalene derivatives could behave as anion *sponges*, very much as amine disubstituted naphthalene derivatives behave as proton sponges [287].

The *proton sponge* concept become popular in 1988 following the remarkable review from Staab and Saupe. This experimental study explained the high basicity of these complexes based on the *cooperative spatial interactions between reactive structural elements which can lead to unusual and gradually varying properties which could not be expected from an isolated treatment of the various functional groups*[67]. The variation of the pKa was evaluated over the influence of: steric effects, the size of the aromatic rings, the electronegativity of the amines, and others, finding pKa values in a wide range between 4.61 up to 16.3 (see tables 1 and 3 from reference [67]). From a theoretical point of view, Elguero and coworkers explained the exacerbated basicity of amine substituted naphthalene compounds considering three aspects: (1) the decrease of the repulsion of the N lone pairs that occurs after protonation, (2) the stability induced by the N:  $\text{H}^+$ : N intramolecular HB, and (3) the reduction of steric repulsion[288, 289]. Other experimental and theoretical studies have shown to be in agreement with these results [289–292].

The geometrical and wave function analysis of the complexes formed between 1,8-di $\text{Be}Y'_1$ -naphthalene derivatives and common anions can be found in appendix B.5 and are represented in figure 4.17. The most stable complexes are those where the anion is located between the Be atoms. The NBO analysis describes the interaction as a charge transfer from the  $\text{LP}_{\text{L}^-}$  towards the  $\text{p}_{\text{Be}}$  AO. The QTAIM method locates a  $\text{BCP}_{\text{BeL}^-}$  with values of  $\rho$  of the order of  $0.01\text{au}$ , but the sign of  $\nabla^2\rho$  is different depending on the complexes, for some of them  $\nabla^2\rho$  was found to be positive and for others negative. The ELF analysis finds a  $V(\text{L},\text{B})$  disynaptic basin with populations higher than  $1.5e^-$ . These data demonstrate that the interaction between the Be atoms and the anions has similarities with BerBs. It is a weak electrostatic interaction that can be increased by the electronegative character of  $Y'_1$  and the basicity of  $\text{L}^-$ , which also increases the covalent character (negative  $\nabla^2\rho$ ).

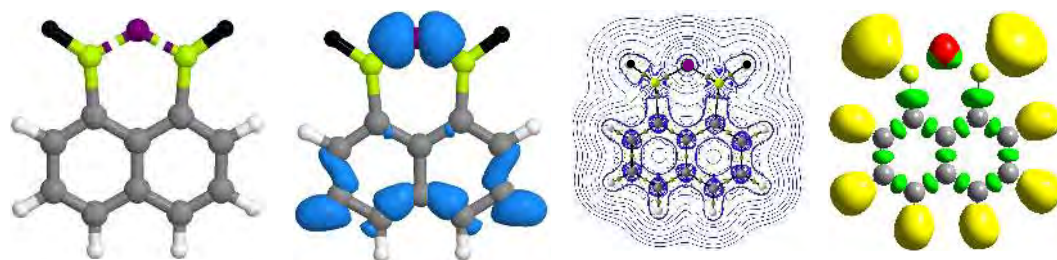


Figure 4.17: Wave function analysis for the  $[L: 1,8\text{-diBeY}'_1\text{naphthalene}]^-$  complexes. The L anion is shown in purple. Same conventions as in figure 4.15 page 129.

There is not a linear relation between the anion affinities ( $E_{\text{L}}^-$ ) of the  $(L: 1,8\text{-diBeY}'_1\text{naphthalene})^-$  complex and their Be-Be bond distances, neither for different  $Y'_1$  substituents (figure 4.18b) or L anions (figure 4.18a). This in agreement with the trends followed by  $E_{\text{ea}}$  or the pKa for the  $1,8\text{-diBeY}'_1\text{naphthalene}$  neutral complexes and the amine substituted naphthalenes [67], respectively.

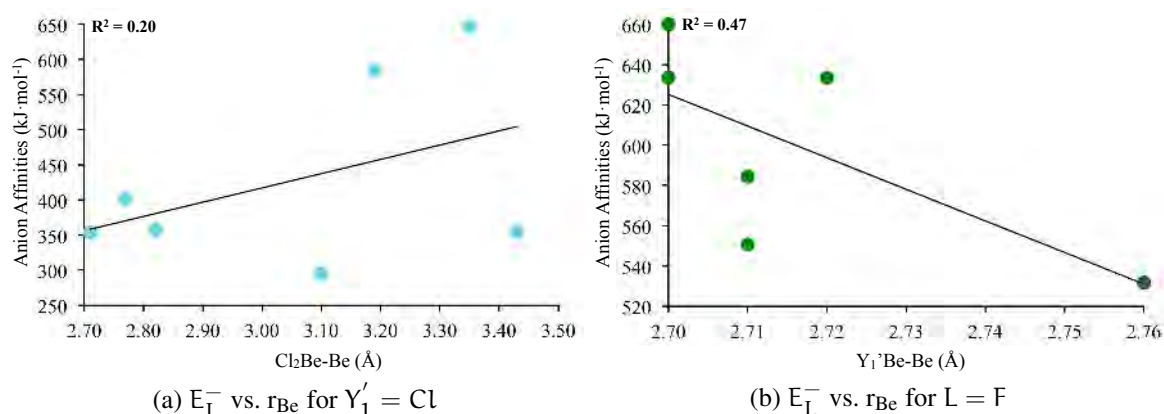


Figure 4.18: Linear correlation between  $E_{\text{L}}^-$  and Be-Be bond distances ( $r_{\text{Be}}$ ) for (a)  $[L: 1,8\text{-diBeClnaphthalene}]^-$  complexes, with  $L = \text{Br}^-, \text{CN}^-, \text{Cl}^-, \text{F}^-, \text{NO}_2^-, \text{NO}_3^-$  and  $\text{SO}_4^{2-}$ . (b)  $[F: 1,8\text{-diBeY}'_1\text{naphthalene}]^-$  complexes, with  $Y'_1 = \text{H}, \text{F}, \text{Cl}, \text{CN}, \text{CF}_3$  and  $\text{C}(\text{CF}_3)_3$ . Be-Be bond distances are in Å and were calculated at B3LYP/6-31+G(d,p) level of theory.  $E_{\text{L}}^-$  are in  $\text{kJ}\cdot\text{mol}^{-1}$  and were calculated at B3LYP/6-311G(3df,2p) level of theory.

The anion affinities of  $1,8\text{-diBeY}'_1\text{naphthalene}$  complexes are shown in figure 4.19.  $E_{\text{L}}^-$  increase with the proton affinities of the L anion and with the  $Y'_1$  substituents electronegativity. Therefore, the highest anion affinity was found for the  $[1,8\text{-diBeClnaphthalene}:\text{SO}_4]^{2-}$  and the lowest for the  $[1,8\text{-diBeHnaphthalene}:\text{Br}]^-$  complexes. The values shown in this figure are among the largest anion affinities reported so far in the literature for single neutral molecules [293–300].

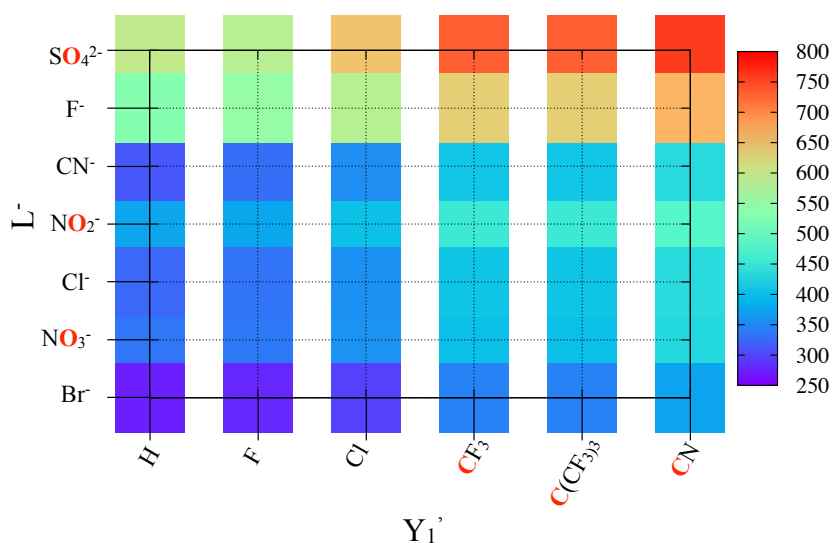


Figure 4.19: Anion affinities for  $[L: 1,8\text{-diBeY}'_1\text{naphthalene}]^-$  complexes.  $E_L^-$  are in  $\text{kJ}\cdot\text{mol}^{-1}$  and were calculated at B3LYP/6-311G(3df,2p) level of theory. The atoms interacting with Be are highlighted in red.

#### 4.2.4 Conclusions

*Beryllium naphthalene derivatives show negative electron affinities that induces the formation of one-electron Be bonds after electron attachment. In addition, these systems behave as what we have named anion sponges, holding among the largest anion affinities for neutral compounds reported so far in the literature.*

Electron attachment of beryllium naphthalene compounds is an exothermic reaction due to the electron deficiency of Be derivatives. The extra electron is localized between the Be atoms, forming a one-electron Be-Be bond. The wave function analysis describes this bond as a strong covalent interaction.

Beryllium naphthalene complexes behave as anion sponges due to the high electron affinity of the beryllium fragments. The interaction between  $\text{BeY}'_1$  and the anion is explained by a charge transfer from the  $\text{LP}_{L^-}$  towards the  $\text{p}_{\text{Be}}$ , sharing characteristics with BerBs. The anion affinities are in the range between  $250 - 800 \text{ kJ}\cdot\text{mol}^{-1}$ , depending on the acidity of the Be moiety or the basicity of the anion. The high anion affinities of  $1,8\text{-diBeY}'_1$  naphthalene derivatives open the possibility to apply these complexes as anion receptors and sensors, especially in the development of new electronic devices.

#### Conclusiones

*Las afinidades electrónicas de los derivados de Berilio-naftaleno son negativas, de tal manera que es posible formar enlaces Be-Be de un-electrón. Además, estos complejos se compor-*



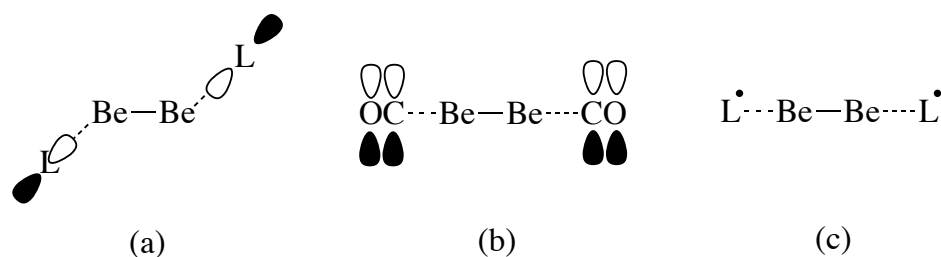
*tan como esponjas de aniones, cuyas afinidades aniónicas se encuentran entre las mayores reportadas en la literatura para complejos neutros.*

La formación de los aniones de los derivados de Berilio-naftaleno es una reacción exotérmica debido a la deficiencia electrónica de los fragmentos de Be. El electrón extra se encuentra localizado entre los átomos de Be, formando un enlace Be-Be de un-electrón. De acuerdo con los análisis de la función de onda, la naturaleza de este enlace es covalente.

Los complejos de Berilio-naftaleno se comportan como esponjas de aniones debido a la alta afinidad electrónica de los fragmentos de Be. La interacción entre  $\text{BeY}'_1$  y diferentes tipos de aniones (L) ha sido explicada considerando una transferencia de carga desde  $\text{LP}_{\text{L}}$  hacia los orbitales  $\text{p}_{\text{Be}}$ , por lo tanto, tienen características comunes con los BerBs. Las afinidades aniónicas de estos compuestos varían entre  $250 - 800 \text{ kJ}\cdot\text{mol}^{-1}$ , lo cual depende de la acidez del fragmento de Be o de la basicidad del anión. Las altas afinidades aniónicas de los derivados de Berilio-naftaleno los proponen como posibles compuestos para ser utilizados en el diseño de receptores y sensores de aniones, con aplicaciones en el desarrollo de nuevos dispositivos electrónicos.

### 4.3 FOUR-ELECTRONS Be BONDS

Four-electrons Be bonds are the bonds formed by the four valence electrons of the metals in the  $\text{Be}_2$  molecule. Section 3.2.2 describes the properties of the dimer, but in this thesis the complexes formed between the dimer and neutral electron-donor species (L) are studied, considering complexes of the type  $\text{L}:\text{Be}-\text{Be}:\text{L}$ . The nature of the  $\text{Be}:\text{L}$  interaction is used to classify  $\text{L}:\text{Be}-\text{Be}:\text{L}$  derivatives into three groups, see scheme 4.8. Group-I consists of the complexes with  $\text{L} = \text{H}_2\text{O}$  and  $\text{NH}_3$ . The interaction between L and Be in this group has a  $\text{LP}_{\text{L}} \rightarrow \text{p}_{\text{Be}}$  nature (4.8a). Group-II is represented by the complex with  $\text{L} = \text{CO}$  (4.8b). The  $\text{CO}:\text{Be}$  interaction takes place via the conjugation of the  $\pi_{\text{CO}} \backslash \pi_{\text{Be}}$  orbitals. The complexes between  $\text{Be}_2$  and N-heterocyclic carbenes studied in reference [43] can be also classified within this group. Finally, group-III is formed by the complexes where L is a neutral radical, with  $\text{L} = \text{CN}\cdot, \text{F}\cdot, \text{OH}\cdot, \text{CH}_3\cdot, \text{CH}_3\text{O}\cdot$  and  $\text{NH}_2\cdot$  (4.8c), where the complex with  $\text{L} = \text{F}$  studied in reference [44] is considered.



Scheme 4.8:  $\text{L}:\text{Be}-\text{Be}:\text{L}$  complexes in (a) group-I with  $\text{L}=\text{NH}_3$  and  $\text{H}_2\text{O}$ , (b) group-II with  $\text{L}=\text{CO}$  and group-III with  $\text{L}=\text{CN}\cdot, \text{F}\cdot, \text{OH}\cdot, \text{CH}_3\cdot, \text{CH}_3\text{O}\cdot$  and  $\text{NH}_2\cdot$ .

### 4.3.1 Methodology

The  $\text{Be}_2$  molecule is accurately described by Full Configuration Interaction (FCI). However, the L: Be-Be: L complexes are too large systems to be described with this method. Thus, we used the CASPT2//CASSCF/cc-pVTZ approach to study the L: Be-Be: L derivatives, which represents one of the best method to study medium size multi-reference systems. The  $\text{Be}_2$  moiety in these complexes has a different oxidation state depending on L. The dimer remains neutral in the complexes in group-I, it becomes a monocation in group-II and a dication in group-III (see table S6 from appendix B.6).

Some of the complexes in group-III present among the strongest Be-Be bond reported in the literature [41–44]. This strong interaction is attributed to the zero occupation of the  $\sigma_{\text{Be-Be}}^*$  orbital, which is depleted by a charge transfer process towards the valence orbitals of the radical ligands, turning L into closed-shell molecules. See appendix B.6-table S6 for the NBO charges and electron configurations of the  $\text{Be}_2$  moiety in these complexes. Therefore, these complexes are characterized by single-reference wave functions ( $\tau_1$  diagnostic,  $\tau_1 < 0.015$ ) and were evaluated at the CCSD(T)/cc-pVTZ level of theory. The energetic and geometric characteristics of the complex with L = F were described by Frenking and coworkers in reference [44]. This work could be considered as representative of the complexes in group-III, and in addition to this, the bonding properties do not require a further analysis. Henceforth, this thesis is focused in the nature of the Be-Be bond of the complexes in groups-I and -II. In the following, the L label makes reference solely to the substituents in these groups.

The complexes in groups-I and -II have a multi-reference character as the isolated dimer. The AS used in their description was chosen considering the nature of the Be: L interactions:

- Group-I. The geometry optimization and energetics were calculated using a (8,10) AS. The active orbitals include the Lone Pair (LP) of L in the direction of the Be atoms and the valence electrons of the Be atoms. See figures S1 and S3 from appendix B.6.
- Group-II. There is a  $\pi$ -conjugation between the  $\pi_{\text{Be}}$  and the  $\pi_{\text{CO}}$  orbitals. The (12,16) AS includes the full  $\pi_{\text{CO}}$  and valence Be orbitals. This large AS is computationally very demanding, so we had to decrease its size:

– (12,16):  $2\sigma_{\text{Be}}$ ,  $3\sigma_{\text{Be}}$ ,  $2\cdot(\pi_{\text{Be}})$ ,  $4\cdot(\pi_{\text{CO}})$ ,  $2\sigma_{\text{Be}}^*$ ,  $3\sigma_{\text{Be}}^*$ ,  $2\cdot(\pi_{\text{Be}}^*)$  and  $4\cdot(\pi_{\text{CO}}^*)$ .

– (12,14):  $2\sigma_{\text{Be}}$ ,  $2\cdot(\pi_{\text{Be}})$ ,  $4\cdot(\pi_{\text{CO}})$ ,  $2\sigma_{\text{Be}}^*$ ,  $2\cdot(\pi_{\text{Be}}^*)$  and  $4\cdot(\pi_{\text{CO}}^*)$ .

– (12,12):  $2\sigma_{\text{Be}}$ ,  $\pi_{\text{Be}}$ ,  $4\cdot(\pi_{\text{CO}})$ ,  $2\sigma_{\text{Be}}^*$ ,  $\pi_{\text{Be}}^*$  and  $4\cdot(\pi_{\text{CO}}^*)$ .

– (10,12):  $2\cdot(\pi_{\text{Be}})$ ,  $4\cdot(\pi_{\text{CO}})$ ,  $2\cdot(\pi_{\text{Be}}^*)$  and  $4\cdot(\pi_{\text{CO}}^*)$ .

The most relevant orbitals of CO: Be-Be: CO and their occupations are represented in figure S5 from appendix B.6. Table S2 from appendix B.6 compares the four AS at

DF-CASSCF/3-21G (Density Fitting- CASSCF) level of theory. The energy difference between (12,16) and (12,14) AS amounts just to  $18\text{kJ}\cdot\text{mol}^{-1}$ , and this difference increases to  $48\text{kJ}\cdot\text{mol}^{-1}$  and  $51\text{kJ}\cdot\text{mol}^{-1}$  with the (12,12) and (10,12) ASs, respectively. However, the DF-CASSCF(12,16)/3-21G calculation is 10 times slower than DF-CASSCF(12,14)/3-21G, indicating that the DF-CASSCF(12,16)/cc-pVTZ calculation is not computationally worth for the amount of electron correlation that could be recovered. The geometries were optimized considering the (10,12) and (12,12) ASs, finding negligible differences among them, and which are of the order of  $0.001\text{\AA}$  for bond distances. The (10,12) AS correctly describes the degeneracy of the  $\pi_{\text{Be}}$  orbitals, for what it was chosen for the geometry optimization and the wave function analyses. According to the previous results, the best compromise between computational effort-accuracy to describe the CO: Be-Be: CO complexes is CASPT2/CASSCF(12,14)/cc-pvTZ//CASPT2/CASSCF(10,12)/cc-pvTZ.

The calculations were performed with MOLPRO 2015. The  $^1[\text{CO: Be-Be: CO}]$  and  $^3[\text{CO: Be-Be: CO}]$  complexes were studied under  $D_{2h}$  and  $C_{2v}$  symmetry constraints, respectively. The complexes in group-I were analyzed without symmetry constraints. The nature of the bond was studied by the analysis of  $\Psi_{\text{CASSCF}}$ .

The CO: Be-Be: CO complex was used to estimate the Basis Set Superposition Error (BSSE) associated to the Be-Be BDE of the L: Be-Be: L derivatives. Two dissociation channels were considered:

1.  $\text{CO: Be-Be: CO} \rightarrow 2\text{COBe}$ , where  $AB = \text{CO: Be-Be: CO}$  and  $A = B = \text{COBe}$ . Equation 2.128 from section 2.6.6 was employed due to the geometry deformation associated to the formation of the COBe complexes

$$\text{BDE}^{\text{CP}}(AB) = E_{\text{AB}}^{\text{AB}}(AB) - 2E_{\text{AB}}^{\text{A}}(A) + 2[E_{\text{AB}}^{\text{A}}(A) - E_{\text{A}}^{\text{A}}(A)] \quad (4.7)$$

2.  $\text{CO: Be-Be: CO} \rightarrow 2\text{CO} + 2\text{Be}$ , where  $AB = \text{CO: Be-Be: CO}$ ,  $A = \text{CO}$ ,  $B = \text{Be}$ . The geometry deformation has not an important role in this reaction and equation 2.127 from section 2.6.6 was then applied

$$\text{BDE}^{\text{CP}}(AB) = E_{\text{AB}}^{\text{AB}}(AB) - 2E_{\text{A}}^{\text{AB}}(A) - 2E_{\text{B}}^{\text{AB}}(B) \quad (4.8)$$

The counterpoise corrections to the BDEs were found to be negligible. The values are below chemical accuracy and represent 1.4% of the total energy in the first reaction and 2.6% in the second. Therefore, the BDEs reported in this section are not corrected for BSSE.

#### 4.3.2 The $\text{Be}_2$ molecule

The description of the Be dimer using CASPT2/CASSCF is very sensible to the size of the ASs. Figure 4.20a compares the FCI results respect to four AS proposed in the literature [54]:

- (4,16):  $2\sigma + 2\sigma^* + 3\sigma + 3\sigma^* + 2\cdot(1\pi) + 2\cdot(1\pi^*) + 4\sigma + 4\sigma^* + 2(2\pi) + 2(2\pi^*)$ .

- (4,8):  $2\sigma + 2\sigma^* + 3\sigma + 3\sigma^* + 2 \cdot (1\pi) + 2 \cdot (1\pi^*)$ .
- (4,4):  $2\sigma + 2\sigma^* + 3\sigma + 3\sigma^*$ .
- (2,2):  $2\sigma^* + 3\sigma$ .

The geometries and energetics of the  $\text{Be}_2$  molecule are collected in table S4 from appendix B.6, and the dissociation curves for the four ASs are shown in figure 4.20a. The (2,2) AS overestimates the bond strength in more than  $40\text{kJ}\cdot\text{mol}^{-1}$  due to the constraints of this subspace. The main configuration in  $\Psi_{(2,2)}$  is  $|(2\sigma)^2(2\sigma^*)^2\rangle$ , but due to the restriction in the AS there is also an important contribution from an  $n^{\text{th}}.1\Sigma = |(2\sigma)^2(3\sigma)^2\rangle$  excited state,  $|\Psi_{\text{CASPT2}}\rangle = |0.91^1\Sigma - 0.41n^{\text{th}}.1\Sigma\rangle$ . The excited states of  $\text{Be}_2$  have a shorter and stronger Be-Be bond than the ground state, suggesting that the large Be-Be BDE at CASSCF(2,2) level of theory is caused by the significant contribution from the  $n^{\text{th}}.1\Sigma$  excited state. The  $\text{Be}_2$  molecule does not exist at CASSCF(4,4) and CASSCF(4,8) level of theory, see figure 4.20a. These spaces are not flexible enough to describe the  $s \rightarrow p$  excitations of the dimer at the equilibrium distances, but on the contrary they accurately describe the Be atoms at the dissociation limit. Thus, the ground state energy of  $\text{Be}_2$  is underestimated by these subspaces. The (4,16) AS is flexible enough to describe correctly the electron correlation in both, at the equilibrium and at the dissociation products regions, being the only AS considered in this thesis that shows a bonding character at CASSCF level of theory for the  $\text{Be}_2$  molecule. On the contrary, CASPT2 dissociation curves are attractive for the four AS. The CASPT2 geometries and energetics values are in good agreement with experimental data (see table S4(a) from appendix B.6). Reference [54] performs a deeper analysis on the multi-reference character of the Be dimer.

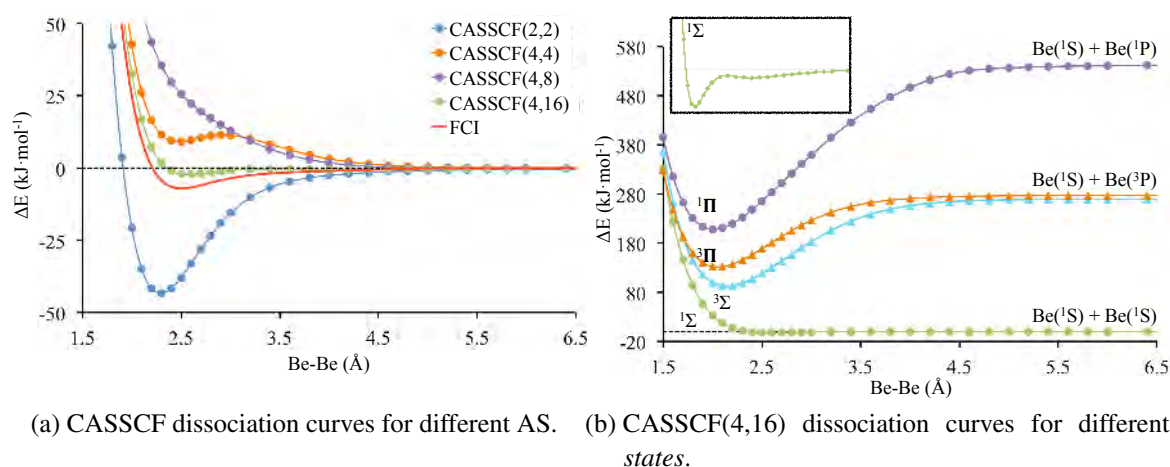


Figure 4.20: (a) Ground state dissociation curve of the  $\text{Be}_2$  molecule for different ASs size. The calculations were performed with the cc-pVTZ basis set. (b) Ground and excited state dissociation curves of the  $\text{Be}_2$  molecule at CASSCF(4,16)/cc-pVTZ level of theory.

The highly correlated  $\text{Be}_2$  interaction energy has been attributed to the low lying  $p_{\text{Be}}$  orbitals, which also have an important effect in the stability of the  $\text{Be}_2$  excited states. Figure

4.20b shows the first two triplets and the first singlet excited states.  $\text{Be}_2$  adiabatic excitation energies ( $T_e$ ) and BDE are shown in table S4(a) from appendix B.6. The ground  $^1\Sigma$  state has a  $|(2\sigma)^2(2\sigma^*)^2\rangle$  electron configuration that dissociates into two neutral Be atoms ( $\text{Be}(^1S) + \text{Be}(^1S)$ ). The first triplet state,  $^3\Sigma$ , lies adiabatically  $90 \text{ kJ}\cdot\text{mol}^{-1}$  higher in energy with respect to the ground state, and the Be-Be bond in this specie is 17 times stronger than the one of the ground state. The  $^3\Pi$  state is just  $20 \text{ kJ}\cdot\text{mol}^{-1}$  higher in energy than the  $^3\Sigma$  state, and both dissociate into the same products  $\text{Be}(^3P) + \text{Be}(^3P)$ . The electron configuration for the  $^3\Sigma$  and  $^3\Pi$  states is  $|(2\sigma^*)^1(3\sigma)^1\rangle$  and  $|(2\sigma^*)^1(\pi)^1\rangle$  for the  $^3\Sigma$  and  $^3\Pi$ , respectively. The first singlet excited state is more than  $200 \text{ kJ}\cdot\text{mol}^{-1}$  higher in energy than the ground state. The electron configuration of the  $^1\Pi$  state is  $|(2\sigma^*)^1(3\bar{\sigma})^1\rangle$  and dissociates into  $\text{Be}(^1S) + \text{Be}(^1P)$ , the bar over the singly occupied orbitals denotes a beta spin.

The wave function analyses of the ground and excited states of  $\text{Be}_2$  are in agreement with the energetics. The ground state of the  $\text{Be}_2$  molecule is characterized by a small  $\rho$  and a negative sign of  $\nabla^2\rho$ , indicating that even though the interaction is weak, it has a covalent character. The ELF method fails in the description of the Be dimer. According to this analysis, the  $\text{Be}_2$  molecule is bonded through a closed-shell interaction between the Be atoms, not showing a  $V(\text{Be}, \text{Be})$  disynaptic basin (see figure 4.21a). However, the nature of the Be-Be bond is different for the excited states and the ground state at CASSCF(2,2) level of theory. The QTAIM method locates a (3,-3) saddle point (Non-Nuclear Attractor (NNA)) between the Be atoms. Then, the two Be atoms are no longer linked through a  $\text{BCP}_{\text{Be-Be}}$ , but instead, through two  $\text{BCP}_{\text{Be-NNA}}$  (see figure 4.21b). The value of  $\rho$  at the  $\text{BCP}_{\text{Be-NNA}}$  of the CASSCF(2,2) ground and excited states is twice than at the  $\text{BCP}_{\text{Be-Be}}$  in the ground state. Finally, the ELF analysis does locate a  $V(\text{Be}, \text{Be})$  basin in the excited and the CASSCF(2,2) ground state, with populations  $1.70e^-$ ,  $1.90e^-$  and  $2.4e^-$  for the  $^1\Sigma$  CASSCF(2,2),  $^3\Sigma$  and  $^1\Pi$  states, respectively. The similarities between  $\Psi_{\text{Excited-States}}$  and  $\Psi_{\text{CAS}(2,2)}$  support that the ultra-short bond predicted by this AS is a consequence of the mixing between the ground and excited states wave functions.

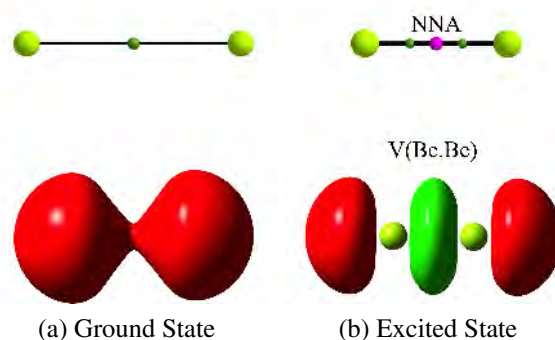
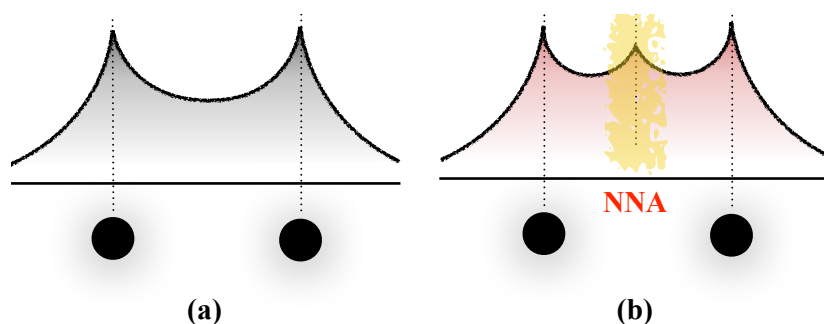


Figure 4.21: Representation of the CASSCF(n,m)/cc-pVTZ wave function analysis for (a) (4,4), (4,8) and (4,16) ground states, and (b) (2,2) ground and excited states of the  $\text{Be}_2$  molecule. The first row shows the molecular graph, green and pink dots are BCPs and NNAs, respectively. The second row shows the ELF representation, green lobes correspond to disynaptic basins between heavy atoms and red lobes denote monosynaptic basins associated with lone-pairs.

The same bond analysis performed for the  $\text{Be}_2$  molecules was done for the  $\text{L: Be-Be: L}$  complexes. Therefore, next section describes the origin and characteristics of NNA.

#### 4.3.2.1 Pseudo-Nuclei

Pseudo-nuclei correspond to positions in which there is an accumulation of  $\rho$  in the absence of a nucleus. Thus, in the QTAIM framework they are described as a (3-3) point of  $\rho$ , not coinciding with the position of a nucleus. Scheme 4.9 compares the topology of  $\rho$  along a bond internuclear distance for a system (a) without and (b) with a NNA. Originally, the existence of NNA was argued both theoretically and experimentally. The first theoretical evidence was obtained at Hartree Fock (HF) level of theory for  $\text{Li}_2$  [301] and later, the existence of this NNA was attributed to the used of a finite basis set [302]. The Maximum Entropy Method (MEM) was applied using the experimental electron density for  $\text{Li}_2$  [303, 304] and afterward these NNAs were associated with an error of the method itself [305]. Only recently, it has been theoretically demonstrated that NNA are not a consequence of the lack of flexibility of: the basis set or the electron correlation [306, 307]. Moreover, the experimental occurrence of NNAs has been evidenced by high resolution X-ray diffraction and Electron Density Distribution (EDD) [308]. Therefore, at present, there are not doubts about the existence of pseudo-nuclei, but it remains unclear why some systems show a NNA and some others do not.

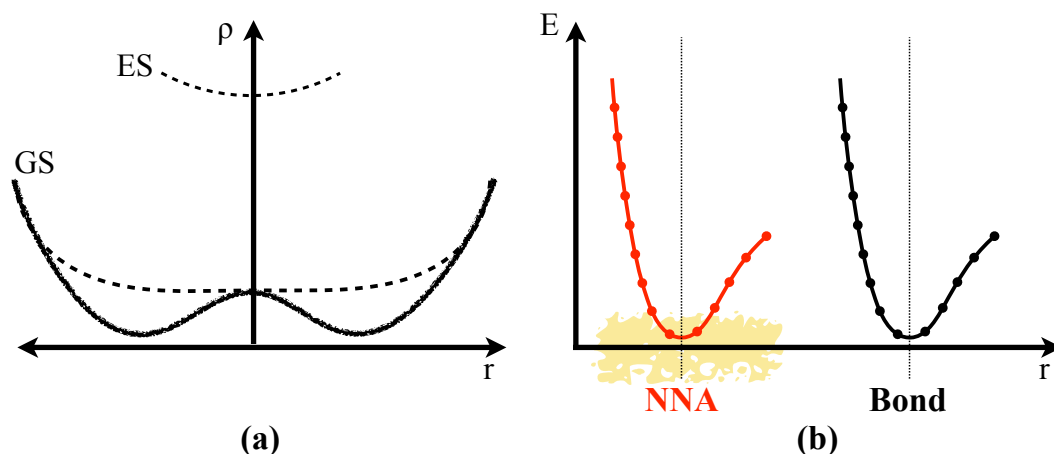


Scheme 4.9: Representation of a system (a) without and (b) with a NNA.

The origin of NNA has been explained considering two different approaches, relying on the same idea: *the existence of pseudo-nuclei is associated to the formation of chemical bonds*.

1. *Catastrophe Theory*, in 1992 Bersuker and coworkers proposed a model where the origin of NNAs was attributed to the coupling between the ground and excited states by an electron-electron interaction of the valence electrons. Therefore, the small energetic gap between the electronic states of metallic species, justifies why NNAs are more common in such systems [306]. See scheme 4.10a.
2. *Promolecular Model*, in 1999 Pendás and collaborators used the promolecular model to explain the formation of NNAs. According to this model, in the formation of homonu-

clear bonds ( $A-A$ ) there is a particular distance, where the  $BCP_{AA}$  splits into a NNA and two BCPs between the NNA and each  $A$  atom. The ground state of a system will show a NNA, only if the equilibrium distance lies in the predicted range of formation of the pseudo-nuclei (NNA window, see scheme 4.10b). This window appears at shorter distances for higher values of  $Z$ , also explaining why NNAs are more common in the ground state of alkali-metal homonuclear systems [307].



Scheme 4.10: Formation of a NNA considering (a) catastrophe theory and (b) promolecular model. GS and ES stand for ground and excited states, respectively. The NNA window is highlighted in yellow.

Earlier studies on NNAs were mainly focussed in homonuclear bonds. More recent studies have shown the presence of NNAs in heteronuclear systems, such as diatomic molecules [309, 310], molecular electriles [311, 312], and solvated electrons [313–315].

The existence of a NNA in the ground state of  $Be_2$  depends on its aggregation state.  $Be_2$  in solid state have been studied by means of MEM [316] and crystal calculations [307]. The two methods locate NNAs in the metal, which is in agreement with the prediction done by the promolecular model [307]. Conversely, molecular  $Be_2$  does not show a NNA at the equilibrium geometry. This absence could be attributed to the the longer Be-Be bond of the molecule compared to the solid, which situates molecular  $Be_2$  outside of the predicted NNA window [307, 310].

#### 4.3.3 Properties of the four-electrons Be-Be bonds

The name four-electrons Be-Be bond is only valid for the complexes in group-I, where the  $Be_2$  moiety remains neutral, but it is not longer correct for the complex in group-II where  $Be_2$  is a monocation. However, the label four-electrons Be-Be bond is preserved to highlight the 4 valence electrons of the isolated Be dimer.

#### 4.3.3.1 Geometries and Electron Configuration

The geometries of the ground and excited states of L: Be-Be: L compounds are shown and described in appendix B.6 figure 1. The most important characteristics are summarized in the following:

- *Be-Be bond distance*, this bond distance is shorter in the L: Be-Be: L complexes than in the isolated Be dimer. For L = CO the Be-Be bond distance becomes 0.5 Å shorter than in the free dimer, while for group-I this bond distance decreases by 0.4 Å.
- *Trans-type geometry*, this is the most stable structure for group-I complexes because it allows a better interaction between the  $LP_L$  and the  $p_{Be}$  orbitals (see scheme 4.8a in page 134). The analogue isomer for L = CO does not correspond to a minimum of the PES.
- *Linear geometry*. The global minimum for L = CO corresponds to a linear molecule. The stability of the linear structure is associated with the enhancement of the conjugation of the  $\pi_{CO}$  and  $\pi_{Be}$  orbitals (see scheme 4.8b in page 134).
- *Excited States*, the Be-Be bond distance in the excited states also becomes shorter with respect to their analogues in the isolated dimer. The most dramatic variation was found for the complex in group-II, where the shortest Be-Be bond distance is no longer that of the excited states, but it corresponds to the one in the ground state.
- *The Be-L interaction*, the Be: L bond distances are within 1.77 and 1.66 Å depending on the L substituent. The complex with L = CO has the shortest Be: L bond in this thesis, 1.66 Å. This value is very close to the one reported for N-heterocyclic carbenes (1.68 Å) [43]. These short Be: L distances are due the  $\pi$ -conjugation between the  $\pi_L$  and  $\pi_{Be}$  orbitals (see figures 4.22a and 4.22c in page 146).

The Be-Be bond length of the complexes studied in this thesis are larger than the ones reported for L = NRC [43] and L = F [44]. This bond length in the fluorine complex is not comparable with the one in the compounds of groups-I and -II. In the F: Be-Be: F complex, the Be<sub>2</sub> moiety is in its +2 oxidation state, that necessarily should present a shorter Be-Be bond than the neutral dimer [23, 317]. Applying the same criteria, the complexes with the NRC ligand can be compared with that carrying CO (Be<sub>2</sub> is a monocation), but not with those including NH<sub>2</sub> and H<sub>2</sub>O ligands where the dimer exists as a neutral moiety. Therefore, to the best of our knowledge, the complexes with L = NH<sub>3</sub> and H<sub>2</sub>O in group-I have the shortest Be-Be bond reported for the neutral dimer.

The Be-Be bond distance is shorter in the complexes with L = NRC than with L = CO. Since, as it was stated before the strong Be-Be bond in this type of complexes is due to a  $\pi$ -conjugation between  $\pi_L$  and  $\pi_{Be}$  orbitals, which is expected to be larger in the N-heterocyclic carbenes than in the CO molecules.



The establishment of L: Be<sub>2</sub> interactions induces changes in both the L: Be-Be: L geometries and the electronic configuration of the complexes, particularly in the Be<sub>2</sub> moiety. Tables S1 and S3 in appendix B.6 collect the CASSCF electronic configurations. The ground state of the Be<sub>2</sub> moiety in group-I complexes shares the electronic configuration of the isolated dimer,  $|(2\sigma_{\text{BeBe}})^2(2\sigma_{\text{BeBe}}^*)^2\rangle$ . However, whereas in the free dimer the second highest coefficient corresponds to the  $|(2\sigma_{\text{BeBe}})^2(2\sigma_{\text{BeBe}}^*)^0(3\sigma_{\text{BeBe}})^2\rangle$  configuration, in the complexes of group-I the second biggest contribution comes from a configuration in which the  $\pi_{\text{Be}}$  orbitals are involved,  $|\Psi_{\text{CASPT2}}\rangle = |0.8[(2\sigma_{\text{BeBe}})^2(2\sigma_{\text{BeBe}}^*)^2] + 0.15[(2\sigma_{\text{BeBe}})^2(2\sigma_{\text{BeBe}}^*)^0(\pi_{\text{BeBe}})^2]\rangle$ . The ground state electron configuration of the complex in group-II is completely different than in the isolated dimer. The  $\pi_{\text{Be}}$  orbitals are highly stabilized by a conjugation with the  $\pi_{\text{CO}}^*$  orbitals. Then, the ground state wave function which is doubly degenerated is  $|\Psi_{\text{CASPT2}}\rangle = |0.32[(2\sigma_{\text{BeBe}})^2(\pi_{\text{BeBe}} + \pi_{\text{CO}}^*)^2] + 0.32[(2\sigma_{\text{BeBe}})^2(\pi_{\text{BeBe}} + \pi_{\text{CO}}^*)^2]\rangle$ . When the geometry of CO: Be-Be: CO is constrained to the trans-type structure, the  $\pi_{\text{CO}} \backslash \pi_{\text{Be}}$  conjugation is eliminated and the system behaves as the complexes in group-I. Finally, for the complex in group-II, the state with the same electron configuration as the isolated dimer is an excited state lying 877 kJ·mol<sup>-1</sup> higher in energy at CASSCF(12,14)/cc-pVTZ level of theory.

The nature of the ground-state wave function of the L: Be-Be: L complexes supports that there is a stabilization of the  $\pi_{\text{Be}}$  orbitals compared to the isolated dimer. As a consequence, the first triplet state for the complexes in group-I is no longer the <sup>3</sup>Σ but the <sup>3</sup>Π state, and there is a decrease in the excitation energy of the <sup>1</sup>Π state with respect to the free dimer (see figure 8 in appendix B.6). The ground state of the complex in group-II is highly correlated. The first singlet excited state is just 4 kJ·mol<sup>-1</sup> higher in energy than the doubly degenerated ground state. The electronic configuration of this third <sup>1</sup>Σ state is  $|(2\sigma_{\text{BeBe}})^2(\pi_{\text{BeBe}} + \pi_{\text{CO}}^*)^1(\bar{\pi}_{\text{BeBe}} + \bar{\pi}_{\text{CO}}^*)^1\rangle$ . The first triplet state for L = CO ( $|(2\sigma_{\text{BeBe}})^2(\pi_{\text{BeBe}} + \pi_{\text{CO}}^*)^1(\pi_{\text{BeBe}} + \pi_{\text{CO}}^*)^1\rangle$ ) is only 16 kJ·mol<sup>-1</sup> higher in energy. In agreement with the energetics, the first four states for L = CO share almost the same geometry, showing differences in the Be-Be and Be-CO bond distances in the order of 0.001 Å. Appendix B.6 figures S8 and S9 show the state energy diagrams for the ground and excited states of the complexes in groups-I and -II, and the excitation energies can be found in table 1 in the same appendix.

#### 4.3.3.2 Wave Function Analysis

All wave function analysis methods employed in this thesis confirm that there is a stronger Be-Be bond in the L: Be-Be: L complexes than in the isolated Be dimer. As was previously stated, the existence and strength of the bond in the Be<sub>2</sub> molecule has been attributed to  $s \rightarrow p$  excitations. The NBO analysis of the L: Be-Be: L complexes shows an increase in the population of the  $p_{\text{Be}}$  orbitals, with occupation values twice as large as those found in the isolated atom. These results are consistent with the shorter Be-Be bond distance of the L: Be-Be: L complexes and the variations in the electronic configurations compared with the isolated Be<sub>2</sub> molecule. The differences between the complexes in groups-I and -II are

also illustrated by NBO. For both groups of complexes, there is a Be-Be bonding orbital (BD), which does not exist in the free Be<sub>2</sub> molecule. Both BD orbitals have populations of 2e<sup>-</sup>, but whilst in group-I complexes this orbital is formed by sp hybrid orbitals, in group-II it is formed by pure s<sub>Be</sub> orbitals. The location of the remaining valence electrons also differentiates the two groups of complexes. For group-I these electrons are localized as Lone Pairs of the Be atom, while for the monocation in group-II, there are two singly occupied orbitals, π<sub>Be</sub> and π<sub>CO</sub><sup>\*</sup> (see table S6 from appendix B.6). The ELF description is in agreement with the NBO results, the ground state of group-I has a V(Be, Be) basin with a population around of 1.7 e<sup>-</sup> and two singly occupied V(Be) monosynaptic basins, while for the second group there are V(Be, Be) and V(Be, C) basins with high populations of 2.4e<sup>-</sup> and 3.22e<sup>-</sup>, respectively. The ELF and NBO results are in appendix B.6 (figure 2 and table S7).

The most surprising results come from the QTAIM analysis. The molecular graphs for the ground state of the L: Be-Be: L complexes shows the existence of a NNA, which is only present in the excited states of the isolated dimer. Then, instead of single BCP<sub>Be-Be</sub> there are two BCP<sub>Be-NNA</sub>, with a value of ρ double than for the BCP<sub>Be-Be</sub> in the isolated dimer. The values of ∇<sup>2</sup>ρ are always negative indicating that the interaction between Be and NNA has a covalent character (see appendix B.6 figure 2 and table S7). The presence of NNA in L: Be-Be: L complexes is not limited only to the ground state. As in the isolated molecule, the first singlet and triplet states also show pseudo-nuclei. The QTAIM outcomes are in appendix B.6 (figures 2 and S10–S12).

Low-lying excited states have been used to explain the formation of NNA (see section 4.3.2.1) and the excited states of the L: Be-Be: L complexes are lower in energy than in the isolated dimer. However, independently on the number of states included in the state-average Ψ<sub>CASSCF</sub>, the systems always show a NNA with an almost constant value of ρ, see table 3. These results suggest that the formation of NNA is in principle not related to the existence of low-lying excited states.

The decrease of the Be-Be bond distance in the L: Be-Be: L complexes, places the Be<sub>2</sub> moiety in the predicted NNA *window* for Be<sub>2</sub> (see figure 2 in [307]), suggesting that the origin of the NNA could be related to the internuclear distances, rather than to the interaction among different electronic states. The formation of the NNA was evaluated along the Be<sub>2</sub> dissociation curve of the CO: Be-Be: CO complex (see figure A.5 in the electronic version of this thesis for an animation of ∇<sup>2</sup>ρ across the dissociation curve). The NNA for this complex is present in a similar range of internuclear distances as for the isolated dimer, 1.4 – 2.1 Å against 1.4 – 2.2 Å, respectively. These results suggest that the NNA *window* slightly changes with the formation of non-covalent interactions, which is consistent with the presence of NNA in Li-electrides in reference [312].

Table 3: Value of  $\rho$  in the NNA for the L: Be-Be: L complexes at the SA(q)CASSCF(n,m)/cc-pVTZ level of theory. The AS for group-I complexes is (8,10) and for group-II is (10,12),  $q$  is equal to the number of states included in the state-average calculation and all values are in au.

q/L	NH <sub>2</sub>	H <sub>2</sub> O	CO <sup>[A]</sup>
1	0.06	0.06	0.07
2	0.05	0.05	0.07
3	0.06	0.06	0.07
4	-	-	0.07

<sup>[A]</sup> For L = CO symmetry constraints were decreased to C<sub>2</sub>, allowing for the simultaneous description of the first four states.

The value of  $\rho$  in the NNA for L = CO was also evaluated including the ground and the first triplet states in the SA-CASSCF. The value of  $\rho$  at the BCP<sub>Be-NNA</sub> remained the same for the singlet-state and state-average wave functions.

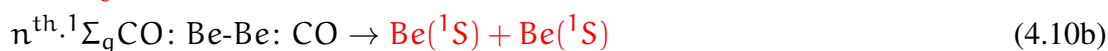
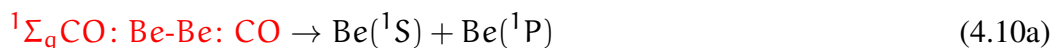
#### 4.3.3.3 Bond Dissociation Energies

The stability of the complexes was studied by considering two dissociation channels:

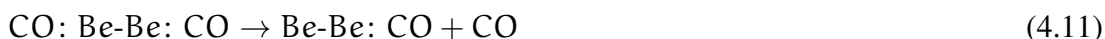


BDE<sub>1</sub> and BDE<sub>2</sub> for the complexes in groups-I and -II are reported in appendix B.6 (table 1 and figures S8 and S9). Whereas the free Be<sub>2</sub> molecule has a very weak bond, the L: Be-Be: L derivatives have a strong Be-Be bond, ratified by they larger BDE. The Be-Be bond en these complexes are up to 10 and 20 times stronger for the complexes in groups-I and -II, with respect to the isolated Be dimer, respectively.

The most favorable dissociation products for group-I complexes are two L: Be compounds (BDE<sub>2</sub>). In these products, the wave function of the Be:L compounds does not show a bonding Be:L orbital, indeed, the L: Be bond distance and the Be electronic configuration ([He]1s<sup>2</sup>2s<sup>2</sup>) are equal in reactant and products, indicating that the L: Be systems are bonded by a closed-shell interaction. Therefore, the dissociation mechanisms for the complexes in group-I are analogous to that of the isolated dimer, but with a higher energetic barrier. Group-II complex shows a different dissociation mechanism because reactant and products are in different electronic states. This suggest that the CO: Be-Be: CO reaction mechanism should involve at least a state-crossing between the two main dissociation channels in equations 4.10 (the ground state of reactant and products is highlighted in red).



According to the previous experimental and theoretical work performed by Randall and co-workers [42], there is a third possible dissociation channel for CO: Be-Be: CO, its decomposition into CO: Be-Be + CO. The main peaks of the IR spectra correspond to the mono- and disubstituted complexes, which were identified as Be-Be: CO and CO: Be-Be: CO at HF level of theory. However, theoretically, reaction 4.11 was found to be exothermic by  $20\text{kJ}\cdot\text{mol}^{-1}$  [42], indicating that the mono-substituted complex is more stable than the disubstituted one.



The multi-reference description of the CO: Be-Be: CO compounds does not support, however, the previous HF results. The multi-reference results show that reaction 4.11 is endothermic by  $121\text{kJ}\cdot\text{mol}^{-1}$ , in contrast with the exothermic reaction estimated by HF. Additionally, the ground state of CO: Be-Be: CO is a singlet, whilst HF method predicts a triplet ground state, and the CASPT2//CASSCF(12,14)/cc-pVTZ BDE of CO: Be-Be: CO is  $132\text{kJ}\cdot\text{mol}^{-1}$  higher than the one determined by HF [42]. Taking into account the energetics of the CO: Be-Be: CO complex, the experimentally detected monosubstituted species should be formed from the reaction between Be<sub>2</sub> and CO ( $\Delta E = -38\text{kJ}\cdot\text{mol}^{-1}$ ). Indicating that the CO: Be-Be: CO compound is energetically stable against the dissociation in Be-Be: CO + CO.

The energetics are in agreement with the strong Be-Be bond predicted by the geometric and the wave function analyses. The strength of the Be-Be bond for the L: Be-Be: L complexes follows the trend for L, CO > NH<sub>3</sub> > H<sub>2</sub>O, but yet in all of them the Be-Be bonds are weaker than the N-heterocyclic carbene or the fluorine derivatives [43, 44]. Nevertheless, the BDE of complexes in group-I are the strongest Be-Be bond reported for the neutral Be dimer.

A conspicuous results with respect to the BDE are the main dissociation channels. The main dissociation products for group-I are the L: Be complexes, where the Be: L interaction was found to be similar to BeRLs,  $\text{LP}_L \rightarrow \text{p}_{\text{Be}}$ . The CO ligand is known as good  $\sigma$ -donor and  $\pi$ -acceptor, however, the CO electron donor capacity is smaller than that of the ligands in group-I. For example, the CO proton affinity is  $300\text{kJ}\cdot\text{mol}^{-1}$  lower than that of NH<sub>3</sub> ( $854\text{kJ}\cdot\text{mol}^{-1}$ ) [318]. Therefore, the CO: Be molecule does not exist due to the weak  $\sigma$ -donor capacity of the CO ligand. The NRC ligands exemplify this behavior because they share characteristics with the two types of complexes studied in this thesis, groups-I and -II. At the equilibrium distance, the NRC ligands behaves as the complex in group-II, the interaction between the Be atoms and the ligands occurs by a conjugation of the  $\pi_L$  and  $\pi_{\text{Be}}$  orbitals (see figures 4.22a and 4.22c). On the contrary, the NRC dissociation products are highly stabilized by a  $\text{LP}_L \rightarrow \text{p}_{\text{Be}}$  electron donation, and in turns, the NRC derivatives behaves as the complexes in group-I (see figures 4.22b and 4.22d).

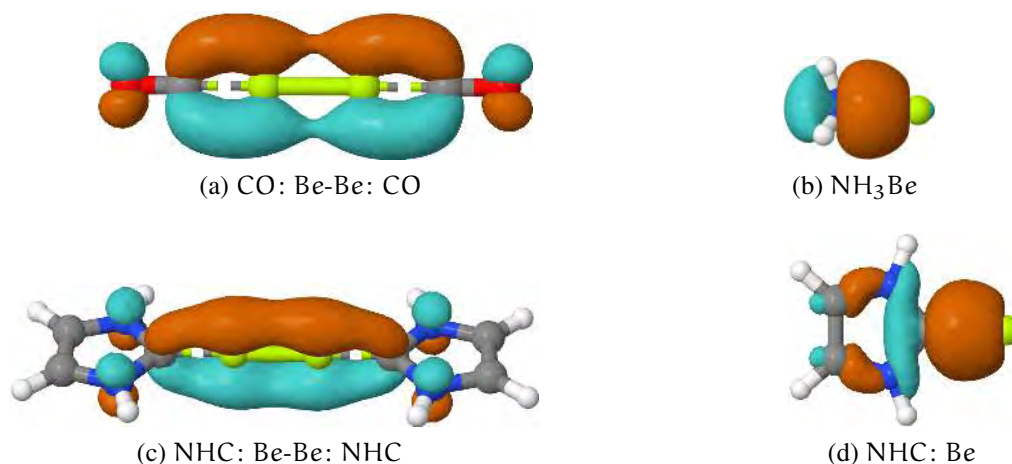


Figure 4.22: Molecular Orbitals associated to the Be: L interaction for the (a) CO: Be-Be: CO (b), NH<sub>3</sub>Be (c), NRC: Be-Be: NRC and (d) NRC: Be (with R=H) complexes.

#### 4.3.4 Conclusions

*The interaction of Be<sub>2</sub> with Lewis bases considerably increases the strength of the Be-Be bond, but the oxidation state of the Be dimer also changes depending on the nature of the LB.*

The strongest Be-Be interaction take places in complexes where Be<sub>2</sub> interacts with radical ligands. The origin of this strong interaction is the depopulation of the  $\sigma_{\text{Be-Be}}^*$  orbital, as a consequence of a charge transfer towards the valence orbitals of the radical ligands.

The interaction between Be<sub>2</sub> and closed-shell electron donor species also increases the strength of the Be-Be bond, since this interaction strongly stabilizes the  $\pi_{\text{Be}}$  orbitals. This stabilization is stronger in ligands with  $\pi$  systems, because of a conjugation between the  $\pi_{\text{Be}}$  and  $\pi_{\text{L}}$  orbitals, changing the oxidation state of Be<sub>2</sub> to Be<sub>2</sub><sup>+</sup>. In the complexes where the Be atom interacts with the LP of the LB, the Be-Be bond is weaker than in those complexes formed by  $\pi$  interaction. However, in these complexes characterized by a LP  $\rightarrow$  p<sub>Be</sub> interaction, the Be<sub>2</sub> moiety remains neutral and are the strongest Be-Be bonds reported in the literature for the neutral Be dimer, to our knowledge.

The short Be-Be bond distance in the L: Be-Be: L systems increases the charge accumulation between the Be atoms, inducing the formation of a NNA in the ground state of these complexes. This investigation did not find a connection between the existence of NNAs and low-lying excited states. Future studies will attempt to describe the role of core and valence electrons in the formation of NNA, in order to rationalize how do the NNA windows varies along the periodic table, and also the NNA absence in H<sub>2</sub> and He<sub>2</sub> for any bond distance [307, 310].

### Conclusiones

*El enlace de Be-Be se vuelve más fuerte cuando Be<sub>2</sub> interactúa con Bases de Lewis, sin embargo, esta interacción no sólo aumenta la fortaleza del enlace, sino que también modifica el estado de oxidación del dímero de Be dependiendo de la naturaleza de la BL.*

La mayor interacción Be-Be ocurre cuando el complejo se forma entre Be<sub>2</sub> y ligandos radicalarios. Este fuerte enlace se debe a la despoblación del orbital  $\sigma_{\text{Be-Be}}^*$ , como consecuencia de una transferencia de carga hacia los orbitales de valencia de los ligandos radicalarios.

La interacción entre Be<sub>2</sub> y especies donadoras de electrones de capa-cerrada también aumenta la fortaleza del enlace Be-Be, debido a que esta interacción estabiliza enormemente los orbitales  $\pi_{\text{Be}}$ . Esta estabilización es mayor cuando los ligandos poseen orbitales  $\pi$ , ya que existe una conjugación entre los orbitales  $\pi_{\text{Be}}$  y  $\pi_{\text{L}}$ , de tal manera que aumenta la fortaleza del enlace Be-Be y también cambia su estado de oxidación respecto a la molécula aislada (Be<sub>2</sub>). Cuando el dímero de Be interactúa con los LP del ligando, el enlace Be-Be es más débil que en aquellos compuestos formados por interacciones  $\pi$ . Sin embargo, en estos complejos caracterizados por una interacción  $\text{LP} \rightarrow p_{\text{Be}}$ , el fragmento Be<sub>2</sub> se mantiene neutro, correspondiendo a los enlaces Be-Be más fuertes reportados en la literatura para el dímero neutro, según nuestro conocimiento.

La acumulación de carga entre los átomos de Be en complejos del tipo L: Be-Be: L aumenta como consecuencia de la corta distancia de enlace Be-Be en estos complejos, lo cual promueve la formación de Pseudo-Núcleos o Atractores No-Nucleares (NNA, por sus siglas en inglés Non Nuclear Attractors) en el estado fundamental de los compuestos L: Be-Be: L. Nuestro estudio no encontró ninguna asociación entre la existencia de NNAs y estados excitados bajos en energía. En el futuro intentaremos describir la importancia de los electrones de core y de valencia en la formación de NNAs, de tal manera que sea posible explicar la periodicidad de las ventanas de NNA, así como la ausencia de NNAs en H<sub>2</sub> y He<sub>2</sub> a cualquier distancia de enlace [307, 310].



## THE TOTAL POSITION SPREAD TENSOR: A NEW TOOL FOR THE ANALYSIS OF CHEMICAL BONDS

---

The theoretical framework of the Total Position Spread Tensor (TPS) ( $\Lambda$ ) is described in section 2.8.5. This method has been widely applied to describe the metal-insulator properties of periodic systems, but its application to molecular environments has not been studied. The TPS is a global quantity with a component on each cartesian coordinate, which describes the electron fluctuation along each cartesian direction when the system is perturbed; such a perturbation could be for instance the dissociation of a chemical bond. Diatomic molecules of first and second row elements are suitable systems to illustrate the behavior of the TPS: the evaluation of the TPS components is easier due to their linear geometry, the theoretical description can be done using high-level ab-initio methods because of their small size and they allow to study different types of chemical bonds. For molecules with linear geometries, two main components of the tensor can be defined: (1) parallel to the bond direction ( $\Lambda_{\parallel}$ ) and (2) perpendicular to the bond ( $\Lambda_{\perp}$ ). The first component describes the electron fluctuation associated with the chemical bond, while the second the variations in the surroundings of the bond. Besides studying some diatomic molecules, the TPS was applied to analyze the bonding properties of the  $\text{Be}_2$  moiety in the  $\text{L}:\text{Be}-\text{Be}:\text{L}$  complexes too. In particular, the  $\text{CO}:\text{Be}-\text{Be}:\text{CO}$  compound has been chosen to illustrate the TPS behavior of this group of molecules, since its evaluation is easier compared to systems with  $\text{L} = \text{NH}_3$  or  $\text{H}_2\text{O}$  due to its linear symmetry.

The perpendicular ( $\Lambda_{\perp}$ , see scheme 5.1a) and parallel ( $\Lambda_{\parallel}$ , see scheme 5.1b) components of both the Spin-Summed of the Total Position Spread Tensor (SS-TPS) (see equation 2.158) and Spin-Partitioned of the Total Position Spread Tensor (SP-TPS) (see equation 2.165) were evaluated for four groups of molecules, which were classified according to the type of the interaction:

1. *Covalent bonds*: the  $\text{H}_2$ ,  $\text{Li}_2$  and  $\text{N}_2$  molecules.
2. *Charge-Shift bonds*: the  $\text{F}_2$  molecule was studied as representative of this type of interaction.
3. *Ionic bonds*: the  $\text{LiF}$  molecule was chosen to illustrate the behavior of the TPS for these bonds.
4. *Weak bonds* depending on the type of weak interactions:
  - a) The  $\text{He}_2$  molecule for the Van der Waals interaction.



- b) The non-dynamical bond in the isolated  $\text{Be}_2$  molecule and in the  $\text{CO}:\text{Be}-\text{Be}:\text{CO}$  complex.



Scheme 5.1: Representation of the TPS (a) perpendicular to the bond direction ( $\Lambda_{\perp}$ ) and (b) in the bond direction ( $\Lambda_{\parallel}$ ).

## 5.1 METHODOLOGY

The SS-TPS and SP-TPS tensors were calculated using Full Configuration Interaction (FCI) and Complete Active Space Self Consistent Field (CASSCF) methods. The selection of the method was based on the size of the system. The FCI calculations were performed using a sequence of programs: the initial HF guesses were computed using the Dalton quantum computational package [319], followed by transformations of the orbital basis from Atomic Orbitals (AO) to Molecular Orbitals (MO), and finally the FCI calculations were performed using the in-house Neptunus program [320–323]. The FCI calculations were done using the frozen core approximation. The CASSCF calculations were carried out with the MOLPRO 2015 computational package [89, 324, 325]. Table 4 shows the method and basis set used for the molecules studied in this chapter.

Table 5 compares the theoretical and experimental values of the equilibrium distances ( $R_e$ ) and the Bond Dissociation Energy (BDE) for the diatomic molecules. For molecules composed by the atoms H, He, Li or Be there is a very good agreement between the reference data and the FCI results. The absolute errors are around  $0.04\text{\AA}$  for  $R_e$  and  $2\text{ kJ}\cdot\text{mol}^{-1}$  for the BDE, those all within chemical accuracy. However, the errors are higher for the molecules involving F or N. The basis set used for these molecules (see table 4) is not flexible enough to describe them correctly, and the use of a bigger basis set is not affordable at FCI level of theory.  $R_e$  and BDE for the  $\text{CO}:\text{Be}-\text{Be}:\text{CO}$  complex were described in section 4.3.3.

Table 12 in appendix B.7 compares the SS-TPS and the SP-TPS of the molecules at dissociation distances with respect to the corresponding isolated atoms. At long bond distances, both tensors converge to the sum of the atomic values, showing the size-consistency of the method. The systems studied in this chapter are closed-shell molecules with a singlet ground state and thus, the spin-partitions of the tensor are grouped in *same spin* ( $\Lambda_{\alpha\alpha+\beta\beta}$ ) and *different spin* ( $\Lambda_{\alpha\beta+\beta\alpha}$ ) components.

Table 4: Description of the method and basis set for the molecules studied in the analysis of the TPS. The basis set used for the analysis of diatomic molecules is the ANO basis set optimized by Roos and coworkers [326], while the cc-pVTZ by Dunning et al is used for the CO: Be-Be: CO [327].

MOLECULE	METHOD	BASIS SET
H <sub>2</sub>	FCI	7s3p3d3f
Li <sub>2</sub>	FCI	7s6p4d3f
N <sub>2</sub>	FCI	3s2p
LiF	FCI	3s2p/3s2p
F <sub>2</sub>	FCI	3s2p
He <sub>2</sub>	FCI	7s4p3d
Be <sub>2</sub>	FCI	7s7p4d3f
CO: Be-Be: CO	CASSCF(10,12)	Be = 3s2p1d C, O = 4s3p2d1f

Table 5: Bond dissociation energies (BDE) and equilibrium distances ( $R_e$ ) for the diatomic molecules studied in this thesis. The equilibrium distances are in Å, the BDE are in  $\text{kJ}\cdot\text{mol}^{-1}$  and all values were calculated at FCI level of theory. The experimental values are shown within parenthesis.

MOLECULE	$R_e$ (Å)	BDE ( $\text{kJ}\cdot\text{mol}^{-1}$ )
H <sub>2</sub> [328]	0.74 (0.74)	456 (458)
Li <sub>2</sub> [329]	2.70 (2.67)	101 (99)
N <sub>2</sub> [330]	1.14 (1.10)	671 (944)
F <sub>2</sub> [331]	1.57 (1.41)	79 (157)
LiF 1 <sup>1</sup> Σ [332]	1.64 (1.57)	506 (575)
He <sub>2</sub> [333]	2.99 (2.97)	0.08 (0.09)
Be <sub>2</sub> [23]	2.51 (2.45)	8 (9)

*The electron rearrangement after the formation of a chemical bond is different for each type of interaction (see chapter 3), indicating that there is a characteristic wave function associated to each type of chemical bond. Thus, the results are generalized for each type of chemical bond. For a detailed analysis of each molecule see appendices B.7 and B.8.*

## 5.2 COVALENT BONDS

The SS-TPS and SP-TPS along the dissociation curves of the molecules in this group can be found in appendix B.7 figures 1-3 and in appendix B.8 figures 1-2. Figure 5.1 represents the behavior of both tensors, SS-TPS and SP-TPS, for all molecules in this group. The most dramatic changes appear in  $\Lambda_{\parallel}$ . Generally, *the lowest values of the SS-TPS and the SP-TPS occur in regions close to the nuclei, because there is a negligible electron mobility. The parallel component of the SS-TPS shows a maximum in the area where the bond is broken ( $R_{\text{break}}$ , the second derivative of the energy becomes zero), while the parallel components of the SP-TPS diverges as  $R_{\text{bond}}^2$  when  $R_{\text{bond}} \rightarrow \infty$  ( $R_{\text{bond}}$  corresponds to the bond distance).*

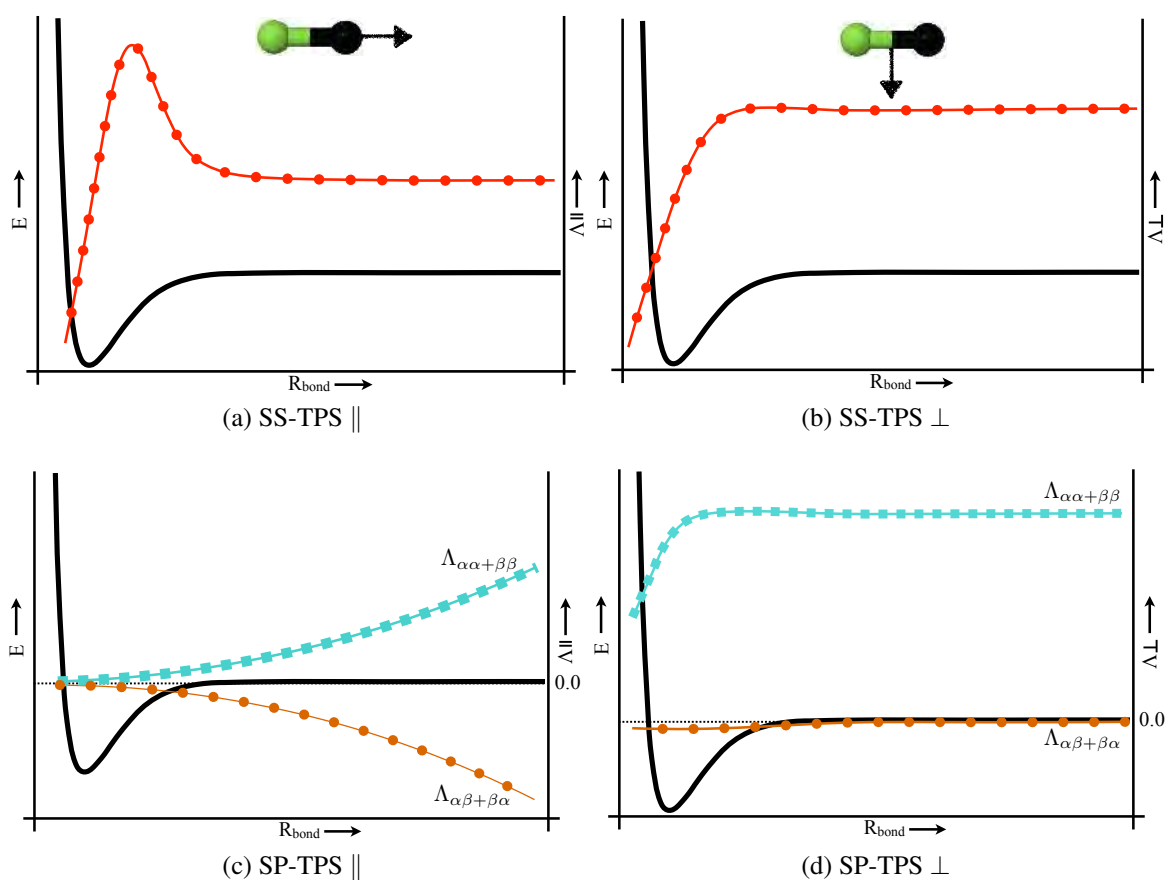


Figure 5.1: SS-TPS ( $\circ$ -red) and SP-TPS ( $\square$ -cyan  $\Lambda_{\alpha\alpha+\beta\beta}$  and  $\circ$ -orange  $\Lambda_{\alpha\beta+\beta\alpha}$ ) for covalent bonds. (a) SS-TPS  $\parallel$ , (b) SS-TPS  $\perp$ , (c) SP-TPS  $\parallel$  and (d) SP-TPS  $\perp$ . The dissociation energy curve is represented in full-black line.

**The SS-TPS.** The dissociation curves of the molecules in this group could be divided into two regions by considering  $R_{\text{break}}$ :

- $R_{\text{bond}} < R_{\text{break}}$ . The parallel and perpendicular components increase with the value of  $R_{\text{bond}}$  due to the decrease of the nuclei constraints over the electron fluctuation. At the equilibrium distance, the values of both,  $\Lambda_{\parallel}$  and  $\Lambda_{\perp}$  are less than atomic values

because the electron fluctuation is still limited by the influence of the nuclei. In the  $R_{\text{break}}$  region,  $\Lambda_{\parallel}$  shows a maximum, while  $\Lambda_{\perp}$  reaches the sum of the atomic values.

- $R_{\text{bond}} > R_{\text{break}}$ ,  $\Lambda$  goes quickly to the sum of the atomic values.

**The SP-TPS** gives qualitative information about the electron correlation in the system:  $\Lambda_{\alpha\alpha+\beta\beta}$  and  $\Lambda_{\alpha\beta+\beta\alpha}$  could be translated as measures of the exchange-correlation energy ( $E_{\text{corr}}^{\text{XC}}$ ) and the coulomb-correlation energy ( $E_{\text{corr}}^{\text{ee}}$ ), respectively. The exchange and coulomb electron correlation were defined in section 2.1.4, and the relation between them has been used to define strongly correlated systems, which occurs when  $|E_{\text{corr}}^{\text{XC}}| \sim |E_{\text{corr}}^{\text{ee}}|$  [334]. Therefore, the SP-TPS could be used as an indicator of the multi-reference character of  $\Psi$ . For covalent bonds, the general behavior is that the parallel component diverges as  $R_{\text{bond}}^2$  when  $R_{\text{bond}} \rightarrow \infty$ , being the same-spin component slightly bigger than the different-spin. Two regions can be defined considering  $\Psi$ :

- $R_{\text{eq}} < R_{\text{bond}} < R_{\text{break}}$ . The ground state of the molecule is represented by a closed-shell configuration where the valence electrons are localized in a bonding orbital  $\Psi_{\text{MO}} = \phi_{\text{A}} + \phi_{\text{B}}$ . Therefore, a single determinant wave function describes correctly the system, and  $|E_{\text{corr}}^{\text{XC}}| > |E_{\text{corr}}^{\text{ee}}|$ .
- $R_{\text{bond}} > R_{\text{break}}$ . The homolytic dissociation of a covalent bonded system results in open-shell products with multi-reference character, which is represented by the  $R_{\text{bond}}^2$  divergence of the same- and different-spin partitions.

**The SP-TPS $_{\perp}$  components** are less impressive compared with the SP-TPS $_{\parallel}$ .  $\Lambda_{\perp(\alpha\beta+\beta\alpha)}$  is close to zero almost everywhere in the dissociation curve. Therefore,  $\Lambda_{\perp(\alpha\alpha+\beta\beta)}$  is the main contribution to the  $\Lambda_{\perp}$ , showing both the same behavior. This means that the small electron fluctuation outside of the bonding region is mainly associated to  $E_{\text{corr}}^{\text{XC}}$ .

### 5.3 CHARGE-SHIFT BONDS

The SS-TPS and SP-TPS of the  $\text{F}_2$  molecule are shown in appendix B.7 figure 4 and in appendix B.8 figures 1-2. The spin-partitioned shows the same behavior as for covalent bonds, while the difference between the two type of interactions can be seen by considering the SS-TPS. *Whereas for covalent bonds the maximum of electron fluctuation is in the bond breaking region, for charge-shift bond it is at the equilibrium distance* (see figure 5.2a).

Section 3.1.2 describes the nature of charge-shift bonds. The Pauli repulsion of the  $\pi$  cloud in the ground state is stabilized by a high electron delocalization, which is described by the maximum of  $\Lambda_{\parallel}$  at the equilibrium distance. Valence Bond Theory (VBT) describes this type of bond as a resonance between a covalent and an ionic configuration. Thus,  $\Psi$  is not

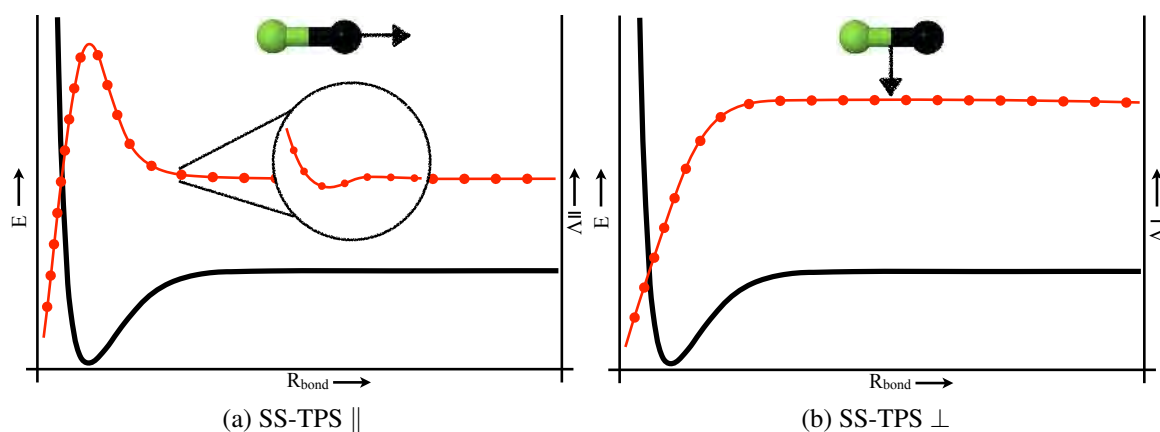


Figure 5.2: SS-TPS (○-red) for charge-shift bonds, (a) SS-TPS  $\parallel$  and (b) SS-TPS  $\perp$ . The dissociation energy curve is represented in full-black line.

longer described by a pure covalent or ionic configuration, but by a mixture of these states. This property has been modeled by studying the  $H_2$  molecule within the  $\Psi_{OV B}$  framework, but considering a scale factor ( $k$ ) between the neutral ground and the ionic  $^1\Sigma_g$  states [335] (where OVB stands for orthogonal VBT). The analysis of the SS-TPS considering  $\Psi_{OV B}$  shows that the maximum of the tensor occurs at shorter distances when the value of  $k$  decreases, which is equivalent to say that  $\Lambda$  is shifted to the equilibrium distances when the gap between the covalent and ionic states becomes smaller (see figure 4 in appendix B.7). Therefore, the  $F_2$  maximum of  $\Lambda_{\parallel}$  at the equilibrium distance is caused by the mixture of the covalent and ionic configurations.

$\Lambda_{\parallel}$  for  $N_2$  has the same behavior than covalent bonds. The maximum of the tensor is in the  $R_{break}$  region, but after that maximum, there is a shallow minimum that is also found for the  $F_2$  molecule (see figure 5.2a). The physical meaning of this minimum may be explained as a relaxation of the system when the Pauli repulsion vanishes due to the bond dissociation. Considering again the  $\Psi_{OV B}$  analysis for the  $H_2$  system, for  $k = 1.0$  the system corresponds to the covalent  $H_2$  molecule and  $\Lambda_{\parallel}$  does not show this minimum. However, the minimum appears for values of  $k$  between  $0.7 - 0.5$  or, otherwise stated, when the charge-shift character increases. The SS-TPS description of the  $F_2$  molecule is characteristic of a pure charge-shift bond, while it is not yet completely understood for  $N_2$ . The wave function analysis of the molecule is shown in figure 5.3, and all of them suggest that  $N_2$  is a strong covalent molecule. The Quantum Theory of Atoms in Molecules (QTAIM) method finds a  $BCP_{NN}$ ,  $\rho$  is on the order of 0.1 and  $\nabla^2\rho$  is negative. The Electron Localization Function (ELF) analysis locates a  $V(N, N)$  disynaptic basin, with a high electron population and small values of  $\langle cov\Omega_i, \Omega_j \rangle$ . On the contrary to the wave function analysis, the Resonance Energy (RE) has an important contribution to the BDE of  $N_2$ , but this contribution is not as big as in bonds including halogen atoms [176]. Therefore, taking into consideration all previous bond analyses, the  $F_2$  molecule is represented by  $k \sim 0.5$  where there is a maximum interaction between the covalent and the ionic state, while  $N_2$  is represented by  $k \sim 0.7$  where the interaction between the states is bigger than in a pure covalent bond, but it cannot be considered a charge-shift bond yet.

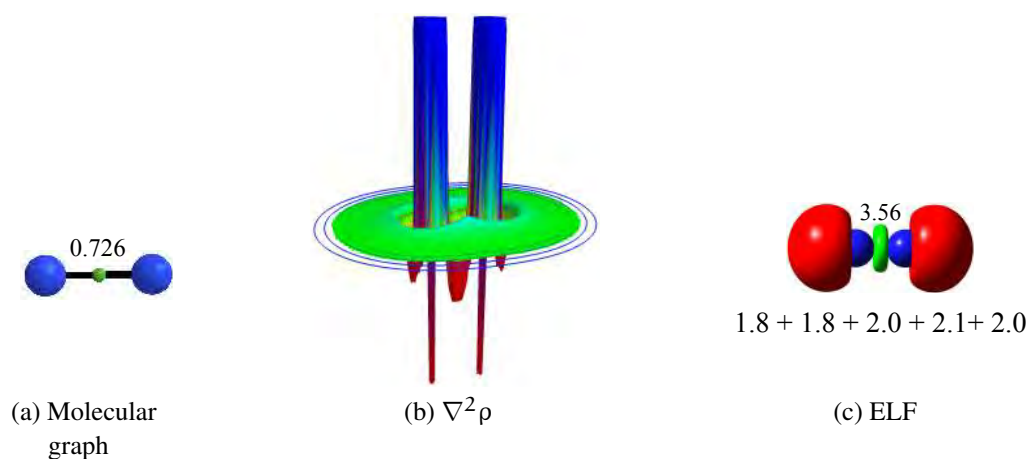
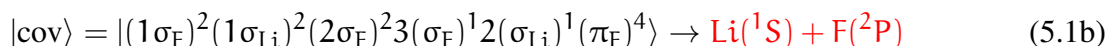
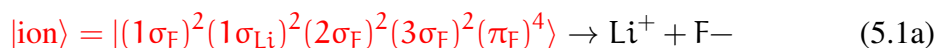


Figure 5.3: Wave function analysis of the  $N_2$  molecule, (a) molecular graph with the  $BCP_{NN}$  in green and its value of  $\rho$ ; (b) the relief map of  $\nabla^2\rho$ , the color scale is: blue  $> 1$ , cyan  $> 0.5$ , green  $> -0.5$ , yellow  $> -1$ , red  $< -1$ ; (c) ELF representation of the basins and their population, the color scale is: monosynaptic basins associated with lone pairs are in red, and disynaptic or trisynaptic basins involving heavy atoms are in green, and below is shown the diagonal elements of the covariance matrix. The calculations were performed at B3LYP/cc-pVTZ level of theory.

## 5.4 IONIC BONDS

The dissociation of ionic systems is more complicated than the dissociation of covalent systems because the reactants and products are in different states. Therefore, the dissociation mechanism must involve a state crossing between the covalent and the ionic states (see section 3.1.1). For LiF a state crossing is forbidden (non-crossing rule), instead there is an avoided crossing around  $5.8\text{\AA}$  (see appendix B.7 figure 6). Appendix B.7 figures 7-8 and appendix B.8 figures 3,5 show the SS-TPS and the SP-TPS for the LiF molecule, and a representative example can be found in figure 5.4. The configuration of the ionic and covalent states for LiF are shown in equation 5.1, emphasizing in red the ground state configuration of reactants and products.



**The  $\perp$  component of the SS-TPS** for ionic bonded systems gives more information about  $\Psi$  than for covalent bonds. When the LiF bond distance is shorter than the avoided crossing position, the tensor of the ground state shows values smaller than for the excited state, indicating a higher electron fluctuation in  $|\text{cov}\rangle$  than in  $|\text{ion}\rangle$ . Before the avoided crossing,  $\Lambda_\perp$  of the  $|\text{ion}\rangle$  configuration increases to reach the values of the ionic products, while  $\Lambda_\perp$  of

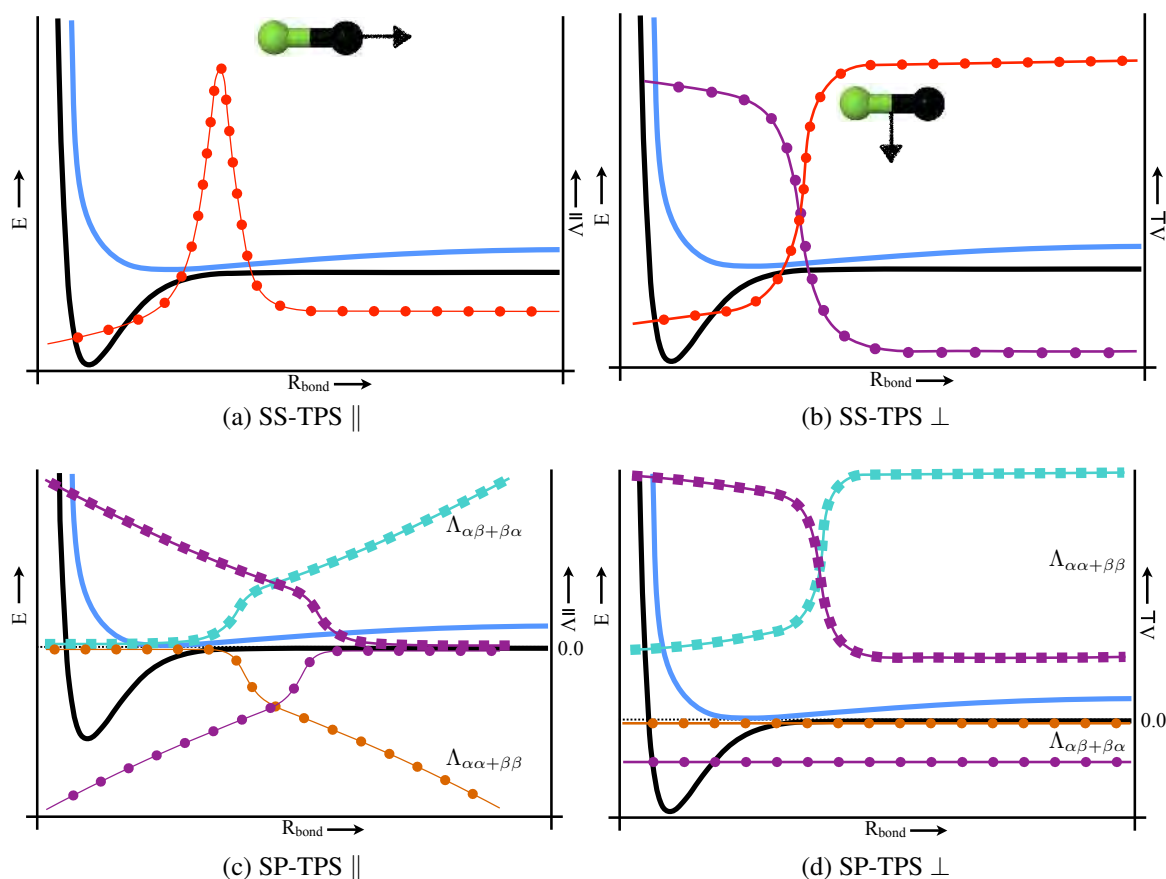


Figure 5.4: Representation of the TPS for ionic bonds. SS-TPS is in  $\circ$ -red for the ground state and in  $\circ$ -purple for the first excited state. SP-TPS for the ground state:  $\Lambda_{\alpha\alpha+\beta\beta}$  is in  $\circ$ -orange and  $\Lambda_{\alpha\beta+\beta\alpha}$  is in  $\square$ -cyan. SP-TPS for the first excited state:  $\Lambda_{\alpha\alpha+\beta\beta}$  is in  $\square$ -purple and  $\Lambda_{\alpha\beta+\beta\alpha}$  is in  $\circ$ -purple. (a) SS-TPS  $\parallel$ , (b) SS-TPS  $\perp$ , (c) SP-TPS  $\parallel$  and (d) SP-TPS  $\perp$ . The dissociation energy curve is represented as a solid black line for the ground state and as a solid blue line for the first excited state.

the  $|\text{cov}\rangle$  configuration decreases to reach the values of the closed-shell products until they crossed at 5.8 Å. Finally, both of them converge to the corresponding sum of atomic values (see figure 5.4b). The main contribution to SS-TPS $\perp$  is from the  $\Lambda_{\perp(\alpha\alpha+\beta\beta)}$  partition, showing both the same behavior ( $\Lambda_{\perp(\alpha\beta+\beta\alpha)}$  is almost a constant close to zero, see figure 5.4d). The values of the  **$\parallel$  component of the SS-TPS** remain close the atomic values almost along all the dissociation curve, except in the avoiding crossing region where the tensor presents a maximum, indicating that the maximum of electron fluctuation for ionic bonds is at the avoiding crossing between the ionic and the covalent states, see figure 5.4a.

The  **$\parallel$  component of the SP-TPS** illustrates the multi- or single- reference character of the wave function in the dissociation of the LiF. The behavior of this tensor is summarized as follow:

1. Ground State:

- SP-TPS  $\sim 0 \Rightarrow R_{\text{bond}} < 5.8\text{\AA}$ .
- SP-TPS diverges as  $R_{\text{bond}}^2 \Rightarrow R_{\text{bond}} > 5.8\text{\AA}$ .

## 2. Excited State:

- SP-TPS diverges as  $R_{\text{bond}}^2 \Rightarrow R_{\text{bond}} < 5.8\text{\AA}$ .
- SP-TPS  $\sim 0 \Rightarrow R_{\text{bond}} > 5.8\text{\AA}$ .

For Li-F bond distances shorter than the avoided-crossing distance ( $5.8\text{\AA}$ ), the ground state is characterized by a single-reference ionic wave function  $|\text{ion}\rangle$ , while the excited state is described by an open-shell covalent wave function  $|\text{cov}\rangle$ . The closed-shell character of the ground state is described by SP-TPS  $\sim 0$  and the multi-reference of the excited state by the  $R_{\text{bond}}^2$  divergence of the tensors. The situation is reversed for bond distances longer than  $5.8\text{\AA}$ , the ground state becomes the open-shell neutral atoms and the excited state the closed-shell ionic atoms. The first one shows a  $R_{\text{bond}}^2$  divergence of the SP-TPS  $\parallel$ , whilst in the second the SP-TPS  $\parallel$  approaches to values close to zero.

## 5.5 WEAK BONDS

The bond dissociation processes described so far involved dramatic changes in  $\Psi$ , because the electronic configurations change from a bonding to an anti-bonding state. Therefore, also dramatic variations were found in the TPS. This is not the case of weak interactions, wherein some systems there is not even an overlap of the moieties wave functions at the equilibrium distance and the interaction is mainly electrostatic. The behavior of the TPS for weak interactions is studied considering the  $\text{He}_2$  and the  $\text{Be}_2$  molecules. For a long time, both interactions were considered Van der Waals, but recently the  $\text{Be}_2$  molecule has been described as a non-dynamical bond [54]. In the next sections the results for  $\text{He}_2$ ,  $\text{Be}_2$  are discussed, as well as the disubstituted complexes formed between  $\text{Be}_2$  and CO, CO: Be-Be: CO.

### 5.5.1 Van der Waals Interactions: $\text{He}_2$ .

The  $\text{He}_2$  molecule is bonded by weak Van der Waals dispersion forces, supported by the very long He-He bond distance and the small BDE shown in table 5. Therefore, the electron fluctuation associated with the dissociation of this dimer should not be remarkable. The SS-TPS $\parallel$  of the He atom is equal to  $0.75\text{au}^2$  (the sum of the atomic values is equal to  $1.51\text{au}^2$ ). When the separation between the He atoms is shorter than the equilibrium distance, the parallel component shows a small peak at  $2\text{\AA}$  ( $\Lambda_{\parallel} = 1.52\text{au}^2$ ), while for bond distances longer than the equilibrium distance, the tensor quickly converges to the sum of the atomic values. The



behavior of  $\text{SS-TPS}_\perp$  is similar to the parallel component. Therefore, the SS-TPS for Van der Waals interactions shows almost a constant value when the bond is stretched, indicating a negligible electron fluctuation. The  $\text{SP-TPS}_\parallel$  is also almost constant for the He dimer. The  $\Lambda_{\parallel(\alpha\beta+\beta\alpha)}$  component is close to zero along the dissociation curve, which is a consequence of the closed-shell character of the interaction. This means that the main contribution to the  $\text{SS-TPS}_\parallel$  is from the  $\Lambda_{\parallel(\alpha\alpha+\beta\beta)}$  component, indicating that the exchange-correlation energy has an important contribution to the  $\text{He}_2$  interaction energy. See appendix B.7 figure 10 and appendix B.8 figure 5 for a graphic representation of the TPS and a deeper analysis of the  $\text{He}_2$  molecule. The only region where the  $\text{He}_2$  TPS shows a significant variation is at very short bond distances, below  $1\text{\AA}$ . This region does not have a physical meaning for the gas phase molecule, nor it is correctly described with the basis set used for the calculation. Therefore, we decided not to perform an analysis of this region of the dissociation curve.

### 5.5.2 Be bonds: $\text{Be}_2$ and CO: Be-Be: CO.

The bonding properties of the beryllium dimer are described in reference [54] and in section 4.3.2. The bond in the Be dimer is originated by the mixture of the low-lying  $p_{\text{Be}}$  with the  $2s_{\text{Be}}$  orbitals, which is not possible for the highly energetic  $p_{\text{He}}$  orbitals. The TPS analysis is in agreement with this description, figure 5.5 shows a representation of the parallel component of the SS-TPS and SP-TPS tensors. The  $\Lambda_\parallel$  component for  $\text{Be}_2$  is different from a constant, thus  $\text{He}_2$  and  $\text{Be}_2$  do not share the same type of interaction: *the Be-Be bond is not a closed-shell interaction*. According to the SS-TPS, the  $\text{Be}_2$  molecule shows a maximum of electron fluctuation in the equilibrium region as the  $\text{F}_2$  molecule. Nevertheless, the high electron fluctuation of  $\text{Be}_2$  is associated to the  $s \rightarrow p$  excitations at the equilibrium distance [54] and not to Pauli repulsion, which is illustrated by the SP-TPS.

The  $\text{SP-TPS}_\parallel$  along the bond direction for  $\text{Be}_2$  and  $\text{F}_2$  are completely different. At short bond distances the same and different-spin tensors of the beryllium dimer diverge as  $R_{\text{bond}}^2$ , whilst for  $\text{F}_2$  the tensor diverges at long bonds distances. This means that while  $\text{F}_2$  has a multi-reference character at the dissociation limit due to the formation of open-shell products, the multi-reference character of the  $\Psi_{\text{Be}_2}$  is at the equilibrium distance. The ground state of  $\text{Be}_2$  needs to be described by more than one Slater determinant, in order to represent correctly the mixture between the  $s_{\text{Be}}$  and  $p_{\text{Be}}$  orbitals. At long distances, the  $\text{Be}_2$  products are closed-shell atoms and the  $\text{SP-TPS}_\parallel$  becomes constant.

The situation is different when  $\text{Be}_2$  interacts with a Lewis Base (LB), in complexes such as L: Be-Be: L. The Be: L non-covalent interaction increase up to 20 times the strength of the Be-Be bond with respect to the isolated dimer, which is caused by a stabilization of the  $\pi_{\text{Be}}$  orbitals. Section 4.3.3 describes the bonding properties of the L: Be-Be: L complexes, with L =  $\text{NH}_3$ ,  $\text{H}_2\text{O}$  and CO. The most dramatic effect was found for L = CO, where the system is highly stabilized by a  $\pi$ -conjugation between the  $\pi_{\text{CO}}$  and the  $\pi_{\text{Be}}$  orbitals. Appendix B.6-figure S9 and appendix B.6-figure 2 show the state energy diagram and the wave function analysis for the CO: Be-Be: CO complex, respectively. The most remarkable

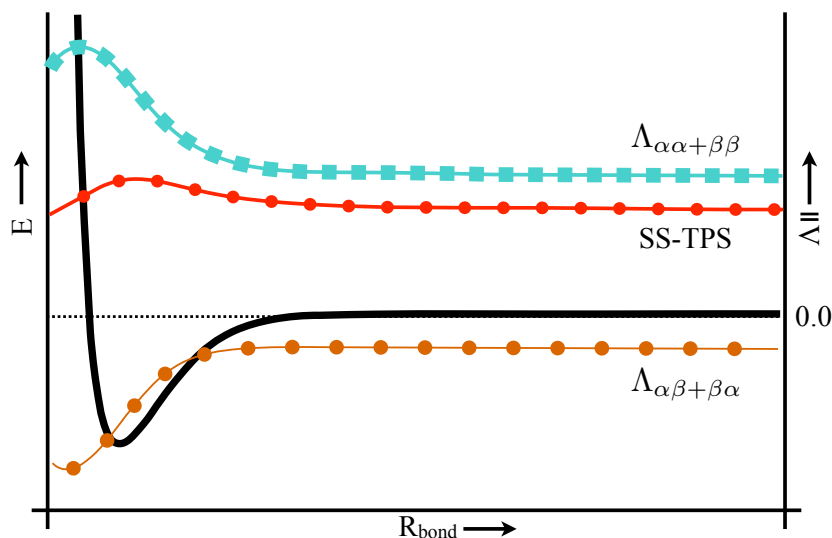
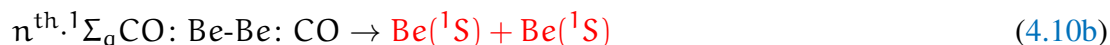
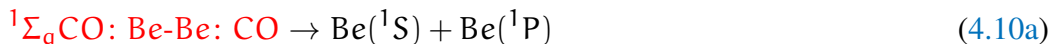


Figure 5.5: Representation of the TPS for non-dynamical bonds the SS-TPS is in  $\circ$ -red. The SP-TPS is in  $\square$ -cyan for  $\Lambda_{\alpha\alpha+\beta\beta}$  and in  $\circ$ -orange for  $\Lambda_{\alpha\beta+\beta\alpha}$ . The dissociation energy curve is represented as a solid black line.

finding is that at the equilibrium distance two singlet states are degenerated ( $|\Psi_{\text{CASPT2}}\rangle = |0.32[(2\sigma_{\text{BeBe}})^2(\pi_{\text{BeBe}} + \pi_{\text{CO}_x}^*)^2] + 0.32[(2\sigma_{\text{BeBe}})^2(\pi_{\text{BeBe}} + \pi_{\text{CO}_y}^*)^2]\rangle$ ) and the  $\text{Be}_2$  moiety is bonded through a Non-Nuclear Attractor (NNA).

The dissociation of this complex is not simple, the doubly degenerated ground state is highly correlated and, reactants and products are in different electronic states (see section 4.3.3.3 and equation 4.10).



**The parallel component of the TPS** for the  $\text{CO: Be-Be: CO}$  system is shown in figure 5.6. Consider that this dissociation path only corresponds to the region before the avoided crossing in equations 4.10. Figure 5.6a shows both the SS-TPS and the value of  $\rho$  at the  $\text{BCP}_{\text{Be-Be}}$ . The pink triangles represent the area where the system is bonded through a NNA. According to  $\Lambda_{||}$  there are two maxima of electron mobility associated to this type of interaction: the first at the equilibrium and the second at long bond distances. It is clear that the second maximum is due to the dissociation of the molecule, which is in agreement with the almost zero value of  $\rho$  at the  $\text{BCP}_{\text{Be-Be}}$ . The area around the equilibrium distance of this system is a complicated section of the Potential Energy Surface (PES), and there are at least three possible explanations for this maximum of the TPS:

1. The formation of the NNA.
2. The doubly degenerated ground state (see appendix B.6 figure S9).
3. The  $s \rightarrow p$  excitations associated to the ground state of the Be-Be bond.

Figure 2 in reference [307] shows that homonuclear diatomic molecules from  $H_2$  to  $F_2$  have a NNA, which appears in different ranges of the dissociation curve depending on the atomic number. The analysis of the SS-TPS for the  $Li_2$ ,  $N_2$ ,  $F_2$  or  $Be_2$  systems does not show a maximum associated to the formation of a NNA, and it is probably not the case for the CO: Be-Be: CO either. This suggests that the behavior of the tensor in the equilibrium region might be attributed by both, the  $s \rightarrow p$  excitations in the  $Be_2$  moiety and the doubly degenerated ground state.

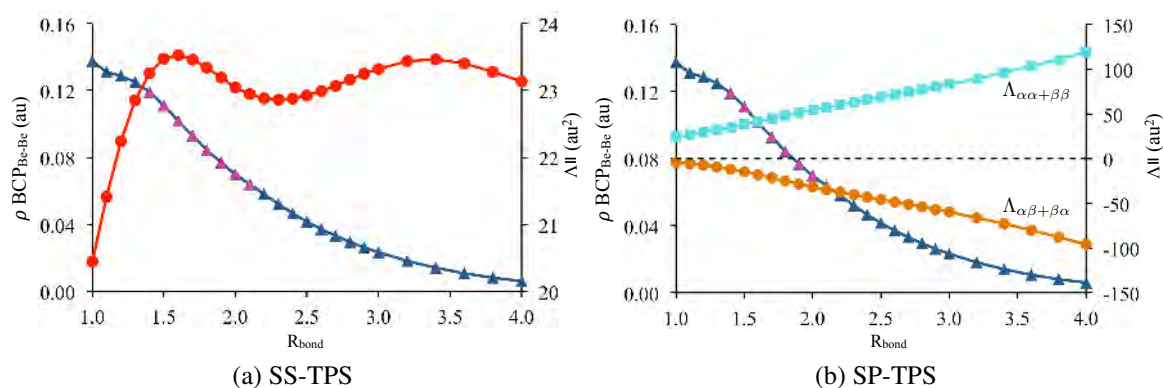


Figure 5.6: Representation of the parallel component of the SS-TPS and SP-TPS for the  $^1\Sigma_g$  ground state of the CO: Be-Be: CO complex. (a) The SS-TPS is shown in  $\circ$ -red and, (b) the SP-TPS is in  $\square$ -cyan for  $\Lambda_{\alpha\alpha+\beta\beta}$  and in  $\circ$ -orange for  $\Lambda_{\alpha\beta+\beta\alpha}$ . The value of  $\rho$  in the  $\text{BCP}_{Be-Be}$  is represented with  $\triangle$ -blue and the  $\text{BCP}_{Be-NNA}$  with  $\triangle$ -pink. The calculations were performed at CASSCF(10,12)/cc-pVTZ//CASPT2/CASSCF(10,12)/cc-pVTZ level of theory.

The SP-TPS is shown in figure 5.6b. The behavior of the tensors in the region between 1 – 4 Å is different from both covalent and the  $Be_2$  bonds; the tensors show an increasing multi-reference character across all the dissociation curve. The reactant in equation 4.10a is a multi-reference molecule, which requires more than one Slater determinant to describe the degeneracy of the doubly occupied  $\pi_{Be-Be}$  orbital and its  $\pi$ -conjugation with the  $\pi_{CO}$  orbitals. The multi-reference character at long distances is enhanced by the formation of neutral radical products ( $\cdot CO: Be\cdot$ ). For distances beyond 4 Å, the crossing between the  $^1\Sigma_g$  and  $n^{th} \cdot ^1\Sigma_g$  states ( $n^{th} \cdot ^1\Sigma_g$  corresponds to the state that dissociates as the isolated dimer) should produce a third maximum in the SP-TPS, which for longer bond distances should evolve to the constant values of 2Be plus 2CO atoms.

### 5.5.3 Conclusions

*The behavior of the SS-TPS and the SP-TPS in molecular dissociation is an intrinsic property of each type of chemical interaction, showing the regions with the highest electron fluctuation and the electron-correlated character.*

The SS-TPS shows a maximum when there is a considerable electron rearrangement. For the bond dissociation of covalent interactions, this occurs when the electron configuration changes from the bonding to the anti-bonding state, indicating the region where there is no longer a chemical interaction. In contrast, for ionic bond dissociations, this maximum takes place at the avoided crossing where the ionic ground state becomes covalent. The SS-TPS for charge-shift and non-dynamical bonds shows a maximum of electron fluctuation at equilibrium distances, but for the first case is a consequence of the resonance between the ionic and covalent states, while for non-dynamical bonds is due to the mixture between valence occupied and unoccupied orbitals. Finally, the variation of the SS-TPS for Van der Waals systems is negligible due to the closed-shell nature of the interaction.

The SS-TPS has proven to be able to monitor the electron fluctuation in the dissociation of chemical bonds, while the SP-TPS does it for the electron spin. Indeed, the partition of the tensor gives information about the relevance of electron correlation in the wave function. For systems with multi-reference character both the same- and different- spin partitions diverge as  $R_{\text{bond}}^2$  when the bond is dissociated, while for single-reference wave functions both partitions remain constant.

### Conclusiones

*El comportamiento de la Suma de Espín del Tensor de la Propagación de la Posición Total (SS-TPS, por sus siglas en inglés Spin-Summed of the Total Position Spread Tensor) y la Partición de Espín del Tensor de la Propagación de la Posición Total (SP-TPS, por sus siglas en inglés Spin-Partitioned of the Total Position Spread Tensor) en sistemas moleculares es una propiedad intrínseca de cada tipo de enlace químico, los cuales permiten identificar aquellas regiones con mayor movilidad electrónica y aquellas donde la correlación electrónica es de gran importancia.*

El SS-TPS presenta un máximo cuando existe una reorganización electrónica importante. Para la disociación de enlaces covalente, este máximo ocurre cuando la configuración electrónica cambia del estado enlazante al antienlazante, indicando la región en la cual ya no existen interacciones químicas. Por el contrario, en la disociación de enlaces iónicos, este máximo ocurre en el cruce evitado entre los estados covalentes e iónicos. De acuerdo con el SS-TPS para enlaces de tipo “charge-shift” y no-dinámicos, el máximo de fluctuación electrónica en el perfil de disociación para este tipo de enlaces sucede a la distancia de equilibrio, sin embargo, en el primer caso es debido a una resonancia entre los estados covalentes e iónicos, mientras que para los enlaces no-dinámicos se debe a una mezcla entre orbitales de valencia ocupados y desocupados. Finalmente, el SS-TPS no presenta ninguna característica extraordinaria para interacciones del tipo Van der Waals, lo cual se debe al carácter de capa cerrada de esta interacción.

El SS-TPS ha demostrado ser capaz de describir la fluctuación electrónica asociada a la disociación de enlaces químicos, mientras que el SP-TPS describe las fluctuaciones de es-

pín electrónico. La partición del tensor proporciona información sobre la importancia de la correlación electrónica en la función de onda. Para sistemas con carácter multi-referencial, las particiones de igual- y diferente espín divergen como  $R_{\text{bond}}^2$  cuando el enlace se disocia, mientras que para funciones de onda mono-referenciales ambas particiones se mantienen constantes.

## Part V

### RÉSUMÉ SUBSTANTIEL

"Theories cannot claim to be indestructible. They are only the plough which the ploughman uses to draw his furrow and which he has every right to discard for another one, of improved design, after the harvest."

*Paul Sabatier. Nobel Lecture - 1912.*



## RÉSUMÉ SUBSTANTIEL

---

Le concept de liaison chimique est considéré comme le concept le plus important en chimie, car il permet d'expliquer la structure, la réactivité et les propriétés d'un système, de comprendre les tendances dans un groupe de molécules ou de concevoir de nouveaux complexes avec des caractéristiques spécifiques. Gilbert Lewis a introduit en 1916 le concept moderne de liaison chimique, définissant que les atomes sont liés par des *paires d'électrons*, et même aujourd'hui les structures de Lewis sont très populaires parmi les chimistes pour représenter la structure électronique d'une molécule. Cependant, les anciens concepts en chimie furent révisés après la naissance de la mécanique quantique, en établissant de nouvelles interactions, par exemple : par transfert de charge, halogène, pnictogène, non dynamique, d'un électron et d'autres types de liaison. L'objectif principal de cette thèse est d'étudier de nouveaux types d'interactions chimiques impliquant l'atome de béryllium.

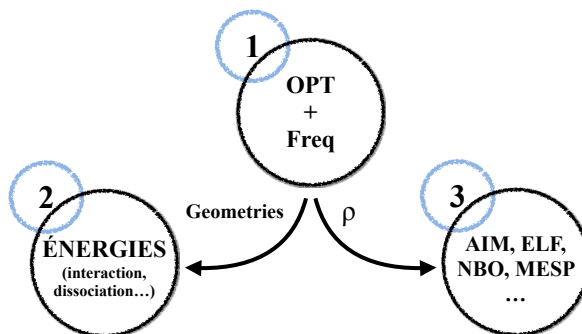
L'atome de Be a une chimie riche en raison de ses orbitales  $p_{Be}$  de basse énergie, donc il est possible de trouver de divers composés de Be avec plusieurs applications. Par exemple, l'oxyde de béryllium (BeO) présente une conductivité thermique, une capacité calorifique et une résistivité électrique très élevée. Il est donc utilisé dans l'industrie électronique, la fabrication d'isolateurs, de résistances, de bougies et de tubes d'hyperfréquences. Les alliages de béryllium présentent une chaleur spécifique, une conductivité thermique et un point de fusion élevée, une faible densité et une rigidité. Par exemple, l'alliage de Be avec du cuivre est utilisé pour les contacts électriques, les ressorts, les pinces, les interrupteurs, les soufflets et les manomètres Bourdon. Le béryllium métallique est un excellent générateur de neutrons en raison de sa faible masse atomique et de son faible rayonnement X. Il est donc utilisé comme initiateur de la fission nucléaire. Enfin, l'hydrure de béryllium et les halogénures de béryllium présentent une affinité très élevée pour les espèces donneuses d'électrons, en raison de leur forte carence en électrons. On a trouvé également que certains composés de Be étaient cancérogènes et provoquaient la Maladie Chronique du Béryllium (CBD, pour l'acronyme en anglais Chronic Beryllium Disease) [9–11, 18].

La toxicité élevée du Be a limité le nombre d'études expérimentales, augmentant l'importance de la théorie dans la description de composés de Be. Cette thèse rapporte l'analyse théorique de trois nouveaux types de liaisons de Be en utilisant des méthodes ab-initio et la Théorie de la Fonctionnelle de la Densité (DFT, pour l'acronyme en anglais Density functional Theory), et l'application du *Tenseur d'Etendue (Spread) de la Position Totale* (TPS, pour l'acronyme en anglais Total-Position Spread Tensor) aux systèmes moléculaires.

La méthodologie employée dans la présente thèse est résumée dans le schéma 4.2. Les points stationnaires de la Surface d'Énergie Potentielle (PSE, pour l'acronyme en anglais Potential Energy Surface) ont été localisés par des optimisations géométriques et ont été classés



comme des minima locaux ou globaux ou comme des points de selle par une évaluation des fréquences vibratoires harmoniques. Pour certaines de ces espèces ont également été calculées les propriétés thermodynamiques. La densité électronique des structures optimisées a été utilisée pour effectuer une analyse des fonctions d'onde, de même manière que les énergétiques ont été affinées au niveau le plus performant de la théorie. Le chapitre 2 décrit toutes les méthodes appliquées dans cette thèse.



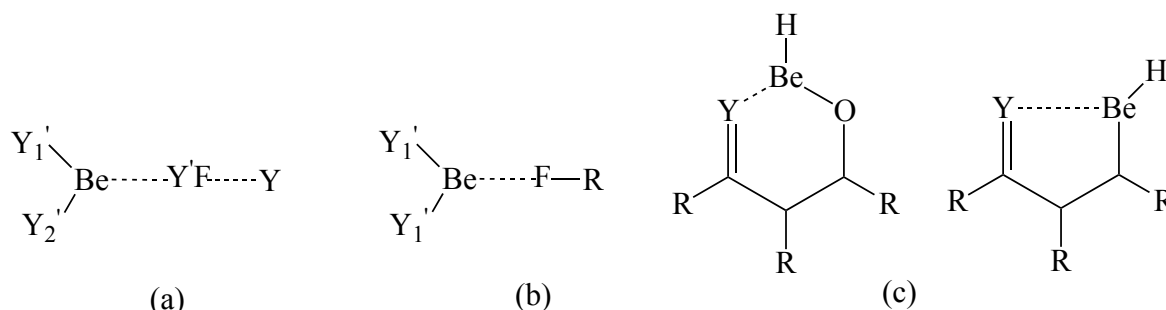
Scheme 4.2 : Schéma de la méthodologie utilisée dans cette thèse : (1) la géométrie est relâchée à un point stationnaire caractérisé par un calcul de fréquence vibratoire. (2) L'énergie a été recalculée au niveau le plus performant de la théorie. (3) Enfin, une analyse de la fonction d'onde du système est réalisée pour caractériser les propriétés des liaisons (plus de détails peuvent être trouvés dans la page 109).

## LIAISONS BÉRYLLIUM

Les Liaisons Béryllium (BerB) ont été caractérisés en 2009 par Yáñez et ses collègues, elles sont définies comme des liaisons non covalentes entre un groupe Be agissant comme un Acide de Lewis (LA, pour l'acronyme en anglais Lewis Acid) et une Base de Lewis (LB, pour l'acronyme en anglais Lewis Bases). Il y a une relation étroite entre les BerB et les Liaisons Hydrogène (HB, pour l'acronyme en anglais Hydrogen Bond), la nature des deux interactions étant principalement électrostatique [6–8]. Cependant, on a constaté que les BerB sont jusqu'à cinq fois plus fortes que HB, parce que les orbitales  $p_{Be}$  faibles favorisent le transfert de charge du LB vers le LA, quelque chose d'impossible pour les orbitales  $p_H$  de haute énergie.

Les Liaisons Béryllium atteignent des énergies d'interactions allant jusqu'à  $150\text{kJ}\cdot\text{mol}^{-1}$ . Les interactions non covalentes se renforcent avec la capacité Accepteur d'électrons de la LA ou le potentiel donneur d'électrons de la LB. Par conséquent, les BerB sont plus fortes dans  $\text{BeCl}_2$  que dans  $\text{BeH}_2$  et plus fortes dans  $\text{NH}_3$  que dans  $\text{H}_2\text{O}$  [19]. Une caractéristique importante des BerB est leur capacité à modifier les propriétés chimiques intrinsèques de la LB avec laquelle Be interagit, par exemple : la force des interactions covalentes [50–52, 231, 232], l'acidité de LA et LB [58, 59, 233] et la réactivité de la LB [58, 232, 234–237].

Cette thèse porte sur l'effet des BerB sur trois types de processus chimiques (voir schéma 4.1) : (1) la formation de liaisons halogènes (XB) dans les composés fluorés (4.1a), (2) la formation d'une espèce radicale neutre (4.1b) et (3) la formation des Liaisons Béryllium Intracellulaires (IBerB, pour l'acronyme en anglais Intramolecular Beryllium Bonds) (4.1c).



Scheme 4.1 : Représentation des BerB étudiées dans cette thèse. (a) Les complexes  $\text{BeY}'_1\text{Y}'_2: \text{Y}'\text{F}: \text{Y}$  impliqués dans la formation des liaisons halogènes. (b) Les complexes  $\text{Be}(\text{Y}'_1)_2: \text{F}-\text{R}$  impliqués dans la formation de radicaux neutres. (c) IBERB dans des dérivés de malonaldéhyde et de tropolone (plus de détails peuvent être trouvés dans la page 108).

Les complexes considérés dans l'étude des liaisons halogènes et IBERB sont des molécules à couches fermées décrites correctement par des méthodes de référence unique. Les structures dans l'analyse de XB ont été optimisées en utilisant le niveau théorique MP2/aug-cc-pVDZ, alors que les géométries IBERB ont été calculées avec B3LYP et la base 6-31G+(d,p). Les énergies finales ont été calculées en augmentant le niveau théorique au CCSD(T)/aug-cc-pVDZ//MP2/aug-cc-pVDZ et B3LYP/6-311G(2df,p)//B3LYP/6-31G+(d,p) pour XB et IBERB respectivement. La situation est différente pour les complexes de Be précurseurs de radicaux, parce que la rupture homolytique d'une liaison est un processus de références multiples. Dans la réaction :



la fonction d'onde des produits radicaux pourrait avoir un caractère multi-référentiel, mais selon nos résultats les produits de  $(\text{Y}'_1)_2\text{BeF}\cdot + \text{R}\cdot$  sont correctement décrits par des méthodes de référence unique, comme la méthode G4 a été choisie pour étudier la réaction 4.1. Le processus de dissociation a été étudié au niveau de théorie de CASPT2/CASSCF(14,9)/cc-pVTZ [336].

L'analyse de la fonction d'onde a été réalisée au niveau théorique B3LYP avec la même base utilisée dans l'optimisation de la géométrie.

Les liaisons halogènes sont des interactions non covalentes entre un halogène (X) et un LB. Traditionnellement, les deux espèces ont été classées comme espèces donneuses d'électrons, mais il y a une région déficiente en électrons ( $\sigma_{\text{hole}}$ ) dans les halogènes qui leur permet de se comporter comme accepteurs d'électrons. Le  $\sigma_{\text{hole}}$  est originaire de la demi occupation d'une orbitale p de l'halogène et peut être trouvé dans tout le groupe à l'exception du fluor.

En raison de son électronégativité élevée, le fluor retire la densité électronique de l'entourage et complète ses orbitales de valence. Cela signifie qu'il n'y a pas d'orbitale p à moitié remplie qui empêche la formation de XB avec l'atome de fluor [204–208].

La formation des BerB entre  $\text{BeY}'_1\text{Y}'_2$  et  $\text{Y}'\text{F}$  (avec  $\text{Y}'_1 = \text{H}, \text{F}, \text{Cl}$ ,  $\text{Y}'_2 = \text{H}, \text{F}, \text{Cl}$  et  $\text{Y}' = \text{CH}_3\text{O}(\text{MeO}), \text{Cl}, \text{NO}_2\text{F}, \text{NO}_3\text{F}, \text{NCF}$ ), génèrent un  $\sigma_{\text{hole}}$  dans les atomes de fluor. En effet, les BerB augmentent l'électronégativité de  $\text{Y}'$ , en évitant le transfert de charges vers l'atome de fluor et en préservant l'orbitale demi remplie de l'halogène. La force du  $\sigma_{\text{hole}}$  dépend de la force des BerB et de l'électronégativité du substituant  $\text{Y}'$ , les deux effets ont été étudiés en considérant le système  $\text{Be}(\text{Y}'_1)_2: \text{CH}_{3-n}\text{F}_n\text{OF}$  dans la figure 4.3. La force des BerB est augmentée en augmentant l'acidité de  $\text{Be}(\text{Y}'_1)_2$  allant de  $\text{Y}'_1 = \text{H}$  à  $\text{Y}'_1 = \text{Cl}$  et la puissance d'attraction d'électrons de  $\text{Y}'$  qui augmente avec  $n$ . Les valeurs les plus élevées de  $V_{\text{max}}$  (maximum du potentiel électrostatique dans  $\sigma_{\text{hole}}$ ) ont été trouvées pour  $\text{Y}'_1 = \text{Cl}$  (rouge-□ ligne) comparé à  $\text{Y}'_1 = \text{H}$  (bleu-○ ligne) et aussi pour un substituant  $\text{Y}'$  d'électronégativité très élevée ( $n = 3$ ). Cependant, il y a une coopérativité négative entre les deux effets : quand l'électronégativité de  $\text{Y}'$  est augmentée, le  $\sigma_{\text{hole}}$  devient plus fort mais la BerB est plus faible. La figure 4.3 montre que tandis que la valeur de  $V(r)$  (ligne complète) augmente avec  $n$  il y a une diminution de  $\Delta V(r)$  (lignes pointillées,  $\Delta V(r) = V(r)_{\text{BerB}} - V(r)_{\text{no-BerB}}$ ).

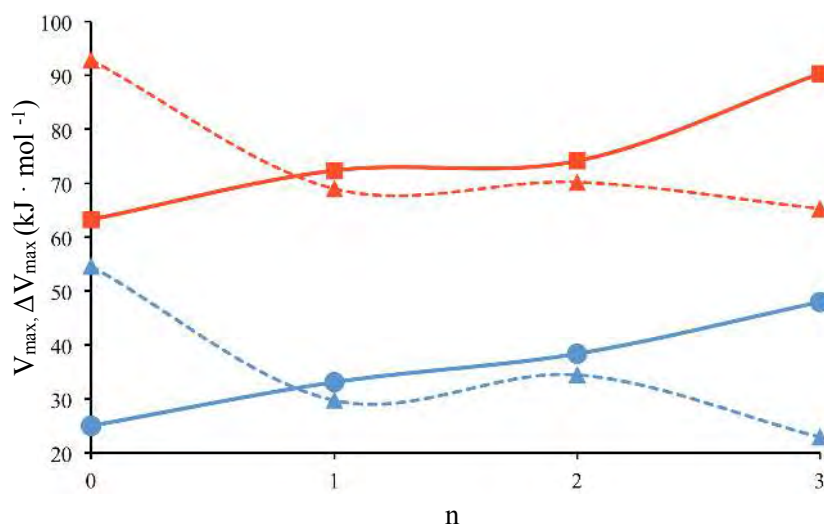


FIGURE 4.3 : Effet du degré de substitution dans la valeur de  $V_{\text{max}}$  du  $\sigma_{\text{hole}}$  pour les complexes  $\text{Be}(\text{Y}'_1)_2: \text{CH}_{3-n}\text{F}_n\text{OF}$  ( $n = 0, 1, 2, 3$ ). Les complexes formés avec  $\text{Y}'_1 = \text{H}$  sont représentés en bleu et  $\text{Y}'_1 = \text{Cl}$  en rouge. Les carrés bleus et les cercles rouges représentent les valeurs de  $V_{\text{max}}$  dans le  $\sigma_{\text{hole}}$  et les triangles  $\Delta V(r)$ . Toutes les valeurs sont en  $\text{kJ} \cdot \text{mol}^{-1}$  et ont été calculées au niveau théorique B3LYP/aug-cc-pVDZ (plus de détails peuvent être trouvés dans la page 114).

La génération d'un  $\sigma_{\text{hole}}$  dans les complexes  $\text{BeY}'_1\text{Y}'_2: \text{Y}'\text{F}$  permet la formation d'un XB du type  $\text{BeY}'_1\text{Y}'_2: \text{Y}'\text{F}: \text{Y}$ , ce qui n'est pas possible sans la BerB. La formation du XB dépend non seulement de la force de la LA ou de la LB, mais aussi de la coopérativité entre les interactions non covalentes, BerB et XB. Lorsque l'acidité de F est plus petite que le groupe Be, la LB préfère interagir avec le métal au lieu de l'halogène, voir  $\text{BeH}_2: \text{CH}_3\text{OF}: \text{NH}_3$

dans la figure 4.6. Lorsque F est plus acide que  $\text{BeY}'_1$ , il existe une formation d'un XB, qui est ratifié par la présence d'un FY Point Critique de Liaison (BCP, pour l'acronyme en anglais Bond Critical Point) avec  $\rho$  du même ordre de grandeur que les liaisons non covalentes (0.01 au), voir la figure 5 en annexe B.1. La formation de complexes  $\text{BeY}'_1\text{Y}'_2 : \text{Y}'\text{F} : \text{Y}$  ratifie la présence d'un  $\sigma_{\text{hole}}$  en dérivés fluorés *et ouvre la possibilité de concevoir de nouveaux matériaux où le fluor se lie par des liaisons halogènes.*

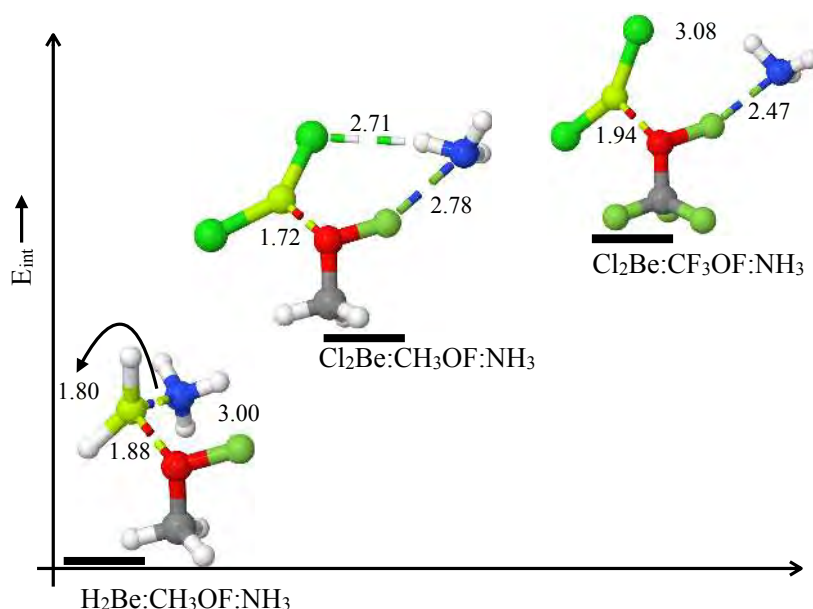


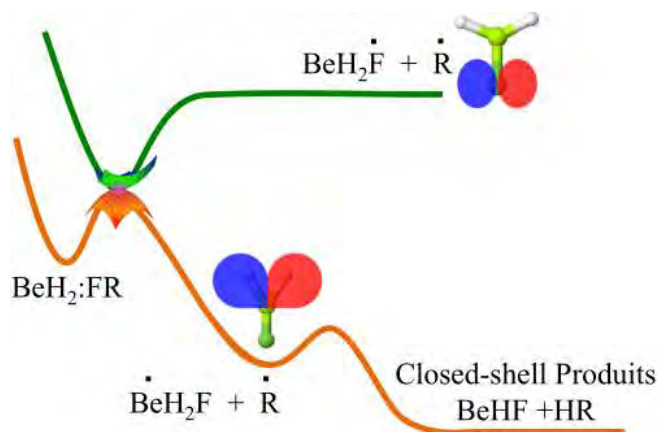
FIGURE 4.6 : Représentation des géométries et des tendances des énergies d'interactions dans les complexes  $\text{BeH}_2 : \text{CH}_3\text{OF} : \text{NH}_3$ ,  $\text{BeCl}_2 : \text{CH}_3\text{OF} : \text{NH}_3$  et  $\text{BeCl}_2 : \text{CF}_3\text{OF} : \text{NH}_3$ . L'énergie d'interaction entre F et  $\text{NH}_3$  augmente de gauche à droite, et les distances de liaison les plus pertinentes sont représentées dans AA. Les paramètres géométriques ont été calculés au niveau théorique MP2/aug-cc-pVDZ (plus de détails peuvent être trouvés dans la page 116).

Les espèces radicales jouent un rôle important dans plusieurs processus chimiques : chimie atmosphérique, polymérisation, biochimie et d'autres. La formation de radicaux nécessite une grande quantité d'énergie car une liaison covalente doit être rompue. C'est donc généralement l'étape déterminante dans de nombreuses réactions chimiques. L'Énergie de Dissociation des Liaisons (BDE, pour l'acronyme en anglais Bond Dissociation Energy) ou l'énergie requise pour rompre une liaison peut être modifiée pour améliorer la formation de radicaux. Des études antérieures ont montré que la BDE diminue lorsque le système est protoné [275, 276]. Dans cette thèse sont utilisés les BerB pour supprimer les barrières énergétiques associées à la formation de radicaux.

L'interaction entre  $\text{Be}(\text{Y}'_1)_2$  et les dérivés fluorés (F-R) diminue leur énergie de liaison, transformant la dissociation homolytique de F-R en un *processus exothermique*. Pour expliquer l'exothermicité des complexes  $\text{Be}(\text{Y}'_1)_2 : \text{F}-\text{R}$ , la stabilité des radicaux  $\cdot(\text{Y}'_1)_2\text{BeF}$  et de  $\text{R}\cdot$  a été comparée en considérant la définition de l'Enthalpie de Stabilisation Radicale (RSH

=  $\text{BDH}_{\text{FR}} - \text{BDH}_{\text{BeH}_2:\text{FR}}$  [279] (les valeurs de BDH et RSH peuvent être trouvées en annexe B.2 tableau 1). Les valeurs positives de RSH indiquent que  $\text{BeH}_2\text{F}\cdot$  est plus stable que  $\text{F}\cdot$ , en diminuant l'enthalpie de  $\text{H}_2\text{Be}:\text{F-R}$  par rapport à  $\text{F-R}$ . Les RSH pour les complexes  $\text{BeH}_2:\text{FR}$  sont supérieurs à  $300\text{kJ}\cdot\text{mol}^{-1}$ , ce qui indique que la diminution du BDH est due à une énorme stabilité des radicaux  $\text{H}_2\text{BeF}\cdot$ . L'analyse de la configuration électronique du radical neutre  $\text{BeFH}_2\cdot$  est représentée dans la figure S3 de l'appendice B.2. Les produits de la dissociation naturelle de la molécule  $\text{F}_2$  sont deux atomes de fluor avec une configuration électronique  $[\text{He}]2s^22p^5$ , tandis que le produit de dissociation du complexe  $\text{BeH}_2:\text{FF}$  est le radical neutre  $\cdot\text{BeH}_2\text{F} + \text{F}\cdot$ . L'atome de F dans  $\cdot\text{BeH}_2\text{F}$  a une configuration de gaz noble  $[\text{Ne}]$  et l'Orbitale Moléculaire Occupée Unique (SOMO, pour l'acronyme en anglais Singled Occupied Molecular Orbital) est situé dans l'orbitale  $\sigma_{\text{BeH}}$ . La migration des électrons vers l'atome F stabilise fortement le radical. En effet, l'état excité où F préserve la configuration électronique de la dissociation naturelle se trouve autour de  $400\text{kJ}\cdot\text{mol}^{-1}$  plus élevé en énergie, ce qui est proche de la RSE calculée pour les complexes  $\text{BeH}_2:\text{FR}$ .

La dissociation de  $\text{F-R}$  dans les complexes  $\text{BeH}_2:\text{F-R}$  est exothermique pour  $\text{R} = \text{F}, \text{NH}_2, \text{OH}, \text{NO}$  et  $\text{Cl}$  mais la spontanéité de cette réaction dépend de la barrière énergétique associée à la migration électronique de  $(\text{Y}'_1)_2\text{Be}$  vers l'atome de fluor. Néanmoins, il existe des produits secondaires à couches fermées qui sont énergiquement plus stables que les radicaux,  $\text{HBeF}$  et  $\text{HR}$ . La dissociation s'effectue donc par un mécanisme à deux échelons : d'abord la formation de l'espèce radicalaire et d'autre part sa réorganisation qui conduit aux produits finis à couches fermées, voir schéma 4.4 pour une représentation du mécanisme réactionnel.



Scheme 4.4 : Schéma du profil d'énergie potentielle pour la dissociation de  $\text{BeH}_2:\text{FR}$ . En vert est représentée la formation des produits radicalaires  $\text{BeH}_2\text{F}\cdot + \text{R}\cdot$ . En orange, les produits radicalaires  $\cdot\text{BeH}_2\text{F} + \text{R}\cdot$ , et enfin les produits à couches fermées  $\text{HBeF} + \text{HR}$  (plus de détails peuvent être trouvés dans la page 120).

Les profils de réaction pour  $\text{BeH}_2:\text{FF}$  et  $\text{BeCl}_2:\text{FF}$  sont montrés dans l'annexe B.2 figures 2 et S5. Le chemin réactionnel est semblable pour les deux complexes, il y a une première étape dans laquelle Be se situe entre les atomes F formant un anneau à trois membres et aidant à la rupture de la liaison F-F. La barrière énergétique associée à cette étape est inférieure à l'énergie de point zéro (ZPE, pour l'acronyme en anglais Zero Point Energy) de  $\text{BeH}_2:\text{FF}$  et de  $\text{BeCl}_2:\text{FF}$  et donc les espèces radicalaires devraient être produites spontanément, les

électrons non appariés étant situés sur  $Y_1'$  et sur l'atome F partant. La différence principale entre les deux complexes est que pour  $\text{BeCl}_2:\text{FF}$  le complexe radical est une espèce intermédiaire, tandis que pour  $\text{BeH}_2:\text{FF}$  les radicaux évoluent spontanément (sans seconde État de transition (TS, pour l'acronyme en anglais Transition State)) aux produits à couches fermées. La seconde barrière pour  $\text{BeCl}_2:\text{FF}$  a été estimée à l'aide d'une Interpolation Linéaire en Coordonnées Internes (LIIC, pour l'acronyme en anglais Liner Interpolation in Internal Coordinates) des intermédiaires aux produits à couches fermées. On estime que cette barrière est plus élevée que la ZPE des intermédiaires, indiquant que ce n'est pas nécessairement un processus spontané. Comme on l'a déjà indiqué ci-dessus, on s'attend à ce que  $\text{BeH}_2:\text{FF}$  se dissocie spontanément dans les produits finis de couches fermées, c'est-à-dire qu'aucune barrière énergétique ne sépare les réactifs des intermédiaires, et ces derniers des produits finis. On a cependant constaté que l'augmentation de l'acidité de  $\text{Be}(Y_1')$  augmentait la barrière énergétique séparant les radicaux des produits à couches fermées, soulignant que la réorganisation du produit final pourrait ne pas être spontanée dans les complexes  $\text{BeCl}_2:\text{FF}$ .

La Figure S6 de l'annexe B.2 montre le mécanisme de réaction du complexe  $\text{BeH}_2:\text{FNO}$ . L'état fondamental de ce système a déjà un caractère radical partiel, où les électrons non appariés se trouvent sur les groupes  $\text{BeH}$  et  $\text{NO}$ . En considérant le schéma 4.4, pour ce complexe, le premier minimum local n'existe pas et le TS pour atteindre les produits à couches fermées se trouve sous le ZPE de  $\text{BeH}_2:\text{FNO}$ . Par conséquent, les produits  $\text{HBeF} + \text{HNO}$  sont produits spontanément. La formation spontanée d'espèces radicales assistées par des composés  $\text{Be}$  pourrait être utilisée pour éliminer le goulot d'étranglement des réactions chimiques fondamentales ou pourrait expliquer la forte toxicité du métal en raison du grand nombre de sites LB dans le corps humain.

Les Liaisons Hydrogènes de résonance assistée (RAHB, pour l'acronyme en anglais Resonance Assisted Hydrogen Bonds) sont parmi les HB les plus fortes pour les composés neutres. Elles ont été initialement définies comme une HB où le donneur de protons et l'accepteur de protons sont reliés par un système  $\pi$ , de telle manière que les structures de résonance augmentent la force de la HB [61–63]. Les RAHB sont devenues un concept populaire pour expliquer la réactivité chimique, par exemple pour décrire la forte interaction entre les paires de bases d'ADN. Cependant, la description théorique n'est pas d'accord sur la corrélation entre la délocalisation  $\pi$  et les énergies d'interaction RAHB. En revanche, la force d'interaction des HB a été expliquée par l'augmentation de la basicité et de l'acidité du donneur et de l'accepteur de H causés par les fragments insaturés [64–66, 191–194].

Dans cette thèse, le concept de résonance assistée a été revisité en considérant IBerB dans les dérivés du malonaldéhyde et du tropolone (voir le schéma 4.1c). La force de l'interaction a été estimée en comparant la stabilité relative entre les structures fermées et ouvertes. L'IBerB étant plus forte dans les systèmes non saturés par analogie avec la RAHB (voir les figures 1-4 et 6 de l'annexe B.3). La nature de l'IBerB dans les structures fermées est analysée en tenant compte des phénomènes d'assistance à la résonance, de l'effet du squelette  $\sigma$  et de l'acidité et de la basicité du donneur et accepteur de  $\text{Be}$ , respectivement.

On a constaté que la diminution de l'insaturation affaiblissait la résistance de l'IBerB, mais l'analyse des structures de résonance contributives du système insaturé ne montre aucune structure où participe le groupe Y-Be, ce qui indique que la BerB n'est pas stabilisée par la résonance du système (voir les schémas 4 et 5 de l'annexe B.3). Les affinités du proton ( $H^+A$ ) et de l'hydrure ( $H^-A$ ) des structures fermées sont représentées dans la figure 4.13a. Les systèmes non saturés ont des valeurs supérieures pour  $H^+A$  et inférieures pour  $H^-A$  par rapport aux contre-parties saturées, montrant que l'augmentation de la force de la BerB est due à une augmentation de la basicité de Y et l'acidité de BeH, et non à cause de l'aide de résonance. De façon constante, lorsque Y est échangé de O à NH, la basicité plus élevée du groupe amide augmente la force de la BerB, et aussi, lorsque BeH est attaché à un groupe alkyle au lieu d'un groupe carbonyle, l'acidité du dérivé Be diminue, de même que la force de l'interaction non covalente. L'effet de la flexibilité du squelette  $\sigma$  a été étudié lorsque R forme un cycle à quatre membres et on a constaté que pour les squelettes plus rigides, l'IBerB devient plus faible. La figure 4.13 montre que la contrainte du squelette  $\sigma$  diminue à la fois l'acidité et la basicité du carbonyle et du BeH respectivement. Par conséquent, les *IBerB*, comme leurs analogues les Liaisons Hydrogènes Intramoléculaires, sont plus fortes dans les systèmes non saturés parce que la résonance améliore l'acidité et la basicité du donneur et accepteurs de Be, mais pas due à une participation de l'interaction non covalente dans les structures de résonance comme il a été précédemment proposé.

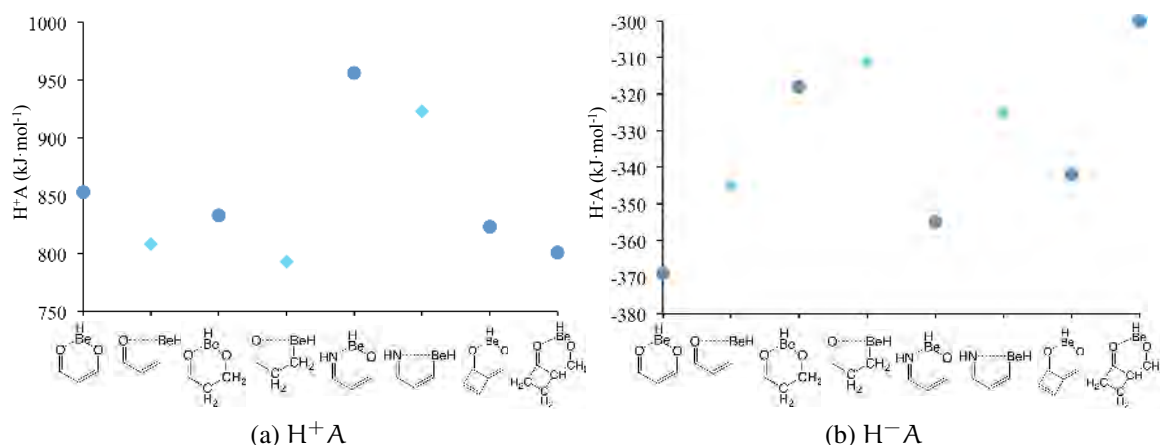
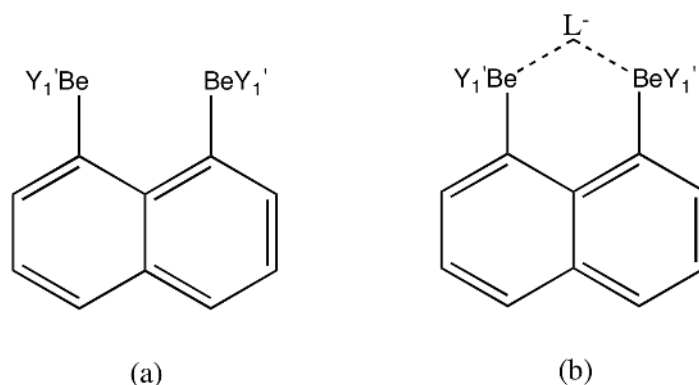


FIGURE 4.13 : (a) Proton ( $H^+A$ ) et (b) hydrure ( $H^-A$ ) affinités des dérivés de malonalaldéhyde. Les cercles bleus correspondent aux structures insaturées et les diamants aux analogues saturés. Toutes les valeurs en  $\text{kJ}\cdot\text{mol}^{-1}$  ont été calculées au niveau de la théorie G4 (plus de détails peuvent être trouvés dans la page 123).

#### LIAISON Be-Be D'UN ÉLECTRON

Les liaisons d'un électron sont les liaisons formées dans les anions par fixation électronique ou dans les cations par perte d'électrons. Le terme a été introduit en 1931 pour expliquer l'interaction dans les dérivés de borane [165]. Il y a plusieurs travaux réalisés sur la capacité de l'atome B pour former des liaisons électroniques, en désignant les orbitales p faible en

énergie comme leurs origines [280–282]. L'atome de Be présente également des orbitales p de basse énergie. Ainsi, on peut définir la *liaison Be-Be d'un électron* comme l'interaction suivant l'attachement électronique dans lequel l'électron non apparié est situé dans le groupe Be. La liaison Be-Be d'un électron a été étudiée dans cette thèse compte tenu des dérivés 1,8-diBeY<sub>1</sub>'naphtalène représentés dans le schéma 4.7a, avec Y<sub>1</sub>' = H, F, Cl, Br, CH<sub>3</sub>, NH<sub>2</sub>, OH, CF<sub>3</sub>, C(CF<sub>3</sub>)<sub>3</sub>, NF<sub>2</sub>, OF, CN, NO<sub>2</sub>, SOH, t-Bu et Ph, ainsi que l'interaction des composés neutres avec les espèces d'anions (L<sup>-</sup>=F<sup>-</sup>, Cl<sup>-</sup>, Br<sup>-</sup>, CN<sup>-</sup>, NO<sub>2</sub><sup>-</sup>, NO<sub>3</sub><sup>-</sup> et SO<sub>4</sub><sup>2-</sup>, voir schème 4.7b).



Scheme 4.7 : Systèmes considérés dans l'étude de dérivés de naphthalène Be-disubstitués. (a) 1,8-diBeY<sub>1</sub>'naphtalène and (b) [L: 1,8-diBeHnaphtalène :]<sup>-</sup> (plus de détails peuvent être trouvés dans la page 127).

Les composés neutres et anioniques ont été trouvés correctement décrits par des méthodes de référence unique. Les géométries ont été optimisées à B3LYP/6-31+G(d,p) et les énergies finales ont été calculées en agrandissant la base pour atteindre le niveau théorique B3LYP/6-311G(3df,2p). L'analyse de la fonction d'onde a été effectuée au même niveau théorique que l'optimisation de la géométrie. On a décrit la nature de la liaison Be-Be d'un électron en utilisant trois approches différentes : la Théorie Quantique des Atomes dans les Molécules (QTAIM, pour l'acronyme en anglais Quantum Theory of Atoms in Molecules) [145], la Fonction de Localisation d'Electrons (ELF, pour l'acronyme en anglais Electron Localization function) [147] et l'Orbitale de Liaison Naturel (NBO, pour l'acronyme en anglais Natural Bond Orbital) [141]. La force de l'interaction a été quantifiée en utilisant l'Analyse de Décomposition Electronique (EDA, pour l'acronyme en anglais Energy Decomposition Analysis) [48, 49].

Les espèces anioniques des dérivés de 1,8-diBeX-naphthalène montrent une très forte liaison Be-Be *mono-électronique* qui est huit fois plus forte et 0.5Å plus courte que dans la molécule Be<sub>2</sub> libre. L'électron supplémentaire au lieu d'être délocalisé sur le noyau de naphthalène aromatique est principalement localisé dans les groupements BeY<sub>1</sub>', de telle manière qu'il compense la déficience en électrons du groupement dans les composés neutres. Contrairement à l'analyse QTAIM pour le neutre, qui ne montre pas un Be-Be BCP, pour l'anion ce point critique existe. Les valeurs de  $\rho$  sont autour de 0.03au et, selon les valeurs négatives de  $\nabla^2\rho$ , l'interaction a un caractère covalent. L'analyse NBO localise une liaison Be-Be correspondant à une Orbitale Moléculaire avec une occupation d'autour 1e<sup>-</sup>, ce qui n'existe



pas dans les complexes neutres. Le calcul ELF de l'espèce neutre ne localise pas de bassins disynaptiques entre les atomes Be, mais les anions montrent  $V(\text{Be}, \text{Be})$  des bassins avec des populations autour de  $1e^-$ . Les propriétés énergétiques sont en accord avec cette analyse de la fonction d'onde. L'EDA prédit la force du Be-Be à environ  $74\text{kJ}\cdot\text{mol}^{-1}$ , avec une contribution maximale de la partie  $\Delta_{\text{orb}}$ , en ratifiant le caractère covalent de l'interaction. La formation d'une liaison Be-Be d'un électron est due à une augmentation de l'affinité électronique ( $E_{\text{ea}}$ ) de l'anion; tandis que pour le naphthalène, la valeur est positive ( $7.5\text{kJ}\cdot\text{mol}^{-1}$ ) pour les dérivés de 1,8-diBeY<sub>1</sub>' naphthalène ces valeurs sont négatives et s'étendent dans une gamme très large de  $-50\text{kJ}\cdot\text{mol}^{-1}$  et  $-230\text{kJ}\cdot\text{mol}^{-1}$ .

Le concept de *éponges de protons* a été introduit pour illustrer la basicité impressionnante des complexes aminés disubstitués de naphthalène [67, 287]. Les affinités de protons exacerbées de ce type de composés ont été expliquées en considérant (1) la diminution de la répulsion des doublets non liants (LP, pour l'acronyme en anglais Lone Pairs) de N qui se produit après la protonation, (2) la stabilité supplémentaire donnée par la formation de la HB intramoléculaire N: H<sup>+</sup>: N et (3) la réduction de la répulsion stérique [288, 289]. Les dérivés de naphthalène disubstitués au béryllium se comportent comme des éponges, mais ils imbibent les anions à la place des protons, donc on les appelle *éponges anioniques*. Les affinités anioniques du [L: 1,8-diBeY<sub>1</sub>'naphthalene]<sup>-</sup> sont représentées dans la figure 4.19. L'affinité anionique augmente avec les affinités protoniques ( $E_{\text{L}}^-$ ) de l'anion L<sup>-</sup> et avec l'électronégativité de Y<sub>1</sub>'. Par conséquent, l'affinité anionique la plus élevée a été trouvée pour le complexe [1,8-diBeCNnaphthalène :SO<sub>4</sub>]<sup>2-</sup> et la plus petite pour le complexe [1,8-diBeHnaphthalène :Br]<sup>-</sup>. Les valeurs montrées dans la figure sont parmi les plus grandes affinités anioniques rapportées dans la littérature pour les molécules neutres, ce qui pourrait conduire à un large éventail d'applications des dérivés 1,8-diBeX-naphthalène comme des récepteurs et des capteurs d'anions.

## Be<sub>2</sub> MOLÉCULE ET L: Be<sub>2</sub>: L COMPLEXES

La caractérisation de la molécule de béryllium est un défi à la fois pour la théorie et les expériences. Les difficultés expérimentales sont liées au fait que Be<sub>2</sub> se dissocie à ses points de fusion et d'ébullition. Be<sub>2</sub> s'oxyde aussi facilement et il est très toxique [238, 239]. Du point de vue théorique, la corrélation électronique joue un rôle très important dans la description du Be<sub>2</sub>. L'utilisation d'approches théoriques faiblement corrélées prédit que le dimère a un caractère répulsif [53, 240–242] ou est lié par une interaction faible de Van der Waals [243–245]. En 1983, le développement des méthodes multi-références a permis de décrire correctement le caractère de liaison de la molécule Be<sub>2</sub> [246] et un an plus tard Bondybey et ses collègues ont rapporté le premier spectre expérimental en phase gazeuse de la molécule Be<sub>2</sub>. Les expériences ont révélé que Be<sub>2</sub> se caractérise par une longueur de liaison courte à l'équilibre (2.45Å) par rapport au complexe de Van der Waals (~5.0 Å) et une petite énergie de dissociation des liaisons (BDE) ( $9.45\text{kJ}\cdot\text{mol}^{-1}$ ) [21, 22], en accord avec les premiers résultats théoriques. La figure 3.8 montre la courbe de dissociation de la molécule Be<sub>2</sub> pour

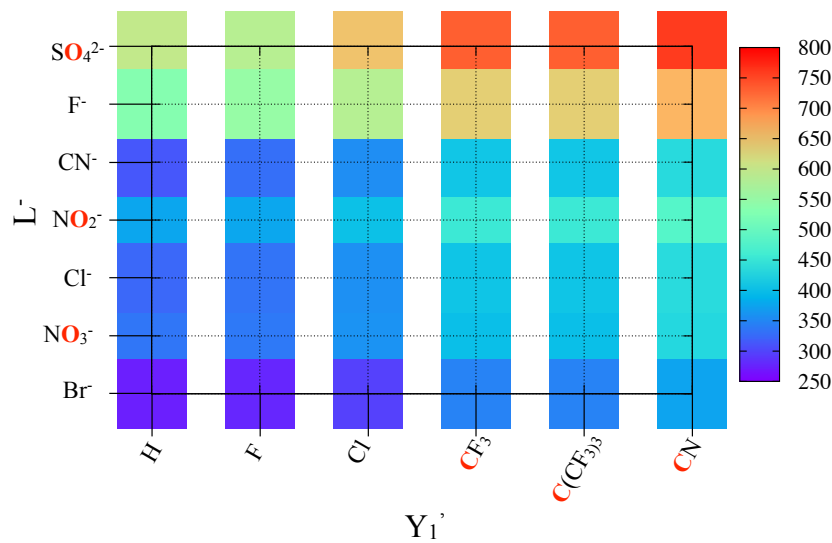


FIGURE 4.19 : Affinité Anionique pour les complexes  $[L: 1,8\text{-diBe}Y_1'\text{naphtalène}]^-$ .  $E_L^-$  est en  $kJ \cdot mol^{-1}$  et fut calculée au niveau théorique B3LYP/6-311G(3df,2p). En rouge sont mis en évidence les atomes interagissant avec Be (plus de détails peuvent être trouvés dans la page 133).

différentes méthodes théoriques. En résumé, la liaison dans la molécule  $Be_2$  a été décrite comme un mélange de deux orbitales quasi-dégénérées  $s_{Be}$  et  $p_{Be}$ , ce type d'interaction a été nommé Liaison Non-Dynamique [54].

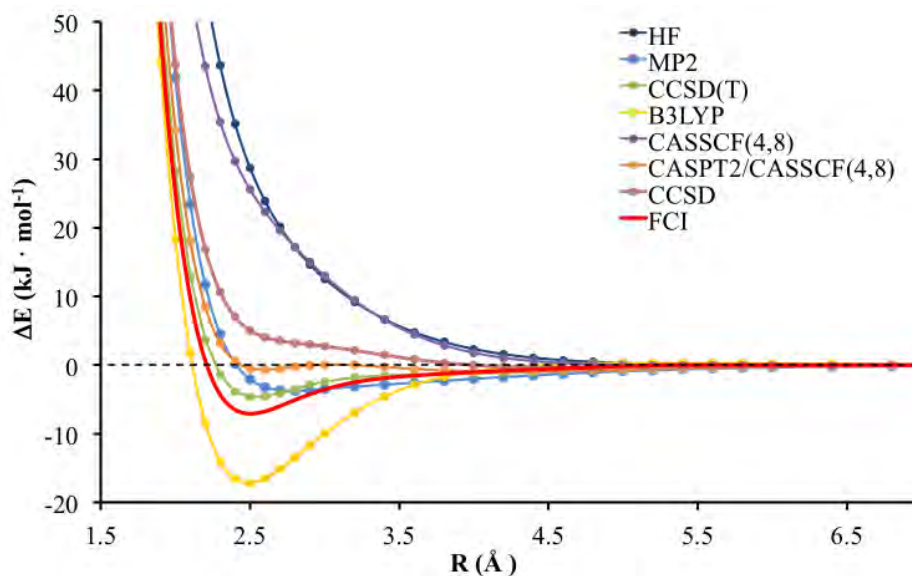


FIGURE 3.8 : Comparaison de différentes méthodes théoriques pour la description de la courbe de dissociation de l'état  $^1\Sigma_g$  du dimère Be. Les calculs ont été effectués avec une base cc-pVTZ (plus de détails peuvent être trouvés dans la page 100).

Le développement de codes plus efficaces et de ressources informatiques plus puissantes a rendu possible la description de complexes Be, évitant les défis expérimentaux associés à la synthèse et à la caractérisation du dimère Be. L'interaction entre les atomes de Be et les es-

pèces donneuses d'électrons augmente la BDE de Be-Be et diminue la longueur de la liaison (voir figure 3.10), étant le travail de référence [41] sur les complexes  $\text{CO}_n : \text{Be-Be} : \text{CO}_n$  parmi les premières études envisageant ce type de complexes. La force de la liaison Be-Be dans les composés Be-carbonyle a été expliquée sur la base de deux arguments différents : (1) la délocalisation entre les orbitales  $\pi_{\text{CO}}$  et  $\pi_{\text{Be}}$  et (2) la formation d'une liaison à trois centres C-Be-Be [249, 250]. En dépit du manque d'information sur la nature de l'interaction, l'intérêt pour les complexes a augmenté, et les  $\text{CO}_n : \text{Be-Be} : \text{CO}_n$  ont également été détectés par spectroscopie IR. Les pics principaux des spectres IR correspondent aux complexes mono- et disubstitués, théoriquement identifiés comme  $\text{Be-Be} : \text{CO}$  et  $\text{CO} : \text{Be-Be} : \text{CO}$ . L'état fondamental des complexes mono et disubstitués a été décrit comme un état triplet, étant les monosubstitués plus stables que les disubstitués, et la différence d'énergie entre les équations 4.11 est juste de  $20 \text{kJ}\cdot\text{mol}^{-1}$  au niveau de la théorie l'Hartree Fock (HF). [42].



Plus tard en 2013, on a constaté que les complexes formés entre  $\text{Be}_2$  et N-carbènes hétérocycliques (NRC) ont une distance Be-Be très courte et ont été identifiés parmi ceux possédant les liaisons Be-Be les plus fortes, mais selon la nature du substituant R, l'état fondamental du complexe correspond à un singlet ou à un triplet [43]. Les systèmes NRC : Be-Be : NRC ont été considérés comme les plus forts complexes de  $\text{Be}_2$ , jusqu'en 2016 lorsque la molécule F : Be-Be : F a été découverte. La BDE de ce complexe est de  $322 \text{kJ}\cdot\text{mol}^{-1}$ , soit 30 fois plus forte que le dimère isolé[44].

Des analyses antérieures des complexes  $\text{Be}_2$  ont été effectuées en utilisant des méthodes de référence unique, mais ces méthodes ne décrivent pas correctement le caractère multi-références des molécules  $\text{Be}_2$ . La nature des interactions Be : L détermine le caractère multi-référence et l'état d'oxydation du groupe  $\text{Be}_2$ . Cette thèse considère trois types de ligands L dans des complexes du type L : Be-Be : L :

- Groupe-I, L est une LB à couche fermée qui interagit avec  $\text{Be}_2$  via l'interaction  $\text{LP}_L \rightarrow \text{p}_{\text{Be}}$ . Le groupe  $\text{Be}_2$  reste neutre et le caractère multi-référentiel du système provient des excitations  $s_{\text{Be}} \rightarrow \text{p}_{\text{Be}}$  dans le dimère de béryllium. L =  $\text{NH}_3$  et  $\text{H}_2\text{O}$  ont été considérés comme des ligands.
- Groupe-II, L est une LB à couche fermée qui interagit avec  $\text{Be}_2$  via la conjugaison des orbitales  $\pi_L \backslash \pi_{\text{Be}}$ . Le groupe  $\text{Be}_2$ , dans ce cas, est un monocation avec une configuration électronique  $(\sigma_{\text{Be-Be}})^2(\pi_{\text{Be-Be}})^1$ . Le caractère multi-référentiel de ces complexes est attribué à la dégénérescence des orbitales  $\pi_{\text{Be-Be}}$ . L = CO a été considéré comme un ligand représentatif pour ces complexes.
- Groupe-III, L est une radical neutre et à couche ouverte qui récupère le caractère de couche fermée en supprimant un électron de l'orbitale  $\sigma_{\text{Be-Be}}^*$ . Ainsi, dans ces complexes  $\text{Be}_2$  est un dication avec une configuration électronique  $(\sigma_{\text{Be-Be}})^2(\sigma_{\text{Be-Be}}^*)^0$ . Le système a un caractère de référence unique et les ligands considérés sont L =  $\text{CN}\cdot$ ,  $\text{F}\cdot$ ,  $\text{OH}\cdot$ ,  $\text{CH}_3\cdot$ ,  $\text{CH}_3\text{O}\cdot$  et  $\text{NH}_2\cdot$ .

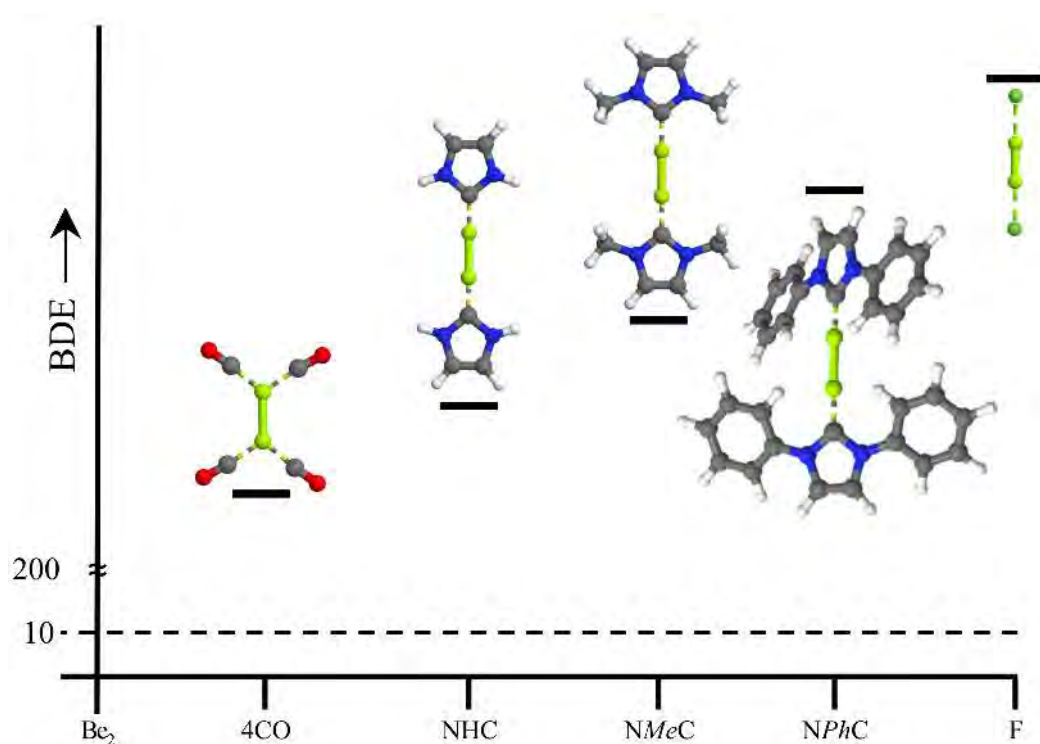
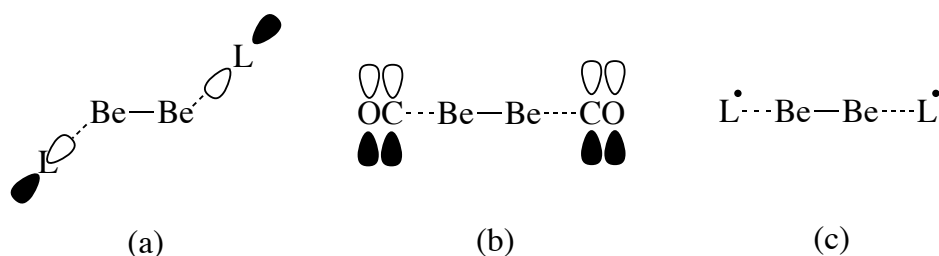


FIGURE 3.10 : Comparaison de la BDE pour les complexes entre  $\text{Be}_2$  et les ligands donneurs d'électrons. Les BDE ont été prises de : 4CO[41], NRC[43] et F[44] (plus de détails peuvent être trouvés dans la page 103).

Le schéma 4.8 illustre les complexes  $\text{L}:\text{Be}-\text{Be}:\text{L}$  et le tableau S6 de l'annexe B.6 recueille les charges NBO. Les complexes dans le groupe-III ont la plus forte interaction Be-Be rapportée dans la littérature, en raison de l'orbite  $\sigma_{\text{Be-Be}}^*$  vide. Ainsi, l'objet de cette thèse est la description de la liaison Be-Be dans le groupe-I et le groupe-II. Pour la description des systèmes  $\text{L}:\text{Be}-\text{Be}:\text{L}$  nous devons utiliser la méthode CASPT2//CASSCF/cc-pVTZ, ce qui représente la meilleure méthode pour décrire correctement les systèmes multi-références de taille moyenne. La nature de la liaison Be-Be a été étudiée en considérant l'analyse QTAIM, ELF et NBO en utilisant la fonction d'onde CASSCF/cc-pVTZ.



Scheme 4.8 : Représentation des complexes  $\text{L}:\text{Be}-\text{Be}:\text{L}$  dans (a) le groupe-I où  $\text{L}=\text{NH}_3, \text{H}_2\text{O}$ , (b) le groupe-II où  $\text{L}=\text{CO}$ , et le groupe-III où  $\text{L}=\text{CN}\cdot, \text{F}\cdot, \text{OH}\cdot, \text{CH}_3\cdot, \text{CH}_3\text{O}\cdot$  et  $\text{NH}_2\cdot$  (plus de détails peuvent être trouvés dans la page 134).

L'interaction Be: L dans le groupe-I et le groupe-II diminue la longueur de la liaison Be-Be autour de 0.5 Å à la fois dans les états fondamentaux et les états excités. Les complexes dans le groupe-I sont disposés selon une géométrie trans par rapport à la liaison Be-Be, les doublets non liants de la LB étant orientés dans la direction des atomes Be, alors que les complexes dans le groupe-II correspond à une molécule linéaire. La configuration électronique du Be<sub>2</sub> change également entre les deux groupes des complexes. Le fragment Be<sub>2</sub> dans l'état fondamental des complexes dans le groupe-I partage la configuration électronique avec le dimère isolé,  $|(2\sigma)^2(2\sigma^*)^2\rangle$ , mais il y a une contribution importante d'une deuxième configuration dans laquelle les orbitales  $\pi_{Be}$  sont impliquées,  $|\Psi_{CASPT2}\rangle = |0.8[(2\sigma)^2(2\sigma^*)^2] + 0.15[(2\sigma)^2(2\sigma^*)^0(1\pi)^2]\rangle$ . En revanche, dans le dimère isolé, la deuxième configuration avec un coefficient plus élevé provient d'une excitation vers une orbitale  $3\sigma$ ,  $|(2\sigma)^2(2\sigma^*)^0(3\sigma)^2\rangle$ . La configuration électronique du complexe dans le groupe-II est complètement différente de celle du dimère isolé, les orbitales  $\pi_{Be}$  sont fortement stabilisées par une conjugaison avec les orbitales  $\pi_{CO}^*$  et l'état fondamental est doublement dégénéré,  $|\Psi_{CASPT2}\rangle = |0.32[(2\sigma_{BeBe})^2(\pi_{BeBe} + \pi_{CO}^*)^2_x] + 0.32[(2\sigma_{BeBe})^2(\pi_{BeBe} + \pi_{CO}^*)^2_y]\rangle$ . L'état avec la même configuration électronique que le dimère isolé étant un état excité  $877\text{kJ}\cdot\text{mol}^{-1}$  plus élevé en énergie. *Ces résultats suggèrent que la liaison Be-Be plus forte dans les complexes L: Be-Be: L est due à une stabilisation des orbitales  $\pi_{Be}$  par rapport au dimère isolé.*

La BDE a été calculée en tenant compte de différentes voies de dissociation. La dissociation la plus favorable pour le groupe-I est la formation de deux molécules Be: L, alors que pour le groupe-II les produits les plus favorables sont deux atomes de Be et deux molécules CO, avec une BDE d'environ  $100\text{kJ}\cdot\text{mol}^{-1}$  et  $174\text{kJ}\cdot\text{mol}^{-1}$  pour le groupe-I et le groupe-II, respectivement. La liaison Be-Be dans les complexes dans le groupe-III est la plus forte en raison de la valeur  $\sigma_{Be-Be}^*$  [43]. Les deuxièmes liaisons les plus fortes sont dans le groupe-II, où Be<sub>2</sub> est un monocation dû à la conjugaison des orbitales  $\pi_L \setminus \pi_{Be}$ . La molécule Be<sub>2</sub> dans le groupe-I reste neutre, de ce fait il possède les plus fortes liaisons Be-Be rapportées dans la littérature à notre connaissance. La description multi-références des complexes avec L = CO ne supporte pas les résultats précédents en utilisant la méthode HF. Selon nos résultats, l'état fondamental du système n'est pas un triplet mais un singulet et la BDE est  $132\text{kJ}\cdot\text{mol}^{-1}$  supérieure à celle prédit par HF. Contrairement aux résultats de HF qui prédisent que les voies dans 4.11 sont proches en énergie, l'approche multi-références CASPT2 // CASSCF (12,14) / cc-pVTZ prédit les complexes disubstitués  $121\text{kJ}\cdot\text{mol}^{-1}$  plus stable. Compte tenu de l'énergie de la dissociation du CO: Be-Be: CO, les espèces monosubstituées détectées expérimentalement devraient être formées à partir de la réaction entre Be<sub>2</sub> et CO ( $\Delta E = -38\text{kJ}\cdot\text{mol}^{-1}$ ).

La diminution de la distance Be-Be dans les complexes L: Be-Be: L induit la formation d'un pseudo-noyau ou d'un Attracteur Non-Nucléaire (NNA, pour l'acronyme en anglais Non-Nuclear Attractor). Selon QTAIM, les NNA sont des positions où il y a un maximum de densité électronique ou un point de selle (3, -3) en l'absence d'un noyau [301, 303, 304, 306–308]. La formation des NNA a été associée à des distances de liaison particulières qui augmentent l'accumulation de densité électronique entre les atomes formant la liaison (*fenêtre*

NNA). La *fenêtre* NNA a été calculée pour plusieurs molécules diatomiques et à différents niveaux de théorie [307, 310]. Pour les isolés Be<sub>2</sub>, la distance de liaison Be-Be est en dehors de la *fenêtre* de NNA prédite, tandis que pour les complexes avec la LB, les distances d'équilibre sont à l'intérieur de ces fenêtres, et donc ils montrent un NNA. *Les résultats de cette thèse soutiennent que l'occurrence du NNA est liée aux distances des noyaux. Les études futures tenteront de décrire le rôle des électrons de noyau et de valence dans la formation du NNA, afin de rationaliser la façon dont les fenêtres de NNA varient le long du tableau périodique, et aussi l'absence de NNA sur H<sub>2</sub> et He<sub>2</sub> pour toute distance d'emprunt.*

#### TENSEUR DE SPREAD DE LA POSITION TOTALE

Le Tenseur de Spread de la Position Totale ( $\Lambda$ ) est une quantité proche du Tenseur de Localisation (LT, pour l'acronyme en anglais Localization Tensor), le TPS est simplement le LT multiplié par le nombre d'électrons dans le système. Le LT a été introduit dans le contexte de la théorie de Khon pour la description des propriétés électriques. La conclusion plus remarquable de cette théorie est la relation entre la nature du métal/isolateur d'un système et la délocalisation de  $\Psi$ , au lieu de la définition classique de la théorie des bandes [56]. En 1999 Resta et Sorella ont proposé une formulation quantitative de la LT pour l'état solide, cette méthode décrit la fluctuation des électrons : LT diverge pour les métaux (fluctuation électronique élevée, petite bande) et est constante pour les isolateurs (faible fluctuation électronique, haute bande), sans le calcul coûteux d'un état excité [156–159]. Le TPS présente l'avantage d'être une méthode de consistance, ce qui suggère qu'elle est un indicateur supérieur pour les systèmes moléculaires par rapport à la LT

Le Spin-Summed TPS (SS-TPS) est défini comme un cumulatif de second ordre de l'opérateur de position  $\hat{R}$

$$\Lambda = \langle \Psi | \hat{R}_i \hat{R}_j | \Psi \rangle - \langle \Psi | \hat{R}_i | \Psi \rangle \langle \Psi | \hat{R}_j | \Psi \rangle \quad (2.157)$$

où  $i$  et  $j$  correspondent à un axe de coordonnées  $x$ ,  $y$  ou  $z$ .  $\hat{R}$  pour un  $N$ -système d'électrons est défini comme :

$$\hat{R} = \sum_{l=1}^N \hat{r}_l(x, y, z) \quad (2.158)$$

Le Spin-Partitioned TPS (SP-TPS) considère le spin électronique, au contraire du SS-TPS. Ainsi,  $\hat{R}$  est défini comme :

$$\hat{R}_\sigma = \sum_{l=1}^N \hat{r}_l \hat{n}_{\sigma l} \quad (2.161)$$

où  $\hat{n}_\sigma$  est l'opérateur du nombre de particules pour  $\alpha$ -spin ( $\hat{n}_\alpha$ ) et  $\beta$ -spin ( $\hat{n}_\beta$ ). Ensuite, l'opérateur de position totale est

$$\hat{R} = \hat{R}_\alpha + \hat{R}_\beta \quad (2.162)$$

et le carré de  $\hat{R}$  est

$$\hat{R}^2 = \hat{R}_\alpha^2 + \hat{R}_\beta^2 + \hat{R}_\alpha \hat{R}_\beta + \hat{R}_\beta \hat{R}_\alpha \quad (2.163)$$

Par conséquent, en considérant les équations 2.157 et 2.163, les partitions spin sont définies comme :

$$\Lambda_{\alpha\alpha} = \langle \Psi | \hat{R}_\alpha^2 | \Psi \rangle - \langle \Psi | \hat{R}_\alpha | \Psi \rangle^2 \quad (2.164a)$$

$$\Lambda_{\beta\beta} = \langle \Psi | \hat{R}_\beta^2 | \Psi \rangle - \langle \Psi | \hat{R}_\beta | \Psi \rangle^2 \quad (2.164b)$$

$$\Lambda_{\alpha\beta} = \langle \Psi | \hat{R}_\alpha \hat{R}_\beta | \Psi \rangle - \langle \Psi | \hat{R}_\alpha | \Psi \rangle \langle \Psi | \hat{R}_\beta | \Psi \rangle \quad (2.164c)$$

$$\Lambda_{\beta\alpha} = \langle \Psi | \hat{R}_\beta \hat{R}_\alpha | \Psi \rangle - \langle \Psi | \hat{R}_\beta | \Psi \rangle \langle \Psi | \hat{R}_\alpha | \Psi \rangle \quad (2.164d)$$

et le SS-TPS est égal à la somme des quatre composantes

$$\Lambda = \Lambda_{\alpha\alpha} + \Lambda_{\beta\beta} + \Lambda_{\alpha\beta} + \Lambda_{\beta\alpha} \quad (2.165)$$

Le SS-TPS et le SP-TPS ont été utilisés dans la présente thèse pour évaluer de différents types de liaisons chimiques. Le SS-TPS mesure comment est la fluctuation des électrons quand il y a une perturbation dans le système, tandis que le SP-TPS montre comment est la fluctuation de spin. Il existe une relation entre le TPS et la polarisation du système, le tenseur pourrait être considéré comme une mesure qualitative de la polarisabilité, qui a une relation profonde avec la description des liaisons chimiques.

Les molécules diatomiques sont un système approprié pour illustrer le comportement du TPS pour différents types des liaisons chimiques, la linéarité de ces molécules permet de définir facilement les deux composantes principales du tenseur : (1) dans la direction de liaison ( $\Lambda_{\parallel}$ ) et (2) parallèle à la liaison ( $\Lambda_{\perp}$ ). La première composante décrit la fluctuation électronique associée à la liaison chimique tandis que la seconde les variations dans l'environnement de la liaison. La taille des molécules diatomiques est également un avantage parce que des méthodes ab-initio de haut niveau avec un set suffisant flexible de bases peuvent être utilisées. Une deuxième application du TPS a été effectuée pour expliquer la nature de la liaison Be-Be dans les complexes L: Be-Be: L, le complexe linéaire CO: Be-Be: CO a été choisi pour illustrer le comportement du TPS dans ce type de molécules en raison de l'évaluation plus facile des composants du TPS.

Les composantes perpendiculaires ( $\Lambda_{\perp}$ , voir la figure 5.1a) et parallèles ( $\Lambda_{\parallel}$ , voir la figure 5.1b) de SS-TPS et SP-TPS ont été évaluées pour quatre groupes selon le type d'interaction :

1. *Des liaisons covalentes*, ont été évalué H<sub>2</sub>, Li<sub>2</sub> et N<sub>2</sub>.
2. *Des liaisons Charge-Shift*, a été évalué F<sub>2</sub>.
3. *Des liaisons ioniques*, a été évalué LiF.
4. *Des faible liaisons*, ont été évalué de différents types d'interactions faibles :

- a) L'interaction de Van der Waals dans la molécule  $\text{He}_2$ .
- b) L'interaction non-dynamique dans le dimère  $\text{Be}_2$  et dans la molécule  $\text{CO}$ :  $\text{Be-Be}$ :  $\text{CO}$ .



Scheme 5.1 : Représentation du TPS (a) perpendiculaire à la direction de la liaison ( $\Lambda_{\perp}$ ) et (b) dans la direction de la liaison ( $\Lambda_{\parallel}$ ) (plus de détails peuvent être trouvés dans la page 150).

### Liaisons Covalentes

Le SS-TPS et le SP-TPS pour les molécules de ce groupe sont présentés dans l'annexe B.7 figures 1-3 et en annexe B.7 figures 1-2, et une représentation est dans la figure 5.1. Les changements les plus spectaculaires sont dans  $\Lambda_{\parallel}$ , les plus petites valeurs des SS-TPS et SP-TPS sont dans les régions proches des noyaux où il y a un minimum de mobilité électronique. Le SS-TPS montre un maximum dans la zone où la liaison est rompue ( $R_{\text{rupture}}$ , la seconde dérivée de l'énergie devient nulle). Le SP-TPS diverge comme  $R_{\text{liaison}}^2$  lorsque la distance de liaison est augmentée.

Le SS-TPS, la courbe de dissociation des molécules de ce groupe pourrait être divisée en deux régions considérant la rupture de la liaison chimique ( $R_{\text{rupture}}$ ) :

- $R_{\text{liaison}} < R_{\text{rupture}}$ , les composantes parallèles et perpendiculaires augmentent avec la valeur de  $R_{\text{liaison}}$ , en raison de la diminution des contraintes des noyaux. Dans la région  $R_{\text{rupture}}$ ,  $\Lambda_{\parallel}$  montre un maximum tandis que  $\Lambda_{\perp}$  atteint la valeur atomique. Les valeurs des deux,  $\Lambda_{\parallel}$  et  $\Lambda_{\perp}$ , à la distance d'équilibre sont plus petites que les valeurs atomiques, parce que la fluctuation des électrons est limitée par l'influence du noyau.
- $R_{\text{liaison}} > R_{\text{rupture}}$ ,  $\Lambda$  va rapidement aux valeurs atomiques.

le SP-TPS, donne des informations sur la corrélation de l'électron dans le système,  $\Lambda_{\alpha\alpha+\beta\beta}$  mesure  $E_{\text{corr}}^{\text{XC}}$  et  $\Lambda_{\alpha\beta+\beta\alpha}$  mesure  $E_{\text{corr}}^{\text{ee}}$ . Des systèmes fortement corrélés ont été définis  $|E_{\text{corr}}^{\text{XC}}| \sim |E_{\text{corr}}^{\text{ee}}|$  [334], donc le SP-TPS pourrait être utilisé comme un indicateur du caractère multi-référentiel de  $\Psi$ . La composante  $\parallel$  diverge comme  $R_{\text{bond}}^2$  quand  $R_{\text{bond}} \rightarrow \infty$ , étant la même composante de spin légèrement plus grande que le spin différent. Deux régions peuvent être définies considérant  $\Psi$  :



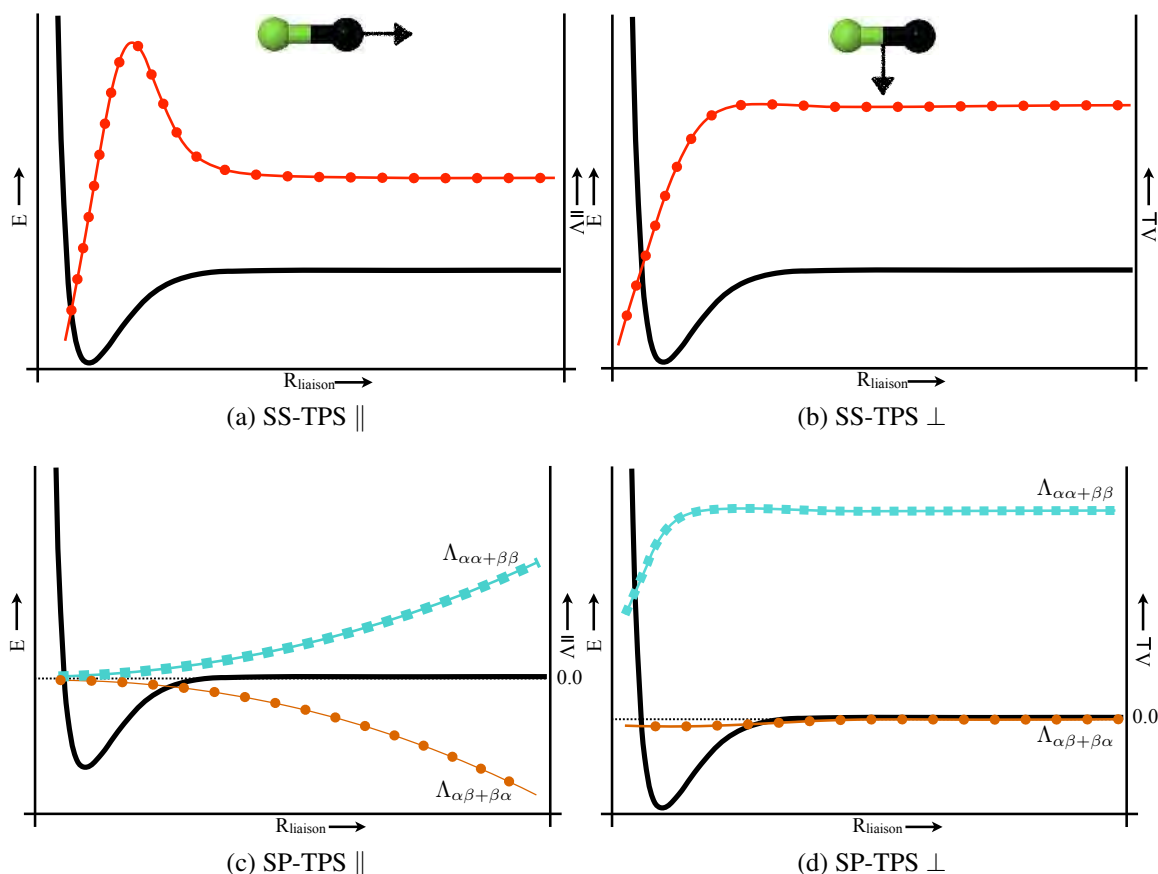


FIGURE 5.1 : SS-TPS (○-rouge) et SP-TPS (□-blue  $\Lambda_{\alpha\alpha+\beta\beta}$  et ○-orange  $\Lambda_{\alpha\beta+\beta\alpha}$ ) pour les liaisons covalentes, (a) SS-TPS  $\parallel$ , (b) SS-TPS  $\perp$ , (c) SP-TPS  $\parallel$  et (d) SP-TPS  $\perp$ . La courbe d'énergie de dissociation est représentée par un trait noir (plus de détails peuvent être trouvés dans la page 152).

- $R_{\text{eq}} < R_{\text{liaison}} < R_{\text{rupture}}$ , l'état fondamental de la molécule est représenté par une configuration à couche fermée dans laquelle les électrons de valence sont localisés dans une orbitale de liaison  $\Psi_{\text{MO}} = \phi_A + \phi_B$ , décrite correctement pour une fonction d'onde de déterminante unique,  $|E_{\text{corr}}^{\text{XC}}| > |E_{\text{corr}}^{\text{ee}}|$ .
- $R_{\text{liaison}} > R_{\text{rupture}}$ , la dissociation homolytique d'un système lié covalent conduit à des produits à couches ouvertes caractère multi-référentiel, représenté par la divergence de  $R_{\text{bond}}^2$  des composantes de même spin et de différent spin.

**Les composantes SP-TPS  $\perp$**  sont moins impressionnantes que les  $\parallel$ . Le SP-TPS  $\perp$  de spin différent est proche de zéro dans presque toute la courbe de dissociation, alors  $\Lambda_{\alpha\alpha+\beta\beta}$  est la principale contribution à la SS-TPS montrant le même comportement expliqué précédemment pour le SS-TPS. Par conséquent, la fluctuation des petits électrons à l'extérieur de la région de liaison est principalement associée à  $E_{\text{corr}}^{\text{XC}}$ .

### Liaisons de Transfert de Charge

Le SS-TPS et SP-TPS de la molécule  $F_2$  est présentée en annexe B.7 figure 4 et en annexe B.7 figures 1-2. Le SP-TPS montre le même comportement que pour les liaisons covalentes, la différence entre les deux types d'interactions peut être vu en considérant le SS-TPS, *tandis que pour les liaisons covalentes, le maximum de la fluctuation des électrons est lorsque la liaison est rompue, pour les liaisons par transfert de charge elles sont dans la distance d'équilibre* (voir figure 5.2a).

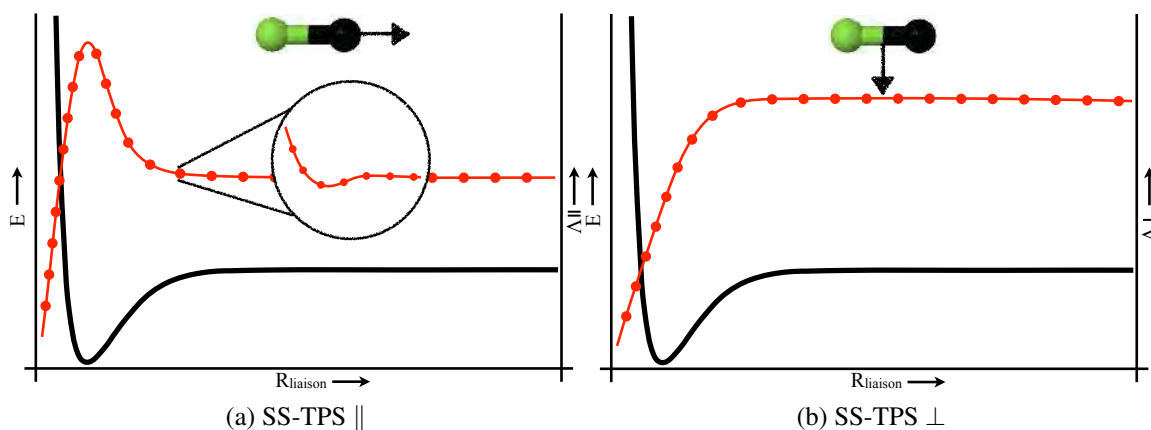


FIGURE 5.2 : SS-TPS (○-rouge) pour les liaisons de transfert de charge, (a) SS-TPS  $\parallel$  et (b) SS-TPS  $\perp$ . La courbe d'énergie de dissociation est représentée en ligne pleine-noire (plus de détails peuvent être trouvés dans la page 154).

La section 3.1.2 décrit ce type d'interaction. La répulsion de Pauli du nuage  $\pi$  dans l'état fondamental est équilibrée avec une délocalisation électronique élevée, décrite par le maximum de la  $\Lambda_{\parallel}$  dans la distance d'équilibre. La définition de la liaison a été basée sur la Théorie de la Liaison de Valence (VBT, pour l'acronyme en anglais Valence Bond Theory). Les liaisons de transfert de charge sont des interactions où il y a une résonance entre la configuration covalente et ionique,  $\Psi$  n'est plus décrite par une contribution covalente ou ionique pure mais par mélange de ces états. Cette propriété a été modélisée en étudiant la molécule  $H_2$  dans le cadre de la  $\Psi_{OVB}$ , mais en tenant compte d'un facteur d'échelle ( $k$ ) entre l'état fondamental neutre et l'état ionique  $\Sigma_g$  (OVB est orthogonale VBT [335]). L'analyse montre que le maximum du tenseur se produit à des distances plus courtes lorsque la valeur de  $k$  diminue, c'est-à-dire  $\Lambda$  est déplacée vers les distances d'équilibre lorsque l'intervalle entre les états covalent et ionique devient plus petit (voir figure 4 en annexe B.7). Par conséquent, le maximum dans l'équilibre du  $\Lambda_{\parallel}$  pour la molécule  $F_2$  est dû au mélange des configurations covalente et ionique.

$\Lambda_{\parallel}$  pour  $N_2$  a le même comportement que les liaisons covalentes classiques. Le maximum du tenseur est dans la région  $R_{rupture}$ , mais après le maximum il montre un minimum étroit qui est également le cas de la molécule  $F_2$  (voir figure 5.2a). Considérant à nouveau l'analyse  $\Psi_{OVB}$  pour la molécule  $H_2$ , pour  $k = 1.0$  le système est le dimère H et  $\Lambda_{\parallel}$  ne montre pas ce minimum, mais il commence à apparaître lorsque la valeur de  $k$  diminue ou quand

le caractère transfert de charge est augmenté, et ceci peut décrire la relaxation du système lorsque la répulsion de Pauli est interrompue en raison de la dissociation. La description SS-TPS de la molécule  $F_2$  est une liaison par transfert de charge pure, mais elle n'est pas claire pour la molécule  $N_2$ . L'analyse de la fonction d'onde de la molécule est montrée dans la figure 5.3, et tout coïncide  $N_2$  est une molécule covalente forte. L'analyse QTAIM trouve un  $BCP_{NN}$  avec  $\rho$  dans l'ordre de 0.1 et  $\nabla^2\rho$  est négatif. ELF localise un  $V(N, N)$  bassin disynaptique avec une population d'électrons élevée et les valeurs  $\langle cov\Omega_i, \Omega_j \rangle$  sont petites. Cependant, il a été trouvé que l'énergie de liaison N-N a une contribution de RE mais n'est pas aussi grande que dans des liaisons entre des halogènes [176]. Par conséquent, en considérant le résultat du SS-TPS pour le  $\Psi_{OVB}$ , le minimum apparaît pour une gamme de  $k$  entre 0.7 – 0.5. La molécule  $F_2$  est représentée par  $k \sim 0.5$  où il y a interaction maximale entre l'état covalent et ionique, et  $N_2$  est représenté par  $k \sim 0.7$  où l'interaction entre les états est plus grande que dans une liaison covalente pure, mais n'est pas encore une liaison de transfert de charge.

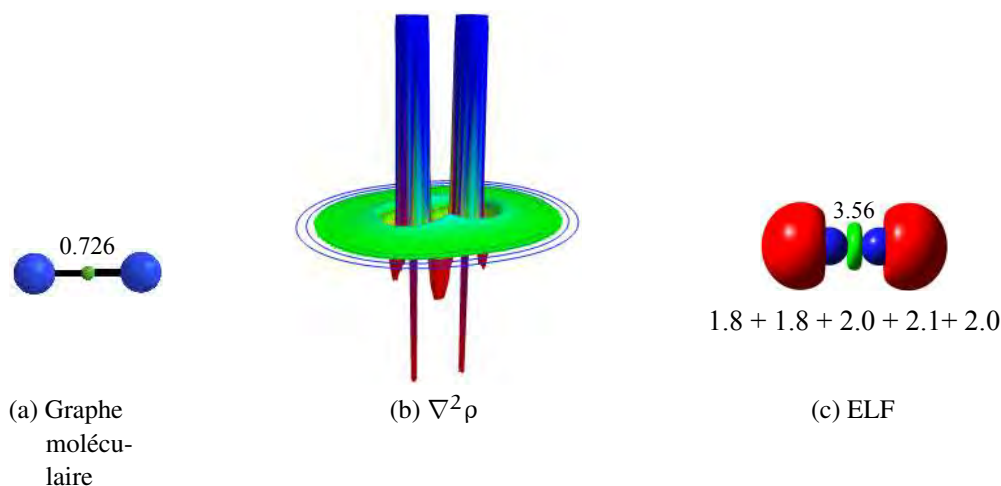
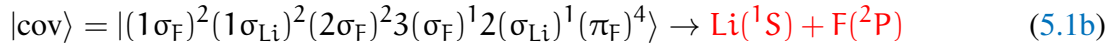
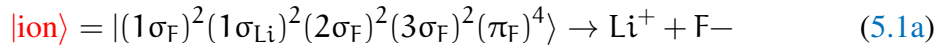


FIGURE 5.3 : Analyse de la fonction d'onde de la molécule  $N_2$ , (a) graphique moléculaire avec le  $BCP_{NN}$  en vert et la valeur de  $\rho$ ; (b) la carte en relief de  $\nabla^2\rho$ , l'échelle de couleur est : bleu  $> 1$ , cyan  $> 0.5$ , vert  $> -0.5$ , jaune  $> -1$ , rouge  $< -1$ ; (c) la représentation ELF des bassins et de sa population, l'échelle de couleurs est : les bassins monosynaptiques associés aux paires seules sont en rouge, et les bassins disynaptiques ou trisynaptiques impliquant des atomes lourds sont en vert et en dessous sont représentés les éléments diagonaux de la matrice de covariance. Les calculs ont été effectués au niveau théorique de B3LYP / cc-pVTZ (plus de détails peuvent être trouvés dans la page 155).

### *Liaisons Ioniques*

La dissociation des systèmes ioniques est plus compliquée que la dissociation des systèmes covalents, parce que les réactifs et les produits sont dans des états différents. Donc, le mécanisme de dissociation doit impliquer un passage d'état entre les états covalent et ionique (voir

la section 3.1.1), pour LiF le croisement évité est d'environ 5.8Å (voir annexe B.7 figure 6). Les figures 7-8 en annexe B.7 et figures 7-8 en annexe B.8 montrent le SS-TPS et le SP-TPS pour LiF, et une représentation est dans la figure 5.4. La configuration des états ionique et covalent pour le LiF est montrée dans l'équation 5.1, en soulignant en rouge la configuration de l'état fondamental des réactifs et des produits.



**La composante  $\perp$**  du SS-TPS des systèmes liés ioniques donne plus d'informations sur  $\Psi$  que pour les liaisons covalentes. Pour les distances au-dessous du croisement évité, le tenseur de l'état fondamental présente des valeurs plus petites que pour l'état excité, montrant une fluctuation plus élevée des électrons dans  $|\text{cov}\rangle$  que dans  $|\text{ion}\rangle$ , avant le croisement évité le TPS de la configuration  $|\text{ion}\rangle$  augmente pour atteindre les valeurs des produits ioniques et le TPS de la configuration  $|\text{cov}\rangle$  diminue pour atteindre les valeurs des produits à couche fermée, Jusqu'à ce qu'ils traversent à 5.8Å, et finalement convergent vers les valeurs atomiques correspondantes (voir figure 5.4b). La contribution principale à la perpendiculaire SS-TPS est de la composante  $\Lambda_{\alpha\alpha+\beta\beta}$ , montrant le même comportement que  $\Lambda_{\perp}$  et,  $\Lambda_{\alpha\beta+\beta\alpha}$  est presque une constante proche de zéro (voir figure 5.4d). Les valeurs de **la composante  $\parallel$**  du SS-TPS restent proches des valeurs atomiques pour pratiquement toute la courbe de dissociation, sauf dans la zone du croisement évité où le tenseur présente un maximum, indiquant que *le maximum de la fluctuation des électrons pour les liaisons ioniques est dans le croisement évité entre les états ionique et covalent*, voir figure 5.4a.

**La composante  $\parallel$  du SP-TPS** illustre le caractère de référence multiple ou unique dans la dissociation de LiF, le comportement du tenseur est résumé comme suit :

1. État Fondamental :

- SP-TPS  $\sim 0 \Rightarrow R_{\text{bond}} < 5.8\text{Å}$ .
- SP-TPS  $R_{\text{bond}}^2 \Rightarrow R_{\text{bond}} > 5.8\text{Å}$ .

2. État Excité :

- SP-TPS  $R_{\text{bond}}^2 \Rightarrow R_{\text{lia}} < 5.8\text{Å}$ .
- SP-TPS  $\sim 0 \Rightarrow R_{\text{bond}} > 5.8\text{Å}$ .

Pour  $R_{\text{liaison}} < 5.8\text{Å}$  l'état fondamental est une fonction d'onde ionique à référence unique  $|\text{ion}\rangle$  tandis que l'état excité est une fonction d'onde covalente à couche ouverte  $|\text{cov}\rangle$ . Le caractère couche fermée de l'état fondamental est décrit par SP-TPS  $\sim 0$  et la multi-référence de l'état excité par la divergence  $R_{\text{liaison}}^2$  du tenseur. La situation est inversée pour  $R_{\text{liaison}} > 5.8\text{Å}$ , l'état fondamental devient les atomes neutres à couches ouvertes et l'état

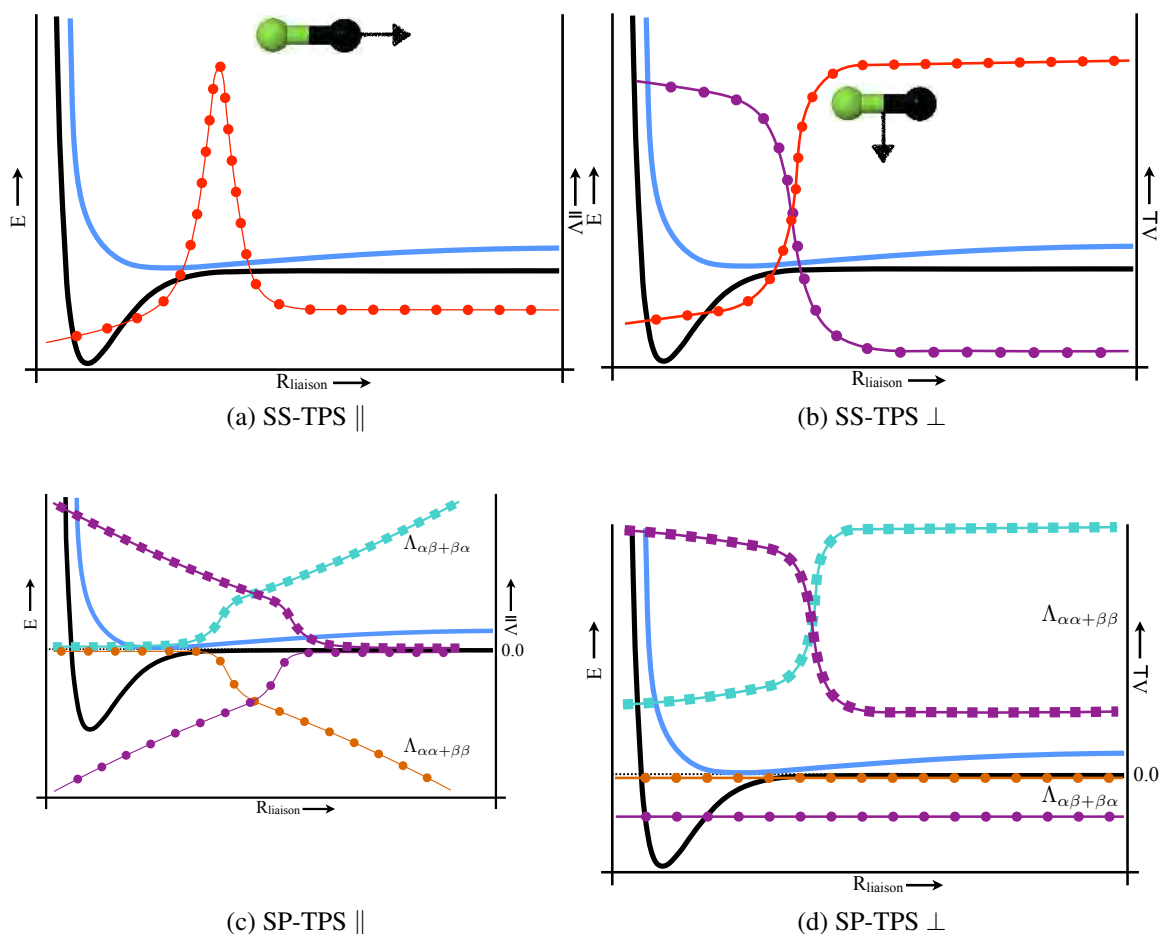


FIGURE 5.4 : Représentation du TPS pour les liaisons ioniques. SS-TPS est dans  $\circ$ -rouge pour l'état fondamental et dans  $\circ$ -violet pour le premier état excité. SP-TPS pour l'état fondamental :  $\square$ -bleu et  $\circ$ -orange. SP-TPS pour le premier état excité :  $\square$ -violet et  $\circ$ -violet. (a) SS-TPS  $\parallel$ , (b) SS-TPS  $\perp$ , (c) SP-TPS  $\parallel$  et (d) SP-TPS  $\perp$ . La courbe d'énergie de dissociation est représentée par un trait noir pour l'état fondamental et par un trait bleu pour le premier état excité (plus de détails peuvent être trouvés dans la page 156).

excité les atomes ioniques à couches fermées, le premier montrant une divergence  $R_{\text{liaison}}^2$  du SP-TPS  $\parallel$  et dans le second le SP-TPS  $\parallel$  va à des valeurs proches de zéro.

### Liaisons Faibles

La formation et la rupture des liaisons décrites jusqu'ici impliquaient des changements spectaculaires de  $\Psi$ , passant d'un état liant à un état anti-liant, donc des variations dramatiques ont été trouvées dans le TPS, mais ce n'est pas le cas des interactions faibles où dans certains systèmes il n'y a même pas un chevauchement de  $\Psi$  dans l'équilibre et l'interaction est principalement électrostatique. Les molécules  $\text{He}_2$  et  $\text{Be}_2$  ont été utilisées pour montrer le comportement du TPS pour les interactions faibles. Pendant longtemps, les deux interactions

ont été considérées comme Van der Waals, mais on a montré que Be-Be est une liaison non dynamique [54]. Ensuite, les sections suivantes traitent des résultats pour les deux molécules diatomiques et pour le complexe entre Be<sub>2</sub> et deux (CO) molécules.

### *Van der Waals Interactions : He<sub>2</sub>.*

L'interaction He-He est essentiellement électrostatique, la molécule est liée par de faibles forces de dispersion de Van der Waals, et le tableau 5 montre une longue distance de liaison He-He, et un petit BDE. Par conséquent, la fluctuation des électrons associée à la dissociation de ce dimère ne devrait pas être remarquable. Le SS-TPS de l'atome He est égal à  $0.75\text{au}^2$  (la somme des valeurs atomiques est égale à  $1.51\text{au}^2$ ), la composante parallèle pour les valeurs inférieures à la distance d'équilibre du dimère montre un maximum à  $2\text{au}^2$ , mais pour d'autres distances de liaison  $\Lambda_{\parallel}$  reste constant à  $1.52\text{au}^2$ , et après la distance d'équilibre le tenseur converge rapidement vers la valeur atomique.  $\Lambda_{\perp}$  a un comportement similaire que la composante parallèle. donc, le SS-TPS pour les interactions de Van der Waals *montre presque une valeur constante quand la liaison est étirée, indiquant une fluctuation négligeable des électrons*. Le SP-TPS est également une constante pour le dimère He, mais le caractère de couche fermée de l'interaction est décrit par la valeur presque nulle de  $\Lambda_{\alpha\beta+\beta\alpha}$  à travers la courbe de dissociation. Ainsi, la contribution principale au SS-TPS vient de la même partition de spin et l'interaction entre le dimère He est principalement due à l'énergie d'échange-corrélation. Voir annexe B.7 figure 10 et annexe B.8 figure 5 pour la représentation graphique du TPS et une analyse plus approfondie de la molécule He<sub>2</sub>.

### *Liaisons Be : Be<sub>2</sub> et CO: Be-Be: CO.*

Les propriétés de liaison du dimère de béryllium sont décrites dans la référence [54] et dans la section 4.3.2, la liaison faible dans le dimère est due à un mélange de l'orbitale basse  $p_{\text{Be}}$  avec l'orbitale  $2s_{\text{Be}}$ , ce qui n'est pas possible dans le He<sub>2</sub> parce que les orbitales  $p_{\text{He}}$  sont beaucoup plus hautes en énergie. L'analyse TPS est en accord avec cette description, la figure 5.5 montre une représentation des tenseurs SS-TPS et SP-TPS pour la composante parallèle. La composante  $\Lambda_{\parallel}$  pour le Be<sub>2</sub> est différente d'une constante, donc He<sub>2</sub> et Be<sub>2</sub> ne partagent pas le même type d'interaction, *la liaison Be-Be n'est pas une interaction à couche fermée*. Selon le SS-TPS, la molécule Be<sub>2</sub> montre un maximum de fluctuation électronique dans la région d'équilibre comme la molécule F<sub>2</sub>, néanmoins la fluctuation électronique élevée du Be<sub>2</sub> est associée aux excitations  $s \rightarrow p$  et non à la répulsion de Pauli, ce qui peut être confirmé par le SP-TPS.

Le SP-TPS dans le sens de liaison pour Be<sub>2</sub> et F<sub>2</sub> sont complètement différents. À *courtes* distances, le tenseur de même et différent spin du dimère de béryllium diverge comme  $R_{\text{liaison}}^2$  alors que pour F<sub>2</sub> le tenseur diverge à *longues* distances, montrant que F<sub>2</sub> a une multi-référence à de longues distances en raison de la formation de produits à couches ouvertes. Le caractère multi-référentiel du  $\Psi_{\text{Be}_2}$  est à l'équilibre parce qu'il est nécessaire d'utiliser plus

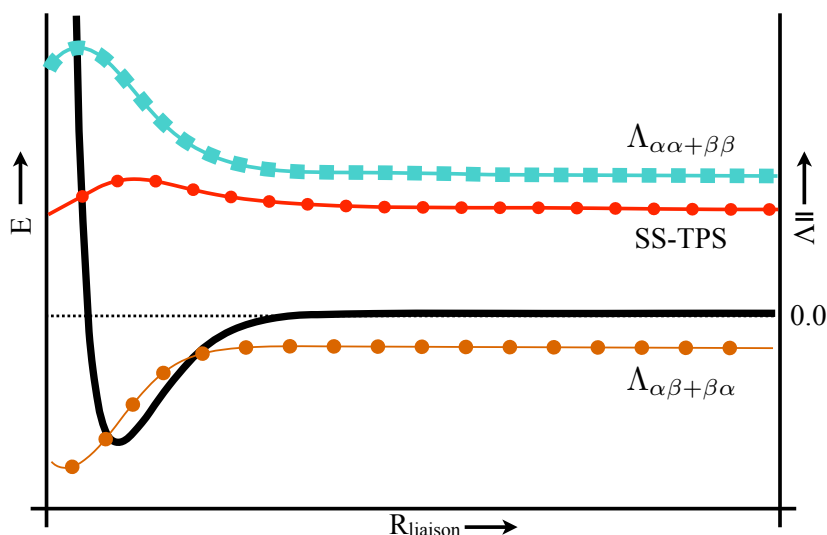


FIGURE 5.5 : Représentation du TPS pour les liaisons non dynamiques le SS-TPS est en  $\circ$ -rouge. Le SP-TPS est dans  $\square$ -cyan pour  $\Lambda_{\alpha\alpha+\beta\beta}$  et dans  $\circ$ -orange pour  $\Lambda_{\alpha\beta+\beta\alpha}$ . La courbe d'énergie de dissociation est représentée par un trait noir en gras (plus de détails peuvent être trouvés dans la page 159).

d'un déterminant pour représenter le mélange entre les orbitales  $s_{Be}$  et  $p_{Be}$ . Sur les longues distances, les produits de  $Be_2$  sont des atomes à couches fermées et le SP-TPS devient une constante.

La situation est différente lorsque  $Be_2$  interagit avec un LB. L'interaction  $Be:L$  non covalente augmente la force de  $Be-Be$  en plus de 10 fois en raison de la stabilisation des orbitales  $\pi_{Be}$ . La section 4.3.3 décrit le lien entre  $L:Be-Be:L$  avec  $L = NH_3, H_2O$  et  $CO$ . L'effet le plus spectaculaire a été trouvé pour  $L = CO$  où la conjugaison  $\pi_{CO}$  avec les orbitales moléculaires  $\pi_{Be}$  a fortement stabilisé le système, mais comme cela a été expliqué dans la section 4.3.3.3 la dissociation de ce complexe n'est pas simple (voir équation 4.10). L'annexe B.6 figure S9 montre une représentation du système, fut remarqué que dans les distances d'équilibre sont dégénérées deux états singulet.

**La composante parallèle du TPS** pour le système  $CO:Be-Be:CO$  est représentée dans la figure 5.6, mais elle ne représente que la réaction avant l'état de croisement entre les équations 4.10. La figure 5.6a montre à la fois le SS-TPS et la valeur de  $\rho$  dans le  $B_{CP_{Be-Be}}$ , les triangles roses montrent la zone où le système est lié par un NNA. Selon  $\Lambda_{||}$  il y a deux maximum de mobilité d'électrons associés à ce type d'interaction : le premier dans les distances d'équilibre et le second aux longues distances de liaison. Il est clair que les seconds maxima sont dus à la dissociation de la molécule, ce qui est en accord avec la valeur presque nulle de  $\rho$  dans le  $B_{CP_{Be-Be}}$ . La zone autour de la distance d'équilibre de ce système est une section compliquée du PES, et au moins il y a trois explications possibles pour le maximum du TPS dans cette région :

1. La formation du NNA.

2. L'état fondamental doublement dégénéré (voir annexe B.6 figure S9).
3. Les excitations  $s \rightarrow p$  associées à la liaison Be-Be.

La figure 2 dans [307] montre que les molécules diatomiques homonucléaires de H à F ont un NNA, qui apparaît dans de différentes zones de la courbe de dissociation. L'analyse du TPS dans les systèmes  $\text{Li}_2$ ,  $\text{N}_2$ ,  $\text{F}_2$  or  $\text{Be}_2$  n'ont pas montré un maximum associé à la formation d'un NNA, et ce n'est probablement pas le cas pour  $\text{CO}:\text{Be}-\text{Be}:\text{CO}$ . Par conséquent, cela suggère que le comportement du tenseur dans la région d'équilibre est attribué à la fois par les excitations  $s \rightarrow p$  dans le groupement  $\text{Be}_2$  et l'état fondamental doublement dégénéré (semblable à la LiF croisement évité).

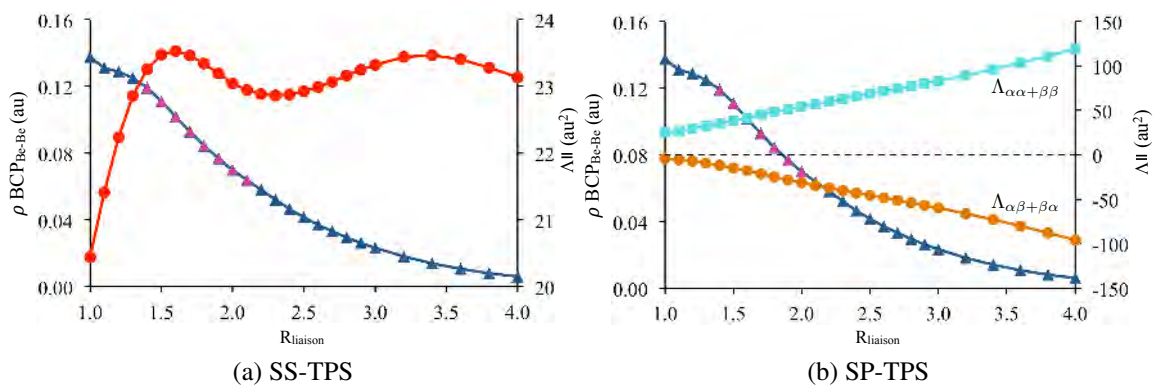


FIGURE 5.6 : Représentation de la composante parallèle du SS-TPS et du SP-TPS pour l'état fondamental  $^1\Sigma_g$  du complexe  $\text{CO}:\text{Be}-\text{Be}:\text{CO}$ . (a) Le SS-TPS est représenté en  $\circ$ -rouge et (b) le SP-TPS est en  $\square$ -cyan pour  $\Lambda_{\alpha\alpha+\beta\beta}$  et en  $\circ$ -orange pour  $\Lambda_{\alpha\beta+\beta\alpha}$ . La valeur de  $\rho$  dans le  $\text{BCP}_{\text{Be-Be}}$  est représentée avec  $\triangle$ -bleu et le  $\text{BCP}_{\text{Be-NNA}}$  avec  $\triangle$ -rose. Les calculs ont été effectués au niveau de la théorie  $\text{CASSCF}(10,12)/\text{cc-pVTZ}//\text{CASPT2}/\text{CASSCF}(10,12)/\text{cc-pVTZ}$  (plus de détails peuvent être trouvés dans la page 160).

Le **SP-TPS** est représenté dans la figure 5.6b, le comportement des tenseurs dans la région entre  $1 - 4\text{\AA}$  est différent des liaisons covalentes et non dynamiques. Les tenseurs montrent une augmentation de la multi-référence à l'intérieur de toute la courbe de dissociation, les réactifs dans l'équation 4.10a sont un système à couche fermée qui requiert plus d'un déterminant de l'entaille pour décrire l'orbitale dégénérée doublement occupée  $\pi_{\text{Be-Be}}$  et la conjugaison avec les orbitales  $\pi_{\text{CO}}$ . Le caractère multi-référence à de longues distances est encore amélioré par les produits radicaux neutres ( $\cdot\text{CO}:\text{Be}\cdot$ ). Pour les distances supérieures à  $4\text{\AA}$ , le croisement entre les états  $^1\Sigma_g$  et  $n\cdot^1\Sigma_g$  ( $n\cdot^1\Sigma_g$  correspond à l'état qui dissocie en tant que dimère libre Be) devrait produire un maximum dans le SP-TPS pour atteindre la valeur constante des atomes Be, comme le cas de la molécule  $\text{Be}_2$  dans la figure 5.5.

*Le comportement du SS-TPS et du SP-TPS dans la dissociation moléculaire est une propriété intrinsèque de chaque type d'interaction chimique, montrant les régions avec la plus forte fluctuation d'électrons et où le système a un fort caractère corrélé.*





## Part VI

### BIBLIOGRAPHY

"Begin at the beginning," the King said very gravel, "and go on till you come to the end: then stop."

*Lewis Carroll. Alice in Wonderland - 1865.*



## BIBLIOGRAPHY

---

- (1) Helgaker, T.; Jørgensen, P.; Olsen, J., *Molecular Electronic-structure Theory*; John Wiley & Sons: 2014.
- (2) Lewis, G. N. *Journal of the American Chemical Society* **1916**, *38*, 762–785.
- (3) Pauling, L. *Journal of the American Chemical Society* **1931**, *53*, 1367–1400.
- (4) Pauling, L., *The nature of the chemical bond and the structure of molecules and crystals: an introduction to modern structural chemistry*; Cornell university press: 1960; Vol. 18.
- (5) Frenking, G.; Shaik, S., *The chemical bond: fundamental aspects of chemical bonding*; John Wiley & Sons: 2014; Vol. 1.
- (6) Müller-Dethlefs, K.; Hobza, P. *Chemical Reviews* **2000**, *100*, 143–168.
- (7) Zahradník, R.; Hobza, P.; Müller-Dethlefs, K. *Collection of Czechoslovak Chemical Communications* **2006**, *71*, 443–531.
- (8) Hobza, P.; Müller-Dethlefs, K., *Non-Covalent Interactions, Theory and Experiment*; RSC Theoretical and Computational Chemistry Series; The Royal Society of Chemistry: 2009, pp 1–226.
- (9) Hinz, I.; Koeber, K.; Kreuzbichler, I.; Kuhn, P.; Seidel, A.; Hinz, I.; Kugler, H. K.; Wagner, J., *Be Beryllium: Supplement Volume A1 The Element. Production, Atom, Molecules, Chemical Behavior, Toxicology*, 8th ed.; Gmelin Handbook of Inorganic and Organometallic Chemistry-8<sup>th</sup> edition Be/A/1: Be Beryllium (System-Nr. 26); Springer-Verlag Berlin Heidelberg: 1986.
- (10) Walsh, K. A., *Beryllium Chemistry and Processing*; ASM International: 2009.
- (11) Hawumba, J. F.; Hung, Y.-T.; Wang, L. K., *Chapter 15 Toxicity, Sources, and Control of Selenium, Nickel, and Beryllium in the Environment*; Chen, J. P., Wang, L. K., Wang, M.-H. S., Hung, Y.-T., Shamma, N. K., Eds.; Remediation of Heavy Metals in the Environment. Advances in Industrial and Hazardous Wastes Treatment. CRC Press: 2016, pp 483–412.
- (12) Harris, L.; Yakel, H. *Acta Crystallographica* **1967**, *22*, 354–360.
- (13) Niemeyer, M.; Power, P. P. *Inorganic chemistry* **1997**, *36*, 4688–4696.
- (14) Gottfriedsen, J.; Blaurock, S. *Organometallics* **2006**, *25*, 3784–3786.
- (15) Dressel, M. P.; Nogai, S.; Berger, R. J.; Schmidbaur, H. *Zeitschrift für Naturforschung B* **2003**, *58*, 173–182.
- (16) Neumüller, B.; Petz, W.; Dehnicke, K. *Zeitschrift für anorganische und allgemeine Chemie* **2008**, *634*, 662–668.

- (17) Ceconi, F.; Ghilardi, C. A.; Ienco, A.; Mariani, P.; Mealli, C.; Midollini, S.; Orlandini, A.; Vacca, A. *Inorganic chemistry* **2002**, *41*, 4006–4017.
- (18) Newman, L. S.; Lloyd, J.; Daniloff, E. *Environmental health perspectives* **1996**, *104*, 937.
- (19) Yáñez, M.; Sanz, P.; Mó, O.; Alkorta, I.; Elguero, J. *Journal of Chemical Theory and Computation* **2009**, *5*, 2763–2771.
- (20) J.M., B. J.; W. D., H. J.; W., W. J. *The Journal of Chemical Physics* **1975**, *62*, 3122–3130.
- (21) Bondybey, V. E.; English, J. H. *The Journal of Chemical Physics* **1984**, *80*, 568–570.
- (22) Bondybey, V. *Chemical Physics Letters* **1984**, *109*, 436–441.
- (23) Merritt, J. M.; Kaledin, A. L.; Bondybey, V. E.; Heaven, M. C. *Physical Chemistry Chemical Physics* **2008**, *10*, 4006–4013.
- (24) McNaught, A. D.; Wilkinson, A., IUPAC. *Compendium of Chemical Terminology (the "Gold Book")*, 2nd ed., 1997.
- (25) Reine, S.; Saue, T., *European summerschool in quantum chemistry*, 9th ed., 2015.
- (26) Karpfen, A. *Theoretica chimica acta* **1978**, *50*, 49–65.
- (27) Armstrong, D. R.; Jamieson, J.; Perkins, P. G. *Theoretica chimica acta* **1979**, *51*, 163–172.
- (28) Hinze, J.; Friedrich, O.; Sundermann, A. *Molecular Physics* **1999**, *96*, 711–718.
- (29) Abdurahman, A.; Shukla, A.; Dolg, M. *The Journal of Chemical Physics* **2000**, *112*, 4801–4805.
- (30) Li, H.; Roy, R. J. L. *The Journal of Chemical Physics* **2006**, *125*, 044307.
- (31) Bernath, P. F.; Shayesteh, A.; Tereszchuk, K.; Colin, R. *Science* **2002**, *297*, 1323–1324.
- (32) Shayesteh, A.; Tereszchuk, K.; Bernath, P.; Colin, R. *The Journal of Chemical Physics* **2003**, *118*, 3622–3627.
- (33) Akishin, P.; Spiridonov, V. P. *Kristallografiya* **1957**, *2*, 475–472.
- (34) Kaupp, M.; Schleyer, P.; Stoll, H.; Preuss, H. *Journal of the American Chemical Society* **1991**, *113*, 6012–6020.
- (35) Ramondo, F.; Bencivenni, L.; Spoliti, M. *Journal of Molecular Structure: THEOCHEM* **1992**, *277*, 171–184.
- (36) Helal, W.; Evangelisti, S.; Leininger, T.; Monari, A. *Chemical Physics Letters* **2013**, *568*, 49–54.
- (37) Meng, B.; Bruna, P. J.; Wright, J. S. *Molecular Physics* **1993**, *79*, 1305–1325.
- (38) Heaven, M. C.; Merritt, J. M.; Bondybey, V. E. *Annual review of physical chemistry* **2011**, *62*, 375–393.
- (39) Kalemos, A. *The Journal of Chemical Physics* **2016**, *145*, 214302.

- 
- (40) Bauschlicher, C. W.; Rosi, M. *Chemical physics letters* **1989**, *159*, 485–488.
- (41) Sunil, K. *Journal of the American Chemical Society* **1992**, *114*, 3985–3986.
- (42) Andrews, L.; Tague Jr, T. J.; Kushto, G. P.; Davy, R. D. *Inorganic Chemistry* **1995**, *34*, 2952–2961.
- (43) Couchman, S. A.; Holzmann, N.; Frenking, G.; Wilson, D. J.; Dutton, J. L. *Dalton Transactions* **2013**, *42*, 11375–11384.
- (44) Cui, Z.-h.; Yang, W.-s.; Zhao, L.; Ding, Y.-h.; Frenking, G. *Angewandte Chemie* **2016**, *128*, 7972–7977.
- (45) Lee, E. P.; Wright, T. G. *The Journal of Physical Chemistry A* **2000**, *104*, 974–981.
- (46) Merritt, J. M.; Bondybey, V. E.; Heaven, M. C. *Science* **2009**, *324*, 1548–1551.
- (47) Jeziorski, B.; Moszynski, R.; Szalewicz, K. *Chemical Reviews* **1994**, *94*, 1887–1930.
- (48) Morokuma, K. *The Journal of Chemical Physics* **1971**, *55*, 1236–1244.
- (49) Ziegler, T.; Rauk, A. *Theoretical Chemistry Accounts: Theory, Computation, and Modeling (Theoretica Chimica Acta)* **1977**, *46*, 1–10.
- (50) Montero-Campillo, M. M.; Lamsabhi, A. M.; M6, O.; Y61nez, M. *Journal of Molecular Modeling* **2013**, *19*, 2759–2766.
- (51) M6, O.; Y61nez, M.; Alkorta, I.; Elguero, J. *Journal of Chemical Theory and Computation* **2012**, *8*, 2293–2300.
- (52) Albrecht, L.; Boyd, R. J.; M6, O.; Y61nez, M. *Physical Chemistry Chemical Physics* **2012**, *14*, 14540–14547.
- (53) R6eggen, I.; Alm6f, J. *International Journal of Quantum Chemistry* **1996**, *60*, 453–466.
- (54) El Khatib, M.; Bendazzoli, G. L.; Evangelisti, S.; Helal, W.; Leininger, T.; Tenti, L.; Angeli, C. *The Journal of Physical Chemistry A* **2014**, *118*, 6664–6673.
- (55) Koch, D; Fertitta, E; Paulus, B *The Journal of Chemical Physics* **2016**, *145*, 024104.
- (56) Kohn, W. *Physical Review* **1964**, *133*, A171.
- (57) Martin, R. M., *Electronic structure: basic theory and practical methods*; Cambridge university press: 2004.
- (58) Y61nez, M.; M6, O.; Alkorta, I.; Elguero, J. *Chemistry-A European Journal* **2013**, *19*, 11637–11643.
- (59) Mart6n-S6mer, A.; M6, O.; Y61nez, M.; Guillemin, J.-C. *Dalton Transactions* **2015**, *44*, 1193–1202.
- (60) Politzer, P.; Murray, J. S.; Concha, M. C. *Journal of Molecular Modeling* **2007**, *13*, 643–650.
- (61) Gilli, G.; Bellucci, F.; Ferretti, V.; Bertolasi, V. *Journal of the American Chemical Society* **1989**, *111*, 1023–1028.

- (62) Bertolasi, V.; Gilli, P.; Ferretti, V.; Gilli, G. *Journal of the American Chemical Society* **1991**, *113*, 4917–4925.
- (63) Gilli, P.; Bertolasi, V.; Ferretti, V.; Gilli, G. *Journal of the American Chemical Society* **1994**, *116*, 909–915.
- (64) González, L.; Mó, O.; Yáñez, M. *The Journal of Organic Chemistry* **1999**, *64*, 2314–2321.
- (65) Sanz, P.; Mó, O.; Yáñez, M.; Elguero, J. *Chemistry -A European Journal* **2008**, *14*, 4225–4232.
- (66) Krygowski, T. M.; Zachara-Horeglad, J. E.; Palusiak, M. *The Journal of Organic Chemistry* **2010**, *75*, 4944–4949.
- (67) Staab, H. A.; Saupe, T. *Angewandte Chemie International Edition in English* **1988**, *27*, 865–879.
- (68) Schrödinger, E. *Physical Review* **1926**, *28*, 1049–1070.
- (69) Schrödinger, E. *Annalen der Physik* **1926**, *384*, 361–376.
- (70) Hartree, D. R. *Proceedings of the Cambridge Philosophical Society* **1928**, *24*, 89.
- (71) Fock, V. *Zeitschrift für Physik* **1930**, *61*, 126–148.
- (72) Slater, J. C. *Physical Review* **1930**, *35*, 210–211.
- (73) Roothaan, C. C. J. *Reviews of Modern Physics* **1951**, *23*, 69–89.
- (74) Hall, G. G. *Proceedings of the Royal Society of London A: Mathematical, Physical and Engineering Sciences* **1951**, *205*, 541–552.
- (75) Pople, J. A.; Nesbet, R. K. *The Journal of Chemical Physics* **1954**, *22*, 571–572.
- (76) Szabo, A.; Ostlund, N. S., *Modern quantum chemistry: introduction to advanced electronic structure theory*; Courier Corporation: 2012.
- (77) Schrödinger, E. *Annalen der Physik* **1926**, *385*, 437–490.
- (78) Rayleigh, J. W. S., *Theory of Sound, Volume 1*, 2nd Edition Revised and Enlarged; Dover Publications: 1945.
- (79) Møller, C.; Plesset, M. S. *Physical Review* **1934**, *46*, 618.
- (80) Pople, J. A.; Binkley, J. S.; Seeger, R. *International Journal of Quantum Chemistry* **1976**, *10*, 1–19.
- (81) Pople, J. A.; Seeger, R.; Krishnan, R. *International Journal of Quantum Chemistry* **1977**, *12*, 149–163.
- (82) Krishnan, R.; Schlegel, H.; Pople, J. *The Journal of Chemical Physics* **1980**, *72*, 4654–4655.
- (83) Langhoff, S. R.; Davidson, E. R. *International Journal of Quantum Chemistry* **1974**, *8*, 61–72.
- (84) Ahlrichs, R.; Scharf, P.; Ehrhardt, C. *The Journal of Chemical Physics* **1985**, *82*, 890–898.

- 
- (85) Pople, J. A.; Head-Gordon, M.; Raghavachari, K. *The Journal of Chemical Physics* **1987**, *87*, 5968–5975.
- (86) Siegbahn, P. E.; Almlöf, J.; Heiberg, A.; Roos, B. O. *The Journal of Chemical Physics* **1981**, *74*, 2384–2396.
- (87) Roos, B. O. *International Journal of Quantum Chemistry* **1980**, *18*, 175–189.
- (88) Karlström, G. et al. *Computational Materials Science* **2003**, *28*, 222–239.
- (89) Werner, H.-J. et al. MOLPRO, version 2015.1, A Package of Ab-initio Programs., Cardiff, UK, 2015.
- (90) Roos, B. O.; Taylor, P. R.; Si, P. E., et al. *Chemical Physics* **1980**, *48*, 157–173.
- (91) Malmqvist, P. A.; Rendell, A.; Roos, B. O. *Journal of Physical Chemistry* **1990**, *94*, 5477–5482.
- (92) Werner, H.-J.; Meyer, W. *The Journal of Chemical Physics* **1980**, *73*, 2342–2356.
- (93) Werner, H.-J.; Meyer, W. *The Journal of Chemical Physics* **1981**, *74*, 5794–5801.
- (94) Andersson, K.; Malmqvist, P. A.; Roos, B. O.; Sadlej, A. J.; Wolinski, K. *Journal of Physical Chemistry* **1990**, *94*, 5483–5488.
- (95) Andersson, K.; Malmqvist, P.-Å.; Roos, B. O. *The Journal of Chemical Physics* **1992**, *96*, 1218–1226.
- (96) Finley, J.; Malmqvist, P.-Å.; Roos, B. O.; Serrano-Andrés, L. *Chemical Physics Letters* **1998**, *288*, 299–306.
- (97) Ghigo, G.; Roos, B. O.; Malmqvist, P.-Å. *Chemical Physics Letters* **2004**, *396*, 142–149.
- (98) Roos, B. O.; Andersson, K. *Chemical Physics Letters* **1995**, *245*, 215–223.
- (99) Roos, B. O.; Andersson, K.; Fülcher, M. P.; Serrano-Andrés, L.; Pierloot, K.; Merchán, M.; Molina, V. *Journal of Molecular Structure: THEOCHEM* **1996**, *388*, 257–276.
- (100) Forsberg, N.; Malmqvist, P.-Å. *Chemical Physics Letters* **1997**, *274*, 196–204.
- (101) Roos, B. O.; Andersson, K. *Chemical physics letters* **1995**, *245*, 215–223.
- (102) Forsberg, N.; Malmqvist, P.-Å. *Chemical physics letters* **1997**, *274*, 196–204.
- (103) Forsberg, N.; Malmqvist, P.-Å. *Chemical physics letters* **1997**, *274*, 196–204.
- (104) Ghigo, G.; Roos, B. O.; Malmqvist, P.-Å. *Chemical physics letters* **2004**, *396*, 142–149.
- (105) Knowles, P. J.; Hampel, C.; Werner, H.-J. *The Journal of Chemical Physics* **1993**, *99*, 5219–5227.
- (106) Bartlett, R. J. *The Journal of Physical Chemistry* **1989**, *93*, 1697–1708.
- (107) Raghavachari, K.; Trucks, G. W.; Pople, J. A.; Head-Gordon, M. *Chemical Physics Letters* **1989**, *157*, 479–483.



- 
- (108) Christiansen, O.; Koch, H.; Jørgensen, P. *The Journal of Chemical Physics* **1996**, *105*, 1451–1459.
- (109) Lee, T. J.; Taylor, P. R. *International Journal of Quantum Chemistry* **1989**, *36*, 199–207.
- (110) Hohenberg, P.; Kohn, W. *Physical Review* **1964**, *136*, B864–B871.
- (111) Kohn, W.; Sham, L. J. *Physical Review* **1965**, *140*, A1133.
- (112) Ceperley, D. M.; Alder, B. J. *Physical Review Letters* **1980**, *45*, 566–569.
- (113) Vosko, S. H.; Wilk, L.; Nusair, M. *Canadian Journal of Physics* **1980**, *58*, 1200–1211.
- (114) Becke, A. D. *Physical Review A* **1988**, *38*, 3098.
- (115) Lee, C.; Yang, W.; Parr, R. G. *Physical Review B* **1988**, *37*, 785.
- (116) Zhao, Y.; Truhlar, D. G. *The Journal of Chemical Physics* **2006**, *125*, 194101.
- (117) Becke, A. D. *The Journal of Chemical Physics* **1993**, *98*, 1372–1377.
- (118) Becke, A. D. *Physical Review A* **1988**, *38*, 3098–3100.
- (119) Slater, J. C. *Physical Review* **1930**, *36*, 57–64.
- (120) Boys, S. F. *Proceedings of the Royal Society of London A: Mathematical, Physical and Engineering Sciences* **1950**, *200*, 542–554.
- (121) Hehre, W. J., *Ab-initio Molecular Orbital Theory*; Wiley-Interscience: 1986.
- (122) Ditchfield, R.; Hehre, W. J.; Pople, J. A. *The Journal of Chemical Physics* **1971**, *54*, 724–728.
- (123) Hehre, W. J.; Ditchfield, R.; Pople, J. A. *The Journal of Chemical Physics* **1972**, *56*, 2257–2261.
- (124) Hariharan, P.; Pople, J. *Molecular Physics* **1974**, *27*, 209–214.
- (125) Binning, R.; Curtiss, L. *Journal of Computational Chemistry* **1990**, *11*, 1206–1216.
- (126) McLean, A.; Chandler, G. *The Journal of Chemical Physics* **1980**, *72*, 5639–5648.
- (127) Krishnan, R.; Binkley, J. S.; Seeger, R.; Pople, J. A. *The Journal of Chemical Physics* **1980**, *72*, 650–654.
- (128) Hariharan, P. C.; Pople, J. A. *Theoretical Chemistry Accounts: Theory, Computation, and Modeling (Theoretica Chimica Acta)* **1973**, *28*, 213–222.
- (129) Francl, M. M.; Pietro, W. J.; Hehre, W. J.; Binkley, J. S.; Gordon, M. S.; DeFrees, D. J.; Pople, J. A. *The Journal of Chemical Physics* **1982**, *77*, 3654–3665.
- (130) Rassolov, V. A.; Pople, J. A.; Ratner, M. A.; Windus, T. L. *The Journal of Chemical Physics* **1998**, *109*, 1223–1229.
- (131) Frisch, M. J.; Pople, J. A.; Binkley, J. S. *The Journal of Chemical Physics* **1984**, *80*, 3265–3269.
- (132) Clark, T.; Chandrasekhar, J.; Spitznagel, G. W.; Schleyer, P. V. R. *Journal of Computational Chemistry* **1983**, *4*, 294–301.

- 
- (133) Jr., T. H. D. *The Journal of Chemical Physics* **1989**, *90*, 1007–1023.
- (134) Kendall, R. A.; Dunning Jr, T. H.; Harrison, R. J. *The Journal of Chemical Physics* **1992**, *96*, 6796–6806.
- (135) Woon, D. E.; Dunning Jr, T. H. *The Journal of Chemical Physics* **1993**, *98*, 1358–1371.
- (136) Pople, J. A.; Head-Gordon, M.; Fox, D. J.; Raghavachari, K.; Curtiss, L. A. *The Journal of Chemical Physics* **1989**, *90*, 5622–5629.
- (137) Curtiss, L. A.; Jones, C.; Trucks, G. W.; Raghavachari, K.; Pople, J. A. *The Journal of Chemical Physics* **1990**, *93*, 2537–2545.
- (138) Curtiss, L. A.; Raghavachari, K.; Trucks, G. W.; Pople, J. A. *The Journal of Chemical Physics* **1991**, *94*, 7221–7230.
- (139) Curtiss, L. A.; Raghavachari, K.; Redfern, P. C.; Rassolov, V.; Pople, J. A. *The Journal of Chemical Physics* **1998**, *109*, 7764–7776.
- (140) Curtiss, L. A.; Redfern, P. C.; Raghavachari, K. *The Journal of Chemical Physics* **2007**, *126*, 084108.
- (141) Reed, A. E.; Curtiss, L. A.; Weinhold, F. *Chemical Reviews* **1988**, *88*, 899–926.
- (142) Reed, A. E.; Weinhold, F. *The Journal of Chemical Physics* **1983**, *78*, 4066–4073.
- (143) Reed, A. E.; Weinstock, R. B.; Weinhold, F. *The Journal of Chemical Physics* **1985**, *83*, 735–746.
- (144) Foster, J.; Weinhold, F. *Journal of the American Chemical Society* **1980**, *102*, 7211–7218.
- (145) Becke, A.; Matta, C. F.; Boyd, R. J., *The Quantum Theory of Atoms in Molecules: from Solid State to DNA and Drug Design*; John Wiley & Sons: 2007.
- (146) Blanco, M.; Martín Pendás, A; Francisco, E *Journal of Chemical Theory and Computation* **2005**, *1*, 1096–1109.
- (147) Becke, A. D.; Edgecombe, K. E. *The Journal of Chemical Physics* **1990**, *92*, 5397–5403.
- (148) Silvi, B.; Savin, A., et al. *Nature* **1994**, *371*, 683–686.
- (149) Bader, R. F.; Stephens, M. E. *Journal of the American Chemical Society* **1975**, *97*, 7391–7399.
- (150) Bader, R., *Comparison of Loge and Virial Methods of Partitioning Molecular Charge Distributions*; Springer: 1975, pp 15–38.
- (151) Mitoraj, M.; Michalak, A. *Journal of Molecular Modeling* **2007**, *13*, 347–355.
- (152) Nalewajski, R. F.; Formosinho, S. J.; Varandas, A. J.; Mrozek, J. *International Journal of Quantum Chemistry* **1994**, *52*, 1153–1176.
- (153) Nalewajski, R. F.; Mrozek, J. *International Journal of Quantum Chemistry* **1994**, *51*, 187–200.

- (154) Nalewajski, R. F.; Mrozek, J.; Michalak, A. *International Journal of Quantum Chemistry* **1997**, *61*, 589–601.
- (155) Mrozek, J.; Nalewajski, R. F.; Michalak, A. *Polish Journal of Chemistry* **1998**, *72*, 1779–1791.
- (156) Resta, R.; Sorella, S. *Physical Review Letters* **1999**, *82*, 370.
- (157) Souza, I.; Wilkens, T.; Martin, R. M. *Physical Review B* **2000**, *62*, 1666.
- (158) Resta, R. *Physical Review letters* **2005**, *95*, 196805.
- (159) Resta, R. *The European Physical Journal B-Condensed Matter and Complex Systems* **2011**, *79*, 121–137.
- (160) Resta, R. The insulating state of matter., <http://www-dft.ts.infn.it/%7Eresta/gtse/lec10.pdf>.
- (161) Kenney, J.; Keeping, E. *Mathematics of Statistics, Princeton, NJ* **1951**.
- (162) Press, W.; Teukolsky, S.; Vetterling, W.; Flannery, B. *Numerical Recipes in C++: The Art of Scientific Computing* **2002**, 615–620.
- (163) Slater, J. C. *Physical Review* **1931**, *38*, 1109.
- (164) Slater, J. C. *Physical Review* **1931**, *37*, 481.
- (165) Pauling, L. *Journal of the American Chemical Society* **1931**, *53*, 3225–3237.
- (166) Lennard-Jones, J. E. *Transactions of the Faraday Society* **1929**, *25*, 668–686.
- (167) Hückel, E. *Zeitschrift für Physik* **1930**, *60*, 423–456.
- (168) Mulliken, R. S. *Chemical Reviews* **1931**, *9*, 347–388.
- (169) Slater, J. C. *Physical Review* **1931**, *37*, 481.
- (170) Hund, F. *Zeitschrift für Physik* **1932**, *73*, 1–30.
- (171) Bader, R. F. *Oxford University Press, Oxford Henkelman G, Arnaldsson A, Jónsson H (2006) A fast and robust algorithm for Bader decomposition of charge density. Comput Mater Sci* **1990**, *36*, 354–360.
- (172) Savin, A.; Nesper, R.; Wengert, S.; Fässler, T. F. *Angewandte Chemie International Edition in English* **1997**, *36*, 1808–1832.
- (173) Frenking, G.; Shaik, S., *The Chemical Bond: Chemical Bonding Across the Periodic Table*; John Wiley & Sons: 2014; Vol. 2.
- (174) Landis, C. R.; Weinhold, F. *The Chemical Bond: Fundamental Aspects of Chemical Bonding* **2014**, 91–120.
- (175) Cottrell, T. L., *The Strengths Of Chemical Bonds*, Second Edition; Butterworths scientific publications; Butterworths Scientific Publications: 1958.
- (176) Shaik, S.; Danovich, D.; Silvi, B.; Lauvergnat, D. L.; Hiberty, P. C. *Chemistry - A European Journal* **2005**, *11*, 6358–6371.
- (177) Creighton, T. E., *Proteins: Structures and Molecular Properties*; Macmillan: 1993.

- 
- (178) Strekowski, L.; Wilson, B. *Mutation Research/Fundamental and Molecular Mechanisms of Mutagenesis* **2007**, *623*, 3–13.
- (179) Maréchal, Y., *The Hydrogen Bond and the Water Molecule: The Physics and Chemistry of Water, Aqueous and Bio-media*; Elsevier: 2006.
- (180) Ajayan, P. M.; Tour, J. M. *Nature* **2007**, *447*, 1066–1068.
- (181) Priimagi, A.; Cavallo, G.; Metrangolo, P.; Resnati, G. *Accounts of chemical research* **2013**, *46*, 2686–2695.
- (182) Politzer, P.; Murray, J. S.; Concha, M. C. *Journal of Molecular Modeling* **2007**, *13*, 643–650.
- (183) Elstner, M.; Hobza, P.; Frauenheim, T.; Suhai, S.; Kaxiras, E. *The Journal of Chemical Physics* **2001**, *114*, 5149–5155.
- (184) Grimme, S.; Antony, J.; Ehrlich, S.; Krieg, H. *The Journal of Chemical Physics* **2010**, *132*, 154104.
- (185) Zhao, Y.; Schultz, N. E.; Truhlar, D. G. *Journal of Chemical Theory and Computation* **2006**, *2*, 364–382.
- (186) Zhao, Y.; Truhlar, D. G. *Theoretical Chemistry Accounts: Theory, Computation, and Modeling (Theoretica Chimica Acta)* **2008**, *120*, 215–241.
- (187) Espinosa, E.; Alkorta, I.; Elguero, J.; Molins, E. *The Journal of Chemical Physics* **2002**, *117*, 5529–5542.
- (188) Su, P.; Li, H. *The Journal of Chemical Physics* **2009**, *131*, 014102.
- (189) Fuster, F.; Silvi, B. *Theoretical Chemistry Accounts: Theory, Computation, and Modeling (Theoretica Chimica Acta)* **2000**, *104*, 13–21.
- (190) Kollman, P. A.; Allen, L. C. *Journal of the American Chemical Society* **1970**, *92*, 6101–6107.
- (191) Alkorta, I.; Eleguero, J.; Mó, O.; Yáñez, M.; Del Bene, J. E. *Molecular Physics* **2004**, *102*, 2563–2574.
- (192) Sanz, P.; Mó, O.; Yáñez, M.; Elguero, J. *The Journal of Physical Chemistry A* **2007**, *111*, 3585–3591.
- (193) Trujillo, C.; Sánchez-Sanz, G.; Alkorta, I.; Elguero, J.; Mó, O.; Yáñez, M. *Journal of Molecular Structure* **2013**, *1048*, 138–151.
- (194) Nekoei, A.-R.; Vatanparast, M. *New Journal of Chemistry* **2014**, *38*, 5886–5891.
- (195) Fonseca-Guerra, C.; Zijlstra, H.; Gàbor, P.; Bickelhaupt, F. M. *Chemistry - A European Journal* **2011**, *17*, 12612–12622.
- (196) Wolters, L. P.; Smits, N. W. G.; Guerra, C. F. *Physical Chemistry Chemical Physics* **2015**, *17*, 1585–1592.
- (197) Guillaumes, L.; Simon, S.; Fonseca-Guerra, C. *ChemistryOpen* **2015**, *4*, 318–327.
- (198) Beck, J. F.; Mo, Y. *Journal of Computational Chemistry* **2007**, *28*, 455–466.

- (199) Zarycz, M. N. C.; Provasi, P. F. *Magnetic Resonance in Chemistry* **2015**, *53*, 120–129.
- (200) Guevara-Vela, J. M.; Romero-Montalvo, E.; Costales, A.; Pendás, A. M.; Rocha-Rinza, T. *Physical Chemistry Chemical Physics* **2016**, *18*, 26383–26390.
- (201) Guthrie, F. *Journal of the Chemical Society* **1863**, *16*, 239–244.
- (202) Remsen, I; Norris, J. *American Chemical Journal* **1896**, *18*, 90–96.
- (203) Dumas, J.-M.; Peurichard, H; Gomel, M. *Journal of Chemical Research, Synopses* **1978**, 54–57.
- (204) Clark, T.; Hennemann, M.; Murray, J. S.; Politzer, P. *Journal of Molecular Modeling* **2007**, *13*, 291–296.
- (205) Politzer, P.; Lane, P.; Concha, M. C.; Ma, Y.; Murray, J. S. *Journal of Molecular Modeling* **2007**, *13*, 305–311.
- (206) Murray, J. S.; Lane, P.; Politzer, P. *Journal of Molecular Modeling* **2009**, *15*, 723–729.
- (207) Politzer, P.; Murray, J. S.; Clark, T. *Physical Chemistry Chemical Physics* **2013**, *15*, 11178–11189.
- (208) Kolar, M.; Hostas, J.; Hobza, P. *Physical Chemistry Chemical Physics* **2014**, *16*, 9987–9996.
- (209) Riley, K. E.; Murray, J. S.; Fanfrlík, J.; Řezáč, J.; Solá, R. J.; Concha, M. C.; Ramos, F. M.; Politzer, P. *Journal of Molecular Modeling* **2011**, *17*, 3309–3318.
- (210) Lu, Y.-X.; Zou, J.-W.; Yu, Q.-S.; Jiang, Y.-J.; Zhao, W.-N. *Chemical Physics Letters* **2007**, *449*, 6–10.
- (211) Metrangolo, P.; Murray, J. S.; Pilati, T.; Politzer, P.; Resnati, G.; Terraneo, G. *CrytEngComm* **2011**, *13*, 6593–6596.
- (212) Voth, A. R.; Hays, F. A.; Ho, P. S. *Proceedings of the National Academy of Sciences* **2007**, *104*, 6188–6193.
- (213) Beale, T. M.; Chudzinski, M. G.; Sarwar, M. G.; Taylor, M. S. *Chemical Society Reviews* **2013**, *42*, 1667–1680.
- (214) Kilah, N. L.; Wise, M. D.; Serpell, C. J.; Thompson, A. L.; White, N. G.; Christensen, K. E.; Beer, P. D. *Journal of the American Chemical Society* **2010**, *132*, 11893–11895.
- (215) Legon, A. C. *Physical Chemistry Chemical Physics* **2010**, *12*, 7736–7747.
- (216) Chudzinski, M. G.; McClary, C. A.; Taylor, M. S. *Journal of the American Chemical Society* **2011**, *133*, 10559–10567.
- (217) Priimagi, A.; Cavallo, G.; Metrangolo, P.; Resnati, G. *Accounts of Chemical Research* **2013**, *46*, 2686–2695.
- (218) Meazza, L.; Foster, J. A.; Fucke, K.; Metrangolo, P.; Resnati, G.; Steed, J. W. *Nature Chemistry* **2013**, *5*, 42–47.

- 
- (219) Maity, S. K.; Bera, S.; Paikar, A.; Pramanik, A.; Haldar, D. *Chemical Communications* **2013**, *49*, 9051–9053.
- (220) Murray, J. S.; Concha, M. C.; Lane, P.; Hobza, P.; Politzer, P. *Journal of Molecular Modeling* **2008**, *14*, 699–704.
- (221) Del Bene, J. E.; Alkorta, I.; Elguero, J. *The Journal of Physical Chemistry A* **2008**, *112*, 7925–7929.
- (222) Eskandari, K.; Zariny, H. *Chemical Physics Letters* **2010**, *492*, 9–13.
- (223) Eskandari, K.; Lesani, M. *Chemistry- A European Journal* **2015**, *21*, 4739–4746.
- (224) Alkorta, I.; Blanco, F.; Deyà, P. M.; Elguero, J.; Estarellas, C.; Frontera, A.; Quiñonero, D. *Theoretical Chemistry Accounts* **2010**, *126*, 1–14.
- (225) Zhao, Q.; Feng, D.; Hao, J. *Journal of Molecular Modeling* **2011**, *17*, 2817–2823.
- (226) Grabowski, S. J. *Theoretical Chemistry Accounts* **2013**, *132*, 1347.
- (227) Eskandari, K. *Journal of Molecular Modeling* **2012**, *18*, 3481–3487.
- (228) Zhong, A.; Chen, D.; Li, R. *Chemical Physics Letters* **2015**, *633*, 265–272.
- (229) Martín-Sómer, A.; Lamsabhi, A. M.; Mó, O.; Yáñez, M. *Computational and Theoretical Chemistry* **2012**, *998*, 74–79.
- (230) Eskandari, K. *Computational and Theoretical Chemistry* **2016**, *1090*, 74–79.
- (231) Albrecht, L.; Boyd, R. J.; Mó, O.; Yáñez, M. *The Journal of Physical Chemistry A* **2014**, *118*, 4205–4213.
- (232) Alkorta, I.; Elguero, J.; Mó, O.; Yáñez, M.; Del Bene, J. E. *Physical Chemistry Chemical Physics* **2015**, *17*, 2259–2267.
- (233) Mó, O.; Yáñez, M.; Alkorta, I.; Elguero, J. *Journal of Molecular Modeling* **2013**, *19*, 4139–4145.
- (234) Lamsabhi, A. M.; Vallejos, M. M.; Herrera, B.; Mó, O.; Yáñez, M. *Theoretical Chemistry Accounts* **2016**, *135*, 147.
- (235) Marín-Luna, M.; Alkorta, I.; Elguero, J. *Tetrahedron* **2016**, *72*, 1978–1983.
- (236) Montero-Campillo, M. M.; Yáñez, M.; Lamsabhi, A. M.; Mó, O. *Chemistry A European Journal* **2014**, *20*, 5309–5316.
- (237) Mykolayivna-Lemishko, K.; Montero-Campillo, M. M.; Mó, O.; Yáñez, M. *The Journal of Physical Chemistry A* **2014**, *118*, 5720–5726.
- (238) Herzberg, G. *Zeitschrift für Physik* **1929**, *57*, 601–630.
- (239) Herzberg, L. *Zeitschrift für Physik* **1933**, *84*, 571–592.
- (240) Bartlett Jr, J.; Furry, W. *Physical Review* **1931**, *38*, 1615.
- (241) Fraga, S.; Ransil, B. J. *The Journal of Chemical Physics* **1962**, *36*, 1127–1142.
- (242) Bender, C. F.; Davidson, E. R. *The Journal of Chemical Physics* **1967**, *47*, 4972–4978.

- (243) Dykstra, C. E.; Schaefer III, H. F.; Meyer, W. *The Journal of Chemical Physics* **1976**, *65*, 5141–5146.
- (244) Chiles, R. A.; Dykstra, C. E. *The Journal of Chemical Physics* **1981**, *74*, 4544–4556.
- (245) Pacchioni, G.; Koutecký, J. *Chemical Physics* **1982**, *71*, 181–198.
- (246) Harrison, R.; Handy, N. *Chemical Physics Letters* **1983**, *98*, 97–101.
- (247) Krapp, A.; Bickelhaupt, F. M.; Frenking, G. *Chemistry - A European Journal* **2006**, *12*, 9196–9216.
- (248) Monari, A.; Vetere, V.; Bendazzoli, G. L.; Evangelisti, S.; Paulus, B. *Chemical Physics Letters* **2008**, *465*, 102–105.
- (249) Kar, T; Nandi, P.; Sannigrahi, A. *Chemical physics letters* **1994**, *220*, 133–137.
- (250) Sannigrahi, A.; Kar, T *Journal of Molecular Structure: THEOCHEM* **2000**, *496*, 1–17.
- (251) Yuan, C.; Zhao, X.-F.; Wu, Y.-B.; Wang, X. *Angewandte Chemie* **2016**, n/a–n/a.
- (252) Zhao, X.-F.; Li, H.; Yuan, C.-X.; Li, Y.-Q.; Wu, Y.-B.; Wang, Z.-X. *Journal of Computational Chemistry* **2016**, *37*, 261–269.
- (253) Zhang, Q.; Li, W.-L.; Zhao, L.; Chen, M.; Zhou, M.; Li, J.; Frenking, G. *Chemistry - A European Journal* **2017**, n/a–n/a.
- (254) Brea, O.; Alkorta, I.; Corral, I.; Mó, O.; Yáñez; Elguero, J., *Intramolecular beryllium bonds. Further insights into resonance assistance phenomena*; Novoa, J., Ed.; Intermolecular interactions in crystals: Fundamentals of Crystal Engineering; The Royal Society of Chemistry: 2017.
- (255) Wang, N. X.; Wilson, A. K. *The Journal of Chemical Physics* **2004**, *121*, 7632–7646.
- (256) Wang, N. X.; Wilson, A. K. *Molecular Physics* **2005**, *103*, 345–358.
- (257) El-Azhary, A. A.; Suter, H. U. *The Journal of Physical Chemistry* **1996**, *100*, 15056–15063.
- (258) Halkier, A.; Klopper, W.; Helgaker, T.; Jørgensen, P.; Taylor, P. R. *The Journal of Chemical Physics* **1999**, *111*, 9157–9167.
- (259) Lozynski, M.; Rusinska-Roszak, D.; Mack, H.-G. *The Journal of Physical Chemistry A* **1998**, *102*, 2899–2903.
- (260) Lazarou, Y. G.; Prosmittis, A. V.; Papadimitriou, V. C.; Papagiannakopoulos, P. *The Journal of Physical Chemistry A* **2001**, *105*, 6729–6742.
- (261) Mó, O.; Yáñez, M.; Eckert-Maksić, M.; Maksić, Z. B.; Alkorta, I.; Elguero, J. *The Journal of Physical Chemistry A* **2005**, *109*, 4359–4365.
- (262) Izgorodina, E. I.; Coote, M. L.; Radom, L. *The Journal of Physical Chemistry A* **2005**, *109*, 7558–7566.
- (263) Jurecka, P.; Spöner, J.; Cerny, J.; Hobza, P. *Physical Chemistry Chemical Physics* **2006**, *8*, 1985–1993.

- 
- (264) Tsuzuki, S.; Honda, K.; Uchimaru, T.; Mikami, M. *The Journal of Chemical Physics* **2006**, *124*, 114304.
- (265) Frisch, M. J. et al. Gaussian09 Revision C.01., Gaussian Inc. Wallingford CT 2009.
- (266) Keith, T. A.; TK-Gristmill, S. AIMAll (Version 13.10.19)., Overland Park KS, USA, 2013.
- (267) Glendening, E. D.; Reed, A. E.; Carpenter, J. E.; Weinhold, F. NBO Version 3.1., Theoretical Chemistry Institute, University of Wisconsin, Madison, 1980.
- (268) Noury, S.; Krokidis, X.; Fuster, F.; Silvi, B. *Computers & Chemistry* **1999**, *23*, 597–604.
- (269) Matito, E.; Silvi, B.; Duran, M.; Solà, M. *The Journal of Chemical Physics* **2006**, *125*, 024301.
- (270) Feixas, F.; Matito, E.; Duran, M.; Solà, M.; Silvi, B. *Journal of Chemical Theory and Computation* **2010**, *6*, 2736–2742.
- (271) Lu, T.; Chen, F. *Journal of Computational Chemistry* **2012**, *33*, 580–592.
- (272) Plumley, J. A.; Evanseck, J. D. *The Journal of Physical Chemistry A* **2009**, *113*, 5985–5992.
- (273) Alkorta, I.; Elguero, J.; Del Bene, J. E.; Mó, O.; Yáñez, M. *Chemistry - A European Journal* **2010**, *16*, 11897–11905.
- (274) Alcamí, M.; Mó, O.; Yáñez, M. *Mass Spectrometry Reviews* **2001**, *20*, 195–245.
- (275) Morris, M.; Chan, B.; Radom, L. *The Journal of Physical Chemistry A* **2012**, *116*, 12381–12387.
- (276) Morris, M.; Chan, B.; Radom, L. *The Journal of Physical Chemistry A* **2014**, *118*, 2810–2819.
- (277) Allred, A. *Journal of Inorganic and Nuclear Chemistry* **1961**, *17*, 215–221.
- (278) Boyd, R. J.; Glover, J. N. M.; Pincock, J. A. *Journal of the American Chemical Society* **1989**, *111*, 5152–5155.
- (279) Henry, D. J.; Parkinson, C. J.; Mayer, P. M.; Radom, L. *The Journal of Physical Chemistry A* **2001**, *105*, 6750–6756.
- (280) Hoefelmeyer, J. D.; Gabbai, F. P. *Journal of the American Chemical Society* **2000**, *122*, 9054–9055.
- (281) Hübner, A.; Diehl, A. M.; Diefenbach, M.; Endeward, B.; Bolte, M.; Lerner, H.-W.; Holthausen, M. C.; Wagner, M. *Angewandte Chemie International Edition* **2014**, *53*, 4832–4835.
- (282) Kusevska, E.; Montero-Campillo, M. M.; Mó, O.; Yáñez, M. *Chemistry - A European Journal* **2016**, *22*, 13697–13704.
- (283) TURBOMOLE V7.02 2016, a development of University of Karlsruhe and Forschungszentrum Karlsruhe GmbH, 1989-2007, TURBOMOLE GmbH, since 2007; available from <http://www.turbomole.com>.



- (284) Te Velde, G.; Bickelhaupt, F. M.; Baerends, E. J.; Fonseca Guerra, C.; van Gisbergen, S. J. A.; Snijders, J. G.; Ziegler, T. *Journal of Computational Chemistry* **2001**, *22*, 931–967.
- (285) Fonseca Guerra, C.; Snijders, J. G.; te Velde, G.; Baerends, E. J. *Theoretical Chemistry Accounts* **1998**, *99*, 391–403.
- (286) Baerends, E. et al. ADF2013, SCM., Vrije Universiteit, Amsterdam, The Netherlands, 2013.
- (287) Alder, R. W.; Bowman, P. S.; Steele, W. R. S.; Winterman, D. R. *Chemical Communications (London)* **1968**, 723–724.
- (288) Llamas-Saiz, A.; Foces-Foces, C.; Elguero, J. *Journal of Molecular Structure* **1994**, *328*, 297–323.
- (289) Alkorta, I.; Elguero, J. *Structural Chemistry* **2000**, *11*, 335–340.
- (290) Platts, J. A.; Howard, S. T.; Wozniak, K. *The Journal of Organic Chemistry* **1994**, *59*, 4647–4651.
- (291) Howard, S. T. *Journal of the American Chemical Society* **2000**, *122*, 8238–8244.
- (292) Pozharskii, A. F.; Ozeryanskii, V. A., *Proton Sponges*; PATAI'S Chemistry of Functional Groups; John Wiley & Sons, Ltd: 2009.
- (293) Haartz, J. C.; McDaniel, D. H. *Journal of the American Chemical Society* **1973**, *95*, 8562–8565.
- (294) Veljković, M.; Nešković, O.; Zmbov, K. F.; Borshchevsky, A. Y.; Vaisberg, V. E.; Sidorov, L. N. *Rapid Communications in Mass Spectrometry* **1991**, *5*, 37–39.
- (295) Jenkins, H. D. B.; Krossing, I.; Passmore, J.; Raabe, I. *Journal of Fluorine Chemistry* **2004**, *125*, 1585–1592.
- (296) Melaïmi, M.; Solé, S.; Chiu, C.-W.; Wang, H.; Gabbai, F. P. *Inorganic Chemistry* **2006**, *45*, 8136–8143.
- (297) Li, S.; Dixon, D. A. *The Journal of Physical Chemistry A* **2006**, *110*, 6231–6244.
- (298) Dorsey, C. L.; Jewula, P.; Hudnall, T. W.; Hoefelmeyer, J. D.; Taylor, T. J.; Honesty, N. R.; Chiu, C.-W.; Schulte, M.; Gabbai, F. P. *Dalton Transactions* **2008**, 4442–4450.
- (299) Chen, Z.; Amine, K. *Journal of The Electrochemical Society* **2009**, *156*, A672–A676.
- (300) Hudnall, T. W.; Chiu, C.-W.; Gabbai, F. P. *Accounts of Chemical Research* **2009**, *42*, 388–397.
- (301) Besnainou, S.; Roux, M.; Daudel, R. *Comptes Rendus Hebdomadaires des Seances de l'Academie des Sciences* **1955**, *241*, 311–313.
- (302) Bader, R. F. W.; Nguyen-Dang, T. T.; Tal, Y. *Reports on Progress in Physics* **1981**, *44*, 893.
- (303) Larsen, F. K.; Hansen, N. K. *Acta Crystallographica Section B* **1984**, *40*, 169–179.
- (304) Sakata, M.; Sato, M. *Acta Crystallographica Section A* **1990**, *46*, 263–270.

- 
- (305) De Vries, R. Y.; Briels, W. J.; Feil, D. *Physical Review Letters* **1996**, *77*, 1719–1722.
- (306) Bersuker, G. I.; Peng, C.; Boggs, J. E. *The Journal of Physical Chemistry* **1993**, *97*, 9323–9329.
- (307) Pendás, A. M.; Blanco, M. A.; Costales, A.; Sánchez, P. M.; Luaña, V. *Physical Review Letters* **1999**, *83*, 1930–1933.
- (308) Platts, J. A.; Overgaard, J.; Jones, C.; Iversen, B. B.; Stasch, A. *The Journal of Physical Chemistry A* **2011**, *115*, 194–200.
- (309) Terrabuio, L. A.; Teodoro, T. Q.; Rachid, M. G.; Haiduke, R. L. A. *The Journal of Physical Chemistry A* **2013**, *117*, 10489–10496.
- (310) Terrabuio, L. A.; Teodoro, T. Q.; Matta, C. F.; Haiduke, R. L. A. *The Journal of Physical Chemistry A* **2016**, *120*, 1168–1174.
- (311) Dale, S. G.; Otero-de-la Roza, A.; Johnson, E. R. *Physical Chemistry Chemical Physics* **2014**, *16*, 14584–14593.
- (312) Postils, V.; Garcia-Borràs, M.; Solà, M.; Luis, J. M.; Matito, E. *Chemical Communications* **2015**, *51*, 4865–4868.
- (313) Taylor, A.; Matta, C. F.; Boyd, R. J. *Journal of chemical theory and computation* **2007**, *3*, 1054–1063.
- (314) Taylor, A.; Boyd, R. J. *Physical Chemistry Chemical Physics* **2008**, *10*, 6814–6819.
- (315) Timerghazin, Q. K.; Peslherbe, G. H. *The Journal of Chemical Physics* **2007**, *127*, 064108.
- (316) Iversen, B. B.; Larsen, F. K.; Souhassou, M.; Takata, M. *Acta Crystallographica Section B: Structural Science* **1995**, *51*, 580–591.
- (317) Bauschlicher, C. W.; Rosi, M. *Chemical Physics Letters* **1989**, *159*, 485–488.
- (318) NIST Computational Chemistry Comparison and Benchmark Database., Release 18, October 2016, Editor: Russell D. Johnson III.
- (319) Aidas, K et al. *Wiley Interdisciplinary Reviews: Computational Molecular Science* **2014**, *4*, 269–284.
- (320) Bendazzoli, G. L.; Evangelisti, S. NEPTUNUS, a Full CI Program Written by G. L. Bendazzoli and S. Evangelisti, with Contributions by A. Monari, L. Gagliardi.
- (321) Bendazzoli, G. L.; Evangelisti, S. *The Journal of Chemical Physics* **1993**, *98*, 3141–3150.
- (322) Bendazzoli, G. L.; Evangelisti, S. *International Journal of Quantum Chemistry* **1993**, *48*, 287–301.
- (323) Gagliardi, L.; Bendazzoli, G. L.; Evangelisti, S. *Journal of Computational Chemistry* **1997**, *18*, 1329–1343.
- (324) El Khatib, M.; Leininger, T.; Bendazzoli, G. L.; Evangelisti, S. *Chemical Physics Letters*, *591*, 58–63.

- (325) Huran, A. W.; Leininger, T.; Bendazzoli, G. L.; Evangelisti, S. *Chemical Physics Letters* **2016**, *664*, 120–126.
- (326) Widmark, P.-O.; Malmqvist, P.-Å.; Roos, B. O. *Theoretica Chimica Acta* **1990**, *77*, 291–306.
- (327) Jr., T. H. D. *The Journal of Chemical Physics* **1989**, *90*, 1007–1023.
- (328) Kol/os, W.; Wolniewicz, L. *The Journal of Chemical Physics* **1965**, *43*, 2429–2441.
- (329) Velasco, R.; Ottinger, C.; Zare, R. N. *The Journal of Chemical Physics* **1969**, *51*, 5522–5532.
- (330) Christian, R. H.; Duff, R. E.; Yarger, F. L. *The Journal of Chemical Physics* **1955**, *23*, 2045–2049.
- (331) DeCorpo, J. J.; Steiger, R. P.; Franklin, J. L.; Margrave, J. L. *The Journal of Chemical Physics* **1970**, *53*, 936–938.
- (332) Brewer, L.; Brackett, E. *Chemical Reviews* **1961**, *61*, 425–432.
- (333) Ogilvie, J.; Wang, F. Y. *Journal of Molecular Structure* **1992**, *273*, 277–290.
- (334) Gebhard, F., *The Mott Metal-Insulator Transition*; Springer Tracts in Modern Physics, Vol. 137; Springer Berlin Heidelberg: Berlin, Heidelberg, 2000.
- (335) Malrieu, J.-P.; Angeli, C.; Cimiraglia, R. *Journal of Chemical Education* **2008**, *85*, 150.
- (336) Fukui, K. *Accounts of Chemical Research* **1981**, *14*, 363–368.

Part VII

APPENDIX



## APPENDIX

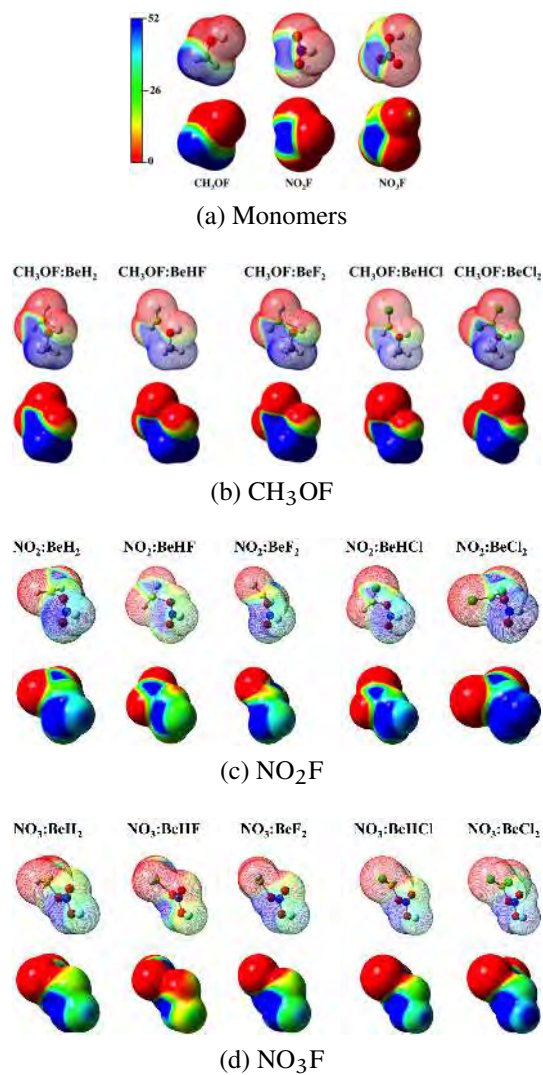


Figure A.1: Molecular electrostatic potentials of  $\text{BeY}'_1\text{Y}'_2: \text{Y}'\text{F}$ , with  $\text{Y}'_1 = \text{H, F and Cl}$ ;  $\text{Y}'_2 = \text{H, F and Cl}$ ;  $\text{Y}' = \text{CH}_3\text{O, NO}_2 \text{ and NO}_3$ . (a) Isolated monomers  $\text{Y}'$ . (b) Complexes with  $\text{Y}' = \text{CH}_3\text{O}$ . (c) Complexes with  $\text{Y}' = \text{NO}_2$ . (d) Complexes with  $\text{Y}' = \text{NO}_3$ . The values of the potentials are in  $\text{kJ}\cdot\text{mol}^{-1}$ .

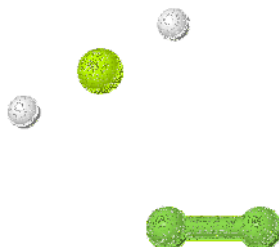


Figure A.2: Animation of the dissociation profile of the  $\text{BeH}_2:\text{FF}$  complexes calculated at CASPT2//CASSCF(14,9)/cc-pVTZ level of theory. **Please use the Adobe Acrobat Reader program for a correct visualization of the animation.**

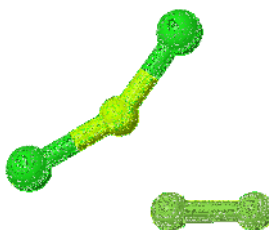


Figure A.3: Animation of the dissociation profile of the  $\text{BeCl}_2:\text{FF}$  complexes calculated at CASPT2//CASSCF(14,9)/cc-pVTZ level of theory. **Please use the Adobe Acrobat Reader program for a correct visualization of the animation.**

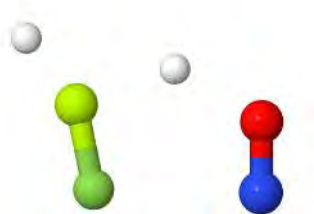


Figure A.4: Animation of the dissociation profile of the  $\text{BeH}_2:\text{FNO}$  complexes calculated at CASPT2//CASSCF(12,9)/cc-pVTZ level of theory. Please use the Adobe Acrobat Reader program for a correct visualization of the animation.

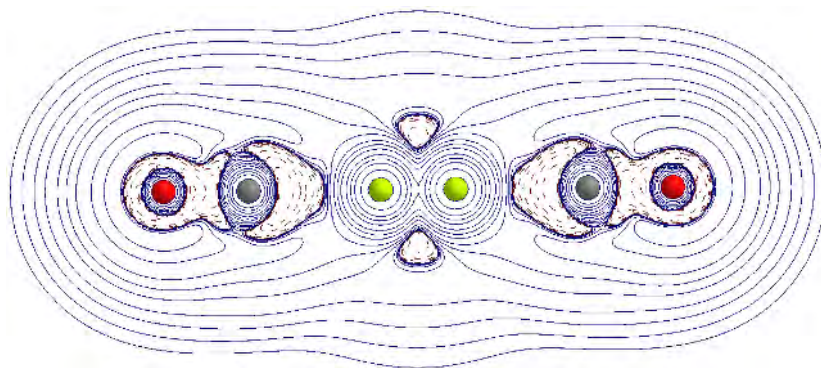


Figure A.5: Animation of the variation of  $\nabla^2\rho$  in the unrelaxed scan of the Be-Be bond distance of the  $\text{CO}:\text{Be-Be}:\text{CO}$  complex at CASPT2//CASSCF(12,12)/cc-pVTZ level of theory. Red and blue areas correspond to negative and positive values of  $\nabla^2$  respectively. The pink dot represents the pseudo-nuclei. Please use the Adobe Acrobat Reader program for a correct visualization of the animation.





# B

## APPENDIX

---

The results of this thesis are published in the following papers



## B.1 ARTICLE I

*Creating  $\sigma$ -Holes through the Formation of Beryllium Bonds*

Published in: Chemistry - A European Journal, **2015**, 21,12676-12682.



## Molecular Modeling

Creating  $\sigma$ -Holes through the Formation of Beryllium BondsOriana Brea,<sup>[a]</sup> Otilia M3, <sup>[a]</sup> Manuel Y3ñez, \*<sup>[a]</sup> Ibon Alkorta, \*<sup>[b]</sup> and Jos3 Elguero<sup>[b]</sup>

**Abstract:** Through the use of ab initio theoretical models based on MP2/aug-cc-pVDZ-optimized geometries and CCSD(T)/aug-cc-pVTZ and CCSD(T)/aug-c-pVDZ total energies, it has been shown that the significant electron density rearrangements that follow the formation of a beryllium bond may lead to the appearance of a  $\sigma$ -hole in systems that previously do not exhibit this feature, such as CH<sub>3</sub>OF, NO<sub>2</sub>F, NO<sub>3</sub>F, and other fluorine-containing systems. The creation of the  $\sigma$ -hole is another manifestation of the bond activation–reinforcement (BAR) rule. The appearance of a  $\sigma$ -hole on the F atoms of CH<sub>3</sub>OF is due to the enhancement of the electronegativity of the O atom that participates in the beryllium bond. This atom recovers part of the charge trans-

ferred to Be by polarizing the valence density of the F into the bonding region. An analysis of the electron density shows that indeed this bond becomes reinforced, but the F atom becomes more electron deficient with the appearance of the  $\sigma$ -hole. Importantly, similar effects are also observed even when the atom participating in the beryllium bond is not directly attached to the F atom, as in NO<sub>2</sub>F, NO<sub>3</sub>F, or NCF. Hence, whereas the isolated CH<sub>3</sub>OF, NO<sub>2</sub>F, and NO<sub>3</sub>F are unable to yield F...Base halogen bonds, their complexes with BeX<sub>2</sub> derivatives are able to yield such bonds. Significant cooperative effects between the new halogen bond and the beryllium bond reinforce the strength of both noncovalent interactions.

## Introduction

Noncovalent interactions<sup>[1]</sup> play a fundamental role in our world because they are responsible for the formation of both natural molecular assemblies, such as DNA and artificial molecular aggregates, as the so-called metal–organic frameworks (MOFs),<sup>[2]</sup> or “soft matter”, a term usually employed to describe materials that are held together by noncovalent interactions involving energies of the order of the thermal energy,  $kT$ .<sup>[3]</sup> These noncovalent interactions usually involve closed-shell systems and in most cases are dominated by electrostatic interactions. Nevertheless, in practically all situations, perhaps with the only exception of van der Waals complexes, there is also a significant polarization of the electron densities of the moieties that interact, one of which behaves as a Lewis base and the other as a Lewis acid. Such polarizations can cover a rather wide range of interaction energies, from very weak linkages as those observed in some hydrogen,<sup>[4]</sup> dihydrogen,<sup>[5]</sup> pnictogen,<sup>[6]</sup> chalcogen,<sup>[7]</sup> halogen,<sup>[8]</sup> or tetrel<sup>[9]</sup> bonds, to rather strong ones

as those observed in dative bonds between Lewis bases and borane or its derivatives, or between Lewis bases and BeX<sub>2</sub> derivatives. Although, as reported recently by P. Politzer et al.,<sup>[10]</sup> fundamental concepts as molecular orbitals are mathematical entities that should not be taken as physical realities, the aforementioned polarization of the lone pairs of the Lewis base towards the Lewis acid is generally described in the framework of the molecular orbital theory as a charge-transfer process. For instance, a A–H...Y hydrogen bond (HB) involves the lone pairs of the proton acceptor, Y, and the  $\sigma_{AH}^*$  antibonding orbital of the proton donor, whereas in X<sub>2</sub>Be...Y, the beryllium bonds<sup>[11]</sup> imply a charge transfer from the lone pairs of Y into both the empty p orbitals of Be and the  $\sigma_{BeX}^*$  antibonding orbital of the BeX<sub>2</sub> molecule.

One of the most important consequences of the polarization effects associated with noncovalent interactions is the appearance of cooperative effects<sup>[4b,12]</sup> or synergetic stabilities,<sup>[13]</sup> when more than one of these noncovalent interactions coincide within the same molecular aggregate. Cooperativity is particularly significant when one of the interactions stabilizing the molecular aggregate is a beryllium bond.<sup>[14]</sup> This synergetic stability is actually the direct consequence of the changes induced on the intrinsic reactivity of the interacting sub-units, associated with the inevitable modification of their electron donor or electron acceptor capacity. Indeed, the system acting as a Lewis base should undergo an increase in its intrinsic acidity, whereas the basicity of the Lewis acid should also increase. Depending of the strength of the interaction, it has been shown that it is possible to change a typical base, such as aniline, for instance, in a very strong Bronsted acid.<sup>[15]</sup> These acidity enhancements open the possibility of having spontaneous

[a] O. Brea, Prof. O. M3, Prof. M. Y3ñez  
Departamento de Qu3mica  
M3dulo 13, Universidad Aut3noma de Madrid  
Campus de Excelencia UAM-CSIC  
Cantoblanco, 28049 Madrid (Spain)  
Fax: (+34)91-497-5238  
E-mail: manuel.yanez@uam.es

[b] Prof. I. Alkorta, Prof. J. Elguero  
Instituto de Qu3mica M3dica (IQM-CSIC)  
Juan de la Cierva, 3, 28006 Madrid (Spain)  
E-mail: ibon@iqm.csic.es

Supporting information for this article is available on the WWW under <http://dx.doi.org/10.1002/chem.201500981>.

proton transfers between the Lewis base, changed into a Bronsted acid, and a Lewis acid, with an enhanced basicity, thus forming spontaneously an ion pair in the gas phase.<sup>[16]</sup> When both active sites are located on the same molecular system, yielding a ditopic compound, the formation of polymeric structures is also feasible.<sup>[17]</sup>

As mentioned above, many of the noncovalent interactions known are rather weak, and their formation is closely related with the existence of what have been called an “ $\sigma$ -hole”, an “electron-deficient outer lobe of a half-filled p (or nearly p) orbital involved in forming a covalent bond”,<sup>[18]</sup> which leads to a region of positive electrostatic potential. The existence of this  $\sigma$ -hole is one of the signatures of halogen bonds<sup>[19]</sup> but is also found in other noncovalent interactions,<sup>[6c, 8c, 17, 20]</sup> and helps to explain the directionality of hydrogen bonds, cooperative effects in hydrogen bonding, and the occurrence of blue-shifting.<sup>[21]</sup> However, the formation of a  $\sigma$ -hole on a halogen atom, for instance, requires a substantial shift of electron density from the p orbital of the halogen triggered by the group attached to it. Hence, fluorine very often does not form halogen bonds, although some reports suggest that it has the capability of doing so if attached to sufficiently electron-withdrawing substituents.<sup>[22]</sup> Nevertheless, when the group attached to fluorine is not very electron withdrawing, such as in methyl hypofluorite ( $\text{CH}_3\text{OF}$ ), the  $\sigma$ -hole does not appear and no stable complexes can be found between this compound and typical Lewis bases, such as ammonia.

The aim of this study is to investigate whether the formation of a beryllium bond between these kinds of fluorine derivatives may lead to the formation of a  $\sigma$ -hole at the F atom and therefore to the possibility of forming  $\text{F}\cdots\text{Base}$  halogen bonds, which is impossible for the isolated compound. A similar question would be, can FCl form  $\text{F}\cdots\text{Base}$  halogen bonds? FCl is a paradigmatic example of a compound capable of yielding quite stable  $\text{Cl}\cdots\text{Base}$  halogen bonds, because F acts as a strong electron-withdrawing system able to create a deep  $\sigma$ -hole on the Cl atom, but obviously no  $\sigma$ -hole can be found at the F atom. Can we reverse the situation profiting the fact that FCl can also behave as a Cl Lewis base towards the  $\text{BeX}_2$  Lewis acid?

## Computational details

The geometries of the isolated molecules and the different complexes were optimized at the  $\text{MP2}^{[23]}/\text{aug-cc-pVDZ}^{[24]}$  level of theory. The same theoretical Scheme was employed to obtain the corresponding harmonic vibrational frequencies and to evaluate the thermal corrections. To assess the reliability of this theoretical model, the optimized geometries of a reduced set of complexes were refined at the  $\text{MP2}/\text{aug-cc-pVTZ}$  level but the changes observed were never significant.

The interaction energies,  $E_{\text{int}}$ , defined as the difference between the energy of the complex and the energy of the monomers with the geometry they have within the complex were calculated at the  $\text{CCSD(T)}/\text{aug-cc-pVDZ}/\text{MP2}/\text{aug-cc-pVDZ}$  level of theory. The accuracy of this model was assessed, using

some suitable examples, by comparing these results with those obtained at the  $\text{CCSD(T)}/\text{aug-cc-pVTZ}$  level.

The electron density,  $\rho(\mathbf{r})$ , for the sake of an easy inclusion of electron correlation effects, was obtained by means of  $\text{B3LYP}/\text{aug-cc-pVDZ}$  single-point calculations. These electron densities were then used to analyze the bonding characteristics of the formed complexes by using the quantum theory of atoms in molecules (QTAIM)<sup>[25]</sup> and the natural bond orbital (NBO) approach.<sup>[26]</sup> In the framework of the QTAIM approach we have obtained the molecular graphs of the complexes under investigation. The molecular graph is the ensemble of the critical points of  $\rho(\mathbf{r})$ , namely, maxima, which are associated with the position of the nuclei, the first and second order saddle points, which are associated with bond and ring critical points (BCP and RCP, respectively), and the bond paths, which are the lines of maximum density that connect two maxima through the bond critical point. An alternative perspective within the framework of the QTAIM approach is based on the use of atomic energy components.<sup>[27]</sup> QTAIM defines atomic basins as regions bounded by zero flux surfaces, and the integration over these basins yields very accurate atomic information. In particular, it has been shown that the variation of atomic energies provides reliable information on the stabilization and destabilization of the interacting subunits in weakly bound molecular aggregates,<sup>[27b,c]</sup> and can also reflect cooperative effects.<sup>[14b,d]</sup> The atomic energy changes for the clusters are calculated with respect to the energy of each atom as it exists in the monomers that form the cluster. The QTAIM calculations were carried out using the AIMAll program package.<sup>[28]</sup>

The NBO method describes the molecular bonding in terms of localized hybrids obtained as local block eigenvectors of the one-particle density matrix. This partition permits the identification of charge-transfer mechanisms by means of a second order perturbation analysis between the occupied orbitals of the base and the empty orbitals of the acid,<sup>[26b]</sup> as implemented in the Gaussian 09 suite of programs<sup>[29]</sup> (NBO-3.0 version). This suite of programs was also used to calculate (at the  $\text{B3LYP}/\text{aug-cc-pVDZ}$  level of theory) the molecular electrostatic potentials (MEPs), which were represented on the electron density isosurface of 0.001 au that roughly correspond to the van der Waals surface. The maxima and minima of the MEP on the surface were calculated using the Multiwfn program.<sup>[30]</sup>

## Results and discussion

### Formation of a $\sigma$ -hole

In the first part of our study, we used methyl hypofluorite ( $\text{CH}_3\text{OF}$ ) as a paradigmatic example of halogen derivative in which no  $\sigma$ -hole is detected on the halogen center. Indeed, any attempt to find stable complexes between  $\text{CH}_3\text{OF}$  and typical conventional bases, such as ammonia or  $\text{NCH}$ , fail because the complex evolves spontaneously towards the two separated subunits. The absence of  $\sigma$ -hole is evident when looking at the corresponding molecular electrostatic potential, which is found to be negative all around the halogen atom (see Figure 1a). However, this situation changes significantly when  $\text{CH}_3\text{OF}$

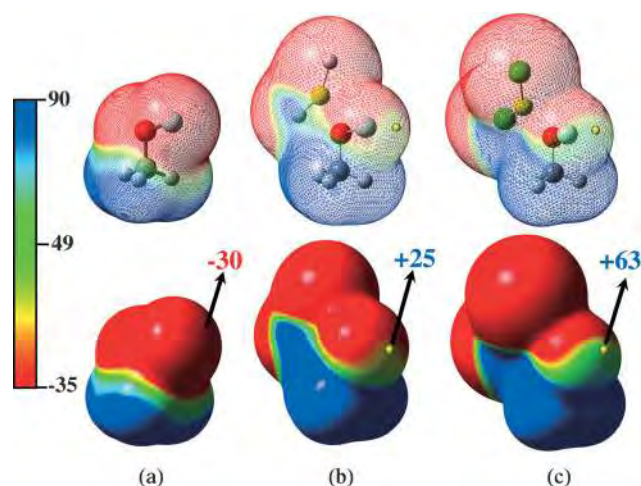


**Figure 1.** Molecular electrostatic potentials of a) isolated  $\text{CH}_3\text{OF}$ , b)  $\text{BeH}_2:\text{CH}_3\text{OF}$  adduct, and c)  $\text{BeCl}_2:\text{CH}_3\text{OF}$  adduct. The yellow dots indicate the location of the maximum value of the potential associated to the  $\sigma$ -hole. The values of the potentials are in  $\text{kJ mol}^{-1}$ .

forms a beryllium bond with  $\text{BeH}_2$ . As illustrated in Figure 1 b), the potential changes along the axis defined by the O–F bond, and it becomes slightly positive, indicating that a  $\sigma$ -hole has been formed. These changes are more apparent when using a stronger Lewis acid as  $\text{BeCl}_2$ , in which case the  $\sigma$ -hole becomes almost three times deeper (see Figure 1 c).

The formation of the  $\sigma$ -hole on the fluorine atom of the  $\text{BeH}_2:\text{CH}_3\text{OF}$  and  $\text{BeCl}_2:\text{CH}_3\text{OF}$  complexes can be understood by comparing the electron density distribution of the isolated  $\text{CH}_3\text{OF}$  molecule and the  $\text{CH}_3\text{OF}$  molecule within the complexes. The formation of the beryllium bond implies a significant polarization of the oxygen lone pair towards the Be atom. These polarization effects result in a concomitant enhancement of the electronegativity of the oxygen atom, which tries to recover part of the density polarized towards the Be atom from the bonds (O–F and O–C), in which it participates. Indeed, an inspection of the molecular graphs of the  $\text{BeH}_2:\text{CH}_3\text{OF}$  and  $\text{BeCl}_2:\text{CH}_3\text{OF}$  complexes (see Figure 2) shows that in both complexes the electron density at the O–C BCP decreases and the corresponding bond lengthens (0.01 and 0.02 Å, respectively), whereas the electron density at the O–F BCP increases and the bond shortens (0.025 and 0.03 Å, respectively). These findings are in perfect agreement with the

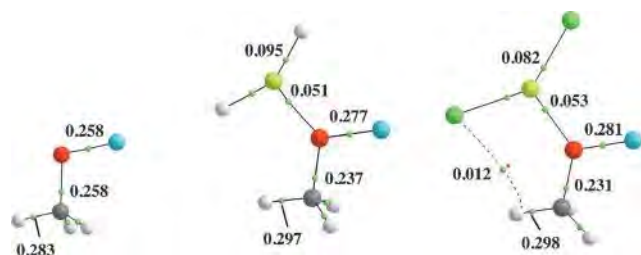


**Figure 2.** Molecular graphs of  $\text{CH}_3\text{OF}$  and its complexes with  $\text{BeH}_2$  and  $\text{BeCl}_2$ . Green and red dots correspond to BCPs and RCPs, respectively. Electron densities are in au.

predictions of the bond activation–reinforcement (BAR) rule,<sup>[31]</sup> which establishes that when the basic site (O) is more electronegative than the atom attached to it (C), the former is able to recover part of the charge by depopulating the O–C bond. Conversely, when the basic site (O) is less electronegative than the atom bonded to it (F), the O polarizes the valence density of the F into the bonding region. In this latter case, the bond becomes reinforced, but the F atom becomes more electron deficient, leading to the appearance of a  $\sigma$ -hole. Consistent with the fact that upon  $\text{BeX}_2$  attachment the F atom becomes more electron deficient, its atomic energy decreases significantly in absolute value (see Table S1 of the Supporting Information).

### Formation of F...N halogen bonds

In principle then, one should expect the  $\text{BeH}_2:\text{CH}_3\text{OF}$  and  $\text{BeCl}_2:\text{CH}_3\text{OF}$  complexes to be able to form halogen bonds when interacting with a conventional Lewis base. The optimized structures and the corresponding molecular graphs of

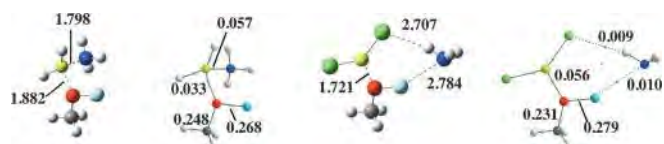


**Figure 3.** Optimized geometry and molecular graph for complexes  $\text{BeH}_2:\text{CH}_3\text{OF}:\text{NH}_3$  and  $\text{BeCl}_2:\text{CH}_3\text{OF}:\text{NH}_3$ . Bond lengths are in Å. In the molecular graphs, the green and red dots denote BCPs and RCPs, respectively. Electron densities are in au.

the complexes formed with  $\text{NH}_3$  are presented in Figure 3. It is apparent that no halogen bond appears when  $\text{BeH}_2:\text{CH}_3\text{OF}$  interacts with ammonia, with a F...N internuclear distance slightly longer than 3 Å. Conversely, the rather short Be...N distance (1.798 Å) indicates the formation of a beryllium bond between the  $\text{BeH}_2$  moiety and the Lewis base, confirming the ability of Be to be tetracoordinated.<sup>[32]</sup> This is indeed reflected in the molecular graph, which shows the existence of two beryllium bonds, Be...O and Be...N, the charge density at the BCP being significantly larger in the latter. This seems to indicate that, in the competition between the two acidic sites,  $\text{NH}_3$  prefers to bind to Be, since the  $\sigma$ -hole created at the F atom is rather shallow.

This picture is consistent with the one obtained by means of the NBO approach, which shows that the interaction of Be with  $\text{CH}_3\text{OF}$  and  $\text{NH}_3$  is so strong that two very polar Be–O (94% O, 6% Be) and Be–N (90% N, 10% Be) bonds are formed, whereas no interaction between the F and the N atoms is detected. The situation is however reversed in complex  $\text{BeCl}_2:\text{CH}_3\text{OF}:\text{NH}_3$ , in which the  $\sigma$ -hole on the F atom is much deeper and a clear F... $\text{NH}_3$  halogen bond is formed. This is confirmed by the appearance of a BCP between F and N, and by the more negative value of the atomic energy component of the F atom, since in the halogen bond it behaves as an electron acceptor (see Table S1 of the Supporting Information). It is worth noting, however, that the Lewis base does not lie in



the direction of the O–F bond, because a secondary interaction, a hydrogen bond between one of the hydrogens of ammonia and one of the Cl atoms of the  $\text{BeCl}_2$  moiety, also contributes to stabilizing the complex. The existence of this second noncovalent interaction is reflected by the appearance of a RCP (See Figure 3).

The situation is different when the Lewis base is HCN, because in this case the formation of a dihydrogen bond between one of the hydrogens of  $\text{BeH}_2$  and the hydrogen of the HCN moiety, or of a beryllium bond between  $\text{BeCl}_2$  and the N atom of the NCH monomer dominate (see Figure S1 of the Supporting Information). Hence, in spite of the existence of a  $\sigma$ -hole on the F atom of the  $\text{BeX}_2\cdot\text{MeOF}$  ( $X = \text{H}, \text{Cl}$ ) binary complexes, the  $\text{F}\cdots\text{N}$  halogen bond is not formed.

### Complexes involving FCl, $\text{NO}_2\text{F}$ , $\text{NO}_3\text{F}$ , and NCF

The FCl molecule is a paradigmatic example of systems able to yield halogen bonds through the  $\sigma$ -hole associated with its Cl atom. However, no examples of complexes with  $\text{ClF}\cdots\text{Base}$  halogen bonds are known because no  $\sigma$ -hole exists on the F atom (see Figure 4a). Nevertheless, FCl yield stable complexes

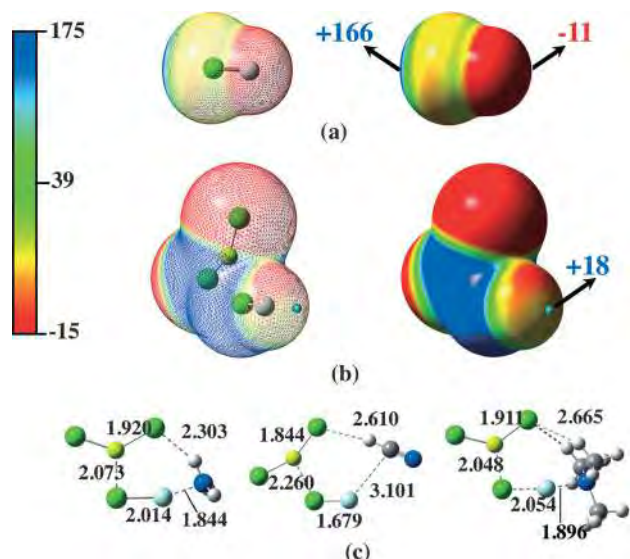


**Figure 4.** Molecular electrostatic potentials of a) isolated FCl and b)  $\text{BeCl}_2\cdot\text{ClF}$  adduct. The values of the potentials are in  $\text{kJ mol}^{-1}$ . The blue dots indicate the location of the maximum value of the potential associated to the  $\sigma$ -hole. c) Optimized geometries of the complexes  $\text{BeCl}_2\cdot\text{N-base}$  (N-base =  $\text{NH}_3$ , NCH,  $\text{N}(\text{CH}_3)_3$ ). Bond lengths are in Å.

with  $\text{BeCl}_2$ , in which the Cl atom behaves as the basic site and, as found above for  $\text{CH}_3\text{OF}$ , a  $\sigma$ -hole appears at the F atom (see Figure 4b), whereas its atomic energy becomes less negative (see Table S1 of the Supporting Information). Hence, not surprisingly the binary  $\text{BeCl}_2\cdot\text{ClF}$  complex forms ternary complexes with ammonia that are stabilized through  $\text{F}\cdots\text{NH}_3$  halogen bonds. As it was found above for the complexes involving  $\text{CH}_3\text{OF}$ , the  $\text{Cl-F}\cdots\text{N}$  arrangement is not linear because of the  $\text{N-H}\cdots\text{Cl}$  hydrogen bond formed between ammonia and  $\text{BeCl}_2$

(see Figure 4c). Similar stable complexes are formed when the Lewis base is NCH or trimethylamine. In addition, in these two cases, hydrogen bonds between the nitrogen Lewis base and the  $\text{BeCl}_2$  molecule contribute to stabilizing the complex.

As previously reported,  $\text{NO}_2\text{F}$  is another system unable to yield halogen bonds.<sup>[20a]</sup> We have verified that the same situation appears for  $\text{NO}_3\text{F}$ . Though in this compound the F atom is attached to an oxygen atom, whereas in  $\text{NO}_2\text{F}$  it is attached to the N atom; any attempt to find a complex between  $\text{NO}_3\text{F}$  and  $\text{NH}_3$  stabilized through a  $\text{F}\cdots\text{N}$  halogen bond failed because the complex spontaneously dissociated into the two neutral monomers. Once more, however, the adducts of both compounds with  $\text{BeCl}_2$  do present a  $\sigma$ -hole and yield stable aggregates with  $\text{NH}_3$ , as shown in Figure 5. It is important to empha-

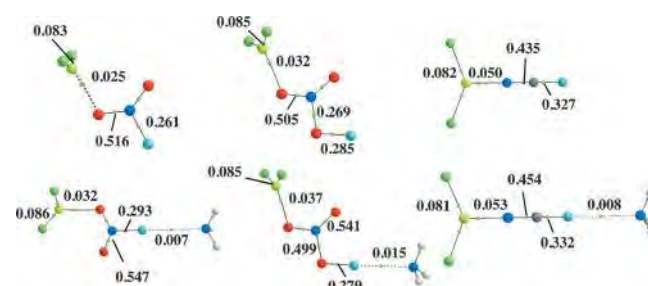


**Figure 5.** Molecular graphs of the binary complexes between  $\text{BeCl}_2$  and  $\text{NO}_2\text{F}$ ,  $\text{NO}_3\text{F}$  and NCF, and the ternary complexes formed when these binary complexes interact with ammonia through a  $\text{F}\cdots\text{N}$  halogen bond. Green dots correspond to BCPs. Electron densities are in au.

size that although in all these cases the beryllium bond involves an atom that is not directly bound to the F center, the polarization effects (described above) are transmitted through the chain of bonds and the F atom becomes again electron deficient, as nicely illustrated by the decrease in its atomic energy (see Table S1 of the Supporting Information). Even though this decrease is smaller than the one observed for  $\text{CH}_3\text{OF}$ , it is significant enough to create the  $\sigma$ -hole.

It is worth noting that in all cases there is a clear cooperativity between the new halogen bond formed and the beryllium bond, whose strength in the ternary complexes increases with respect to the binary ones. This is clearly reflected by the increment of the electron density at the corresponding BCP (see Figure 5), as well as in the shortening (0.105 Å) of the  $\text{Be}\cdots\text{O}$  internuclear distance from  $\text{BeCl}_2\cdot\text{NO}_2\text{F}$  to  $\text{BeCl}_2\cdot\text{NO}_2\text{F}\cdot\text{NH}_3$  and from  $\text{BeCl}_2\cdot\text{NO}_3\text{F}$  to  $\text{BeCl}_2\cdot\text{NO}_3\text{F}\cdot\text{NH}_3$  (0.044 Å). Consistently, the interaction energies associated with beryllium bonds are systematically larger in the triads than those in the binary complexes (See Table 1).

Note that for  $\text{BeCl}_2\cdot\text{X}\cdot\text{N-base}$  ( $X = \text{ClF}, \text{MeOF}$ , N-base =  $\text{NH}_3$ , NCH) the value of the  $E_{\text{int}}$ (halogen bond) does not measure only the strength of the halogen bond formed in the corresponding triads, because, as discussed above, these complexes are also stabilized by concomitant hydrogen bonds. Conversely, for those triads in which  $X = \text{NO}_2\text{F}, \text{NO}_3\text{F}$ , or NCF, the  $E_{\text{int}}$ (halogen bond) is indeed a direct measure of the strength of the halogen bond formed in the triad. Note also the good

**Table 1.** CCSD(T)/aug-cc-pVDZ calculated interaction energies ( $E_{int}$ ,  $\text{kJ mol}^{-1}$ ) associated with the beryllium bonds ( $E_{int}(\text{BeCl}_2 \cdots \text{X})$ ) in binary and ternary complexes. The interaction energies associated with halogen bonds ( $E_{int}(\text{BeCl}_2 \cdots \text{X} \cdots \text{N-base})$ ) can only be reported for ternary complexes, since the binary  $\text{X} \cdots \text{N-base}$  complexes do not exist.

Complex	Beryllium bond $E_{int}(\text{BeCl}_2 \cdots \text{X})$	Halogen bond $E_{int}(\text{BeCl}_2 \cdots \text{X} \cdots \text{N-base})$
binary complexes		
$\text{BeCl}_2 \cdots \text{ClF}$	-23.2 [-30.5] <sup>[a]</sup>	-
$\text{BeCl}_2 \cdots \text{MeOF}$	-93.1 [-98.6] <sup>[a]</sup>	-
$\text{BeCl}_2 \cdots \text{NO}_2\text{F}$	-31.8	-
$\text{BeCl}_2 \cdots \text{NO}_3\text{F}$	-48.3	-
$\text{BeCl}_2 \cdots \text{NCF}$	-102.0	-
ternary complexes		
$\text{BeCl}_2 \cdots \text{ClF} \cdots \text{NH}_3$	-157.0 [-162.1] <sup>[a]</sup>	-117.3 [-116.7] <sup>[a]</sup>
$\text{BeCl}_2 \cdots \text{ClF} \cdots \text{NCH}$	-36.5 [-40.7] <sup>[a]</sup>	-14.4 [-13.4] <sup>[a]</sup>
$\text{BeCl}_2 \cdots \text{MeOF} \cdots \text{NH}_3$	-112.7	-17.2
$\text{BeCl}_2 \cdots \text{NO}_2\text{F} \cdots \text{NH}_3$	-49.5 [-50.2] <sup>[a]</sup>	-8.1 [-9.2] <sup>[a]</sup>
$\text{BeCl}_2 \cdots \text{NO}_2\text{F} \cdots \text{NCH}$	-48.4	-9.1
$\text{BeCl}_2 \cdots \text{NO}_3\text{F} \cdots \text{NH}_3$	-62.0	-14.6
$\text{BeCl}_2 \cdots \text{NO}_3\text{F} \cdots \text{NCH}$	-59.2	-11.5
$\text{BeCl}_2 \cdots \text{NCF} \cdots \text{NH}_3$	-113.6	-14.7
$\text{BeCl}_2 \cdots \text{NCF} \cdots \text{NCH}$	-113.7	-15.0

[a] Values calculated at the CCSD(T)/aug-cc-pVTZ level of theory.

agreement between the calculated values when the two different basis sets are used, which indicates that the CCSD(T)/aug-cc-pVDZ model can be considered reasonably reliable for the study of these interactions.

The aforementioned cooperativity also explains the changes observed in both the beryllium and the halogen bonds when the  $\text{BeCl}_2 \cdots \text{NCF} \cdots \text{NH}_3$  complex is formed. In this particular case, the isolated NCF molecule has a very shallow  $\sigma$ -hole and yields a weakly bound  $\text{NCF} \cdots \text{NH}_3$  complex with a  $\text{F} \cdots \text{N}$  internuclear distance of 3.141 Å. Upon association with  $\text{BeCl}_2$ , not only the beryllium bond but also the halogen bond become reinforced; the halogen bond shrinks by 0.199 Å, whereas the electron density at the BCP increases from 0.005 to 0.008 au (see Figure S2 of the Supporting Information). Also consistently, the  $E_{int}$ (halogen bond) for the  $\text{NCF} \cdots \text{NH}_3$  complex is estimated to be  $8.6 \text{ kJ mol}^{-1}$  smaller than that of the  $\text{BeCl}_2 \cdots \text{NCF} \cdots \text{NH}_3$  reported in Table 1.

### Substituent effects

In this section we analyze the evolution of the  $\sigma$ -hole when the H atoms of the  $\text{CH}_3\text{OF}$  compound are replaced successively by F atoms in both the  $\text{CH}_{3-n}\text{F}_n\text{OF}$  ( $n=1, 2, 3$ ) isolated systems and in the corresponding binary complexes with  $\text{BeCl}_2$ . As could be anticipated, the successive substitution of H atoms by F atoms leads to a decrease (in absolute value) of the electrostatic potential around the F atom of the O–F group. Thus, whereas the unsubstituted parent compound does not exhibit any  $\sigma$ -hole on the fluorine atom, the mono- and disubstituted fluoro-derivatives present a very shallow one; only for the trisubstituted derivative does a deeper  $\sigma$ -hole appear (See Figure 6a).

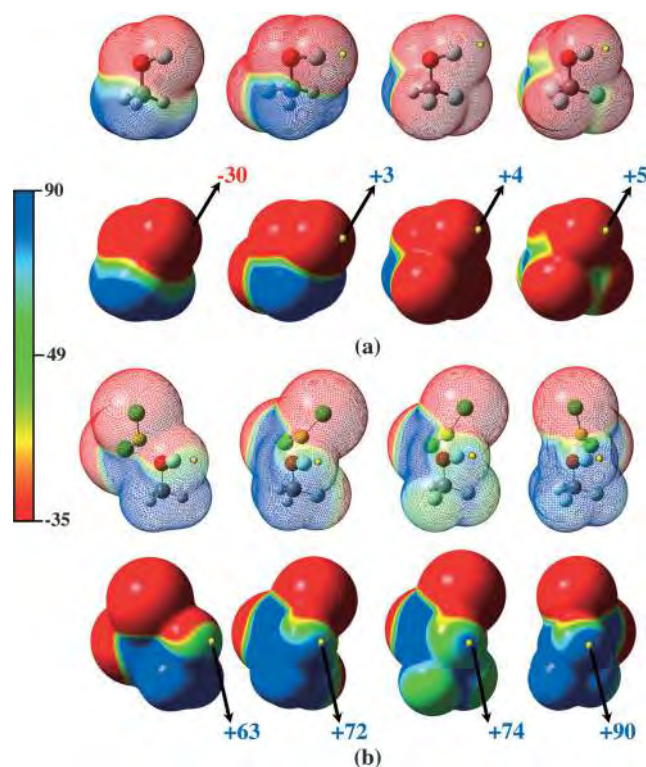


**Figure 6.** Molecular electrostatic potentials of a) isolated  $\text{CH}_{3-n}\text{F}_n\text{OF}$  ( $n=1, 2, 3$ ) derivatives and b) binary  $\text{BeCl}_2 \cdots \text{CH}_{3-n}\text{F}_n\text{OF}$  ( $n=0, 1, 2, 3$ ) complexes. The values of the potentials are in  $\text{kJ mol}^{-1}$ . The yellow dots indicate the location of the maximum value of the potential associated to the  $\sigma$ -hole when it exists.

The situation changes significantly on going from the isolated  $\text{CH}_{3-n}\text{F}_n\text{OF}$  ( $n=0, 1, 2, 3$ ) derivatives to the corresponding complexes with  $\text{BeCl}_2$ , because a rather deep  $\sigma$ -hole appears in all cases (see Figure 6b). Interestingly, the curves showing the variation of the depth of the  $\sigma$ -hole with the number of F substituents for both the isolated systems ( $\blacklozenge$  in Figure 7) and for the binary  $\text{BeCl}_2 \cdots \text{CH}_{3-n}\text{F}_n\text{OF}$  ( $n=1, 2, 3$ ) complexes ( $\blacktriangle$  in Figure 7) are however almost parallel, mainly for  $n \geq 1$  (see Figure 7). This can also be seen by looking at the difference between the values of  $V_{\text{hole}}$  for the  $\text{BeCl}_2 \cdots \text{CH}_{3-n}\text{F}_n\text{OF}$  ( $n=0, 1, 2, 3$ ) complexes with respect to the value of  $V_{\text{hole}}$  for the  $\text{CH}_{3-n}\text{F}_n\text{OF}$  ( $n=0, 1, 2, 3$ ) isolated monomers ( $\blacksquare$  in Figure 7). It is apparent that the most significant change occurs on going from the unsubstituted parent compound to the monosubstituted derivative, and both curves cross between the unsubstituted and the monosubstituted derivative. This is so because in the unsubstituted parent compound, no  $\sigma$ -hole exists, but it is created upon association with  $\text{BeCl}_2$ . Whereas for  $n \geq 1$ , the effect of the  $\text{BeCl}_2$  attachment is to deepen the already existing  $\sigma$ -hole, and the value of  $\Delta V_{\text{hole}}$  is necessarily smaller than the value of  $V_{\text{hole}}$ , whereas it is the other way around for the unsubstituted compound.

Furthermore, the increase in the number of F substituents has a marginal effect on the variation of the depth of the  $\sigma$ -hole ( $\blacksquare$ , Figure 7), which is rather similar for  $n=1, 2$  and is slightly smaller for  $n=3$ . This is consistent with the variations

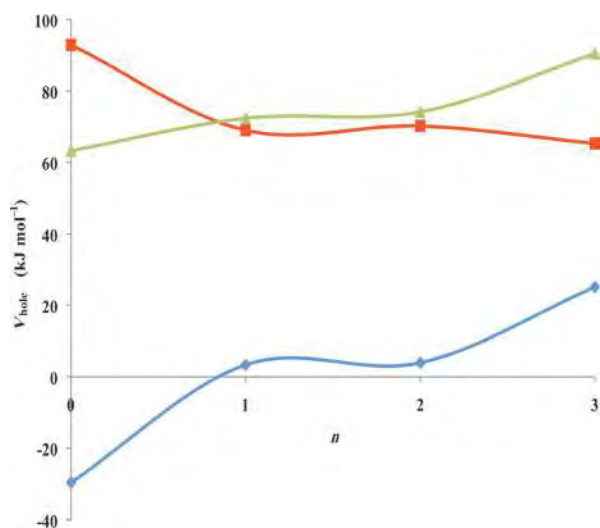


**Figure 7.** Molecular electrostatic potential at the  $\sigma$ -hole,  $V_{\text{hole}}$ , for  $\text{BeCl}_2\cdot\text{CH}_{3-n}\text{F}_n\text{OF}$  ( $n=1, 2, 3$ ) binary complexes.  $\Delta V_{\text{hole}}$  measures the change on this potential on going from the isolated  $\text{CH}_{3-n}\text{F}_n\text{OF}$  ( $n=0, 1, 2, 3$ ) compounds to the corresponding complexes with  $\text{BeCl}_2$ . Note that for  $n=0$  the system does not present a  $\sigma$ -hole and therefore the potential is negative.  $\blacklozenge = V_{\text{hole}}$  (isolated);  $\blacksquare = V_{\text{hole}}$ ; and  $\blacktriangle = V_{\text{hole}}$  ( $\text{BeCl}_2$  adduct).

observed for the F atomic energy components as a function of  $n$ . As can be deduced from the values in Table S1 of the Supporting Information, this variation is very similar (280 and 275  $\text{kJ mol}^{-1}$ , respectively) for  $n=1, 2$  and slightly smaller (238  $\text{kJ mol}^{-1}$ ) for  $n=3$ . The electron density of the different complexes actually shows that the strength of the beryllium bond decreases as the number of F substituents in the  $\text{CH}_{3-n}\text{F}_n\text{OF}$  moiety increases, because the electron donor capacity of the oxygen atom decreases (see Figure 8). However,

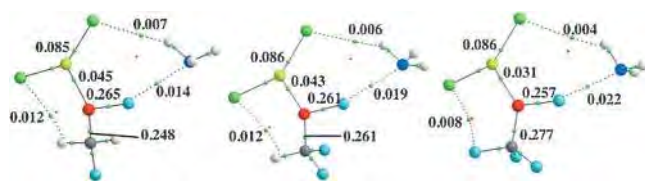


**Figure 8.** Molecular graphs of  $\text{BeCl}_2\cdot\text{CH}_{3-n}\text{F}_n\text{OF}\cdot\text{NH}_3$  ( $n=1, 2, 3$ ) ternary complexes. In the molecular graphs, the green and red dots correspond to BCPs and RCPs, respectively. Electron densities are in a.u.

the concomitant effect of both factors (the formation of the beryllium bond and the increase in the fluorine substitution) results in a deepening of the  $\sigma$ -hole (see Figure 6). As indicated above, this leads to the obvious enhancement of the interaction with ammonia but also to a reinforcement of the O–F bond, as shown by the values of the electron densities at the corresponding BCPs (see Figure 8). It should also be noted that the increase of the strength of the halogen bond results in a greater linearity of the O–F...N arrangement (see Figure S3 in the Supporting Information), which leads to an increase of the distance between the  $\text{NH}_3$  molecule from the Cl atom of the  $\text{BeCl}_2$  moiety closer to it. Consequently, a systematic weaken-

ing of the Cl...H–N hydrogen bond with fluorine substitution is also observed.

## Conclusion

We have shown that the significant electron density rearrangements that follow the formation of a beryllium bond may lead to the appearance of a  $\sigma$ -hole in systems that, when isolated, do not exhibit this feature, such as  $\text{CH}_3\text{OF}$ ,  $\text{NO}_2\text{F}$ ,  $\text{NO}_3\text{F}$  and other fluorine-containing systems. The creation of the  $\sigma$ -hole is another manifestation of the BAR rule.<sup>[31]</sup> The appearance of  $\sigma$ -hole on the F atoms of the aforementioned fluoro-derivatives is due to the significant polarization of the atom X of the X–F bond towards the beryllium atom when a  $\text{Be}\cdots\text{X}$  beryllium bond is formed. This necessarily leads to an enhancement of the electronegativity of X, which tries to recover part of this density from the bonds in which it participates. According to the BAR rule, when this atom is less electronegative than the atom attached to it (F in our case), it polarizes the valence density of the F into the bonding region. Consequently, the X–F bond becomes reinforced and the F atom becomes more electron deficient, which is nicely reflected in a significant decrease in absolute value of its atomic energy, and a  $\sigma$ -hole is created on the F halogen atom. These effects are also observed even in those cases in which the atom X involved in the beryllium bond is not directly bound to the F atom. Hence, compounds like  $\text{CH}_3\text{OF}$ ,  $\text{NO}_2\text{F}$ ,  $\text{NO}_3\text{F}$ , in which the F atom does not exhibit a  $\sigma$ -hole and therefore do not yield  $\text{F}\cdots\text{Base}$  halogen bonds, are able to form these kinds of linkages when associated to a strong electron acceptor as  $\text{BeX}_2$  derivatives. Furthermore, the coincidence of both noncovalent interactions in the same molecular aggregate leads to significant cooperative effects between the new halogen bond and the beryllium bond, which reinforce the strength of both noncovalent interactions.

## Acknowledgements

This work was partially supported by the Ministerio de Economía y Competitividad (Projects No. CTQ2012-35513-C02 and CTQ2013-43698-P), by the STSM COST Action CM1204, and by the Project FOTOCARBON-CM S2013/MIT-2841 of the Comunidad Autónoma de Madrid. OB acknowledges a FPU grant from the Ministerio de Educación, Cultura y Deporte of Spain. Computational time at Centro de Computación Científica (CCC) of Universidad Autónoma de Madrid is also acknowledged.

**Keywords:** beryllium · cooperative effects · halogen bonds · molecular modeling · noncovalent interactions

- [1] a) P. Hobza, R. Zahradník, K. Müller-Dethlefs, *Collect. Czech. Chem. Commun.* **2006**, *71*, 443–531; b) P. Hobza, K. Müller-Dethlefs, *Non-covalent Interactions: Theory and Experiment*, RSC, London, **2009**.
- [2] L. R. MacGillivray, *Metal–Organic Frameworks: Design and Application*, John Wiley & Sons, Singapore, **2010**.
- [3] a) J. V. Yakhmi, *J. Mater. Educ.* **2011**, *33*, 149–160; b) G. R. Whittell, M. D. Hager, U. S. Schubert, I. Manners, *Nat. Mater.* **2011**, *10*, 176–188.
- [4] a) G. C. Pimentel, A. L. McClelland, *The Hydrogen Bond*, W. H. Freeman and Co., San Francisco, **1960**; b) P. A. Kollman, L. C. Allen, *Chem. Rev.*

- 1972, 72, 283–303; c) G. A. Jeffrey, *An Introduction to Hydrogen Bonding*, Oxford University Press, New York, 1997; d) S. J. Grabowski, *Hydrogen Bonding: New Insights*, Springer, Dordrecht (The Netherlands), 2006.
- [5] a) V. I. Bakhmutov, *Dihydrogen Bonds: Principles, Experiments and Applications*, John Wiley & Sons, Hoboken, 2008; b) R. Custelcean, J. E. Jackson, *Chem. Rev.* **2001**, 101, 1963–1980.
- [6] a) S. Zahn, R. Frank, E. Hey-Hawkins, B. Kirchner, *Chem. Eur. J.* **2011**, 17, 6034–6038; b) J. E. Del Bene, I. Alkorta, G. Sánchez-Sanz, J. Elguero, *J. Phys. Chem. A* **2011**, 115, 13724–13731; c) S. Scheiner, *Acc. Chem. Res.* **2013**, 46, 280–288; d) G. Sánchez-Sanz, C. Trujillo, M. Solimannejad, I. Alkorta, J. Elguero, *Phys. Chem. Chem. Phys.* **2013**, 15, 14310–14318.
- [7] a) P. Sanz, O. Mó, M. Yáñez, *J. Phys. Chem. A* **2002**, 106, 4661–4668; b) P. Sanz, O. Mó, M. Yáñez, *Chem. Eur. J.* **2002**, 8, 3999–4007; c) W. Z. Wang, B. M. Ji, Y. Zhang, *J. Phys. Chem. A* **2009**, 113, 8132–8135.
- [8] a) P. Metrangolo, G. Resnati, *Chem. Eur. J.* **2001**, 7, 2511–2519; b) P. Politzer, P. Lane, M. C. Concha, Y. Ma, J. S. Murray, *J. Mol. Model.* **2007**, 13, 305–311; c) P. Politzer, J. S. Murray, T. Clark, *Phys. Chem. Chem. Phys.* **2013**, 15, 11178–11189.
- [9] a) A. Bauzá, T. J. Mooibroek, A. Frontera, *Angew. Chem. Int. Ed.* **2013**, 52, 12317–12321; *Angew. Chem.* **2013**, 125, 12543–12547; b) L. M. Azofra, S. Scheiner, *J. Chem. Phys.* **2015**, 142, 034307.
- [10] P. Politzer, J. S. Murray, T. Clark, *J. Mol. Model.* **2015**, 21, 52.
- [11] a) M. Yáñez, P. Sanz, O. Mó, I. Alkorta, J. Elguero, *J. Chem. Theory Comput.* **2009**, 5, 2763–2771; b) E. Fernández Villanueva, O. Mó, M. Yáñez, *Phys. Chem. Chem. Phys.* **2014**, 16, 17531–17536.
- [12] a) H. Kleeberg, D. Klein, W. A. P. Luck, *J. Phys. Chem.* **1987**, 91, 3200–3203; b) O. Mó, M. Yáñez, J. Elguero, *J. Chem. Phys.* **1992**, 97, 6628–6638.
- [13] I. Alkorta, F. Blanco, P. M. Deyà, J. Elguero, C. Estarellas, A. Frontera, D. Quiñero, *Theor. Chem. Acc.* **2010**, 126, 1–14.
- [14] a) O. Mó, M. Yáñez, I. Alkorta, J. Elguero, *J. Chem. Theory Comput.* **2012**, 8, 2293–2300; b) L. Albrecht, R. J. Boyd, O. Mó, M. Yáñez, *Phys. Chem. Chem. Phys.* **2012**, 14, 14540–14547; c) M. M. Montero-Campillo, A. M. Lamsabhi, O. Mó, M. Yáñez, *J. Mol. Model.* **2013**, 19, 2759–2766; d) L. Albrecht, R. J. Boyd, O. Mó, M. Yáñez, *J. Phys. Chem. A* **2014**, 118, 4205–4213; e) I. Alkorta, J. Elguero, O. Mó, M. Yáñez, J. E. Del Bene, *Phys. Chem. Chem. Phys.* **2015**, 17, 2259–2267.
- [15] M. Yáñez, O. Mó, I. Alkorta, J. Elguero, *Chem. Eur. J.* **2013**, 19, 11637–11643.
- [16] a) M. Yáñez, O. Mó, I. Alkorta, J. Elguero, *Chem. Phys. Lett.* **2013**, 590, 22–26; b) O. Mó, M. Yáñez, I. Alkorta, J. Elguero, *Mol. Phys.* **2014**, 112, 592–600.
- [17] I. Alkorta, J. Elguero, M. Yáñez, O. Mó, *Phys. Chem. Chem. Phys.* **2014**, 16, 4305–4312.
- [18] J. S. Murray, P. Lane, P. Politzer, *J. Mol. Model.* **2009**, 15, 723–729.
- [19] T. Clark, M. Hennemann, J. S. Murray, P. Politzer, *J. Mol. Model.* **2007**, 13, 291–296.
- [20] a) M. Solimannejad, V. Ramezani, C. Trujillo, I. Alkorta, G. Sánchez-Sanz, J. Elguero, *J. Phys. Chem. A* **2012**, 116, 5199–5206; b) K. J. Donald, M. Tawfik, *J. Phys. Chem. A* **2013**, 117, 14176–14183; c) Q. Z. Li, X. Guo, X. Yang, W. Z. Li, J. B. Cheng, H. B. Li, *Phys. Chem. Chem. Phys.* **2014**, 16, 11617–11625.
- [21] M. Hennemann, J. S. Murray, P. Politzer, K. E. Riley, T. Clark, *J. Mol. Model.* **2012**, 18, 2461–2469.
- [22] a) P. Politzer, J. S. Murray, M. C. Concha, *J. Mol. Model.* **2007**, 13, 643–650; b) Y. X. Lu, J. W. Zou, Q. S. Yu, Y. J. Jiang, W. N. Zhao, *Chem. Phys. Lett.* **2007**, 449, 6–10; c) P. Metrangolo, J. S. Murray, T. Pilati, P. Politzer, G. Resnati, G. Terraneo, *CrystEngComm* **2011**, 13, 6593–6596; d) W. Li, Y. L. Zeng, X. Y. Zhang, S. J. Zheng, L. P. Meng, *Phys. Chem. Chem. Phys.* **2014**, 16, 19282–19289; e) K. Eskandari, M. Lesani, *Chem. Eur. J.* **2015**, 21, 4739–4746.
- [23] a) J. S. Binkley, J. A. Pople, *Int. J. Quantum Chem.* **1975**, 9, 229–236; b) D. J. DeFrees, B. A. Levi, S. K. Pollack, W. J. Hehre, J. S. Binkley, J. A. Pople, *J. Am. Chem. Soc.* **1979**, 101, 4085–4089.
- [24] T. H. Dunning, *J. Chem. Phys.* **1989**, 90, 1007–1023.
- [25] a) R. F. W. Bader, *Atoms in Molecules. A Quantum Theory*, Clarendon Press, Oxford, 1990; b) C. F. Matta, R. J. Boyd, *The Quantum Theory of Atoms in Molecules*, Wiley-VCH, Weinheim, 2007.
- [26] a) A. E. Reed, R. B. Weinstock, F. Weinhold, *J. Chem. Phys.* **1985**, 83, 735–746; b) A. E. Reed, L. A. Curtiss, F. Weinhold, *Chem. Rev.* **1988**, 88, 899–926.
- [27] a) U. Koch, P. L. A. Popelier, *J. Phys. Chem.* **1995**, 99, 9747–9754; b) A. Taylor, J. Taylor, G. W. Watson, R. J. Boyd, *J. Phys. Chem. B* **2010**, 114, 9833–9839; c) L. Albrecht, R. J. Boyd, *J. Phys. Chem. A* **2012**, 116, 3946–3951.
- [28] T. A. Keith, *AIMAll* (Version 13.05.06), Gristmill Software, Overland Park, KS, **2013**, aim.tkgristmill.com, 2013.
- [29] Gaussian 09, Revision C.01, M. J. Frisch, G. W. Trucks, H. B. Schlegel, G. E. Scuseria, M. A. Robb, J. R. Cheeseman, G. Scalmani, V. Barone, B. Menonucci, G. A. Petersson, H. Nakatsuji, M. Caricato, X. Li, H. P. Hratchian, A. F. Izmaylov, J. Bloino, G. Zheng, J. L. Sonnenberg, M. Hada, M. Ehara, K. Toyota, R. Fukuda, J. Hasegawa, M. Ishida, T. Nakajima, Y. Honda, O. Kitao, H. Nakai, T. Vreven, J. A. Montgomery, Jr., J. E. Peralta, F. Ogliaro, M. Bearpark, J. J. Heyd, E. Brothers, K. N. Kudin, V. N. Staroverov, R. Kobayashi, J. Normand, K. Raghavachari, A. Rendell, J. C. Burant, S. S. Iyengar, J. Tomasi, M. Cossi, N. Rega, J. M. Millam, M. Klene, J. E. Knox, J. B. Cross, V. Bakken, C. Adamo, J. Jaramillo, R. Gomperts, R. E. Stratmann, O. Yazyev, A. J. Austin, R. Cammi, C. Pomelli, J. W. Ochterski, R. L. Martin, K. Morokuma, V. G. Zakrzewski, G. A. Voth, P. Salvador, J. J. Dannenberg, S. Dapprich, A. D. Daniels, Ö. Farkas, J. B. Foresman, J. V. Ortiz, J. Cioslowski, D. J. Fox, Gaussian, Inc., Wallingford, CT, 2009.
- [30] T. Lu, F. Chen, *J. Comput. Chem.* **2012**, 33, 580–592.
- [31] M. Alcami, O. Mó, M. Yáñez, *Mass Spectrom. Rev.* **2001**, 20, 195–245.
- [32] a) T. M. McCleskey, D. S. Ehler, T. S. Keizer, D. N. Asthagiri, L. R. Pratt, R. Michalczyk, B. L. Scott, *Angew. Chem. Int. Ed.* **2007**, 46, 2669–2671; *Angew. Chem.* **2007**, 119, 2723–2725; b) B. L. Scott, T. M. McCleskey, A. Chaudhary, E. Hong-Geller, S. Gnanakaran, *Chem. Commun.* **2008**, 2837–2847; c) T. M. McCleskey, B. L. Scott, *J. Occup. Environ. Hyg.* **2009**, 6, 751–757.

Received: March 12, 2015

Published online on July 21, 2015

# CHEMISTRY

## A **European** Journal

### Supporting Information

#### **Creating $\sigma$ -Holes through the Formation of Beryllium Bonds**

Oriana Brea,<sup>[a]</sup> Otilia M $\acute{o}$ ,<sup>[a]</sup> Manuel Y $\acute{a}$ ñez,<sup>\*[a]</sup> Ibon Alkorta,<sup>\*[b]</sup> and Jos $\acute{e}$  Elguero<sup>[b]</sup>

chem\_201500981\_sm\_miscellaneous\_information.pdf

**Table S1.** Atomic energy (AE, kJ mol<sup>-1</sup>) of the fluorine atom participating in the halogen bond<sup>a</sup> (in red) and its change ( $\Delta$ AE, kJ mol<sup>-1</sup>) upon formation of the halogen bond.

System	AE	$\Delta$ AE
BeCl <sub>2</sub> :CH <sub>3</sub> OF	683	
BeCl <sub>2</sub> : CH <sub>3</sub> OF:NH <sub>3</sub>	646	-37
BeCl <sub>2</sub> : NO <sub>2</sub> F	690	
BeCl <sub>2</sub> : NO <sub>2</sub> F:NH <sub>3</sub>	384	-306
BeCl <sub>2</sub> : NO <sub>3</sub> F	449	
BeCl <sub>2</sub> : NO <sub>3</sub> F:NH <sub>3</sub>	429	-20
BeCl <sub>2</sub> : NCF	65	
BeCl <sub>2</sub> : NCF:NH <sub>3</sub>	-128	-193
BeCl <sub>2</sub> : CH <sub>2</sub> FOF	732 [280] <sup>b</sup>	
BeCl <sub>2</sub> : CH <sub>2</sub> FOF:NH <sub>3</sub>	400	-332
BeCl <sub>2</sub> : CHF <sub>2</sub> OF	638 [275] <sup>b</sup>	
BeCl <sub>2</sub> : CHF <sub>2</sub> OF:NH <sub>3</sub>	311	-327
BeCl <sub>2</sub> : CF <sub>3</sub> OF	565 [231] <sup>b</sup>	
BeCl <sub>2</sub> : CF <sub>3</sub> OF:NH <sub>3</sub>	251	-314

<sup>a</sup> The value of the AE is calculated taken as a reference the value in the corresponding isolated monomer. Hence, a positive value indicates a destabilization of the corresponding atom.

<sup>b</sup>Values within brackets give the change in the Atomic energy component of the F atom of BeCl<sub>2</sub>:CH<sub>3-n</sub>F<sub>n</sub>OF (n = 1, 2, 3) binary complexes with respect to BeCl<sub>2</sub>:CH<sub>3</sub>OF.

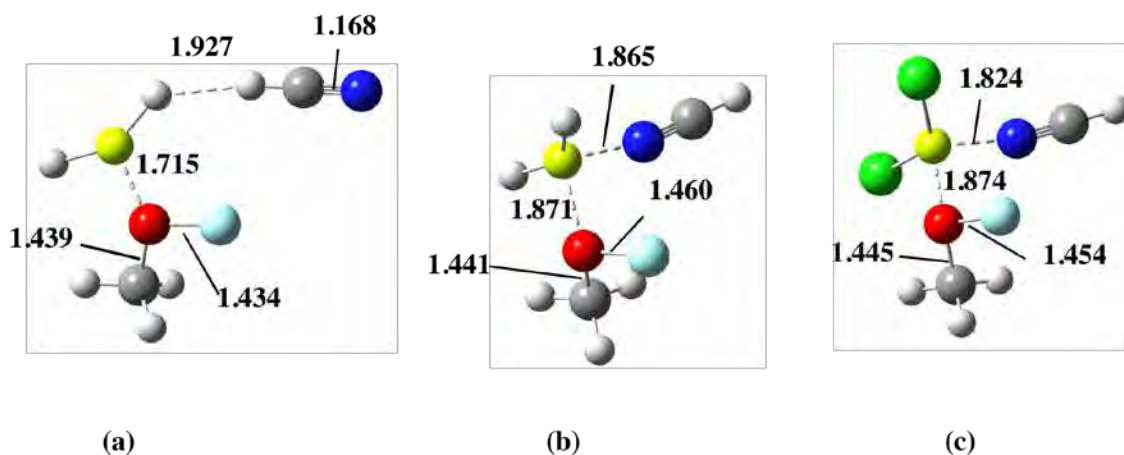


**Figure S1.** Optimized structures of the ternary complexes  $\text{BeH}_2:\text{CH}_3\text{OF}:\text{NCH}$  and  $\text{BeCl}_2:\text{CH}_3\text{OF}:\text{NCH}$ . Bond distances are in Å. The  $\text{BeH}_2:\text{CH}_3\text{OF}:\text{NCH}$  complex presents two stable conformations, conformer (a) being  $250 \text{ kJ mol}^{-1}$  higher in energy than conformer (b).

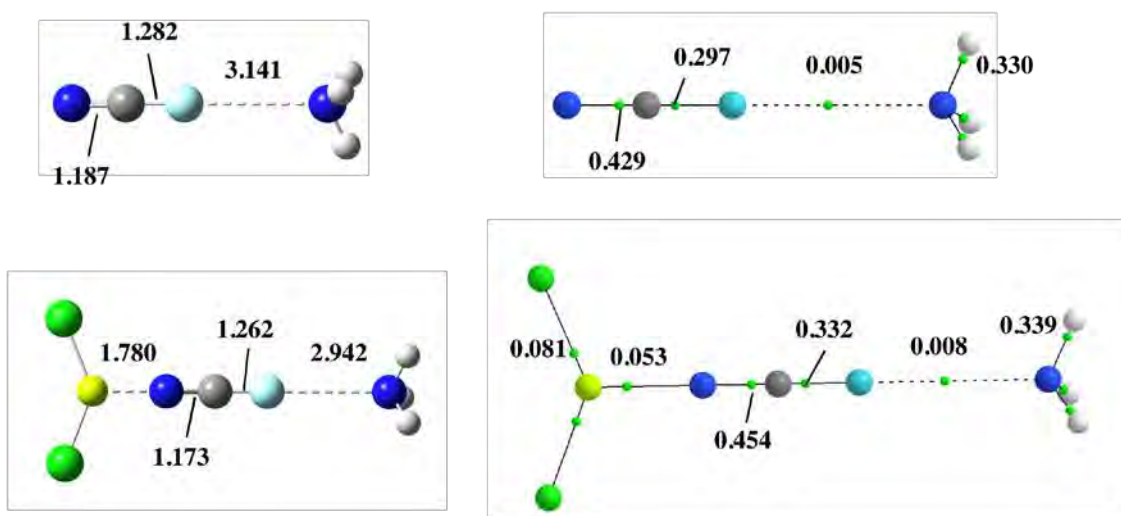


**Figure S2.** Optimized geometry and molecular graph of the  $\text{NCF}\cdots\text{NH}_3$  binary complex and the  $\text{BeCl}_2:\text{NCF}:\text{NH}_3$  triad. Bond distances are in Å. In the molecular graph green dots denote BCPs. Electron densities are in au.

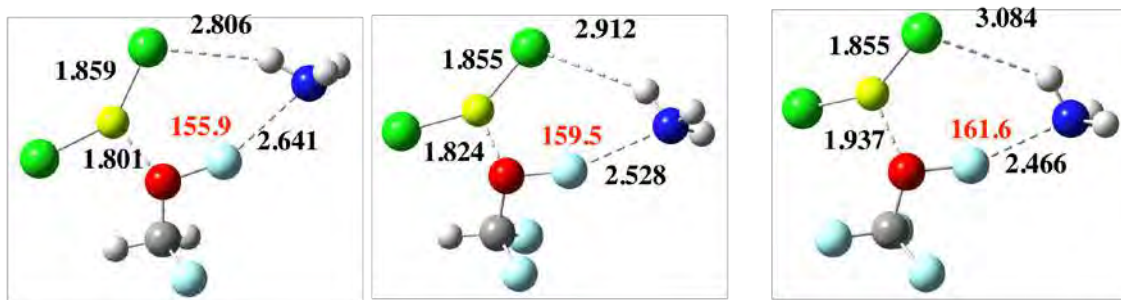


**Figure S3.** Optimized structures of the ternary complexes  $\text{BeCl}_2:\text{CH}_{3-n}\text{F}_n\text{OF}:\text{NH}_3$  ( $n = 1, 2, 3$ ). Bond distances are in Å. In red the OFN angle in degrees.





## B.2 ARTICLE II

*Exergonic and Spontaneous Production of Radicals through Beryllium Bonds*

Published in: *Angewandte Chemie*, **2016**, *128*, 8878-8881.



# Exergonic and Spontaneous Production of Radicals through Beryllium Bonds

Oriana Brea, Ibon Alkorta, Otilia Mó, Manuel Yáñez,\* José Elguero, and Inés Corral

**Abstract:** High-level *ab initio* calculations show that the formation of radicals, by the homolytic bond fission of  $Y-R$  ( $Y=F, OH, NH_2$ ;  $R=CH_3, NH_2, OH, F, SiH_3, PH_2, SH, Cl, NO$ ) bonds is dramatically favored by the association of the molecule with  $BeX_2$  ( $X=H$  and  $Cl$ ) derivatives. This finding is a consequence of two concomitant effects, the significant activation of the  $Y-R$  bond after the formation of the beryllium bond, and the huge stabilization of the  $F^\bullet$  ( $OH^\bullet, NH_2^\bullet$ ) radical upon  $BeX_2$  attachment. In those cases where  $R$  is an electronegative group, the formation of the radicals is not only exergonic, but spontaneous.

Since the moment the first free radical was discovered back in 1900,<sup>[1]</sup> the interest in these species has steadily increased because radicals are involved in a plethora of chemical phenomena, and nowadays their role as intermediates is well established in a huge number of chemical reactions, as well as in the metabolism of biochemical systems.

The formation of neutral radicals usually involves the homolytic bond cleavage of covalent bonds, a process that requires a rather large amount of energy.<sup>[2]</sup> Boryl, aminyl, phosphinyl radicals, among others, are used as photoinitiating or initiating species<sup>[3]</sup> even though the formation of these radicals is often hindered by the high amount of energy needed to break a B–H, a N–H, or a P–H bond.<sup>[4]</sup> Clearly the energy demanded would be much lower when dealing with weak linkages, but even in those cases the amount of energy required is very high. In fact the dissociation of a rather weak covalent bond, such as F–F, still requires  $157 \text{ kJ mol}^{-1}$ .<sup>[2]</sup>

However, the strength of a covalent linkage can be altered by protonation,<sup>[5]</sup> reflecting the relationship between bond energies and electronegativity proposed by Pauling,<sup>[6]</sup> but also through the binding of a Lewis acid via non-covalent interactions, which normally induces a distortion of the electron density of the two interacting subunits. These distortions are particularly large for molecular linkers based on beryllium bonds,<sup>[7]</sup> in which the  $BeXY$  moiety acts as Lewis acid.

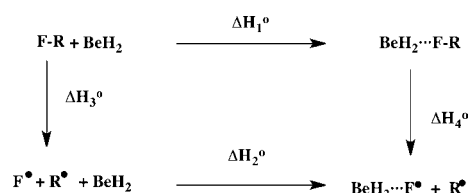
These electron density redistributions are at the origin of 1) very large cooperative effects between beryllium bonds and other non-covalent interactions,<sup>[8,9]</sup> 2) huge acidity enhancements of the Lewis bases participating in the beryllium bond,<sup>[10]</sup> 3) the spontaneous formation of ion-pairs in the gas-phase.<sup>[11]</sup>

Herein, through the use of high-level molecular orbital multi-configurational calculations, which are described in the Supporting Information, we will show that beryllium bonds also strongly favor the formation of radicals. For this purpose, the following compounds: F–R, OH–R and  $NH_2$ –R ( $R=CH_3, NH_2, OH, F, SiH_3, PH_2, SH, Cl, NO$ ) and their complexes with  $BeH_2$  have been investigated.

As illustrated in Figure 1, for the set F–R ( $R=CH_3, NH_2, OH, F, NO$ ), the electron density at the F–R bond critical point clearly decreases on going from the isolated Lewis base to the base in the  $BeH_2$  complex. This F–R bond activation is obviously reflected in a significant lengthening of the corresponding bond (see Table S1 of the Supporting Information). Similar results are found for the HO–R,  $H_2N$ –R derivatives (see Figures S1 and S2 of the Supporting Information).

However, the most important finding is the dramatic decrease of the F–R, O–R, and N–R bond dissociation energies on going from the isolated bases to the complex as illustrated in Table 1. Even more importantly, for some systems (F– $NH_2$ , F–OH,  $F_2$ , F–SH, F–Cl, F–NO) the bond dissociation is not only an exothermic but also an exergonic process!

The origin of such a dramatic change in the strength of these bonds can be traced through the thermodynamic cycle shown in Scheme 1.



Scheme 1.

The  $\Delta H_3^\circ$  and  $\Delta H_4^\circ$  are the F–R bond dissociation enthalpies for the isolated FR molecule and for the  $BeH_2 \cdots FR$  complex, respectively (see Table 1).  $\Delta H_1^\circ$  and  $\Delta H_2^\circ$  measure the stabilization of FR and  $F^\bullet$  upon  $BeH_2$  attachment, respectively. This cycle, clearly illustrates that the dramatic decrease observed in the F–R dissociation energy is not only a consequence of the weakening of the

[\*] M. Sc. O. Brea, Prof. Dr. O. Mó, Prof. Dr. M. Yáñez, Prof. Dr. I. Corral  
Universidad Autónoma de Madrid  
Departamento de Química, Facultad de Ciencias  
Módulo 13, Campus de Excelencia UAM-CSIC  
Cantoblanco, 28049 Madrid (Spain)  
E-mail: manuel.yanez@uam.es

Prof. Dr. I. Alkorta, Prof. Dr. J. Elguero  
Instituto de Química Médica (CSIC).  
C/ Juan de la Cierva, 3, 28006 Madrid (Spain)

Supporting information and the ORCID identification number(s) for the author(s) of this article can be found under <http://dx.doi.org/10.1002/anie.201603690>.

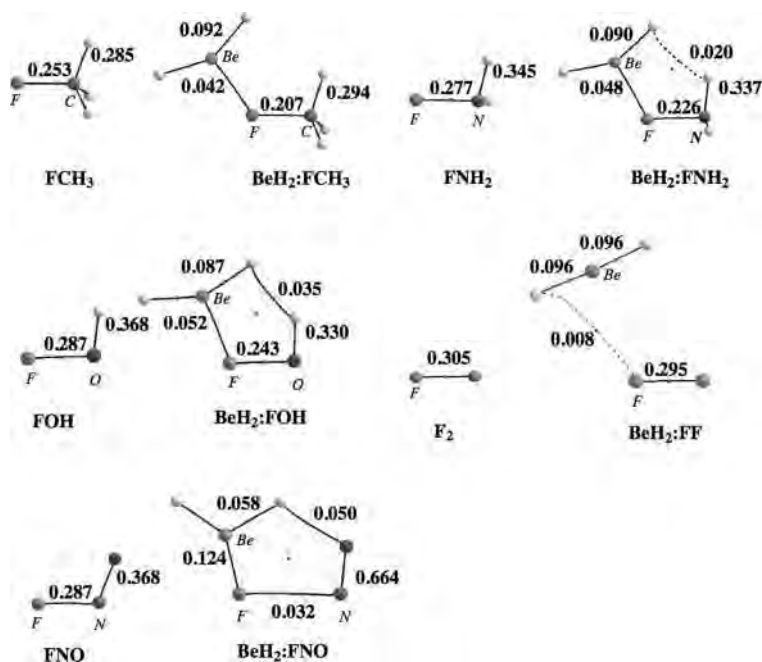


**Figure 1.** Molecular graphs of F–R (R = CH<sub>3</sub>, NH<sub>2</sub>, OH, F, NO) compounds and their complexes with BeH<sub>2</sub>. Small gray dots on bonds indicate the bond critical points, a small gray dot in a ring system indicates the ring critical point. Electron densities are in a.u.

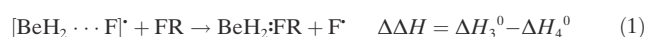
**Table 1:** G4 calculated F–R bond dissociation enthalpies ( $\Delta H$ ) and Gibbs energies ( $\Delta G$ ) at 298.2 K, as defined in Scheme 1, for the isolated compounds and for their complexes with BeH<sub>2</sub>.

$\Delta\Delta H = \Delta H_3^0 - \Delta H_4^0$  and  $\Delta\Delta G = \Delta G_3^0 - \Delta G_4^0$  measure the changes in these two thermodynamic magnitudes upon association with BeH<sub>2</sub>. All the dissociation energies were calculated considering the ground state  $\cdot\text{BeH}_2\text{F}$  radical product.

F–R	Isolated				BeH <sub>2</sub> Complex		Variation	
	$\Delta H_1^0$	$\Delta H_3^0$	$\Delta G_3^0$	$\Delta H_{\text{exp}}^{[a]}$	$\Delta H_4^0$	$\Delta G_4^0$	$\Delta\Delta H$	$\Delta\Delta G$
F–CH <sub>3</sub>	–36.7	459.6	420.9	460 ± 8	124.3	79.9	335.3	341.0
F–NH <sub>2</sub>	–39.6	289.8	255.1		–42.6	–88.9	332.4	344.0
F–OH	–38.1	200.5	169.7		–133.4	–176.9	333.9	346.6
F–F <sup>[b]</sup>	–2.96	143.6	113.8	156.9	–212.6	–234.6	356.2	348.4
F–SiH <sub>3</sub>	–22.3	633.3	594.6	638 ± 5	283.6	234.7	349.7	359.9
F–PH <sub>2</sub>	–23.1	465.7	429.8	461.5 ± 10.5	116.8	73.4	348.9	356.0
F–SH	–25.4	347.8	316.8		1.2	–40.4	346.6	357.2
F–Cl	–42.1	256.4	274.0	256.2	–73.5	–106.4	329.9	380.4
F–NO	–102.1	257.0	224.4		–12.8	–53.5	269.8	278.0

The stabilization enthalpy of F $\cdot$  ( $\Delta H_2^0$ ) at G4 level of theory is –372.0 kJ mol<sup>–1</sup>. [a] Values taken from Ref. [2]. [b] Calculated at CCSD(T)/cc-TZVP level of theory. At this level the stabilization enthalpy of F $\cdot$  is –359.2 kJ mol<sup>–1</sup>.

bond, but it is mostly due to the huge stabilization undergone by the F $\cdot$  radical as compared with the stabilization of the FR compound. Note that the Reaction (1):



is related to what Radom et al. have defined as radical stabilization energy (RSE).<sup>[12]</sup> As shown in Table 1, the RSE ( $\Delta\Delta H$ ) of  $[\text{BeH}_2 \cdots \text{F}]^{\cdot}$  is enormous for the different R substituents considered in Reactions (1).

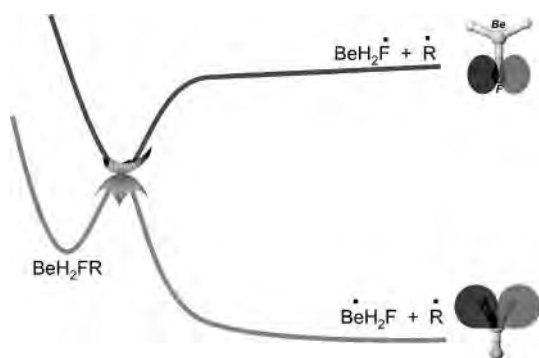
This huge RSE results in a substantial decrease of the enthalpy of Reaction (2):



which for some of species in Table 1 becomes even exothermic. Why? Since, the  $\text{BeH}_2\text{F}^{\cdot} + \text{R}^{\cdot}$  dissociation limit must lie necessarily higher in energy than the  $\text{BeH}_2\text{F-R}$  complex, the only possibility of having an exothermic formation of radicals is through a crossing with a second state whose dissociation limit is lower in energy (see Scheme 2). An exploration of the nature of the wavefunction through a multi-configurational approach shows that this lower dissociation limit corresponds to  $\cdot\text{BeH}_2\text{F} + \text{R}^{\cdot}$ , that is, a radical in which the unpaired electron migrates from the F atom to BeH<sub>2</sub> moiety (See Figure S3 of the Supporting Information and the accompanying explanation). Indeed, the structure in which the unpaired electron is located at the F atom corresponds to an excited state of the system, which lies about 400 kJ mol<sup>–1</sup>, above the ground state.

The conclusion is that the radical initially formed by the homolytic cleavage of the  $\text{BeH}_2\text{F-R}$  bond (Reaction (2)) in which  $\text{BeH}_2\text{F}^{\cdot}$  is formed, eventually evolves into a much more stable electronic arrangement in which the unpaired electron is mainly localized at the BeH<sub>2</sub> moiety. This process requires however to overpass an activation barrier dictated by the crossing point of the two states involved (see Scheme 2). Therefore, although the dissociation of the  $\text{BeH}_2\text{F-R}$  complex into two radicals is, in several cases exergonic, it is not necessarily a barrierless, and therefore, a spontaneous process. The height of the aforementioned barrier can only be reliably estimated by using multireference methods, because in the area near the crossing of both states, the wavefunction character is necessarily a mixture of several configurations. As suitable model systems to investigate this point we have chosen the  $\text{BeH}_2\text{F-F}$  complex, whose dissociation is the most exergonic process, the  $\text{BeCl}_2\text{F-F}$  one, in which we have changed the electron acceptor capacity of the Lewis acid by replacing BeH<sub>2</sub> with BeCl<sub>2</sub>, and finally the  $\text{BeH}_2\text{F-NO}$  complex, where the NO radical formed is a rather stable molecule.

The results obtained for the  $\text{BeH}_2\text{F-F}$  complex are presented in Figure 2. The curves correspond to the F–F bond cleavage in the isolated F<sub>2</sub> molecule and in the  $\text{BeH}_2\text{FF}$  complex. The curve for the isolated F<sub>2</sub> has the expected shape



Scheme 2.

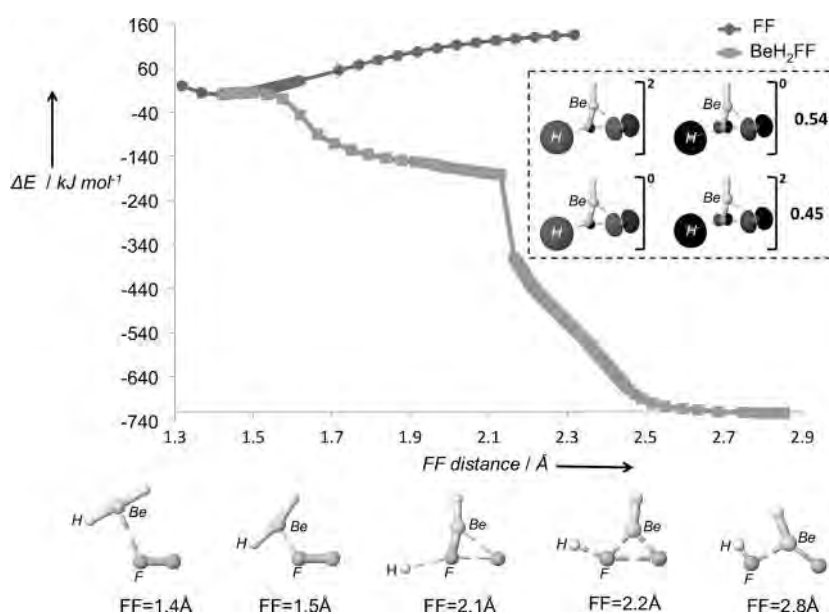


**Figure 2.** Potential energy curves corresponding to the dissociation of the F–F bond in the  $F_2$  isolated molecule (dots) and in the  $BeH_2:FF$  complex (squares). Inset: the character of the wavefunction for an F–F distance of 2.1 Å. FF and  $BeH_2:FF$  dissociation profiles were computed, respectively at CASPT2//CASSCF(10,6)/cc-TZVP, and CASPT2//CASSCF(14,9)/cc-TZVP levels of theory.

of an asymmetric parabola, which leads in the asymptotic limit to  $F^\bullet + F^\bullet$ . However, the curve for the  $BeH_2:FF$  complex goes through a negligible activation barrier (ca.  $4 \text{ kJ mol}^{-1}$ ) to yield  $\bullet BeH_2F + F^\bullet$ . The inset in the Figure 2 shows the two main configurations, of almost equal weight, which describe the system along the dissociation of the F–F bond and that ultimately corresponds to a biradical wavefunction with the two unpaired electrons sitting on the F atom and  $BeH_2F$  moiety (see Figure S4 for the evolution of the wavefunction over the reaction pathway). For longer  $F \cdots F$  distances the system tries to stabilize the  $F^\bullet$  so formed, by abstracting a H atom from the  $BeH_2F$  moiety, eventually yielding  $FH + FBeH$  as the final products. The situation changes only slightly when  $BeH_2$  is replaced by  $BeCl_2$ : the barrier becomes slightly higher, but still low enough to conclude that the dissociation process is still spontaneous, and the reaction mechanism goes

through a radical intermediary (see Figure S5 of the Supporting Information).

The case of the  $BeH_2:FNO$  system is particularly interesting, because NO is a rather stable radical. As a consequence, the effect of  $BeH_2$  attachment is already evident in the initial complex which is actually two radical species interacting via hydrogen bond ( $BeH_2F:NO$ ). Also in this case, the limit  $FBeH + HNO$ , in which the NO radical abstracts a H atom from the  $[BeH_2F]^\bullet$  radical lies lower in energy, however the evolution from  $[BeH_2F]^\bullet + NO^\bullet$  to  $FBeH + HNO$  requires surpassing an activation barrier of  $32 \text{ kJ mol}^{-1}$  (See Figure S6). Note that the process is barrierless in practice, since the zero point energy of the complex is higher (ca.  $52 \text{ kJ mol}^{-1}$ ) than the barrier height.

We can then conclude that beryllium bonds strongly facilitate the formation of radicals from  $Y-R$  ( $Y = F, OH, NH_2$ ;  $R = CH_3, NH_2, OH, F, SiH_3, PH_2, SH, Cl, NO$ ) molecules as a consequence of two concomitant effects, the significant activation of the  $Y-R$  bond, and the huge stabilization of the  $F^\bullet$  ( $OH^\bullet, NH_2^\bullet$ ) radical upon  $BeX_2$  attachment. In those cases where R is an electronegative group, the formation of the radicals is not only exergonic but spontaneous. There is still a final question to be answered, is always the homolytic dissociation of the  $Y-R$  bond dominant? To answer this question let us take FCl as a model compound. In Table 2 we show the homolytic and heterolytic dissociation energies for the isolated molecule and for the complexes in which FCl interacts: a) with  $BeH_2$ , FCl acting as a fluorine Lewis base ( $BeH_2:FCl$ ), b) with methanimine, FCl acting as a Cl Lewis acid ( $FCl:NH=CH_2$ ), c) with both, acting simultaneously as a fluorine Lewis base and as a Cl Lewis acid ( $BeH_2:FCl:NH=CH_2$ ; see Table 2).

As expected, the heterolytic dissociation of the FCl molecule is much more endo-

**Table 2:** G4 calculated F–Cl heterolytic and homolytic bond dissociation enthalpies ( $\Delta H$ ,  $\text{kJ mol}^{-1}$ ).

Reaction	$\Delta H$
$FCl \rightarrow F^\bullet + Cl^\bullet$	1305.3
$FCl \rightarrow F^- + Cl^+$	256.4
$BeH_2:FCl \rightarrow BeH_2F^\bullet + Cl^\bullet$	1014.5
$BeH_2:FCl \rightarrow [BeH_2F]^\bullet + Cl^\bullet$	–73.5
$FCl:NH=CH_2 \rightarrow F^\bullet + [Cl:NH=CH_2]^\bullet$	619.6
$FCl:NH=CH_2 \rightarrow F^- + [Cl:NH=CH_2]^+$	257.6
$BeH_2:FCl:NH=CH_2 \rightarrow [BeH_2:F]^\bullet + [Cl:NH=CH_2]^\bullet$	379.2
$BeH_2:FCl:NH=CH_2 \rightarrow [BeH_2:F]^- + [Cl:NH=CH_2]^+$	–21.7

thermic than its homolytic dissociation. Upon association to  $BeH_2$  both processes are favored, the effect being slightly larger in the case of the homolytic bond fission. Nevertheless,

as a result of the very large heterolytic bond dissociation energy of the isolated molecule, the heterolytic F–Cl cleavage in the  $\text{BeH}_2\text{:FCl}$  complex is still extremely endothermic, whereas the homolytic one becomes exothermic. The association with methanimine leads to a dramatic decrease of the heterolytic bond dissociation energy, because the imine strongly stabilizes the  $\text{Cl}^+$  cation, whereas the homolytic bond dissociation remains practically unchanged. When the  $\text{BeH}_2\text{:FCl:NH=CH}_2$  triad is considered, the decrease in the heterolytic bond dissociation energy ( $926.1 \text{ kJ mol}^{-1}$ ) is enormous, due to two concomitant effects, the stabilization of the  $\text{Cl}^+$  cation and the  $\text{F}^-$  anion by the imine and the moieties, respectively. However, the decrease of the homolytic bond dissociation energy is much smaller, because as indicated above only the stabilization of the  $\text{F}^\cdot$  by  $\text{BeH}_2$  is significant. Still, the homolytic bond dissociation is slightly exothermic, whereas the heterolytic bond cleavage is still endothermic. However, it must be taken into account that in the heterolytic bond fission two ions of opposite sign are forming, that will attract leading to a  $[\text{BeH}_2\text{:F}]^- \text{:}[\text{Cl:NH=CH}_2]^+$  ion pair, which as shown before in the literature, is a very favorable process.<sup>[9b]</sup>

### Acknowledgements

Work supported by the MINECO, Comunidad de Madrid, and the EU Framework Programme Horizon 2020: Projects CTQ2012-35513-C02-01, CTQ2013-43698-P, FOTOCAR-BON-CM S2013/MIT-2841, and COST Action CM1204.

**Keywords:** ab initio calculations · beryllium · gas-phase reactions · noncovalent interactions · spontaneous radical formation

**How to cite:** *Angew. Chem. Int. Ed.* **2016**, *55*, 8736–8739  
*Angew. Chem.* **2016**, *128*, 8878–8881

- [1] M. Gomberg, *J. Am. Chem. Soc.* **1900**, *22*, 757–771.
- [2] a) *NIST Chemistry Webbook. Standard Reference Database Number 69*, Eds. P. Linstrom, W. G. Mallard, National Institute of Standards and Technology, Gaithersburg, **2013**; b) S. J. Blanksby, G. B. Ellison, *Acc. Chem. Res.* **2003**, *36*, 255–263; c) O. Mó, M. Yáñez, M. Eckert-Maksić, Z. B. Maksić, I. Alkorta, J. Elguero, *J. Phys. Chem. A* **2005**, *109*, 4359–4365.
- [3] a) M. Lucarini, G. F. Pedulli, L. Valgimigli, *J. Org. Chem.* **1996**, *61*, 4309–4313; b) J. Lalevée, M. A. Tehfe, X. Allonas, J. P. Fouassier, *Macromolecules* **2008**, *41*, 9057–9062; c) J. C. Walton, *Angew. Chem. Int. Ed.* **2009**, *48*, 1726–1728; *Angew. Chem.* **2009**, *121*, 1754–1756.
- [4] J. Hioe, A. Karton, J. M. L. Martin, H. Zipse, *Chem. Eur. J.* **2010**, *16*, 6861–6865.
- [5] R. J. Boyd, J. N. M. Glover, J. A. Pincock, *J. Am. Chem. Soc.* **1989**, *111*, 5152–5155.
- [6] L. Pauling, *The Nature of the Chemical Bond*, Cornell University Press, Ithaca, **1939**.
- [7] M. Yáñez, P. Sanz, O. Mó, I. Alkorta, J. Elguero, *J. Chem. Theory Comput.* **2009**, *5*, 2763–2771.
- [8] a) L. Albrecht, R. J. Boyd, O. Mó, M. Yáñez, *Phys. Chem. Chem. Phys.* **2012**, *14*, 14540–14547; b) O. Mó, M. Yáñez, I. Alkorta, J. Elguero, *J. Chem. Theory Comput.* **2012**, *8*, 2293–2300.
- [9] a) L. Albrecht, R. J. Boyd, O. Mó, M. Yáñez, *J. Phys. Chem. A* **2014**, *118*, 4205–4213; b) I. Alkorta, J. Elguero, O. Mó, M. Yáñez, J. E. Del Bene, *Phys. Chem. Chem. Phys.* **2015**, *17*, 2259–2267.
- [10] a) O. Mó, M. Yáñez, I. Alkorta, J. Elguero, *J. Mol. Model.* **2013**, *19*, 4139–4145; b) M. M. Montero-Campillo, A. M. Lamsabhi, O. Mó, M. Yáñez, *J. Mol. Model.* **2013**, *19*, 2759–2766; c) M. Yáñez, O. Mó, I. Alkorta, J. Elguero, *Chem. Eur. J.* **2013**, *19*, 11637–11643.
- [11] a) M. Yáñez, O. Mó, I. Alkorta, J. Elguero, *Chem. Phys. Lett.* **2013**, *590*, 22–26; b) O. Mó, M. Yáñez, I. Alkorta, J. Elguero, *Mol. Phys.* **2014**, *112*, 592–600.
- [12] a) D. J. Henry, C. J. arkinson, P. M. Mayer, L. Radom, *J. Phys. Chem. A* **2001**, *105*, 6750–6756.

Received: April 18, 2016

Published online: June 16, 2016

## Supporting Information

### **Exergonic and Spontaneous Production of Radicals through Beryllium Bonds**

*Oriana Brea, Ibon Alkorta, Otilia M<sup>o</sup>, Manuel Y<sup>a</sup>ñez,\* Jos<sup>e</sup> Elguero, and In<sup>e</sup>s Corral*

ange\_201603690\_sm\_miscellaneous\_information.pdf



**The supplementary information contains the following information:**

1. Computational details.
2. Tables S1- S3.
3. Figures S1- S7.

## Computational Details

The dissociation energies of all the systems included in this study were calculated by means of the G4 ab initio composite model,<sup>[1]</sup> which provides total energies effectively at the CCSD(T,full)/G3LargeXP + HF limit level. For those systems, however, showing a clear multireference character, the CASPT2//CASCF(14,9)/cc-pVTZ protocol<sup>[2,3]</sup> was employed instead for the geometry optimizations. Although the reliability of the G4 theory in this context is ratified by the excellent agreement between the calculated dissociation energies for the isolated Y-R (Y = F, OH, NH<sub>2</sub>) bases and the experimental values, we have decided to assess the correctness of this approach also when the dissociation of the BeH<sub>2</sub>F-R complexes is concerned, since this composite model is based on the use of B3LYP/6-31G(2df,p) optimized geometries. In our assessment we have used as a reference total energies obtained at the CCSD(T)/cc-pVTZ level and using MP2/cc-pVTZ optimized geometries, and as illustrated in Table S2 the agreement between both theoretical models is very good. Tables S1 and S2 also compare the performance of different monoconfigurational methods on the prediction of the geometries of the beryllium complexes taking the multireference method CASPT2 as benchmark. As shown in tables S1 and S2, the differences between the CCSD(T) and CASPT2 geometries and dissociation energies are minimal, which is consistent with the calculated T1 diagnostic<sup>[4]</sup> for [BeH<sub>2</sub>F]·.

To accurately describe the dissociative potential energy curves (minimum energy paths), that unavoidably require to account for the multireference character of the dissociating system, particularly at the region close to the crossing of the two states, we have carried out CASPT2//CASCF(14,9) calculations. Smaller active spaces such as (10,6) were instead used to optimize the beryllium complexes. Final energies were computed using the larger (14,9) active space. Details on the composition of the active spaces used can be found in Figure S7.

The analysis of the electron density redistribution triggered by the formation of the beryllium bonds was done by using the atoms in molecules (AIM) theory.<sup>[5]</sup> In this formalism it is possible to calculate the electron density at the bond critical points, which allows to identify bond weakening or bond reinforcement processes depending on whether the corresponding electron density decreases or increases respectively.

[1] L. A. Curtiss, P. C. Redfern and K. Raghavachari, *J. Chem. Phys.* **2007**, *126*, 12.

[2] B. O. Roos, in *Ab initio Methods in Quantum Chemistry II*, ed. K. P. Lawley, Wiley, Chichester, **1987**.

[3] K. Andersson, P. Å. Malmqvist and B. O. Roos, *J. Chem. Phys.* **1992**, *96*, 1218.

[4] T. J. Lee and P. R. Taylor, *Int. J. Quant. Chem.* **1989**, *36*, 199-207.

[5] R. F. W. Bader, *Atoms in Molecules. A Quantum Theory*, Clarendon Press, Oxford, **1990**.

Table S1. Comparison of the performance of different methods in the prediction of the geometries of the lewis bases and beryllium complexes studied. Bond distances are in Angstroms (Å) and Angles in degrees (°). All calculations were performed with the cc-pVTZ basis set, except for DFT calculations that used the 6-31G(2df,p) basis set.

Molecule	B3LYP			MP2			CCSD(T)			CASPT2//CASSCF (10,6) / (5,3)*		
	BeF	FR	BeX	BeF	FR	BeX	BeF	FR	BeX	BeF	FR	BeX
<b>FF</b>	-	1.40	-	-	1.40	-	-	1.42	-	-	1.42	-
<b>BeH<sub>2</sub>FF**</b>	2.61	1.39	1.33	2.65	1.40	1.33	2.62	1.42	1.33	2.65	1.43	1.33
<b>FOH</b>	-	1.43	-	-	1.42	-	-	1.44	-	-	1.41	-
<b>BeH<sub>2</sub>FOH</b>	1.67	1.47	1.37	1.76	1.44	1.34	1.72	1.47	1.38	1.74	1.47	1.37
<b>FNH<sub>2</sub></b>	-	1.43	-	-	1.42	-	-	1.43	-	-	1.41	-
<b>BeH<sub>2</sub>FNH<sub>2</sub></b>	1.69	1.48	1.34	1.73	1.47	1.34	1.71	1.47	1.37	1.71	1.47	1.36
<b>FNO</b>	-	1.52	-	-	1.53	-	-	1.50	-	-	1.52	-
<b>BeH<sub>2</sub>FNO</b>	1.42	2.31	1.36	1.43	2.30	1.35	1.40	2.63	1.35	1.40	2.71	1.34
<b>[BeH<sub>2</sub>F]·</b>	1.37	-	1.43	1.38	-	1.43	1.38	-	1.44	1.39	-	1.43

Molecule	B3LYP		MP2		CCSD(T)		CASPT2//CASSCF (10,6) / (5,3)*	
	XBeX	BeFR	XBeX	BeFR	XBeX	BeFR	XBeX	BeFR
<b>BeH<sub>2</sub>FF**</b>	178	180	177	119	176	111	176	112
<b>BeH<sub>2</sub>FOH</b>	149	110	151	109	148	109	150	109
<b>BeH<sub>2</sub>FNH<sub>2</sub></b>	148	117	149	103	148	116	148	116
<b>BeH<sub>2</sub>FNO</b>	114	103	116	105	108	101	106	102
<b>[BeH<sub>2</sub>F]·</b>	68	-	63	-	65	-	65	-

\* The [BeH<sub>2</sub>F]· radical was optimized at CASPT2//CASSCF(5,3) level of theory, and the BeH<sub>2</sub>FNO complex at CASPT2//CASSCF(12,9).

\*\* The B3LYP functional fails to accurately describe the shape of the PES for the BeH<sub>2</sub>FF complex. The B3LYP BeH<sub>2</sub>FF geometry actually corresponds to a second order transition state of the CASPT2 PES.

Table S2. Comparison of the performance of different methods in the prediction of the dissociation energies [ $\text{BeH}_2:\text{FR} \rightarrow (\text{BeH}_2\text{F})\cdot + \text{R}\cdot$ ]. All values are in  $\text{kJ mol}^{-1}$  and the calculations were performed with cc-pVTZ basis set, except for the G4 energies.

Molecule	G4	CCSD(T)	CASPT2//CAS SCF(10,6)	CASPT2//CASS CF(14,9)
$\text{BeH}_2\text{FF}$	-217.7	-212.0	-227.2	-222.7
$\text{BeH}_2\text{FOH}$	-133.4	-131.8	-147.3	-118.0
$\text{BeH}_2\text{FNH}_2$	-42.6	-43.9	+22.7	-35.5
$\text{BeH}_2\text{FNO}$	-12.8	-0.5	-	6.0*

\* The  $\text{BeH}_2\text{FNO}$  energies were calculated using a (12,9) active space.

Table S3. T1 and D1 diagnostics calculated at CCSD(T)/cc-pVTZ level of theory.

Molecules	T1*	D1*
$\text{BeH}_2\text{FF}$	0.01051735	0.02911799
$\text{BeH}_2\text{FOH}$	0.01600998	0.05538680
$\text{BeH}_2\text{FNH}_2$	0.01307411	0.04304478
$\text{BeH}_2\text{FNO}$	0.03219209	0.13364582
$\text{BeH}_2\text{F}\cdot$	0.01747493	0.04011864

\*For values of  $T1 > 0.02$  and  $D1 > 0.05$  the system is considered to be multireference.

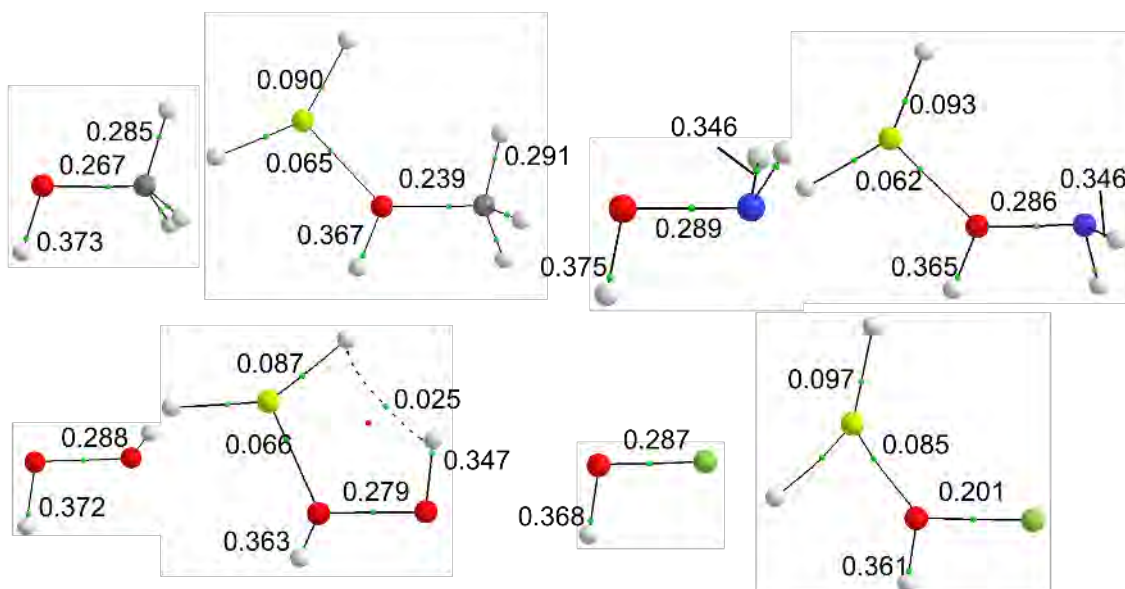


Figure S1. Molecular graphs for OH-R (R =  $\text{CH}_3$ ,  $\text{NH}_2$ ,  $\text{OH}$ ,  $\text{F}$ ) Lewis bases and their complexes with  $\text{BeH}_2$ . Electron densities are in a.u. Bond and ring critical points are indicated with green and red dots, respectively.

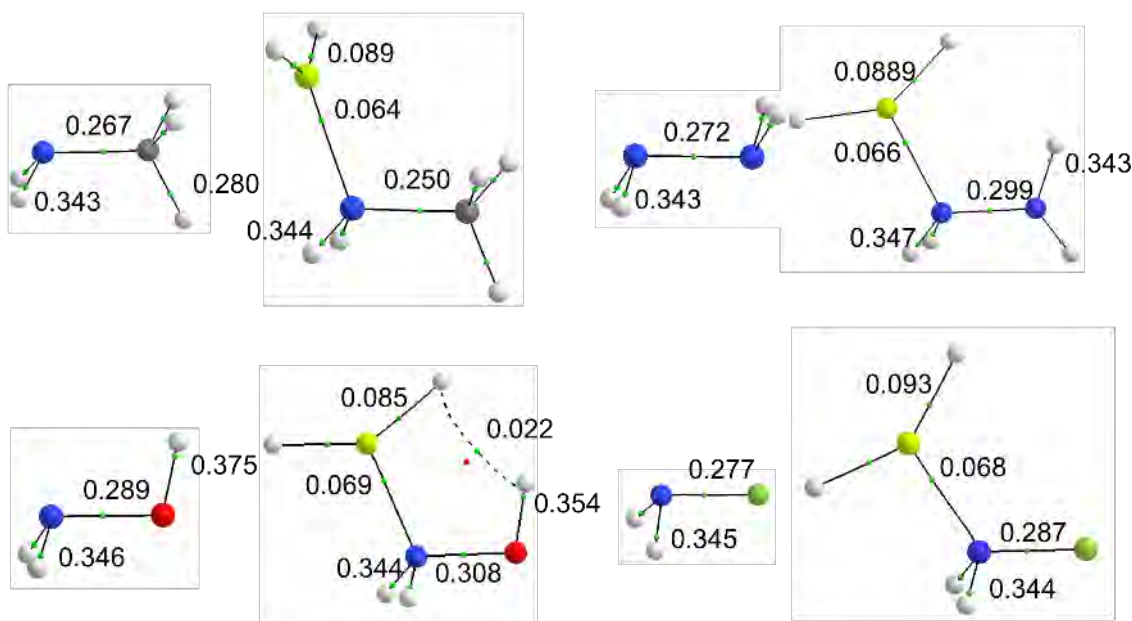


Figure S2. Molecular graphs for  $\text{NH}_2\text{-R}$  ( $\text{R} = \text{CH}_3, \text{NH}_2, \text{OH}, \text{F}$ ) Lewis bases and their complexes with  $\text{BeH}_2$ . Electron densities are in a.u. Bond and ring critical points are indicated with green and red dots, respectively.

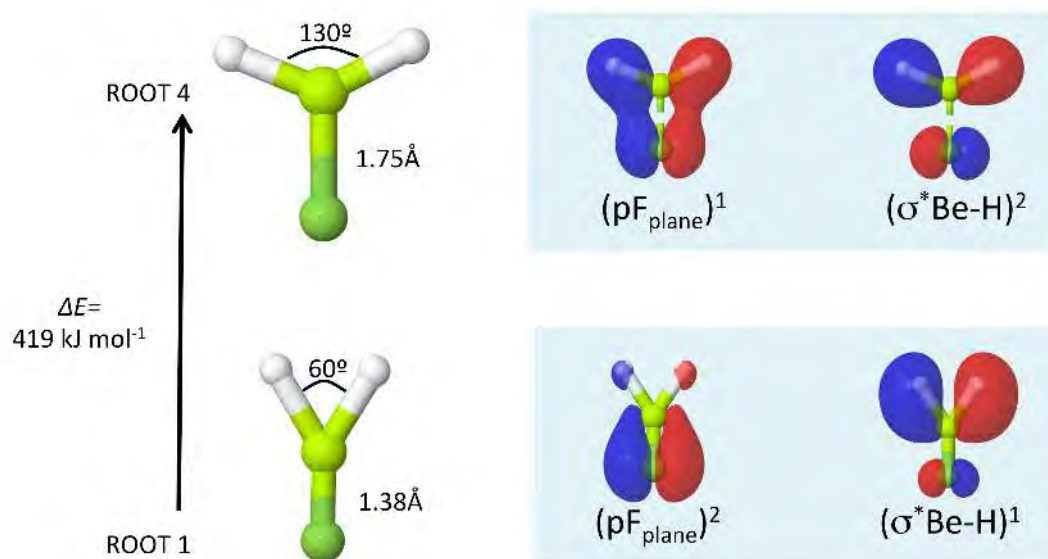


Figure S3. Comparison of the geometries and energies of  $\cdot\text{BeH}_2\text{F}$  ground state and the  $\text{BeH}_2\text{F}\cdot$  excited state. The ground state corresponds to the system with the spin localized in the  $\text{BeH}_2$  moiety, while in the third excited state it is in the F atom. On the right, the most relevant orbitals and their occupation. The calculation was performed at SA(6)-CASPT2//CASSCF(9,6)/cc-pVTZ level of theory.

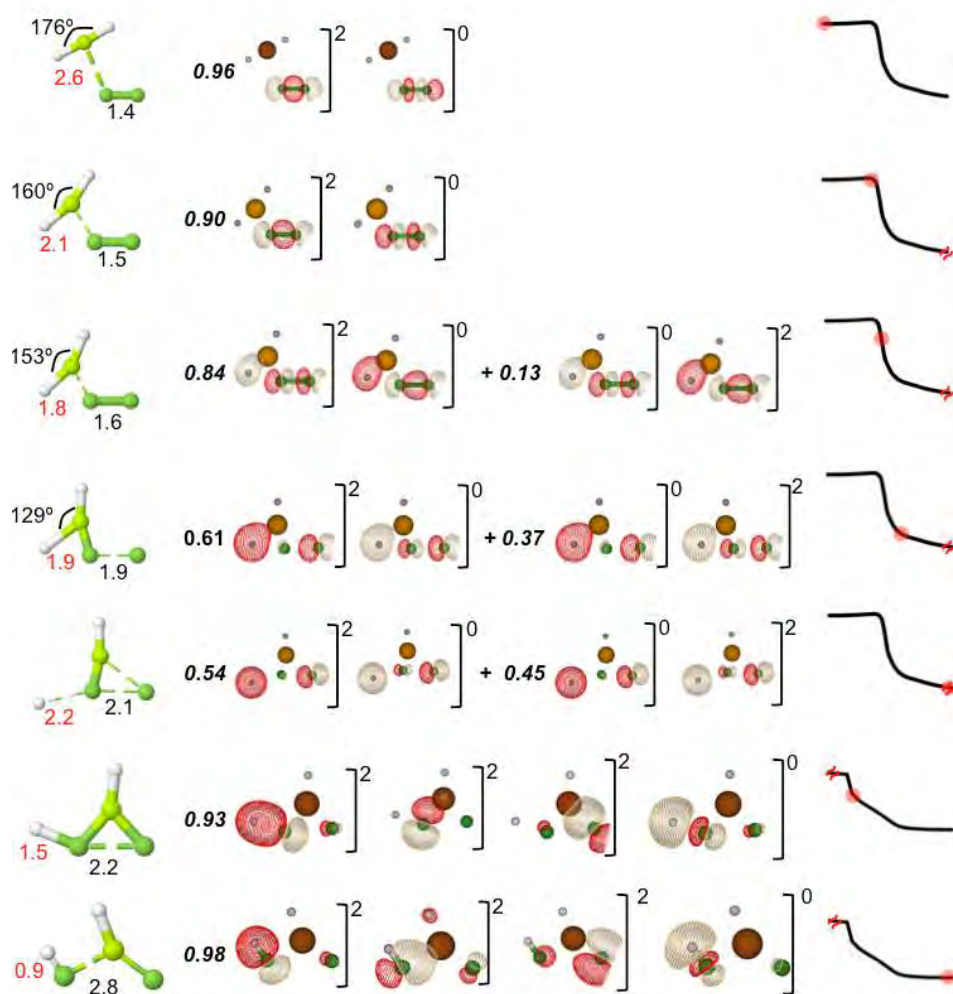


Figure S4. Wavefunction analysis (in bold the configuration's weight) and geometrical parameters along the IRC path for the  $\text{BeH}_2\text{FF}$  system. From the reactant to the transition state (TS) (F-F distance equal to 1.5 Å) there are not significant changes in the electronic configuration, after the TS the system evolves to a biradical state and finally reaches the neutral products  $\text{HF}:\text{BeHF}$ . The bond distances are in Angstroms (Å) and angles in degrees (°). The calculation was performed at CASPT2//CASSCF(14,9)/cc-pVTZ level of theory.

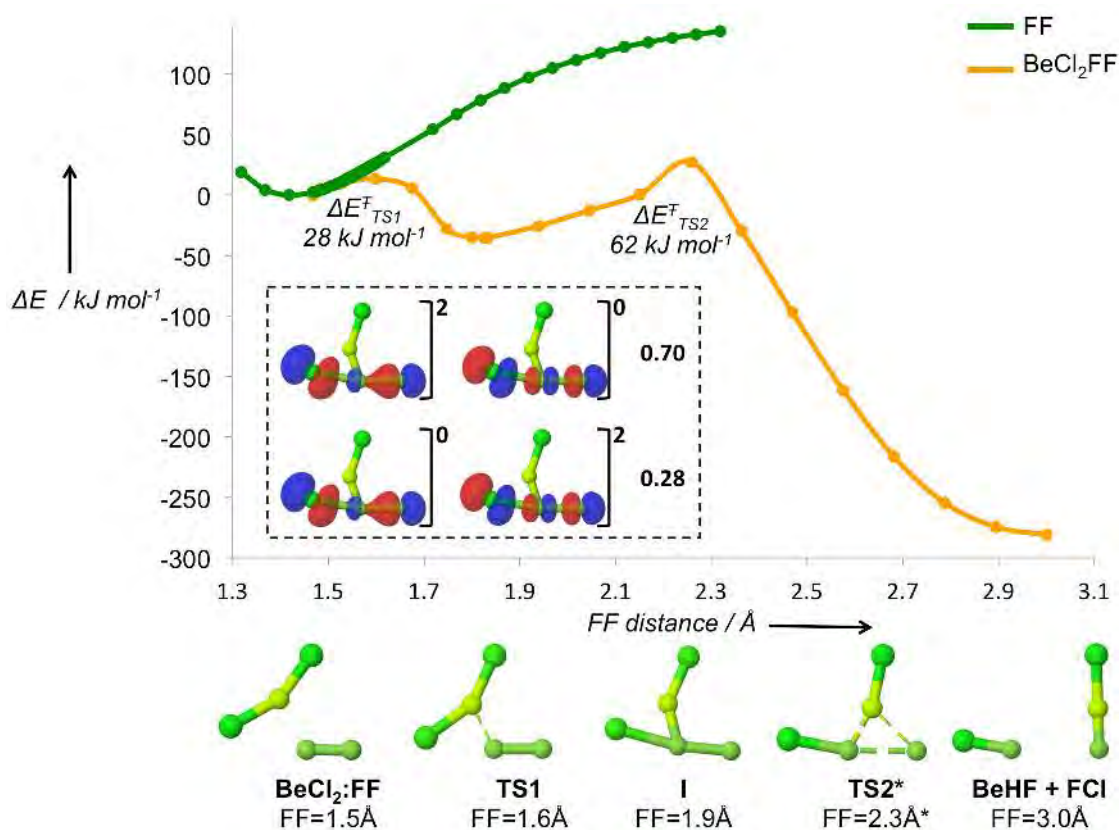


Figure S5. Potential energy curves corresponding to the dissociation of the F–F bond for the  $\text{F}_2$  isolated molecule (green curve) and for the  $\text{BeCl}_2\text{:FF}$  complex (orange curve). The inset represents the orbitals for the radical intermediate that later evolves to the neutral products  $\text{ClF}:\text{BeClF}$ . The IRC calculation for the  $\text{BeCl}_2\text{:FF}$  was performed at CASPT2//CASSCF(14,9)/cc-pVTZ and for  $\text{F}_2$  CASPT2//CASSCF(10,6)/cc-pVTZ level of theory. \*The second transition state was approximated by a linear geometry interpolation between the intermediary (I) and the neutral products.

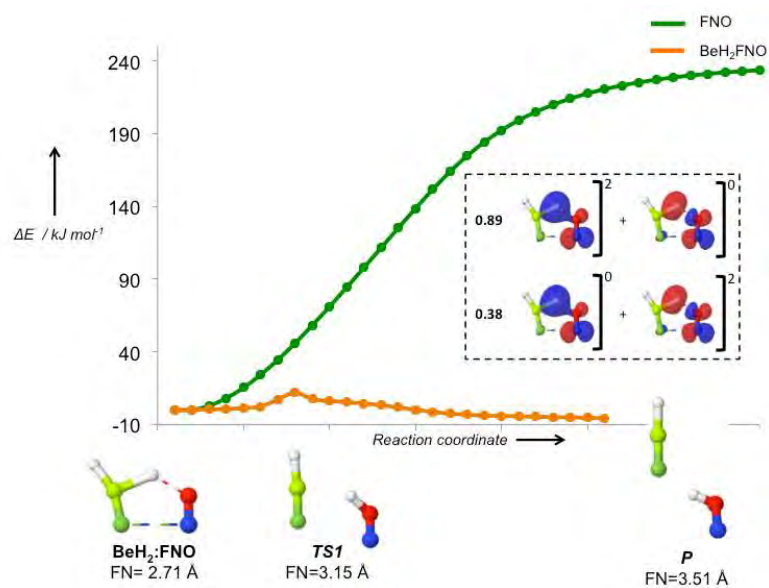


Figure S6. Potential energy curves corresponding to the dissociation of the F-NO bond for isolated FNO (green curve) and for the  $\text{BeH}_2\text{:FNO}$  complex (orange curve). The inset represents the orbitals for the  $\text{BeH}_2\text{:FNO}$  complex that evolves through TS1 to the neutral products (HNO + BeHF). The calculations were performed at CASPT2//CASSCF(12,9)/cc-pVTZ level of theory.



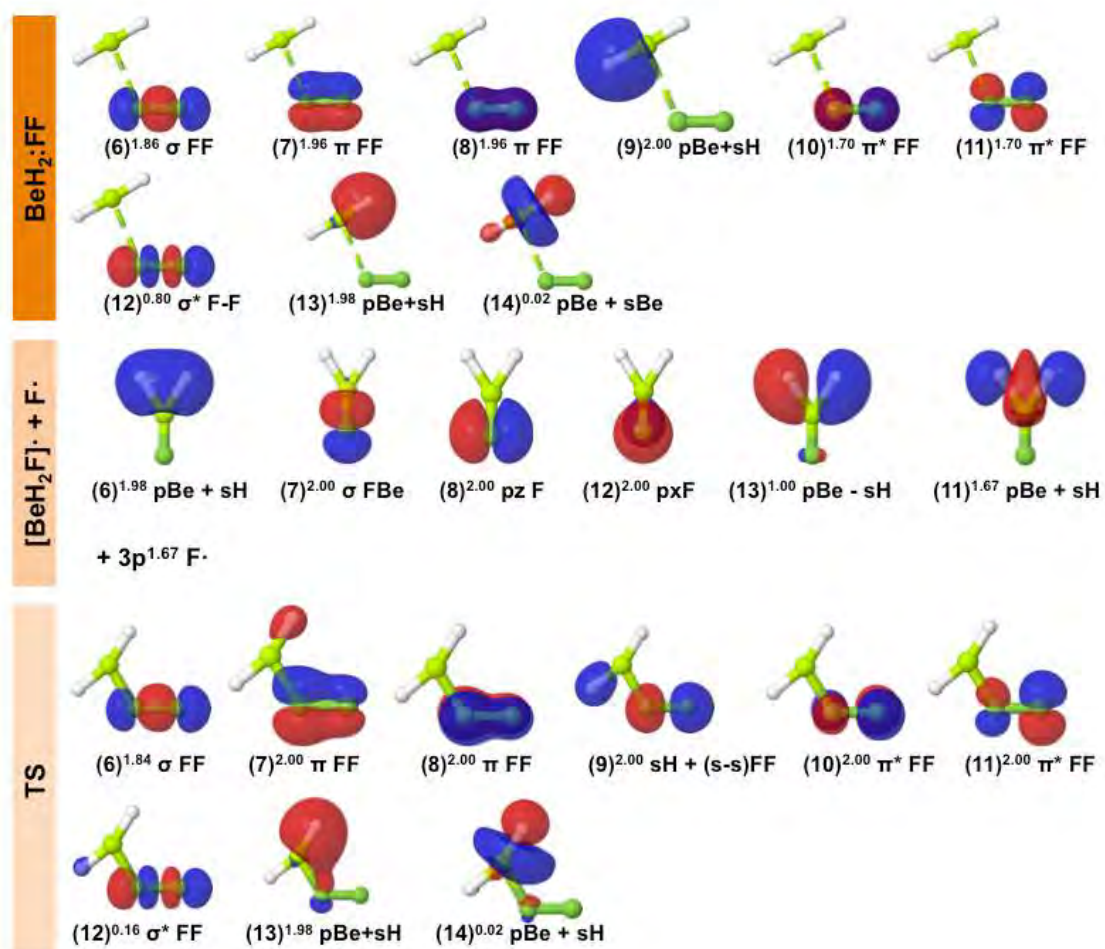


Figure S7. SA(3)-CASSCF(14,9) active space used for the description of the reactant: BeH<sub>2</sub>FF, product: ·BeH<sub>2</sub>F + F· and transition state. The MOs occupations are presented as superscripts.

---

## B.3 CHAPTER BOOK

*Intramolecular beryllium bonds. Further insights into resonance assistance phenomena*



## CHAPTER X

### **Intramolecular beryllium bonds. Further insights into resonance assistance phenomena**

O. Brea<sup>a</sup>, I. Alkorta<sup>b</sup>, I. Corral<sup>a</sup>, O. Mó<sup>a</sup>, M. Yáñez<sup>a\*</sup> and J. Elguero<sup>b</sup>

<sup>a</sup> Universidad Autónoma de Madrid, Departamento de Química, Facultad de Ciencias, Módulo 13, Campus de Excelencia UAM-CSIC, Cantoblanco, Madrid, 28049, Spain

<sup>b</sup> Instituto de Química Médica, CSIC, Juan de la Cierva, 3, Madrid, 28006, Spain

\*Corresponding contributor. E-mail: [manuel.yanez@uam.es](mailto:manuel.yanez@uam.es)

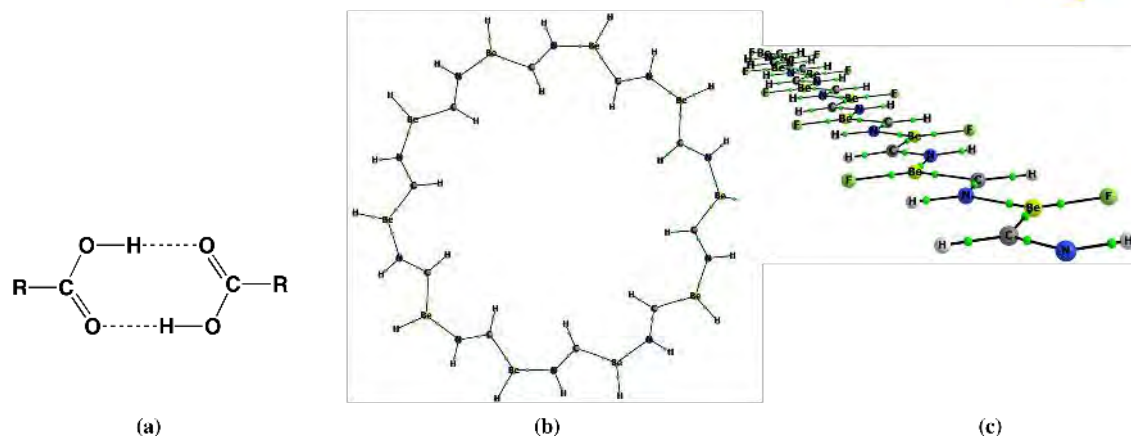
## Abstract

Beryllium bonds are acid-base closed-shell interactions in which the Lewis acid is a BeXY derivative. These molecular linkers share common characteristics with hydrogen bonds (HBs), though they produce strong distortions on the electron density distribution of the Lewis base participating in the interaction. The characteristics of intramolecular beryllium bonds (IMBeBs) in which a basic site interacts with a BeH group of the same molecule have been analyzed through DFT and high-level ab initio calculations. IMBeBs are stronger than the intramolecular HBs in analogous environments, and also stronger in unsaturated compounds. However, this larger strength does not arise from resonance assisted phenomena, but from a larger basicity of the basic site and a larger Lewis acidity of the BeH group when belonging to an unsaturated moiety. Hence, it is the high strength of the beryllium bond what triggers an enhancement of the resonance within the system, and not the resonance stabilization of the system that renders the IMBeB stronger. The dimerization of malonaldehyde-like structures is also analyzed. These dimers are stabilized by Be-H-Be bonds similar to the ones responsible for the stability of diborane. The substitution of H by halogen atoms, alkyl and phenyl groups in these bridges is also investigated.

## X.1 Introduction

A significant number of phenomena in chemistry are related to the interaction between close-shell systems. To this category belong most of the non-covalent interactions known up to date, such as hydrogen bonds,<sup>1-3</sup> halogen bonds,<sup>4-6</sup> di-hydrogen bonds,<sup>7, 8</sup> pnictogen bonds,<sup>9-12</sup> tetrel,<sup>13, 14</sup> and chalcogen interactions,<sup>15-17</sup> and beryllium bonds.<sup>18, 19</sup> All the aforementioned linkages can be classified as acid-base interactions in the Lewis sense, because in all cases one of the interacting subunits behaves as a Lewis base able to transfer some electronic charge to the second interacting subunit acting as a Lewis acid. For the particular case of the well known hydrogen bonds,  $X-H \cdots A$ , the proton acceptor, A, is the system which behaves as a Lewis base by donating charge from its electron lone-pairs to the antibonding X-H orbitals of the proton donor, leading to a lengthening of the corresponding X-H bond and to a red-shifting of its X-H stretching frequency, both effects being signatures of these kinds of non-covalent interactions. In beryllium bonds, the Lewis acid is a BeXY derivative,<sup>18</sup> whereas the Lewis base is any compound with some electron donor capacity, namely systems having sites with lone-pairs of electrons. In this case the charge donation from the base goes not only to the Be-X or Be-Y antibonding orbitals, resulting in a lengthening of the corresponding bonds, but also to the empty *p* orbitals of Be atom, leading to a hybridization change of this atomic center reflected in a significant bending of the X-Be-Y moiety.<sup>18</sup>

Particularly interesting situations arise when the center acting as a Lewis base and that behaving as a Lewis acid form part of the same molecular compound, usually known as ditopic systems.<sup>20-23</sup> When the electron affinity of the acidic center is significant and the electron donor capacity of the basic center is also high, the aforementioned coincidence opens the possibility of self-assembling, and the formation of polymers becomes an important issue. Paradigmatic examples can be found in the carboxylic acid dimers<sup>24-27</sup> stabilized through two intermolecular hydrogen bonds (HBs) in which the carbonyl group of one of the monomers behaves as a basic center with respect to the hydroxyl group acting as the Lewis acid of the second monomer (see scheme 1a). This is also the case, for instance of (iminomethyl)beryllium hydride which is able to form *n*-mers which may be cyclic (see scheme 1b) or linear (see scheme 1c),<sup>28</sup> because the terminal imino group is an excellent electron donor and the terminal Be-X (X = H, F) is a very good electron acceptor, so the formation of quite strong  $Be \cdots N$  beryllium bonds give a substantial stability to the dimers, trimers, tetramers and in general *n*-mers. In scheme 1 the structures of the cyclic and linear decamers are shown.<sup>28</sup>



**Scheme X.1** Self-assembled structures triggered the formation of: (a) hydrogen bonds, (b) and (c) beryllium bonds.

Many other ditopic ligands are the building blocks of a large series of coordination polymers<sup>29</sup> and linear coordination supramolecules<sup>30, 31</sup> or lead to rather interesting molecular aggregates,<sup>32, 33</sup> or play a role in supramolecular gel chemistry.<sup>34</sup> Ditopic ligands have been also employed for solvent extraction of cations and anions profiting their ability to behave simultaneously as a base and as an acid.<sup>35</sup>

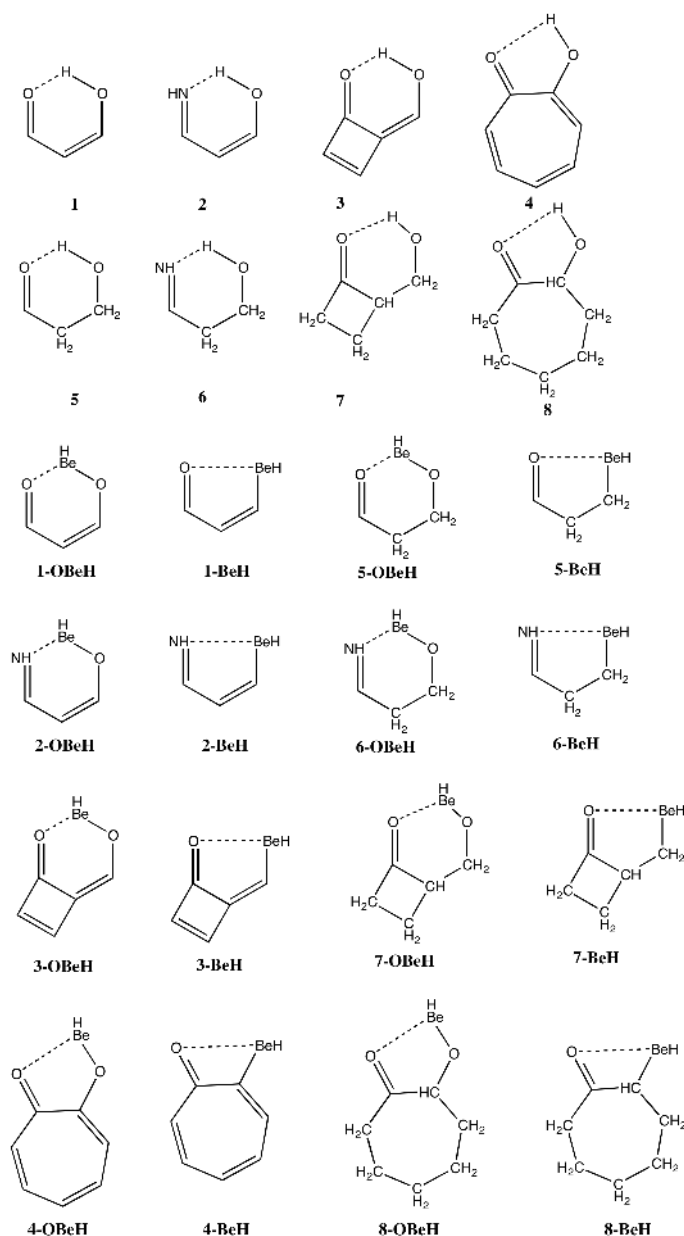
However, in more flexible ditopic systems it is also possible to observe intramolecular interactions between the two active sites. This kind of interactions are not possible, for instance, in normal carboxylic acids where the planarity and the rigidity of the acidic function prevents the hydroxyl group to approach sufficiently to the carbonyl group to form an intramolecular HB, but it is possible in many other compounds, such as malonaldehyde<sup>36, 37</sup> and its derivatives, tropolone,<sup>38, 39</sup> in diols, sugars and a pleiade of other organic and inorganic compounds. These intramolecular linkages are not exclusive of HBs, but can also involve chalcogen-chalcogen interactions<sup>15, 40</sup> or intramolecular halogen bonds.<sup>41-43</sup> One of the signatures of intramolecular interactions is the difficulty to establish quantitatively their energetic contribution to the stability of the molecule and, for this reason, the information about of the strength of intramolecular bonds is usually obtained through indirect magnitudes, such as the internuclear distances between the interacting centers, the electron density within the bonding region, or the shifting of some specific vibrational frequencies. This difficulty in accurately evaluating the interaction energy of an intramolecular interaction is closely related with the vagueness or ambiguity on the factors that may contribute to the strength of the interaction. A typical example of these foggy bases behind some useful concepts is the so called resonance assisted hydrogen bonds (RAHBs).<sup>44-50</sup> Indeed the strength of intramolecular HBs in unsaturated systems is clearly larger than in the saturated analogues. This clear evidence is usually explained by claiming that these linkages are stronger because they enhance the resonance in the unsaturated compound,<sup>44</sup> which is however not a so convincing argument.<sup>51, 52</sup> As a matter of fact several papers, among them several from our group,<sup>51-</sup>

<sup>60</sup> put in question not the effect but its interpretation as a resonance enhancement. The new viewpoint could be summarized by asserting that it is the unsaturated nature of the compound the factor behind the larger strength of the intramolecular linkage. In other words, the intramolecular HB is not stronger due to a resonance assisted effect, but is due to the fact that the interaction is assisted by the resonance of the system, due to several concomitant features. On the one hand, because the rigidity of the skeleton of an unsaturated compound strongly facilitates the interaction between the HB donor and the HB acceptor, and this is well reflected by the magnetic properties of the system, which are very sensible to structural details. On the other hand, because the presence of an unsaturation in the system modulates both the intrinsic basicity and the intrinsic acidity of the two active centers involved, enhancing the acid-base interaction.

The aim of the present chapter is three-fold: a) to investigate, for the first time, the nature and characteristics of intramolecular beryllium bonds in molecular environments similar to those in which different intramolecular hydrogen bonds have been found and characterized, b) to analyze these new intramolecular linkages to gain further insight into possible resonance assisted phenomena, and c) to explore whether these compounds are able to dimerize forming Be-Be bonds, and what are the characteristics of these bonds, taking into account that Be<sub>2</sub> is only bound by a very weak interaction arising only from electron correlation.

For this purpose, and in order to ensure that we are going to have a similar molecular environment to directly compare intramolecular beryllium bonds with intramolecular HBs, we have used as suitable model systems the Be derivatives which can be formed by making replacements in the acidic group (the hydroxyl group) of malonaldehyde (**1**), some of its derivatives (**2**, **3**) and tropolone (**4**) as well as in the corresponding saturated analogues (**5-7**)(see scheme 2). Two approaches were used to build up the compounds with intramolecular beryllium bonds: the substitution of the H atom of the hydroxyl group by a BeH group (compounds **n-OB<sub>n</sub>BeH**, **n** = 1,8) and the substitution of the whole hydroxyl group by a BeH group (compounds **n-BeH**, **n** = 1,8), as shown in scheme 2.





**Scheme X.2** Systems characterized by the existence of intramolecular hydrogen bonds (**1-8**) and the related compounds able to present intramolecular beryllium bonds, which are obtained from the former, by replacing the H atom of the OH group by a -BeH substituent (compounds **n-OBcH**, **n** = 1-8) or replacing the whole -OH group by a -BeH group (compounds **n-BcH**, **n** = 1-8).

## X.2 Computational Details

The geometries of the different compounds and complexes investigated in this study have been optimized by using the B3LYP functional associated with a 6-31+G(d,p) basis set expansion. The B3LYP approach combines the Becke's three-parameter<sup>61</sup> nonlocal hybrid exchange potential<sup>61</sup> with the nonlocal correlation functional of Lee, Yang and Parr<sup>62</sup> and it has been found to be rather reliable for the description of

intermolecular beryllium bonds.<sup>18</sup> Nevertheless, in order to ensure the reliability of this model for the description of intramolecular beryllium bonds, we have assessed the results obtained at the B3LYP/6-31+G(d,p) by using as a reference the G4 theory<sup>63</sup> for two derivatives, namely **1-OB<sub>e</sub>H** and **1-BeH**, as suitable examples. The G4 approach is a high-level ab initio composite method which uses B3LYP/6-31G(2df,p) optimized geometries and thermal corrections, and high-level empirical corrections, to yield final energies at an effective CCSD(T,full)/G3LargeXP + HF limit level.<sup>63</sup> This method is very well suited for the calculation of different thermodynamic magnitudes. Indeed, an assessment of the method on 454 experimental energies, yielded an average absolute deviation from experiment of 3.47 kJ mol<sup>-1</sup> (0.83 kcal mol<sup>-1</sup>). However, since the G4 composite method, as mentioned above, is based also on the use of B3LYP optimized structures, we have assessed the reliability of these geometries by comparing them with those obtained at the MP2/6-31+G(d,p) level for the same two reference compounds. The agreement between both B3LYP and MP2 optimized geometries is rather good, although, in general, the B3LYP method tends to overbind the Be atom to the C=O basic site, but this effect does not compromise the conclusions of our analysis, based on general trends.

One signature of beryllium bonds is that they produce a significant distortion on the electron density distribution of the Lewis base participating in the interaction.<sup>64</sup> In order to quantitatively analyze these electron density perturbations we have used two different, but somehow complementary methods, namely the atoms in molecules (AIM) theory<sup>65</sup> and the Natural Bond Orbital (NBO) approach.<sup>66</sup> The AIM theory is based on the topological analysis of the electron density,  $\rho(\mathbf{r})$  and its Laplacian,  $\nabla^2\rho(\mathbf{r})$ . The topology of  $\rho(\mathbf{r})$  of any chemical system is characterized by the presence of maxima, associated with the position of the nuclei, saddle points located between two maxima or inside cyclic structures, usually named bond critical points (BCPs) and ring critical points (RCPs), respectively, and minima associated with the existence of cage structures. On top of that, the so called molecular graphs, which are the representation of the bond paths, defined as the lines of maximum density connecting two maxima and containing a BCP, provide an accurate description of the molecular structure since these molecular graphs are able to account for bent bonds, usually associated with ring-strain phenomena and which cannot be identified from the optimized geometries. Also importantly, the changes observed in the values of the electron density at the BCPs permit to quantitatively measure bond strengthening or bond weakening effects. These AIM calculations have been carried out by using the AIMAll program package.<sup>67</sup>

The NBO approach is very well suited to analyze the formation of the new linkages between a basic site and an acidic site, because it permits to quantify charge transfers between occupied and empty orbitals within a given molecular system, through the calculation of the second-order orbital interaction energies involved in

the interaction between these orbitals. Furthermore, this method, based on the use of localized natural orbitals, permits to describe the bonding of a molecule in terms of hybrid orbitals and core and lone pairs obtained as local block eigenvectors of the one-particle density matrix. The NBO approach also allows to calculate the Wiberg bond order (WBO)<sup>68</sup> which is a good index to measure the strength of a chemical bond. All the NBO calculations have been done by using the NBO-3.1 program package.<sup>69</sup>

## X.3 Results and Discussion

### X.3.1 Intramolecular beryllium bonds in malonaldehyde-like systems

The optimized structures of compounds **1-OBeH** and **1-BeH** are shown in Figure 1. The first conspicuous fact is that in all these compounds a rather strong O-Be intramolecular bond is formed, since the O-Be distances are much smaller than the sum of the van der Waals radii of both atoms, and in all cases a BCP is located within the O-Be bonding region with electron densities of the same order of magnitude as the normal covalent bonds between Be and H atoms. A relative idea of the strength of these intramolecular O-Be bonds can be achieved by comparing the relative stability of the cyclic forms shown in Figure 1 with the conformers in which the alkyl chain is extended and no contact between the BeH group and the oxygen atom of the carbonyl group can be established. From now on these open structures will be named adding **(t)** to the name of the corresponding cyclic conformer.

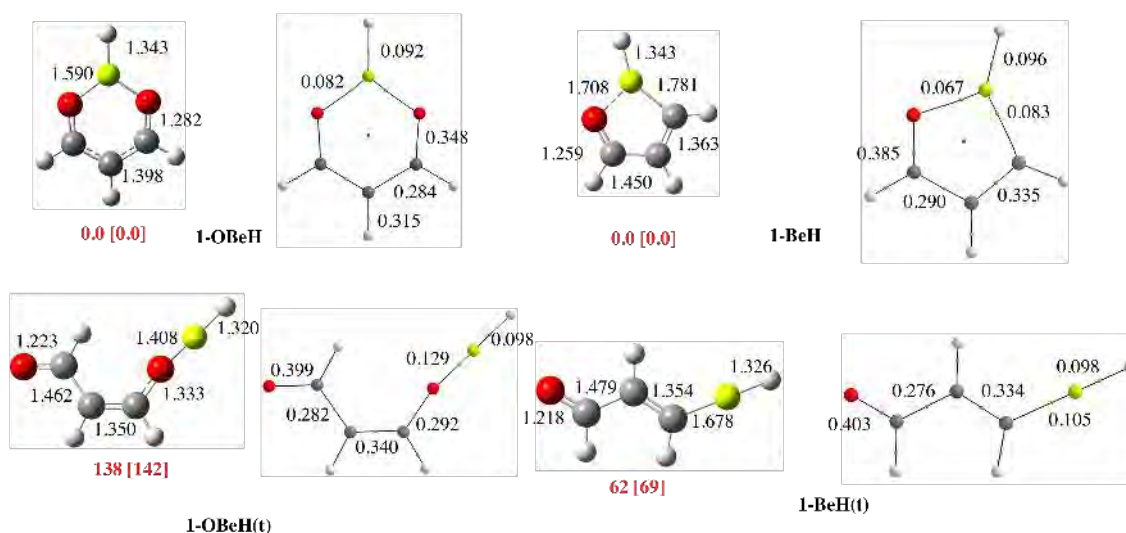
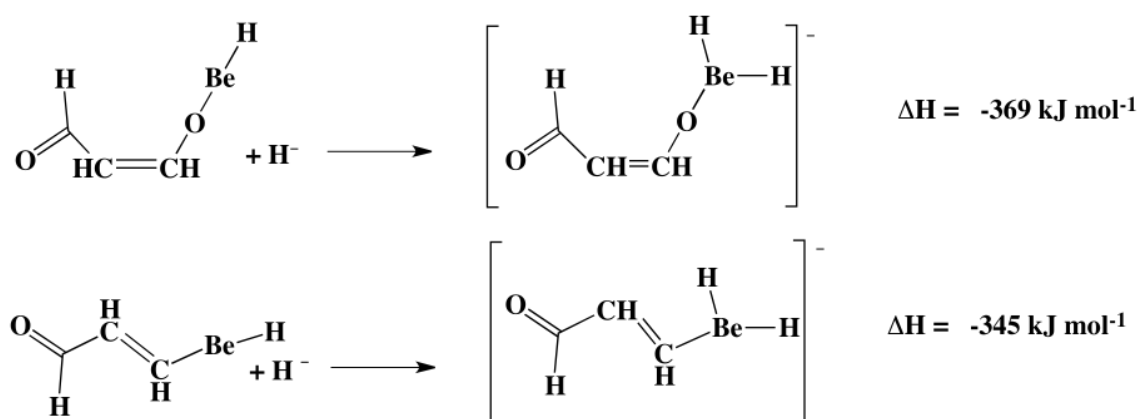


**Figure X.1** B3LYP/6-31+G(d,p) optimized structures and molecular graphs of unsaturated compounds showing a O...Be intramolecular beryllium bonds and their corresponding open conformers. In red, the relative stabilities of the open forms with respect to the cyclic ones are given in kJ mol<sup>-1</sup>. Values in square brackets were calculated at the G4 level of theory. Internuclear distances are in Å. In the molecular graphs, green and red dots denote BCPs and RCPs respectively. Electron densities are in a.u.

It can be seen that both **1-OB<sub>e</sub>H** and **1-BeH** cyclic structures are more stable than the corresponding open forms, indicating that the new intramolecular O···Be bond significantly contributes to the stabilization of the former with respect to the latter. A comparison between the molecular graphs shows that on going from the open to the cyclic structure a significant decrease of the electron density at the O-BeH and the C-BeH bonds takes place. This bond weakening is reflected in a sizable lengthening of these bonds in the cyclic structure, but this destabilizing feature is counterbalanced by the formation of the new Be···O intramolecular beryllium bond. A comparison of the Be···O internuclear distance, the value of the electron density at the corresponding BCP, and the WBO (0.27 vs. 0.11) shows that the intramolecular beryllium bond is stronger in the **1-OB<sub>e</sub>H** than in **1-BeH**. Consistently, the energy gap between the cyclic structure and the open one is also significantly larger for **1-OB<sub>e</sub>H** than for **1-BeH**. It is worth noting that the agreement between the relative energies obtained using the high-level G4 approach and the less computationally demanding B3LYP/6-31+G(d,p) theoretical model is rather good.

The stronger Be···O beryllium bond in **1-OB<sub>e</sub>H** is a consequence of two concomitant facts: the larger intrinsic basicity of the carbonyl group and the larger intrinsic acidity of the BeH group of this structure with respect to those of the **1-BeH** compound. It is rather obvious that the BeH group of **1-OB<sub>e</sub>H** should be a better Lewis acid than the same group in **1-BeH** compound, because in the former the Be atom is attached to an electron withdrawing group (C-O) whereas in the latter is attached to a carbon atom. Indeed, this prediction is corroborated by the G4 calculated hydride affinity of the corresponding open forms (see scheme 3).



**Scheme X.3** Hydride affinities of compounds **1-OB<sub>e</sub>H(t)** and **1-BeH(t)** calculated at the G4 level of theory.

The enhanced basicity of the C=O group of **1-OB<sub>e</sub>H** is also confirmed by the G4 calculated proton affinity of compound **1-OB<sub>e</sub>H(t)** (853 kJ mol<sup>-1</sup>) which is 45 kJ mol<sup>-1</sup> larger than that of compound **1BeH(t)** (808 kJ

$\text{mol}^{-1}$ ). All these findings are consistent with the results of the NBO analysis. According to this approach, the intramolecular beryllium bond in **1-OB<sub>e</sub>H** molecule is a consequence of a strong dative bond (with a second-order interaction energy of  $99 \text{ kJ mol}^{-1}$ ) from one of the oxygen lone-pairs of the carbonyl group into the empty  $p$  orbital (actually a  $sp^2$  hybrid) of Be atom. It is the population of the  $p$  orbital of the metal which is responsible for the bending of the O-Be-H, because the hybridization of the Be atom, changes from  $sp$  in the open forms, where no beryllium bond is possible, to  $sp^2$  in the cyclic structures. A similar charge transfer into the  $\sigma_{\text{BeH}}^*$  antibonding orbital, with a second order interaction energy of  $133 \text{ kJ mol}^{-1}$ , is responsible for the lengthening of the Be-H bond that is observed on going from the open form to the cyclic one. For **1-BeH**, the aforementioned charge donation from the CO group to Be is smaller, due as mentioned above to a smaller electron donor capacity of the former and a smaller electron acceptor ability of the latter. Hence, the second order interaction energy between the oxygen lone-pair and the empty  $p$  orbital of Be is only  $67 \text{ kJ mol}^{-1}$ , and the one corresponding to the interaction with the  $\sigma_{\text{BeH}}^*$  antibonding orbital  $110 \text{ kJ mol}^{-1}$ .

The strength of the  $\text{C}=\text{O}\cdots\text{Be}$  interaction in **1-OB<sub>e</sub>H** is responsible for the symmetric arrangement of the O-Be-O bridge, which differs from the behavior observed for malonaldehyde, where the O-H-O bridge is clearly non symmetric with an O-H distance much larger for the intramolecular hydrogen bond than for the O-H group acting as proton donor. We will come back later on to this question.

The situation is different when dealing with the corresponding saturated analogues, whose optimized structures and molecular graphs are shown in Figure 2.

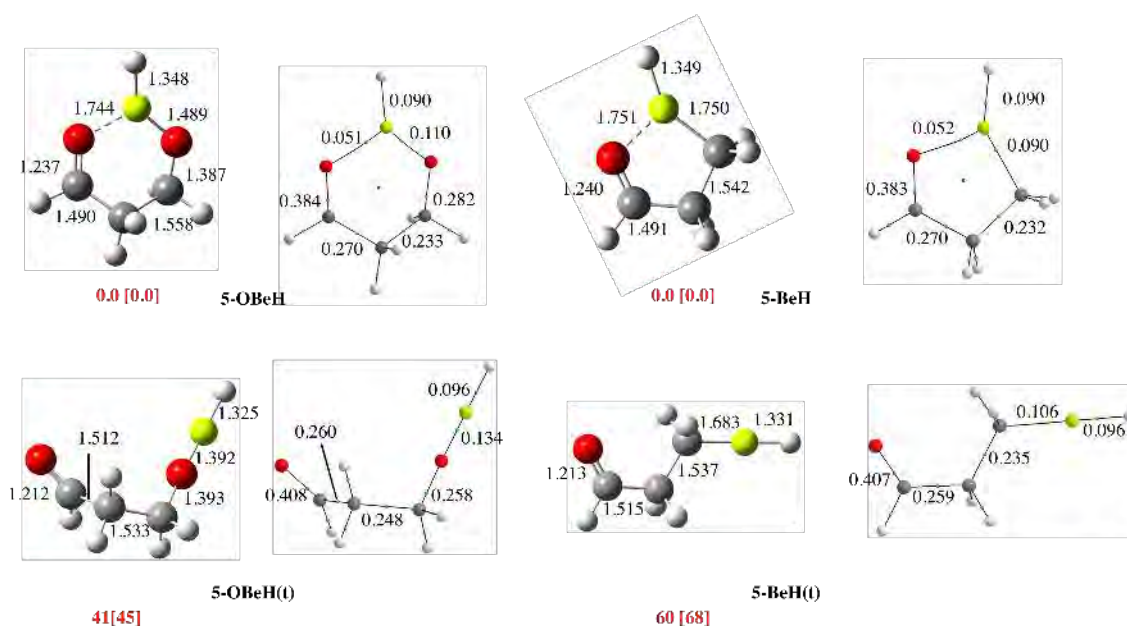
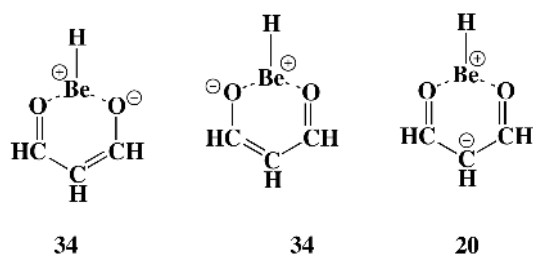


**Figure X.2** B3LYP/6-31+G(d,p) optimized structures and molecular graphs of saturated compounds showing a  $\text{O}\cdots\text{Be}$  intramolecular beryllium bonds and their corresponding open conformers. Same conventions as in Figure 1.

A comparison of Figures 1 and 2 clearly shows that the O···Be intramolecular beryllium bond in both **5-OB<sub>e</sub>H** and **5-BeH** compounds is weaker than in the corresponding unsaturated counterparts, **1-OB<sub>e</sub>H** and **1-BeH**. The same was observed when the intramolecular hydrogen bond of malonaldehyde was compared with that in its saturated analogue, which was frequently used as an argument in favor of resonance assistance in malonaldehyde. However, the main reason of the substantial decrease in the strength of the O···Be beryllium bond in **5-OB<sub>e</sub>H**, and **5-BeH** as compared with the one in **1-OB<sub>e</sub>H** and **1-BeH**, respectively is again twofold: i) the decrease in the electron donor ability of the carbonyl group in **5-OB<sub>e</sub>H** and **5-BeH** as compared with those of **1-OB<sub>e</sub>H** and **1-BeH**, respectively; ii) the concomitant decrease of the Lewis acidity of the corresponding BeH group. Indeed, the G4 calculated proton affinities for **5-OB<sub>e</sub>H(t)** and **5-BeH(t)** (833 and 793 kJ mol<sup>-1</sup>, respectively) are clearly lower than those for the unsaturated counterparts **1-OB<sub>e</sub>H(t)**, **1-BeH(t)** (853 and 808 kJ mol<sup>-1</sup>, respectively), as well as the corresponding hydride affinities (318 and 311 kJ mol<sup>-1</sup>, to be compared with the values in Scheme 3).

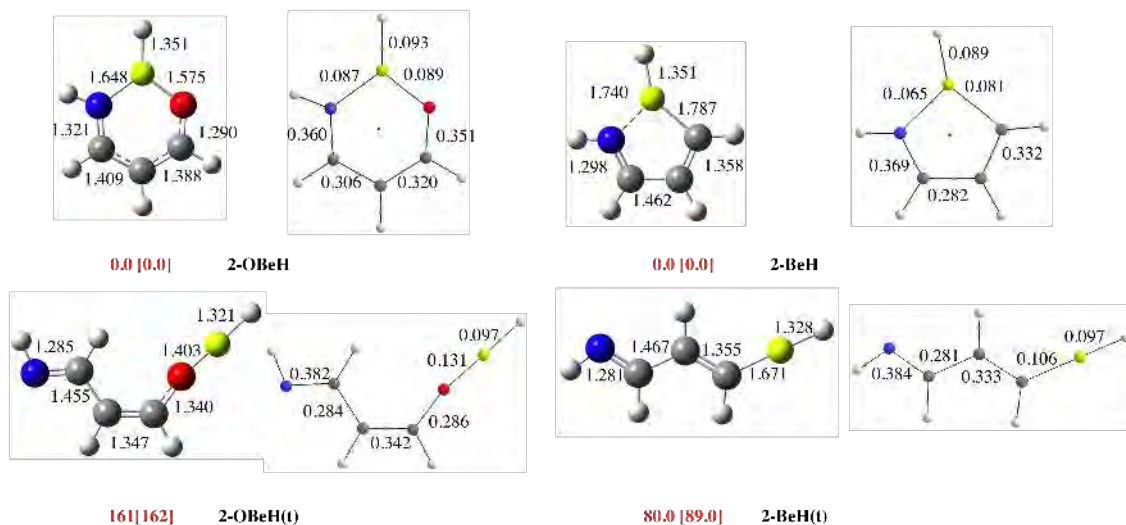
However, in contrast with the unsaturated analogues, in both **5-OB<sub>e</sub>H** and **5-BeH** the intramolecular beryllium bond is of similar strength attending not only, to the O···Be distances but also to the densities at the BCPs and the WBOs (0.1 vs. 0.095), being only slightly stronger in the **5-OB<sub>e</sub>H** molecule. Still the basicity of the **5-OB<sub>e</sub>H** is 40 kJ mol<sup>-1</sup> greater than that of **5-BeH**, but, as indicated above, the acidity of **5-BeH** is 8 kJ mol<sup>-1</sup> larger than that of **5-OB<sub>e</sub>H**. These opposite effects partially counterbalance each other, with the result that the O···Be intramolecular bond is only slightly stronger in **5-OB<sub>e</sub>H** than in **5-BeH**. In this respect, it is important to note that whereas the energy gap between the **5-BeH** (cyclic) and the **5-BeH(t)** (open) forms is very similar to that between the corresponding unsaturated analogues, **1-BeH** and **1-BeH(t)** (See figures 1 and 2), the energy gap between **5-OB<sub>e</sub>H** and the **5-OB<sub>e</sub>H(t)** is much smaller than the one between **1-OB<sub>e</sub>H** and **1-OB<sub>e</sub>H(t)**. This seems to point out to an extra-stabilization of the unsaturated **1-OB<sub>e</sub>H** cyclic structure, likely due to some resonant effects. Indeed, as we have discussed in previous paragraphs, the formation of the intramolecular O···Be beryllium bond implies a rather large charge transfer from the oxygen lone-pairs of the carbonyl group to the empty orbitals of Be. This results in a deep distortion of the electron density distribution of the rest of the molecule, which is apparent by comparing the molecular graphs of the **1-OB<sub>e</sub>H** (cyclic) and the **1-OB<sub>e</sub>H(t)** (open) structures. Upon cyclization of the system a significant weakening of the covalent O-Be linkage and accordingly a reinforcement of the corresponding C-O bond is observed. Concomitantly, the densities at the C-C bonds are also affected, and the two clearly localized C-C bonds in the open **1-OB<sub>e</sub>H(t)** structure (one single and the other double) become in the cyclic **1-OB<sub>e</sub>H** identical by symmetry, with a density slightly higher than that associated to a C-C single bond (see Figure 1).

This electron density redistribution is in agreement with the picture that is obtained through the use of the Natural Resonance Theory (NRT)<sup>70</sup> in the framework of the NBO approach, which shows that the unsaturated **1-OB<sub>e</sub>H** cyclic structure is stabilized by the participation of the three different resonant structures depicted in Scheme 4.



**Scheme X.4** Natural Resonance Theory weights (%) of the most important resonant structures contributing to the stability of **1-OB<sub>e</sub>H** derivative. Note that the NBO describes the BeH group as an independent unit.

We can then conclude that the higher relative stability of the cyclic **1-OB<sub>e</sub>H** with respect to the saturated counterpart **5-OB<sub>e</sub>H** is due to resonance, as it is the stability of malonaldehyde and its derivatives.<sup>71</sup> Note however, that, as we have been claiming for similar systems showing intramolecular hydrogen bonds, the existence of this resonance does not result in a stronger intramolecular beryllium bond, but the other way around, is the much stronger beryllium bond, resulting from a larger intrinsic basicity of the basic site (C=O group) and from a larger Lewis acidity of the -BeH group, which leads to a symmetric structure with two identical Be···O linkages resulting necessarily in an enhancement of the resonance within the system. In summary, as indicated in ref. 60 concerning hydrogen bonds, the quasi-aromaticity observed in the unsaturated compounds is consistent with hydrogen-bonding-assisted resonance rather than with RAHB. This argument is also consistent with the fact that the beryllium bond does not participate as such in any of the resonant structures stabilizing the system, since any of the resonant forms present O-Be bonds.



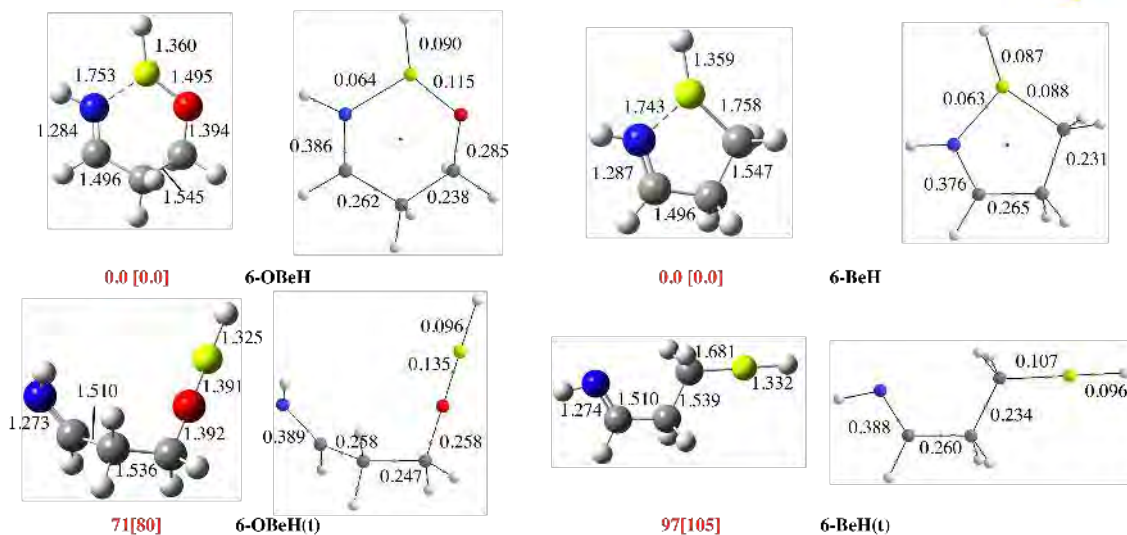
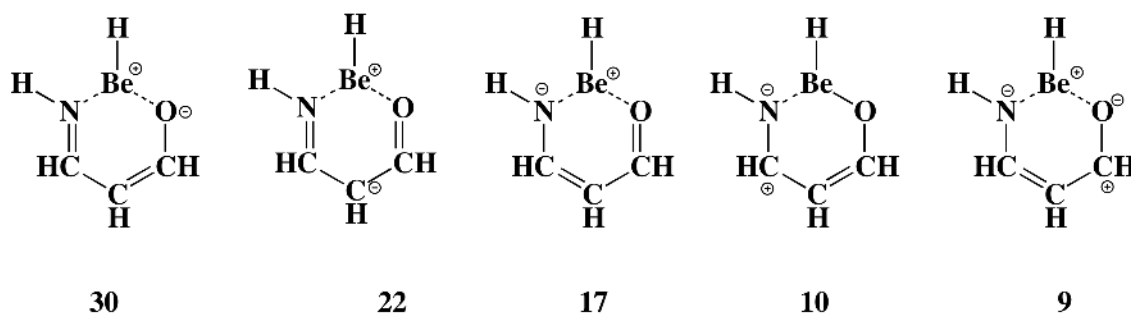


**Figure X.3** B3LYP/6-31+G(d,p) optimized structures and molecular graphs of unsaturated and saturated compounds showing a N $\cdots$ Be intramolecular beryllium bond and their corresponding open conformers. Same conventions as in Figure 1.

In order to gain some insight on the effect of changing the nature of the basic center involved in the formation of the intramolecular beryllium bond, we have included in our survey the derivatives that could be obtained from the set discussed above, by replacing their carbonyl group by a C=NH group, and which will be stabilized through the formation of Be $\cdots$ NH intramolecular beryllium bonds, namely **2-OBeH**, **2-BeH**, **6-OBeH** and **6-BeH**. The optimized structures of these compounds and their molecular graphs are shown in Figure 3. The trends observed are similar to those discussed above for Be $\cdots$ O bonds and for similar reasons. The intramolecular beryllium bond in **2-OBeH** is stronger than in **2-BeH** due to a larger basicity of the =NH group (956 vs. 923 kJ mol<sup>-1</sup>) and to a larger Lewis acidity of the -BeH group in the former, reflected in a larger hydride affinity (355 vs. 325 kJ mol<sup>-1</sup>). Again, the differences between these intramolecular beryllium bonds are much smaller between **6-OBeH** and **6-BeH**, because the intrinsic basicity of the imino groups in the extended conformers, **6-OBeH(t)** and **6-BeH(t)** are equal (933 kJ mol<sup>-1</sup>) and only the hydride affinity of **6-OBeH(t)** (299 kJ mol<sup>-1</sup>) is slightly larger than that of **6-BeH(t)** (295 kJ mol<sup>-1</sup>). It is worth noting that the energy gaps between the cyclic and the open forms of these series of compounds are larger than the ones calculated for the carbonyl containing analogues discussed above. This is an indication that the Be $\cdots$ NH intramolecular bonds are stronger than the Be $\cdots$ O, due to a much larger intrinsic basicity of the imino group with respect to the carbonyl one (956 vs. 853 kJ mol<sup>-1</sup> for **2-OBeH(t)** and **1-OBeH(t)**, respectively, and 923 vs. 807 kJ mol<sup>-1</sup> for **2-BeH(t)** and **1-BeH(t)**, respectively). Nevertheless, this effect is partially counterbalanced by a concomitant decrease of the hydride affinity of the BeH group in the nitrogen containing compounds with respect to the oxygen containing analogues.



Again, as it was found above for the couple **1-OBeH**/**1-BeH**, the gap between the cyclic **2-OBeH** and the open structures **2-OBeH(t)**, is larger than the one between **2-BeH** and **2-BeH(t)**, because the **2-OBeH** is stabilized through resonance effects associated with the participation of the five dominant resonant forms depicted in Scheme 5.



**Scheme X.5** Natural Resonance Theory weights (%) of the most important resonant structures contributing to the stability of **2-OBeH** derivative. Note that, with the only exception of form **10**, the NBO describes the BeH group as an independent unit.

Again, as in the case of the **1-OBeH**, the enhanced stability of the cyclic **2-OBeH** compound is a direct consequence of resonance triggered by the large strength of the  $\text{Be}\cdots\text{NH}$  intramolecular bond. The relative stabilities of the other three cyclic compounds, namely **6-OBeH**, **2-BeH** and **6-BeH** with respect to the corresponding open forms, are rather similar. In these cases, where resonance effects have a negligible role, the differences between the cyclic and the open structures are mainly due, although not exclusively, to the formation of the intramolecular beryllium bond.

### X.3.2 Effects of the rigidity of the molecular skeleton

At this point we considered it of interest to investigate what would be the effect of imposing some rigidity to the system exhibiting an intramolecular beryllium bond. For this purpose, we consider a system in which the malonaldehyde-like moiety is fused to a four membered ring, as in species **3-OBeH** and **3-BeH** and in their saturated counterparts **7-OBeH** and **7-BeH**.

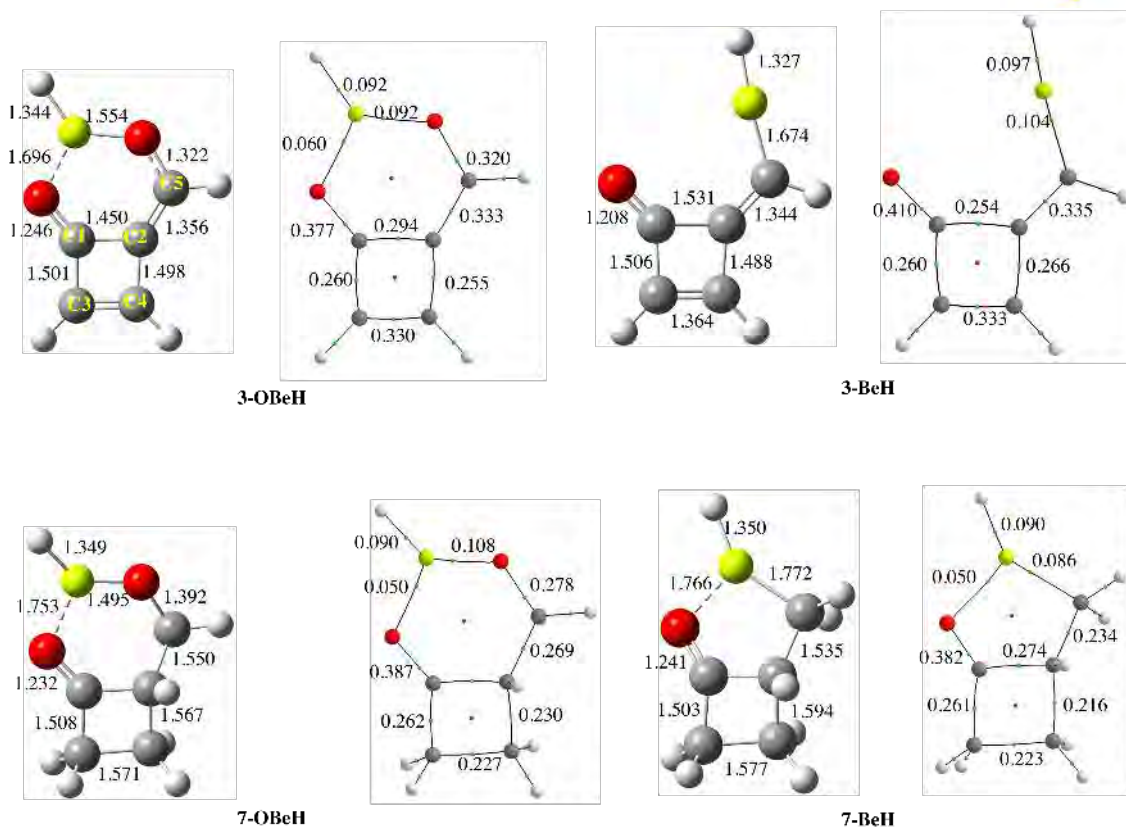


**Figure X.4** B3LYP/6-31+G(d,p) optimized structures and molecular graphs of compounds related to (*Z*)-4-(hydroxymethylene)cyclobut-2-enone (**3**) and 2-(hydroxymethyl)cyclobutanone (**7**). Compounds **3-OBcH** and **7-OBcH** are obtained by replacing the H atom of the OH group in compounds **3** and **7** by a BeH group. Compounds **3-BeH** and **7-BeH** are obtained by replacing the OH group in compounds **3** and **7** by a BeH group. Same conventions as in Figure 1.

From the structures and molecular graphs in Figure 4, it is apparent the effect of the geometrical constraints imposed by the four membered ring in the strength of the beryllium intramolecular bond. Indeed, whereas in compound **1-OBcH** the beryllium atom is symmetric located between the two oxygen atoms, in compound **3-OBcH** this symmetric arrangement is not possible because the C1-C2 bond which belongs to the four membered ring is forced to be essentially a single bond, and as a consequence the C2-C5 is essentially a much shorter double bond. The consequence is that the O $\cdots$ Be intramolecular beryllium bond is necessarily much longer and much weaker in compound **3-OBcH** than in compound **1-OBcH**. It is then the rigidity of the sigma skeleton, the factor that strongly influences the strength of this intramolecular linkage, very much in the same way as it was suggested to occur when dealing with the intramolecular hydrogen bond in (*Z*)-4-(hydroxymethylene)cyclobut-2-enone (**3** in scheme 2) as compared with that in malonaldehyde (**1** in scheme 2).<sup>54</sup>

The effect of the rigidity of the four membered ring is even more dramatic in compound **3-BeH**, whose

equilibrium conformation, differently to what has been found above for the **1-BeH** analogue, does not exhibit any intramolecular beryllium bond, because the rigidity imposed by the four membered cycle forces the distance between the Be atom and the carbonyl oxygen to be too large as to interact in an effective way. We found however a structure for this system that does present a beryllium bond (see Figure 5). However, the formation of this cyclic structure requires a significant lengthening of the C-Be bond, and consequently this local minimum lies  $7 \text{ kJ mol}^{-1}$  above the non-cyclic equilibrium conformation, in terms of Gibbs free energies.

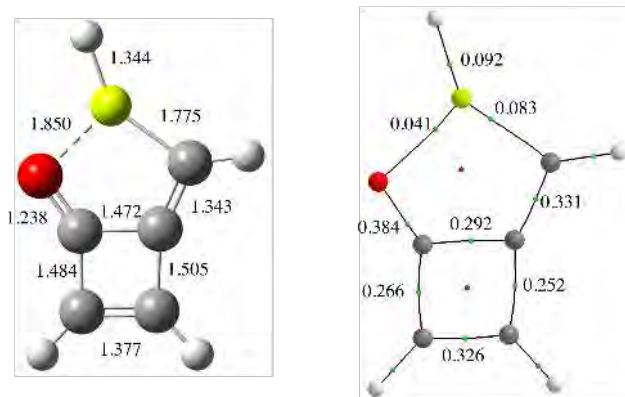


**Figure X.5** Local minimum of the **3-BeH** compound exhibiting a  $\text{Be}\cdots\text{O}$  intramolecular bond. This minimum lies  $7 \text{ kJ mol}^{-1}$  above the global minimum. Same conventions as in Figure 1.

As it was found for the previous two series of compounds, the intramolecular beryllium bond in the **7-OB<sub>e</sub>H** saturated species (see Figure 5) is weaker than in the corresponding unsaturated one, **3-OB<sub>e</sub>H**. Once more this is a consequence of a higher intrinsic basicity of the carbonyl group of the **3-OB<sub>e</sub>H** unsaturated compound ( $823 \text{ kJ mol}^{-1}$ ) and of a concomitant higher hydride affinity of its BeH group ( $-342 \text{ kJ mol}^{-1}$ ) with respect to those of the corresponding saturated derivative ( $801$  and  $-300 \text{ kJ mol}^{-1}$ , respectively). However, whereas the rigidity of the  $\sigma$ -skeleton in **3-BeH** hinders the formation of the beryllium intramolecular bond, the larger flexibility of the aliphatic chain in the corresponding saturated analogue, **7-BeH**, facilitates the formation of this non-covalent linkage.

### X.3.3 Intramolecular beryllium bonds in tropolone-like systems

The third set of compounds considered in our survey could be considered as derivatives of tropolone (**4** in scheme 2) and 2-hydroxycycloheptanone (**8** in scheme 2), respectively in which the H atom of the OH group has been replaced by a BeH group to yield compounds **4-OB<sub>e</sub>H** and **8-OB<sub>e</sub>H**, respectively or the whole OH group was replaced by a BeH group, to yield compounds **4-BeH** and **8-BeH**, respectively. This set represents a different molecular environment, where the basic sites, as in the compounds studied in the previous section, are attached to a cyclic structure, the difference being not only the size of the ring, a seven-

membered ring instead of a four-membered ring, but the possibility of having an aromatization of the seven-membered cyclic system, triggered by the formation of the intramolecular beryllium bond.

The structures and molecular graphs of these four compounds are shown in Figure 6. The first conspicuous fact is that whereas tropolone, which is stabilized by a intramolecular O-H $\cdots$ O hydrogen bond, presents a cycle with a clear alternation of single and double bonds, the **4-OB<sub>e</sub>H** compound presents an almost totally aromatic ring where the only typically single C-C bond is the one to which the two oxygen atoms of the system are attached. The remaining C-C bonds of the seven membered ring exhibit almost identical bond lengths, in agreement with the fact that the electron densities at the BCPs are also practically equal. As it was discussed above for **1-OB<sub>e</sub>H**, the large basicity of tropolone (894.1 kJ mol<sup>-1</sup>) 40 kJ mol<sup>-1</sup> larger than that of **1-OB<sub>e</sub>H(t)** system results in a very strong Be $\cdots$ O intramolecular beryllium bond, in which, as it was found above for **1-OB<sub>e</sub>H**, the Be atom sits symmetrically between both oxygen atoms.

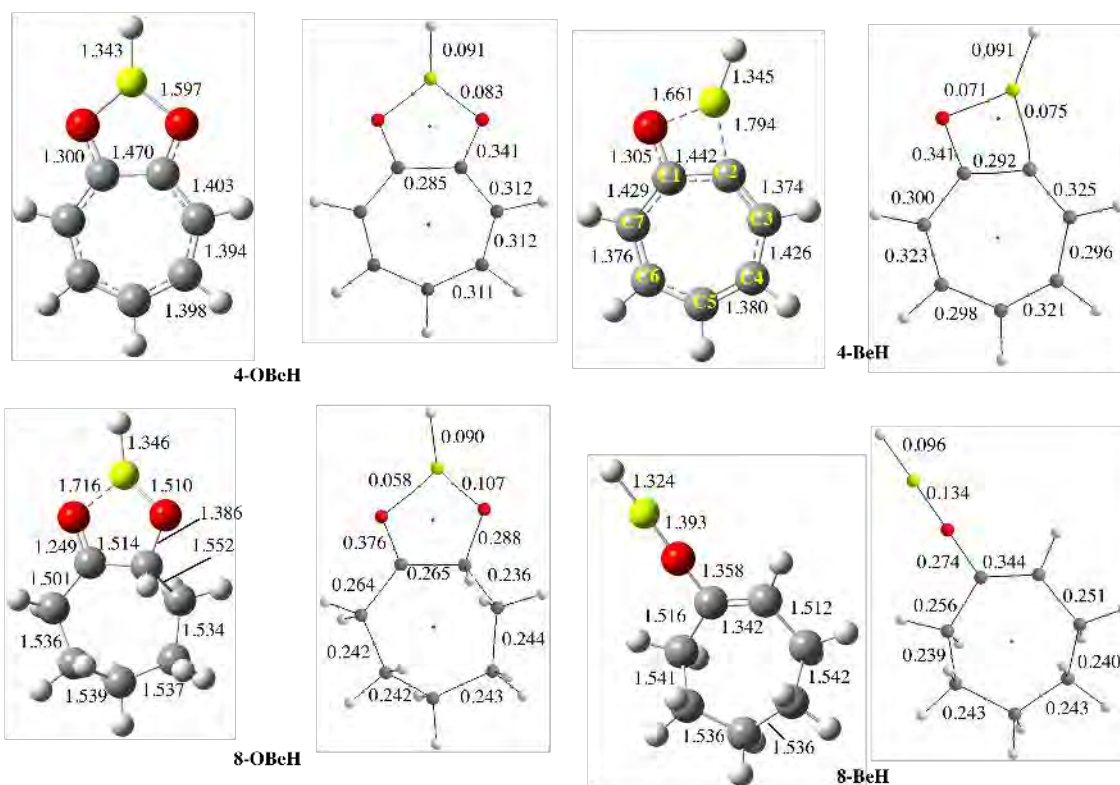


**Figure X.6** B3LYP/6-31+G(d,p) optimized structures and molecular graphs of compounds related to tropolone (**4**) and 2-hydroxycycloheptanone (**8**). Compounds **4-OB<sub>e</sub>H** and **8-OB<sub>e</sub>H** are obtained by replacing the H atom of the OH group in compounds **3** and **8** by a BeH group. Compounds **4-BeH** and **8-BeH** are obtained by replacing the OH group in compounds **4** and **8** by a BeH group. Same conventions as in Figure 1.

The high strength of the beryllium bond formed leads therefore to a symmetrization of the **4-OB<sub>e</sub>H** system, which is not observed in tropolone, ratifying that it is the strength of the intramolecular interaction the key

factor in the resonance stabilization of the system, and not the other way around. As illustrated in Figure 6, this effect is almost totally destroyed on going to the **4-BeH**, where the formation of the O···Be intramolecular bond requires to almost cleave the C2-Be bond. This forces a much higher localization within the seven-membered ring, because the weakening of the C2-Be bond necessarily results in a strengthening of the C2-C3 bond, which becomes a clear double bond, forcing an alternation around the cycle.

As in previous cases, the intramolecular beryllium bond is weaker in the saturated derivative **8-OBBeH**, which is a direct consequence of the significantly decrease of the intrinsic basicity of the carbonyl group and the concomitant decrease in the Lewis acidity of the -BeH group on going from the unsaturated to the saturated compound. In fact, the intrinsic basicity of tropolone ( $891 \text{ kJ mol}^{-1}$ ), which can be considered as a good model system to estimate the intrinsic basicity of the carbonyl group of **4-OBBeH** is significantly higher than that of 2-hydroxycycloheptanone ( $815 \text{ kJ mol}^{-1}$ ), which is a good model for the basicity of this group in compound **8-OBBeH**. On the other hand, our calculated intrinsic acidity of cyclohepta-2,4,6-trienol ( $1525 \text{ kJ mol}^{-1}$ ) which would be a good measure of the intrinsic acidity of **4-OBBeH**, is found to be  $35 \text{ kJ mol}^{-1}$  larger than that of cycloheptanol, which is a good model for the acidity of compound **8-OBBeH**.

Our attempts to locate a local minimum for **8-BeH** featuring an intramolecular beryllium bond, similar to the one found for the unsaturated analogue, **4-BeH**, failed, because they collapsed to the structure depicted on Figure 6, in which the C-Be bond cleavage initiated in compound **4-BeH** becomes complete in the saturated analogue, **8-BeH**. Consequently, Be is covalently attached to the carbonyl oxygen atom only. This is reflected not only in an electron density at the O-Be BCP almost twice as large in **8-BeH** than in **4-BeH**, but also in the fact that for **4-BeH** only a dative bond from the lone-pairs of the oxygen to beryllium is found, whereas for compound **8-BeH**, a very polar covalent bond, with 91% participation of the sp hybrids at the oxygen atom and 9% of the  $sp^2$  orbitals at the beryllium atom is found. This possibility is very unlikely when dealing with the unsaturated analogue **4-BeH**, because the complete breaking of the C2-Be bond and the eventual migration of the BeH group towards the oxygen atom would lead a carbene-like structure which would be rather unstable.

### X.3.4 Beryllium bridges. Dimerization of malonaldehyde-like systems

In this section we investigate the dimerization of Be-containing malonaldehyde-like systems, namely **1-OBBeH** and **1-BeH** compounds, trying to see whether the self-assembly of these systems leads to the formation of Be-Be bonds.  $\text{Be}_2$  dimer itself is a very weakly bound species, the most recent experimental value for its dissociation energy being  $935 \text{ cm}^{-1}$ ,<sup>72</sup> and for which only 12 vibrational states have been

resolved.<sup>73, 74</sup>  $\text{Be}_2$  has been also a challenge for chemical theory.<sup>72-85</sup> Although the most recent studies indicate that the bonding arises from electron correlation effects.<sup>84</sup> In other words, in the absence of electron correlation effects, the  $\text{Be}_2$  system would be unbound, which is the prediction of basic molecular orbital theory. We have shown for many different cases the ability of beryllium compounds to form very stable complexes in which they behave as very good electron acceptors reflecting the electron-deficient character of beryllium derivatives. This nature is also behind the strong intramolecular beryllium bonds that we have analyzed and discussed in preceding sections. The question we want to address now is whether these compounds, in which the propensity of Be to accept electrons is at least partially satisfied through the formation of an intramolecular beryllium bond are able to self-assemble through the direct interaction between the beryllium atoms. For this purpose we have optimized the structures of the dimers of **1-OB<sub>2</sub>H** and **1-BeH**. As illustrated in Figure 7, the dimerization leads to the formation of Be-H-Be bridges, very much as the ones that stabilizes diborane, so the two monomers lie in the same plane, whereas the two hydrogens of the bridge lie in a perpendicular one. These bridges are characterized by BCPs whose electron densities are about 40% lower than in normal Be-H bonds as in beryllium dihydride ( $\rho_{\text{BCP}} = 0.102$  a.u.).

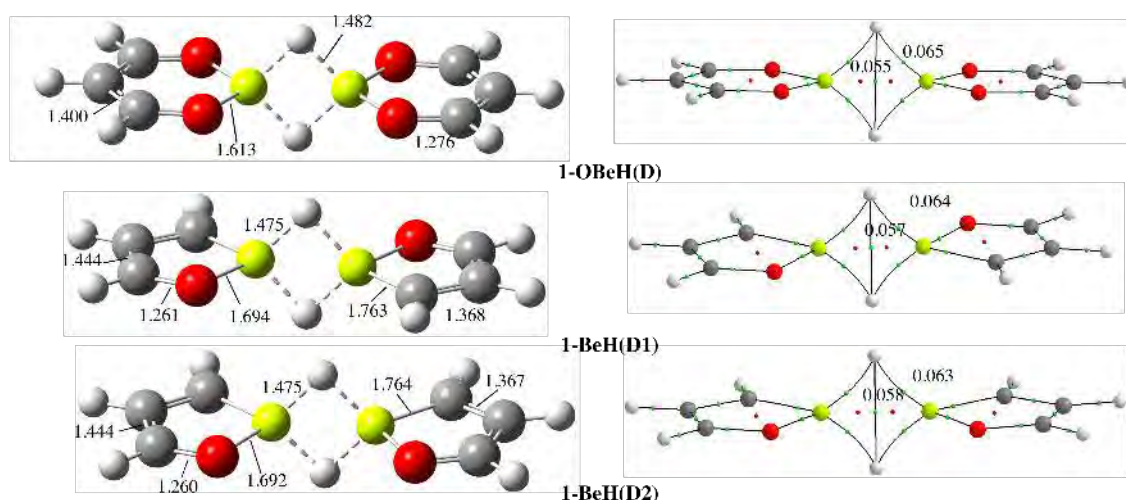


**Figure X.7** B3LYP/6-31+G(d,p) optimized structures and molecular graphs of the dimers of **1-OB<sub>2</sub>H** and **1-BeH** compounds. Note that for the latter two different isomers, practically degenerate, namely **1-BeH(D1)** and **1-BeH(D2)**, are local minima on the potential energy surface. Same conventions as in Figure 1.

The immediate consequence is that the length of the Be-H bond increases by about 0.14 Å with respect to the isolated monomers. Rather interestingly, the effects on the other two bonds in which the Be atom participates is the opposite in **1-OB<sub>2</sub>H(D)** dimer that in the **1-BeH(D1)** and **1-BeH(D2)**, ones. As showed in Figure 7, in the former the O-Be distances increase 0.023 Å with respect to the isolated monomers, whereas in the latter the O-Be and C-Be distances shrink by 0.014 and 0.017 Å, respectively. It is also worth noting that the Be-H-Be bridges are rather similar for both **1-OB<sub>2</sub>H** and **1-BeH** dimers. Coherently the WBOs for

all these Be-H linkages are equal (0.446). No BCP is found between the two beryllium atoms, although it is observed between the two hydrogen atoms involved in the bridge. This AIM result is in contrast with the values of the WBOs, which are negligible small between the two hydrogens of the bridge, but sizably large (0.26 and 0.29, respectively) between the two Be atoms. The bonding within the bridge is viewed as two three-center bonds, shown in Figure 8, which involve 17% participation of  $sp^3$  orbitals of both Be atoms and 65% participation of the 1s orbital of the H atom. Each of these three-center bonds is populated by  $1.97 e^-$ . The nature of these bridges is not substantially different from those responsible for the stability of diborane, the only significant difference being the relative participation of the orbitals of boron in the bonding, which amounts to 28%, reflecting the larger electronegativity of the boron atom with respect to the Be atom. The calculated dimerization enthalpy of these Be-containing dimers is significantly high ( $-105 \text{ kJ mol}^{-1}$ ) and of the same order of magnitude than that of diborane ( $-141 \text{ kJ mol}^{-1}$ ).<sup>86</sup>

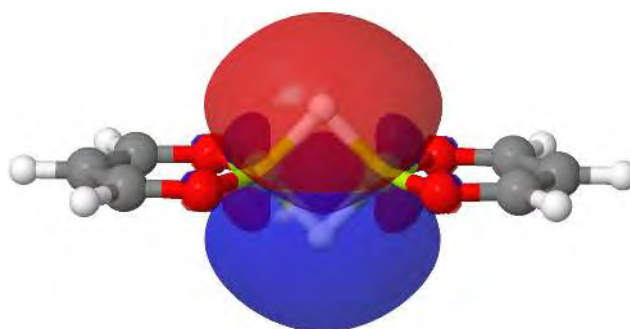


**Figure X.8** Three-center localized natural orbitals responsible for the formation of two Be-H-Be bridges in dimer **1-OBcH(D1)**.

Two different dimers are possible for the **1-BeH** compound, depending on the relative orientation of the two monomers (see Figure 7). Quite interestingly however both structures, **1-BeH(D1)** and **1-BeH(D2)**, are practically degenerate in terms of Gibbs free energies, the latter being only  $1 \text{ kJ mol}^{-1}$  lower in energy than the former, with binding energies higher ( $-164 \text{ kJ mol}^{-1}$ ) than that of **1-OBcH(D)**. In view of the identical stability of both conformers we considered it of interest to calculate the transition state between both structures (See Figure 9).

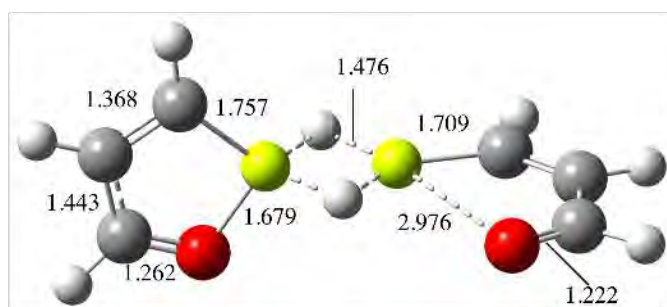


**Figure X.9** B3LYP/6-31+G(d,p) optimized structures for the transition state connecting **1-BeH(D1)** and **1-BeH(D2)** dimers. Bond distances are in Å.

The calculated barrier height for the **1-BeH(D1)/1-BeH(D2)** isomerization is  $82 \text{ kJ mol}^{-1}$ . One could naively expect a very low activation barrier associated with the rotation of one of the monomers to be perpendicular to the plane of the other monomer, however, although this is indeed the displacement connecting the minima with the TS, this rotation forces the oxygen of the rotating moiety to lie in the same plane of the Be-H-Be bridge and too much close to one of the hydrogens. This strong repulsion leads to a significant distortion of the rotating monomer and a significant lengthening of the Be-O bond, what explains the rather high activation barrier. The main conclusion then is that in the gas phase the **1-BeH** dimerization should lead to a 50/50 mixture of both conformers in equilibrium, because no interconversion between them should be expected.

The dimerization of the corresponding saturated systems obeys rather similar patterns as the ones just described in the preceding paragraphs. In this case, due to the lack of symmetry in the corresponding monomers, there are two different dimers for both the **5-OBeH** and the **5-BeH** compounds. For the sake of conciseness we present in Figure 10 only the ones associated with the **5-OBeH** compound. As in the case of the unsaturated counterparts the two dimers, namely **5-OBeH(D1)** and **5-OBeH(D2)** are very close in energy, the latter being  $2.4 \text{ kJ mol}^{-1}$  less stable than the former.

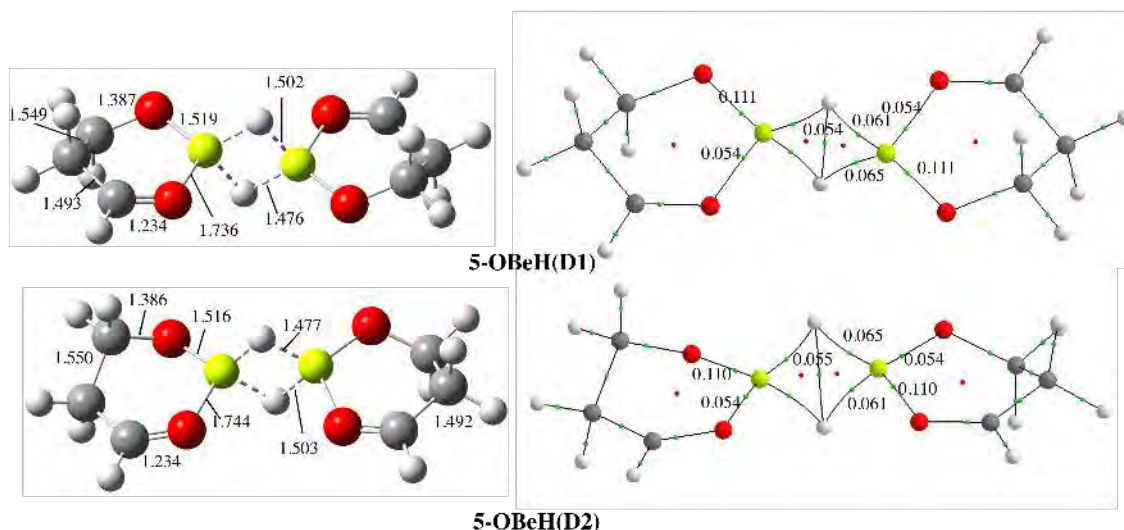


**Figure X.10** B3LYP/6-31+G(d,p) optimized structures and molecular graphs of the dimers of **5-OBeH** compound. Two different isomers, practically degenerate, namely **5-OBeH(D1)** and **5-OBeH(D2)**, are local minima on the potential energy surface. Same conventions as in Figure 7.

It is interesting to remark the great similarity of the Be-H-Be bridges in these saturated dimers and their corresponding unsaturated analogues (see Figure 7) as far as internuclear distances and electron densities are concerned. Also the three-center bonds obtained through the NBO analysis are essentially identical, with



negligible differences in the participation of the Be orbitals, which for the unsaturated derivative, as mentioned above is 17%, whereas for the saturated analogue is 18%. As a matter of fact, their binding energies are almost identical to that of the unsaturated analogue ( $-102 \text{ kJ mol}^{-1}$ ). The question that arises quite naturally is whether these bridge linkers also are formed when the hydrogen atoms are replaced by other atoms or functional groups. To answer this question we have considered three different cases, i) the substitution of the H atoms by another atom more electronegative, chlorine atoms, ii) the substitution of the H atom by a group with a clear inductive effect, such as the methyl group, and iii) the substitution by a bulkier and aromatic group, such as the phenyl group.

The structures and molecular graphs of chlorine containing complexes have been plotted in Figure 11 for the unsaturated systems. The results are similar for the corresponding saturated analogues and therefore they are not going to be discussed in detail.

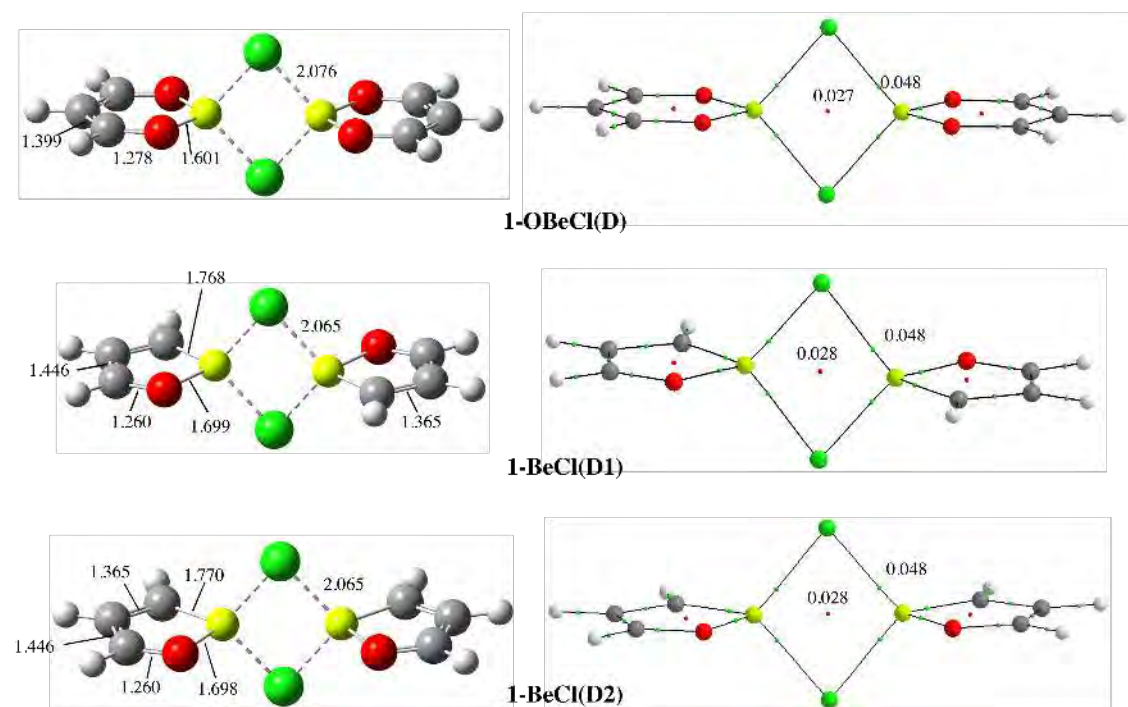
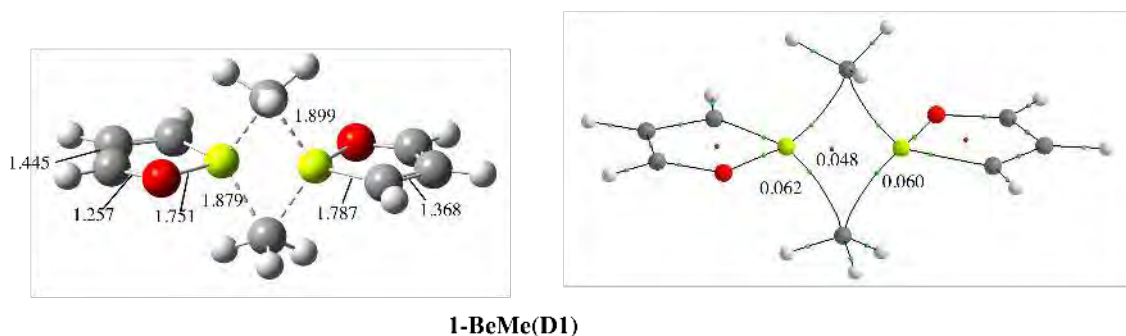


**Figure X.11** B3LYP/6-31+G(d,p) optimized structures and molecular graphs of the dimers obtained when the H atoms of **1-OBcH** and **1-BeH** derivatives are substituted by chlorine atoms. Two different isomers, practically degenerate, namely **1-BeCl(D1)** and **1-BeCl(D2)**, are local minima on the potential energy surface. Bond distances are in Å. Same conventions as in Figure 7.

As illustrated in Figure 11, the replacement of H by chlorine atoms does not alter significantly the bonding pattern of the corresponding dimers, in which the two monomers are held together through Be-Cl-Be bridges. As expected the length of the Be-Cl links are larger than the Be-H ones due to the larger size of the chlorine atoms, and, for the same reason the electron densities are necessarily smaller. However, the NBO

analysis indicates that the interaction between Be and Cl in these bridges is stronger than between Be and H in the bridges of the **1-OB<sub>2</sub>H(D)**, as reflected in a larger WBO (0.517 vs. 0.446). In fact, whereas in **1-OB<sub>2</sub>H(D)** dimers, as indicated above, the interaction is a dative bond from the H electron density into the empty Be orbitals, in the **1-OB<sub>2</sub>Cl(D)**, **1-BeH(D1)** and **1-BeH(D2)**, the NBO analyses finds a very polar covalent bond between a sp<sup>3</sup> hybrid in Cl atom, with a contribution of 91%, and a sp<sup>3</sup> hybrid in Be with a contribution of 9%. Consistently the electron densities at the BCPs of the bridges are equal in all these dimers. Also, the Gibbs free energy gap between the two conformers **1-BeH(D1)** and **1-BeH(D2)** is negligible small, the latter being 0.9 kJ mol<sup>-1</sup> lower in free energy than the former.

Upon methyl substitution the changes in the bonding of the dimers are not significant with respect to the unsubstituted parent dimer. In Figure 12, as a suitable example we present the structure and the molecular graph of the **1-BeMe(D1)**. The electron densities at the BCPs are rather similar to the unsubstituted dimer, whereas the WBO of the Me-H bonds within the bridge is 0.390. As expected the localized Be-CH<sub>3</sub> bond is less polar than for the chlorine derivative with a participation of the sp<sup>3</sup> orbitals of Be of 14%.



**1-BeMe(D1)**

**Figure X.12** B3LYP/6-31+G(d,p) optimized structures and molecular graphs of the dimer obtained when the H atoms of **1-BeH** derivative are substituted by methyl groups. Same conventions as in Figure 7.

The substitution by phenyl groups does not alter either the bonding patterns observed in the dimers discussed so far. The **1-OB<sub>2</sub>Ph(D)** chosen as a suitable example to illustrate the characteristics of the dimers with phenyl substituents has, as the unsubstituted **1-OB<sub>2</sub>H(D)** or the chlorine containing analogue **1-OB<sub>2</sub>Cl(D)**, *D*<sub>2h</sub> symmetry. The Be-C<sub>6</sub>H<sub>5</sub> bonds are similar to those seen in the methyl derivative, with WBOs of 0.399. The bonding of the aromatic ring to both beryllium atoms, as in previous cases, occurs actually through Be-C-Be three-center bonds. These bonds have a significant contribution from the sp<sup>2</sup> hybrid of the phenyl carbon atom which amounts to 77%, reducing the participation of the Beryllium bonds to 11%. This significant participation of the carbon orbital has a non-negligible effect in the aromaticity of the phenyl derivative. This is actually reflected in a substantial negative charge (-0.49 e<sup>-</sup>) of both phenyl groups. On the other hand, as shown in Figure 13, the electron density at the BCPs between the carbon atom participating in the bridge and its two neighbors in the aromatic ring (0.301 a.u.) is smaller than the density

at the other C-C BCPs within the ring. This bonding pattern resembles that of a Wheland intermediate, with the difference that these intermediates were postulated for electrophilic aromatic substitutions and therefore they are cationic, whereas in the present case they are electron rich, with a negative charge close to half of an electron, as mentioned above.

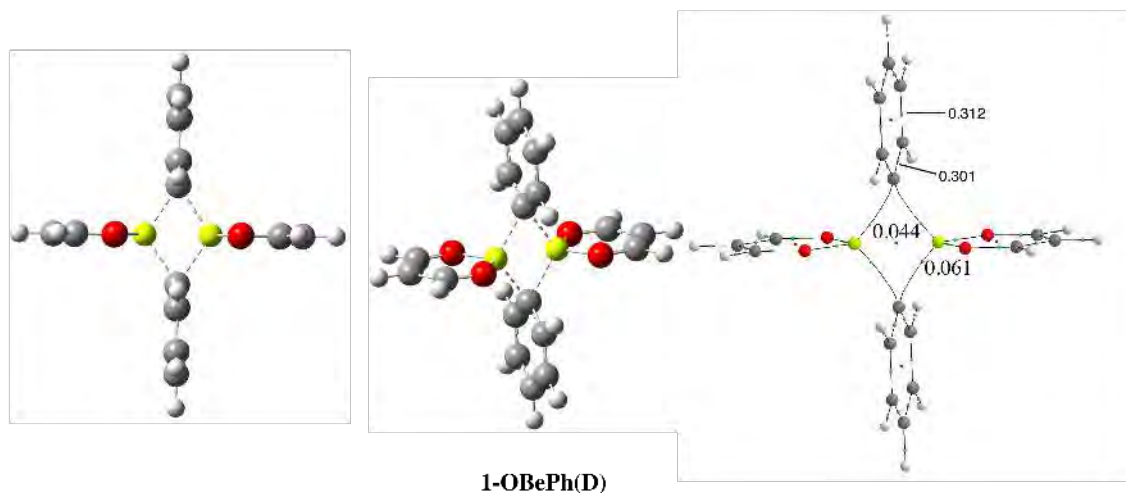


**Figure X.13** Two different perspectives of the B3LYP/6-31+G(d,p) optimized structures of the dimer of obtained when the H atoms of **1-BeH** derivative are substituted by phenyl groups. The third graphic corresponds to the molecular graph. Same conventions as in Figure 7.

#### X.4 Concluding Remarks

The intramolecular beryllium bonds have the same intrinsic characteristics as the intermolecular ones. These characteristics are a direct consequence of the charge transfer from the lone pairs of the basic site to the  $\sigma_{\text{BeX}}^*$  antibonding orbital and to the empty  $p$  orbitals of Be atom. As a consequence, and similarly to what has been observed for the intermolecular case, the  $\text{BeX}_2$  moiety distorts significantly, departing from linearity, while the Be-X bonds become longer. In some cases, this charge donation is so large that a new covalent linkage between the Be atom and the basic site of the molecule is formed. In general the intramolecular beryllium bonds share many similarities with hydrogen bonds within the same molecular environment, though the former are in general stronger and therefore produce stronger distortions on the electron density distribution within the system. This electron density redistribution for unsaturated compounds leads to a significant enhancement of the resonance within the  $\pi$ -system, because the formation of the Be bond necessarily implies a weakening of the bonds in which the basic site participates, and therefore leads to a complete rearrangement of the remaining bonds of the system. It is important then to emphasize that the resonance enhancement is larger in systems that exhibit an intramolecular beryllium bond, than in similar systems which are stabilized through an intramolecular hydrogen bond, just because the former interactions are stronger than the latter. It is also worth noting that there is a reasonably good

linear correlation between the strength of these two kinds of interactions, as measured by the electron density at the corresponding BCPs, as shown in Figure 14, for some of the systems included in this study.

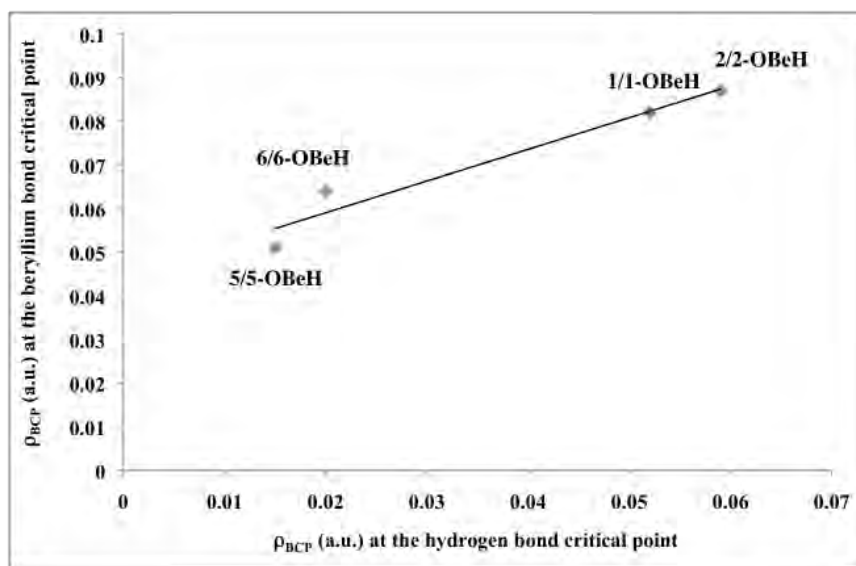


**Figure X.14** Linear correlation between the electron density at the beryllium bond critical point and at the hydrogen bond critical point [ $\rho_{\text{BCP}}(\text{Be}) = 0.7265 \rho_{\text{BCP}}(\text{HB}) + 0.0445$ ;  $r^2 = 0.946$ ] for compounds in which the hydrogen bond has been replaced by a beryllium bond (see Scheme 1 for nomenclature).

More importantly, the larger strength of the intramolecular beryllium bonds in unsaturated derivatives with respect to the saturated analogues does not arise from a resonance assisted mechanism but it is essentially due to two concomitant intrinsic effects: a larger basicity of the basic site and a larger acidity of the -BeH group in the unsaturated derivative. The immediate consequence is that the larger the strength of the intramolecular interaction the larger the stabilization of the system by resonance. This is rather well illustrated by the fact that the equilibrium structure in malonaldehyde is not symmetric, whereas that of the BeH containing analogue, **1-OBcH**, is. Therefore the resonance stabilization of the latter is much larger than the resonance stabilization of the former, because the intramolecular beryllium bond is stronger than the hydrogen bonds.

The self-assembly of Be-containing malonaldehyde-like structures takes place through the formation of Be-H-Be bridges, but non-direct Be-Be interactions are observed. These bridges are rather similar, and only slightly weaker than those stabilizing diborane. The substitution of the H atom in these bridges by either halogen atoms, such as Cl, alkyl groups or phenyl groups does not alter this arrangement and the two moieties appear still connected through Be-X-Be (X = Cl, CH<sub>3</sub>, C<sub>6</sub>H<sub>5</sub>) bridges.

## Acknowledgement

This work has been also partially supported by the Ministerio de Economía y Competitividad (Projects No. CTQ2015-63997-C2-1-P and CTQ2013-43698-P), by the STSM COST Action CM1204, and by the Project FOTOCARBON-CM S2013/MIT-2841 of the Comunidad Autónoma de Madrid. OB acknowledges the Ministerio de Ciencia, Cultura y Deportes of Spain by a FPU grant. Computational time at Centro de Computación Científica (CCC) of Universidad Autónoma de Madrid is also acknowledged.

## References

1. G. C. Pimentel and A. L. McClelland, *The hydrogen bond*, W.H. Freeman and Co. , San Francisco, 1960.
2. G. A. Jeffrey, *An Introduction to Hydrogen Bonding*, Oxford University Press New York, 1997.
3. S. J. Grabowski, *Hydrogen bonding. New Insights*, 2006.
4. P. Metrangolo and G. Resnati, *Chem. Eur. J.*, 2001, **7**, 2511-2519.
5. T. Clark, M. Hennemann, J. S. Murray and P. Politzer, *J. Mol. Mod.*, 2007, **13**, 291-296.
6. P. Politzer, J. S. Murray and T. Clark, *Phys. Chem. Chem. Phys.*, 2013, **15**, 11178-11189.
7. I. Alkorta, J. Elguero and C. Foces-Foces, *Chem. Comm.* 1996, 1633-1634.
8. V. I. Bakhmutov, *Dihydrogen Bond: Principles, Experiments, and Applications*, John Wiley & Sons, 2008.
9. S. Zahn, R. Frank, E. Hey-Hawkins and B. Kirchner, *Chem. Eur. J.*, 2011, **17**, 6034-6038.
10. J. E. Del Bene, I. Alkorta, G. Sánchez-Sanz and J. Elguero, *J. Phys. Chem. A*, 2011, **115**, 13724-13731.
11. S. Scheiner, *Acc. Chem. Res.*, 2013, **46**, 280-288.
12. S. Scheiner, *Int. J. Quant. Chem.*, 2013, **113**, 1609-1620.
13. A. Bauzá, T. J. Mooibroek and A. Frontera, *Angew. Chem. Int. Ed.*, 2013, **52**, 12317-12321.
14. I. Alkorta, I. Rozas and J. Elguero, *J. Phys. Chem. A*, 2001, **105**, 743-749.
15. P. Sanz, O. Mó and M. Yáñez, *J. Phys. Chem. A*, 2002, **106**, 4661-4668.
16. P. Sanz, O. Mó and M. Yáñez, *New J. Chem.*, 2002, **26**, 1747-1752.
17. W. Z. Wang, B. M. Ji and Y. Zhang, *J. Phys. Chem. A*, 2009, **113**, 8132-8135.
18. M. Yáñez, P. Sanz, O. Mó, I. Alkorta and J. Elguero, *J. Chem. Theor. Comput.*, 2009, **5**, 2763-2771.
19. E. Fernández Villanueva, O. Mó and M. Yáñez, *Phys. Chem. Chem. Phys.*, 2014, **16**, 17531-17536.
20. D. Parker, *J. Chem. Soc. Chem. Commun.*, 1985, 1129-1131.
21. F. Zhang, T. Morawitz, S. Bieller, M. Bolte, H. W. Lerner and M. Wagner, *Dalton Trans.*, 2007, 4594-4598.
22. F. Tancini and E. Dalcanale, *Polymerization with Ditopic Cavitand Monomers, in Supramolecular Polymer Chemistry.*, Wiley-VCH Verlag GmbH & Co, 2011.
23. T. K. Kim, K. J. Lee, M. Choi, N. Park, D. Moon and H. R. Moon, *New J. Chem.*, 2013, **37**, 4130-4139.
24. R. Muallem, E. Sominska, V. Kelner and A. Gedanken, *J. Chem. Phys.*, 1992, **97**, 8813-8814.
25. A. Witkowski, *J. Chem. Phys.*, 1970, **52**, 4403-4407.
26. A. Winkler and P. Hess, *J. Am. Chem. Soc.*, 1994, **116**, 9233-9240.
27. F. O. Koller, M. Huber, T. E. Schrader, W. J. Schreier and W. Zinth, *Chem. Phys.*, 2007, **341**, 200-206.
28. I. Alkorta, J. Elguero, M. Yáñez and O. Mó, *Phys. Chem. Chem. Phys.*, 2014, **16**, 4305-4312.
29. R. Dobrawa and F. Wurthner, *J. Polym. Sci. Part A: Polym. Chem.*, 2005, **43**, 4981-4995.
30. Y. Yan and J. B. Huang, *Coord. Chem. Rev.*, 2010, **254**, 1072-1080.

31. A. D. Burrows, M. F. Mahon, P. R. Raithby, A. J. Warren, S. J. Teat and J. E. Warren, *Crystengcomm*, 2012, **14**, 3658-3666.
32. F. Wurthner, C. C. You and C. R. Saha-Moller, *Chem. Soc. Rev.*, 2004, **33**, 133-146.
33. B. Lippert and P. J. S. Miguel, *Chem. Soc. Rev.*, 2011, **40**, 4475-4487.
34. J. W. Steed, *Chem. Comm.*, 2011, **47**, 1379-1383.
35. D. J. White, N. Laing, H. Miller, S. Parsons, S. Coles and P. A. Tasker, *Chem. Comm.*, 1999, 2077-2078.
36. W. F. Rowe, R. W. Duerst and E. B. Wilson, *J. Am. Chem. Soc.*, 1976, **98**, 4021-4023.
37. R. S. Brown, *J. Am. Chem. Soc.*, 1977, **99**, 5497-5499.
38. N. Sanna, F. Ramondo and L. Bencivenni, *J. Mol. Struct.*, 1994, **318**, 217-235.
39. M. A. Rios and J. Rodriguez, *Can. J. Chem.*, 1991, **69**, 201-204.
40. P. Sanz, O. M6 and M. Y6ñez, *Phys. Chem. Chem. Phys.*, 2003, **5**, 2942-2947.
41. D. L. Widner, Q. R. Knauf, M. T. Merucci, T. R. Fritz, J. S. Sauer, E. D. Speetzen, E. Bosch and N. P. Bowling, *J. Org. Chem.*, 2014, **79**, 6269-6278.
42. M. Yahia-Ouahmed, V. Tognetti and L. Joubert, *Comp. Theor. Chem.*, 2015, **1053**, 254-262.
43. B. V. Pandiyan, P. Deepa and P. Kolandaivel, *Phys. Chem. Chem. Phys.*, 2015, **17**, 27496-27508.
44. G. Gilli, F. Bellucci, V. Ferretti and V. Bertolasi, *J. Am. Chem. Soc.*, 1989, **111**, 1023-1028.
45. V. Bertolasi, L. Nanni, P. Gilli, V. Ferretti, G. Gilli, Y. M. Issa and O. E. Sherif, *New J. Chem.*, 1994, **18**, 251-261.
46. V. Bertolasi, P. Gilli, V. Ferretti and G. Gilli, *J. Chem. Soc. Perkin Trans. 2*, 1997, 945-952.
47. P. Gilli, V. Bertolasi, V. Ferretti and G. Gilli, *J. Am. Chem. Soc.*, 2000, **122**, 10405-10417.
48. B. K. Paul, N. Ghosh, R. Mondal and S. Mukherjee, *Photochem. & Photobiol. Sci.*, 2015, **14**, 1147-1162.
49. M. Dracinsky, L. Cechova, P. Hodgkinson, E. Prochazkova and Z. Janeba, *Chem. Comm.*, 2015, **51**, 13986-13989.
50. D. Rusinska-Roszak and G. Sowinski, *J. Phys. Chem. A*, 2015, **119**, 3674-3687.
51. I. Alkorta, J. Elguero, O. M6, M. Y6ñez and J. D. Bene., *Mol. Phys.*, 2004, **102**, 2563-2574.
52. P. Sanz, O. M6, M. Y6ñez and J. Elguero, *J. Phys. Chem. A*, 2007, **111**, 3585-3591.
53. Y. R. Mo, *J. Mol. Mod.*, 2006, **12**, 221-228.
54. P. Sanz, O. M6, M. Y6ñez and J. Elguero, *ChemPhysChem*, 2007, **8**, 1950-1958.
55. J. F. Beck and Y. R. Mo, *J. Comput. Chem.*, 2007, **28**, 455-466.
56. Y. R. Mo, *Journal of Physical Chemistry A*, 2012, **116**, 5240-5246.
57. R. W. Gora, M. Maj and S. J. Grabowski, *Physical Chemistry Chemical Physics*, 2013, **15**, 2514-2522.
58. A. R. Nekoei and M. Vatanparast, *New J. Chem.*, 2014, **38**, 5886-5891.
59. K. Sutter, G. A. Aucar and J. Autschbach, *Chem. Eur. J.*, 2015, **21**, 1-19.
60. M. P. Romero-Fernandez, M. Avalos, R. Babiano, P. Cintas, J. L. Jimenez and J. C. Palacios, *Tetrahedron*, 2016, **72**, 95-104.
61. A. D. Becke, *J. Chem. Phys.*, 1993, **98**, 5648-5652.
62. C. Lee, W. Yang and R. G. Parr, *Phys. Rev. B*, 1988, **37**, 785-789.
63. L. A. Curtiss, P. C. Redfern and K. Raghavachari, *J. Chem. Phys.*, 2007, **126**, 12.
64. O. Brea, O. M6, M. Y6ñez, I. Alkorta and J. Elguero, *Chem. Eur. J.*, 2015, **21**, 12676-12682.
65. R. F. W. Bader, *Atoms in Molecules. A Quantum Theory*, Clarendon Press, Oxford, 1990.
66. A. E. Reed, L. A. Curtiss and F. Weinhold, *Chem. Rev.*, 1988, **88**, 899-926.
67. T. A. Keith, *AIMAll (Version 13.05.06)*, (2013) AIMAll (Version 13.05.06) Gristmill Software, Overland Park, KS, 2013; aim.tkgristmill.com.
68. K. B. Wiberg, *Tetrahedron*, 1968, **24**, 1083-1088.
69. F. Weinhold, *NBO Program*, (2001) University of Wisconsin System, Madison.
70. E. D. Glendening and F. Weinhold, *J. Comput. Chem.*, 1998, **19**, 593-609.
71. M. Palusiak, S. Simon and M. Sola, *Chem. Phys.*, 2007, **342**, 43-54.

72. V. V. Meshkov, A. V. Stolyarov, M. C. Heaven, C. Haugen and R. J. LeRoy, *J. Chem. Phys.*, 2014, **140**.
73. J. M. Merritt, V. E. Bondybey and M. C. Heaven, *Science*, 2009, **324**, 1548-1551.
74. K. Patkowski, V. Spirko and K. Szalewicz, *Science*, 2009, **326**, 1382-1384.
75. M. R. A. Blomberg and P. E. M. Siegbahn, *Int. J. Quant. Chem.*, 1978, **14**, 583-592.
76. S. Evangelisti, G. L. Bendazzoli and L. Gagliardi, *Chem. Phys.*, 1994, **185**, 47-56.
77. J. Starck and W. Meyer, *Chem. Phys. Lett.*, 1996, **258**, 421-426.
78. R. J. Gdanitz, *Chem. Phys. Lett.*, 1999, **312**, 578-584.
79. J. M. L. Martin, *Chem. Phys. Lett.*, 1999, **303**, 399-407.
80. M. W. Schmidt, J. Ivanic and K. Ruedenberg, *J. Phys. Chem. A*, 2010, **114**, 8687-8696.
81. J. Koput, *Phys. Chem. Chem. Phys.*, 2011, **13**, 20311-20317.
82. W. Helal, S. Evangelisti, T. Leininger and A. Monari, *Chem. Phys. Lett.*, 2013, **568**, 49-54.
83. J. M. Matxain, F. Ruiperez and M. Piris, *J. Mol. Mod.*, 2013, **19**, 1967-1972.
84. M. El Khatib, G. L. Bendazzoli, S. Evangelisti, W. Helal, T. Leininger, L. Tenti and C. Angeli, *J. Phys. Chem. A*, 2014, **118**, 6664-6673.
85. M. J. Deible, M. Kessler, K. E. Gasperich and K. D. Jordan, *J. Chem. Phys.*, 2015, **143**, 084116.
86. L. T. Redmon, G. D. Purvis and R. J. Bartlett, *J. Am. Chem. Soc.*, 1979, **101**, 2856-2862.

## B.4 ARTICLE III

*On the existence of intramolecular one-electron Be-Be bonds*

Published in: Chemistry Communication, **2016**, 52, 9656-9659.







Cite this: *Chem. Commun.*, 2016, 52, 9656

Received 24th May 2016,  
Accepted 27th June 2016

DOI: 10.1039/c6cc04350j

[www.rsc.org/chemcomm](http://www.rsc.org/chemcomm)

## On the existence of intramolecular one-electron Be–Be bonds†

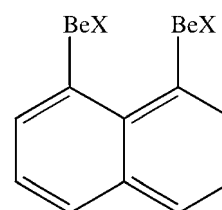
Oriana Brea,<sup>a</sup> Otilia Mó,<sup>a</sup> Manuel Yáñez,\*<sup>a</sup> Ibon Alkorta<sup>b</sup> and José Elguero<sup>b</sup>

**Although the Be–Be bond is extremely weak in Be<sub>2</sub> dimers, we have shown that rather stable Be–Be one-electron sigma bonds are formed upon electron attachment to 1,8-diBeX-naphthalene derivatives. Wavefunction analyses corroborate the formation of Be–Be covalent linkages in which the extra electron is accommodated between the Be atoms as reflected in the dramatic shortening of the Be–Be distance with respect to the corresponding neutral molecule.**

The possible existence of Be<sub>2</sub> molecules has attracted the interest of chemists for many years, since the MO theory predicts for this element a behavior similar to the noble gases, where no neutral stable diatomic molecules could be formed.<sup>1–10</sup> However, the existence of close lying empty 2p orbitals in Be opens up the possibility of an energetically feasible sp hybridization, not possible for noble gases, and therefore the possibility of forming stable derivatives like BeH<sub>2</sub> or BeCl<sub>2</sub>. But still the existence and stability of Be<sub>2</sub> molecules opened a question for many years. Back in 1984, the first evidence of the existence of Be<sub>2</sub> in the gas phase was reported in the literature,<sup>11,12</sup> though the dissociation energy of this dimer was extremely small (11 kJ mol<sup>-1</sup>).<sup>13–15</sup> For many years the nature of the bonding between two Be atoms remained unknown, until recent high-level *ab initio* calculations showed that the bonding is essentially due to non-dynamical correlation effects which mix two quasi-degenerate orbitals with a rather low occupancy.<sup>16</sup> However, Be is an electron deficient system and beryllium derivatives behave like very strong Lewis acids, when interacting with a great variety of Lewis bases, yielding rather strong linkages, called beryllium bonds.<sup>17</sup> The formation of beryllium bonds actually triggers a significant distortion of the BeX<sub>2</sub> compound, which departs significantly from linearity, because the electron density is accepted into the

empty p orbitals of Be, which necessarily results in a change in its hybridization from pure sp to sp<sup>n</sup> (1 < n ≤ 2).<sup>17</sup> This intrinsic acidity of –BeX groups also leads to the formation of intramolecular beryllium bonds, provided that within the same molecule a Lewis-basic center able to interact with a –BeX group exists.<sup>18</sup> When two –BeX groups coincide in the same compound, one should not expect them to interact in a bonding manner due to the aforementioned electron-deficient character, but they could still behave like very good electron acceptors. The question we have tried to address in this communication is what would be the electronic structure of such a kind of system after accepting an extra electron. If both –BeX groups are physically close, very likely the extra electron should be trapped between both electron-deficient Be–X groups. Is this indeed the case? To answer this question we have considered as appropriate candidates 1,8-disubstituted naphthalene derivatives in which the substituents at positions 1 and 8 are BeX (X = H, F, Cl, Br, CH<sub>3</sub>, NH<sub>2</sub>, OH, CF<sub>3</sub>, C(CF<sub>3</sub>)<sub>3</sub>, NF<sub>2</sub>, OF, CN, NO<sub>2</sub>, SOH, *t*-Bu, Ph) groups (see Scheme 1). We will show, through the use of high-level *ab initio* and density functional theory (DFT) calculations, that, indeed in most cases, although in not all of them, the global minimum of the corresponding radical anion is stabilized through the formation of a rather strong one-electron σ Be–Be bond.

For this purpose, the structures of the neutral 1,8-disubstituted naphthalene derivatives and their radical anions have been fully optimized at the B3LYP/6-31+G(d,p) level of theory. The same approach was used to obtain the harmonic vibrational



**Scheme 1** 1,8-Disubstituted naphthalene derivatives included in this study. X = H, F, Cl, Br, CH<sub>3</sub>, OH, CF<sub>3</sub>, C(CF<sub>3</sub>)<sub>3</sub>, N(CH<sub>3</sub>)<sub>2</sub>, OCH<sub>3</sub>, NF<sub>2</sub>, OF, CN, NO, SOCH<sub>3</sub>, *t*-Bu, Ph.

<sup>a</sup> Departamento de Química, Facultad de Ciencias, Universidad Autónoma de Madrid, Campus de Excelencia UAM-CSIC, Módulo 13, Cantoblanco, 28049-Madrid, Spain. E-mail: manuel.yanez@uam.es

<sup>b</sup> Instituto de Química Médica, C/Juan de la Cierva, 3, CSIC, 28006-Madrid, Spain

† Electronic supplementary information (ESI) available: Geometrical details, electron affinities, other energetic data, molecular graphs and ELF plots. See DOI: 10.1039/c6cc04350j

frequencies, which confirm that all the structures reported correspond to local minima of the corresponding potential energy surfaces. In order to have more reliable relative energies, the final total energies have been obtained using the same B3LYP functional but with a much extended 6-311+G(3df,2p) basis set. This theoretical model was assessed by comparing the B3LYP optimized structures with those obtained at the CCSD(T)/cc-pVDZ level of theory, for the anions in which X = H, F, as suitable model systems. As shown in Fig. S1 of the ESI† the agreement between both sets of values can be considered as excellent, in particular in what concerns the interaction involving both Be atoms. Also importantly, the relative stability of the two isomers does not change on going from the B3LYP to the CCSD(T) calculation. We have also verified that the structure of these systems does not change appreciably when using multireference CASSCF methods (see Fig. S2 of the ESI†), confirming that these kinds of systems are well described by methods accounting for electron correlation effects, but based on a single configuration, such as MP2, CCSD(T) or G4 theory. Finally, we have also verified that when a more flexible cc-pVTZ basis set is used the effect on the optimized structures is marginal (see Fig. S3 of the ESI† and the corresponding discussion). Three different approaches, namely the Atoms in Molecules (AIM) theory,<sup>19</sup> the Natural Bond Orbital (NBO) method<sup>20</sup> and the Electron Localization Function (ELF)<sup>21</sup> have been used to analyze the bonding in the systems under investigation, and to confirm the formation of one-electron Be–Be bonds upon electron attachment.

In principle, the neutral 1,8-disubstituted naphthalene derivatives may have different conformations depending on the relative position of the –BeX groups with respect to the aromatic rings (see Fig. 1). However for the parent compound (X = H) as well as for two other derivatives chosen as suitable examples (X = F, CN), the most stable one corresponds to the conventional structure **1** in which the Be atom and the central atom of the substituents X lie on the plane of the naphthalene ring. The other local minima are higher in terms of free energy (see Table S1 of the ESI†), so we can conclude that the most stable structure for 1,8-disubstituted naphthalene derivatives corresponds to the conventional conformation **1**.

The attachment of one electron to these three kinds of conformations leads to the three anions shown in Fig. 2, namely **A1**, **A2** and **A3**. The first conspicuous fact is that electron attachment to structures of type **1** leads to anions in

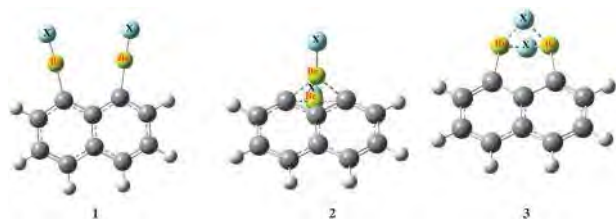


Fig. 1 Different types of local minima of neutral 1,8-diBeX derivatives of naphthalene. Type 1 structures were found to be the global minimum in all cases investigated.



Fig. 2 Different stationary points of the radical anions of 1,8-diBeX derivatives of naphthalene. Structures **A3** are found to be transition states rather than local minima.

which the Be–Be distance decreases dramatically. The formation of **A2** and **A3** anions, in contrast does not entail significant structural changes with respect to the corresponding neutrals, in particular in what concerns the Be–Be distance that actually lengthens slightly rather than shortening. On the other hand only **A1**- and **A2**-type structures correspond to minima of the potential energy surface, whereas all the **A3**-type structures are predicted to be transition states, whose imaginary frequency corresponds to a vibrational mode that would connect two identical **A1** minima in which the positions of the BeX groups are interchanged. The most important finding however is that for the majority of the substituents the anion formed from the most stable neutral, **A1**, is also the most stable anionic species (see Table S3 of the ESI†). For X = H, CH<sub>3</sub>, CF<sub>3</sub>, *t*-Bu, Ph, however the **A2** anion is slightly more stable than **A1** in terms of free energies (see Table S3, ESI†). However, it should be remembered that also in these cases, the dominant neutral structure is predicted to be of the 1-type, and therefore, electron attachment should produce **A1**-type structures, which would eventually isomerize to the most stable **A2**-type anions. However, the activation barrier associated with such a process is rather high (81 kJ mol<sup>-1</sup> in terms of free energies for X = H) and therefore even in the aforementioned cases in which the **A2** structure is found to be slightly more stable than the **A1** one, the isomerization would not occur under normal conditions because of the high activation barriers involved. Hence, one should expect, regardless of the nature of the substituent, that electron attachment should produce **A1**-type structures in all the cases.

Let us now analyze in more detail the bonding in **A1** anions. The most significant finding, as mentioned above, is the significant shortening of the Be–Be distance (see Table 1), pointing to a significant change in the bonding pattern on going from the neutral system to the anion. This shortening is particularly dramatic for X = *t*-Bu and C(CF<sub>3</sub>)<sub>3</sub>, because these bulky substituents force the Be–Be distance to be very large in the neutral system, whereas in the anion, the formation of the one-electron Be–Be bond (*vide infra*) leads always to Be–Be distances around 2.3 Å independent of the nature of the X substituent. Note that these Be–Be distances are only 0.3 Å longer than normal (two-electron) Be–Be bonds as the one in FBe–BeF<sup>22</sup> (see also Table S2 of the ESI†). This shortening is consistent with the existence of a Be–Be stretching displacement around 250–330 cm<sup>-1</sup>. It is also very important to emphasize that whereas G4 calculations<sup>23</sup> predict a positive electron affinity for naphthalene (7.5 kJ mol<sup>-1</sup>, so that the anion should not exist), for the 1,8-diBeX derivatives

**Table 1** Shortening of the Be–Be internuclear distance ( $\Delta R(\text{Be–Be})$ ) upon electron attachment; electron density at the Be–Be bond critical point; character of the hybrids involved in the one-electron Be–Be bond, together with its electron population and the corresponding Wiberg bond order (WBO)

X	$\Delta R(\text{Be–Be})$ (in Å)	$\rho_{\text{BCP}}$ (a.u.)	Hybrids character	Electron population	WBO
H	0.676	0.033	s(78.4%) p 0.27(21.5%)	0.922	0.195
F	0.667	0.033	s(79.6%) p 0.25(20.2%)	0.932	0.235
Cl	0.801	0.036	s(78.8%) p 0.27(21.1%)	0.937	0.226
Br	0.843	0.038	s(78.5%) p 0.27(21.4%)	0.937	0.223
CH <sub>3</sub>	0.645	0.032	s(81.3%) p 0.24(18.6%)	0.884	0.189
OH	0.538	0.030	s(80.9%) p 0.23(19.0%)	0.929	0.230
CF <sub>3</sub>	0.607	0.035	s(81.9%) p 0.22(18.0%)	0.893	0.200
C(CF <sub>3</sub> ) <sub>3</sub>	1.243	0.033	s(78.7%) p 0.27(21.2%)	0.875	0.215
N(CH <sub>3</sub> ) <sub>2</sub>	0.633	0.032	s(80.7%) p 0.24(19.2%)	0.884	0.206
OCH <sub>3</sub>	0.569	0.031	s(81.8%) p 0.22(18.1%)	0.911	0.223
NF <sub>2</sub>	0.849	0.035	s(79.9%) p 0.25(20.3%)	0.879	0.202
OF	0.578	0.034	s(81.2%) p 0.23(18.7%)	0.870	0.202
CN	0.883	0.034	s(80.9%) p 0.23(19.0%)	0.852	0.173
NO <sup>a</sup>	—	—	—	—	0.030
SOMe	0.597	0.034	s(81.4%) p 0.23(18.5%)	0.928	0.233
<i>t</i> -Bu	0.926	0.033	s(82.1%) p 0.22(17.8%)	0.883	0.204
Ph	0.741	0.033	s(82.5%) p 0.21(17.4%)	0.854	0.182

<sup>a</sup> For X = NO both neutral and anion can be seen as the result of the interaction between a (NO)<sub>2</sub> dimer and the C<sub>10</sub>H<sub>6</sub>Be<sub>2</sub> moiety, so no Be–Be is formed (see Fig. S4 of the ESI<sup>†</sup>).

investigated the calculated electron affinity of the corresponding neutral systems goes from  $-53.7$  (X = OCH<sub>3</sub>) up to  $-220.3$  kJ mol<sup>-1</sup> (X = C(CF<sub>3</sub>)<sub>3</sub>) (see Table S4 of the ESI<sup>†</sup>). The existence of this stabilizing Be–Be interaction is also reflected in the molecular graphs of the A1-anions which show the existence of a Be–Be bond critical point (see Fig. 3 and Fig. S4 of the ESI<sup>†</sup>), with an electron density that is typically around 0.033 a.u. (see Table 1) that does not exist in the neutral compounds.

Furthermore, as shown also in Fig. 3 both the energy density and the Laplacian of the energy density at the Be–Be BCP are always negative indicating that this interaction has a non-negligible covalent character, also confirmed by the ratio  $-G(r)/V(r)$  which is typically around 0.14.<sup>24</sup> This is totally consistent, also, with the description of the bonding provided by the NBO analysis, which shows the existence, in all cases, of a Be–Be bonding molecular orbital with a large contribution of the 2s orbitals of Be (around 80%), and with a population always around one electron, and which, as illustrated in the second row of Fig. 3 is totally localized between the two Be atoms. Also consistently, the Wiberg bond order (WBO)<sup>25</sup> is not negligible (see Table 1). These two pictures are in harmony with the one that can be obtained by means of the ELF approach. Indeed, as it is clearly illustrated in the third row of Fig. 3 (see also Fig. S5 of the ESI<sup>†</sup>), in all the A1-type anions, a Be–Be disynaptic-basin is systematically located, with a population always around one electron, ratifying that A1-type anions are stabilized through the formation of one-electron Be–Be bonds.

It is also worth mentioning that in A2-type isomers, there are no Be–Be bonds. As illustrated by the corresponding molecular graphs the two Be atoms bridge between C1 and C8 of the naphthalene molecule, but no BCP is found between both Be atoms (see Fig. S6 of the ESI<sup>†</sup>).

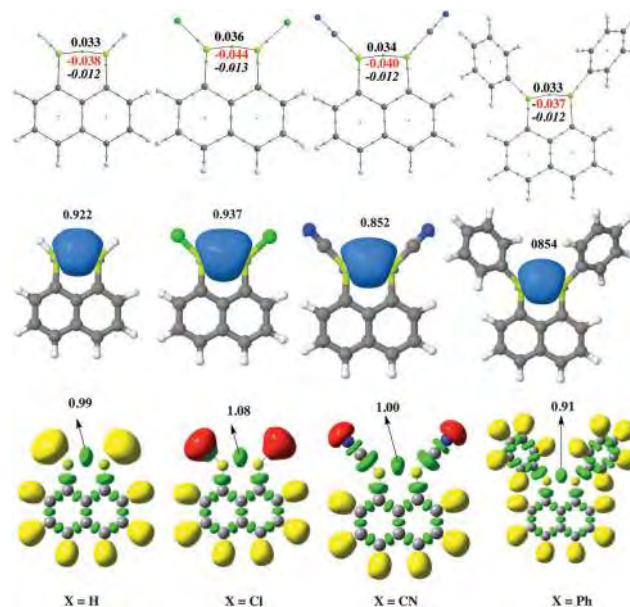
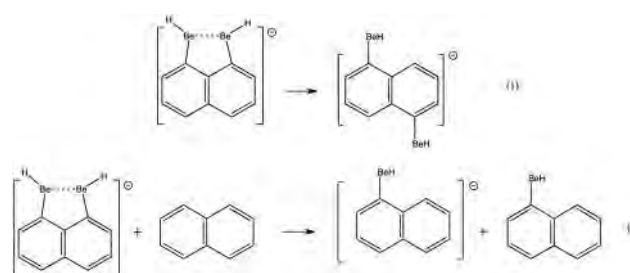


**Fig. 3** Molecular graphs (first row) for 1,8-diBeX-naphthalene radical anions (X = H, Cl, CN, Ph). Green and red dots correspond to bond and ring critical points respectively. For the Be–Be bond critical point the electron density, its Laplacian (in red) and the energy density (in italics) are given. Both values in are a.u. The second row shows the one-electron localized MO between both Be atoms obtained through the NBO approach. Its population (in e<sup>-</sup>) is also given. The third row presents the ELF plots for the same systems. Yellow lobes correspond to disynaptic basins involving hydrogen atoms. Green lobes correspond to disynaptic basins between heavy atoms and red basins denote monosynaptic basins associated with lone-pairs. The population (e<sup>-</sup>) of the Be–Be disynaptic basin is shown.

In order to have an idea of the strength of this one-electron linkage, we have used the two isodesmic reactions shown in Scheme 2. In order to ensure the reliability of these estimates, the calculation of the reaction energies was carried out at the G4-level of theory, which typically yields values with errors smaller than 4 kJ mol<sup>-1</sup>.

The energetics also confirms the existence of these one-electron Be–Be bonds. The localized molecular orbital energy decomposition analysis (LMOEDA)<sup>26</sup> (see details in the ESI<sup>†</sup>) shows that in the 1,8-diBeX-naphthalene radical anions, the Be–Be interaction exhibits a significant covalent character. Consistently, G4 theory predicts the isodesmic reaction (1) of Scheme 2 to be endothermic by 61 kJ mol<sup>-1</sup>. This value, which



**Scheme 2** Isodesmic reactions to estimate the energy of the one-electron Be–Be bond.

can be taken as a reasonable estimate of the strength of the one-electron Be–Be bond in the **A1** anion for X = H, should be corrected by the energy change of the C–Be bonds, which in the reactants are weaker than in the products. Our estimate of this effect is 15 kJ mol<sup>-1</sup> (see Table S5 of the ESI<sup>†</sup>), which would yield for the Be–Be bond an energy of 76 kJ mol<sup>-1</sup>. The value obtained when reaction (2) is used is 89 kJ mol<sup>-1</sup>, so we can infer that the energy associated with this one-electron Be–Be sigma bond for the parent compound (X = H) is typically around 80 kJ mol<sup>-1</sup>, and it should be slightly stronger for electron withdrawing substituents. Again these values are consistent with those obtained in with the LMOEDA, which gives for the Be–Be bond in the [(CH<sub>3</sub>BeH)<sub>2</sub>]<sup>-</sup> dimer an energy of -74 kJ mol<sup>-1</sup> (see details in the ESI<sup>†</sup>). It can then be concluded that even though a direct interaction between two Be atoms leads to an extremely weak bond, rather stable one-electron Be–Be bonds similar to B–B bonds recently reported in the literature<sup>27,28</sup> are formed upon electron attachment to 1,8-diBeX-naphthalene derivatives, showing that this property can be considered a signature of this kind of compounds when they involve electron deficient atoms as substituents. Finally the formal similarity between 1,8-diBeX-naphthalene derivatives and proton sponges such as 1,8-bis(dimethylamino)naphthalene is worth noting.<sup>29</sup> The latter interact strongly with protons through the Lewis base N(CH<sub>3</sub>)<sub>2</sub> substituents, whereas the former interact with electrons through the Lewis acid BeX substituents.

This work was supported by the Projects CTQ2015-63997-C2 and CTQ2013-43698-P, FOTOCARBON-CM S2013/MIT-2841 by the COST Action CM1204.

## Notes and references

- M. R. A. Blomberg and P. E. M. Siegbahn, *Int. J. Quantum Chem.*, 1978, **14**, 583.
- M. A. Robb and S. Wilson, *Mol. Phys.*, 1980, **40**, 1333.
- S. Wilson, *Mol. Phys.*, 1983, **49**, 1489.
- G. A. Petersson and W. A. Shirley, *Chem. Phys. Lett.*, 1989, **160**, 494.
- S. Evangelisti, G. L. Bendazzoli and L. Gagliardi, *Chem. Phys.*, 1994, **185**, 47.
- J. Starck and W. Meyer, *Chem. Phys. Lett.*, 1996, **258**, 421.
- J. M. L. Martin, *Chem. Phys. Lett.*, 1999, **303**, 399.
- J. A. W. Harkless and K. K. Irikura, *Int. J. Quantum Chem.*, 2006, **106**, 2373.
- K. Patkowski, V. Spirko and K. Szalewicz, *Science*, 2009, **326**, 1382.
- J. Koput, *Phys. Chem. Chem. Phys.*, 2011, **13**, 20311.
- V. E. Bondybey and J. H. English, *J. Chem. Phys.*, 1984, **80**, 568.
- V. E. Bondybey, *Chem. Phys. Lett.*, 1984, **109**, 436.
- J. M. Merritt, V. E. Bondybey and M. C. Heaven, *Science*, 2009, **324**, 1548.
- S. Sharma, T. Yanai, G. H. Booth, C. J. Umrigar and G. K. L. Chan, *J. Chem. Phys.*, 2014, **140**, 104112.
- M. J. Deible, M. Kessler, K. E. Gasperich and K. D. Jordan, *J. Chem. Phys.*, 2015, **143**, 084116.
- M. El Khatib, G. L. Bendazzoli, S. Evangelisti, W. Helal, T. Leininger, L. Tenti and C. Angeli, *J. Phys. Chem. A*, 2014, **118**, 6664.
- M. Yáñez, P. Sanz, O. Mó, I. Alkorta and J. Elguero, *J. Chem. Theory Comput.*, 2009, **5**, 2763.
- O. Brea, I. Alkorta, I. Corral, O. Mó, M. Yáñez and J. Elguero, in *Intermolecular interactions in crystals: Fundamentals of Crystal Engineering*, ed. J. Novoa, Royal Society of Chemistry, Cambridge, 2016.
- R. F. W. Bader, *Atoms in Molecules. A Quantum Theory*, Clarendon Press, Oxford, 1990.
- A. E. Reed, L. A. Curtiss and F. Weinhold, *Chem. Rev.*, 1988, **88**, 899.
- A. Savin, R. Nesper, S. Wengert and T. F. Fäslser, *Angew. Chem., Int. Ed. Engl.*, 1997, **36**, 1808.
- Z. Cui, W. Yang, L. Zhao, Y. Ding and G. Frenking, *Angew. Chem., Int. Ed.*, 2016, **55**, 7841.
- L. A. Curtiss, P. C. Redfern and K. Raghavachari, *J. Chem. Phys.*, 2007, **126**, 084108.
- D. Cremer and E. Kraka, *Croat. Chem. Acta*, 1984, **57**, 1259.
- K. B. Wiberg, *Tetrahedron*, 1968, **24**, 1083.
- P. Su and H. Li, *J. Chem. Phys.*, 2009, **131**, 014102.
- J. D. Hoefelmeyer and F. P. Gabbai, *J. Am. Chem. Soc.*, 2000, **122**, 9054.
- A. Hubner, A. M. Diehl, M. Diefenbach, B. Endeward, M. Bolte, H. W. Lerner, M. C. Holthausen and M. Wagner, *Angew. Chem., Int. Ed.*, 2014, **53**, 4832.
- R. W. Alder, P. S. Bowman, W. R. S. Steele and D. R. Winterman, *Chem. Commun.*, 1968, 723.

**On the existence of intramolecular one-electron Be-Be bonds.**

Oriana Brea, Otilia Mó, Manuel Yáñez, Ibon Alkorta, José Elguero

*Contribution from the Departamento de Química, Facultad de Ciencias, Módulo 13, Universidad Autónoma de Madrid, Campus de Excelencia UAM-CSIC, Cantoblanco, 28049-Madrid, Spain and the Instituto de Química Médica, C/ Juan de la Cierva, 3, CSIC, 28006-Madrid. Spain*

**Supporting Information (A total of 11 pages)**

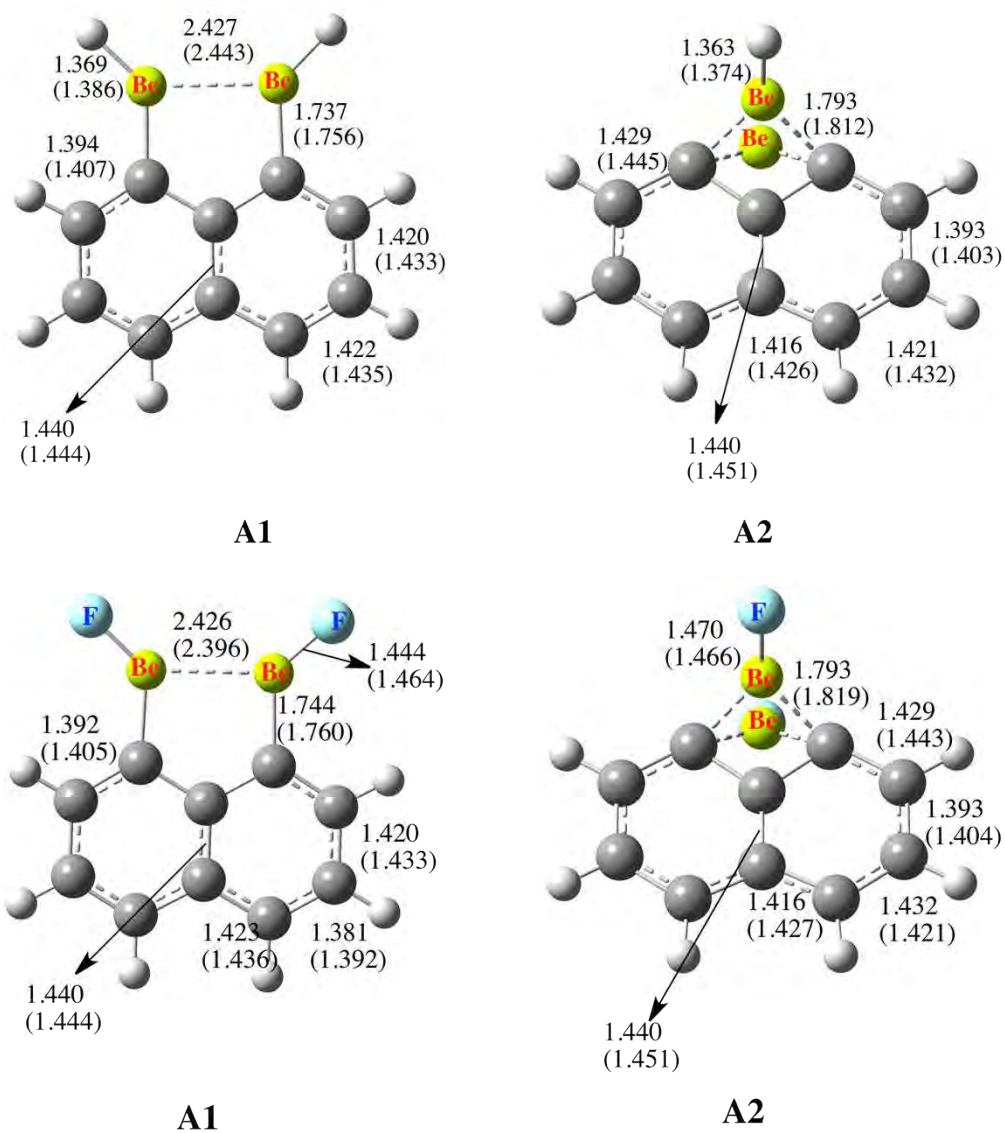


**Figure S1.** Comparison between B3LYP/6-31+G(d,p) and CCSD(T)/cc-pVDZ (values within parenthesis) optimized geometries of the stable anions of 1,8-BeX-naphthalene derivatives (X = H, F). Bond lengths in Å. In spite of the fact that in isomers **A2** the Be-Be distances are around 2.2 Å, in both cases, no bond critical point is found between both Be atoms.

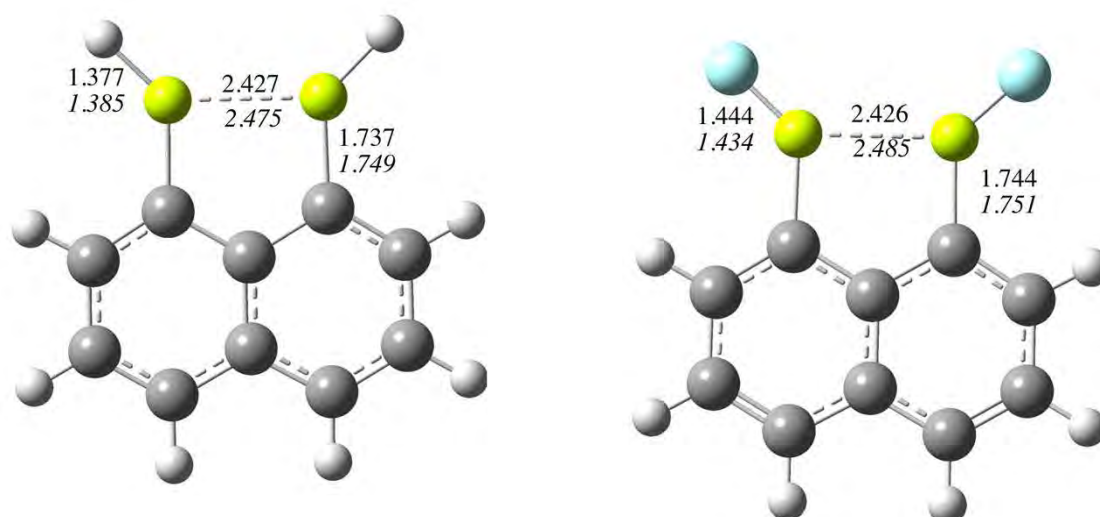


**Figure S2.** Comparison of the optimized geometrical parameters which characterize the formation of the one-electron Be-Be bond in 1,8-BeX-naphthalene anions (X = H, F), obtained through B3LYP/6-31+G(d,p) and CASSCF(5,6)/6-31+G(d,p) calculations. The latter are written in italics.



### Basis set effects

The effect on enlarging the size of the basis set on the structural characteristics of the one-electron Be–Be bonds was investigated at two different levels of theory. In the first assessment, we have compared the structures obtained when a B3LYP/6-31+G(d,p) theoretical model is used with those obtained at the B3LYP/cc-pVTZ level, for some 1,8-BeX-naphthalene anionic derivatives, taken as suitable examples (see Figure S3a). The second assessment was done using high-level ab initio methods. Taking into account that geometry optimizations at the CCSD(T)/cc-pVTZ are too expensive for systems of the size consider in this study, this assessment was made by using the RI-CC2 method, in which only singles and doubles excitations are taking into account. The results of this comparison are shown in Figure S3b.

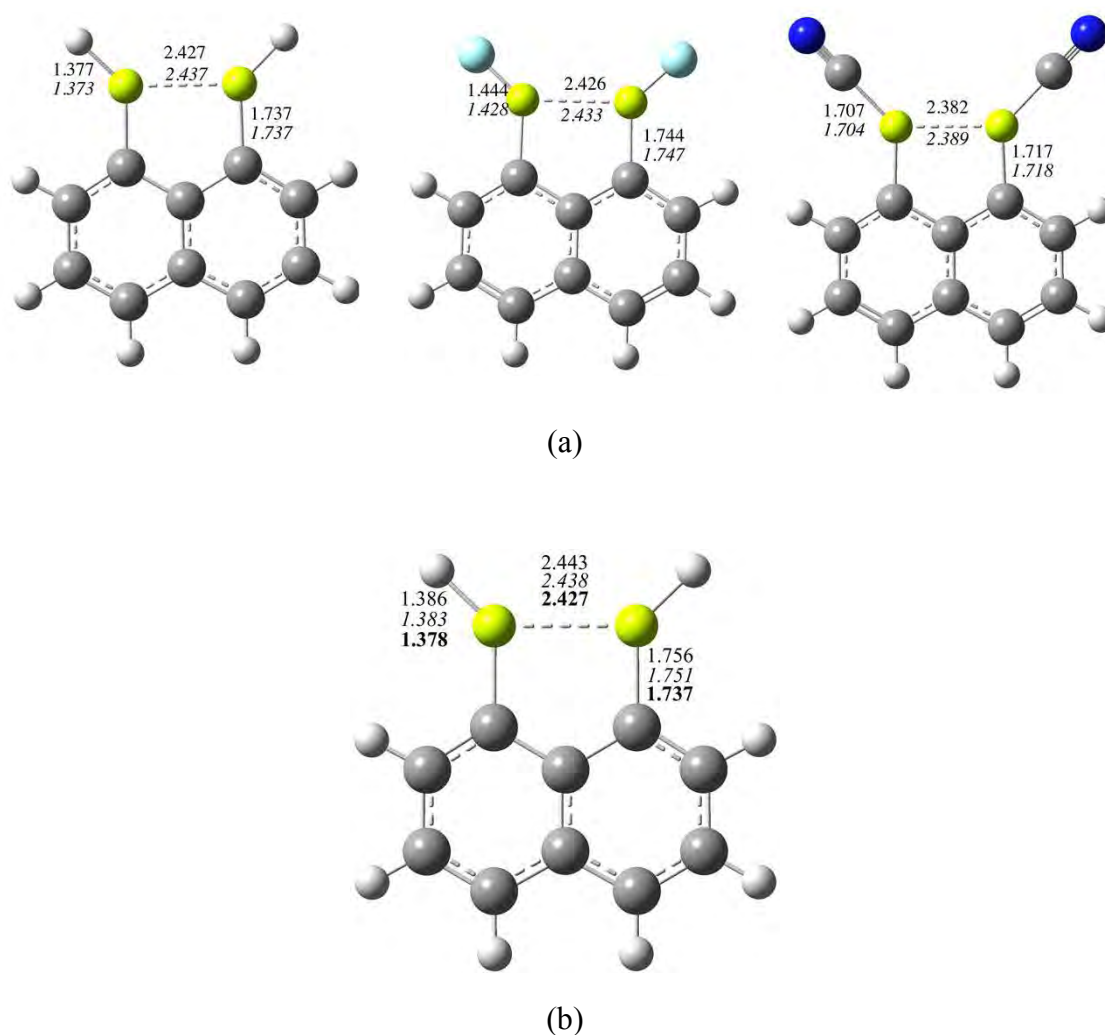


**Figure S3.** (a) Effect of enlarging the basis set from a split-double zeta 6-31+G(d,p) to a triple zeta cc-pVTZ on the geometrical parameters associated to the existence of a Be-Be one-electron bond, when the B3LYP hybrid functional is used. Values in italic correspond to those obtained with the cc-pVTZ basis set expansion. (b) Comparison between CCSD(T)/cc-pVDZ geometrical parameters, with those obtained at the RI-CC2/cc-pVDZ (italic) and at the the RI-CC2/cc-pVTZ (bold) levels of theory, respectively.

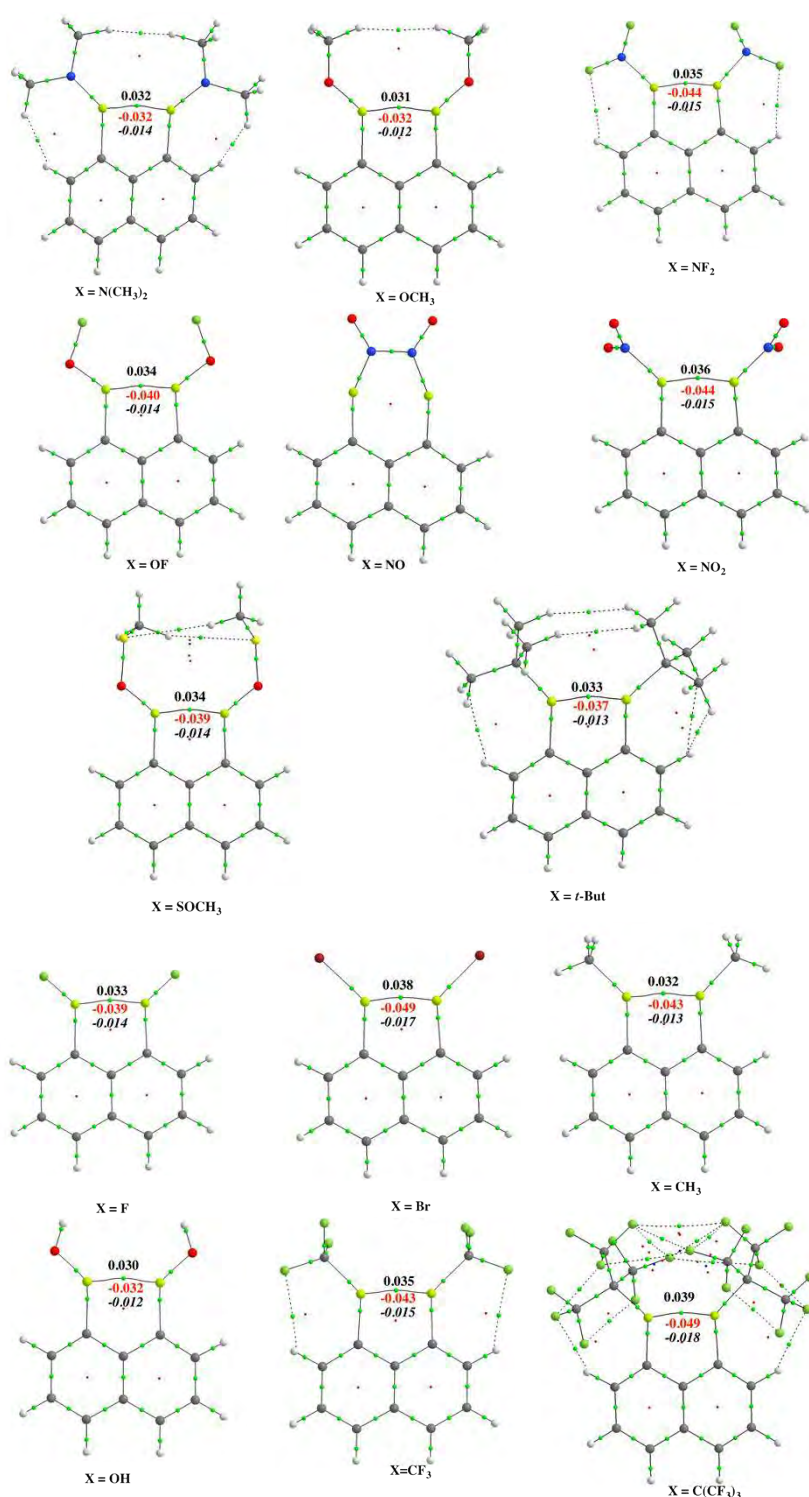


**Figure S4.** Molecular graphs for 1,8-BeX-naphthalene A1-type anions ( X = F, Br, CH<sub>3</sub>, OH, CF<sub>3</sub>, C(CF<sub>3</sub>)<sub>3</sub>, N(CH<sub>3</sub>)<sub>2</sub>, OCH<sub>3</sub>, NF<sub>2</sub>, OF, NO, NO<sub>2</sub>, SOCH<sub>3</sub>, *t*-But), showing the existence of a one-electron Be-Be bond, with the only exception of X =NO, where the systems is stabilized through a N-N bond between the two substituents. Green and red dots correspond to bond and ring critical points respectively. For the Be-Be bond critical point, the electron density and its Laplacian (in red) as well as the energy density (in italics) are given in a.u.

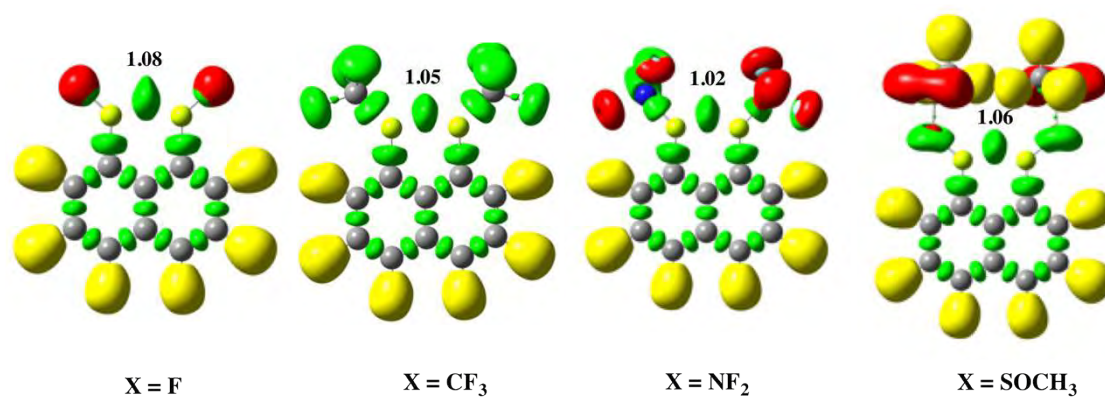


**Figure S5.** ELF plots for 1,8-BeX-naphthalene anions ( $X = \text{F}, \text{CF}_3, \text{NF}_2, \text{SOCH}_3$ ). Yellow lobes correspond to disynaptic basins involving hydrogen atoms. Green lobes correspond to disynaptic basins between heavy atoms and red basins denote monosynaptic basins associated with lone-pairs. The population ( $e^-$ ) of the Be-Be disynaptic basin is shown.

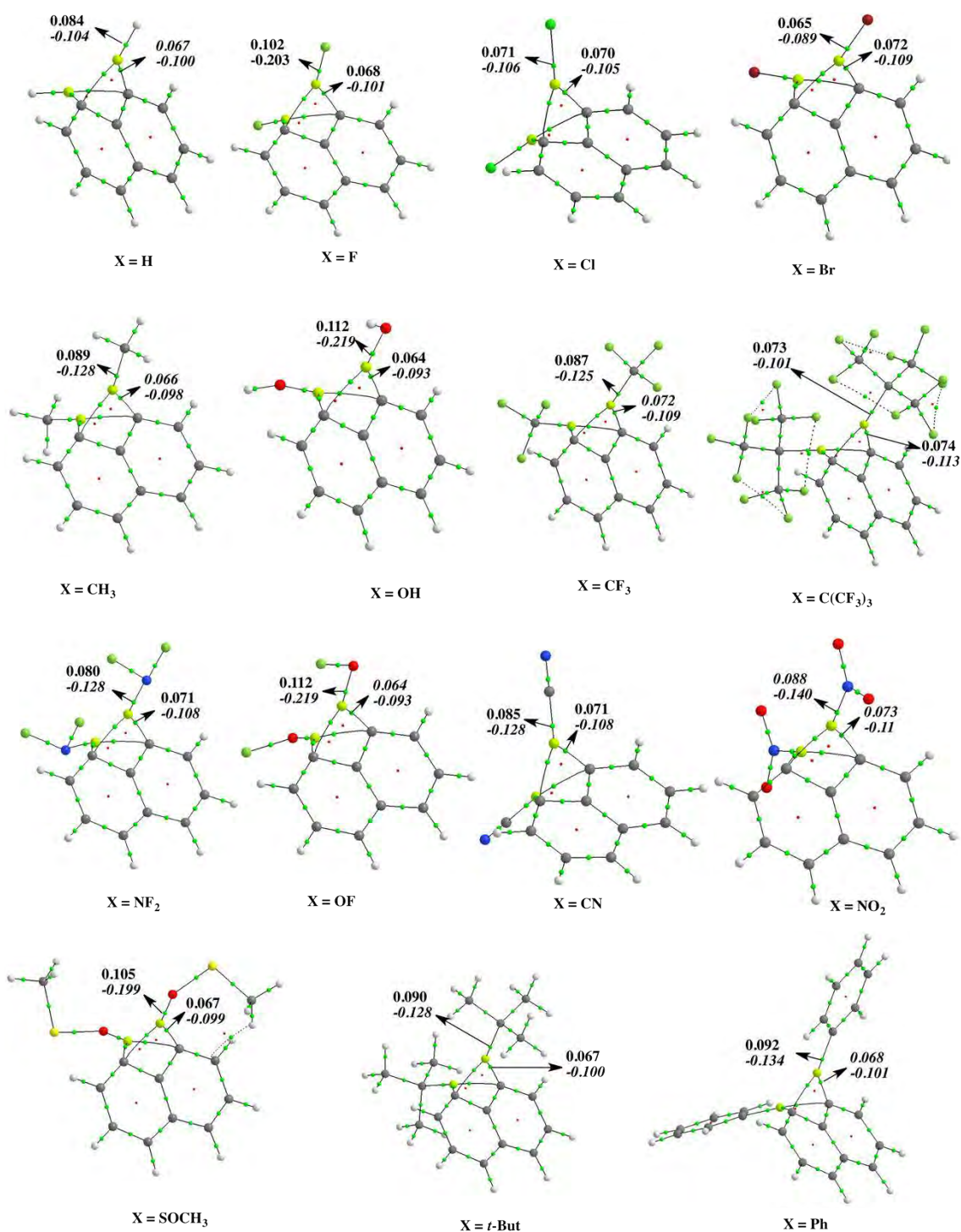


**Figure S6.** Molecular graphs for 1,8-BeX-naphthalene A2-type anions (X = H, F, Cl, Br, CH<sub>3</sub>, OH, CF<sub>3</sub>, C(CF<sub>3</sub>)<sub>3</sub>, NF<sub>2</sub>, OF, CN, NO<sub>2</sub>, SOCH<sub>3</sub>, *t*-But, Ph). Green and red dots correspond to bond and ring critical points respectively. For the Be-Be bond critical point the electron density and the energy density (in italics) are given. Both values in a.u.

**Table S1.** B3LYP/6-31+G(d,p) relative free energy of isomers **2** and **3** with respect to isomer **1** minima for 1,8-BeX-naphthalene derivatives. Negative values (in kJ mol<sup>-1</sup>), indicate that the corresponding isomer is more stable than isomer **1**.

	<b>Isomer 2</b>	<b>Isomer 3</b>
<b>X</b>		
<b>H</b>	36	40
<b>F</b>	55	56
<b>Cl</b>	185	223
<b>Br</b>	177	215
<b>CF<sub>3</sub></b>	208	143
<b>N(CH<sub>3</sub>)<sub>2</sub></b>	-	49
<b>OH</b>	136	45
<b>NF<sub>2</sub></b>	75	16
<b>OF</b>	200	169
<b>CN</b>	5	93
<b>NO</b>	-	191

**Table S2.** Be-Be distances (Å) for 1,8-BeX-naphthalene derivatives and its anions

<b>X</b>	R (Be-Be) (neutral)	R (Be-Be) anion <sup>a</sup>
<b>H</b>	3.103	2.427
<b>F</b>	3.093	2.426
<b>Cl</b>	3.168	2.367
<b>Br</b>	3.172	2.329
<b>CH<sub>3</sub></b>	3.102	2.412
<b>NH<sub>2</sub></b>	2.979	2.418
<b>OH</b>	3.002	2.464
<b>CF<sub>3</sub></b>	2.978	2.371
<b>C(CF<sub>3</sub>)<sub>3</sub></b>	3.548	2.305
<b>NF<sub>2</sub></b>	3.206	2.357
<b>OF</b>	3.370	2.375
<b>CN</b>	3.265	2.382
<b>NO<sub>2</sub></b>	3.161	2.344
<b>SOH</b>	3.008	2.312
<b>t-Bu</b>	3.369	2.443
<b>Ph</b>	3.156	2.415

<sup>a</sup> Note that these values are only  $\approx 0.3$  Å longer than normal (two-electron) Be-Be bonds as the one in FBe–BeF (G. Frenking et al. *Angew. Chem. Int. Ed.* 2016, doi:10.1002/anie.201601890). Note also that these distances are only slightly longer than those in Be<sub>2</sub><sup>+</sup> (2.246 Å) and Be<sub>2</sub><sup>2+</sup> (2.130 Å).

**Table S3.** B3LYP/6-311+G(3df,2p)//B3LYP/6-31+G(d,p) relative energy of **A2** with respect to **A1** minima for 1,8-BeX-naphthalene anions. Negative values (in kJ mol<sup>-1</sup>) indicate that **A1** is more stable than **A2**

<b>X</b>	<b>ΔH</b>	<b>ΔG</b>
<b>H</b>	13.8	10.2
<b>F</b>	-20.3	-23.6
<b>Cl</b>	-10.6	-14.1
<b>Br</b>	-9.9	-10.9
<b>CH<sub>3</sub></b>	9.8	12.6
<b>OH</b>	-20.6	-24.1
<b>CF<sub>3</sub></b>	10.1	6.8
<b>C(CF<sub>3</sub>)<sub>3</sub></b>	29.0	29.2
<b>N(CH<sub>3</sub>)<sub>2</sub></b>	-0.9	-1.4
<b>OCH<sub>3</sub></b>	-20.8	-23.5
<b>NF<sub>2</sub></b>	-1.9	-3.0
<b>OF</b>	-5.5	-9.0
<b>NO</b>	-77.1	-63.5
<b>CN</b>	5.1	0.6
<b>SOCH<sub>3</sub></b>	-15.4	-15.4
<b>t-But</b>	19.0	14.9
<b>Ph</b>	10.9	8.3

**Table S4.** Electron affinity (EA, kJ mol<sup>-1</sup>) of the 1,8-BeX-naphthalene derivatives investigated and Be-Be stretching frequency ( $\nu_{\text{BeBe}}$ , cm<sup>-1</sup>) of the corresponding **A1**-type anion.

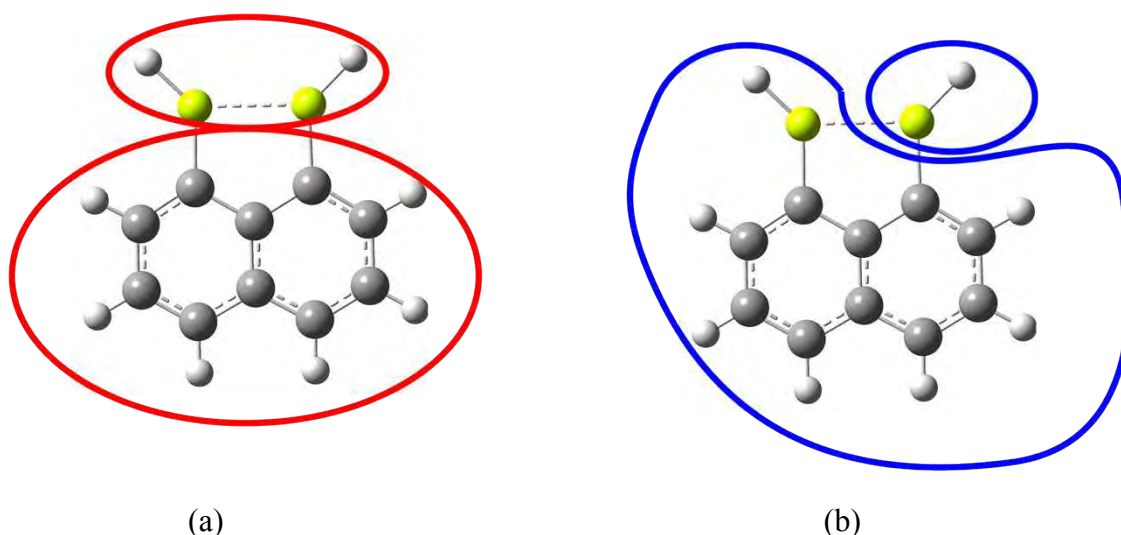
<b>X</b>	<b>EA (neutral)</b>	<b><math>\nu_{\text{BeBe}}</math> (anion)</b>
<b>H</b>	-93.9	332
<b>F</b>	-99.8	278
<b>Cl</b>	-138.6	223
<b>Br</b>	-155.5	171
<b>CH<sub>3</sub></b>	-66.8	273
<b>OH</b>	-57.6	275
<b>CF<sub>3</sub></b>	-191.7	269
<b>C(CF<sub>3</sub>)<sub>3</sub></b>	-220.3	301
<b>N(CH<sub>3</sub>)<sub>2</sub></b>	-67	370
<b>OCH<sub>3</sub></b>	-53.7	247
<b>NF<sub>2</sub></b>	-137.9	156
<b>OF</b>	-148.3	275
<b>NO</b>	-124.0	313
<b>CN</b>	-214.7	198
<b>SOCH<sub>3</sub></b>	-93.9	256
<b>t-But</b>	-98.4	158
<b>Ph</b>	-106.5	131

**Table S5.** B3LYP/6-311+G(3df,2p) energies of 1,5-diBeH-naphthalene anion in its equilibrium conformation and with the C-Be distances equal to those of 1,8-diBeH-naphthalene anion.

<b>R (C-Be)</b>	<b>E<sub>total</sub> (a.u.)</b>	<b>□E (kJ·mol<sup>-1</sup>)</b>
<b>equilibrium</b>	-415.5097376	0
<b>1.737</b>	-415.5040365	15

### Localized Molecular Orbital Energy Decomposition Analysis (LMOEDA).

In order to characterize the Be-Be interactions in the anions under investigation, through the use of the LMOEDA,<sup>a</sup> we have considered two approaches. In the first one, we have taken the unsubstituted parent compound 1,8 BeH-naphthalene anion and we have defined two different fragmentations. In fragmentation (a) we have defined HBeBeH as one of the fragments and the C<sub>10</sub>H<sub>8</sub> moiety as another fragment. In fragmentation (b) we have taken only one of the BeH groups as the first fragment and C<sub>10</sub>H<sub>8</sub>BeH as the second fragment (see the following Scheme)



Scheme. Molecular fragmentation considered in the LMOEDA calculation for the 1,8 BeH-naphthalene anion. (a) HBeBeH + C<sub>10</sub>H<sub>8</sub> and (b) BeH + C<sub>10</sub>H<sub>8</sub>BeH fragments.

The values of the Energy Decomposition Analysis (EDA) for the two fragmentations are given in the following Table S6.

Table S6. Energy decomposition analysis of 1,8 BeH-naphthalene anion. The fragments correspond to those proposed in the Scheme. All values are in kJ·mol<sup>-1</sup>.

Fragmentation	Eelst	Epauli	Eorb	Eint
(a)	-880.4	1288.6	-1021.5	-613.3
(b)	-762.5	1764.9	-1377.4	-375.1
Be-Be	-322.3	1120.6	-866.68	-68.4

Taking into account that in fragmentation (b) we have only the interaction associated with the formation of one C-Be bond between the C<sub>10</sub>H<sub>8</sub>BeH and a BeH group, and that in fragmentation (a) we have the interaction between HBe-BeH and the C<sub>10</sub>H<sub>8</sub>

moiety, with the formation of two C–Be bonds, the difference between the energies of fragmentation (b) –  $\frac{1}{2}$  of the energies of fragmentation (a), give us the energies associated with the Be–Be interaction. It can be seen that this value is rather close to the one estimated using the isodesmic reactions (1) and (2). Also importantly, the EDA shows that the orbital contribution to the interaction energy is clearly dominant.

In the second approach we have calculated the  $(\text{HBeCH}_3)_2$  (anion) with  $C_{2v}$  symmetry at B3LYP/6-31+G(d,p). The structure obtained present a Be-Be distance of 2.544 Å, whereas the neutral dimer dissociates spontaneously into the two monomers.



Figure S7.  $(\text{HBeCH}_3)_2$  anion structure calculated at B3LYP/6-31+G(d,p) level of theory with  $C_{2v}$  symmetry.

The LMOEDA partition considering one of the monomers as neutral and the other as an anion yields the following results:

Table S7. Energy decomposition analysis for the fragmentations of the  $(\text{HBeCH}_3)_2$  anion. The dimer is fragmented in a neutral and an anion monomer. All values are in  $\text{kJ}\cdot\text{mol}^{-1}$ .

Fragmentation	$E_{\text{elst}}$	$E_{\text{XC}}$	$E_{\text{rep}}$	$E_{\text{pol}}$	$E_{\text{DISP}}$	$E_{\text{int}}$
$\text{HBeCH}_3 + (\text{HBeCH}_3)^{-1}$	-173.8	-133.4	422.1	-182.2	-34.8	-133.4

The distortion energy of the monomers to adopt the geometry of the complex is 3.3  $\text{kJ}\cdot\text{mol}^{-1}$  for the anion and 56.7  $\text{kJ}\cdot\text{mol}^{-1}$  for the neutral molecule. So, the sum of the distortion energy plus the interaction energy obtained with LMOEDA amount 73.4  $\text{kJ}\cdot\text{mol}^{-1}$ . This value is similar to the ones provided in the article for the isodesmic reactions.

<sup>a</sup> Peifeng Su and Hui Li, "Energy decomposition analysis of covalent bonds and intermolecular interactions" J. Chem. Phys. **2009**, 131, 014102





---

## B.5 ARTICLE IV

### *Beryllium-Based Anion Sponges: Close Relatives of Proton Sponges*

Published in: Chemistry - A European Journal, **2016**, 22, DOI:10.1002/chem.201604325.



## Anion Sponges | Hot Paper |

## Beryllium-Based Anion Sponges: Close Relatives of Proton Sponges

Oriana Brea,<sup>[a]</sup> Inés Corral,<sup>[a]</sup> Otilia Mó,<sup>[a]</sup> Manuel Yáñez,<sup>\*[a]</sup> Ibon Alkorta,<sup>[b]</sup> and José Elguero<sup>[b]</sup>

**Abstract:** Through the use of high-level ab initio and density functional calculations it is shown that 1,8-diBeX-naphthalene (X=H, F, Cl, CN, CF<sub>3</sub>, C(CF<sub>3</sub>)<sub>3</sub>) derivatives behave as anion sponges, very much as 1,8-bis(dimethylamino)naphthalene derivatives behave as proton sponges. The electron-deficient nature of the BeX substituents, which favors strong charge transfer from the anion towards the former, results in anion affinities that are among the largest ones reported for single neutral molecules.

A great majority of non-covalent interactions involve a charge transfer from one of the interacting subunits, acting as a Lewis base, towards a second subunit acting as a Lewis acid. This is actually the case of conventional hydrogen bonds, A–H...X in which the hydrogen bond acceptor, X, acts as a Lewis base transferring some electron charge typically from its lone-pairs into the A–H antibonding orbital of the hydrogen bond donor, acting as a Lewis acid. This is also the signature of the so-called beryllium bonds,<sup>[1]</sup> base...BeXZ, in which the BeXZ derivative behaves as an extremely strong Lewis acid, due to the electron-deficient nature of the Be atom. This charge transfer is not only reflected in significant interaction energies, but in dramatic structural changes of both the BeXZ derivative, which usually departs significantly from linearity, whereas the Be–X and Be–Z bonds also lengthen appreciably, and the corresponding Lewis base, which, in some specific cases cleaves heterolytically and spontaneously producing an ion-pair, or homolytically yielding two radicals in exergonic and spontaneous processes.<sup>[2]</sup>

The capacity of Be atoms within a molecular framework to accept electronic density into their low-lying empty p orbitals is also behind their ability to form rather stable anions.<sup>[3]</sup> This is the case of 1,8-diBeX-naphthalene derivatives, whose anionic

forms are characterized by very short Be–Be distances, through the formation of one-electron  $\sigma_{\text{Be-Be}}$  bonds, as ratified by the analysis of their electron density distribution. Indeed, the atoms in molecules (AIM) theory shows the existence of a bond critical point (BCP) between both Be atoms, with negative values of both the Laplacian and the energy density, ratifying the covalent character of the interaction. Consistently, the electron localization function (ELF) method also locates a V(Be,Be) disynaptic basin with a population of one electron or more, whereas the natural bond orbital (NBO) approach, shows the existence of a  $\sigma_{\text{Be-Be}}$  bonding orbital with a population of about  $1 e^-$ .<sup>[3]</sup> These findings seem to indicate that this kind of compounds should be able to act as good anion receptors. It is important to emphasize that anion sensors have attracted an increasing attention in the last decades for many reasons, among them because they lead to a better performance of lithium-based batteries,<sup>[4]</sup> they act as anion carriers for anion-selective electrodes,<sup>[5]</sup> as anion sensors,<sup>[6]</sup> as selective fluorescent sensing of anions,<sup>[7]</sup> or as receptors for the selective capture of specific or toxic anions.<sup>[8]</sup>

Different strategies have been suggested to design strong and selective anion receptors.<sup>[9]</sup> To explore whether 1,8-diBeX-naphthalene derivatives are good anion receptors, herein we have theoretically investigated the characteristics and stability of complexes formed when 1,8-diBeX-naphthalene (X=H, F, Cl, CN, CF<sub>3</sub>, C(CF<sub>3</sub>)<sub>3</sub>) derivatives interact with some of the most common anions that can be found in the natural media,<sup>[10]</sup> namely, F<sup>-</sup>, Cl<sup>-</sup>, Br<sup>-</sup>, CN<sup>-</sup>, NO<sub>2</sub><sup>-</sup>, NO<sub>3</sub><sup>-</sup>, SO<sub>4</sub><sup>2-</sup>.

The geometries of the complexes have been optimized, with density functional theory (DFT), through the use of the B3LYP hybrid functional<sup>[11]</sup> together with a 6-31+G(d,p) basis set expansion. The same level of theory was used to calculate their harmonic vibrational frequencies to confirm that the structures obtained were local minima of the potential energy surface. Final energies were obtained in single-point calculations by using the same functional with a more flexible 6-311+G(3df,2p) basis set expansion on the aforementioned B3LYP/6-31+G(d,p) optimized geometries. To assess the reliability of this theoretical model, a subset of these [1,8-diBeX-naphthalene]Y anions (X=H, Y=F<sup>-</sup>, Cl<sup>-</sup>, Br<sup>-</sup>, CN<sup>-</sup>, NO<sub>2</sub><sup>-</sup>, NO<sub>3</sub><sup>-</sup>, SO<sub>4</sub><sup>2-</sup>; X=F, Cl, CN, Y=F<sup>-</sup>) was investigated using the G4MP2 high-level ab initio approach,<sup>[12]</sup> which typically provides thermodynamic magnitudes with an accuracy of  $\pm 4 \text{ kJ mol}^{-1}$ . The very good correlation between the B3LYP/6-311+G(3df,2p) results and the G4MP2 outcomes confirms the reliability of the B3LYP/6-311+G(3df,2p) approach for the purposes of this study (see the Supporting Information, Figure S1 and the related discus-

[a] O. Brea, Dr. I. Corral, Prof. Dr. O. Mó, Prof. Dr. M. Yáñez  
Departamento de Química, Facultad de Ciencias  
Universidad Autónoma de Madrid  
Módulo 13, Campus de Excelencia UAM-CSIC, Cantoblanco, 28049 Madrid  
(Spain)  
E-mail: manuel.yanez@uam.es

[b] Prof. Dr. I. Alkorta, Prof. Dr. J. Elguero  
Instituto de Química Médica, CSIC  
C/ Juan de la Cierva, 3, 28006 Madrid (Spain)

Supporting information and ORCID(s) from the author(s) for this article are available on the WWW under <http://dx.doi.org/10.1002/chem.201604325>.

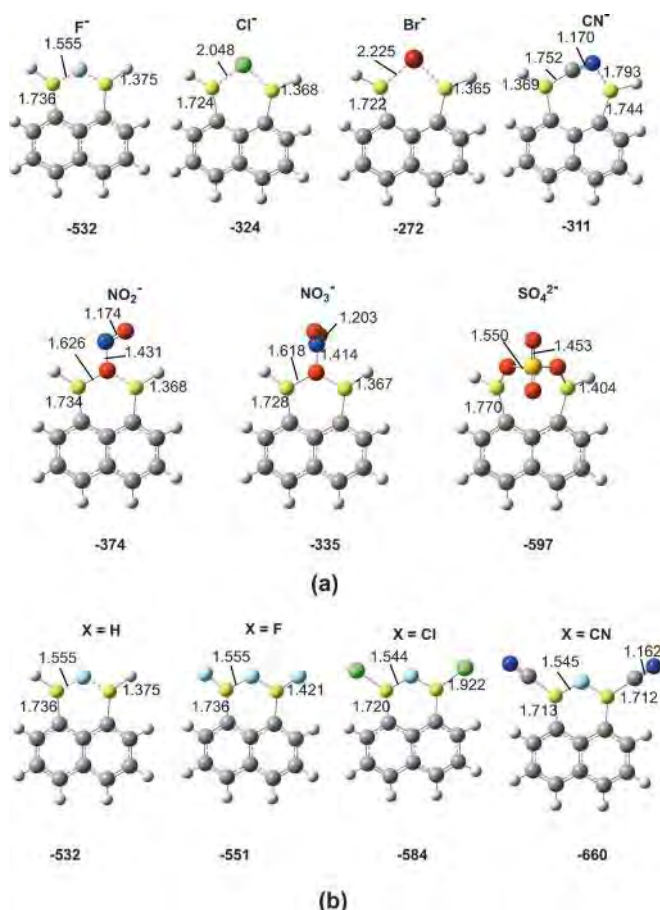


**Figure 1.** G4MP2 optimized geometries of: a) [1,8-diBeH-naphthalene]Y complexes (Y = F<sup>−</sup>, Cl<sup>−</sup>, Br<sup>−</sup>, CN<sup>−</sup>, NO<sub>2</sub><sup>−</sup>, NO<sub>3</sub><sup>−</sup>, SO<sub>4</sub><sup>2−</sup>); b) [1,8-diBeX-naphthalene]F<sup>−</sup> complexes (X = H, F, Cl, CN). Only the interatomic distances [Å] directly related with the interaction between the Be atoms and the anions are reported. The corresponding G4MP2 anion affinities [kJ mol<sup>−1</sup>] are given in bold.

sion). Figure 1 shows the equilibrium structure of a selection of the anionic complexes investigated, together with the G4MP2

calculated anion affinity. The optimized structures of all the complexes under scrutiny are summarized in the Supporting Information, Table S1.

The global minimum of the potential energy surface (PES) for complexes involving monoatomic anions, F<sup>−</sup>, Cl<sup>−</sup>, and Br<sup>−</sup> corresponds to a chelated structure in which the anion interacts with both Be atoms of the 1,8-diBeX-naphthalene moiety. However for CN<sup>−</sup> anion, the global minimum corresponds to the structure in which each Be atom interacts with a different atom of the anion (Figure 1), whereas the two stationary points of C<sub>2</sub> symmetry (Supporting Information, Figure S2) in which only the C atom or only the N atom bridges between the two Be atoms of 1,8-diBeX naphthalene derivative are found to be second-order saddle points. The situation is slightly more complicated when dealing with NO<sub>2</sub><sup>−</sup>, NO<sub>3</sub><sup>−</sup>, and SO<sub>4</sub><sup>2−</sup> anions, because the structure of the global minimum strongly depends on the nature of the anion. For NO<sub>2</sub><sup>−</sup> and for SO<sub>4</sub><sup>2−</sup> two local minima, but with opposite relative stabilities, are found to be stable. For NO<sub>2</sub><sup>−</sup>, the global minimum corresponds to the structure in which only one of the oxygen atoms is chelated by the two Be atoms (Figure 1), whereas the structures with one to one oxygen–beryllium interactions (Supporting Information, Figure S2) lie about 30–50 kJ mol<sup>−1</sup> higher in energy (Supporting Information, Table S2). For SO<sub>4</sub><sup>2−</sup> it is the other way around, and the second arrangement, in which each Be atom interacts with a different oxygen atom of the anion, is preferred with respect to the structure in which one oxygen atom interacts with both Be atoms in a C<sub>s</sub> arrangement (Supporting Information, Figure S2 and Table S2). Interestingly, for NO<sub>3</sub><sup>−</sup> only the structure similar to the first structure described above for NO<sub>2</sub><sup>−</sup> is found to be a minimum, whereas the dicoordinated structure (Supporting Information, Figure S2) is found to be a transition state (TS).

The most relevant finding however is that the calculated anion affinities for the different 1,8-diBeX-naphthalene derivatives investigated are very high and over a wide range; the values are between 200–800 kJ mol<sup>−1</sup> (Table 1).

**Table 1.** Y<sup>−</sup> anion affinities [kJ mol<sup>−1</sup>] of 1,8-diBeX-naphthalene derivatives.<sup>[a]</sup>

X	H		F		Cl		CN		CF <sub>3</sub>		C(CF <sub>3</sub> ) <sub>3</sub>	
Y	A	B	A	B	A	B	A	B	A	B	A	B
F <sup>−</sup>	516.4	531.7	534.9	550.6	563.6	584.4	639.8	660.0	613.9	633.6	644.5	633.6
		<i>541.4</i>		<i>558.7</i>		<i>585.9</i>		<i>658.2</i>				
Cl <sup>−</sup>	286.5	323.8	296.9	333.0	320.4	355.3	401.1	431.8	372.5	404.6	372.4	404.6
		<i>323.0</i>										
Br <sup>−</sup>	228.8	271.8	237.5	276.6	257.7	295.7	338.7	372.6	309.6	345.0	300.0	345.0
		<i>268.1</i>										
CN <sup>−</sup>	284.4	311.6	293.2	329.5	319.0	353.9	399.9	430.6	374.3	406.4	394.2	406.4
		<i>321.0</i>										
NO <sub>2</sub> <sup>−</sup>	336.2	374.5	341.4	375.1	368.4	400.8	452.2	480.3	423.3	452.8	427.4	452.8
		<i>370.2</i>										
NO <sub>3</sub> <sup>−</sup>	293.3	334.9	301.1	337.0	323.3	358.0	396.2	427.1	366.0	398.5	344.9	398.5
		<i>329.4</i>										
SO <sub>4</sub> <sup>2−</sup>	561.2	597.4	563.5	585.8	627.8	646.8	745.6	758.5	718.2	732.5	770.7	732.5
		<i>583.9</i>										

[a] A-type columns: values calculated at the B3LYP/6–311 + G(3df,2p)//B3LYP/6–31 + G(d,p) level of theory. B-type columns: values calculated at the G4MP2 level of theory. Values in italic correspond to G4MP2 values extrapolated using the correlation equation shown in the Supporting Information, Figure S1. These values have an estimated error of ± 5 kJ mol<sup>−1</sup>.

Indeed, the calculated fluoride affinities for  $X=H, F, Cl, CN$ , are more than  $100 \text{ kJ mol}^{-1}$  higher than previous values reported in the literature for strong anion capturers, such as  $SbF_5$  ( $F^-$  affinity  $503 \text{ kJ mol}^{-1}$ ),<sup>[13]</sup>  $AsF_5$  ( $F^-$  affinity  $464 \text{ kJ mol}^{-1}$ ),<sup>[14]</sup> or boron-containing Lewis acids, such as tris(perfluorophenyl)borane ( $F^-$  affinity  $406 \text{ kJ mol}^{-1}$ )<sup>[15]</sup> or 1,8-diborylnaphthalenes.<sup>[16]</sup> They are also more than  $300 \text{ kJ mol}^{-1}$  higher than those of  $BF_3$  or bidentate diboranes<sup>[17]</sup> and of the same order as those reported for  $MO_3$  metal oxides,<sup>[18]</sup> which have been shown to exhibit the highest fluoride affinities so far reported before for neutral systems. As a matter of fact, the calculated fluoride affinities for the 1,8-diBeX naphthalene derivatives considered in this study are only surpassed by those  $Sb_nF_{5n}$  ( $n=1-4$ ), which are among the strongest Lewis acids known.<sup>[19]</sup> Although the information on other anion affinities is very scarce or inexistent, our calculated chloride affinities are also much larger than previous values reported in the literature for other Lewis acids.<sup>[20]</sup>

These high anion affinities are consistent with the characteristics of the electron density distribution of the complexes formed. For the monoatomic anions the AIM analysis shows the existence of a bond critical point (BCP) between the anion and both Be atoms (Figure 2). BCPs are also found between

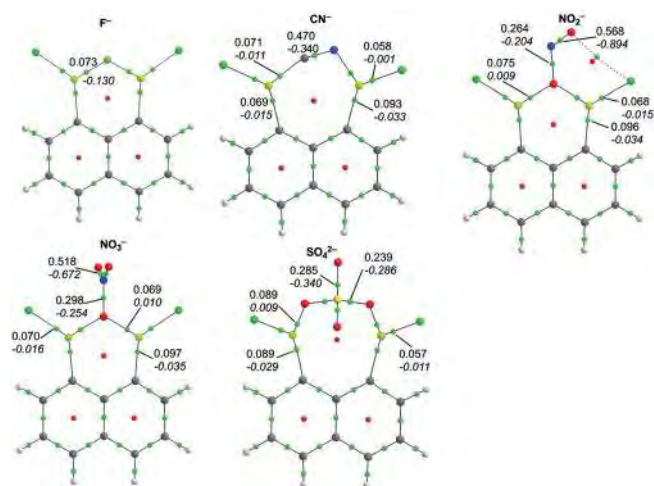


**Figure 2.** Molecular graphs of [1,8-diBeX-naphthalene] $Y^-$  anions ( $X=Cl$ ;  $Y=Cl^-, CN^-, NO_2^-, NO_3^-, SO_4^{2-}$ ). Green and red dots correspond to bond and ring critical points, respectively. The energy density (in italics) and the electron density are given. Both values in are a.u.

the two Be atoms and the polyatomic anions, but the most significant finding is the large decrease in the electron density at the bond of the anion directly interacting with both Be atoms, whose bond length increases also significantly. For instance, for the complex between 1,8-diBeCl-naphthalene and  $NO_2^-$  the electron density at the BCP of the N–O interacting with both Be atoms is 0.3 a.u. smaller.

These dramatic changes are also in harmony with the NBO description which shows that upon the formation of the complex there is a significant amount of charge transfer from the lone pairs of the anion towards the p empty orbitals of Be, as

well as towards the  $\sigma_{BeX}^*$  antibonding orbital. The population of the empty p orbital changes the hybridization of the Be atom and consistently the C-Be-X arrangement, which in the neutral compound is linear, becomes significantly bent and the charge transfer towards the  $\sigma_{BeX}^*$  antibonding orbital results in longer Be–X bonds in the anionic forms than in the neutral. Also consistently, the ELF analysis shows the appearance in all cases of disynaptic basins, with a significantly large electron population, between the Be atoms and the atoms of the anion participating in the interaction (Figure 3).

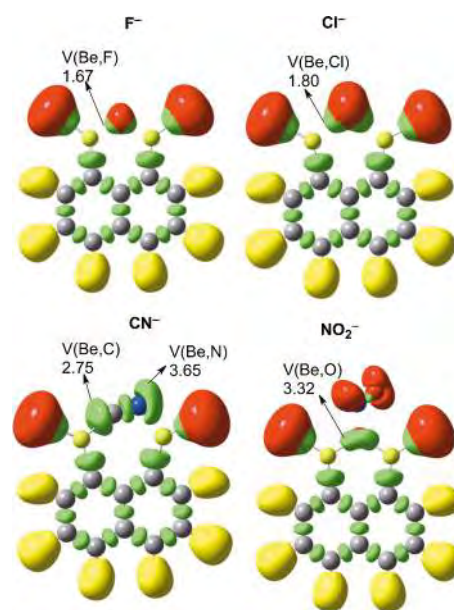


**Figure 3.** ELF plots for [1,8-diBeX-naphthalene] $Y^-$  anions ( $X=Cl$ ;  $Y=F, Cl, CN, NO_2$ ). Yellow lobes correspond to disynaptic basins involving hydrogen atoms. Green lobes correspond to disynaptic basins between heavy atoms and red lobes denote monosynaptic basins associated with lone pairs. The population ( $e^-$ ) of the disynaptic basins involving Be atoms is shown.

The results discussed above allow us to conclude that, as 1,8-bis(dimethylamino)naphthalene derivatives behave as very strong Lewis bases (receiving the name of proton sponges) because the huge charge transferred from the lone pairs of the amino groups toward the bare proton strongly stabilizes the cationic protonated species, the 1,8-diBeX-naphthalene derivatives behave as anion sponges through the strong charge transfer from the anion towards the electron deficient BeX substituents. The most significant consequence is that the calculated anion affinities for these systems are among the largest ones ever reported before for single neutral molecules.

## Acknowledgements

This work was supported by the Projects CTQ2015-63997-C2, CTQ2013-43698-P, FOTOCARBON-CM S2013/MIT-2841, and by the COST Action CM1204. The authors wish to thank J. M. Segovia for his contributions to the graphical material.

**Keywords:** ab initio calculations · anion affinities · anion sponges · beryllium · density functional calculations

- [1] M. Yáñez, P. Sanz, O. Mó, I. Alkorta, J. Elguero, *J. Chem. Theory Comput.* **2009**, *5*, 2763–2771.
- [2] O. Brea, O. Mó, M. Yáñez, I. Alkorta, J. Elguero, *Chem. Commun.* **2016**, 52, 9656–9659.
- [3] O. Brea, I. Alkorta, O. Mó, M. Yáñez, J. Elguero, I. Corral, *Angew. Chem.* **2016**, *128*, 8878–8881.
- [4] J. Liu, Z. H. Chen, S. Busking, K. Amine, *Electrochem. Commun.* **2007**, *9*, 475–479.
- [5] H. Hattori, M. Hoshino, T. Wakii, A. Yuchi, *Anal. Chem.* **2004**, *76*, 5056–5062.
- [6] V. Amendola, L. Fabbri, L. Mosca, *Chem. Soc. Rev.* **2010**, *39*, 3889–3915.
- [7] Y. Zhang, M. X. Li, M. Y. Lu, R. H. Yang, F. Liu, K. A. Li, *J. Phys. Chem. A* **2005**, *109*, 7442–7448.
- [8] a) H. Zhao, F. P. Gabbai, *Nat. Chem.* **2010**, *2*, 984–990; b) R. Tepper, B. Schulze, M. Jager, C. Friebe, D. H. Scharf, H. Gols, U. S. Schubert, *J. Org. Chem.* **2015**, *80*, 3139–3150.
- [9] M. Samet, A. Fattahi, S. R. Kass, *Org. Biomol. Chem.* **2015**, *13*, 2170–2176.
- [10] G. Sposito, *The Chemistry of Soils*, Oxford University Press, New York, **2006**.
- [11] a) A. D. Becke, *J. Chem. Phys.* **1993**, *98*, 1372–1377; b) C. Lee, W. Yang, R. G. Parr, *Phys. Rev. B* **1988**, *37*, 785–789.
- [12] L. A. Curtiss, P. C. Redfern, K. Raghavachari, *J. Chem. Phys.* **2007**, *126*, 084108.
- [13] K. O. Christe, D. A. Dixon, D. McLemore, W. W. Wilson, J. A. Sheehy, J. A. Boatz, *J. Fluorine Chem.* **2000**, *101*, 151–153.
- [14] J. C. Haartz, D. H. McDaniel, *J. Am. Chem. Soc.* **1973**, *95*, 8562–8565.
- [15] Z. H. Chen, K. Amine, *J. Electrochem. Soc.* **2009**, *156*, A672–A676.
- [16] a) T. W. Hudnall, C. W. Chiu, F. P. Gabbai, *Acc. Chem. Res.* **2009**, *42*, 388–397; b) M. Melaïmi, S. Sole, C. W. Chiu, H. D. Wang, P. Gabbai, *Inorg. Chem.* **2006**, *45*, 8136–8143.
- [17] a) M. Veljković, O. Nešković, K. F. Zmbov, A. Y. Borshchevsky, V. E. Vaisberg, L. N. Sidorov, *Rapid Commun. Mass Spectrom.* **1991**, *5*, 37–39; b) C. L. Dorsey, P. Jewula, T. W. Hudnall, J. D. Hoefelmeyer, T. J. Taylor, N. R. Honesty, C. W. Chiu, M. Schulte, F. P. Gabbai, *Dalton Trans.* **2008**, 4442–4450.
- [18] S. G. Li, D. A. Dixon, *J. Phys. Chem. A* **2006**, *110*, 6231–6244.
- [19] H. D. B. Jenkins, I. Krossing, J. Passmore, I. Raabe, *J. Fluorine Chem.* **2004**, *125*, 1585–1592.
- [20] A. Kraft, J. Beck, I. Krossing, *Chem. Eur. J.* **2011**, *17*, 12975–12980.

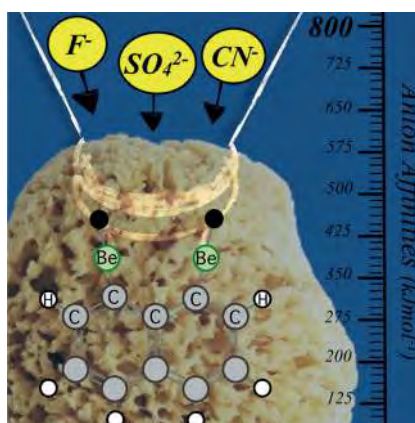
Received: September 13, 2016

Accepted Article published: October 21, 2016

Published online on ■ ■ ■, 0000

## COMMUNICATION

**Soaking it up:** The great capacity of beryllium centers in 1,8-diBeX-naphthalene compounds (X = H, F, Cl, CN, CF<sub>3</sub>, C(CF<sub>3</sub>)<sub>3</sub>) to accept electron density results in anion affinities that are among the largest ever reported for single neutral molecules.

**Anion Sponges**

O. Brea, I. Corral, O. M<sup>o</sup>, M. Y<sup>a</sup>ñez,\*  
I. Alkorta, J. Elguero



**Beryllium-Based Anion Sponges: Close  
Relatives of Proton Sponges**  



# CHEMISTRY

## A **European** Journal

### Supporting Information

#### **Beryllium-Based Anion Sponges: Close Relatives of Proton Sponges**

Oriana Brea,<sup>[a]</sup> Inés Corral,<sup>[a]</sup> Otilia Mó,<sup>[a]</sup> Manuel Yáñez,<sup>\*[a]</sup> Ibon Alkorta,<sup>[b]</sup> and José Elguero<sup>[b]</sup>

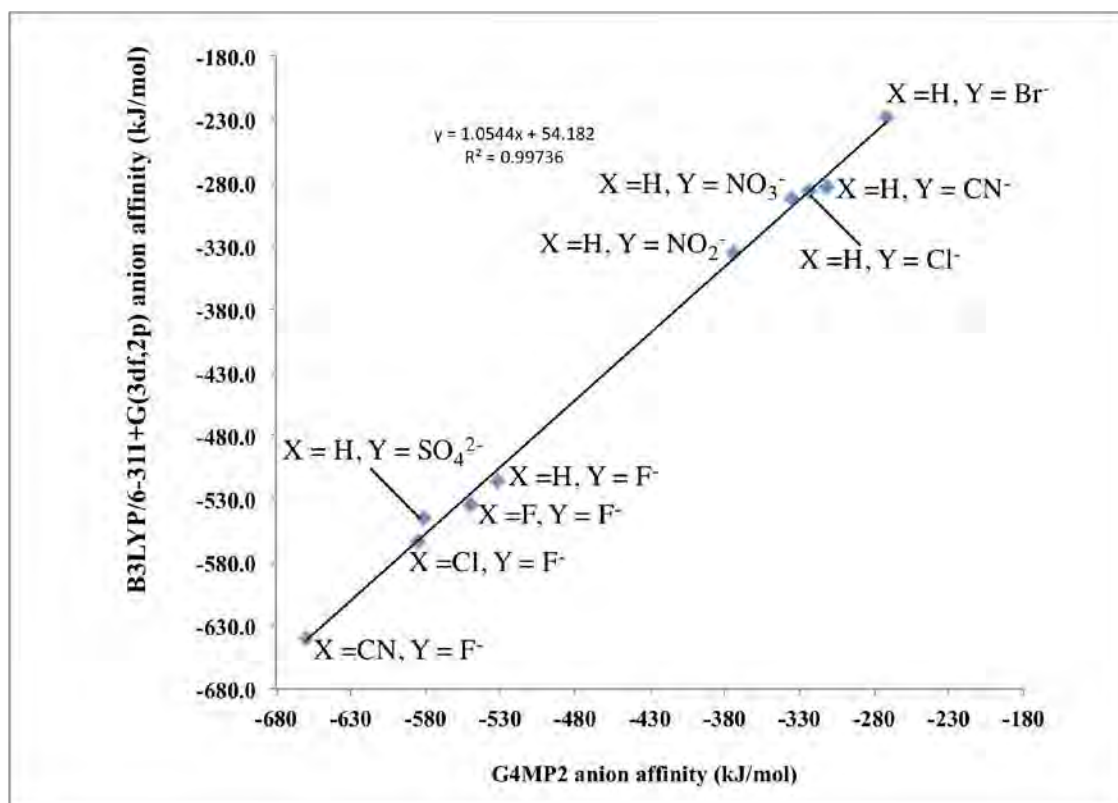
chem\_201604325\_sm\_miscellaneous\_information.pdf

*Contribution from the Departamento de Química, Facultad de Ciencias, Módulo 13, Universidad Autónoma de Madrid, Campus de Excelencia UAM-CSIC, Cantoblanco, 28049-Madrid, Spain and the Instituto de Química Médica, C/ Juan de la Cierva, 3, CSIC, 28006-Madrid. Spain*

**Supporting Information (A total of 30 pages)**

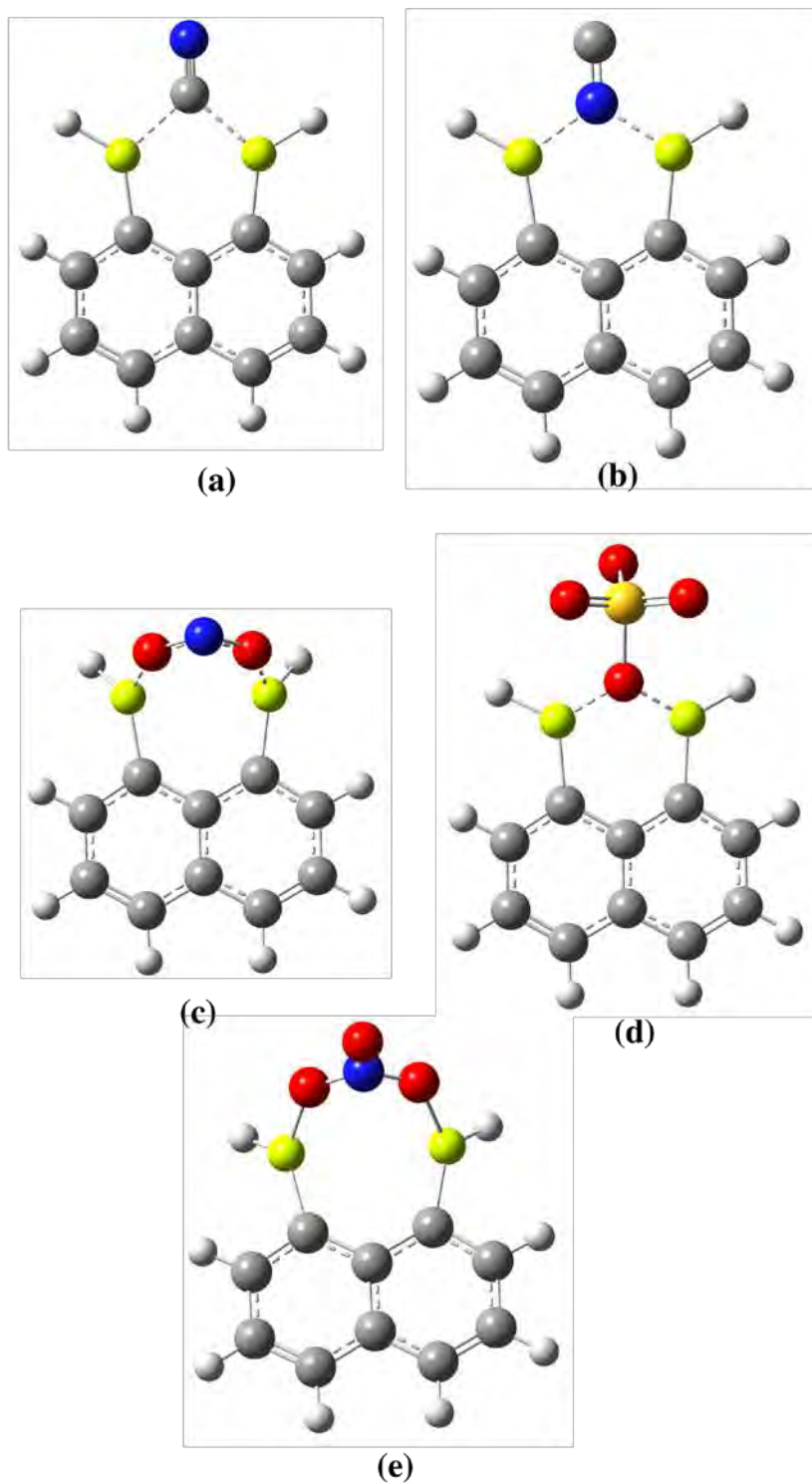
**Table of Contents:**

Figure S1 .....	S2
Figure S2 .....	S3
Table S1 .....	S4
Table S2 .....	S30



**Figure S1.** Linear correlation between B3LYP/6-311+G(3df,2p) and G4MP2 anion affinities for 1,8-diBeX-naphthalene derivatives.

The correlation in Figure S1, shows that the calculated B3LYP/6-311+G(3df,2p) anion affinities for the anions considered in our survey follow the same trend as those calculated with the G4MP2 composite ab initio method, even though B3LYP slightly underestimates anion affinities by  $27 \text{ kJ}\cdot\text{mol}^{-1}$  on average.



**Figure S2.** Stationary points of the PES of some complexes between 1,8-diBeX-naphthalene derivatives and different anions. Structures (a) and (b) correspond to second-order saddle points when X = H and the anion is  $\text{CN}^-$ . Structures (c) and (d) are high-lying local minima of the 1,8-diBeX-naphthalene: $\text{NO}_2^-$  and 1,8-diBeX-naphthalene: $\text{SO}_4^{2-}$  complexes. Structure (e) in which each Be atom of the 1,8-diBeX-naphthalene moiety interacts with a different oxygen atom of the  $\text{NO}_3^-$  is a transition state on the corresponding potential energy surface.

F	3.87382300	-1.88516100	1.55480200
F	1.62998700	-2.70044900	0.42290000
F	1.29470900	-2.02058100	-1.61319100
F	3.10414700	-3.12352800	-1.09951500
F	-1.34808800	-2.40569600	0.04311400
F	-3.05207400	-2.33541400	1.40383500
F	-3.29174800	-3.08836400	-0.61687300
F	-4.38588400	0.08792700	1.45664600
F	-4.89551800	0.74526700	-0.55162800
F	-5.31223400	-1.29132500	0.06175100
F	-3.86920700	-1.25063100	-2.52532600
F	-2.92454900	0.68134400	-2.30758700
F	-1.70725400	-1.11699300	-2.28810200

**Table S2.** B3LYP/6-311+G(3df,2p) relative stability (in  $\text{kJ mol}^{-1}$ ) of the di-coordinated respect to the mono-coordinated complexes of  $\text{NO}_2^-$  and  $\text{SO}_4^{=}$  anions with 1,8-diBeX-naphthalene ( $X = \text{H, F, Cl, CN, CF}_3, \text{C}(\text{CF}_3)_3$ ) derivatives

X	$\text{NO}_2^-$		$\text{SO}_4^{=}$	
	$\Delta\text{H}$	$\Delta\text{G}$	$\Delta\text{H}$	$\Delta\text{G}$
H	34.9	35.8	-16.1	-15.1
	[49.4] <sup>a</sup>	[52.3] <sup>a</sup>	[-16.0] <sup>a</sup>	[-13.0] <sup>a</sup>
F	37.7	33.5	-17.8	-16.4
Cl	39.2	36.4	-12.2	-19.4
CN	48.4	44.2	-1.7	-8.8
$\text{CF}_3$	39.8	40.4	3.2	-4.9
$\text{C}(\text{CF}_3)_3$	16.4	15.0	-5.3	-15.1

<sup>a</sup> Values obtained at the G4MP2 level of theory.

---

## B.6 ARTICLE V

*Modulation of the strength of Be-Be bonds by Lewis Base coordination.*

In preparation.



# Modulation of the strength of Be-Be bonds by Lewis Base coordination.

Oriana Brea<sup>ab</sup>, Ibon Alkorta<sup>c</sup>, Otilia M<sup>o</sup><sup>a</sup>, Thierry Leininger<sup>b</sup>, José Elguero<sup>c</sup>, Stefano Evangelisti<sup>b</sup>, Manuel Yáñez<sup>a</sup>, Inés Corral<sup>a</sup>

<sup>a</sup> Universidad Autónoma de Madrid. Departamento de Química, Facultad de Ciencias, Módulo 13, Campus de Excelencia UAM-CSIC, Cantoblanco, 28049-Madrid, Spain.

<sup>b</sup> Université de Toulouse III – Paul Sabatier. Laboratoire de Chimie et Physique Quantiques. 118, Route de Narbonne, 31400 Toulouse, France.

<sup>c</sup> Instituto de Química Médica. C/ Juan de la Cierva, 3, CSIC, 28006-Madrid. Spain

**Abstract:** The interaction between Be dimer and Lewis bases (LB) has been studied using high-level ab-initio methods. The nature of the LB:Be interaction determines the oxidation state of the metal atoms and thus the strength of the interaction of the Be<sub>2</sub> dimer within the L:Be-Be:L complexes. The Be<sub>2</sub> remains as a neutral moiety when the metal interacts with LB with available Lone Pairs. It is oxidized to a monocation when interacting with LB presenting  $\pi$  orbitals that conjugate with the p orbitals of Be, and it exists as a dication when the LB are radical species. The Bond Dissociation energies were found to be up to 7, 12 and 30 times stronger for L:Be-Be:L complexes containing neutral monocationic and dicationic Be<sub>2</sub> moieties compared to the isolated dimer.

The concept of chemical bond is central to Chemistry and hence to Computational Chemistry. Despite the great advances in chemical bond theory and the extraordinary development of computational architectures the bond description for some systems still remains a challenge for this discipline; Be dimer being a paradigmatic example.

The impossibility to identify stable dimers in the gas phase until 1984 led to believe that beryllium gas was composed of isolated atoms,<sup>[1]</sup> consistently with the repulsive nature of the Be-Be molecule predicted at that time by theory.<sup>[2]</sup> In 1984 Bondybey and co-workers registered the first experimental spectrum of Be<sub>2</sub>. These experiments also determined that Be atoms in the dimer are weakly bonded with a bond distance of 2.45 Å and a Bond Dissociation Energy (BDE) of 9.46 kJ·mol<sup>-1</sup><sup>[3]</sup>, triggering a debate on the nature of the bond in this exotic system.

It has only been recently shown that Be-Be bond in the dimer can be described as *non-dynamical bond*,<sup>[4]</sup> the wave function of the system showing a non-negligible multiconfigurational character. The complex nature of the weak Be-Be bond in the isolated dimer, which complicates both the experimental and theoretical characterization of this system, pushed both theoreticians and experimentalists to design new Be<sub>2</sub> with stronger Be-Be interactions via its complexation with electron donor ligands, such as for instance N-heterocyclic carbene (NRC) and fluorine.<sup>[6a]</sup>

To date, the complexes showing the strongest (321.98 kJ·mol<sup>-1</sup>) and the shortest (1.95Å) Be-Be bond are those

where the Be<sub>2</sub> respectively interacts with two fluorine atoms and two NRC ligands.<sup>[6]</sup>

The idea behind inducing stronger Be-Be bonds via ligand complexation is not new. An old theoretical study using CO as ligands predicted a Be-Be double bond in the (CO)<sub>2</sub>:Be-Be:(CO)<sub>2</sub> complex, with a very short bond distance between the metals amounting to 1.938 Å.<sup>[7]</sup> This unusually strong Be-Be bond attracted the attention of experimentalists, who were able to spectroscopically identify the complex together with other Be-carbonyls derivatives.<sup>[8]</sup> Years later, Sannigrahi et al. revisited the characterization of (CO)<sub>n</sub>:Be-Be:(CO)<sub>n</sub> complexes (with n=1,2) with multicenter bond indexes analysis and rejected the HF double bond description, based on the electron deficient nature of the Be atom. These authors instead proposed for complex with n=1 a three center two electron BeBeC bond, and a ( $\sigma_{\text{Be-Be}}$ )<sup>2</sup> ( $\pi_{\text{C-Be-Be-C}}$ )<sup>2</sup> configuration for the n=2 complex, compatible with the short bond distances and the high bond orders found in previous theoretical works.<sup>[9]</sup>

Unfortunately, all the information about Be-carbonyls derivatives comes from theoretical studies performed in the 90's based on monoconfigurational calculations, unable to properly describe the complex nature of Be<sub>2</sub> bond. Another limitation of this type of methods is the inaccurate description they provide for triplet states that for some complexes like NRC:Be-Be:NRC, and CO:Be-Be correspond to the ground state.<sup>[6a, 10]</sup> In this communication, we made use of high level ab-initio multi- and mono-configurational methods to characterize L:Be-Be:L complexes considering three categories of ligands:

- *Group-I:* which includes closed-shell ligands, such as L = NH<sub>3</sub> and H<sub>2</sub>O, with available lone pairs.
- *Group-II:* which groups closed-shell LB, such as L = CO, presenting  $\pi$  bonds, allowing the conjugation with Be p orbitals.
- *Group-III:* where L are open-shell neutral radical species. Within this category the ligands L = CN·, F·, OH·, CH<sub>3</sub>·, CH<sub>3</sub>O· and NH<sub>2</sub>· were considered.

The computational details for the geometry optimizations, the calculation of the dissociation energies and the characterization of the bonds in the complexes can be found in the SI.



The equilibrium geometries for the global minima of the singlet ground and first triplet excited states of *group-I* and *-II* complexes are collected in Figure 1. Taking into account the simplicity of the bonds in *group-III* complexes and that previous works already reported<sup>[6b]</sup> on their geometries and bonding, in the following they will be dropped from the discussion except for comparisons with *group-I* and *-III* complexes.

As already discussed, ligand complexation in all the cases leads to a remarkable decrease of the Be-Be bond compared to the isolated dimer. Interestingly, this decrease is more pronounced (0.5 Å) in the case of *group-II* complexes compared to *group-I* (0.4 Å), but the complexes in these two categories provide longer both distances compared to *group-III* (F:Be-Be:F, 2.05 Å)<sup>[6b]</sup> and to complexes including NRC ligands (R=H, Be-Be: 1.95 Å and R=Ph, Be-Be: 1.98 Å).<sup>[6a]</sup>

Also interestingly, the minima of the potential energy surfaces for *group-I* complexes correspond to trans-type isomers respect to the Be-Be bond, with the lone pairs of the LB oriented in the direction of the Be atoms. At contrast, the geometry of the complex with CO is linear allowing p<sub>Be</sub> orbitals to conjugate with the π<sub>CO</sub> orbitals of the ligands. All the attempts to optimize equivalent trans-type isomers for L=CO, preventing the π conjugation between the metals and the ligands, failed and converged to the linear system, (see figure S7).

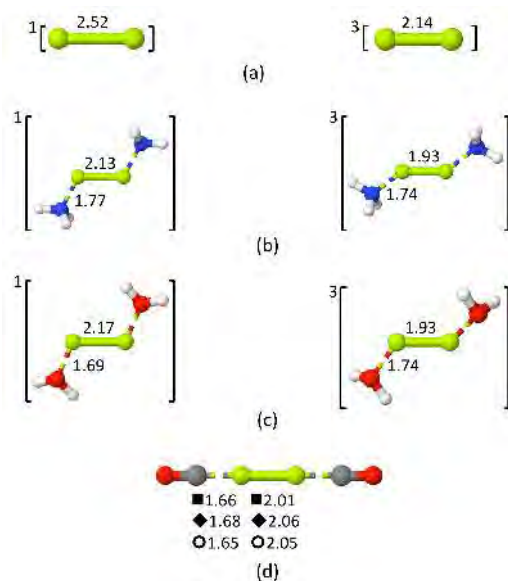


**Figure 1.** CASPT2//CASSCF(n,m)/cc-PVTZ optimized geometries for the first singlet (GS) and triplet states of the Be-Be and L:Be-Be:L systems: (a) n=4 and m=16 (b) L= NH<sub>3</sub>, n=8 and m=10; (c) L= H<sub>2</sub>O, n=8 and m=10; (d) L=CO, n=10 and m=12, ■ represents the <sup>1</sup>Σ<sub>g</sub> state, ◆ the <sup>2</sup><sup>1</sup>Σ<sub>g</sub> state, and ○ the <sup>3</sup>Σ<sub>u</sub>. The Be-Be and Be-L interatomic distances are reported in Å.

The triplet excited states of the complexes in *group-I* present shorter bond distances than their corresponding ground state, at difference with *group-II* complexes, where the ground state of the complex with L=CO is characterized by shorter Be-Be bond distance compared to the triplets.

In order to rationalize these structural trends, we have analyzed the electronic configurations and NBO charges provided by our multiconfigurational calculations.

Tables S1, and S3 report the electronic configurations for *group-I* and *-II* complexes and table S6 collects their respective natural atomic charges. Intriguingly, *group-I* complexes show a neutral Be<sub>2</sub> moiety, whilst according to our NBO calculations Be<sub>2</sub> holds almost +1 and +2 charges in the cases of *group-II* and *group-III* complexes. The NBO picture is fully consistent with the analysis of the wave functions of the three groups of complexes, which also clearly reflects the charge transfer from the Be<sub>2</sub> moiety towards the ligands in the case of *group-II* and *group-III* complexes. In fact, the configuration of the Be dimer evolves from (2σ<sub>Be-Be</sub>)<sup>2</sup> (2σ\*<sub>Be-Be</sub>)<sup>2</sup> in *group-I* complexes to (2σ<sub>Be-Be</sub>)<sup>2</sup> (π<sub>Be</sub>+π\*<sub>CO</sub>)<sup>2</sup> in *group-II*, where some electron density has been transferred already to the ligands, to (2σ<sub>Be-Be</sub>)<sup>2</sup> (2σ\*<sub>Be-Be</sub>)<sup>0</sup> in *group-III* complexes, where the two electrons of the 2σ\*<sub>Be-Be</sub> orbital have been ceded from the metal dimer to the ligands recovering their closed shell electronic structure. All in all, the different charge and electronic configuration of the Be<sub>2</sub> moiety in the three groups of complexes would then explain the trend in the Be-Be bond distance when moving from *group-I* to *group-III* complexes.

**Table 1.** Energetic and bond analysis properties for the L:Be-Be:L complexes. Te corresponds to the adiabatic energy difference between the singlet and triplet state (Te = E<sub>sing</sub> - E<sub>trip</sub>). The BDE1 corresponds to the binding energy dissociation into 2L + 2Be, while the BDE2 is the binding energy associated to the 2LBe products. ρ is the electron density and ∇<sup>2</sup>ρ the electron density laplacian at the BCP. P is population of the disynaptic basins. WBO are the Wiberg Bond Orders. All energetic values are in kJ·mol<sup>-1</sup> and the bond analysis in au.

L	Energy (kJ·mol <sup>-1</sup> )			Bond Analysis (au)			
	Te	BDE1	BDE2	ρ <sub>NNA-Be</sub>	∇ <sup>2</sup> ρ <sub>NNA-Be</sub>	P <sub>Be-Be</sub>	WBO
/	-108	15.4	/	0.026 <sup>[a]</sup>	-0.014	/	0.11
NH <sub>3</sub>	-4	135	100	0.054	-0.048	1.78	0.50
H <sub>2</sub> O	-30	97	99	0.054	-0.049	1.72	0.47
CO	-16	174	231	0.069	-0.062	2.43	0.83

[a] For the isolated Be<sub>2</sub> molecule the BCP corresponds to a Be-Be critical point.

Te between the ground and the third singlet state for the CO:Be-Be:CO complex amounts to 4 kJ·mol<sup>-1</sup>.

The electronic configurations' analysis of the singlet and triplet complexes also allows for the interpretation of the structural differences among these electronic states and between *group-I* and *group-II* complexes.

As already discussed, the Be<sub>2</sub> moiety in *group-I* complexes shares the same electronic configuration as the isolated dimer (2σ<sub>Be-Be</sub>)<sup>2</sup> (2σ\*<sub>Be-Be</sub>)<sup>2</sup>, while in the complex with CO two electrons have been relocated from the 2σ\*<sub>Be-Be</sub> orbital into

the  $(\pi_{\text{Be-Be}} + \pi_{\text{C-O}}^*)$  orbital leading to the final configuration  $(2\sigma_{\text{Be-Be}})^2 (\pi_{\text{Be-Be}} + \pi_{\text{C-O}}^*)^2$ . The electronic configuration for the triplet states of both groups of complexes is defined by a single excitation from the HOMO orbital,  $(2\sigma_{\text{Be-Be}}^*)$  in *group-I* or  $(\pi_{\text{Be-Be}} + \pi_{\text{C-O}}^*)$  in *group-II* complexes, towards bonding or antibonding  $\pi_{\text{Be-Be}}$  orbitals. This electron promotion reinforces the Be-Be bond in *group-I* complexes due to the emptying of the antibonding  $(2\sigma_{\text{Be-Be}}^*)$  orbital, whereas it weakens the same bond in *group-II* complexes due to the antibonding character of the final  $\pi_{\text{Be-Be}}$  orbital.

Lewis base coordination was found to have also an effect on higher lying excited states. The excitation energies of  $\text{Be}_2$  and  $\text{L}:\text{Be-Be}:\text{L}$  are collected in Table 1 and excited state diagrams for  $\text{L} = \text{NH}_3$ ,  $\text{H}_2\text{O}$  and  $\text{CO}$  complexes can be found in figures S8 and S9 of the SI. In general, Lewis base coordination was found to significantly stabilize  $\pi_{\text{Be-Be}}$  orbitals, although to different extents depending on the nature of the ligand coordinated. Similarly to the isolated dimer, the second singlet state in *group-I* complexes is described by the  $(2\sigma_{\text{Be-Be}})^2 (2\sigma_{\text{Be-Be}}^*)^1 (\bar{\pi}_{\text{Be-Be}})^1$  configuration, although it lies much lower in energy (the bar over the singly occupied orbital denotes a beta spin). At contrast for the *group-II* complex  $\text{CO}:\text{Be-Be}:\text{CO}$ , the configuration contributing most to the wave function of the first singlet excited state  $3^1\Sigma_g$  is  $(2\sigma_{\text{Be-Be}})^2 (\pi_{\text{Be-Be}} + \pi_{\text{C-O}}^*)^1 (\bar{\pi}_{\text{Be-Be}} + \bar{\pi}_{\text{C-O}})^1$ , due to the greater stabilization of the  $\pi_{\text{Be-Be}}$  orbitals as a consequence of their conjugation with the  $\pi_{\text{CO}}$  orbitals of the ligands. At this point, it must be noted that the first excited state  $3^1\Sigma_g$  for the  $\text{CO}:\text{Be-Be}:\text{CO}$  complex lies only 4 kJ/mol higher in energy than the doubly degenerate  $1^1\Sigma_g$  GS, whilst the equivalent excited state corresponding to the ground state in the isolated dimer and in *group-I* complexes and defined by the  $(2\sigma_{\text{Be-Be}})^2 (2\sigma_{\text{Be-Be}}^*)^2$  configuration lies 877  $\text{kJ}\cdot\text{mol}^{-1}$  over the ground state.

Also important, our multiconfigurational calculations predict the doubly degenerate  $1^1\Sigma_g$  electronic state as the ground state, the triplet lying 16  $\text{kJ}\cdot\text{mol}^{-1}$  over it. This result contradicts previous Hartree-Fock calculations, which find a triplet ground state for the complex in *group-II*,<sup>[8]</sup> demonstrating the limitations of monoconfigurational approaches to describe Be-carbonyl compounds.

The multiconfigurational nature of the  $\text{Be}_2$  molecule and its complexes with *group-I* and *group-II* ligands hampers its description, resulting their characterization a real challenge for theory. In an effort to further characterize these systems we have analyzed the bond in *group-I* and *group-II* complexes using several wave function analysis approaches, whose results are shown in Table 1 and Figure 2. Consistently with the structural analysis of these complexes, all the properties calculated to estimate the bond strength predict a stronger Be-Be interaction in the  $\text{L}:\text{Be-Be}:\text{L}$  complexes than in the isolated dimer. Surprisingly, the QTAIM (Quantum Theory of Atoms in Molecules) analysis locates a maximum of the electron density, defined as a (3,-3) saddle point or Non-Nuclear Attractor (NNA), between the Be atoms, instead of the usual Be-Be Bond Critical Point (BCP). Two additional BCPs

between the NNA and each Be atom were also found in the molecular graph (See Figure 2). The occurrence of NNAs has been ascribed to particular ranges of internuclear distances that would enhance the accumulation of electron density between the interacting atoms. Thus, the decrease in the Be-Be bond distance upon ligand interaction complexes position these complexes in the range of bond lengths predicted by Pendás and coworkers where  $\text{Be}_2$  shows a NNA.<sup>[11]</sup>

The value of  $\rho$  at the BCPs between the NNA and the Be atoms is twice for *group-I* and almost triple for *group-II* compared to  $\rho$  at the Be-Be BCP of the isolated  $\text{Be}_2$  (See Table 1), and for all the systems considered  $\nabla^2\rho$  was found to be negative, indicating the covalent character of the Be-NNA interaction. At contrast with isolated Be-Be for which ELF analysis does not show a disynaptic basin,  $\text{L}:\text{Be-Be}:\text{L}$  complexes present disynaptic basins with populations around of  $1.8e^-$  for *group-I* and  $2.4e^-$  for *group-II* (see Table 1 and Figure 2).

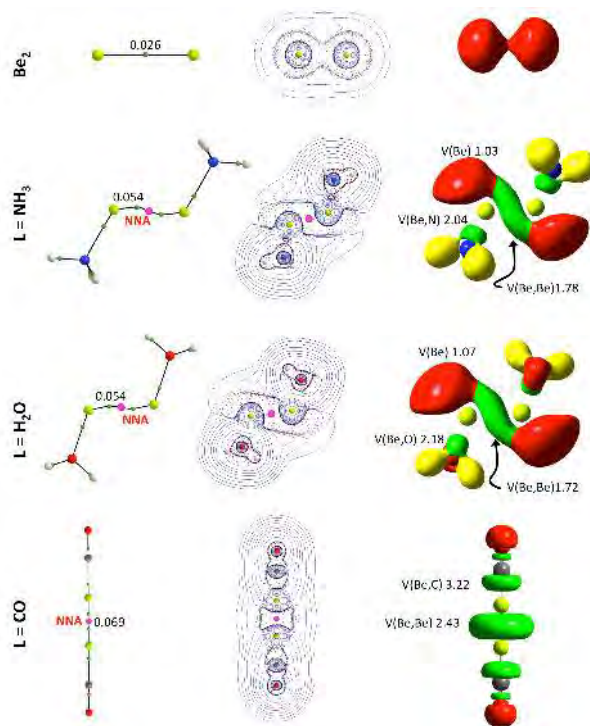


**Figure 2.** Wave function analysis for the  $\text{Be}_2$  and the  $\text{L}:\text{Be-Be}:\text{L}$  complexes ( $\text{L} = \text{NH}_3$ ,  $\text{H}_2\text{O}$ ,  $\text{CO}$ ). First column collects the molecular graphs, green and pink dots denote bond and NNA critical points, respectively. For the NNA-Be bond critical points the electron density is given in au. The second column shows the electron density Laplacian, red and blue areas represent negative and positive values of the Laplacian, respectively. The third column presents the ELF plots for the same systems, yellow lobes correspond to disynaptic basins involving hydrogen atoms, green lobes correspond to disynaptic basins between heavy atoms, and red basins denote monosynaptic basins associated with lone-pairs. The population of the Be-Be and Be:L disynaptic basin is shown.

Tables 1 and S6 show the results from the NBO analysis. The NBO method does not locate a Be-Be bonding orbital for the isolated Be dimer and predicts a bond order of almost zero (see Table 1). After Be<sub>2</sub> association with Lewis bases, this method predicts the existence of a Be-Be bonding orbital, mainly formed by a combination of the s<sub>Be</sub> orbital from each Be atom and bond orders comprised between 0.5 and 1.0. The difference between the *group-I* and *group-II* complexes lies in the second pair of valence electrons, which for L=NH<sub>3</sub> and L=H<sub>2</sub>O they are localized as lone pairs of Be, and for L=CO an unpaired electron is localized in a π\*<sub>C-O</sub> orbital and the other in a p<sub>Be</sub> orbital, coinciding with the analysis of the MS-CASPT2/CASSCF wave function.

Further studies on the Be-NNA-Be interaction using a new wave function analysis method developed in our group are in course.<sup>[12]</sup>

Finally, we have estimated the Bond Dissociation Energies (BDE) for the complexes of interest at CASPT2//CASSCF(n,m)/cc-pVTZ level of theory. Two possible dissociation channels were considered:



Our calculations predict dissociation into 2Be:L slightly favored for *group-I* complexes. The wave function of the Be:L compounds does not show a bonding Be:L orbital. Indeed, the electronic configuration of Be remains as in the isolated atom (1s<sup>2</sup>2s<sup>2</sup>), suggesting a closed-shell interaction between Be and L. For *group-II* complexes with L=CO, 2CO + 2Be dissociation is preferred. For the CO:Be-Be:CO system, a third dissociation channel leading to Be-Be:CO + CO was considered (BDE3). These products, resulting from an exothermic dissociation process (BDE3 = -20kJ·mol<sup>-1</sup>) according to HF results, were also detected experimentally.<sup>[10]</sup> Our CASPT2 results, however, predict the CO:Be-Be:CO complex to be stable against its dissociation into Be-Be:CO, with an endothermic BD3 amounting to 120 kJ·mol<sup>-1</sup>, and support the alternative route proposed at HF level of theory<sup>[6]</sup> for the formation of the experimentally detected monosubstituted complex via the reaction between Be<sub>2</sub> and CO (ΔE<sub>HF</sub> = -63kJ·mol<sup>-1</sup> and ΔE<sub>CASPT2</sub> = -38kJ·mol<sup>-1</sup>). The BDE reported in Table 1 for *group-I* and *group-II* complexes are almost 7 and 12 times higher than those calculated for Be<sub>2</sub> molecule, but lie below the BDEs previously reported for NRC and F ligands,<sup>[6]</sup> either because the oxidation state of the Be<sub>2</sub> is different (recall that *group-I* and *group-II* complexes present a neutral and cationic Be<sub>2</sub> moieties at difference with F:Be-Be:F and NRC:Be-Be:NRC where the Be<sub>2</sub> moiety presents +2 and +1 charges) or due to the stronger π<sub>NRC-Be</sub> conjugation allowed in NRC ligands compared to CO.

The results described above allow us to conclude that the BDE for *group I*-Be<sub>2</sub> complexes reported in this communication, resulting from the electron density accumulation at the NNA between Be atoms, are among the strongest reported so far in the literature, only surpassed by

NRC or F complexes, where the Be<sub>2</sub> moiety has been oxidized by the ligands.

#### Acknowledgements

This work has been supported by the Projects CTQ2015-63997-C2 and CTQ2013-43698-P, FOTOCARBON-CM S2013/MIT-2841 and by the COST Action CM1204. A generous allocation of computational time at Centro de Computación Científica (CCC) of Universidad Autónoma de Madrid is also acknowledged.

#### References

- [1] a) G. Herzberg, *Zeitschrift für Physik* **1929**, *57*, 601-630; b) L. Herzberg, *Zeitschrift für Physik* **1933**, *84*, 571-592.
- [2] a) J. H. Bartlett, W. H. Furry, *Physical Review* **1931**, *38*, 1615-1622; b) C. F. Bender, E. R. Davidson, *The Journal of Chemical Physics* **1967**, *47*, 4972-4978; c) S. Fraga, B. J. Ransil, *The Journal of Chemical Physics* **1962**, *36*, 1127-1142; d) M. J. Stephen, *The Journal of Chemical Physics* **1964**, *40*, 669-673.
- [3] a) V. E. Bondybey, *Science* **1985**, *227*, 125-131; b) V. E. Bondybey, *Chemical Physics Letters* **1984**, *109*, 436-441; c) V. E. Bondybey, J. H. English, *The Journal of Chemical Physics* **1984**, *80*, 568-570.
- [4] a) M. El Khatib, G. L. Bendazzoli, S. Evangelisti, W. Helal, T. Leininger, L. Tenti, C. Angeli, *The Journal of Physical Chemistry A* **2014**, *118*, 6664-6673; b) D. Koch, E. Fertitta, B. Paulus, *The Journal of Chemical Physics* **2016**, *145*, 024104.
- [5] M. C. Heaven, J. M. Merritt, V. E. Bondybey, *Annual Review of Physical Chemistry* **2011**, *62*, 375-393.
- [6] a) S. A. Couchman, N. Holzmann, G. Frenking, D. J. D. Wilson, J. L. Dutton, *Dalton Transactions* **2013**, *42*, 11375-11384; b) Z.-h. Cui, W.-s. Yang, L. Zhao, Y.-h. Ding, G. Frenking, *Angewandte Chemie International Edition* **2016**, *55*, 7841-7846.
- [7] K. K. Sunil, *Journal of the American Chemical Society* **1992**, *114*, 3985-3986.
- [8] L. Andrews, T. J. Tague, G. P. Kushto, R. D. Davy, *Inorganic Chemistry* **1995**, *34*, 2952-2961.
- [9] a) T. Kar, P. K. Nandi, A. B. Sannigrahi, *Chemical Physics Letters* **1994**, *220*, 133-137; b) A. B. Sannigrahi, T. Kar, *Journal of Molecular Structure: THEOCHEM* **2000**, *496*, 1-17.
- [10] L. Andrews, T. J. Tague Jr., G. P. Kushto, R. D. Davy, *Inorg. Chem.* **1995**, *34*, 2952-2961.
- [11] A. M. Pendás, M. A. Blanco, A. Costales, P. M. Sánchez, V. Luaña, *Physical Review Letters* **1999**, *83*, 1930-1933.
- [12] a) O. Brea, M. El Khatib, C. Angeli, G. L. Bendazzoli, S. Evangelisti, T. Leininger, *Journal of Chemical Theory and Computation* **2013**, *9*, 5286-5295; b) O. Brea, M. El Khatib, G. L. Bendazzoli, S. Evangelisti, T. Leininger, C. Angeli, *The Journal of Physical Chemistry A* **2016**, *120*, 5230-5238.

**Contribution from the Universidad Autónoma de Madrid, Departamento de Química, Facultad de Ciencias, Módulo 13, Campus de Excelencia UAM–CSIC, Cantoblanco, 28049-Madrid, Spain. The Instituto de Química Médica. C/ Juan de la Cierva, 3, CSIC, 28006–Madrid, Spain. The Université de Toulouse III – Paul Sabatier. Laboratoire de Chimie et Physique Quantiques. 118, Route de Narbonne, 31400–Toulouse, France**

## CONTENTS

s1 Computational Details	S3
s2 Active Space and Electron Configurations	S3
s3 Beryllium Dimer	S10
s4 Wave Function Analysis	S12
s5 Bond Dissociation Energy NRC: Be-Be: NRC	S15

## LIST OF FIGURES

Figure S1	CASPT2//CASSCF(8,10)/cc-pVTZ active space used for the description of the $^1[\text{NH}_3:\text{Be}-\text{Be}:\text{NH}_3]$ complex	S4
Figure S2	CASPT2//CASSCF(8,10)/cc-pVTZ active space used for the description of the $^3[\text{NH}_3:\text{Be}-\text{Be}:\text{NH}_3]$ complex	S4
Figure S3	CASPT2//CASSCF(8,10)/cc-pVTZ active space used for the description of the $^1[\text{H}_2\text{O}:\text{Be}-\text{Be}:\text{H}_2\text{O}]$ complex	S4
Figure S4	CASPT2//CASSCF(8,10)/cc-pVTZ active space used for the description of the $^3[\text{H}_2\text{O}:\text{Be}-\text{Be}:\text{H}_2\text{O}]$ complex	S4
Figure S5	SA(2)CASPT2//CASSCF(n,m)/cc-pVTZ active space used for the description of the $^1[\text{CO}:\text{Be}-\text{Be}:\text{CO}]$ complex	S6
Figure S6	SA(2)CASPT2//CASSCF(n,m)/cc-pVTZ active space used for the description of the $^3[\text{CO}:\text{Be}-\text{Be}:\text{CO}]$ complex	S7
Figure S7	Single point calculation for the trans-type isomer of the ground state of the $\text{CO}:-\text{Be}-\text{Be}:\text{CO}$ complex.	S7
Figure S8	State energy diagram of the complexes with $\text{L}=\text{NH}_3$ and $\text{H}_2\text{O}$	S9
Figure S9	State energy diagram of the complex with $\text{L}=\text{CO}$	S9
Figure S10	Wave function analysis of the $^M[\text{NH}_3:\text{Be}-\text{Be}:\text{NH}_3]$ complexes	S13
Figure S11	Wave function analysis of the $^M[\text{H}_2\text{O}:\text{Be}-\text{Be}:\text{H}_2\text{O}]$ complexes	S14
Figure S12	Wave function analysis of the $^M[\text{CO}:\text{Be}-\text{Be}:\text{CO}]$ complexes	S14

## LIST OF TABLES

Table S1	Electron configuration of the $^M[\text{L}:\text{Be}-\text{Be}:\text{L}]$ complexes, with $\text{L} = \text{NH}_3$ and $\text{H}_2\text{O}$	S5
Table S2	Comparison of the performance of different active spaces for the $^1[\text{CO}:\text{Be}-\text{Be}:\text{CO}]$ complex	S6
Table S3	Electron configuration of the $^M[\text{CO}:\text{Be}-\text{Be}:\text{CO}]$ complexes	S8
Table S4	Energetic and geometric properties and electron configuration of the $\text{Be}_2$ molecule	S10

Table S5	Bonding properties of the $^1\Sigma_g$ Be <sub>2</sub> molecule . . . . .	S11
Table S6	NBO Analysis for the L:Be-Be:L complexes and the isolated dimer . . . . .	S12
Table S7	Wave function analysis of the $^M$ [L:Be–Be:L] complexes . . . . .	S13
Table S8	BDE for the NRC: Be-Be: NRC complexes at MP2/cc-pVTZ//B3LYP/cc-pVTZ level of theory. . . . .	S15

## S1 COMPUTATIONAL DETAILS

The geometries of singlet and triplet states of the complexes study in this communication were optimized in the CASPT2//CASSCF(*n,m*)/cc-pVTZ framework,<sup>1–5</sup> with an active space (AS) equal to (8,10) for L=H<sub>2</sub>O and NH<sub>3</sub>, and for L=CO were considered two AS: (10,12) and (12,12), finding negligible differences in the order of 1E<sup>-3</sup> for the bond distances. The same level of theory was employed to calculate the harmonic vibrational frequencies, which were used to confirm that the structures obtained are local minima of the potential energy surface. For the CO:Be–Be:CO complexes final energies were determined by single-point calculations increasing the active space to (12,14). The AS are detailed in section S2. Finally, the Bond Dissociation Energies (BDE) were calculated considering the fragments at 20Å in order to have the same active space in the equilibrium and in the dissociation distances. The complexes formed with Be<sub>2</sub> and radical species are closed-shell due to the charge transfer from Be→L, therefore they were studied considering CCSD(T)/cc-pVTZ level of theory.<sup>6,7</sup> All calculations were performed with MOLPRO 2015 computational package.<sup>8</sup>

The nature of the Be-Be bond in the L:Be-Be:L complexes was analyzed using the CASSCF wave function at the same level of theory than the geometry optimization. Different complementary approaches were used to analyze the wave function: Quantum Theory of Atoms in Molecules Theory (QTAIM),<sup>9</sup> Electron Localized Functional (ELF)<sup>10</sup> and Natural Bond Orbital (NBO).<sup>11</sup> The QTAIM methodology is based in a representation of the electron density ( $\rho(r)$ ) in real space, in such a way that is possible to define atomic regions inside of the molecule, allowing to determine the energy of an atom inside of a molecule and to explain how atoms are linked between each other to built the molecule. The topological analysis of  $\rho(r)$  and  $\nabla^2\rho(r)$  defines and characterize the critical points of the electron density: Bond Critical Points (BCP) are saddle points of  $\rho(r)$  connecting two atoms and the magnitude of  $\rho(r)$  at the BCP is related to the strength of the interaction between the atoms. The sign of  $\nabla^2\rho(r)$  in a BCP describe how is built the electron density between the atoms, negative values of  $\nabla^2\rho(r)$  indicate a concentration of  $\rho(r)$  around the BCP (covalent interaction) while positive values of  $\nabla^2\rho(r)$  represent a depletion of  $\rho(r)$  around the BCP (ionic bonds). The BCP are connected by bond paths that are calculated following the path where  $\rho$  is maxima, giving a more realistic representation of the chemical bonds, the molecular graphs are the ensemble of all bond paths and critical points.

The NBO analysis is a multistep procedure based in the orbital localization of the one-electron density matrix to obtain the NBO orbitals, this method recovers classical chemical concepts that are very useful to describe chemical bonds: the Lewis structure, atomic charges, hybridization, bond indexes, and others. The NBO calculations have been done with the NBO-6.0 program package.<sup>12</sup>

The ELF method is a topological analysis of the electron localization function, the real space is partitioned using the gradient path as QTAIM, but as a difference, it analyzes the regions where is a maximum of probability to locate an electron pair (basin). The classification of the basins are related to the number of atoms in which are centered: mono-synaptic basins are centered over an atom (Lone or core pairs) and di(poly-)synaptic basins are centered over two (or more than two) atoms. The population of di-synaptic basins has been associated to the strength of the interaction between the atoms. The ELF calculations have been carried out by using the TopMod package.<sup>13</sup>

## S2 ACTIVE SPACE AND ELECTRON CONFIGURATIONS

### s2.1 L = NH<sub>3</sub> and H<sub>2</sub>O

The active space for the complexes is composed by the lone pairs of the Lewis bases interacting with the Be and the valence orbitals of the beryllium atoms, with an active space equal to (8,10).

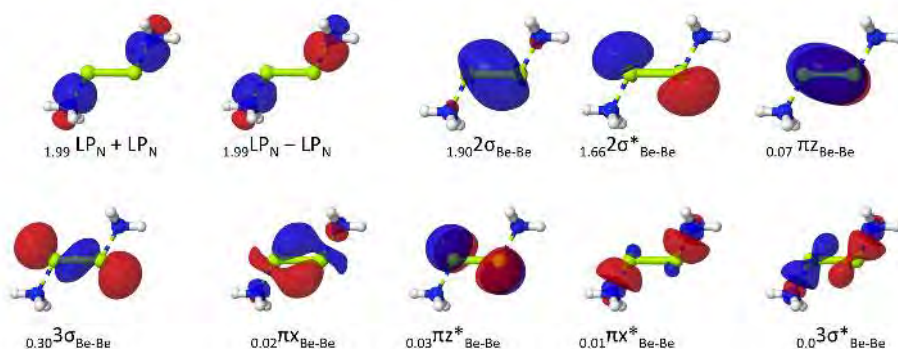


**Figure S1:** CASPT2//CASSCF(8,10)/cc-pVTZ active space used for the description of the  $^1[\text{NH}_3:\text{Be}-\text{Be}:\text{NH}_3]$  complex. The orbital occupation is showed in subscript.

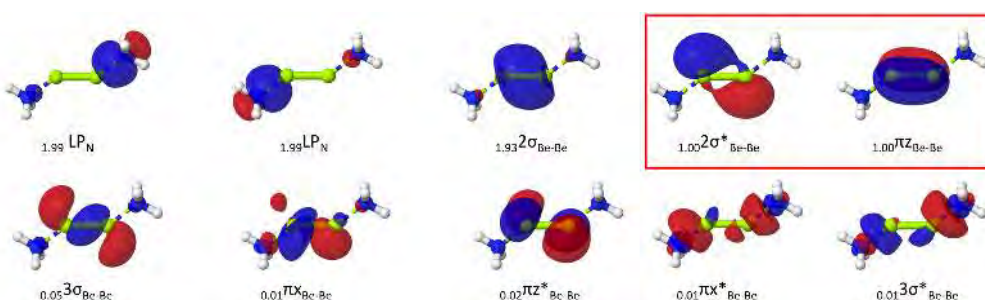


**Figure S2:** CASPT2//CASSCF(8,10)/cc-pVTZ active space used for the description of the  $^3[\text{NH}_3:\text{Be}-\text{Be}:\text{NH}_3]$  complex. The orbital occupation is showed in subscript and the singlet occupied molecular orbitals are highlight in red squares.

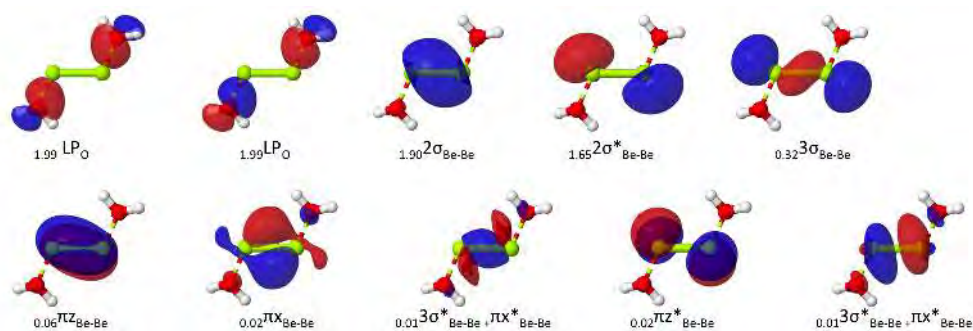


**Figure S3:** CASPT2//CASSCF(8,10)/cc-pVTZ active space used for the description of the  $^1[\text{H}_2\text{O}:\text{Be}-\text{Be}:\text{H}_2\text{O}]$  complex. The orbital occupation is showed in subscript.

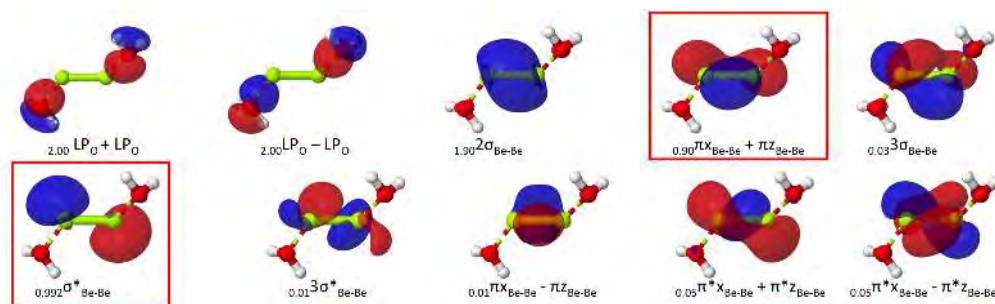


**Figure S4:** CASPT2//CASSCF(8,10)/cc-pVTZ active space used for the description of the  $^3[\text{H}_2\text{O}:\text{Be}-\text{Be}:\text{H}_2\text{O}]$  complex. The orbital occupation is showed in subscript and the singlet occupied molecular orbitals are highlight in red squares.

**Table S1:** Electron configuration of the  $M[L:Be-Be:L]$  complexes, with  $L = NH_3$  and  $H_2O$  and  $M$  equal to multiplicity. The calculations were performed at CASPT2/CASSCF(8,10)/cc-pVTZ level of theory.

$M_L$	Configuration	Weight
$^1[NH_3]$	$(LP_N)^2 (2\sigma_{Be})^2 (2\sigma^*_{Be})^2 (3\sigma_{Be})^0 (\pi_{zBe})^0 (\pi_{xBe})^0 (\pi_{yBe})^0 (\pi^*_{zBe})^0 (\pi^*_{xBe})^0 (\pi^*_{yBe})^0$	0.78
	$(LP_N)^2 (LP_N)^2 (2\sigma_{Be})^2 (2\sigma^*_{Be})^0 (3\sigma_{Be})^2 (\pi_{zBe})^0 (\pi_{xBe})^0 (\pi_{yBe})^0 (\pi^*_{zBe})^0 (\pi^*_{xBe})^0 (\pi^*_{yBe})^0$	0.14
$^3[NH_3]$	$(LP_N)^2 (LP_N)^2 (2\sigma_{Be})^2 (2\sigma^*_{Be})^1 (3\sigma_{Be})^0 (\pi_{zBe})^1 (\pi_{xBe})^0 (\pi_{yBe})^0 (\pi^*_{zBe})^0 (\pi^*_{xBe})^0 (\pi^*_{yBe})^0$	0.93
	$(LP_O)^2 (LP_O)^2 (2\sigma_{Be})^2 (2\sigma^*_{Be})^2 (3\sigma_{Be})^0 (\pi_{zBe})^0 (\pi_{xBe})^0 (\pi_{yBe})^0 (\pi^*_{zBe})^0 (\pi^*_{xBe})^0 (\pi^*_{yBe})^0$	0.78
$^1[H_2O]$	$(LP_O)^2 (LP_O)^2 (2\sigma_{Be})^2 (2\sigma^*_{Be})^0 (3\sigma_{Be})^2 (\pi_{zBe})^0 (\pi_{xBe})^0 (\pi_{yBe})^0 (\pi^*_{zBe})^0 (\pi^*_{xBe})^0 (\pi^*_{yBe})^0$	0.15
	$(LP_O)^2 (LP_O)^2 (2\sigma_{Be})^2 (2\sigma^*_{Be})^1 (3\sigma_{Be})^0 (\pi_{zBe})^1 (\pi_{xBe})^0 (\pi_{yBe})^0 (\pi^*_{zBe})^0 (\pi^*_{xBe})^0 (\pi^*_{yBe})^0$	0.92



## s2.2 L = CO

The *ideal* active space for these complexes is composed by two  $\pi_{\text{CO}}$ , two  $\pi^*_{\text{CO}}$  and the valence electrons of the beryllium atoms, which corresponds to (12,16) AS. However, CASPT2 calculation with this CI matrix is not feasible, as a consequence we had to reduce the size of the active space. We considered four possible AS:

- (10,12):  $2 \cdot (\pi_{\text{Be}})$ ,  $4 \cdot (\pi_{\text{CO}})$ ,  $2 \cdot (\pi^*_{\text{Be}})$  and  $4 \cdot (\pi^*_{\text{CO}})$ .
- (12,12):  $2\sigma_{\text{Be}}$ ,  $\pi_{\text{Be}}$ ,  $4 \cdot (\pi_{\text{CO}})$ ,  $\sigma^*_{\text{Be}}$ ,  $\pi^*_{\text{Be}}$  and  $4 \cdot (\pi^*_{\text{CO}})$ .
- (12,14):  $2\sigma_{\text{Be}}$ ,  $2 \cdot (\pi_{\text{Be}})$ ,  $4 \cdot (\pi_{\text{CO}})$ ,  $2\sigma^*_{\text{Be}}$ ,  $2 \cdot (\pi^*_{\text{Be}})$  and  $4 \cdot (\pi^*_{\text{CO}})$ .
- (12,16):  $2\sigma_{\text{Be}}$ ,  $3\sigma_{\text{Be}}$ ,  $2 \cdot (\pi_{\text{Be}})$ ,  $4 \cdot (\pi_{\text{CO}})$ ,  $2\sigma^*_{\text{Be}}$ ,  $3\sigma^*_{\text{Be}}$ ,  $2 \cdot (\pi^*_{\text{Be}})$  and  $4 \cdot (\pi^*_{\text{CO}})$ .

The energy differences between the four AS at DF-CASSCF(n,m)/3-21G level of theory<sup>14</sup> are reported in Table S2. From these results was decided to perform the geometry optimization at CASPT2//CASSCF(10,12)/cc-pVTZ level of theories, and final energies were calculated as single points at SA(2)CASPT2//CASSCF(12,14)/cc-pVTZ. In the CASSCF(12,14) were included two states because of the degeneracy of the  $\pi_{\text{Be}}$  orbitals.

**Table S2:** Comparison of the performance of different active spaces for the  $^1[\text{CO}:\text{Be}-\text{Be}:\text{CO}]$  complex, the calculations were performed at CASSCF(n,m)/3-21G level of theory.

AS (n,m)	$\Delta E$ (kJ mol <sup>-1</sup> )
(12,16)	0
(12,14)	18
(12,12)	48
(10,12)	51

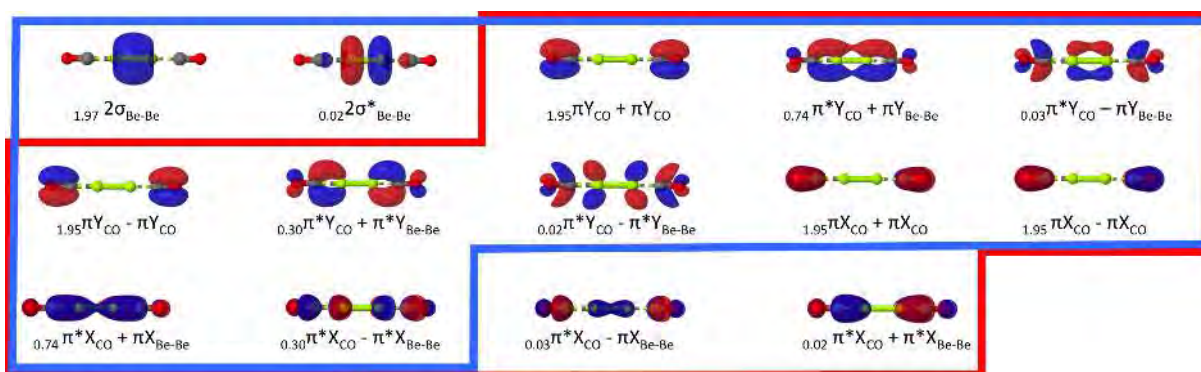


**Figure S5:** SA(2)CASPT2//CASSCF(n,m)/cc-pVTZ active space used for the description of the  $^1[\text{CO}:\text{Be}-\text{Be}:\text{CO}]$  complex. The complete set of orbitals correspond to the (12,14) AS, the orbitals in the blue square correspond to the (12,12) AS, and in red square the de (10,12) AS. The orbital occupation is showed in subscript.

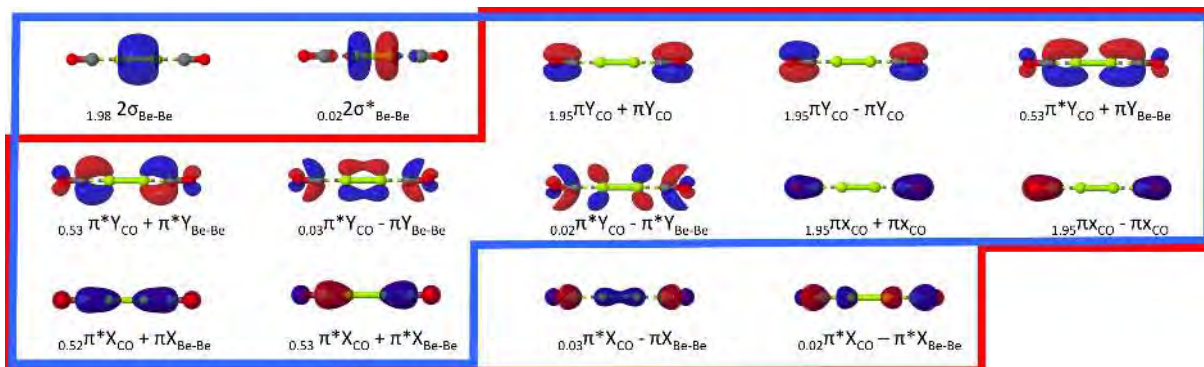


**Figure S6:** SA(2)CASPT2//CASSCF( $n,m$ )/cc-pVTZ active space used for the description of the  $^3[\text{CO}:\text{Be}-\text{Be}:\text{CO}]$  complex. The complete set of orbitals correspond to the (12,14) AS, the orbitals in the blue square correspond to the (12,12) AS, and in red square the de (10,12) AS. The orbital occupation is showed in subscript. The orbital occupation is showed in subscript.

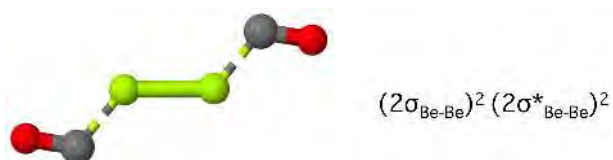


**Figure S7:** Single point calculation for the trans-type isomer of the ground state of the  $\text{CO}:\text{Be}-\text{Be}:\text{CO}$  complex, noticed that the electron configuration of the  $\text{Be}_2$  moiety is equivalent to the isolated dimer. The calculation was performed at SA(2)CASPT2//CASSCF(12,14)/cc-pVTZ level of theory.

**Table S3:** Electron configuration of the  $M^1[\text{CO}_2\text{Be}-\text{Be}:\text{CO}]$  complexes, with  $M$  equal to the multiplicity. The calculations were performed at SA(2)CASPT2//CASSCF(12, 14)/cc-pVTZ level of theory.

$M^1$	Configuration	Weight
$^1[\text{CO}]$	$(2\sigma_{\text{Be}})^2 2(\pi_{\text{xCO}})^2 2(\pi_{\text{yCO}})^2 (\pi_{\text{xBe}} + \pi_{\text{xCO}}^*)^2 (\pi_{\text{xBe}} - \pi_{\text{xCO}}^*)^0 (\pi_{\text{yBe}} + \pi_{\text{yCO}}^*)^0 (\pi_{\text{yBe}} - \pi_{\text{yCO}}^*)^0$ $(2\sigma_{\text{Be}}^*)^0 (\pi_{\text{xBe}}^* + \pi_{\text{xCO}}^*)^0 (\pi_{\text{xBe}}^* - \pi_{\text{xCO}}^*)^0 (\pi_{\text{yBe}}^* + \pi_{\text{yCO}}^*)^0 (\pi_{\text{yBe}}^* - \pi_{\text{yCO}}^*)^0$	0.32
	$(2\sigma_{\text{Be}})^2 2(\pi_{\text{xCO}})^2 2(\pi_{\text{yCO}})^2 (\pi_{\text{xBe}} + \pi_{\text{xCO}}^*)^0 (\pi_{\text{xBe}} - \pi_{\text{xCO}}^*)^0 (\pi_{\text{yBe}} + \pi_{\text{yCO}}^*)^2 (\pi_{\text{yBe}} - \pi_{\text{yCO}}^*)^0$ $(2\sigma_{\text{Be}}^*)^0 (\pi_{\text{xBe}}^* + \pi_{\text{xCO}}^*)^0 (\pi_{\text{xBe}}^* - \pi_{\text{xCO}}^*)^0 (\pi_{\text{yBe}}^* + \pi_{\text{yCO}}^*)^0 (\pi_{\text{yBe}}^* - \pi_{\text{yCO}}^*)^0$	0.32
$^3[\text{CO}]$	$(2\sigma_{\text{Be}})^2 2(\pi_{\text{xCO}})^2 2(\pi_{\text{yCO}})^2 (\pi_{\text{xBe}} + \pi_{\text{xCO}}^*)^1 (\pi_{\text{xBe}} - \pi_{\text{xCO}}^*)^0 (\pi_{\text{yBe}} + \pi_{\text{yCO}}^*)^0 (\pi_{\text{yBe}} - \pi_{\text{yCO}}^*)^0$ $(2\sigma_{\text{Be}}^*)^0 (\pi_{\text{xBe}}^* + \pi_{\text{xCO}}^*)^1 (\pi_{\text{xBe}}^* - \pi_{\text{xCO}}^*)^0 (\pi_{\text{yBe}}^* + \pi_{\text{yCO}}^*)^0 (\pi_{\text{yBe}}^* - \pi_{\text{yCO}}^*)^0$	0.45
	$(2\sigma_{\text{Be}})^2 2(\pi_{\text{xCO}})^2 2(\pi_{\text{yCO}})^2 (\pi_{\text{xBe}} + \pi_{\text{xCO}}^*)^0 (\pi_{\text{xBe}} - \pi_{\text{xCO}}^*)^0 (\pi_{\text{yBe}} + \pi_{\text{yCO}}^*)^1 (\pi_{\text{yBe}} - \pi_{\text{yCO}}^*)^0$ $(2\sigma_{\text{Be}}^*)^0 (\pi_{\text{xBe}}^* + \pi_{\text{xCO}}^*)^0 (\pi_{\text{xBe}}^* - \pi_{\text{xCO}}^*)^0 (\pi_{\text{yBe}}^* + \pi_{\text{yCO}}^*)^1 (\pi_{\text{yBe}}^* - \pi_{\text{yCO}}^*)^0$	0.45

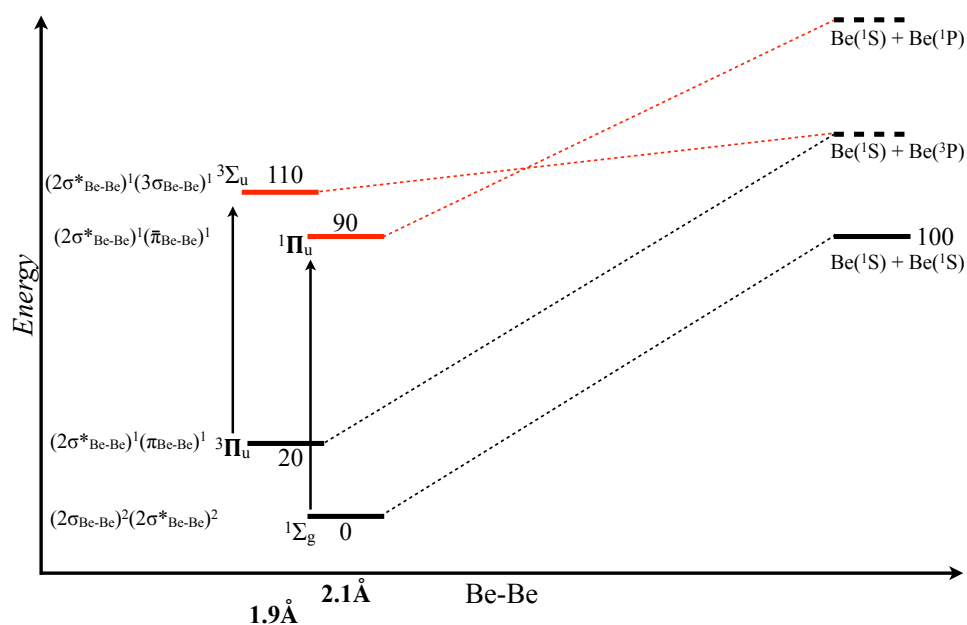


**Figure S8:** State energy diagram of the complexes with L=NH<sub>3</sub> and H<sub>2</sub>O, the vertical excitation energies are in red and the adiabatic excitation energies are in black. The Be-Be electron configuration and bond distances are also shown. The calculations were performed at CASPT2//CASSCF(8,10)/cc-pVTZ level of theory, the energies are kJ·mol<sup>-1</sup> and the bond distances in Å.

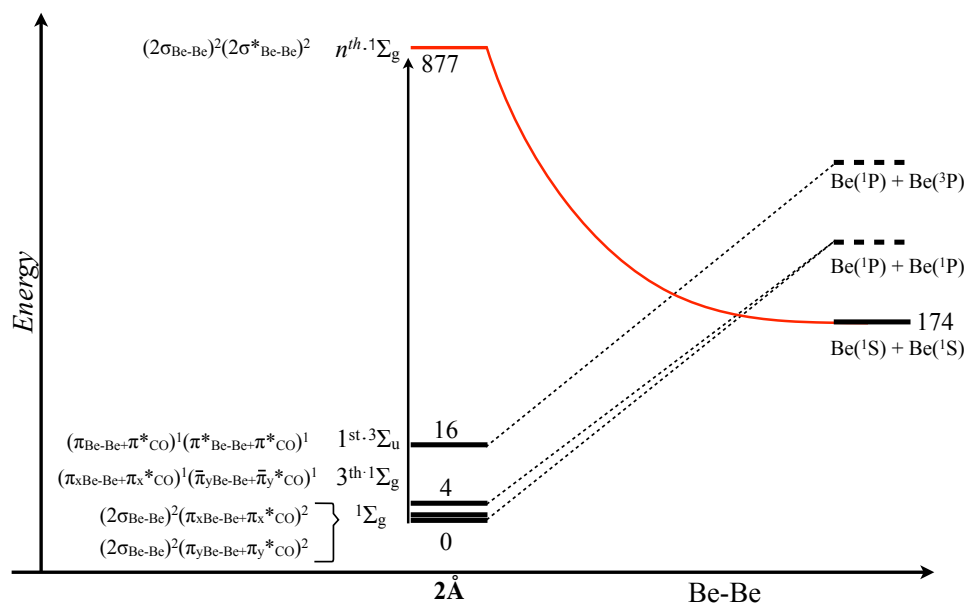


**Figure S9:** State energy diagram of the complex with L=CO, the vertical excitation energies are in red and the adiabatic excitation energies are in black. The Be-Be electron configuration and bond distances are also shown. The calculations were performed at SA(2)CASPT2//CASSCF(12,14)/cc-pVTZ level of theory, the energies are kJ·mol<sup>-1</sup> and the bond distances in Å.

### S3 BERYLLIUM DIMER

The AS to describe the Be<sub>2</sub> seems to be an easy choice: the full valence (4,8), but previous results has shown that the CASSCF(4,8) dissociation curve is repulsive<sup>15</sup> and the AS must be increased to (4,16) to recover the binding character. Reference<sup>15</sup> describes the behavior of the Be<sub>2</sub> for the four AS:

1. (4,16):  $2\sigma + 2\sigma^* + 3\sigma + 3\sigma^* + 2(1\pi) + 2(1\pi^*) + 4\sigma + 4\sigma^* + 2(2\pi) + 2(2\pi^*)$ .
2. (4,8):  $2\sigma + 2\sigma^* + 3\sigma + 3\sigma^* + 2(1\pi) + 2(1\pi^*)$ .
3. (4,4):  $2\sigma + 2\sigma^* + 3\sigma + 3\sigma^*$ .
4. (2,2):  $2\sigma^* + 3\sigma$ .

**Table S4:** Energetic and geometric properties and electron configuration of the Be<sub>2</sub> molecule

Table S4(a): Comparison energetic properties of the Be<sub>2</sub> molecule considering different AS. Bond Dissociation Energy (BDE) and excitation energy  $T_e$  are in (kJ·mol<sup>-1</sup>), and bond distances in Å. All values were calculated at CASPT2//CASSCF(n,m)/cc-pVTZ

State	(n,m)	Be-Be	BDE <sub>CASSCF</sub>	BDE <sub>CASPT2</sub>	$T_e$ (CASSCF)	$T_e$ (CASPT2)
<sup>1</sup> Σ <sub>g</sub>	(2,2)	2.33	45	32	0	0
	(4,4)	2.43	-9	13	0	0
	(4,8)	2.59	-23	1	0	0
	(4,16)	2.52	2	6	0	0
	<b>Ref</b> <sup>16,17</sup>	2.45		9.45	-	-
<sup>3</sup> Σ <sub>u</sub>	(2,2)	2.15	-	-	49	72
	(4,4)	2.17	-	-	60	78
	(4,8)	2.14	150	171	105	96
	(4,16)	2.14	177	180	94	92
	<b>Ref</b> <sup>18</sup>	2.13		186		90
<sup>1</sup> Π <sub>g</sub>	(4,8)	2.00	303	356	226	175
	(4,16)	2.00	339	313	212	225
	<b>Ref</b> <sup>19</sup>	2.00		354		168

Table S4(b): Comparison of the Be<sub>2</sub> molecule electron configuration considering different AS. All values were calculated at CASPT2//CASSCF(n,m)/cc-pVTZ

State	(n,m)	Electron Configuration
<sup>1</sup> Σ <sub>g</sub>	(2,2)	0.91·[(2σ) <sup>2</sup> (2σ*) <sup>2</sup> (3σ) <sup>0</sup> ] – 0.41·[(2σ) <sup>2</sup> (2σ*) <sup>0</sup> (3σ) <sup>2</sup> ]
	(4,4)	0.90·[(2σ) <sup>2</sup> (2σ*) <sup>2</sup> (3σ) <sup>0</sup> ] – 0.38·[(2σ) <sup>2</sup> (2σ*) <sup>0</sup> (3σ) <sup>2</sup> ]
	(4,8)	0.90·[(2σ) <sup>2</sup> (2σ*) <sup>2</sup> (3σ) <sup>0</sup> ] – 0.23·[(2σ) <sup>2</sup> (2σ*) <sup>0</sup> (3σ) <sup>2</sup> ]
	(4,16)	0.89·[(2σ) <sup>2</sup> (2σ*) <sup>2</sup> (3σ) <sup>0</sup> ] – 0.26·[(2σ) <sup>2</sup> (2σ*) <sup>0</sup> (3σ) <sup>2</sup> ]
<sup>3</sup> Σ <sub>u</sub>	(4,8)	0.97·[(2σ) <sup>2</sup> (2σ*) <sup>1</sup> (3σ) <sup>1</sup> ]
	(4,16)	0.96·[(2σ) <sup>2</sup> (2σ*) <sup>1</sup> (3σ) <sup>1</sup> ]
<sup>1</sup> Π <sub>g</sub>	(4,8)	0.65·[(2σ) <sup>2</sup> (2σ*) <sup>1</sup> (1π <sub>x</sub> ) <sup>1</sup> ] – 0.65·[(2σ) <sup>2</sup> (2σ*) <sup>1</sup> ((1π <sub>y</sub> ) <sup>1</sup> )]
	(4,16)	0.64·[(2σ) <sup>2</sup> (2σ*) <sup>1</sup> (1π <sub>x</sub> ) <sup>1</sup> ] – 0.64·[(2σ) <sup>2</sup> (2σ*) <sup>1</sup> ((1π <sub>y</sub> ) <sup>1</sup> )]

**Table S5:** Bonding properties of the <sup>1</sup>Σ<sub>g</sub> Be<sub>2</sub> molecule. The values of ρ and ∇<sup>2</sup>ρ in BCP<sub>Be-Be</sub> is shown in a.u., and with a • are represented the values in BCP<sub>NNA-Be</sub>. The population in the V(Be, Be) basin shown also in a.u., and the bond distances are in Å. The wave function analysis was performed at CASSCF(n,m)/cc-pVTZ, while bond distances at CASPT2//CASSCF(n,m)/cc-pVTZ. The •• represents the presence of a pseudo-nuclei and therefore there are two BCP<sub>Be-NNA</sub>

State	AS	Be-Be	ρ	∇ <sup>2</sup> ρ	pop
<sup>1</sup> Σ <sub>g</sub>	(2,2)	2.33	•• 0.05	•• -0.05	1.71
	(4,4)	2.43	0.04	-0.05	-
	(4,8)	2.59	0.03	-0.01	-
	(4,16)	2.52	0.03	-0.03	-

## S4 WAVE FUNCTION ANALYSIS

**Table S6:** NBO for the L:Be-Be:L complexes and the isolated dimer: the Be<sub>2</sub> atomic charges are in au, the electron configuration of the Be in the complexes and the hybrid character of the Be-Be bond. The occupation of the Be-Be bond is shown within parenthesis.

L-Group	Charge Be <sub>2</sub>	Electron Configuration Be	Be <sub>2</sub> Hybrid Character
/	0.0	[core]2s <sup>1.74</sup> 2p <sup>0.24</sup>	2· (2)LP Be
<i>L-Group-I:</i>			
NH <sub>3</sub>	-0.01333	[core]2s <sup>1.49</sup> 2p <sup>0.46</sup>	(2.0)BD Be-Be: s(92%)p(8%)Be(1) + s(6%)p(93%)Be(2) (2.0)LP Be(2) s(2%)p(98%)
H <sub>2</sub> O	+0.03153	[core]2s <sup>1.64</sup> 2p <sup>0.30</sup>	(2.0)BD Be-Be: s(91%)p(9%)Be(1) + sp(4%)p(93%)Be(2) (2.0)LP Be(2) s(91%)p(9%)
<i>L-Group-II:</i>			
CO	+0.71658	[core]2s <sup>1.03</sup> 2p <sup>0.59</sup>	(2.0)BD Be-Be: s(92%)p(8%)Be(1) + s(92%)p(8%)Be(2) (0.5)RY Be(2) p(100%)
NHC[a]	+0.81694	[core]2s <sup>1.03</sup> 2p <sup>0.52</sup>	(2.0)BD Be-Be: s(93%)p(7%)Be(1) + s(93%)p(7%)Be(2) (0.4)RY Be(2) p(100%)
NMeC[a]	+0.80642	[core]2s <sup>1.04</sup> 2p <sup>0.52</sup>	(2.0)BD Be-Be: s(92%)p(8%)Be(1) + s(92%)p(8%)Be(2) (0.4)RY Be(2) p(100%)
NPhC[a]	+1.18486	[core]2s <sup>1.01</sup> 2p <sup>0.38</sup>	(2.0)BD Be-Be: s(92%)p(7%)BBe(1) + s(92%)p(7%)BBe(2) (0.3)RY Be(2) p(100%)
<i>L-Group-III:</i>			
CN•	+1.75990	[core]2s <sup>0.97</sup> 2p <sup>0.13</sup>	(2.0)BD Be-Be: s(91%)p(9%)Be(1) + s(91%)p(9%)Be(2)
F•	+1.79088	[core]2s <sup>0.91</sup> 2p <sup>0.18</sup>	(2.0)BD Be-Be: s(87%)p(12%)Be(1) + s(87%)p(12%)Be(2)
CH <sub>3</sub> O•	+1.74276	[core]2s <sup>0.94</sup> 2p <sup>0.17</sup>	(2.0)BD Be-Be: s(90%)p(10%)Be(1) + s(90%)p(10%)Be(2)
OH•	+1.75114	[core]2s <sup>0.94</sup> 2p <sup>0.17</sup>	(2.0)BD Be-Be: s(92%)p(7%)Be(1) + s(92%)p(7%)Be(2)
NH <sub>2</sub> •	+1.70728	[core]2s <sup>0.97</sup> 2p <sup>0.17</sup>	(2.0)BD Be-Be: s(92%)p(8%)Be(1) + s(92%)p(8%)Be(2)
CH <sub>3</sub> •	+1.67496	[core]2s <sup>1.02</sup> 2p <sup>0.13</sup>	(2.0)BD Be-Be: s(93%)p(7%)Be(1) + s(93%)p(7%)Be(2)

[a] The geometry was taken from reference<sup>20</sup> and the NBO calculation was performed at B3LYP/cc-pVTZ level of theory.

**Table S7:** Wave function analysis of the  $^M[L:Be-Be:L]$  complexes, with  $L=NH_3$ ,  $H_2O$  and  $CO$  and  $M$  equal to the multiplicity. Values for the Be-Be bond distance ( $r_{Be-Be}$ ), the Be-BCP distance ( $r_{Be-BCP}$ ) and the Be-NNA distance ( $r_{Be-NNA}$ ) are in Å. The values of  $\rho$ ,  $\nabla^2\rho$  and  $\epsilon$  are reported for the BCP between the Be and the NNA, all values are in au. The atomic energy of the Be atom ( $E_{Be}$ ) is reported in au. The population of the Be-Be dysynaptic basin  $V(Be,Be)$  is reported in au.

$^M L$	$r_{Be-Be}$	$r_{Be-BCP}$	$r_{Be-NNA}$	$\rho$	$\nabla^2\rho$	$E_{Be}$	$\epsilon$	$V(Be,Be)$
$^1/$	2.58	/	/	0.026	-0.014	-1.46E <sup>01</sup>	0.000	/
$^3/$	2.14	0.70	0.37	0.064	-0.080	-1.44E <sup>01</sup>	0.000	1.92
$^1NH_3$	2.13	0.70	0.38	0.054	-0.035	-1.44E <sup>01</sup>	0.169	1.78
$^3NH_3$	1.93	0.66	0.36	0.062	-0.004	-1.44E <sup>01</sup>	0.201	1.79
$^1H_2O$	2.17	0.70	0.39	0.054	-0.035	-1.44E <sup>01</sup>	0.172	1.72
$^3H_2O$	1.99	0.66	0.34	0.063	-0.014	-1.44E <sup>01</sup>	0.124	2.03
$^1CO$	2.01	0.69	0.31	0.069	-0.071	-1.43E <sup>01</sup>	0.220	2.43
$^3CO$	2.05	0.70	0.34	0.069	-0.808	-1.43E <sup>01</sup>	0.120	2.17

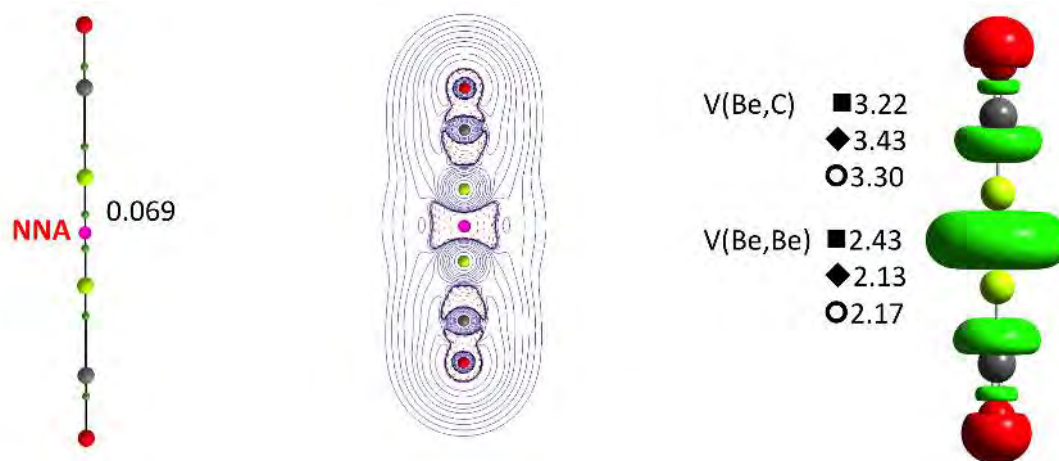


**Figure S10:** Molecular graphs (first row) for the  $^M[NH_3:Be-Be:NH_3]$ , with  $M = 1,3$ . Green and pink dots correspond to BCP and NNAs respectively. The second row shows the two dimension representation of the  $\nabla^2\rho$ , red and blue areas correspond to negative and positive values of  $\nabla^2$  respectively. The ELF plots are in the third row for the same systems. Yellow lobes correspond to dysynaptic basins involving hydrogen atoms or NNA. Green lobes correspond to dysynaptic basins between heavy atoms and red basins denote monosynaptic basins associated with lone-pairs. All values are in au.



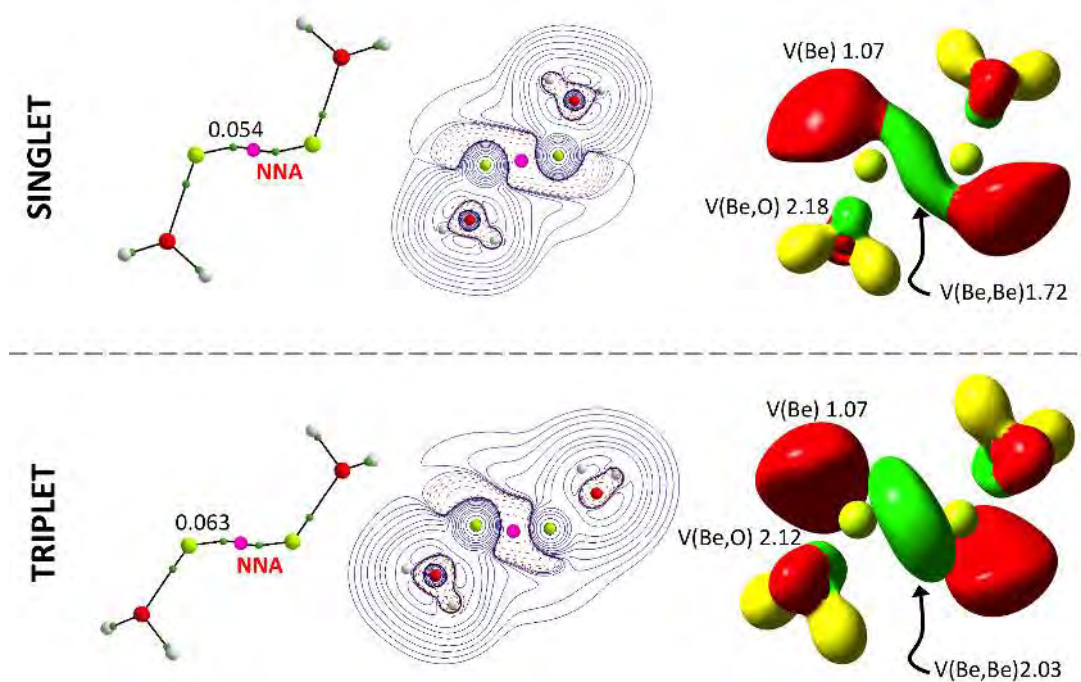


**Figure S11:** Molecular graphs (first row) for the  $M[\text{H}_2:\text{Be}-\text{Be}:\text{H}_2\text{O}]$ , with  $M = 1,3$ . Green and pink dots correspond to BCP and NNAs respectively. The second row shows the two dimension representation of the  $\nabla^2\rho$ , red and blue areas correspond to negative and positive values of  $\nabla^2$  respectively. The ELF plots are in the third row for the same systems. Yellow lobes correspond to disynaptic basins involving hydrogen atoms or NNA. Green lobes correspond to disynaptic basins between heavy atoms and red basins denote monosynaptic basins associated with lone-pairs. All values are in au.

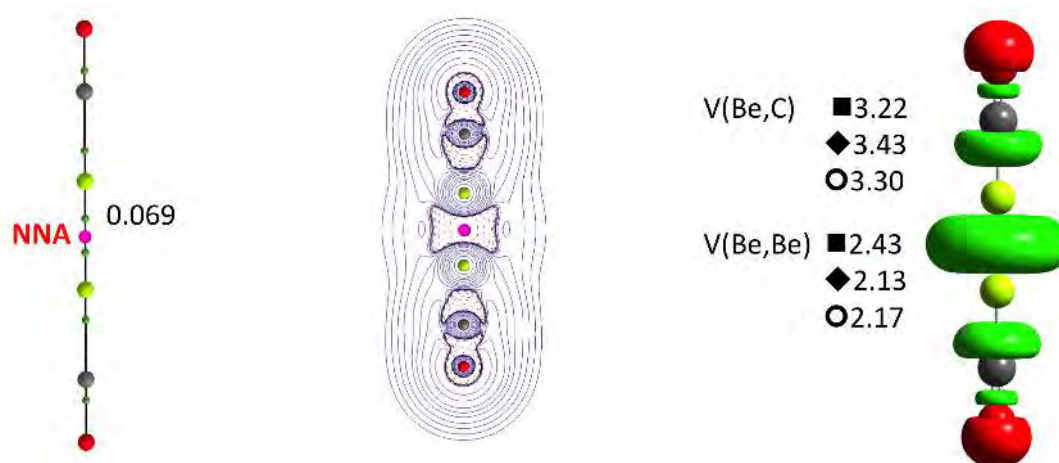


**Figure S12:** Molecular graphs (first row) for the  $M[\text{CO}:\text{Be}-\text{Be}:\text{CO}]$ , with  $M = 1,3$ . Green and pink dots correspond to BCP and NNAs respectively. The second row shows the two dimension representation of the  $\nabla^2\rho$ , red and blue areas correspond to negative and positive values of  $\nabla^2$  respectively. The ELF plots are in the third row for the same systems. Yellow lobes correspond to disynaptic basins involving hydrogen atoms or NNA. Green lobes correspond to disynaptic basins between heavy atoms and red basins denote monosynaptic basins associated with lone-pairs. The ■ represents the  $1\Sigma_g$  state, ◆ the  $2^1\Sigma_g$  state, and ○ the  $3^3\Sigma_u$ . All values are in au.

## S5 BOND DISSOCIATION ENERGY NRC: BE-BE: NRC

**Table S8:** BDE for the NRC: Be-Be: NRC complexes at MP2/cc-pVTZ//B3LYP/cc-pVTZ level of theory.

R-Group	BDE <sub>1</sub>	BDE <sub>2</sub>
H	360	262
Me	415	304
Ph	506	379

## BIBLIOGRAPHY

- <sup>1</sup> Roos, B. O.; Taylor, P. R.; Sigbahn, P. E. *Chemical Physics* **1980**, *48*, 157 – 173.
- <sup>2</sup> Roos, B. O. *The Complete Active Space Self-Consistent Field Method and its Applications in Electronic Structure Calculations*; John Wiley & Sons, Inc., 2007; pp 399–445.
- <sup>3</sup> Andersson, K.; Malmqvist, P. A.; Roos, B. O.; Sadlej, A. J.; Wolinski, K. *The Journal of Physical Chemistry* **1990**, *94*, 5483–5488.
- <sup>4</sup> Andersson, K.; Malmqvist, P. P. E.; Roos, B. O. *The Journal of Chemical Physics* **1992**, *96*, 1218–1226.
- <sup>5</sup> Kendall, R. A.; Dunning, T. H.; Harrison, R. J. *The Journal of Chemical Physics* **1992**, *96*, 6796–6806.
- <sup>6</sup> Watts, J. D.; Gauss, J.; Bartlett, R. J. *The Journal of chemical physics* **1993**, *98*, 8718–8733.
- <sup>7</sup> Deegan, M. J.; Knowles, P. J. *Chemical physics letters* **1994**, *227*, 321–326.
- <sup>8</sup> Werner, H.-J.; et al.; *MOLPRO, version 2015.1, a package of ab initio programs*; 2015.
- <sup>9</sup> Bader, R. *Atoms in Molecules. A Quantum Theory*; Clarendon Press, 1994.
- <sup>10</sup> Savin, A.; Nesper, R.; Wengert, S.; F?ssler, T. F. *Angewandte Chemie International Edition in English* **1997**, *36*, 1808–1832.
- <sup>11</sup> Reed, A. E.; Curtiss, L. A.; Weinhold, F. *Chemical Reviews* **1988**, *88*, 899–926.
- <sup>12</sup> NBO (Version 6.0); 2016. <http://nbo6.chem.wisc.edu/>.
- <sup>13</sup> TopMoD; 2009. <http://www.lct.jussieu.fr/pagesperso/silvi/topmod.html>.
- <sup>14</sup> Gyórfy, W.; Shiozaki, T.; Knizia, G.; Werner, H.-J. *The Journal of Chemical Physics* **2013**, *138*, 104104.
- <sup>15</sup> El Khatib, M.; Bendazzoli, G. L.; Evangelisti, S.; Helal, W.; Leininger, T.; Tenti, L.; Angeli, C. *The Journal of Physical Chemistry A* **2014**, *118*, 6664–6673; PMID: 24866399.
- <sup>16</sup> Bondybey, V. E.; English, J. H. *The Journal of Chemical Physics* **1984**, *80*, 568–570.
- <sup>17</sup> Bondybey, V. *Chemical Physics Letters* **1984**, *109*, 436 – 441.
- <sup>18</sup> Helal, W.; Evangelisti, S.; Leininger, T.; Monari, A. *Chemical Physics Letters* **2013**, *568-569*, 49 – 54.
- <sup>19</sup> Kalemoss, A. *The Journal of Chemical Physics* **2016**, *145*, 214302.
- <sup>20</sup> Cui, Z.-h.; Yang, W.-s.; Zhao, L.; Ding, Y.-h.; Frenking, G. *Angewandte Chemie* **2016**, *128*, 7972–7977.



## B.7 ARTICLE VI

*Behavior of the Position-Spread Tensor in Diatomic Systems.*

Published in: J. Chem. Theory Comput., **2013**, 9, 5286-5295.



# Behavior of the Position–Spread Tensor in Diatomic Systems

Oriana Brea,<sup>†,‡</sup> Muammar El Khatib,<sup>†</sup> Celestino Angeli,<sup>\*,§</sup> Gian Luigi Bendazzoli,<sup>¶</sup> Stefano Evangelisti,<sup>†</sup> and Thierry Leininger<sup>†</sup>

<sup>†</sup>Laboratoire de Chimie et Physique Quantiques, Université de Toulouse et CNRS, 118, Route de Narbonne, F-31062 Toulouse Cedex, France

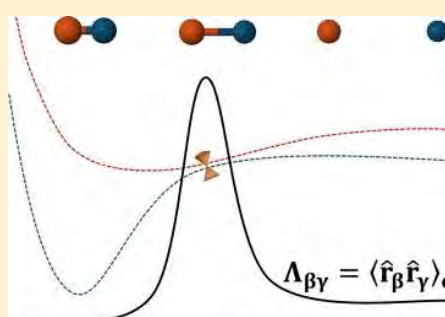
<sup>‡</sup>Departamento de Química, Facultad de Ciencias, Módulo 13, Universidad Autónoma de Madrid, Cantoblanco, 28049 Madrid, Spain

<sup>§</sup>Dipartimento di Scienze Chimiche e Farmaceutiche, Università di Ferrara, Via Borsari 46, I-44121 Ferrara, Italy

<sup>¶</sup>P.A.M. Università di Bologna, Dipartimento di Chimica Industriale “Toso Montanari”, Viale Risorgimento 4, I-40136 Bologna, Italy

## Supporting Information

**ABSTRACT:** The behavior of the Position–Spread Tensor ( $\Lambda$ ) in a series of light diatomic molecules (either neutral or negative ions) is investigated at a Full Configuration Interaction level. This tensor, which is the second moment cumulant of the total position operator, is invariant with respect to molecular translations, while its trace is also rotationally invariant. Moreover, the tensor is additive in the case of noninteracting subsystems and can be seen as an intrinsic property of a molecule. In the present work, it is shown that the longitudinal component of the tensor,  $\Lambda_{\parallel}$ , which is small for internuclear distances close to the equilibrium, tends to grow if the bond is stretched. A maximum is reached in the region of the bond breaking, then  $\Lambda_{\parallel}$  decreases and converges toward the isolated-atom value. The degenerate transversal components,  $\Lambda_{\perp}$ , on the other hand, usually have a monotonic growth toward the atomic value. The Position Spread is extremely sensitive to reorganization of the molecular wave function, and it becomes larger in the case of an increase of the electron mobility, as illustrated by the neutral-ionic avoided crossing in LiF. For these reasons, the Position Spread can be an extremely useful property that characterizes the nature of the wave function in a molecular system.



## 1. INTRODUCTION

The “Localization Tensor” (LT) is a quantity introduced in the context of the theory of Kohn<sup>1</sup> to characterize the electrical conductivity properties. Indeed, in his seminal work, Kohn realized that the most fundamental picture of electrical conductivity is more related to a properly defined delocalization of the wave function than to the simple gap closure. Subsequently, Resta and co-workers, with the introduction of the localization tensor, provided an important tool to give a quantitative formulation of this localization.<sup>2–4</sup> According to their results, one of the key properties of this quantity is the following: it diverges in the thermodynamic limit for a conductor, while remaining finite for an insulator. A remarkable sum rule connecting explicitly the electrical resistivity and the localization tensor was later given by Souza, Wilkens, and Martin<sup>5</sup> (also see ref 6). The LT has been considered as an indicator of the square of the exchange-correlation lengths in the electronic distribution, that is of the extension of the influence of one electron on the other electrons.<sup>7</sup> We have recently applied the LT formalism to the study of low-dimensional systems (linear chains, graphene nanoislands), either at ab initio<sup>8–12</sup> or tight-binding level<sup>13–16</sup> (also see ref 17). A remarkable study of the localization tensor for small molecular systems has been recently reported by Ángyán.<sup>18</sup>

The interest related to the application of the LT to molecular systems is 2-fold: first, one can study the insulator/conductor

properties as a function of the size of a homologous series with the aim to clarify the main molecular features affecting these properties. Such an approach is relevant, for instance, in the field of molecular electronics, where the focus is on the possibility to use the molecules as building blocks in the fabrication of the next generation electronic devices. More generally, the LT is an interesting quantity for the systems that are in the intermediate region between “chemistry” and “solid-state physics”—the subject of nanotechnology. A second interest for the applications of the LT to molecular systems is more strictly related to the electronic structure of the molecules. Indeed, this quantity allows to identify, besides the insulator/conductor nature, intriguing properties of the electronic distribution with a connection to the chemical description of the molecular architecture.

As said, the LT has been introduced to identify the electrical conductivity properties in solid-state physics, and, for this reason, it is a “per electron” quantity. In molecular studies, while this choice maintains its interest for the first application field described above, for its use in the analysis of the molecular wave function, the full quantity (not divided by the number of electrons) seems more appropriate. For this reason, we introduce the Total Position–Spread (TPS) tensor ( $\Lambda$ ),

Received: May 31, 2013

Published: November 5, 2013

**Table 1.** Dissociation Energies (eV) and Equilibrium Distances (bohr) for the Diatomic Molecules Considered in This Study, And Their Basis Set

molecule	basis set	This Work		Reference Data			
		$R_e$ (bohr)	$E_{\text{dis}}$ (eV)	$R_e$ (bohr)	ref	$E_{\text{dis}}$ (eV)	ref
H <sub>2</sub> <sup>+</sup>	(7s3p3d3f)	1.99	2.7896	1.99	40	2.6507	41
H <sub>2</sub>	(7s3p3d3f)	1.40	4.7279	1.40	42	4.7474	42
Li <sub>2</sub>	(7s6p4d3f)	5.10	1.0421	5.05	43	1.0260	43
N <sub>2</sub>	(3s2p)	2.15	6.9511	2.07	44	9.7797	44
F <sub>2</sub>	(3s2p)	2.96	0.8209	2.67	45	1.6261	45
LiF 1 <sup>1</sup> Σ	(3s2p/3s2p)	3.10	5.2604	2.96	46	5.9625	46
He <sub>2</sub>	(7s4p3d)	5.65	0.0008	5.61	47	0.0009	47
HeH <sup>+</sup>	(7s4p3d/6s4p3d)	11.50	0.0001	11.50	48	0.0004	37
Be <sub>2</sub>	(7s7p4d3f)	4.75	0.0906	4.63	49	0.0979	49
BeH <sup>+</sup>	(7s7p4d3f/6s4p3d)	2.75	1.9730	2.67	50	2.2000	50

which is defined as the second moment cumulant of the total electron position operator. In this work, the behavior of  $\Lambda$  for a series of diatomic molecules and ions has been investigated, as a function of the internuclear distance  $R$ . The results of the present study can be summarized as follows. Let us first consider the longitudinal component of the tensor,  $\Lambda_{\parallel}$ , the one in the direction of the internuclear axis,  $z$ . As a general trend, one observes that, close to the equilibrium distance,  $\Lambda_{\parallel}(R)$  is a growing function of  $R$ .  $\Lambda_{\parallel}(R)$  generally reaches a maximum in the region where the bond is broken, and then it becomes a decreasing function of  $R$ . For very large values of  $R$ ,  $\Lambda_{\parallel}(R)$  becomes a constant, given by the sum of the atomic values. The peak in the region of the bond breaking is often very pronounced. The two perpendicular components, denoted from now on as  $\Lambda_{\perp}(R)$  ( $\Lambda_{xx}(R)$  and  $\Lambda_{yy}(R)$ ), are obviously degenerate for symmetry reasons in isolated diatomic molecules. Their behavior generally is less spectacular than the parallel one, and their values are often growing monotonically to the asymptotic limit in a smooth way.

The remaining of the paper is organized as follows: in Section 2, the definition of the TPS tensor is shortly recalled, the computational details are described in Section 3, the numerical values of the TPS tensor are reported and discussed in Section 4, and Section 5 contains some final considerations.

## 2. THE TOTAL POSITION–SPREAD TENSOR

The TPS tensor, indicated by  $\Lambda$ , is defined as the second moment cumulant of the total electron position operator. As detailed in ref 11, one considers the position operator and its tensorial square:

$$\hat{r}_{\beta} = \sum_{p=1}^n \hat{\beta}(p) \quad (1)$$

$$\hat{r}_{\beta}\hat{r}_{\gamma} = \sum_{p,q=1}^n \hat{\beta}(p)\hat{\gamma}(q) \quad (2)$$

where the sums run over the electrons ( $n$  is the total number of electrons) and  $\beta$  and  $\gamma$  represent one of the Cartesian coordinates ( $x$ ,  $y$ , and  $z$ ).

The cumulant of the quadratic fluctuation of the position is

$$\langle \hat{r}_{\beta}\hat{r}_{\gamma} \rangle_c = \langle \Psi | \hat{r}_{\beta}\hat{r}_{\gamma} | \Psi \rangle - \langle \Psi | \hat{r}_{\beta} | \Psi \rangle \langle \Psi | \hat{r}_{\gamma} | \Psi \rangle \quad (3)$$

Finally, the localization tensor is defined as

$$\lambda_{\beta\gamma}^2 = \frac{\langle \hat{r}_{\beta}\hat{r}_{\gamma} \rangle_c}{n} \quad (4)$$

The expression “localization tensor” is somehow misleading, as already pointed out by Ángyán,<sup>19</sup> since very mobile electrons are associated with large values of the tensor. Moreover, as stated in the Introduction, in a molecular context, we believe that the more interesting quantity is not the *per electron* spread, but rather the global value. We stress this fact by denoting Total Position Spread this quantity, with components  $\Lambda_{\beta\gamma} = \langle \hat{r}_{\beta}\hat{r}_{\gamma} \rangle_c$ . The reason for the interest in the global quantity is because only the TPS shows a size consistency property: the TPS of noninteracting fragments is given by the sum of the TPS of the individual fragments, while, obviously, the LT does not have this property. This is true for each individual component of the tensor and, of course, for the trace that becomes a rotational invariant. As a consequence, the trace of the TPS is an additive and rotationally invariant quantity associated with a molecular system.

## 3. COMPUTATIONAL DETAILS

In the present work, we investigate at Full Configuration Interaction (FCI) level the behavior of the ground-state TPS tensor for a series of diatomic systems, belonging to the first two periods of the periodic table: homonuclear diatomic molecules (H<sub>2</sub>, He<sub>2</sub>, Li<sub>2</sub>, Be<sub>2</sub>, N<sub>2</sub>, F<sub>2</sub>) and one heteroatomic molecule that shows an ionic-neutral avoided crossing (LiF). The ionic systems HeH<sup>+</sup> and BeH<sup>+</sup> were also considered. All chosen systems have closed-shell singlet ground states: <sup>1</sup>Σ<sub>g</sub><sup>+</sup> for homonuclear and <sup>1</sup>Σ<sup>+</sup> for heteroatomic systems. Open-shell systems will be the subject of forthcoming investigations.

We used the ANO basis sets optimized by Roos and co-workers,<sup>20</sup> by adopting contractions of different qualities. In particular, we employed the following contractions for the diatomic molecules that have been considered in this study: H<sub>2</sub>, 7s3p3d3f; Li<sub>2</sub>, 7s6p4d3f; He<sub>2</sub>, 7s4p3d; HeH<sup>+</sup>, 7s4p3d – 6s4p3d; Be<sub>2</sub>, 7s7p4d3f; BeH<sup>+</sup>, 7s7p4d3f – 6s4p3d; LiF, N<sub>2</sub> and F<sub>2</sub>, 3s2p. The choice of the basis set is limited by the size of the FCI space, which shows a factorial growth as a function of the number of electrons and the size of the basis set. The initial Hartree–Fock calculations were performed using the computational ab initio Quantum-Chemistry package DALTON.<sup>21,22</sup> The atomic one- and two-electron integrals then were transformed to the molecular basis set, using the Ferrara code.<sup>23</sup> Finally, the Full-CI calculations were performed using our FCI algorithm,<sup>24–26</sup> implemented in the NEPTUNUS

code<sup>27</sup> and interfaced to the previous codes using the common data formats *Q5Cost*.<sup>28–30</sup>

The 1s electrons were kept frozen at the Hartree–Fock level for all atoms but hydrogen and helium. The contribution of these frozen electrons to the TPS tensor was taken into account through a generalization of the formalism discussed in Section 2. However, its value is extremely small, and our preliminary investigations show that the effect of including (or not including) the dynamic electron correlation for these electrons has a negligible effect.

## 4. RESULTS AND DISCUSSION

In Table 1, the equilibrium distance and the dissociation energy obtained at FCI level are compared to the experimental results (when available). For all systems here considered, the ground-state potential energy curve is reported in the Supporting Information. In the case of the ions  $\text{BeH}^-$  and  $\text{HeH}^-$  (for which, to the best of our knowledge, there is no experimental data), we have compared our results with those obtained at FCI level with a larger basis set. From the values reported in Table 1, it is apparent that all results are of a reasonable quality, except for the systems involving nitrogen ( $\text{N}_2$ ) or fluorine ( $\text{F}_2$  and  $\text{LiF}$ ), for which the dissociation energy is seriously underestimated. This fact, in view of the small basis set that we were forced to use in order to treat these molecules at FCI level, is certainly not surprising. We consider now in detail the behavior of the TPS tensor for the different systems.

**4.1. Covalent and Ionic Systems.** Here, we examine the behavior of systems having strong covalent or ionic bonds. The considered systems are the covalent species  $\text{H}_2$ ,  $\text{Li}_2$ ,  $\text{N}_2$ , and  $\text{F}_2$ , and the strongly ionic molecule  $\text{LiF}$ .

In the case of a singlet covalent bond, the equilibrium wave function is known to be a mixture of neutral and ionic forms. The nature of the ground state of the prototype of all molecules showing covalent bonds, the  $\text{H}_2$  molecule, has been analyzed in detail in terms of Orthogonal Valence Bond (OVB) structures in ref 31, and the influence of the relative weight of the ionic and neutral structures in the ground state wave function on the LT has been described in ref 11. In summary, starting from the equilibrium geometry, the weight of the ionic forms slightly decreases by increasing the interatomic distance. However, for these structures, the value of  $\Lambda_{\parallel}$  quickly grows with  $R$ . As a result, the value of  $\Lambda_{\parallel}$  computed for the full ground-state wave function increases as a function of  $R$ . This picture is valid in the region of the bond. When the bond is broken, however, we have a dramatic change in the nature of the wave function, and the weight of the ionic forms quickly goes to zero as  $R$  is increased. The contribution of these forms becomes negligible, and the value of  $\Lambda_{\parallel}$  goes quickly to the asymptotic atomic limit.

For the simple case of  $\text{H}_2$  in the minimal basis set, the longitudinal component of the TPS computed for the approximate UHF wave function shows an interesting behavior and allows one to discuss the dependence of  $\Lambda_{\parallel}$  on  $R$  from a slightly different point of view. Indeed, for  $R$  smaller than the Coulson–Fischer point (computed to be at 2.287 bohr in the 1s basis), the UHF wave function coincides with the RHF wave function; therefore, it is a superposition of the neutral and ionic OVB forms with equal weight. In this case,  $\Lambda_{\parallel}$  is a growing function of  $R$  (scaling as  $R^2$ ). On the other hand, for  $R$  larger than the Coulson–Fischer point, the UHF wave function becomes the broken-symmetry, spin-contaminated, solution for which  $\Lambda_{\parallel}$  slowly approaches the value of the neutral OVB structure (it converges to this value for  $R \rightarrow \infty$ ). Therefore,

starting from  $R_c$  and increasing  $R$ ,  $\Lambda_{\parallel}$  shows a marked increase up to  $R \approx 2.3$  bohr and then a decrease to the sum of the atomic values. This behavior has been confirmed computing  $\Lambda_{\parallel}$  as a function of  $R$  for the UHF wave function with the STO12G basis set used in ref 11 (see the Supporting Information). Obviously, the UHF wave function is only a rough approximation to the FCI wave function and the maximum of  $\Lambda_{\parallel}$  observed in the minimal basis set at the FCI level is at a slightly different value of  $R$  ( $R = 2.76$  bohr, see ref 11), but the simple picture offered by the UHF description allows to identify the main features of  $\Lambda_{\parallel}$ .

This scheme can be rationalized and fully understood by other simple qualitative considerations (see the Appendix). In fact, as can be easily shown, even at the Hückel level, two electrons in two localized orbitals coupled to form a singlet wave function give a vanishing value for  $\Lambda_{\parallel}$ . The same result is also obtained if the two electrons occupy the same localized orbital. In contrast, when the wave function is a combination of the two ionic forms obtained by placing the two electrons in one of the two local orbitals, the value of  $\Lambda_{\parallel}$  is nonzero. Moreover, for a fixed mixing between the two localized ionic forms, the TPS grows as the square of the distance between the two centers.

Let us consider now the case of an “ionic” bond, again by using this simple approach. In such a case, one generally has a mixture between an ionic and a neutral structure, their relative weight being a function of the interatomic distance. Usually, at the equilibrium distance, the ionic structure dominates in the ground state wave function, while at dissociation, it is the neutral structure that describes the ground state (no diatomic molecule dissociates to a pair of ionic atoms). Therefore, there is a distance where the two states undergo an avoided crossing and, in the crossing region, the wave function is a mixture of ionic and neutral forms.

Of course, things become more complicated at the ab initio level, since, in this case, the atomic contributions also must be taken into account (these terms are neglected in the simple approach described above). However, these intra-atomic contributions tend to be significantly smaller than the interatomic ones, so the general picture obtained at Hückel level is still valid when the complete Hamiltonian is considered.

These considerations are confirmed by the calculations reported in the present work. For all covalent systems, a similar behavior is observed and hereafter briefly described. The perpendicular value,  $\Lambda_{\perp}$ , is usually smaller for the molecule at the equilibrium geometry than for the dissociated atoms. This behavior is due to the increased nuclear effective charge experienced by the electrons at short internuclear distances (two nuclei instead of only one), which leads to a spatial contraction of the orbitals in the directions orthogonal to the internuclear axis. This, in turn, induces a reduction of the  $\perp$  component of the TPS tensor. The parallel component,  $\Lambda_{\parallel}$ , starts at small values of  $R$  from a value smaller than the asymptotic limit (for the same reason reported for  $\Lambda_{\perp}$ ) and shows a quick growth by increasing  $R$ . Close to the equilibrium distance, the value becomes close to the asymptotic limit but it keeps growing. At a distance close to the bond-breaking distance,  $\Lambda_{\parallel}$  has a maximum and then it falls down to the isolated-atom limit. One can assume, in a rather conventional way, the bond-breaking distance to be the distance at which the energy slope has a maximum, or, equivalently, where the second derivative of the energy, with respect to the internuclear distance, becomes zero. From Table 2 it is apparent that the



**Table 2. Bond-Breaking Distance (Bohr) Computed as the Distance at Which the Second Derivative of the Energy, with Respect to the Internuclear Distance, Vanishes**

molecule	R
H <sub>2</sub>	2.14
Li <sub>2</sub>	6.90
N <sub>2</sub>	2.68
F <sub>2</sub>	3.46
LiF	4.27
He <sub>2</sub>	6.36
HeH <sup>-</sup>	13.58
Be <sub>2</sub>	5.21
BeH <sup>-</sup>	3.49

position of the TPS maximum is often close to the bond-breaking distance, although it is generally slightly larger. The system where there is a charge transfer from one atom to the other one as a function of the distance (LiF, BeH<sup>-</sup>) does not follow this pattern, since, in this case, the TPS maximum occurs at the distance of the charge jump.

This picture explains the behavior of  $\Lambda$  in the case of covalent bonds, such as H<sub>2</sub>, Li<sub>2</sub>, and N<sub>2</sub>, and it is illustrated in Figures 1–3. The F<sub>2</sub> molecule (see Figure 4) differs from the

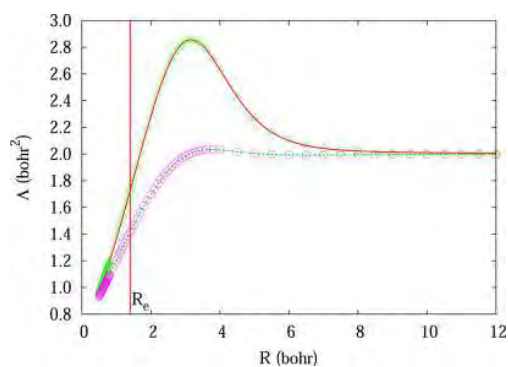


**Figure 1.** Total Position Spread computed for the  $^1\Sigma_g^+$  ground state of the hydrogen dimer at Full CI (FCI) level of theory:  $\Lambda_{\parallel}$ , which is denoted by the red solid line and triangles, and  $\Lambda_{\perp}$ , which is denoted by the green dashed line and circles. The equilibrium geometry is indicated by a vertical line.

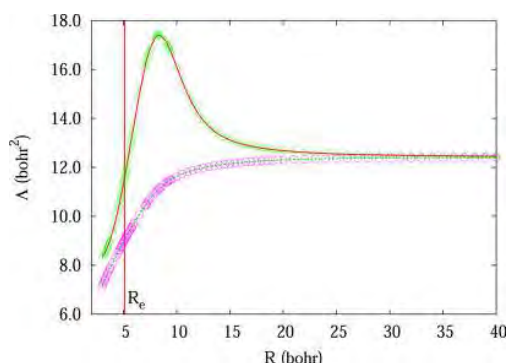


**Figure 2.** Total Position Spread computed for the  $^1\Sigma_g^+$  ground state of the lithium dimer at Full CI (FCI) level of theory:  $\Lambda_{\parallel}$ , which is denoted by the red solid line and triangles, and  $\Lambda_{\perp}$ , which is denoted by the green dashed line and circles. The equilibrium geometry is indicated with a vertical line.

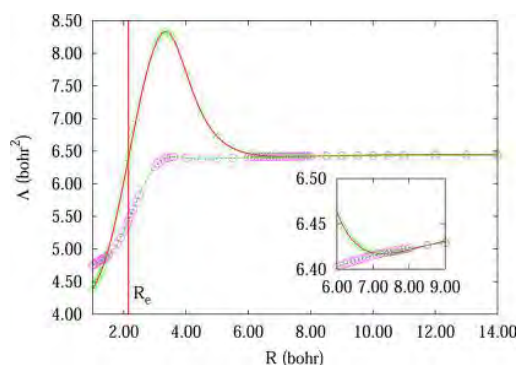


**Figure 3.** Total Position Spread computed for the  $^1\Sigma_g^+$  ground state of the nitrogen dimer at Full CI (FCI) level of theory:  $\Lambda_{\parallel}$ , which is denoted by the red solid line and triangles, and  $\Lambda_{\perp}$ , which is denoted by the green dashed line and circles. In the inset zoom, the local minimum of  $\Lambda$  is reported. The equilibrium geometry is indicated with a vertical line.

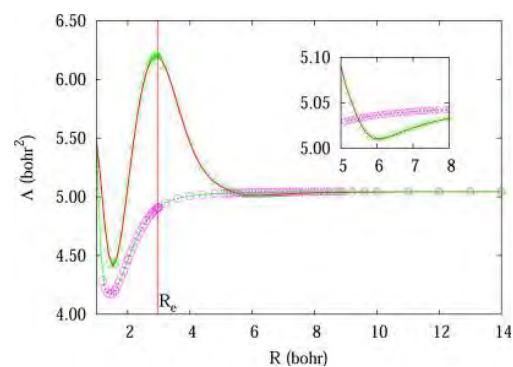


**Figure 4.** Total Position Spread computed for the  $^1\Sigma_g^+$  ground state of the fluorine dimer at Full CI (FCI) level of theory:  $\Lambda_{\parallel}$ , which is denoted by the red solid line and triangles, and  $\Lambda_{\perp}$ , which is denoted by the green dashed line and circles. In the inset zoom, the local minimum of  $\Lambda$  is reported. The equilibrium geometry is indicated with a vertical line.

above scenario, since the maximum is reached for values of  $R$  that are very close to the equilibrium distance. This result is a manifestation of the peculiar nature of the bond in this molecule, as it has been pointed out in valence bond and electron localization function studies,<sup>32,33</sup> where it has been shown that the fluctuation of the electron pair density play an important role for the bond formation, so that it has been termed *charge-shift bonds*. Moreover, after its maximum value,  $\Lambda_{\parallel}$  has a very shallow minimum before reaching its asymptotic value from below. Actually, a similar behavior is also seen in the nitrogen dimer, although the depth of the minimum, in this case, is much smaller.

In order to identify the origin of the appearance of this minimum in F<sub>2</sub> and N<sub>2</sub>, we have reconsidered the analytical OVB approach applied to H<sub>2</sub> with the minimal 1s basis set, which has been fully developed in refs 11 and 31. In order to simulate different bond situations, the off-diagonal element of the Hamiltonian matrix between the neutral and the ionic  $\Sigma_g$  components (eq 20 in ref 31) has been scaled by a factor  $k$ . For  $k < 1$ , after the diagonalization of the  $2 \times 2$  Hamiltonian matrix, the weight of the ionic OVB structure in the ground state is lower than for  $k = 1$  (corresponding to the exact treatment of H<sub>2</sub>) for all geometries. This effect is particularly intense in the

region between the equilibrium geometry and the bond-breaking geometry, where the smaller  $k$  is, the quicker the decrease of the weight of the ionic structures with  $R$ . Such a modification has a marked effect on the qualitative dependence of  $\Lambda_{\parallel}$  on  $R$ , as it is apparent from Figure 5, where  $\Lambda_{\parallel}$  is

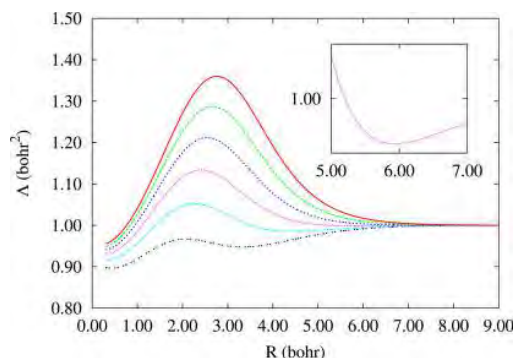


**Figure 5.** Longitudinal Total Position Spread component,  $\Lambda_{\parallel}$ , computed for the  $^1\Sigma_g^+$  ground state of the hydrogen dimer at the minimal basis OVB level of theory with a scaling by a factor  $k$  of the off-diagonal element of the Hamiltonian matrix between the neutral and the ionic  $\Sigma_g$  OVB components.  $k = 1$  for the top curve (red solid line), while  $k = 0.5$  for the bottom curve (black dashed line). The other curves are reported for intermediate values of  $k$  with steps of 0.1. In the inset enlargement, the local minimum of  $\Lambda_{\parallel}$  is reported for the  $k = 0.7$  case (pink dashed curve).

reported as a function of  $R$  for  $k = 0.5, 0.6, 0.7, 0.8, 0.9, 1.0$ . One notes that the maximum observed for  $k = 1$  is lowered and shifted at smaller  $R$  when  $k$  is reduced. Moreover, a minimum appears at long  $R$  values for  $k = 0.5, 0.6, 0.7$  (the inset of Figure 5 reports a zoom in the minimum region for  $k = 0.7$ ).

These results suggest that the minimum observed for  $N_2$  and  $F_2$  (see Figures 3 and 4) can be due to a lower weight of the ionic OVB component in the ground state of these molecules, with respect to the other dimers considered here. The same argument could also explain the fact that the maximum of  $\Lambda_{\parallel}$  in  $F_2$  is at  $R$  close to the equilibrium internuclear distance.

The ionic system LiF has a particularly interesting behavior. The nature of the two relevant states in this system, as in all molecules of the type MX, where M is an alkali metal and X is a halogen, can be understood in terms of two diabatic states: one dissociating to the neutral  $M + X$  atomic limit, and the other one to the ionic  $M^+ + X^-$  limit (which is, for all diatomic molecules, always higher in energy than the  $M + X$  asymptote). For a complete discussion, the reader is referred to ref 34. Similarly to what is observed for  $H_2$ ,<sup>35</sup> the neutral state is dissociative (no bond). In contrast, the ionic diabatic state is strongly bound, due to the strong Coulombic interaction. At short internuclear distances, the ionic diabatic state is lower in energy than the neutral one, and as a result of the low value of the ionization potential of M and of the large value of the electron affinity of X, which makes the energy of the  $M^+ + X^-$  atomic limit not too high in energy, with respect to the  $M + X$  one. Therefore, the two diabatic energies become equal at a distance larger than the equilibrium geometry, in the case of LiF for a value of  $R$  of  $\sim 11.10$  bohr, and the system shows an avoided crossing between the two states (see Figure 6). This behavior has been discussed in detail in a paper by Bauschlicher and Langhoff.<sup>36</sup> The two diabatic states are described, at a first approximation, by an ionic determinant (the ionic state), and a

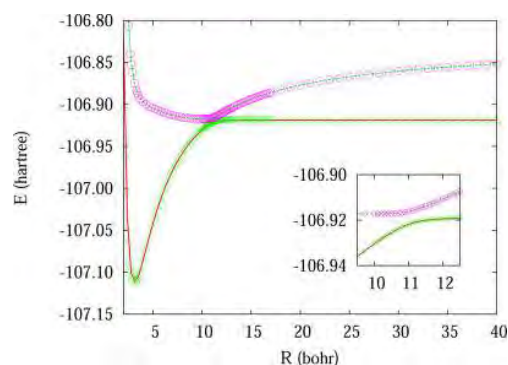


**Figure 6.** Potential energy curve of LiF for the  $^1\Sigma^+$  ground state (red solid line and triangles) and first excited state (green dashed line and circles) at Full CI (FCI) level of theory. In the enlargement shown as an inset, the avoiding crossing region is reported.

singlet combination of purely neutral determinants. The dependence of  $\Lambda_{\perp}$  on  $R$  is reported in Figure 7 for the two

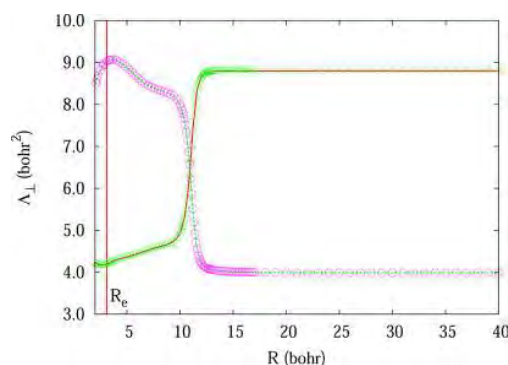


**Figure 7.** Total Position Spread ( $\Lambda_{\perp}$  component), computed for the  $^1\Sigma^+$  ground state (red solid line and triangles) and first excited state (green dashed line and circles) of the lithium fluoride (LiF) molecule at Full CI (FCI) level of theory.

states. One notes that, as intuitively expected,  $\Lambda_{\perp}$  changes suddenly passing the crossing region (for the ground state from the “ionic value” before the crossing, to the “neutral value” after the crossing and vice versa for the excited state). In contrast, the behavior of  $\Lambda_{\parallel}$  (reported in Figure 8) is more complex. As

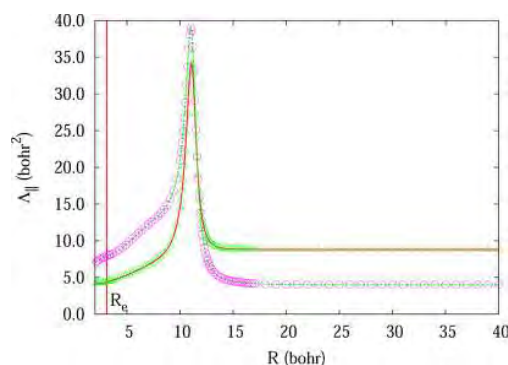


**Figure 8.** Total Position Spread ( $\Lambda_{\parallel}$  component), computed for the  $^1\Sigma^+$  ground state (red solid line and triangles) and first excited state (green dashed line and circles) of the lithium fluoride (LiF) molecule at Full CI level of theory.

described in the Appendix, the ionic and neutral wave functions, taken separately, have a strictly zero longitudinal TPS at the Hückel level. When they are combined, however, their TPS is equal to the product of the squares of the coefficients. From Figure 8, in fact, one sees that the TPS of the two states remains close to the asymptotic values for all  $R$  values except in the avoided-cross region. Close to the cross region, near to 11 bohr with the employed basis set, the Hückel value is expected to have a maximum of  $R^2/4$ , which amounts to  $\sim 30$  bohr<sup>2</sup>. This is in very good agreement with the increase of the TPSs in this region, that is comprised between 25 and 35 bohr<sup>2</sup> for the ground state and the excited state, respectively.

#### 4.2. Molecular Anions and Weakly Bonded Systems.

We will examine now the behavior of systems whose bonds are weak or very weak: the neutral dimers of helium and beryllium ( $\text{He}_2$  and  $\text{Be}_2$ ), and the anions that these atoms form by combination with the hydrogen anion ( $\text{HeH}^-$  and  $\text{BeH}^-$ ).

Among these species,  $\text{Be}_2$  has a TPS that is very much alike that those of the previously considered covalent dimers (see Figure 9). This confirms the fact that, although very weak, the bond in this molecule has essentially a covalent nature.

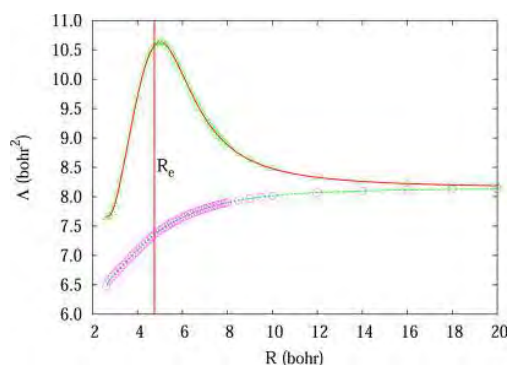


**Figure 9.** Total Position Spread ( $\Lambda_{\parallel}$ , red solid line and triangles;  $\Lambda_{\perp}$ , green dashed line and circles), computed for the  $^1\Sigma_g^+$  ground state of  $\text{Be}_2$  at Full CI (FCI) level of theory. The equilibrium geometry is indicated with a vertical line.

The helium dimer, on the other hand, has a marked TPS peak at very short interatomic distance (see Figure 10). This can be explained by the fact that its value, in the united-atom limit, must converge to that of the beryllium atom. This is

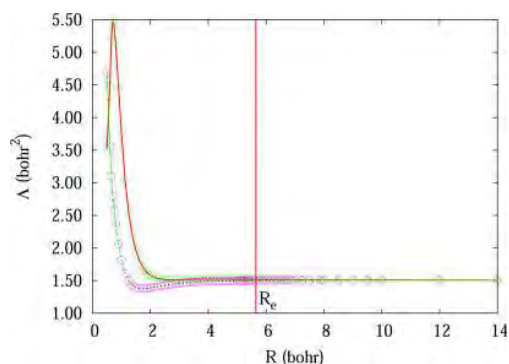


**Figure 10.** Total Position Spread ( $\Lambda_{\parallel}$ , red solid line and triangles;  $\Lambda_{\perp}$ , green dashed line and circles), computed for the  $^1\Sigma_g^+$  ground state of the helium dimer at Full CI (FCI) level of theory. The equilibrium geometry is indicated with a vertical line.

indeed the case, since the short-distance value of the  $\text{He}_2$  system oscillates between 4 and 5.5 bohr<sup>2</sup>, while the corresponding value for a beryllium atom is  $\sim 5$  bohr<sup>2</sup>. The oscillations shown by the helium-dimer values (the longitudinal component in a particular way) at very short distance are most likely due to changes in the configuration structure of the wave function. In view of the fact that our basis set is certainly not suitable for a short distance description of the system (because of the lack of very concentrated atomic orbitals (AOs)), we did not carry this analysis at a deeper level.

As far as the two ions are concerned, their behavior is rather different from those of the neutral systems. In the case of  $\text{HeH}^-$  system, we have an extremely weakly bonded system. The interactions are of the charge-induced dipole type, and the minimum well is only a few  $\text{cm}^{-1}$  deep.<sup>37</sup> The TPS values become very high at short internuclear distances, where they converge to the united-atom limit (see Figure 11). More

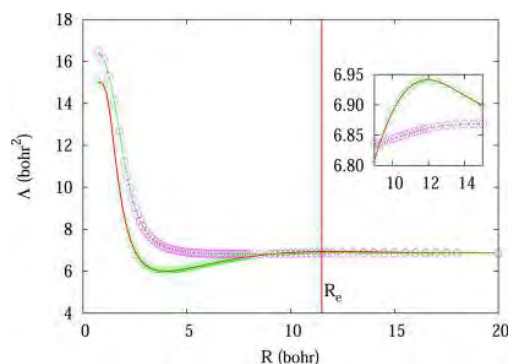


**Figure 11.** Total Position Spread ( $\Lambda_{\parallel}$ , red solid line and triangles;  $\Lambda_{\perp}$ , green dashed line and circles), computed for the  $^1\Sigma^+$  ground state of  $\text{HeH}^-$  at Full CI (FCI) level of theory. In the enlargement shown as an inset, the local maximum of the Total Position Spread  $\Lambda$  is reported. The equilibrium geometry is indicated with a vertical line.

interestingly, there is a maximum of  $\Lambda_{\parallel}$  in the region of the energy minimum, whose depth is much more pronounced than the energy variation. Once again, it is clear that the TPS tensor is very sensitive to variation in the wave function structure that has only a tiny effect on the system energy.  $\text{BeH}^-$  is a hypothetical system having a covalent nature at short distance.<sup>38</sup> The  $\Lambda_{\parallel}$  component (see Figure 12) has a pronounced maximum in the region where the wave function changes its nature, while the  $\Lambda_{\perp}$  component has a minimum in the same region. At the equilibrium distance, both components have values similar to the asymptotic ones, and they become very large for shorter distances.

**4.3. The Long-Distance Behavior of the TPS Tensor.** As discussed in Section 2, the TPS tensor is a quantity that is additive for noninteracting systems. The trace of the TPS tensor is invariant under rotations of the coordinate axes, and therefore it is a scalar quantity characterizing the system as a whole. Because of the symmetry of the systems here considered, the component along the internuclear axis,  $\Lambda_{\parallel}$ , and the two degenerate components orthogonal to this axis,  $\Lambda_{\perp}$ , are additive quantities in the case of noninteracting systems. For this reason, in Table 3, we compared the value of  $\Lambda_{\parallel}$  computed at an internuclear distance of 50 bohr (40 bohr for LiF, as discussed later) with the sum of the atomic values. It should be noticed that in the case of the F atom, a symmetry-broken solution must be considered, in order to have a

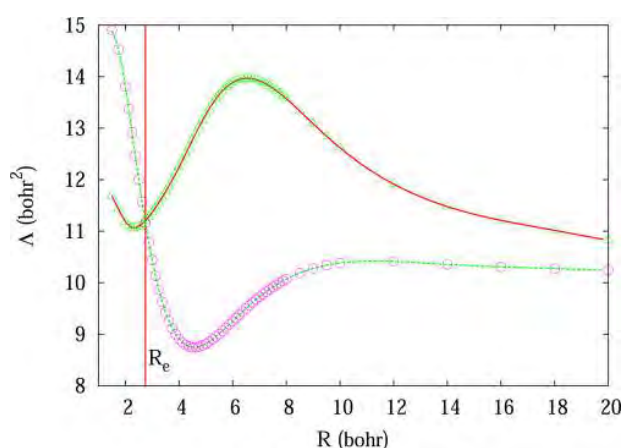


**Figure 12.** Total Position Spread ( $\Lambda_{\parallel}$ , red solid line and triangles;  $\Lambda_{\perp}$ , green dashed line and circles), computed for the  $1\Sigma^+$  ground state of  $\text{BeH}^-$  at Full CI (FCI) level of theory. The equilibrium geometry is indicated with a vertical line.

**Table 3. Total Position Spread ( $\text{bohr}^2$ ) Values for the Diatomic Molecules Close to the Dissociation Limit (50 bohr) Except for LiF (40 bohr), Compared to the Sum of Their Corresponding Values for the Isolated Atoms**

molecule	Value at Dissociation (50 bohr)		Isolated Atoms (Sum of the Atomic Values)	
	$\Lambda_{\parallel}$	$\Lambda_{\perp}$	$\Lambda_{\parallel}$	$\Lambda_{\perp}$
$\text{H}_2$	2.000742	2.000639	2.000668	2.000668
$\text{Li}_2$	12.439117	12.415638	12.423086	12.423086
$\text{N}_2$	6.441467	6.441315	6.440920	6.440920
$\text{F}_2$	5.050114	5.040229	5.050058	5.040210
$\text{LiF} (1^1\Sigma)$	8.805411	8.799939	8.804686	8.799762
$\text{LiF} (2^1\Sigma)$	3.986952	3.985769	3.986199	3.986199
$\text{He}_2$	1.506416	1.506392	1.506400	1.506400
$\text{HeH}^-$	6.870093	6.869880	6.869950	6.869950
$\text{Be}_2$	8.152292	8.148845	8.149992	8.149992
$\text{BeH}^-$	10.193261	10.191089	10.191746	10.191746

situation that is comparable with the  $D_{\infty h}$  and  $C_{\infty v}$  values of the  $\text{F}_2$  and  $\text{LiF}$  molecules, respectively. As an example, one can see in Table 3 that the molecular values of  $\Lambda_{\parallel}$  for  $\text{F}_2$  at a distance of 50 bohr is 5.050114  $\text{bohr}^2$ , while the sum of the atomic values is 5.050058  $\text{bohr}^2$  with an absolute percent difference of  $5.6 \times 10^{-3}\%$ . It is worth noticing that the energies have a much faster convergence to their asymptotic values, since, at a distance of 50 bohr, the percent difference for the energy is  $7.5 \times 10^{-6}\%$  for  $\text{F}_2$ , compared with the sum of the isolated atoms.

For the sake of comparison, we also reported the values of  $\Lambda$  for the isolated atoms in Table 4. All the values are isotropic, with the exception of fluorine, whose  $\Lambda_{\parallel}$  component (one electron in the  $2p_z$  orbital) is slightly larger than the  $\Lambda_{\perp}$  component (two electrons in the  $2p_x$  and  $2p_y$  orbitals). This tiny difference is probably due to a compensation between the size of the orbitals and their occupation numbers. We also notice the very large values for Li and, even larger,  $\text{H}^-$ , and the relatively small increase in  $\Lambda$  in going from F to  $\text{F}^-$ .

We have already discussed the ionic-covalent avoided crossing of  $\text{LiF}$ , that occurs at  $\sim 11$  bohr. At much larger distances, the  $\text{LiF}$  ionic energy curve undergoes further, and much more complex, avoided crossings. This is because, at a very large distance ( $\sim 43$  bohr with the present basis set), the

**Table 4. Isolated-Atom Values of the Total Position Spread ( $\text{bohr}^2$ )<sup>a</sup>**

atom	$\Lambda$
H	1.000334
$\text{H}^-$	6.116750
He	0.753200
$\text{Li}(7s6p4d3f)$	6.211543
$\text{Li}(3s2p)$	6.279657
$\text{Li}^+(3s2p)$	0.297617
Be	4.074996
N	3.220460
$\text{F}(\Lambda_{\parallel})$	2.525029
$\text{F}(\Lambda_{\perp})$	2.520105
$\text{F}^-$	3.688582

<sup>a</sup>All values are isotropic with the exception of F, for which the  $\Lambda_{\parallel}$  (in the z direction) is different from  $\Lambda_{\perp}$  (x and y directions).

energy of the ionic  $\text{Li}(1s^2)^+ + \text{F}(1s^2 2s^2 2p^6)^-$  pair becomes degenerate with the neutral pair  $\text{Li}(1s^2 2p^1) + \text{F}(1s^2 2s^2 2p^5)$ . The latter gives rise to three highly degenerate singlet states (two of which are exactly degenerate) having a  $1^1\Sigma^+$  symmetry. These states are obtained by singlet combinations of pairs of determinants having the singly occupied  $2p$  orbitals in Li and F of the same type, either x, or y, or z. Therefore, the ionic state undergoes avoided crossings with a bunch of three neutral states, and the behavior of the TPS tensor becomes complicated in the regions of the crossings. Since the study of these crossings is well beyond the scope of the present paper, we are not going to discuss further this aspect. For this reason, the  $2^1\Sigma^+$  values reported in Table 3 in the case of  $\text{LiF}$  were computed at a distance of 40 bohr rather than 50 bohr, where the state having a ionic character is no longer the second  $1^1\Sigma^+$  state.

## 5. CONCLUSIONS

The results presented in this work confirm the fact that the TPS tensor is a powerful indicator of the electronic rearrangements in a molecular wave function. Indeed, when a bond is stretched from its equilibrium distance, the longitudinal component of the TPS tensor increases rapidly. The extension of the mutual influence of the electrons keeps increasing, until the bond is broken and then there is a sudden drop-off to the sum of the values found for the two noninteracting atoms. One can therefore conclude that, in the region where the bond is in formation (for  $R$  between  $R_e$  and the distance where the bond is broken), it is characterized by a relatively large extension of the mutual influence of the electrons, while outside this region such influence is more “short range”. This is true for diatomic systems, but preliminary results show its usefulness also for more-complex molecular architectures.

Besides the description of the nature of the chemical bond, another interesting possibility concerns the application of this technique to the study of mixed-valence systems. In this case, the TPS tensor is able to describe the delocalized nature of the mobile electrons (or holes) during the transfer process. Together with the mean value of the position operator, this gives an interesting description of the transfer mechanism.

With the aim to apply the strategy here reported to larger systems, we are currently working on the implementation of the algorithm in the MOLPRO code,<sup>39</sup> in particular for the case of CAS-SCF wave functions. This will open a wider possibility of application, since the number of systems that can be treated at

Full CI (FCI) level is rather limited (however, one should stress the fact that rather large CAS-SCF spaces can be treated by using a FCI formalism, if the orbitals are preliminary computed by a general code, and the inactive orbitals are frozen).

## APPENDIX

In this Appendix, the analytic expression of the TPS tensor is discussed for the case of a two-electron two-center system having point-like orbitals. This simple model is useful in order to understand the behavior of the TPS in the diatomic molecules considered in this article. Let us consider two centers, A and B, placed at a distance  $R$ , with  $\chi_A$  and  $\chi_B$  indicating the two point-like orbitals located in the centers A and B, respectively.

The total position operator,  $\hat{Z}$  ( $z$  being the internuclear axis), is given by

$$\hat{Z} = \hat{z}(1) + \hat{z}(2) \quad (5)$$

where indexes 1 and 2 label electron coordinates. This gives, for its square, the expression

$$\begin{aligned} \hat{Z}^2 &= [\hat{z}(1) + \hat{z}(2)]^2 \\ &= \hat{z}(1)^2 + \hat{z}(2)^2 + \hat{z}(1)\hat{z}(2) + \hat{z}(2)\hat{z}(1) \end{aligned} \quad (6)$$

The first two terms in the last sum correspond to the one-electron part of the operator,  $\hat{Z}_m^2$ , while the last two terms constitute the two-electron part of the operator,  $\hat{Z}_b^2$ :

$$\hat{Z}_m^2 = \hat{z}(1)^2 + \hat{z}(2)^2 \quad (7)$$

and

$$\hat{Z}_b^2 = \hat{z}(1)\hat{z}(2) + \hat{z}(2)\hat{z}(1) \quad (8)$$

The TPS tensor is given by the expression

$$\Lambda_{zz} = \langle \hat{Z}^2 \rangle - \langle \hat{Z} \rangle^2 = \langle \hat{Z}_m^2 \rangle + \langle \hat{Z}_b^2 \rangle - \langle \hat{Z} \rangle^2 \quad (9)$$

Notice that  $\Lambda$  is invariant with respect to a translation of the coordinate origin, although the different terms separately are not. This fact can be used to simplify the calculation of the tensor. For instance, if the system has a center of symmetry, the mean value  $\langle \hat{Z} \rangle$  will be zero if the coordinate origin is chosen to be in the center of symmetry of the system.

We consider first the  $H_2^+$  ion, for which the two relevant wave functions are (only the spatial part is reported):

$$|^2\Psi_g\rangle = \frac{\chi_A(1) + \chi_B(1)}{\sqrt{2}} \quad (\text{doublet } g) \quad (10)$$

and

$$|^2\Psi_u\rangle = \frac{\chi_A(1) - \chi_B(1)}{\sqrt{2}} \quad (\text{doublet } u) \quad (11)$$

In order to compute the cumulant  $\Lambda_{zz}$ , it is convenient to place the origin of the coordinates in the midpoint between A and B: in this way, the mean value of  $\hat{Z}$  vanishes, and the only contribution comes from the mean value of  $\hat{Z}^2$ . Only the one-electron term contributes, and we obtain

$$\begin{aligned} \langle ^2\Psi_g | \hat{Z}_m^2 | ^2\Psi_g \rangle &= \langle ^2\Psi_u | \hat{Z}_m^2 | ^2\Psi_u \rangle \\ &= \frac{R^2}{4} \end{aligned} \quad (12)$$

We switch now to the neutral hydrogen molecule. Let us consider first the two neutral forms (a singlet and a triplet),  $|^1\Psi_g\rangle$  and  $|^3\Psi_u\rangle$ , given by (again, only the spatial part is reported)

$$|^1\Psi_g\rangle = \frac{\chi_A(1)\chi_B(2) + \chi_B(1)\chi_A(2)}{\sqrt{2}} \quad (\text{singlet } g) \quad (13)$$

and

$$|^3\Psi_u\rangle = \frac{\chi_A(1)\chi_B(2) - \chi_B(1)\chi_A(2)}{\sqrt{2}} \quad (\text{triplet } u) \quad (14)$$

We have

$$\langle ^1\Psi_g | \hat{Z}_m^2 | ^1\Psi_g \rangle = \langle ^3\Psi_u | \hat{Z}_m^2 | ^3\Psi_u \rangle = \frac{R^2}{2} \quad (15)$$

while

$$\langle ^1\Psi_g | \hat{Z}_b^2 | ^1\Psi_g \rangle = \langle ^3\Psi_u | \hat{Z}_b^2 | ^3\Psi_u \rangle = -\frac{R^2}{2} \quad (16)$$

In both cases, the one-electron contribution is  $R^2/2$ , while the two-electron one is  $-R^2/2$ . This means that, for the two neutral states, the total value of  $\Lambda$  is equal to zero:

$$\langle ^1\Psi_g | \hat{Z}^2 | ^1\Psi_g \rangle = \langle ^3\Psi_u | \hat{Z}^2 | ^3\Psi_u \rangle = 0 \quad (17)$$

Let us consider now an ionic determinant. We can take, for instance, the determinant  $|^1\Psi_A\rangle$ , in which both electrons are located on the center A:

$$|^1\Psi_A\rangle = \chi_A(1)\chi_A(2) \quad (\text{singlet}) \quad (18)$$

In such a case, it is convenient to place the origin of the coordinates in A: the mean value of both  $\hat{Z}$  and  $\hat{Z}^2$  is zero and, again,  $\Lambda_{zz}$  vanishes.

If, however, a combination of two ionic determinants is considered, the situation is completely different. Let us take, for instance, the out-of-phase combination of the ionic distributions

$$|^1\Psi_A\rangle = \frac{\chi_A(1)\chi_A(2) - \chi_B(1)\chi_B(2)}{\sqrt{2}} \quad (\text{singlet } u) \quad (19)$$

By placing the coordinate origin in the midpoint between A and B, again the mean value of  $\hat{Z}$  will vanish by symmetry. The two contributions to  $\hat{Z}^2$  are

$$\langle ^1\Psi_u | \hat{Z}_m^2 | ^1\Psi_u \rangle = \left(-\frac{R}{2}\right)^2 + \left(\frac{R}{2}\right)^2 = \frac{R^2}{2} \quad (20)$$

while

$$\langle ^1\Psi_u | \hat{Z}_b^2 | ^1\Psi_u \rangle = \left(-\frac{R}{2}\right)^2 + \left(\frac{R}{2}\right)^2 = \frac{R^2}{2} \quad (21)$$

and, therefore,

$$\langle ^1\Psi_u | \hat{Z}^2 | ^1\Psi_u \rangle = \frac{R^2}{2} + \frac{R^2}{2} = R^2 \quad (22)$$

The same result is obtained for the in-phase combination of the ionic distributions (an excited singlet state),

$$|2^1\Psi_g\rangle = \frac{\chi_A(1)\chi_A(2) + \chi_B(1)\chi_B(2)}{\sqrt{2}} \quad (\text{singlet } g) \quad (23)$$

which gives

$$\langle 2^1\Psi_g | \hat{Z}^2 | 2^1\Psi_g \rangle = \frac{R^2}{2} + \frac{R^2}{2} = R^2 \quad (24)$$

We consider now a slightly more-complex situation, where three determinants give a significant contribution to the (singlet) wave function. They are the ionic term  $|^1\Psi_A\rangle$  and the neutral singlet  $|^1\Psi_g\rangle$ , mixed in variable proportions. Therefore, we write

$$\begin{aligned} |^1\Psi(\theta)\rangle &= \sin(\theta)|^1\Psi_A\rangle + \cos(\theta)|^1\Psi_g\rangle \\ &= \frac{\sin(\theta)\chi_A(1)\chi_A(2) + \cos(\theta)\chi_A(1)\chi_B(2) + \chi_B(1)\chi_A(2)}{\sqrt{2}} \end{aligned} \quad (25)$$

In this case, again, it is convenient to place the coordinate origin in the midpoint between A and B. However, one must consider that, now, the contribution that comes from  $\langle \hat{Z} \rangle$  will not vanish and must be taken into account. One has

$$\langle \hat{Z}_m^2 \rangle = \sin^2(\theta) \frac{R^2}{2} + \cos^2(\theta) \frac{R^2}{2} \quad (26)$$

and

$$\langle \hat{Z}_b^2 \rangle = \sin^2(\theta) \frac{R^2}{2} - \cos^2(\theta) \frac{R^2}{2} \quad (27)$$

and, hence,

$$\langle \hat{Z}^2 \rangle = 2 \sin^2(\theta) \frac{R^2}{2} = \sin^2(\theta) R^2 \quad (28)$$

On the other hand,

$$\langle \hat{Z} \rangle = -\sin^2(\theta) R \quad (29)$$

and, therefore,

$$\langle \hat{Z} \rangle^2 = \sin^4(\theta) R^2 \quad (30)$$

The cumulant  $\Lambda_{||}$  as a function of  $\theta$  becomes

$$\Lambda_{zz}(\theta) = R^2[\sin^2(\theta) - \sin^4(\theta)] = r^2 \sin^2(\theta) \cos^2(\theta) \quad (31)$$

The cumulant is zero for  $\theta = 0$  or  $\theta = \pi/2$ , while it reaches a maximum of  $R^2/4$  for a value of  $\theta = \pi/4$ .

## ■ ASSOCIATED CONTENT

### 📄 Supporting Information

Supporting figures showing the FCI potential energy curves of the ground state of the  $H_2$ ,  $Li_2$ ,  $N_2$ ,  $F_2$ ,  $BeH^-$ ,  $He_2$ ,  $HeH^-$ , and  $Be_2$  molecules, the one-electron and two-electron terms of the TPS for the FCI ground state of  $H_2$ , and the longitudinal component of the TPS for the UHF wave function of  $H_2$ . This material is available free of charge via the Internet at <http://pubs.acs.org>.

## ■ AUTHOR INFORMATION

### Corresponding Author

\*E-mail: [anc@unife.it](mailto:anc@unife.it).

## Notes

The authors declare no competing financial interest.

## ■ ACKNOWLEDGMENTS

We thank the University of Toulouse and the French CNRS for financial support. M.E.K. acknowledges the ANR-DFG action ANR-11-INTB-1009 MITLOW for his Ph.D. grant. O.B. acknowledges the support of the Erasmus Mundus program of the European Union (FPA 2010-0147). C.A. has been financed by the Italian MIUR through its PRIN 2009 funds.

## ■ REFERENCES

- (1) Kohn, W. *Phys. Rev.* **1964**, *133*, A171.
- (2) Resta, R.; Sorella, S. *Phys. Rev. Lett.* **1999**, *82*, 370.
- (3) Resta, R. *Phys. Rev. Lett.* **2005**, *95*, 196805.
- (4) Resta, R. *Eur. Phys. J. B* **2011**, *79*, 121.
- (5) Souza, I.; Wilkens, T.; Martin, R. M. *Phys. Rev. B* **2000**, *62*, 1666.
- (6) Resta, R. *Phys. Rev. Lett.* **2006**, *96*, 137601.
- (7) Resta, R. *J. Phys. Chem.* **2006**, *124*, 104104.
- (8) Vetere, V.; Monari, A.; Bendazzoli, G. L.; Evangelisti, S.; Paulus, B. *J. Phys. Chem.* **2008**, *128*, 024701.
- (9) Bendazzoli, G. L.; Evangelisti, S.; Monari, A.; Paulus, B.; Vetere, V. *J. Phys. Conf. Series* **2008**, *117*, 012005.
- (10) Bendazzoli, G. L.; Evangelisti, S.; Monari, A. *Int. J. Quantum Chem.* **2011**, *111*, 3416.
- (11) Angeli, C.; Bendazzoli, G. L.; Evangelisti, S. *J. Chem. Phys.* **2013**, *138*, 054314.
- (12) Giner, E.; Bendazzoli, G. L.; Evangelisti, S.; Monari, A. *J. Chem. Phys.* **2013**, *138*, 074315.
- (13) Monari, A.; Bendazzoli, G. L.; Evangelisti, S. *J. Chem. Phys.* **2008**, *129*, 134104.
- (14) Bendazzoli, G. L.; Evangelisti, S.; Monari, A. *Theor. Chem. Acc.* **2010**, *126*, 257.
- (15) Bendazzoli, G. L.; Evangelisti, S.; Monari, A.; Resta, R. *J. Chem. Phys.* **2010**, *133*, 064703.
- (16) Bendazzoli, G. L.; Evangelisti, S.; Monari, A. *Int. J. Quantum Chem.* **2012**, *112*, 653.
- (17) Monari, A.; Evangelisti, S. Finite size effects in graphene nanostructures. In *Physics and Applications of Graphene: Theory*; InTech Publishing: Wien, Austria, 2011; Chapter 14, pp 303–318.
- (18) Ángyán, J. G. *Curr. Org. Chem.* **2011**, *15*, 3609.
- (19) Ángyán, J. G. *Int. J. Quantum Chem.* **2009**, *109*, 2340.
- (20) Widmark, P.-O.; Malmqvist, P.-Å.; Roos, B. O. *Theor. Chem. Acc.* **1990**, *77*, 291.
- (21) DALTON, a Molecular Electronic Structure Program, Release 2.0 (2005). See <http://www.kjemi.uio.no/software/dalton/dalton.html> (accessed October 5, 2013).
- (22) Aidas, K.; Angeli, C.; Bak, K. L.; Bakken, V.; Bast, R.; Boman, L.; Christiansen, O.; Cimiraglia, R.; Coriani, S.; Dahle, P.; Dalskov, E. K.; Ekström, U.; Enevoldsen, T.; Eriksen, J. J.; Ettenhuber, P. Fernández, B.; Ferrighi, L.; Fliegl, H.; Frediani, L.; Hald, K.; Halkier, A.; Hättig, C.; Heiberg, H.; Helgaker, T.; Hennum, A. C.; Hettner, H.; Hjertenæs, E.; Høst, S.; Høyvik, I.-M.; Iozzi, M. F.; Janšík, B.; Jensen, H. J. A.; Jonsson, D.; Jørgensen, P.; Kauczor, J.; Kirpekar, S.; Kjærgaard, T.; Klopper, W.; Knecht, S.; Kobayashi, R.; Koch, H.; Kongsted, J.; Krapp, A.; Kristensen, K.; Ligabue, A.; Lutnaes, O. B.; Melo, J. I.; Mikkelsen, K. V.; Myhre, R. H.; Neiss, C.; Nielsen, C. B.; Norman, P.; Olsen, J.; Olsen, J. M. H.; Osted, A.; Packer, M. J.; Pawłowski, F.; Pedersen, T. B.; Provasi, P. F.; Reine, S.; Rinkevicius, Z.; Ruden, T. A.; Ruud, K.; Rybkin, V. V.; Salek, P.; Samson, C. C. M.; Sánchez de Meñas, A.; Saue, T.; Sauer, S. P. A.; Schimmelpfennig, B.; Sneskov, K.; Steindal, A. H.; Sylvester-Hvid, K. O.; Taylor, P.; Teale, A. M.; Tellgren, E. I.; Tew, D. P.; Thorvaldsen, A. J.; Thøgersen, L.; Vahtras, O.; Watson, M. A.; Wilson, D. J. D.; Ziolkowski, M.; Ågren, H. *WIREs Comput. Mol. Sci.* in press, DOI: 10.1002/wcms.1172.
- (23) Cimiraglia, R. Private communication.
- (24) Bendazzoli, G. L.; Evangelisti, S. *J. Chem. Phys.* **1993**, *98*, 3141.

- (25) Bendazzoli, G. L.; Evangelisti, S. *Int. J. Quantum Chem.* **1993**, *27*, 287.
- (26) Gagliardi, L.; Bendazzoli, G. L.; Evangelisti, S. *J. Comput. Chem.* **1997**, *18*, 1329.
- (27) Bendazzoli, G. L.; Evangelisti, S. NEPTUNUS, a Full CI program written by G. L. Bendazzoli and S. Evangelisti, with contributions by A. Monari, L. Gagliardi.
- (28) Angeli, C.; Bendazzoli, G. L.; Borini, S.; Cimiraglia, R.; Emerson, A.; Evangelisti, S.; Maynau, D.; Monari, A.; Rossi, E.; Sanchez-Marín, J.; Szalay, P.; Tajti, A. *Int. J. Quantum Chem.* **2007**, *107*, 2082.
- (29) Borini, S.; Monari, A.; Rossi, E.; Tajti, A.; Angeli, C.; Bendazzoli, G. L.; Cimiraglia, R.; Emerson, A.; Evangelisti, S.; Maynau, D.; Sanchez-Marín, J.; Szalay, P. *J. Chem. Inf. Model.* **2007**, *47*, 1271.
- (30) Rampino, S.; Monari, A.; Evangelisti, S.; Rossi, E.; Laganà, A. *Chem. Phys.* **2012**, *47*, 192.
- (31) Angeli, C.; Cimiraglia, R.; Malrieu, J.-P. *J. Chem. Educ.* **2008**, *85*, 150.
- (32) Shaik, S.; Danovich, D.; Silvi, B.; Lauvergnat, D. L.; Hiberty, P. *C. Chem.—Eur. J.* **2005**, *11*, 6358.
- (33) Hiberty, P. C.; Ramozzi, R.; Song, L.; Wu, W.; Shaik, S. *Faraday Discuss.* **2007**, *135*, 261.
- (34) Persico, M. Electronic diabatic states: definition, computation, and applications. In *Encyclopedia of Computational Chemistry*, Vol. 2; John Wiley and Sons: Chichester, U.K., 2010; p 852.
- (35) Angeli, C.; Cimiraglia, R.; Malrieu, J.-P. *Mol. Phys.* **2013**, *111*, 1069.
- (36) Bauschlicher, C. W.; Langhoff, S. R. *J. Chem. Phys.* **1988**, *89*, 4246.
- (37) Bendazzoli, G. L.; Evangelisti, S.; Passarini, F. *Chem. Phys.* **1997**, *215*, 217.
- (38) Verdicchio, M.; Bendazzoli, G. L.; Evangelisti, S.; Leininger, T. J. *Phys. Chem. A* **2013**, *117*, 192.
- (39) Knowles, P.; Werner, H. J. *Molpro Quantum Chemistry Package*; available via the Internet at <http://www.molpro.net> (accessed October 5, 2013).
- (40) Schaad, L. *J. Chem. Phys.* **1970**, *53*, 851.
- (41) Bishop, D. M.; Wetmore, R. W. *Mol. Phys.* **1973**, *26*, 145.
- (42) Kolos, W.; Wolniewicz, L. *J. Chem. Phys.* **1965**, *43*, 2429.
- (43) Velasco, R.; Ottinger, C.; Zare, R. N. *J. Chem. Phys.* **1969**, *51*, 5522.
- (44) Christian, R. H.; Duff, R. E.; Yarger, F. L. *J. Chem. Phys.* **1955**, *23*, 2045.
- (45) DeCorpo, J. J.; Steiger, R. P.; Franklin, J. L. *J. Chem. Phys.* **1970**, *53*, 936.
- (46) Brazier, C. R.; Oliphant, N. H.; Bernath, P. F. *Chem. Rev.* **1961**, *61*, 425.
- (47) Ogilvie, J. F.; Wang, F. Y. H. *J. Mol. Struct.* **1992**, *273*, 277.
- (48) Li, Y.; Lin, C. *Phys. Rev. A* **1999**, *60*, 2009.
- (49) Bondybey, V. E.; English, J. H. *J. Chem. Phys.* **1984**, *80*, 568.
- (50) Kenney, J.; Simons, J. *J. Chem. Phys.* **1975**, *62*, 592.

---

## B.8 ARTICLE VII

### *The Spin-Partitioned Total-Position Spread Tensor: An Application To Diatomic Molecules*

Published in: J. Phys. Chem. A, **2016**, *120*, 5230-5238.





# The Spin-Partitioned Total-Position Spread Tensor: An Application To Diatomic Molecules

Oriana Brea,<sup>†,‡</sup> Muammar El Khatib,<sup>†</sup> Gian Luigi Bendazzoli,<sup>¶</sup> Stefano Evangelisti,<sup>\*,†</sup> Thierry Leininger,<sup>†</sup> and Celestino Angeli<sup>§</sup>

<sup>†</sup>Laboratoire de Chimie et Physique Quantiques-LCPQ/IRSAMC, Université de Toulouse (UPS) et CNRS (UMR-5626), 118, Route de Narbonne, Toulouse Cedex 31062, France

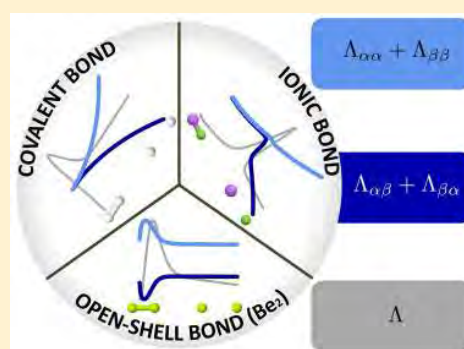
<sup>‡</sup>Departamento de Química, Facultad de Ciencias, Universidad Autónoma de Madrid, Módulo 13 Cantoblanco, 28049 Madrid, Spain

<sup>¶</sup>Dipartimento di Chimica Industriale "Toso Montanari", Università di Bologna, Viale Risorgimento 4, I-40136 Bologna, Italy

<sup>§</sup>Dipartimento di Scienze Chimiche e Farmaceutiche, Università di Ferrara, Via Fossato di Mortara 17, 44121 Ferrara, Italy

## Supporting Information

**ABSTRACT:** The spin partition (SP) of the total-position spread (TPS) tensor is applied to the case of a few light diatomic molecules at full configuration interaction (FCI) level. It appears that the SP-TPS tensor gives informations that are complementary with respect to the corresponding spin-summed (SS) quantity. The spin-summed total position-spread tensor (SS-TPS,  $\Lambda$ ) is defined as the second moment cumulant of the total position operator, and the SP-TPS is its partition in equal ( $\Lambda_{\alpha\alpha+\beta\beta}$ ) and different spin ( $\Lambda_{\alpha\beta+\beta\alpha}$ ) contributions. Then, the SS-TPS allows description of the molecule charge mobility, while the SP-TPS allows description of the spin delocalization. The most relevant Cartesian-component for both tensors (SS-TPS and SP-TPS) is the component along the chemical bond ( $\Lambda^{\parallel}$ ), and it was found that its behavior was related to the type of interaction involved. For covalent bonds the SP-TPS has a squared growth when the bond is stretched, while for ionic bonds there exists a faster-than-linear growth after the avoided-crossing between the covalent and the ionic states. Other exotic bonds, like He<sub>2</sub> and Be<sub>2</sub>, were also considered, and a particular spin delocalization was able to describe the different character of the two weakly bonded molecules, and specially the multireference character of the wave function along the dissociative potential energy curve.



## 1. INTRODUCTION

The introduction of the chemical bond as a description of how atoms link to each other goes back to the last century, when experiment and theory used the bond to explain the structural and energetic properties of the chemical systems. In the last years, the development of computational chemistry has opened the way to a more refined explanation of the intimate nature of the chemical bond and, even if being considered in some cases as an "old" concept, new kinds of bonds have been revealed.<sup>1–3</sup>

The development of theoretical techniques to explore new molecular electronic properties has provided important information about the electronic structure, as it is the case of atoms in molecules (AIM) theory,<sup>4</sup> electron localization function (ELF),<sup>5,6</sup> natural bond orbital (NBO),<sup>7,8</sup> and others. Such a wealth of different analysis of the electronic wave function has contributed to the elucidation of the key aspects of the chemical interactions.

The localization (LT,  $\lambda$ ) and the total position-spread (TPS,  $\Lambda$ ) tensors are quantities that account for the electronic fluctuation, clearly an important quantity to understand the nature of the wave function, in particular, its modification during molecular rearrangements. The LT is a quantity

introduced in the context of the theory of Kohn<sup>9</sup> to characterize electrical conductivity properties. A new formulation of the theory of localization of Kohn was introduced by Resta and co-workers with the localization tensor,<sup>10–12</sup> a quantity that diverges in the thermodynamic limit for conductors, while remaining finite for insulators. A remarkable sum rule connecting explicitly electrical resistivity and the LT has been later given by Souza, Wilkens, and Martin.<sup>13</sup> The LT is also an indicator of the square of the exchange-correlation lengths in the electronic distribution, which refers to the influence of one electron on the other electrons.<sup>14</sup> A few examples of the evaluation of this quantity for various molecular systems have been presented by the present authors<sup>1,15–20</sup> and by others (see ref 18 and references therein).

The interest related to the application of the LT to molecular systems is twofold. On the one hand, one can consider a

**Special Issue:** Piergiorgio Casavecchia and Antonio Lagana Festschrift

**Received:** January 30, 2016

**Revised:** March 23, 2016

**Published:** March 25, 2016

homologous series of molecules and use the LT to study the insulator/conductor properties as a function of the size of the system with the aim to identify the key molecular features controlling these properties, with an important relevance in the field of molecular electronics. On the other hand, the evaluation of the LT for a molecular system is interesting in itself, given that it allows to increase the knowledge of the complex structure of the wave function. In fact, this quantity allows to identify, besides the insulator/conductor nature, intriguing properties of the electronic distribution with a connection to the chemical description of the molecular architecture.

The LT is a “per electron” quantity, and in molecular studies this can pose a limit, given that different electrons with different fluctuation properties are present in a molecule (core, valence, and lone pairs). For these reasons, we prefer to use the TPS tensor,<sup>18</sup> a quantity more appropriate than the LT when considering molecular systems. The TPS is trivially related to the LT, given that it is the second moment cumulant of the total position operator, while the LT is the same quantity divided by the total number of electrons. Unlike the LT, TPS shows a size-consistency property: the TPS of non-interacting fragments is the sum of the TPS of the individual fragments, which is an extremely useful property when dealing with bond breaking or formation.

In previous investigations,<sup>18,21</sup> we used the TPS to monitor the wave function during the dissociation of a set of diatomic molecules. We found that this tensor is clearly sensitive not only to the change in the wave function as a consequence of the bond breaking but also to the nature of the chemical bond, showing a different behavior for covalent and ionic molecules as well as the charge-shift interaction in F<sub>2</sub>.<sup>3,22</sup> Moreover, in one of our recent studies,<sup>19</sup> we realized that the TPS partitioned according to the spin variables is an important quantity to understand spin mobility and to show the differences between charge and spin delocalization. Therefore, our aim in the present work is to report the variation of the spin-partitioned TPS when diatomic molecules are stretched, focused on the behavior of the different chemical bonds.

The paper is organized as follows. Section 2 reports the general formalism of the spin-partitioned TPS, in Section 3 the computational details are shortly described, the results are presented and discussed in Section 4, and, finally, a few conclusions are sketched out in Section 5.

## 2. GENERAL FORMALISM: SPIN-PARTITION OF TOTAL POSITION SPREAD TENSOR

To elaborate the formalism of the spin-partitioned (SP) TPS tensor, let us express the position operator  $\hat{r}$  of an electron as the sum of its  $\alpha$ - and  $\beta$ -spin components. By multiplying the position operator with the particle number operator for  $\alpha$ -spin ( $\hat{n}_\alpha$ ) and  $\beta$ -spin ( $\hat{n}_\beta$ ):

$$\hat{r}(i) = \sum_{\sigma=\alpha,\beta} \hat{r}(i)\hat{n}_\sigma(i) \quad (1)$$

From the one-particle position operator,  $\hat{r}$ , it is possible to define the total position operator,  $\hat{R}$ , as the sum over all electrons in the molecular system:

$$\hat{R} = \sum_{i=1}^n \sum_{\sigma=\alpha,\beta} \hat{r}(i)\hat{n}_\sigma(i) \quad (2)$$

and its corresponding spin-partitioned terms

$$\hat{R}_\sigma = \sum_{i=1}^n \hat{r}(i)\hat{n}_\sigma(i), \text{ where } \hat{R} = \hat{R}_\alpha + \hat{R}_\beta \quad (3)$$

The ordinary, spin-summed TPS tensor (SS-TPS),  $\Lambda$ , is defined as the second moment cumulant<sup>23</sup> of the total position operator:

$$\Lambda = \langle \Psi | \hat{R}^2 | \Psi \rangle - \langle \Psi | \hat{R} | \Psi \rangle^2 \quad (4)$$

The TPS (or SS-TPS) has an incremental behavior when a system experiences a high delocalization of the wave function. This is the reason why we decided to drop the name *localization* tensor in favor of *total position-spread* tensor.<sup>15,18,24</sup> For the particular case when molecules are stretched, large values of the tensor will indicate the most relevant region for the chemical process that could be used as an intrinsic characteristic of the system.

As previously discussed, according to eqs 2 and 3, the operator  $\hat{R}$  can be partitioned as the sum of  $\hat{R}_\alpha$  and  $\hat{R}_\beta$  operators. By taking the square of eq 3 one trivially obtains:

$$\hat{R}^2 = \hat{R}_\alpha^2 + \hat{R}_\beta^2 + \hat{R}_\alpha\hat{R}_\beta + \hat{R}_\beta\hat{R}_\alpha \quad (5)$$

Consequently, from the definition shown in eq 4 it is possible to construct four cumulants:

$$\Lambda_{\alpha\alpha} = \langle \Psi | \hat{R}_\alpha^2 | \Psi \rangle - \langle \Psi | \hat{R}_\alpha | \Psi \rangle^2 \quad (6)$$

$$\Lambda_{\beta\beta} = \langle \Psi | \hat{R}_\beta^2 | \Psi \rangle - \langle \Psi | \hat{R}_\beta | \Psi \rangle^2 \quad (7)$$

$$\Lambda_{\alpha\beta} = \langle \Psi | \hat{R}_\alpha\hat{R}_\beta | \Psi \rangle - \langle \Psi | \hat{R}_\alpha | \Psi \rangle \langle \Psi | \hat{R}_\beta | \Psi \rangle \quad (8)$$

$$\Lambda_{\beta\alpha} = \langle \Psi | \hat{R}_\beta\hat{R}_\alpha | \Psi \rangle - \langle \Psi | \hat{R}_\beta | \Psi \rangle \langle \Psi | \hat{R}_\alpha | \Psi \rangle \quad (9)$$

The sum of all contributions in eqs 6–9 recovers the value of the SS-TPS:

$$\Lambda = \Lambda_{\alpha\alpha} + \Lambda_{\beta\beta} + \Lambda_{\alpha\beta} + \Lambda_{\beta\alpha} \quad (10)$$

**2.1. General Properties.** The two terms  $\Lambda_{\alpha\beta}$  and  $\Lambda_{\beta\alpha}$  are identical, since the commutator between  $\hat{R}_\alpha$  and  $\hat{R}_\beta$  vanishes. When the wave functions have a total  $\hat{S}_z$  spin component equal to zero,  $\Lambda_{\alpha\alpha}$  and  $\Lambda_{\beta\beta}$  are identical. For this reason, we will report in this work the global component  $\Lambda_{\alpha\beta+\beta\alpha}$  and for the same spin component  $\Lambda_{\alpha\alpha}$  plus  $\Lambda_{\beta\beta}$  ( $\Lambda_{\alpha\alpha+\beta\beta}$ ).

It is important to notice that  $\Lambda_{\alpha\alpha}$  and  $\Lambda_{\beta\beta}$  are second-order cumulants themselves and are therefore positive definite. The quantities  $\Lambda_{\alpha\beta}$  and  $\Lambda_{\beta\alpha}$  however, are joint cumulants,<sup>25,26</sup> so they are not necessarily positive definite. This will be seen in the applications where  $\Lambda_{\alpha\alpha}$  and  $\Lambda_{\beta\beta}$  are always positive, while  $\Lambda_{\alpha\beta} + \Lambda_{\beta\alpha}$  do not have a definite sign.

The complete SS-TPS tensor is given by eq 10. If  $\langle \Psi | \hat{R}_\alpha | \Psi \rangle = 0$ , we have

$$\Lambda_{\alpha\alpha} = \langle \Psi | \hat{R}_\alpha^2 | \Psi \rangle, \text{ where } \langle \Psi | \hat{R}_\alpha | \Psi \rangle = 0 \quad (11)$$

and

$$\Lambda_{\alpha\beta+\beta\alpha} = \langle \Psi | \hat{R}_\alpha\hat{R}_\beta | \Psi \rangle, \text{ where } \langle \Psi | \hat{R}_\alpha | \Psi \rangle = 0 \quad (12)$$

while if it is  $\langle \Psi | \hat{R}_\beta | \Psi \rangle = 0$ , we have

$$\Lambda_{\beta\beta} = \langle \Psi | \hat{R}_\beta^2 | \Psi \rangle, \text{ where } \langle \Psi | \hat{R}_\beta | \Psi \rangle = 0 \quad (13)$$

and

$$\Lambda_{\alpha\beta+\beta\alpha} = \langle \Psi | \hat{\mathbf{R}}_{\alpha} \hat{\mathbf{R}}_{\beta} | \Psi \rangle, \text{ where } \langle \Psi | \hat{\mathbf{R}}_{\beta} | \Psi \rangle = 0 \quad (14)$$

Notice that  $\langle \Psi | \hat{\mathbf{R}} | \Psi \rangle = \langle \Psi | \hat{\mathbf{R}}_{\alpha} | \Psi \rangle + \langle \Psi | \hat{\mathbf{R}}_{\beta} | \Psi \rangle$ . However, in general,  $\langle \Psi | \hat{\mathbf{R}}_{\alpha} | \Psi \rangle$  and  $\langle \Psi | \hat{\mathbf{R}}_{\beta} | \Psi \rangle$  will be different. Therefore, by a suitable coordinate translation, it is not possible to annihilate simultaneously both  $\langle \Psi | \hat{\mathbf{R}}_{\alpha} | \Psi \rangle$  and  $\langle \Psi | \hat{\mathbf{R}}_{\beta} | \Psi \rangle$ . Hence, normally one cannot express the different TPS spin contributions via eqs 11–14. In particular, if the coordinates are chosen in such a way that  $\langle \Psi | \hat{\mathbf{R}} | \Psi \rangle = 0$  (and therefore  $\langle \Psi | \hat{\mathbf{R}}_{\alpha} | \Psi \rangle = -\langle \Psi | \hat{\mathbf{R}}_{\beta} | \Psi \rangle$ ) the SS-TPS will be given by  $\Lambda = \langle \Psi | \hat{\mathbf{R}}^2 | \Psi \rangle$ , but eqs 11–14 will not hold. It is only when  $\langle \Psi | \hat{\mathbf{R}}_{\alpha} | \Psi \rangle = \langle \Psi | \hat{\mathbf{R}}_{\beta} | \Psi \rangle$  that eqs 1–10 can simultaneously hold. In fact, in such a case, by a suitable coordinate translation, we can have both  $\langle \Psi | \hat{\mathbf{R}}_{\alpha} | \Psi \rangle = 0$  and  $\langle \Psi | \hat{\mathbf{R}}_{\beta} | \Psi \rangle = 0$ , and therefore  $\langle \Psi | \hat{\mathbf{R}} | \Psi \rangle = \langle \Psi | \hat{\mathbf{R}}_{\alpha} | \Psi \rangle + \langle \Psi | \hat{\mathbf{R}}_{\beta} | \Psi \rangle = 0$ .

**2.2. Long-Distance Behavior.** The long-distance behavior of the longitudinal components of the TPS tensor in a diatomic system is related to the presence of entanglement in the wave function, as discussed in ref 19. Quantum Entanglement exists when two or several particles participate to a quantum state whose wave function cannot be described as a product of the wave functions of the individual particles, even in absence of any interaction among the particles. It means that, even at infinite distances, there is a correlation between the system particles. In the language of Quantum Chemistry, the entanglement is often (although not always) associated with the presence of nondynamical correlation. In this case, several Slater determinants are needed for a correct description of the system, even if their parts are not related by a physical interaction.

Very often, the breaking of a molecular bond gives rise to an entangled wave function. This is the case, for instance, in all singlet systems where the two electrons of a bond give rise, after the breaking process, to two unpaired electrons belonging to different atoms. To keep a singlet wave function, the two electrons must be “non-dynamically” correlated in such a way that an  $\alpha$ -electron on atom one implies a  $\beta$ -electron on atom two, and vice versa. Some examples of this can be found among the systems treated in the present work: the ground states of  $\text{H}_2$ ,  $\text{Li}_2$ , and  $\text{F}_2$ , for instance, or the neutral component of the two lowest states of  $\text{LiF}$ . The divergence, with opposite signs, of  $\Lambda_{\alpha\alpha+\beta\beta}$  and  $\Lambda_{\alpha\beta+\beta\alpha}$  are a manifestation of this entanglement.

A somehow related phenomenon is the absence of rotational invariance in the F atoms obtained in the dissociation of  $\text{F}_2$  or the ground state of  $\text{LiF}$ . An isolated atom is necessarily spherically symmetric, so in the case of a fluorine atom one must average over the three possibilities of a hole in an otherwise completely filled 2p subshell. However, in the case of the dissociation of  $\text{F}_2$ , for instance, at any finite distance the two electrons will be located in the empty  $3\sigma_u$  orbital. This is mainly given by the antisymmetric combination of the  $2p_z$  atomic orbitals,  $z$  being the internuclear axis. By continuity, this will be true for any value of the internuclear separation, even at infinite distance. For this reason the fluorine SS-TPS converge to a limit where the equivalent  $xx$  and  $yy$  components are not degenerate with the  $zz$  one.

**2.3. Single-Determinant Case.** If the wave function can be expressed by a single Slater determinant,  $|\Phi_0\rangle$ , the  $\Lambda_{\alpha\beta}$  component vanishes. To demonstrate it, let us first introduce the resolution of the identity operator,  $\sum_I |\Phi_I\rangle \langle \Phi_I|$ , between the two  $\hat{\mathbf{R}}$  operators in  $\hat{\mathbf{R}}^2$ :

$$\langle \Phi_0 | \hat{\mathbf{R}}^2 | \Phi_0 \rangle = \sum_I \langle \Phi_0 | \hat{\mathbf{R}} | \Phi_I \rangle \langle \Phi_I | \hat{\mathbf{R}} | \Phi_0 \rangle \quad (15)$$

As a consequence of  $\hat{\mathbf{R}}$  being a one-electron operator, the determinants  $|\Phi_I\rangle$  giving a nonvanishing contribution in the sum in eq 15 are either  $|\Phi_0\rangle$  itself or single excitations,  $|\Phi_{I_1}\rangle$ , from the determinant  $|\Phi_0\rangle$ . But a single excitation  $|\Phi_{I_1}\rangle$  cannot be simultaneously an  $\alpha$  and a  $\beta$  excitation from  $|\Phi_0\rangle$ , hence

$$\langle \Phi_0 | \hat{\mathbf{R}}_{\alpha} | \Phi_{I_1} \rangle \langle \Phi_{I_1} | \hat{\mathbf{R}}_{\beta} | \Phi_0 \rangle = 0 \quad (16)$$

This means that the  $\alpha\beta$  and  $\beta\alpha$  contributions vanish:

$$\begin{aligned} \sum_{I_1} \langle \Phi_0 | \hat{\mathbf{R}}_{\alpha} | \Phi_{I_1} \rangle \langle \Phi_{I_1} | \hat{\mathbf{R}}_{\beta} | \Phi_0 \rangle \\ = \sum_{I_1} \langle \Phi_0 | \hat{\mathbf{R}}_{\beta} | \Phi_{I_1} \rangle \langle \Phi_{I_1} | \hat{\mathbf{R}}_{\alpha} | \Phi_0 \rangle \\ = 0 \end{aligned} \quad (17)$$

The only surviving term in the resolution of the identity, eq 15, is when  $|\Phi_I\rangle = |\Phi_0\rangle$ , which implies that

$$\langle \Phi_0 | \hat{\mathbf{R}}_{\alpha} \hat{\mathbf{R}}_{\beta} | \Phi_0 \rangle = \langle \Phi_0 | \hat{\mathbf{R}}_{\alpha} | \Phi_0 \rangle \langle \Phi_0 | \hat{\mathbf{R}}_{\beta} | \Phi_0 \rangle \quad (18)$$

and hence  $\Lambda_{\alpha\beta} = 0$  (see eq 8). The same result holds obviously for  $\Lambda_{\beta\alpha}$ .

### 3. COMPUTATIONAL DETAILS

Electronic structure calculations were performed to build the potential energy curves of the bond breaking of diatomic molecules at the Full Configuration Interaction (FCI) level of theory.

The dependence of the SP-TPS on the internuclear distance  $R$  was studied for the ground state of homoatomic ( $\text{H}_2$ ,  $\text{He}_2$ ,  $\text{Li}_2$ ,  $\text{Be}_2$ ,  $\text{N}_2$ , and  $\text{F}_2$ ) and heteroatomic ( $\text{LiF}$ ) molecules. For  $\text{LiF}$  the first  $^1\Sigma^+$  excited state was also computed, to correctly describe the ionic-neutral avoided-crossing region. All systems under investigation are closed-shell singlet molecules with  $^1\Sigma_g^+$  symmetry, except for the  $\text{LiF}$  case for which the symmetry is  $^1\Sigma^+$ .

The atomic natural orbital (ANO) basis set optimized by Roos and co-workers<sup>27</sup> was used, by adopting different contractions for the considered diatomic molecules. The details of the basis sets employed in this work are shown in Table 1,

**Table 1. Dimension of the Basis Set and Number of Determinants Spanning the Full Configuration Interaction Space for the Molecules Studied in This Work**

molecule	basis set	correlated electrons	active orbitals	symmetry-adapted determinants
$\text{H}_2$	7s3p3d	2	62	674
$\text{Li}_2$	7s6p4d3f	2	130	2474
$\text{N}_2$	3s2p	10	16	2 388 528
$\text{F}_2$	3s2p	14	16	16 361 136
$\text{LiF}$	3s2p	8	16	828 944
$\text{He}_2$	7s4p3d	4	68	681 460
$\text{Be}_2$	7s7p4d3f	4	136	10 670 896

together with the number of the symmetry-adapted Slater determinants spanning the FCI space, and the number of correlated electrons. Note that the use of a small basis set for the F and the N atoms is justified by the fact that one must keep the size of the FCI space manageable.

The initial calculations of the reference wave function (Hartree–Fock (HF)) were done using the Dalton quantum

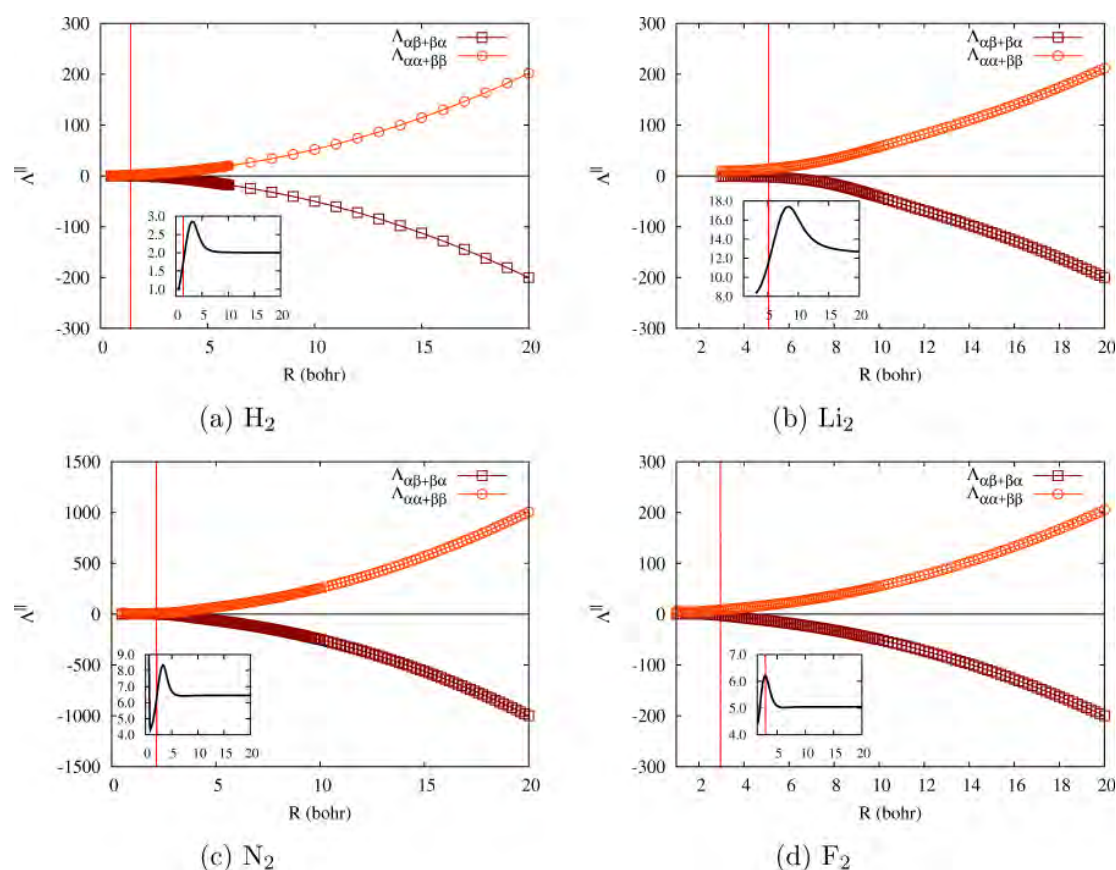


**Figure 1.** Spin-partitioned SP-TPS (parallel component,  $\Lambda^{\parallel}$ ) for the molecules in group:  $\text{H}_2$  (a),  $\text{Li}_2$  (b),  $\text{N}_2$  (c), and  $\text{F}_2$  (d). (insets) The SS-TPS for comparison. The vertical red lines represent the equilibrium internuclear distance.

chemistry package.<sup>28</sup> Then, the one- and two-electron integrals on the atomic orbital (AO) basis were transformed to the HF molecular orbital (MO) basis set. Finally, the FCI calculations were performed using the Neptunus program.<sup>29–32</sup> It is important to note that the 1s orbitals were kept frozen (doubly occupied) in the FCI calculations (frozen-core FCI).

#### 4. RESULTS AND DISCUSSIONS

We present the results relative to three classes of molecules, having different types of bonds. In Group I we classify homoatomic molecules with bonds going from a covalent to a charge-shift nature. Group II contains a single system, the well-known ionic-bonded LiF dimer. In Group III, we consider two “weakly-bonded” systems, the helium and beryllium dimers. In the next sections, the three groups are discussed separately.

**4.1. Group I. Covalent and Charge-Shift Bonds:  $\text{H}_2$ ,  $\text{Li}_2$ ,  $\text{N}_2$ , and  $\text{F}_2$ .** The longitudinal ( $\Lambda^{\parallel}$ ) and perpendicular ( $\Lambda^{\perp}$ ) SP-TPS (both  $\Lambda_{\alpha\alpha+\beta\beta}$  and  $\Lambda_{\alpha\beta+\beta\alpha}$ ) are reported in Figures 1 and 2, respectively, for the  $\text{H}_2$ ,  $\text{Li}_2$ ,  $\text{N}_2$ , and  $\text{F}_2$  (group I) molecules. For the sake of comparison, the SS-TPS is also reported in the insets. The behavior of the SS-TPS has been discussed in detail in ref 18, and only the case of the hydrogen molecule is here shortly recalled, focusing on the parallel component (inset of Figure 1a), given that the perpendicular component ( $\Lambda^{\perp}$ ) does not show any special behavior. Starting from the equilibrium distance, the SS-TPS increases, reaching a maximum value of  $\approx 2.8$  bohr<sup>2</sup>. By further stretching the bond the SS-TPS quickly decreases to recover twice the value of an isolated hydrogen

atom (1 bohr<sup>2</sup>). In the repulsive region,  $\Lambda^{\parallel}$  is lower than in the asymptotic limit as a consequence of the effective charge of the nuclei, which approaches the value of 2 when  $R \rightarrow 0$ . This, in turn, makes the electrons feel a stronger electron–nucleus attraction and leads to a strong spatial contraction of the wave function. This behavior has been rationalized,<sup>18</sup> within an orthogonal valence bond (OVb) representation of the wave function,<sup>21</sup> in terms of the variation in the ground state wave function of the ionic component (for which the SS-TPS shows a dependence proportional to  $R^2$ ), thus confirming that  $\Lambda$  is able to capture important features of the wave function. A similar behavior is observed for the other molecules in the group I ( $\text{Li}_2$ ,  $\text{N}_2$ , and  $\text{F}_2$ ; see Figure 1b–d).

The decomposition of the parallel component of the SS-TPS in its spin components shows interesting results. The same-spin contribution ( $\Lambda_{\alpha\alpha+\beta\beta}$ ) can be translated as a measure of the Fermi correlation, whereas the different-spin contribution ( $\Lambda_{\alpha\beta+\beta\alpha}$ ) gives indication of the Coulomb correlation. It is worth noticing here that a widely accepted definition of a strongly correlated system is when the magnitudes of Coulomb and Fermi correlations are comparable,<sup>33</sup> and this happens when the wave function shows a multireference character. In the systems investigated herein, all SP-TPS components diverge as  $R^2$  if  $R \rightarrow \infty$  ( $\Lambda_{\alpha\alpha+\beta\beta}$  being slightly larger than  $\Lambda_{\alpha\beta+\beta\alpha}$ ), even staying within the insulating regime (the SS-TPS does not show divergences), as happens for finite-size molecular systems (see Section 2.2 for a description of the asymptotic behavior of the TPS). When a chemical bond is broken, in general, the

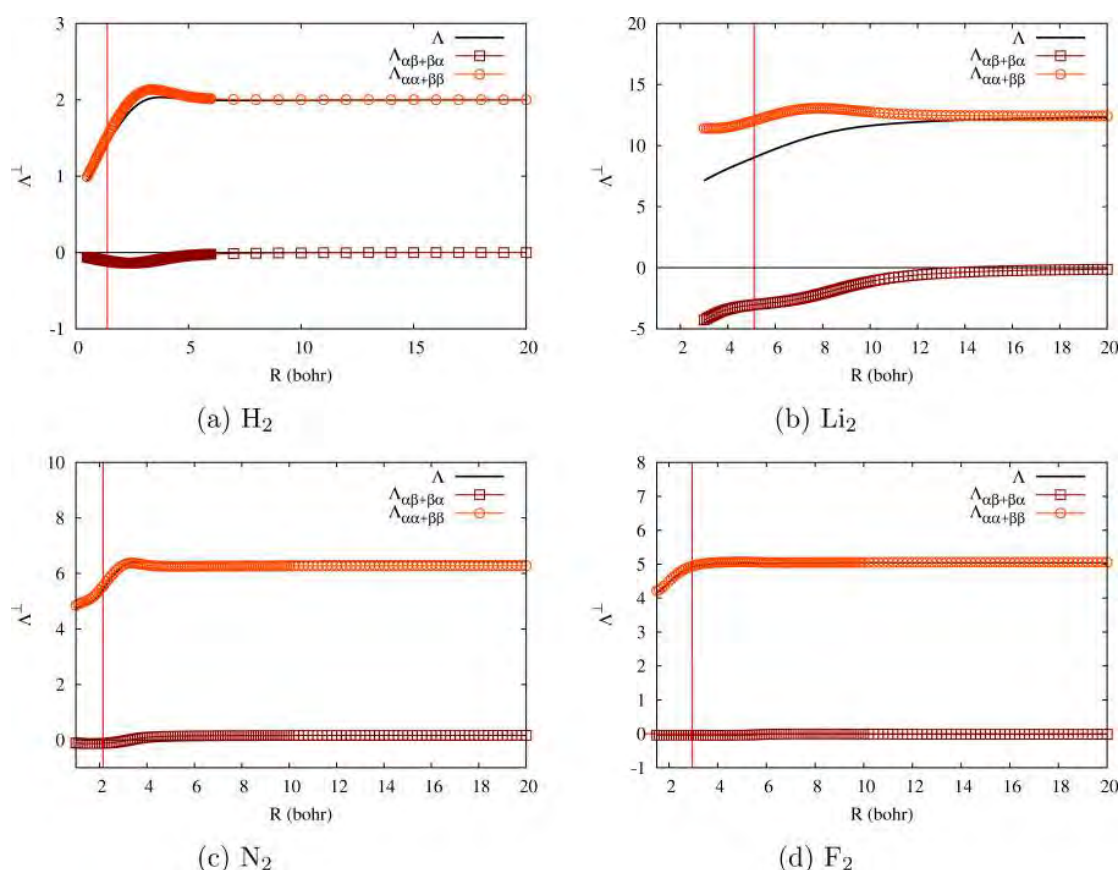


**Figure 2.** Spin-partitioned SP-TPS (perpendicular component,  $\Lambda^\perp$ ) for the molecules in group I:  $\text{H}_2$  (a),  $\text{Li}_2$  (b),  $\text{N}_2$  (c), and  $\text{F}_2$  (d). The vertical red lines represent the equilibrium internuclear distance.

molecular wave functions must be represented by more than one configuration state function, and the SP-TPS is sensitive to this change in the nature of the wave function, as made evident by the  $R^2$  divergence of both the same-spin and different-spin contributions when  $R \rightarrow \infty$ . This behavior will be found again at short internuclear distances in Section 4.3, where we will discuss the case of weakly bonded systems and, in particular, the case of the  $\text{Be}_2$  molecule for which the bond has a multireference character. Such a behavior has been deeply analyzed in ref 19, highlighting a relation with the concept of quantum entanglement.

Concerning the other three molecules of this group, one clearly notes that what was reported for  $\text{H}_2$  remains valid also in these cases, confirming that the intimate nature of the chemical bond in the molecules belonging to this group is quite similar, even for the  $\text{F}_2$  charge-shift bond.

The perpendicular component of the SP-TPS for the group I molecules is reported in Figure 2. In this case the  $R$  dependence of the two components does not show particularly interesting trends.

**4.2. Group II. Ionic Bonds: The Paradigmatic LiF Molecule.** The LiF molecule shows a common example of an ionic bond. The parallel and perpendicular parts of the two relevant SP-TPS components are reported in Figure 3 as a function of the internuclear distance  $R$  for both the ground state and the first excited state of the same symmetry ( $^1\Sigma^+$ ). The parallel component of the SS-TPS is also reported for comparison in the insets.

Let us focus first on the parallel component. The observed behavior can be rationalized considering the nature of the two electronic states and the analysis reported in ref 19 for the simple case of the  $\text{H}_2$  molecule.

Concerning the nature of the two lowest electronic states of  $^1\Sigma^+$  symmetry, they are due to an avoided-crossing between two diabatic states, which can receive a clear description in a valence bond (VB)-like language. One of these states is neutral (dissociating to the ground states of the two atoms), and the other is ionic (dissociating to  $\text{Li}^+\cdots\text{F}^-$ ). The first diabatic state is the lowest in energy at large internuclear distances, while at the equilibrium distance the ionic state is the lowest. The two diabatic states cross at  $R \approx 11$  bohr. The adiabatic ground state coincides with the ionic diabatic state at short internuclear distances and corresponds to the neutral diabatic state for  $R > 11$  bohr (see Figure 4). Obviously, the opposite happens for the excited adiabatic state.

The dependence on  $R$  of a set of VB states has been studied in detail in ref 19 for the  $\text{H}_2$  molecule, for which the problem has been solved analytically in the case where the minimal Slater-type orbital basis is used. This analysis has revealed that both  $\Lambda_{\alpha\alpha+\beta\beta}^\parallel$  and  $\Lambda_{\alpha\beta+\beta\alpha}^\parallel$  diverge as  $R^2$  (with a positive sign in the first case and a negative in the second) for the neutral wave function, while it has a constant asymptote for the  $\text{H}^+\cdots\text{H}^+$  (or  $\text{H}^+\cdots\text{H}^-$ ) wave function. It is worth noticing that for the  $\text{H}^+\cdots\text{H}^+ \pm \text{H}^+\cdots\text{H}^-$  wave functions both SP-TPS components show again an  $R^2$  divergent behavior.

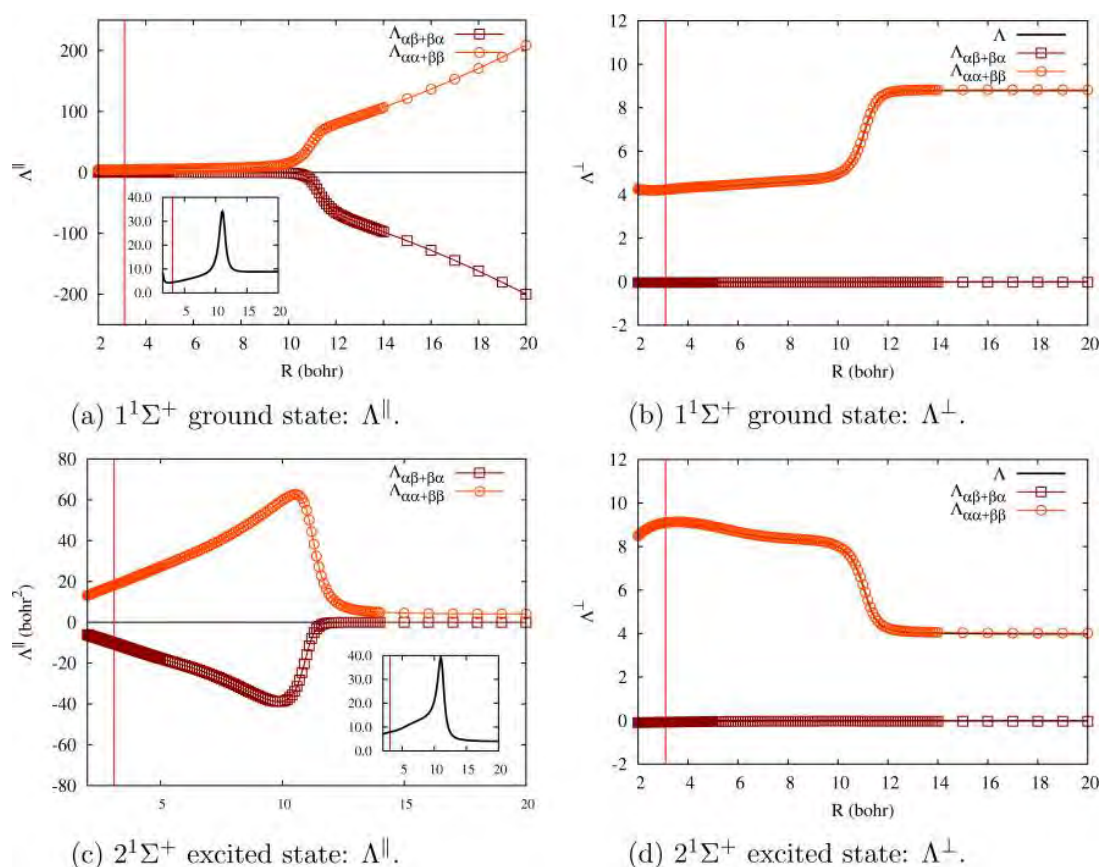


**Figure 3.** Spin-partitioned TPS (parallel and perpendicular components) for the: (a)  $1^1\Sigma^+$  ground state SP-TPS, parallel component (b)  $1^1\Sigma^+$  ground state SP-TPS, perpendicular component, (c)  $2^1\Sigma^+$  ground-state SP-TPS, parallel component and (d)  $2^1\Sigma^+$  ground state SP-TPS, perpendicular component of LiF. (insets) The parallel SS-TPS for comparison. The vertical red lines represent the equilibrium internuclear distance. Note the difference in the scale between (a) and (c).

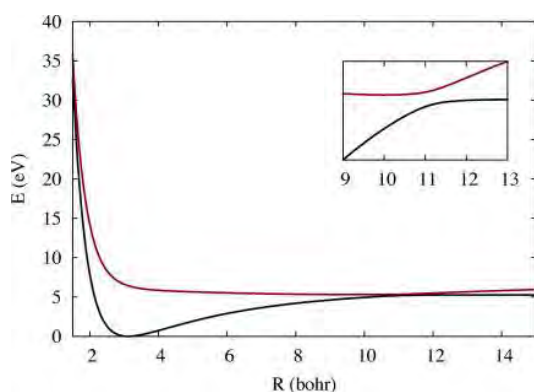


**Figure 4.** Potential energy curve of LiF for the  $1^1\Sigma^+$  ground and first excited states at FCI level of theory. (inset) The avoiding-crossing region is reported.

The considerations reported above allow to explain the results reported in Figure 3a,c. Indeed, for the ground state (Figure 3a) both  $\Lambda_{\alpha\alpha}^{\parallel}$  and  $\Lambda_{\alpha\beta}^{\parallel}$  are almost constant for  $R < 11$  bohr (the state is essentially ionic,  $\text{Li}^+\cdots\text{F}^-$ ), while they diverge for  $R > 11$  bohr (the state is essentially neutral,  $\text{Li}\cdots\text{F}$ ). Strictly the opposite behavior is observed for the excited state (Figure 3c), due to the opposite nature of this state.

Using the same logic, the dependence of both SP-TPS components of the perpendicular part of the SS-TPS (Figure

3b,d) can receive an analogous interpretation. In particular, it is interesting to notice that the perpendicular component of  $\Lambda_{\alpha\beta+\beta\alpha}$  is very small, for any value of the internuclear distance. This fact indicates an absence of correlation between  $\alpha$  and  $\beta$  electrons in the direction orthogonal to the internuclear direction. This is true both for the ground and the first excited state.

**4.3. Group III. "Weak Bonds":  $\text{He}_2$  and  $\text{Be}_2$ .** The two molecules considered in this section,  $\text{He}_2$  and  $\text{Be}_2$ , are only apparently similar, their common character being just the weakest bonds in this investigation. In fact, the nature of the bond in the two cases is deeply different. The helium dimer has an extremely weak bond, whose origin is due to a dispersion van der Waals interaction between the two atoms.<sup>34,35</sup> This gives rise to a very shallow potential-energy curve, with a tiny minimum at an internuclear distance close to six bohr. Beryllium dimer, however, has a comparatively much deeper minimum, due to a multireference nature of the wave function in the equilibrium region. At large distance, however, the  $\text{Be}_2$  wave function becomes atom-like and essentially single-reference (see ref 36 and references therein). The difference between the two wave function structures is clearly reflected by the different SS-TPS behavior in the two cases.

Except for very short internuclear distances, all parts of the TPS tensor for  $\text{He}_2$  are essentially atom-like: the perpendicular and parallel components, both SS and SP, are constant and virtually coincide with the asymptotic values. Since the atomic

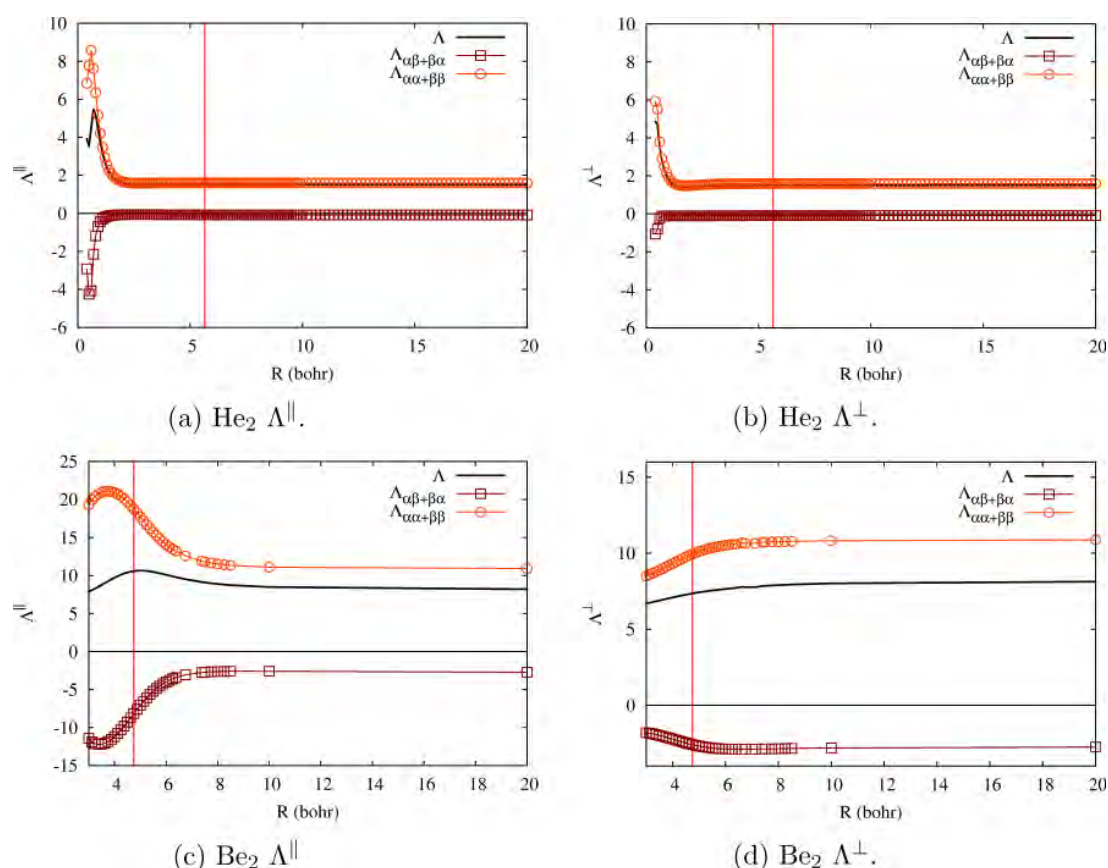


**Figure 5.** Spin-partitioned TPS (parallel and perpendicular components) for the molecules in group III: (a)  $\text{He}_2 \Lambda^{\parallel}$ , (b)  $\text{He}_2 \Lambda^{\perp}$ , (c)  $\text{Be}_2 \Lambda^{\parallel}$ , and (d)  $\text{Be}_2 \Lambda^{\perp}$ . The parallel SS-TPS is also reported for comparison. The vertical red lines represent the equilibrium internuclear distance.

wave function is isotropic, the perpendicular and parallel components are identical. The different-spin components are extremely small, a fact due to the single-determinant nature of the wave function, as discussed in Section 2. As a consequence, the equal-spin and total components are practically identical. At extremely short distances (below one bohr), the TPS values have a quick variation, probably due to a multi-reference nature of the wave function in this region. However, the fact must be stressed that these distances are unphysical for this dimer in normal conditions and could become relevant only at extremely high collision energies (or pressures). Moreover, the contracted ANO basis sets used in this investigation are not suitable to describe correctly the system at very short distances, for which, one should use uncontracted Gaussian orbitals with large exponents, to describe correlation effects in this range of distances. For these reasons, we did not continue our investigation in this direction.

We come now to the case of the beryllium dimer, which is a particularly interesting system. In the past, this molecule was thought to be a van der Waals system, like  $\text{He}_2$ , but in our recent paper its multireference nature was discovered and deeply detailed,<sup>1</sup> to which we address the reader for a more complete discussion. Here we recall some of the main conclusions reported in that work. At long interatomic distances ( $R > 10$  bohr, i.e., well beyond the equilibrium region), the wave function is essentially just the product of the two atomic wave functions. All components of the TPS are constant, in a way that is very much similar to what is observed

for  $\text{He}_2$ . Notice, however, that now the different-spin component is significantly different from zero (compare Figure 5a,b for  $\text{Be}_2$  to Figure 5c,d for  $\text{He}_2$ ). This fact is related to the importance of the electronic correlation in the Be atom, where the pair excitation  $2s^2 \rightarrow 2p^2$  plays a crucial role in the FCI wave function. In the equilibrium-distance region, the wave function is dominated by only two determinants, namely,  $[\text{core}]2\sigma_g^2 2\sigma_u^2$  and  $[\text{core}]2\sigma_g^2 3\sigma_g^2$ , where [core] is given by the doubly occupied  $1s^2$  orbitals of the two atoms. As a consequence, the maximum in the longitudinal SS-TPS is the result of a cancellation between the different-spin and same-spin contributions (see Figure 5c). As discussed in Section 4.1, the situation is somewhat similar to what happens for  $\text{H}_2$  or  $\text{Li}_2$ , with the difference that now the multideterminant wave function is at short interatomic distances, while at long distance the system is essentially a closed shell.

## 5. CONCLUSIONS

In this work we have reported a study of the dependence of the SP-TPS tensor on the internuclear distance for a selected set of diatomic molecules, which complements a similar work on the SS-TPS tensor<sup>18</sup> and the analysis of the behavior of the SP-TPS tensor in other systems, in particular, open-shell systems.<sup>15,16</sup>

We have illustrated this point by applying the formalism to a few light diatomic molecules, ranging from covalent ( $\text{H}_2$ ,  $\text{Li}_2$ , and  $\text{N}_2$ ), charge-shift ( $\text{F}_2$ ), and ionic ( $\text{LiF}$ ) bonds to weakly bonded systems like  $\text{He}_2$  and  $\text{Be}_2$ .



The present results show the ability of the SP-TPS tensor to give interesting information not only about molecular systems with unpaired electrons (where the spin delocalization can reasonably be expected to play a key role) as discussed in previous works but also in the case of “ordinary” molecules, in particular, when the bonds are stretched, leading to an open-shell electronic distribution.

Indeed, all the TPS’ tensors are deeply related to the entanglement of the wave function. In particular, while the SS-TPS measures the charge entanglement of a system, like in the ionic state of  $H_2$ , as discussed in ref 19, the SP components are related to the spin entanglement of the wave function that is present in open-shell wave functions. Moreover, the property that  $\Lambda_{\alpha\beta} + \Lambda_{\beta\alpha}$  exactly vanishes in the case of a single-determinant wave function could be extremely valuable, since it gives the opportunity of a nonambiguous definition of a closed-shell system. As an example of the use of this property, the nature of the bond in two weakly bonded systems ( $He_2$  and  $Be_2$ ) has been interpreted from the point of view of the SP-TPS, confirming that the stabilization of the  $He_2$  system with respect to the atoms is due to dispersion (van der Waals) forces, while in  $Be_2$  a particular type of weak bond appears.

## ■ ASSOCIATED CONTENT

### 📄 Supporting Information

The Supporting Information is available free of charge on the ACS Publications website at DOI: 10.1021/acs.jpca.6b01043.

Atomic Natural Orbital basis set description. Calculated dissociation curves for all the diatomic molecules described in the paper. Data with the energetic and TPS values obtained for all the systems. (PDF)

## ■ AUTHOR INFORMATION

### Corresponding Author

\*E-mail: Stefano.Evangelisti@irsamc.ups-tlse.fr.

### Notes

The authors declare no competing financial interest.

## ■ ACKNOWLEDGMENTS

We thank the Univ. of Toulouse and the French CNRS for financial support. M.E.K. acknowledges the ANR-DFG action ANR-11-INTB-1009 MITLOW for his Ph.D. grant. We acknowledge the support of the Erasmus Mundus programme of the European Union (FPA 2010-0147). O.B. thanks the Spanish “Ministerio de Educación Cultura y Deporte” for her Ph.D. grant. This work was supported by the Programme Investissements d’Avenir under the program ANR-11-IDEX-0002-02, reference ANR-10-LABX-0037-NEXT. Finally, we also thank the HPC resources of CALMIP under the allocation 2011-[p1048].

## ■ REFERENCES

- (1) El Khatib, M.; Bendazzoli, G. L.; Evangelisti, S.; Helal, W.; Leininger, T.; Tenti, L.; Angeli, C. Beryllium Dimer: A Bond Based on Non-Dynamical Correlation. *J. Phys. Chem. A* **2014**, *118*, 6664–6673.
- (2) Zhang, H.; Danovich, D.; Wu, W.; Brai da, B.; Hiberty, P. C.; Shaik, S. Charge-Shift Bonding Emerges as a Distinct Electron-Pair Bonding Family from Both Valence Bond and Molecular Orbital Theories. *J. Chem. Theory Comput.* **2014**, *10*, 2410–2418.
- (3) Shaik, S.; Danovich, D.; Wu, W.; Hiberty, P. C. Charge-Shift Bonding and its Manifestations in Chemistry. *Nat. Chem.* **2009**, *1*, 443–449.
- (4) Bader, R. F. W. A Quantum Theory of Molecular Structure and its Applications. *Chem. Rev.* **1991**, *91*, 893–928.
- (5) Becke, A. D.; Edgecombe, K. E. A Simple Measure of Electron Localization in Atomic and Molecular Systems. *J. Chem. Phys.* **1990**, *92*, 5397–5403.
- (6) Savin, A.; Nesper, R.; Wengert, S.; Fässler, T. F. ELF: The Electron Localization Function. *Angew. Chem., Int. Ed. Engl.* **1997**, *36*, 1808–1832.
- (7) Reed, A. E.; Curtiss, L. A.; Weinhold, F. Intermolecular Interactions from a Natural Bond Orbital, Donor-Acceptor Viewpoint. *Chem. Rev.* **1988**, *88*, 899–926.
- (8) Glendening, E. D.; Landis, C. R.; Weinhold, F. Natural Bond Orbital Methods. *Wiley Interdiscip. Rev. Comput. Mol. Sci.* **2012**, *2*, 1–42.
- (9) Kohn, W. Theory of the Insulating State. *Phys. Rev.* **1964**, *133*, A171–A181.
- (10) Resta, R.; Sorella, S. Electron Localization in the Insulating State. *Phys. Rev. Lett.* **1999**, *82*, 370–373.
- (11) Resta, R. Electron Localization in the Quantum Hall Regime. *Phys. Rev. Lett.* **2005**, *95*, 196805.
- (12) Resta, R. The Insulating State of Matter: a Geometrical Theory. *Eur. Phys. J. B* **2011**, *79*, 121–137.
- (13) Souza, I.; Wilkens, T.; Martin, R. M. Polarization and Localization in Insulators: Generating Function Approach. *Phys. Rev. B: Condens. Matter Mater. Phys.* **2000**, *62*, 1666–1683.
- (14) Resta, R. Kohn’s Theory of the Insulating State: A Quantum-Chemistry Viewpoint. *J. Chem. Phys.* **2006**, *124*, 104104.
- (15) El Khatib, M.; Leininger, T.; Bendazzoli, G. L.; Evangelisti, S. Computing the Position-Spread Tensor in the CAS-SCF Formalism. *Chem. Phys. Lett.* **2014**, *591*, 58–63.
- (16) Fertitta, E.; El Khatib, M.; Bendazzoli, G. L.; Paulus, B.; Evangelisti, S.; Leininger, T. The Spin-Partitioned Total Position-Spread Tensor: An Application to Heisenberg Spin Chains. *J. Chem. Phys.* **2015**, *143*, 244308.
- (17) Bendazzoli, G. L.; El Khatib, M.; Evangelisti, S.; Leininger, T. The total Position Spread in Mixed-Valence Compounds: A Study on the  $\{H_4^+\}$  Model System. *J. Comput. Chem.* **2014**, *35*, 802–808.
- (18) Brea, O.; El Khatib, M.; Angeli, C.; Bendazzoli, G. L.; Evangelisti, S.; Leininger, T. Behavior of the Position-Spread Tensor in Diatomic Systems. *J. Chem. Theory Comput.* **2013**, *9*, 5286–5295.
- (19) El Khatib, M.; Brea, O.; Fertitta, E.; Bendazzoli, G. L.; Evangelisti, S.; Leininger, T. The Total Position-Spread Tensor: Spin Partition. *J. Chem. Phys.* **2015**, *142*, 129902.10.1063/1.4916357
- (20) El Khatib, M.; Brea, O.; Fertitta, E.; Bendazzoli, G. L.; Evangelisti, S.; Leininger, T.; Paulus, B. Spin Delocalization in Hydrogen Chains Described with the Spin-Partitioned Total Position-Spread Tensor. *Theor. Chem. Acc.* **2015**, *134*, 29–36.
- (21) Angeli, C.; Bendazzoli, G. L.; Evangelisti, S. The Localization Tensor for the  $\{H_2\}$  Molecule: Closed Formulae for the Heitler-London and Related Wavefunctions and Comparison with Full Configuration Interaction. *J. Chem. Phys.* **2013**, *138*, 054314.
- (22) Shaik, S.; Danovich, D.; Silvi, B.; Lauvergnat, D. L.; Hiberty, P. C. Charge-Shift Bonding: A Class of Electron-Pair Bonds That Emerges from Valence Bond Theory and is Supported by the Electron Localization Function Approach. *Chem. - Eur. J.* **2005**, *11*, 6358–6371.
- (23) Kubo, R. Generalized Cumulant Expansion Method. *J. Phys. Soc. Jpn.* **1962**, *17*, 1100–1120.
- (24) Ángyán, J. G. Electron Localization and the Second Moment of the Exchange Hole. *Int. J. Quantum Chem.* **2009**, *109*, 2340–2347.
- (25) Severini, T. A. *Elements of Distribution Theory*; Cambridge University Press, 2005; Vol. 17.
- (26) Rao Jammalamadaka, S.; Subba Rao, T.; Terdik, G. Higher Order Cumulants of Random Vectors and Applications to Statistical Inference and Time Series. *Sankhya Indian J. Stat.* **2006**, *68*, 326.
- (27) Widmark, P.-O.; Malmqvist, P.-Å.; Roos, B. Density Matrix Averaged Atomic Natural Orbital (ANO) Basis Sets for Correlated Molecular Wave Functions. *Theor. Chim. Acta* **1990**, *77*, 291–306.
- (28) Aidas, K.; Angeli, C.; Bak, K. L.; Bakken, V.; Bast, R.; Boman, L.; Christiansen, O.; Cimraglia, R.; Coriani, S.; Dahle, P.; et al. The

Dalton Quantum Chemistry Program System. *Wiley Interdiscip. Rev. Comput. Mol. Sci.* **2014**, *4*, 269–284.

(29) Bendazzoli, G. L.; Evangelisti, S. *NEPTUNUS*, a Full CI Program; with Contributions by A. Monari, L. Gagliardi.

(30) Bendazzoli, G. L.; Evangelisti, S. A Vector and Parallel Full Configuration Interaction Algorithm. *J. Chem. Phys.* **1993**, *98*, 3141–3150.

(31) Bendazzoli, G. L.; Evangelisti, S. Computation and Analysis of the Full Configuration Interaction Wave Function of Some Simple Systems. *Int. J. Quantum Chem.* **1993**, *48*, 287–301.

(32) Gagliardi, L.; Bendazzoli, G. L.; Evangelisti, S. Direct-list Algorithm for Configuration Interaction Calculations. *J. Comput. Chem.* **1997**, *18*, 1329–1343.

(33) Gebhard, F. The Mott Metal-Insulator Transition. In *Springer Tracts in Modern Physics*; Springer Berlin Heidelberg: Berlin, Germany, 2000; Vol. 137.

(34) Schöllkopf, W.; Toennies, J. P. Nondestructive Mass Selection of Small Van der Waals Clusters. *Science* **1994**, *266*, 1345–1348.

(35) Chalasinski, G.; Szczesniak, M. M. Origins of Structure and Energetics of Van der Waals Clusters from ab Initio Calculations. *Chem. Rev.* **1994**, *94*, 1723–1765.

(36) Evangelisti, S.; Bendazzoli, G. L.; Gagliardi, L. Full Configuration Interaction Calculations on Be<sub>2</sub>. *Chem. Phys.* **1994**, *185*, 47–56.



## INSIDE COVER I

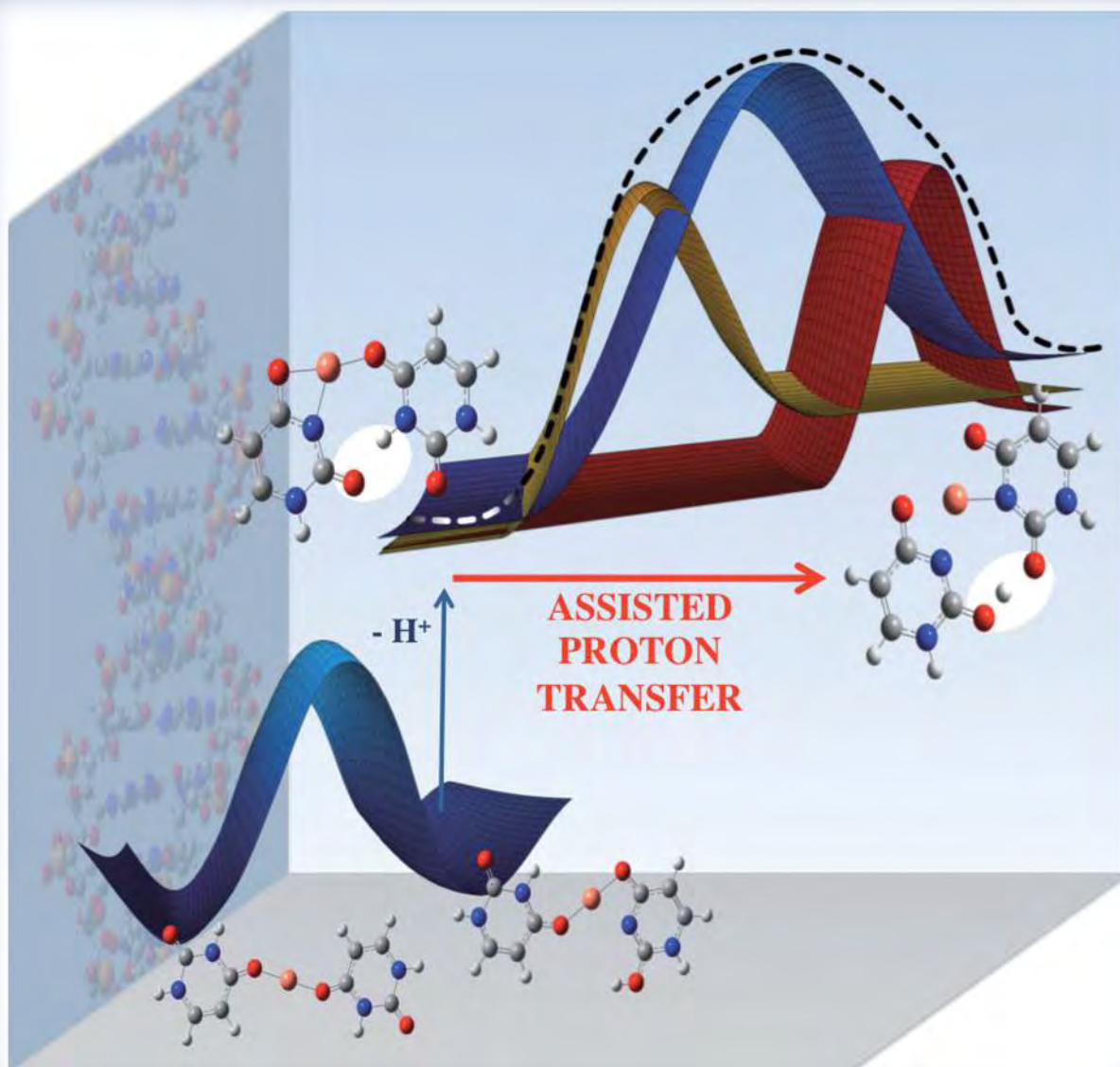
*Why Is the Spontaneous Deprotonation of  $[\text{Cu}(\text{uracil})_2]^{2+}$  Complexes Accompanied by Enolization of the System?*



A EUROPEAN JOURNAL

# CHEMPHYSICHEM

OF CHEMICAL PHYSICS AND PHYSICAL CHEMISTRY



11/2015

A Journal of



On p. 2375, M. Yáñez, A. M. Lamsabhi et al. report that the association of  $\text{Cu}^{2+}$  with a uracil dimer triggers its deprotonation, followed by what appears to be a single enolization process, but is actually a three-step assisted-proton-transfer mechanism.

[www.chemphyschem.org](http://www.chemphyschem.org)

WILEY-VCH



---

## INSIDE COVER II

*Beryllium-Based Anion Sponges: Close Relatives of Proton Sponges*





# CHEMISTRY

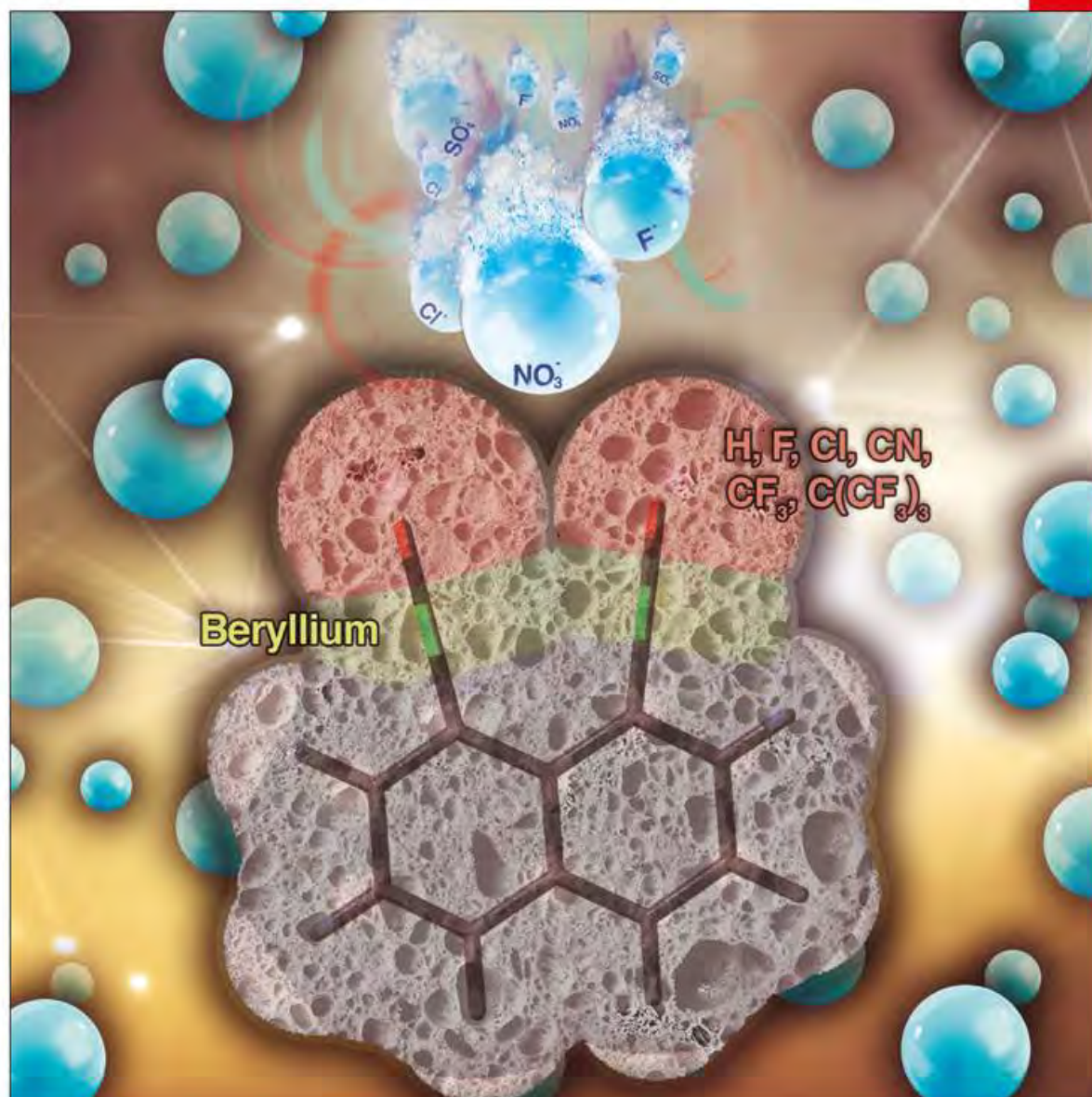
## A European Journal

www.chemeurj.org

A Journal of



2016-22/00



**Cover Picture:**

*M. Yáñez et al.*

Beryllium-Based Anion Sponges: Close Relatives of Proton Sponges

Supported by

ACES Asian Chemical  
Editorial Society

WILEY-VCH